

PROPERTIES OF MIXED ALKALI GERMANATE GLASSES

BY

MELISSANN MARIE ASHTON-PATTON

A THESIS
SUBMITTED TO THE FACULTY OF

ALFRED UNIVERSITY

IN PARTIAL FULFILLMENT OF THE REQUIREMENTS
FOR THE DEGREE OF

DOCTOR OF PHILOSOPHY

IN

GLASS SCIENCE

ALFRED, NEW YORK

APRIL, 2008

Alfred University theses are copyright protected and may be used for education or personal research only. Reproduction or distribution in any format is prohibited without written permission from the author.

PROPERTIES OF MIXED ALKALI GERMANATE GLASSES

BY

MELISSANN MARIE ASHTON-PATTON

B.S. ALFRED UNIVERSITY (2004)

B.A. ALFRED UNIVERSITY (2004)

M.S. ALFRED UNIVERSITY (2005)

SIGNATURE OF AUTHOR _____ (SIGNATURE ON FILE)

APPROVED BY _____ (SIGNATURE ON FILE)
JAMES E. SHELBY, ADVISOR

(SIGNATURE ON FILE)
ALEXIS G. CLARE, ADVISORY COMMITTEE

(SIGNATURE ON FILE)
DOREEN D. EDWARDS, ADVISORY COMMITTEE

(SIGNATURE ON FILE)
MATTHEW M. HALL, ADVISORY COMMITTEE

(SIGNATURE ON FILE)
CHAIR, ORAL DISSERTATION DEFENSE

ACCEPTED BY _____ (SIGNATURE ON FILE)
ALASTAIR N. CORMACK, DEAN
KAZUO INAMORI SCHOOL OF ENGINEERING

ACCEPTED BY _____ (SIGNATURE ON FILE)
WILLIAM M. HALL, ASSOCIATE PROVOST
FOR GRADUATE AND PROFESSIONAL PROGRAMS
ALFRED UNIVERSITY

ACKNOWLEDGEMENTS

I would like to begin by thanking Dr. Linda Jones who didn't ignore this crazy history major when she came into your office wanting to get an engineering degree, if you hadn't taken me seriously I wouldn't be where I am today. Secondly, I would like to thank Dr. Linda Mitchell and Shawn Allen who encouraged me to try engineering.

I would like to thank my family for all their years of support and encouragement. Kevin, thank you for graciously working here in Alfred even though it wasn't your first choice and for supporting me.

A big thank you goes out to all of the grad students and faculty I have had a privilege to collaborate with through the years.

Finally, last but not least, I would like to thank Dr. Shelby. You have been my advisor and mentor for the last 5 years. I have had the privilege and pleasure to learn from your expertise. I would not be the scientist I am today without all the time and energy you have invested into my education. Enjoy being a grandpa! And may the Phillies always come in first and the Braves in second!

TABLE OF CONTENTS

	PAGE
Chapter 1: Introduction	1
Chapter 2: Literature Review	3
2.1 Mixed Alkali Effect	3
2.2 Alkali Germanate Anomaly	5
2.2.1 Ivanov, Evstropiev, Murthy and Ip Theory	6
2.2.2 Henderson and Fleet Theory	7
2.2.3 Current Theory	7
2.3 References	9
Chapter 3: Experimental Procedures	20
3.1 Glass Batching	20
3.2 Glass Melting	20
3.3 Cutting, Grinding and Polishing	21
Chapter 4: General Properties	20
4.1 Introduction	20
4.2 Literature Review	20
4.2.1 Glass Transition Temperature	20
4.2.2 Density	28
4.3 Experimental Procedure	36
4.3.1 Glass Transition Temperature	36
4.3.2 Density	36
4.4 Results	37
4.4.1 Glass Transition Temperature	37
4.4.2 Density	43
4.5 Discussion	52
4.5.1 Glass Transition Temperature	52
4.5.2 Density	55
4.6 Conclusion	58
4.7 References	59
Chapter 5: Infrared Spectra	63
5.1 Introduction	63
5.2 Literature Review	63
5.3 Experimental Procedures	64
5.4 Results	65
5.4.1 Mixed Alkali Glasses	65
5.4.2 Germanate Anomaly	73
5.5 Discussion	76
5.6 Conclusion	80
5.7 References	80
Chapter 6: Electrical Conductivity	64
6.1 Introduction	64
6.2 Literature Review	65
6.2.1 Ionic Conductivity in Glasses	65
6.2.2 Mixed Mobile Ion Effects on Conductivity	74

	PAGE
6.2.3 Germanate Anomaly	75
6.3 Experimental Procedures	87
6.3.1 Sample Preparation	87
6.3.2 Electrical Conductivity Measurements	88
6.3.3 Comparing to NIST Standards.....	89
6.4 Results.....	91
6.4.1 Mixed Alkali Germanate Glasses	91
6.4.2 Germanate Anomaly	107
6.5 Discussion.....	120
6.5.1 Mixed Alkali Effect	120
6.5.2 Germanate Anomaly	129
6.6 Conclusions.....	142
6.7 References.....	143
Chapter 7: Crystallization	150
7.1 Introduction.....	150
7.2 Literature Review.....	150
7.2.1 Crystallization Kinetics.....	150
7.2.2 Previous Work	161
7.3 Experimental Procedure.....	163
7.3.1 Sample Preparation	163
7.3.2 Differential Scanning Calorimetry.....	163
7.3.3 X-Ray Diffraction	165
7.3.4 Environmental Scanning Electron Microscopy	165
7.4 Results.....	166
7.4.1 DSC Studies	166
7.4.2 High Temperature X-Ray Diffraction.....	189
7.5 Discussion.....	202
7.5.1 Kissinger Study.....	202
7.5.2 Effect of Particle Size	205
7.5.3 X-ray Diffraction	210
7.5.4 Comparison to Literature Data.....	212
7.6 Conclusion	213
7.7 References.....	213
Chapter 8: Conclusions	236
APPENDIX A	238

LIST OF TABLES

	PAGE
Table 2-I. Summary of Mixed Alkali Effect on Various Properties ⁴	3
Table 4-I. Maxima and Minima in T_g for the Binary Alkali Germanate Glasses	24
Table 4-II. Approximate Maxima in Density and Minima in Molar Volume for Alkali Germanate Glasses	29
Table 4-III. Glass Transition Temperatures for $\text{Na}_2\text{O}\cdot\text{K}_2\text{O}\cdot\text{GeO}_2$ and $\text{Li}_2\text{O}\cdot\text{Cs}_2\text{O}\cdot\text{GeO}_2$ Glasses	37
Table 4-IV. Glass Transition Temperatures for $0.5x \text{Na}_2\text{O}\cdot 0.5x \text{K}_2\text{O}\cdot(100-x)\text{GeO}_2$, $0.5x \text{Li}_2\text{O}\cdot 0.5x \text{Cs}_2\text{O}\cdot(100-x) \text{GeO}_2$ Glasses	38
Table 4-V. The Densities and Molar Volumes for $x \text{Li}_2\text{O}\cdot(10-x) \text{Cs}_2\text{O}\cdot 90 \text{GeO}_2$ and $x \text{Na}_2\text{O}\cdot(10-x) \text{K}_2\text{O}\cdot 90 \text{GeO}_2$ Glasses	44
Table 4-VI. The Densities and Molar Volumes for $x \text{Li}_2\text{O}\cdot(15-x) \text{Cs}_2\text{O}\cdot 85 \text{GeO}_2$ and $x \text{Na}_2\text{O}\cdot(15-x) \text{K}_2\text{O}\cdot 85 \text{GeO}_2$ Glasses	44
Table 4-VII. Densities and Molar Volumes of $0.5x \text{Na}_2\text{O}\cdot 0.5x \text{K}_2\text{O}\cdot(100-x) \text{GeO}_2$, $0.5x \text{Li}_2\text{O}\cdot 0.5x \text{Cs}_2\text{O}\cdot(100-x) \text{GeO}_2$ Glasses	45
Table 5-I. Band Positions of the Infrared Absorption Water Bands of Germanate Glasses.....	64
Table 6-I. Cation Ratios, Radius Values Taken from Shannon and Prewitt	65
Table 6-II. Electrical Conductivity Properties for the $\text{Li}_2\text{O}\cdot\text{Cs}_2\text{O}\cdot 90 \text{GeO}_2$ Glasses	93
Table 6-III. Electrical Conductivity Properties for $\text{Li}_2\text{O}\cdot\text{Cs}_2\text{O}\cdot 85 \text{GeO}_2$ Glasses	97
Table 6-IV. Electrical Conductivity Properties for the $\text{Na}_2\text{O}\cdot\text{K}_2\text{O}\cdot 90 \text{GeO}_2$ Glasses	100
Table 6-V. Electrical Conductivity Properties for the $\text{Na}_2\text{O}\cdot\text{K}_2\text{O}\cdot 85 \text{GeO}_2$ Glasses	105
Table 6-VI. Electrical Conductivity Properties for $0.5x \text{Li}_2\text{O}\cdot 0.5x \text{Cs}_2\text{O}\cdot(100-x) \text{GeO}_2$ Glasses	108
Table 6-VII. Electrical Conductivity Properties for $0.75x \text{Li}_2\text{O}\cdot 0.25x \text{Cs}_2\text{O}\cdot(100-x) \text{GeO}_2$ Glasses.....	112

	PAGE
Table 6-VIII. Electrical Conductivity Properties for $0.25x \text{Li}_2\text{O} \cdot 0.75x \text{Cs}_2\text{O} \cdot (100-x) \text{GeO}_2$ Glasses.....	112
Table 6-IX. Electrical Conductivity Properties for $0.5x \text{Na}_2\text{O} \cdot 0.5x \text{K}_2\text{O} \cdot (100-x) \text{GeO}_2$ Glasses	114
Table 6-X. Electrical Conductivity Properties for $0.5x \text{K}_2\text{O} \cdot 0.5x \text{Rb}_2\text{O} \cdot (100-x) \text{GeO}_2$ Glasses.	118
Table 7-I. Table Showing the Different Particle Size Ranges Used in the DSC experiment	165
Table 7-II. Heat Treatment Times and Temperatures for All Glasses.....	166
Table 7-III. T_g , T_x , and T_p Values for 15 $\text{Li}_2\text{O} \cdot 85 \text{GeO}_2$ Glasses	166
Table 7-IV. T_g , T_x , and T_p Values for 15 $\text{Cs}_2\text{O} \cdot 85 \text{GeO}_2$ Glasses.....	169
Table 7-V. T_g , T_x , and T_p Values for 7:1 $\text{Li}_2\text{O}:\text{Cs}_2\text{O} \cdot 85 \text{GeO}_2$ Glasses.....	171
Table 7- VI. T_g , T_x , and T_p Values for 3:1 $\text{Li}_2\text{O}:\text{Cs}_2\text{O} \cdot 85 \text{GeO}_2$ Glasses.....	174
Table 7-VII. T_g , T_x , and T_p Values for 1:1 $\text{Li}_2\text{O}:\text{Cs}_2\text{O} \cdot 85 \text{GeO}_2$ Glasses.....	176
Table 7-VIII. T_g , T_x , and T_p Values for 1:3 $\text{Li}_2\text{O}:\text{Cs}_2\text{O} \cdot 85 \text{GeO}_2$ Glasses.....	177
Table 7-IX. T_g , T_x , and T_p Values for 1:7 $\text{Li}_2\text{O}:\text{Cs}_2\text{O} \cdot 85 \text{GeO}_2$ Glasses.....	180
Table 7-X. T_g , T_x , and T_p Values for Different Particle Sizes of 15 $\text{Li}_2\text{O} \cdot 85 \text{GeO}_2$ Glasses	182
Table 7-XI. T_g , T_x , and T_p Values for Different Particle Sizes of 15 $\text{Cs}_2\text{O} \cdot 85 \text{GeO}_2$ Glasses	184
Table 7-XII. T_g , T_x , and T_p Values for Different Particle Sizes of 7:1 $\text{Li}_2\text{O}:\text{Cs}_2\text{O} \cdot 85 \text{GeO}_2$ Glasses.....	184
Table 7-XIII. T_g , T_x , and T_p Values for Different Particle Sizes of 3:1 $\text{Li}_2\text{O}:\text{Cs}_2\text{O} \cdot 85 \text{GeO}_2$ Glasses.....	184
Table 7-XIV. T_g , T_x , and T_p Values for Different Particle Sizes of 1:1 $\text{Li}_2\text{O}:\text{Cs}_2\text{O} \cdot 85 \text{GeO}_2$ Glasses.....	186
Table 7-XV. T_g , T_x , and T_p Values for Different Particle Sizes of 1:3 $\text{Li}_2\text{O}:\text{Cs}_2\text{O} \cdot 85 \text{GeO}_2$ Glasses.....	187

	PAGE
Table 7-XVI. T_g , T_x , and T_p Values for Different Particle Sizes of 1:7 $\text{Li}_2\text{O}:\text{Cs}_2\text{O}\cdot 85 \text{ GeO}_2$ Glasses.....	188
Table 7-XVII. Crystal Phases Resulting from the Low and High Temperature Heat Treatments of 15 $\text{Li}_2\text{O}\cdot 85 \text{ GeO}_2$ Glass.....	190
Table 7-XVIII. Crystal Phases Resulting from the Low Temperature Heat Treatment of 15 $\text{Cs}_2\text{O}\cdot 85 \text{ GeO}_2$ Glass	190
Table 7-XIX. Peak Crystallization Temperature and Activation Energies for Crystallization for All $x \text{ Li}_2\text{O}\cdot(15-x) \text{ Cs}_2\text{O}\cdot 85 \text{ GeO}_2$ Glasses (20 K/min, 63 to 75 μm)	203
Table A-I. Authors, Symbols and References for T_g of $\text{Li}_2\text{O}\cdot\text{GeO}_2$ Glasses.....	238
Table A-II. Authors, Symbols and References for T_g of $\text{Na}_2\text{O}\cdot\text{GeO}_2$ Glasses.....	238
Table A-III. Authors, Symbols and References for T_g of $\text{K}_2\text{O}\cdot\text{GeO}_2$ Glasses.....	238
Table A-IV. Authors, Symbols and References for T_g of $\text{Rb}_2\text{O}\cdot\text{GeO}_2$ Glasses.....	239
Table A-V. Authors, Symbols and References for T_g of $\text{Cs}_2\text{O}\cdot\text{GeO}_2$ Glasses	239
Table A-VI. Authors, Symbols and References for Density of $\text{Li}_2\text{O}\cdot\text{GeO}_2$ Glasses.	239
Table A-VII. Authors, Symbols and References for Density of $\text{Na}_2\text{O}\cdot\text{GeO}_2$ Glasses.	239
Table A-VIII. Authors, Symbols and References for Density of $\text{K}_2\text{O}\cdot\text{GeO}_2$ Glasses	240
Table A-IX. Authors, Symbols and References for Density of $\text{Rb}_2\text{O}\cdot\text{GeO}_2$ Glasses.	240
Table A-X. Authors, Symbols and References for Density of $\text{Cs}_2\text{O}\cdot\text{GeO}_2$ Glasses.	240

LIST OF FIGURES

		PAGE
Figure 4-1.	Glass transition temperature of $\text{Li}_2\text{O}\cdot\text{GeO}_2$ glasses from the literature.....	21
Figure 4-2.	Glass transition temperature all of $\text{Na}_2\text{O}\cdot\text{GeO}_2$ glasses from the literature.....	22
Figure 4-3.	Glass transition temperature of $\text{Na}_2\text{O}\cdot\text{GeO}_2$ containing 60 to 100 mol % GeO_2	23
Figure 4-4.	Glass transition temperature of $\text{K}_2\text{O}\cdot\text{GeO}_2$ glasses from the literature.....	23
Figure 4-5.	Glass transition temperature of $\text{K}_2\text{O}\cdot\text{GeO}_2$ containing 60 to 100 mol % GeO_2	24
Figure 4-6.	Glass transition temperature of $\text{Rb}_2\text{O}\cdot\text{GeO}_2$ glasses from the literature.....	25
Figure 4-7.	Glass transition temperature of $\text{Rb}_2\text{O}\cdot\text{GeO}_2$ containing 60 to 100 mol % GeO_2	25
Figure 4-8.	Glass transition temperature of $\text{Cs}_2\text{O}\cdot\text{GeO}_2$ glasses from the literature.....	26
Figure 4-9.	Glass transition temperatures of mixed alkali $\text{Na}_2\text{O}\cdot\text{K}_2\text{O}\cdot 80 \text{ GeO}_2$ glasses, from the literature.....	27
Figure 4-10.	Glass transition temperatures of mixed alkali $\text{Na}_2\text{O}\cdot\text{K}_2\text{O}\cdot\text{GeO}_2$ glasses.....	29
Figure 4-11.	Density of $\text{Li}_2\text{O}\cdot\text{GeO}_2$ glasses from the literature.....	29
Figure 4-12.	Molar volume of literature $\text{Li}_2\text{O}\cdot\text{GeO}_2$ glasses.	30
Figure 4-13.	Density of $\text{Na}_2\text{O}\cdot\text{GeO}_2$ glasses from the literature.....	30
Figure 4-14.	Molar volume of literature $\text{Na}_2\text{O}\cdot\text{GeO}_2$ glasses.....	31
Figure 4-15.	Density of $\text{K}_2\text{O}\cdot\text{GeO}_2$ glasses from the literature.	31
Figure 4-16.	Molar volume of literature $\text{K}_2\text{O}\cdot\text{GeO}_2$ glasses.....	32
Figure 4-17.	Density of $\text{Rb}_2\text{O}\cdot\text{GeO}_2$ glasses from the literature.....	32

	PAGE
Figure 4-18. Molar volume of literature $\text{Rb}_2\text{O}\cdot\text{GeO}_2$ glasses.....	33
Figure 4-19. Density of $\text{Cs}_2\text{O}\cdot\text{GeO}_2$ glasses from the literature.....	33
Figure 4-20. Molar volume of literature $\text{Cs}_2\text{O}\cdot\text{GeO}_2$ glasses..	34
Figure 4-21. Density of $\text{R}_2\text{O}\cdot\text{GeO}_2$ glasses.....	34
Figure 4-22. Molar volume of $\text{R}_2\text{O}\cdot\text{GeO}_2$ glasses.	35
Figure 4-23. Density of mixed alkali $\text{Na}_2\text{O}\cdot\text{K}_2\text{O}\cdot\text{GeO}_2$ glasses from the literature.....	35
Figure 4-24. Glass transition temperature, found using the intercept method.....	36
Figure 4-25. Glass transition temperatures for the glasses on the $\text{Na}_2\text{O}\cdot\text{K}_2\text{O}\cdot 90$ GeO_2 tie line.....	39
Figure 4-26. Glass transition temperatures for the glasses on the $\text{Na}_2\text{O}\cdot\text{K}_2\text{O}\cdot 85$ GeO_2 tie line.....	39
Figure 4-27. Deviation from additivity for the $\text{Na}_2\text{O}\cdot\text{K}_2\text{O}\cdot 90$ GeO_2 and $\text{Na}_2\text{O}\cdot\text{K}_2\text{O}\cdot 85$ GeO_2 glasses.....	40
Figure 4-28. Glass transition temperatures for the glasses on the $\text{Li}_2\text{O}\cdot\text{Cs}_2\text{O}\cdot 90$ GeO_2 tie line.....	40
Figure 4-29. Glass transition temperatures for the glasses on the $\text{Li}_2\text{O}\cdot\text{Cs}_2\text{O}\cdot 85$ GeO_2 tie line.....	41
Figure 4-30. Deviation from additivity for the $\text{Li}_2\text{O}\cdot\text{Cs}_2\text{O}\cdot 90$ GeO_2 and $\text{Li}_2\text{O}\cdot\text{Cs}_2\text{O}\cdot 85$ GeO_2 glasses.....	41
Figure 4-31. Germanate anomaly, shown for T_g data of the $\text{Na}_2\text{O}\cdot\text{K}_2\text{O}\cdot\text{GeO}_2$ system, down the 1:1 $\text{Na}_2\text{O}:\text{K}_2\text{O}$ line.....	42
Figure 4-32. Germanate anomaly, shown for T_g data of the $\text{Li}_2\text{O}\cdot\text{Cs}_2\text{O}\cdot\text{GeO}_2$ system, down the 1:1 $\text{Li}_2\text{O}:\text{Cs}_2\text{O}$ line.....	42
Figure 4-33. Densities of $x \text{Na}_2\text{O}\cdot(10-x) \text{K}_2\text{O}\cdot 90 \text{GeO}_2$ glasses.....	43
Figure 4-34. Molar volumes of $x \text{Na}_2\text{O}\cdot(10-x) \text{K}_2\text{O}\cdot 90 \text{GeO}_2$ glasses.....	45
Figure 4-35. Densities of $x \text{Na}_2\text{O}\cdot(15-x) \text{K}_2\text{O}\cdot 85 \text{GeO}_2$ glasses.....	46
Figure 4-36. Molar volumes of $x \text{Na}_2\text{O}\cdot(15-x) \text{K}_2\text{O}\cdot 85 \text{GeO}_2$ glasses.....	46

	PAGE
Figure 4-37. Comparison between the molar volumes of the $x \text{Na}_2\text{O} \cdot (100-x-y) \text{K}_2\text{O} \cdot y \text{GeO}_2$, $y = 90$ and 85 mol %.	47
Figure 4-38. Densities of $x \text{Li}_2\text{O} \cdot (10-x) \text{Cs}_2\text{O} \cdot 90 \text{GeO}_2$ glasses.	47
Figure 4-39. Molar volumes of $x \text{Li}_2\text{O} \cdot (10-x) \text{Cs}_2\text{O} \cdot 90 \text{GeO}_2$ glasses.	48
Figure 4-40. Densities of $x \text{Li}_2\text{O} \cdot (15-x) \text{Cs}_2\text{O} \cdot 85 \text{GeO}_2$ glasses.	48
Figure 4-41. Molar volume of $x \text{Li}_2\text{O} \cdot (15-x) \text{Cs}_2\text{O} \cdot 85 \text{GeO}_2$ glasses.	49
Figure 4-42. Comparison between the molar volume of the $x \text{Li}_2\text{O} \cdot (100-x-y) \text{Cs}_2\text{O} \cdot y \text{GeO}_2$, $y = 90$ and 85 mol %.	49
Figure 4-43. Densities of $0.5x \text{Na}_2\text{O} \cdot 0.5x \text{K}_2\text{O} \cdot (100-x) \text{GeO}_2$.	50
Figure 4-44. Molar volumes of $0.5x \text{Na}_2\text{O} \cdot 0.5x \text{K}_2\text{O} \cdot (100-x) \text{GeO}_2$.	50
Figure 4-45. Densities of $0.5x \text{Li}_2\text{O} \cdot 0.5x \text{Cs}_2\text{O} \cdot (100-x) \text{GeO}_2$.	51
Figure 4-46. Molar volumes of $0.5x \text{Li}_2\text{O} \cdot 0.5x \text{Cs}_2\text{O} \cdot (100-x) \text{GeO}_2$.	51
Figure 4-47. Comparison between the $\text{Na}_2\text{O} \cdot \text{K}_2\text{O} \cdot \text{GeO}_2$ and $\text{Li}_2\text{O} \cdot \text{Cs}_2\text{O} \cdot \text{GeO}_2$ glasses containing 90 mol% GeO_2 .	53
Figure 4-48. Comparison between the $\text{Na}_2\text{O} \cdot \text{K}_2\text{O} \cdot \text{GeO}_2$ and $\text{Li}_2\text{O} \cdot \text{Cs}_2\text{O} \cdot \text{GeO}_2$ glasses containing 85 mol % GeO_2 .	53
Figure 4-49. Comparison of the germanate anomaly for T_g data between the $\text{Li}_2\text{O} \cdot \text{Cs}_2\text{O} \cdot \text{GeO}_2$ and the $\text{Na}_2\text{O} \cdot \text{K}_2\text{O} \cdot \text{GeO}_2$ systems.	54
Figure 4-50. Glass transition temperature for the binary Na_2O and K_2O germanate glasses.	54
Figure 4-51. Glass transition temperature for the binary Li_2O and Cs_2O germanate glasses.	55
Figure 4-52. Comparison of the molar volume between the $\text{Na}_2\text{O} \cdot \text{K}_2\text{O} \cdot 90 \text{GeO}_2$ and $\text{Li}_2\text{O} \cdot \text{Cs}_2\text{O} \cdot 90 \text{GeO}_2$ systems.	56
Figure 4-53. Comparison of the molar volume between the $\text{Na}_2\text{O} \cdot \text{K}_2\text{O} \cdot 85 \text{GeO}_2$ and $\text{Li}_2\text{O} \cdot \text{Cs}_2\text{O} \cdot 85 \text{GeO}_2$ systems.	56
Figure 4-54. Comparison between the molar volume for the germanate anomaly.	57

	PAGE
Figure 4-55. Literature values for density of the binary Na ₂ O and K ₂ O alkali-germanate glasses compared to the value for the Na ₂ O•K ₂ O•GeO ₂ mixed alkali glasses.....	57
Figure 4-56. Literature values for density of the binary Li ₂ O and Cs ₂ O alkali-germanate glasses compared to the value for the Li ₂ O•Cs ₂ O•GeO ₂ mixed alkali glasses.....	58
Figure 5-1. Schematic of water used to melt glasses under high vapor pressure of water.....	65
Figure 5-2. Infrared spectra for x Li ₂ O•(10- x) Cs ₂ O•90 GeO ₂ glasses.	66
Figure 5-3. Normalized infrared spectra for x Li ₂ O•(10- x) Cs ₂ O•90 GeO ₂ glasses.....	67
Figure 5-4. Peak position of Band I in the infrared spectra for x Li ₂ O•(10- x) Cs ₂ O•90 GeO ₂ glasses.	68
Figure 5-5. Infrared spectra for x Li ₂ O•(15- x) Cs ₂ O•85 GeO ₂ glasses.	68
Figure 5-6. Normalized infrared spectra for x Li ₂ O•(15- x) Cs ₂ O•85 GeO ₂ glasses.....	69
Figure 5-7. Peak position of Band I in the infrared spectra for x Li ₂ O•(15- x) Cs ₂ O•85 GeO ₂ glasses.	69
Figure 5-8. Infrared spectra for x Na ₂ O•(10- x) K ₂ O•90 GeO ₂ glasses.....	70
Figure 5-9. Normalized infrared spectra for x Na ₂ O•(10- x) K ₂ O•90 GeO ₂ glasses.....	70
Figure 5-10. Peak position of Band I in the infrared spectra for x Na ₂ O•(10- x) K ₂ O•90 GeO ₂ glasses.	71
Figure 5-11. Infrared spectra for x Na ₂ O•(15- x) K ₂ O•85 GeO ₂ glasses.....	72
Figure 5-12. Normalized infrared spectra for x Na ₂ O•(15- x) K ₂ O•85 GeO ₂ glasses.....	72
Figure 5-13. Position of Band I in the infrared spectra for x Na ₂ O•(15- x) K ₂ O•85 GeO ₂ glasses.	73
Figure 5-14. Infrared spectra for 0.5 x Li ₂ O•0.5 x Cs ₂ O•(100- x) GeO ₂ glasses.....	74
Figure 5-15. Infrared spectra for 0.5 x Na ₂ O•0.5 x K ₂ O•(100- x) GeO ₂ glasses.....	74

	PAGE
Figure 5-16. Normalized infrared spectra for $0.5x \text{Li}_2\text{O} \cdot 0.5x \text{Cs}_2\text{O} \cdot (100-x) \text{GeO}_2$ glasses.....	75
Figure 5-17. Normalized infrared spectra for $0.5x \text{Na}_2\text{O} \cdot 0.5x \text{K}_2\text{O} \cdot (100-x) \text{GeO}_2$ glasses.....	75
Figure 5-18. Position of Band I in the infrared spectra for $0.5x \text{R}_2\text{O} \cdot 0.5x \text{R}'_2\text{O} \cdot 85 \text{GeO}_2$ glasses.	76
Figure 5-19. Position of Band I in the infrared spectra for $x \text{R}_2\text{O} \cdot (10-x) \text{R}'_2\text{O} \cdot 90 \text{GeO}_2$ glasses.	77
Figure 5-20. Position of Peak I in the infrared spectra for $x \text{R}_2\text{O} \cdot (15-x) \text{R}'_2\text{O} \cdot 85 \text{GeO}_2$ glasses.	77
Figure 5-21. Position of Band I in the infrared spectra for $x \text{Li}_2\text{O} \cdot y-x \text{Cs}_2\text{O} \cdot (100-x-y) \text{GeO}_2$ glasses, where $y = 10$ or 15	78
Figure 5-22. Position of Band I in the infrared spectra for $x \text{Na}_2\text{O} \cdot y-x \text{K}_2\text{O} \cdot (100-x-y) \text{GeO}_2$ glasses, where $y = 10$ or 15	78
Figure 5-23. Infrared spectra for $8.5 \text{Li}_2\text{O} \cdot 8.5 \text{Cs}_2\text{O} \cdot 83 \text{GeO}_2$ glasses prior and following treatment in a water furnace.....	79
Figure 5-24. Normalized infrared spectra for $8.5 \text{Li}_2\text{O} \cdot 8.5 \text{Cs}_2\text{O} \cdot 83 \text{GeO}_2$ glasses prior and following treatment in a water furnace.....	80
Figure 6-1. Shannon and Prewitt ionic radii of alkali ions.	66
Figure 6-2. Illustration showing the shear energy and the electrostatic barriers for ionic conduction.....	69
Figure 6-3. Radii ratio for the larger ion to the smaller ion.....	74
Figure 6-4. Literature values for the DC electrical conductivity, at 300°C , of $\text{Li}_2\text{O} \cdot \text{GeO}_2$ glasses.....	76
Figure 6-5. Activation energy for DC conductivity of $\text{Li}_2\text{O} \cdot \text{GeO}_2$ glasses.	78
Figure 6-6. Pre-exponential factors for $\text{Li}_2\text{O} \cdot \text{GeO}_2$ glasses.....	78
Figure 6-7. Literature values for the DC electrical conductivity, at 300°C , of $\text{Na}_2\text{O} \cdot \text{GeO}_2$ glasses.	79
Figure 6-8. Activation energy for DC conductivity of $\text{Na}_2\text{O} \cdot \text{GeO}_2$ glasses.	79
Figure 6-9. Pre-exponential factors for $\text{Na}_2\text{O} \cdot \text{GeO}_2$ glasses.....	80

	PAGE
Figure 6-10. Literature values for the DC electrical conductivity, at 300 °C, of K ₂ O•GeO ₂ glasses.	80
Figure 6-11. Activation energy for DC conductivity of K ₂ O•GeO ₂ glasses.	81
Figure 6-12. Pre-exponential factors for K ₂ O•GeO ₂ glasses.	82
Figure 6-13. Literature values for the DC electrical conductivity, at 300 °C, of Rb ₂ O•GeO ₂ glasses.	83
Figure 6-14. Unpublished DC electrical conductivity at 300 °C, for Cs ₂ O•GeO ₂ glasses.	83
Figure 6-15. Activation energy for DC conductivity of Rb ₂ O•GeO ₂ glasses.	84
Figure 6-16. Activation energy for DC conductivity of Cs ₂ O•GeO ₂ glasses.	84
Figure 6-17. Pre-exponential factors for Rb ₂ O•GeO ₂ glasses.	85
Figure 6-18. Pre-exponential factors for Cs ₂ O•GeO ₂ glasses.	85
Figure 6-19. Literature values for the DC electrical conductivity, at 300 °C, of R ₂ O•GeO ₂ glasses.	86
Figure 6-20. Activation energies for electrical conductivity, from the literature, for binary alkali-germanate glasses.	87
Figure 6-21. Illustration of the samples used in the DC conductivity experiments.	87
Figure 6-22. Illustration of the DC conductivity apparatus used in this thesis.	88
Figure 6-23. Illustration of the circuit used in the DC conductivity apparatus.	89
Figure 6-24. NIST standard 624 and the values measured using the equipment used in this study	90
Figure 6-25. DC conductivity for the x Li ₂ O•(10- x) Cs ₂ O•90 GeO ₂ mixed alkali glasses.	92
Figure 6-26. DC conductivity for x Li ₂ O•(10- x) Cs ₂ O•90 GeO ₂ glasses at the glass transition temperature (T_g) and at 300 °C.	93
Figure 6-27. Log plot of the deviation from additivity for the DC electrical conductivity of x Li ₂ O•(10- x) Cs ₂ O•90 GeO ₂ glasses at the glass transition temperature (T_g) and 300 °C.	94

	PAGE
Figure 6-28. Activation energy for DC conductivity of the mixed alkali x $\text{Li}_2\text{O}\cdot(10-x) \text{Cs}_2\text{O}\cdot 90 \text{GeO}_2$ glasses.....	94
Figure 6-29. Deviation from additivity of the activation energy for DC conductivity for the mixed alkali x $\text{Li}_2\text{O}\cdot(10-x) \text{Cs}_2\text{O}\cdot 90 \text{GeO}_2$ glasses.....	95
Figure 6-30. Pre-exponential factor (σ_0) of the Arrhenius equation for the mixed alkali x $\text{Li}_2\text{O}\cdot(10-x) \text{Cs}_2\text{O}\cdot 90 \text{GeO}_2$ glasses..	95
Figure 6-31. DC electrical conductivity for x $\text{Li}_2\text{O}\cdot(15-x) \text{Cs}_2\text{O}\cdot 85 \text{GeO}_2$ glasses.....	96
Figure 6-32. Values for DC electrical conductivity at the glass transition temperature and T_g for x $\text{Li}_2\text{O}\cdot(15-x) \text{Cs}_2\text{O}\cdot 85 \text{GeO}_2$ glasses.....	97
Figure 6-33. The deviation from additivity for the Log of the DC electrical conductivity at 300°C for $x\text{Li}_2\text{O}\cdot 15-x\text{Cs}_2\text{O}\cdot 85 \text{GeO}_2$ glasses.....	98
Figure 6-34. Activation energy for crystallization for x $\text{Li}_2\text{O}\cdot(15-x) \text{Cs}_2\text{O}\cdot 85 \text{GeO}_2$ glasses.....	98
Figure 6-35. Pre-exponential factors (σ_0) for x $\text{Li}_2\text{O}\cdot(15-x) \text{Cs}_2\text{O}\cdot 85 \text{GeO}_2$ glasses.....	99
Figure 6-36. DC electrical conductivity values for x $\text{Na}_2\text{O}\cdot(10-x) \text{K}_2\text{O}\cdot 90 \text{GeO}_2$ glasses.....	100
Figure 6-37. DC conductivity for x $\text{Na}_2\text{O}\cdot(10-x) \text{K}_2\text{O}\cdot 90 \text{GeO}_2$ glasses at the glass transition temperature (T_g) and at 300°C	101
Figure 6-38. Log of the deviation from additivity for the DC electrical conductivity for x $\text{Na}_2\text{O}\cdot(10-x) \text{K}_2\text{O}\cdot 90 \text{GeO}_2$ glasses at the glass transition temperature (T_g) and 300°C . Lines added as an aid to the eye.....	101
Figure 6-39. Activation energy for DC conductivity of the mixed alkali x $\text{Na}_2\text{O}\cdot(10-x) \text{K}_2\text{O}\cdot 90 \text{GeO}_2$ glasses.....	102
Figure 6-40. Deviation from additivity of the activation energy for DC conductivity for the mixed alkali x $\text{Na}_2\text{O}\cdot(10-x) \text{K}_2\text{O}\cdot 90 \text{GeO}_2$ glasses.....	102
Figure 6-41. Pre-exponential (σ_0) factors for x $\text{Na}_2\text{O}\cdot(10-x) \text{K}_2\text{O}\cdot 90 \text{GeO}_2$ glasses.....	103

	PAGE
Figure 6-42. DC electrical conductivity values for $x \text{Na}_2\text{O} \cdot (15-x) \text{K}_2\text{O} \cdot 85 \text{GeO}_2$ glasses.....	103
Figure 6-43. DC conductivity for $x \text{Na}_2\text{O} \cdot (15-x) \text{K}_2\text{O} \cdot 85 \text{GeO}_2$ glasses at the glass transition temperature (T_g) and at 300 °C	104
Figure 6-44. Log of the deviation from additivity for the DC electrical conductivity $x \text{Na}_2\text{O} \cdot (15-x) \text{K}_2\text{O} \cdot 85 \text{GeO}_2$ glasses at the glass transition temperature (T_g) and 300 °C.	104
Figure 6-45. Activation energy for DC conductivity of the mixed alkali $x \text{Na}_2\text{O} \cdot (15-x) \text{K}_2\text{O} \cdot 85 \text{GeO}_2$ glasses.	105
Figure 6-46. Deviation from additivity of the activation energy for DC conductivity for the mixed alkali $x \text{Na}_2\text{O} \cdot (15-x) \text{K}_2\text{O} \cdot 85 \text{GeO}_2$ glasses.....	106
Figure 6-47. Pre-exponential (σ_0) factors for $x \text{Na}_2\text{O} \cdot (15-x) \text{K}_2\text{O} \cdot 85 \text{GeO}_2$ glasses.....	106
Figure 6-48. DC electrical conductivity values for $0.5x \text{Li}_2\text{O} \cdot 0.5x \text{Cs}_2\text{O} \cdot (100-x) \text{GeO}_2$ glasses.....	108
Figure 6-49. DC conductivity for $0.5x \text{Li}_2\text{O} \cdot 0.5x \text{Cs}_2\text{O} \cdot (100-x) \text{GeO}_2$ glasses at the glass transition temperature (T_g) and at 300 °C.....	109
Figure 6-50. Activation energy for $0.5x \text{Li}_2\text{O} \cdot 0.5x \text{Cs}_2\text{O} \cdot (100-x) \text{GeO}_2$ glasses.	109
Figure 6-51. Pre-exponential (σ_0) factors for $0.5x \text{Li}_2\text{O} \cdot 0.5x \text{Cs}_2\text{O} \cdot (100-x) \text{GeO}_2$ glasses.....	110
Figure 6-52. DC electrical conductivity values for $0.75x \text{Li}_2\text{O} \cdot 0.25x \text{Cs}_2\text{O} \cdot (100-x) \text{GeO}_2$ glasses.	110
Figure 6-53. DC electrical conductivity values for $0.25x \text{Li}_2\text{O} \cdot 0.75x \text{Cs}_2\text{O} \cdot (100-x) \text{GeO}_2$ glasses.	111
Figure 6-54. DC conductivity for $0.75x \text{Li}_2\text{O} \cdot 0.25x \text{Cs}_2\text{O} \cdot (100-x) \text{GeO}_2$ and $0.25x \text{Li}_2\text{O} \cdot 0.75x \text{Cs}_2\text{O} \cdot (100-x) \text{GeO}_2$ glasses at 300 °C.	111
Figure 6-55. Activation energies for DC conductivity for $0.75x \text{Li}_2\text{O} \cdot 0.25x \text{Cs}_2\text{O} \cdot (100-x) \text{GeO}_2$ and $0.25x \text{Li}_2\text{O} \cdot 0.75x \text{Cs}_2\text{O} \cdot (100-x) \text{GeO}_2$ glasses.....	113
Figure 6-56. Pre-exponential (σ_0) factors for $0.75x \text{Li}_2\text{O} \cdot 0.25x \text{Cs}_2\text{O} \cdot (100-x) \text{GeO}_2$ and $0.25x \text{Li}_2\text{O} \cdot 0.75x \text{Cs}_2\text{O} \cdot (100-x) \text{GeO}_2$ glasses.....	113

	PAGE
Figure 6-57. DC electrical conductivity values for 0.5x Na ₂ O•0.5x K ₂ O•(100-x) 85 GeO ₂ glasses.....	115
Figure 6-58. DC conductivity for 0.5x Na ₂ O•0.5x K ₂ O•(100-x) GeO ₂ glasses at the glass transition temperature (T _g) and at 300 °C.....	115
Figure 6-59. Activation energy for 0.5x Na ₂ O•0.5x K ₂ O•(100-x) GeO ₂ glasses.	116
Figure 6-60. Pre-exponential (σ ₀) factors for 0.5x Na ₂ O•0.5x K ₂ O•(100-x) GeO ₂ glasses.....	116
Figure 6-61. DC electrical conductivity values for 0.5x K ₂ O•0.5x Rb ₂ O•(100-x) GeO ₂ glasses.....	117
Figure 6-62. DC conductivity for 0.5x K ₂ O•0.5x Rb ₂ O•(100-x) GeO ₂ glasses at the glass transition temperature (T _g) and at 300 °C.....	118
Figure 6-63. Activation energy for 0.5x K ₂ O•0.5x Rb ₂ O•(100-x) GeO ₂ glasses.	119
Figure 6-64. Pre-exponential (σ ₀) factors for 0.5x K ₂ O•0.5x Rb ₂ O•(100-x) GeO ₂ glasses.....	119
Figure 6-65. Comparison of DC conductivity at 300 °C for Li ₂ O•Cs ₂ O•GeO ₂ glasses with 90 and 85 mol % GeO ₂	121
Figure 6-66. Difference between the log of the conductivity at 300 °C and the log of the additive line for Li ₂ O•Cs ₂ O•GeO ₂ glasses with 90 and 85 mol % GeO ₂	122
Figure 6-67. Comparison of the DC conductivity at 300 °C for Na ₂ O•K ₂ O•GeO ₂ glasses with 90 and 85 mol % GeO ₂	122
Figure 6-68. Difference between the log of the conductivity at 300 °C and the log of the additive line for Na ₂ O•K ₂ O•GeO ₂ glasses with 90 and 85 mol % GeO ₂	123
Figure 6-69. Difference between the log of the conductivity at 300 °C and the log of the additive line for mixed alkali glasses with 90 mol % GeO ₂	123
Figure 6-70. Difference between the log of the conductivity at 300 °C and the log of the additive line for mixed alkali glasses with 85 mol % GeO ₂	124
Figure 6-71. Comparison between activation energies of Li ₂ O•Cs ₂ O•GeO ₂ glasses, with 90 and 85 mol % GeO ₂	125

	PAGE
Figure 6-72. Comparison between activation energies of $\text{Na}_2\text{O}\cdot\text{K}_2\text{O}\cdot\text{GeO}_2$ glasses, with 90 and 85 mol % GeO_2	125
Figure 6-73. Pre-exponential factor for all mixed alkali germanate glasses.....	127
Figure 6-74. Comparison between the literature values and this study for the DC conductivity at 300 °C for $\text{Na}_2\text{O}\cdot\text{K}_2\text{O}\cdot 90 \text{ GeO}_2$	128
Figure 6-75. Comparison between the literature values and this study for the DC conductivity at 300 °C for $\text{Na}_2\text{O}\cdot\text{K}_2\text{O}\cdot 85 \text{ GeO}_2$	128
Figure 6-76. DC conductivity for $0.5x \text{ K}_2\text{O}\cdot 0.5x \text{ Rb}_2\text{O}\cdot(100-x) \text{ GeO}_2$, $x \text{ K}_2\text{O}\cdot(100-x) \text{ GeO}_2$ and $x \text{ Rb}_2\text{O}\cdot(100-x) \text{ GeO}_2$ glasses at 300 °C.....	130
Figure 6-77. Comparison between activation energies of $\text{K}_2\text{O}\cdot\text{GeO}_2$, $\text{Rb}_2\text{O}\cdot\text{GeO}_2$ and $\text{K}_2\text{O}\cdot\text{Rb}_2\text{O}\cdot\text{GeO}_2$ glasses.	130
Figure 6-78. DC conductivity for $0.5x \text{ Na}_2\text{O}\cdot 0.5x \text{ K}_2\text{O}\cdot(100-x) \text{ GeO}_2$, $x \text{ Na}_2\text{O}\cdot(100-x) \text{ GeO}_2$ and $x \text{ K}_2\text{O}\cdot(100-x) \text{ GeO}_2$ glasses at 300 °C.....	132
Figure 6-79. Difference between the log of the conductivity at 300 °C and the log of the additive line for mixed alkali glasses for all $\text{Na}_2\text{O}\cdot\text{K}_2\text{O}\cdot\text{GeO}_2$ glasses.	132
Figure 6-80. Comparison between activation energies of $\text{Na}_2\text{O}\cdot\text{GeO}_2$, $\text{K}_2\text{O}\cdot\text{GeO}_2$ and $\text{Na}_2\text{O}\cdot\text{K}_2\text{O}\cdot\text{GeO}_2$ glasses.	133
Figure 6-81. DC conductivity for $0.5x \text{ Li}_2\text{O}\cdot 0.5x \text{ Cs}_2\text{O}\cdot(100-x) \text{ GeO}_2$, $x \text{ Li}_2\text{O}\cdot(100-x) \text{ GeO}_2$ and $x \text{ Cs}_2\text{O}\cdot(100-x) \text{ GeO}_2$ glasses at 300 °C.....	135
Figure 6-82. Comparison between activation energies of $\text{Li}_2\text{O}\cdot\text{GeO}_2$, $\text{Cs}_2\text{O}\cdot\text{GeO}_2$ and $\text{Li}_2\text{O}\cdot\text{Cs}_2\text{O}\cdot\text{GeO}_2$ glasses.	136
Figure 6-83. DC conductivity for $0.75x \text{ Li}_2\text{O}\cdot 0.25x \text{ Cs}_2\text{O}\cdot(100-x) \text{ GeO}_2$, $0.5x \text{ Li}_2\text{O}\cdot 0.5x \text{ Cs}_2\text{O}\cdot(100-x) \text{ GeO}_2$ and $0.25x \text{ Li}_2\text{O}\cdot 0.75x \text{ Cs}_2\text{O}\cdot(100-x) \text{ GeO}_2$ glasses at 300 °C.....	136
Figure 6-84. Difference between the log of the conductivity at 300 °C and the log of the additive line for mixed alkali glasses for all $\text{Li}_2\text{O}\cdot\text{Cs}_2\text{O}\cdot\text{GeO}_2$ glasses.	137
Figure 6-85. Comparison between activation energies of $\text{Li}_2\text{O}\cdot\text{Cs}_2\text{O}\cdot\text{GeO}_2$ glasses, with varying ratios of alkali.	137
Figure 6-86. Comparison between the conductivity at 300 °C and the activation energy of conduction for 1:1 $\text{Li}_2\text{O}:\text{Cs}_2\text{O}\cdot\text{GeO}_2$ glasses.	138

	PAGE
Figure 6-87. Comparison between the conductivity at 300 °C and the activation energy of conduction for 1:3 Li ₂ O:Cs ₂ O•GeO ₂ glasses.	138
Figure 6-88. Comparison between the conductivity at 300 °C and the activation energy of conduction for 3:1 Li ₂ O:Cs ₂ O•GeO ₂ glasses.	139
Figure 6-89. Pre-exponential (σ_0) factors for x Li ₂ O• y Cs ₂ O•(100- x - y) GeO ₂ glasses.....	139
Figure 6-90. DC conductivity for 0.5 x Li ₂ O•0.5 x Cs ₂ O•(100- x) GeO ₂ , x Li ₂ O•(100- x) GeO ₂ and x Cs ₂ O•(100- x) GeO ₂ glasses at 300 °C.....	141
Figure 6-91. Activation energy for 0.5 x K ₂ O•0.5 x Rb ₂ O•(100- x) GeO ₂ glasses.	141
Figure 6-92. Pre-exponential (σ_0) factor for x R ₂ O• y R' ₂ O•(100- x - y) GeO ₂ glasses.....	142
Figure 7-1. Example Kissinger plot for a mixed alkali germanate glass.	156
Figure 7-2. Illustration showing the effect of temperature on the rate of nucleation and crystal growth in glasses.	160
Figure 7-3. Phase diagram for Li ₂ O•GeO ₂	162
Figure 7-4. Phase diagram for Cs ₂ O•GeO ₂	163
Figure 7-5. Glass transition temperature and onset of crystallization, found using the intercept method.	164
Figure 7-6. DSC curves with ramp rates ranging from 5 to 30 K/min curve for 15 Li ₂ O•85 GeO ₂ glasses.....	167
Figure 7-7. T _g , T _x , and T _p values for 15 Li ₂ O•85 GeO ₂ glasses as a result of varying ramp rate.....	167
Figure 7-8. Kissinger plot for 15 Li ₂ O•85 GeO ₂ glass.....	168
Figure 7-9. DSC curves with ramp rates ranging from 5 to 30 K/min curve for 15 Cs ₂ O•85 GeO ₂ glasses.....	169
Figure 7-10. T _g , T _x , and T _p values for 15 Cs ₂ O•85 GeO ₂ glasses as a result of varying ramp rate.....	170
Figure 7-11. Kissinger plot for 15 Cs ₂ O•85 GeO ₂ glass.....	170
Figure 7-12. DSC curves with ramp rates ranging from 5 to 30 K/min curve for 7:1 Li ₂ O:Cs ₂ O•85 GeO ₂ glasses.....	171

	PAGE
Figure 7-13. T_g , T_x , and T_p values for 7:1 $\text{Li}_2\text{O}:\text{Cs}_2\text{O}\cdot 85 \text{ GeO}_2$ glasses as a result of varying ramp rate.	172
Figure 7-14. Kissinger plot for 7:1 $\text{Li}_2\text{O}:\text{Cs}_2\text{O}\cdot 85 \text{ GeO}_2$ glass.	173
Figure 7-15. DSC curves with ramp rates ranging from 5 to 30 K/min curve for 3:1 $\text{Li}_2\text{O}:\text{Cs}_2\text{O}\cdot 85 \text{ GeO}_2$ glasses.	173
Figure 7-16. T_g , T_x , and T_p values for 3:1 $\text{Li}_2\text{O}:\text{Cs}_2\text{O}\cdot 85 \text{ GeO}_2$ glasses as a result of varying ramp rate.	174
Figure 7-17. Kissinger plot for 3:1 $\text{Li}_2\text{O}:\text{Cs}_2\text{O}\cdot 85 \text{ GeO}_2$ glass.	175
Figure 7-18. DSC curves with ramp rates ranging from 5 to 30 K/min curve for 1:1 $\text{Li}_2\text{O}:\text{Cs}_2\text{O}\cdot 85 \text{ GeO}_2$ glasses.	175
Figure 7-19. T_g , T_x , and T_p values for 1:1 $\text{Li}_2\text{O}:\text{Cs}_2\text{O}\cdot 85 \text{ GeO}_2$ glasses as a result of varying ramp rate.	176
Figure 7-20. Kissinger plot for 1:1 $\text{Li}_2\text{O}:\text{Cs}_2\text{O}\cdot 85 \text{ GeO}_2$ glass.	177
Figure 7-21. DSC curves with ramp rates ranging from 5 to 30 K/min curve for 1:3 $\text{Li}_2\text{O}:\text{Cs}_2\text{O}\cdot 85 \text{ GeO}_2$ glasses.	178
Figure 7-22. T_g , T_x , and T_p values for 1:3 $\text{Li}_2\text{O}:\text{Cs}_2\text{O}\cdot 85 \text{ GeO}_2$ glasses as a result of varying ramp rate.	178
Figure 7-23. Kissinger plot for 1:3 $\text{Li}_2\text{O}:\text{Cs}_2\text{O}\cdot 85 \text{ GeO}_2$ glass.	179
Figure 7-24. DSC curves with ramp rates ranging from 5 to 30 K/min curve for 1:7 $\text{Li}_2\text{O}:\text{Cs}_2\text{O}\cdot 85 \text{ GeO}_2$ glasses.	180
Figure 7-25. T_g , T_x , and T_p values for 1:7 $\text{Li}_2\text{O}:\text{Cs}_2\text{O}\cdot 85 \text{ GeO}_2$ glasses as a result of varying ramp rate.	181
Figure 7-26. Kissinger plot for 1:7 $\text{Li}_2\text{O}:\text{Cs}_2\text{O}\cdot 85 \text{ GeO}_2$ glass.	181
Figure 7-27. DSC curves of glasses with different particle sizes for 15 $\text{Li}_2\text{O}\cdot 85 \text{ GeO}_2$ glasses.	183
Figure 7-28. DSC curves of glasses with different particle sizes for 15 $\text{Cs}_2\text{O}\cdot 85 \text{ GeO}_2$ glasses.	183
Figure 7-29. DSC curves of glasses with different particle sizes for 7:1 $\text{Li}_2\text{O}:\text{Cs}_2\text{O}\cdot 85 \text{ GeO}_2$ glasses.	185
Figure 7-30. DSC curves of glasses with different particle sizes for 3:1 $\text{Li}_2\text{O}:\text{Cs}_2\text{O}\cdot 85 \text{ GeO}_2$ glasses.	185

	PAGE
Figure 7-31. DSC curves of glasses with different particle sizes for 1:1 Li ₂ O:Cs ₂ O•85 GeO ₂ glasses.	186
Figure 7-32. DSC curves of glasses with different particle sizes for 1:3 Li ₂ O:Cs ₂ O•85 GeO ₂ glasses.	188
Figure 7-33. DSC curves of glasses with different particle sizes for 1:7 Li ₂ O:Cs ₂ O•85 GeO ₂ glasses.	189
Figure 7-34. HTXRD scans for isothermal heat treatment at 550 °C for the 15 Li ₂ O•85 GeO ₂ glass.	191
Figure 7-35. Diffraction pattern of the room temperature crystals, following the HTXRD experiment and heat treatment at 550 °C, for the 15 Li ₂ O•85 GeO ₂ glass.	191
Figure 7-36. HTXRD scans for isothermal heat treatment at 645 °C for the 15 Li ₂ O•85 GeO ₂ glass.	192
Figure 7-37. Diffraction pattern of the room temperature crystals, following the HTXRD experiment and heat treatment at 645 °C, for the 15 Li ₂ O•85 GeO ₂ glass.	192
Figure 7-38. Diffraction patterns of 15 Li ₂ O•85 GeO ₂ glass powder, following HTXRD with isothermal heat treatments at 550 °C and 645 °C.	193
Figure 7-39. HTXRD scans for isothermal heat treatment at 590 °C for the 15 Cs ₂ O•85 GeO ₂ glass.	193
Figure 7-40. Diffraction pattern of the room temperature crystals, following the HTXRD experiment and heat treatment at 590 °C, for the 15 Cs ₂ O•85 GeO ₂ glass.	194
Figure 7-41. HTXRD scans for isothermal heat treatment at 590 °C for the 7:1 Li ₂ O:Cs ₂ O•85 GeO ₂ glass.	195
Figure 7-42. Diffraction pattern of the room temperature crystals, following the HTXRD experiment and heat treatment at 550 °C, for the 7:1 Li ₂ O:Cs ₂ O•85 GeO ₂ glass.	195
Figure 7-43. HTXRD scans for isothermal heat treatment at 550 °C for the 3:1 Li ₂ O:Cs ₂ O•85 GeO ₂ glass.	196
Figure 7-44. Diffraction pattern of the room temperature crystals, following the HTXRD experiment and heat treatment at 550 °C, for the 3:1 Li ₂ O:Cs ₂ O•85 GeO ₂ glass.	196

	PAGE
Figure 7-45. Comparison between diffraction patterns of 7:1 Li ₂ O:Cs ₂ O•85 GeO ₂ and 3:1 Li ₂ O:Cs ₂ O•85 GeO ₂ , following isothermal heat treatment at 550 °C.....	197
Figure 7-46. Comparison between the diffraction patterns of the crystallized binary glasses and 3:1 Li ₂ O:Cs ₂ O 85 GeO ₂ glasses, following isothermal heat treatment.	197
Figure 7-47. HTXRD scans for isothermal heat treatment at 605 °C for the 1:1 Li ₂ O:Cs ₂ O•85 GeO ₂ glass.	199
Figure 7-48. Diffraction pattern of the room temperature crystals, following the HTXRD experiment and heat treatment at 605 °C, for the 1:1 Li ₂ O:Cs ₂ O•85 GeO ₂ glass.	199
Figure 7-49. HTXRD scans for isothermal heat treatment at 520 °C for the 1:3 Li ₂ O:Cs ₂ O•85 GeO ₂ glass.	200
Figure 7-50. Diffraction pattern of the room temperature crystals, following the HTXRD experiment and heat treatment at 520 °C, for the 1:3 Li ₂ O:Cs ₂ O•85 GeO ₂ glass.	200
Figure 7-51. HTXRD scans for isothermal heat treatment at 495 °C for the 1:7 Li ₂ O:Cs ₂ O•85 GeO ₂ glass.	201
Figure 7-52. Diffraction pattern of the room temperature crystals, following the HTXRD experiment and heat treatment at 495 °C, for the 1:7 Li ₂ O:Cs ₂ O•85 GeO ₂ glass.	201
Figure 7-53. DSC curves for glasses on the x Li ₂ O• (15- x) Cs ₂ O•85 GeO ₂ line, with a 20 K/min heating rate.	203
Figure 7-54. T _g and T _p for all glasses along x Li ₂ O• (15- x) Cs ₂ O•85 GeO ₂ , with a 20 K/min heating rate. Lines added to aid the eye.	204
Figure 7-55. Activation energy of crystallization for x Li ₂ O•(15- x) Cs ₂ O•85 GeO ₂ glasses.....	204
Figure 7-56. ESEM image, of crystals formed in 15 Li ₂ O•85 GeO ₂ glass after the low temperature heat treatment (485 °C).	206
Figure 7-57. ESEM image of crystals formed in 15 Li ₂ O•85 GeO ₂ glass after the high temperature heat treatment (635 °C)	206
Figure 7-58. ESEM image of crystals formed in 7:1 Li ₂ O:Cs ₂ O•85 GeO ₂ glass.....	207
Figure 7-59. ESEM image of crystals formed in 3:1 Li ₂ O:Cs ₂ O•85 GeO ₂ glass.....	208

	PAGE
Figure 7-60. ESEM image of crystals formed in 1:1 Li ₂ O:Cs ₂ O•85 GeO ₂ glass.....	208
Figure 7-61. ESEM image of crystals formed in 1:3 Li ₂ O:Cs ₂ O•85 GeO ₂ glass.....	209
Figure 7-62. ESEM image of crystals formed in 1:7 Li ₂ O:Cs ₂ O•85 GeO ₂ glass.....	209
Figure 7-63. ESEM image of crystals formed in 15 Cs ₂ O•85 GeO ₂ glass.....	210
Figure 7-64. X-ray diffraction patterns for all seven x Li ₂ O•(15- x) Cs ₂ O•85 GeO ₂ compositions following isothermal heat treatment.....	211
Figure 7-65. X-ray diffraction patterns for glasses where the predominate crystal phases are binary cesium germanium oxides.....	212

ABSTRACT

There is little data in the literature pertaining to mixed alkali germanate glasses. The majority of the data exists for the sodium-potassium-germanate glasses, and focuses on the density, glass transition temperature and vibrational spectra. This study explores three of the ten possible mixed alkali germanate glass systems: the lithium-cesium-germanium ternary, the sodium-potassium-germanium ternary, and the potassium-rubidium-germanium ternary. The mixed alkali effect was examined at two different concentrations of germania (85 and 90 mol %). To examine the mixed alkali effect on the germanate anomaly, the alkali oxides were held in a ratio of 1:1 and the germanium was varied from 100 to 75 mol %.

The glass transition temperature and densities behavior of the mixed alkali germanate glasses in this study behaved as expected, exhibiting a maximum in T_g and no mixed alkali effect in density. The glasses with a 1:1 ratio of alkali exhibited properties between the end member glasses.

The infrared spectra from this study show that the hydroxyl content increases as the amount of alkali in the glass increases. The cation identity does effect the band positions and intensities. The infrared bands between 1500 and 4000 cm^{-1} are shown to be a result of water.

Electrical conductivity of mixed alkali germanate glasses exhibited unique behavior. Small additions of alkali (≤ 5 mol %) result in a positive or a linear deviation from additivity, in both the lithium-cesium-germanate system and the sodium-potassium-germanate system. With 10 mol % alkali oxide addition the deviation from additivity increases as the radius ratio of the cations increases. However, with 15 mol % alkali oxide addition, the greater the difference in the radius ratio of the cations, the smaller the deviation from additivity.

A Kissinger study on the lithium-cesium-germanate glasses, yields activation energies consistent with crystallization studies in the literature for other mixed alkali germanate glasses. Glasses with a 1:1 ratio of cesium oxide to lithium oxide, or more cesium oxide than lithium oxide, crystallize into cesium germanium oxide crystals, however if there is more lithium the glasses crystallize into an unknown phase.

CHAPTER 1: INTRODUCTION

Early glass researchers strived to understand why glasses formed and what compounds would result in a glass. Sun's work from 1947 resulted in his *Bond Strength Criterion* for glass formation.¹ Sun predicted that B_2O_3/B_2O , GeO_2 , SiO_2 , V_2O_5 , and P_2O_5 would act as glass formers.

Silicates were the first glasses discovered and are the most thoroughly studied.² When the properties of a glass system behave differently from those of the equivalent silicate system, its behavior is called anomalous, e.g. the boron anomaly,^{3,4} which occurs when alkali oxide is added to amorphous boron oxide. In that case, it is believed that the three coordinated boron ions transform to four coordinated ions without breaking up the glass network, i.e. no formation of non-bridging oxygens, completely changing the expected property behavior.

Similarly, the properties of alkali germanate glasses are different from those of silicate glasses.⁵⁻¹⁰ Depending on the property, there may be either one anomaly, at ≈ 10 to 20 mol % R_2O , or two anomalies, i.e. a low alkali germanate anomaly, which occurs between 2 and 5 mol% alkali oxide and a high alkali anomaly that occurs around 15-18 mol% alkali oxide.⁷ Structural changes accompanying these anomalies are not well understood.

This thesis deals with the mixed alkali effect in germanate glasses. The first three chapters of this thesis (4 through 6) will explore the properties and behaviors of mixed alkali germanate glasses. Each chapter will present data on glasses in two to three of the mixed alkali germanate ternary systems and discuss both the mixed alkali effect and the germanate anomaly. These chapters cover general properties, infrared spectra, and electrical conductivity. Chapter 7 reports the results of a study of the crystallization behavior of $x Li_2O \cdot (100-x) Cs_2O \cdot 85 GeO_2$ glasses and will not include discussion regarding the germanate anomaly.

1. K.H. Sun, "Fundamental Condition of Glass Formation," *J. Am. Ceram. Soc.*, **30** [9] 277-81 (1947).
2. SciGlass 6.5 [CD-ROM] ITC Inc., Newton, MA, 2005.
3. J.E. Shelby, "Properties of B₂O₃-GeO₂ Glasses," *J. Appl. Phys.*, **45** [12] 5272-7 (1974).
4. J.E. Shelby, *Introduction to Glass Science and Technology*; pp. 1-181. The Royal Society of Chemistry, Cambridge, 1997.
5. D. Di Martino, L.F. Santos, A.C. Marques, and R.M. Almeida, "Vibrational Spectra and Structure of Alkali Germanate Glasses," *J. Non-Cryst. Solids*, **293-295** 394-401 (2001).
6. E.I. Kamitsos, Y.D. Yiannopoulos, C.P.E. Varsamis, and H. Jain, "Structure-Property Correlation in Glasses by Infrared Reflectance Spectroscopy," *J. Non-Cryst. Solids*, **222** [1] 59-68 (1997).
7. J.E. Shelby, "Thermal Expansion of Mixed-Alkali Germanate Glasses," *J. Appl. Phys.*, **46** [1] 193-6 (1975).
8. H.-J. Weber, "Bond Volumes in Crystals and Glasses and a Study of the Germanate Anomaly," *J. Non-Cryst. Solids*, **243** [2-3] 220-32 (1999).
9. Y.D. Yiannopoulos, C.P.E. Varsamis, and E.I. Kamitsos, "Medium Range Order in Glass and the 'Germanate Anomaly' Effect," *Chem. Phys. Lett.*, **359** [3-4] 246-52 (2002).
10. Y.D. Yiannopoulos, C.P.E. Varsamis, and E.I. Kamitsos, "Density of Alkali Germanate Glasses Related to Structure," *J. Non-Cryst. Solids*, **293-295** 244-9 (2001).

CHAPTER 2: LITERATURE REVIEW

This chapter will provide an overview of the literature concerning the mixed alkali effect and the germanate anomaly. Chapters 4 through 7 contain literature review sections covering, in detail, the literature that relates directly to the subject of the chapter.

2.1 Mixed Alkali Effect

Properties rarely follow linear trends when one alkali ion is exchanged for another alkali ion in a glass compositional series. The non-linearity in these properties is called a deviation from additivity, which can be either a positive or negative deviation. This effect is commonly known as the “mixed alkali effect,” but also has been called the “neutralization effect,” “the poly-alkali effect,” and the “mixed-mobile ion effect.”¹⁻⁵ Day⁴ divides the mixed alkali effect into four categories: slight (where the departure from additivity is $< \pm 5\%$), small (deviation $\approx \pm 10\text{-}25\%$), moderate ($\approx \pm 50\%$), and major ($\approx \pm 100\%$). Table 2-I provides a summary of various properties for mixed alkali glasses.

Table 2-I. Summary of Mixed Alkali Effect on Various Properties⁴

Property	Deviation from additivity	Miscellaneous note
Density	Small, $\approx \pm 10\%$	
Refractive Index	Small, $\approx \pm 10\%$	
Molar Volume	Slight, $< \pm 5\%$	
Hardness	Small, $\approx \pm 10\%$	
Glass Transition Temperature	Small, $\approx \pm 10\%$	Negative Deviation
Thermal Expansion	Small, $\approx \pm 10\%$	Usually Positive Deviation
Elastic Modulus	Small, $\approx \pm 20\%$	Temperature Dependent
Conductivity	Major, 2-6 orders of magnitude	Negative Deviation
Dielectric Loss	Major, 1-3 orders of magnitude	Negative Deviation
Dielectric Constant	Small-Moderate ($\approx \pm 25\text{-}50\%$)	Usually Negative Deviation Frequency Dependent
Alkali Diffusion Coefficient	Major, 2-4 orders of magnitude	Negative Deviation
Viscosity	Major, 1-2 orders of magnitude	Negative Deviation Temperature Dependent
Gas Permeability	Small, $< 10\%$	Negative Deviation

The greatest deviations from additivity occur for properties that depend on ionic transport.^{1,2,4,6} These deviations are always negative and can vary by orders of magnitude. Bulk properties are affected differently by mixing alkali ions. Properties

such as refractive index, density, and thermal expansion coefficient have very small deviations from additivity.^{2,4}

The most challenging aspect of the mixed alkali effect (MAE) is the development of a theoretical model. The magnitude of the mixed alkali effect is not the same for every pair of alkali. As the difference in the ionic radii of the alkali increases, the deviation from additivity increases.^{1,4,5} Isard has suggested all proposed theories “must be applicable to any oxide glass, simple or complex, and must relate the effect only to the ionic sizes.”¹ Many well known glass scientists still continue to pursue a theory for the mixed alkali effect.^{1,2,4,6-63}

Historically, theories to explain the MAE fall into one of two major categories, i.e. those that emphasize the structural features of the glass network^{14,64} and those that emphasize the differences in the bonding and coordination environment of the alkali ions.^{5,27,28} Theories based on structural features have been unable to describe the lack of the MAE in properties such as molar volume. The past decade has shown progress towards understanding the MAE. Modern theories on the MAE⁶ combine the updated version of the dynamic structure model^{12,13} and ionic transport mechanisms developed by Ngai,^{65,66} Funke,^{20,21} and co-workers. Since their work is relevant for discussion of the MAE, it will be presented in detail in this chapter. The fundamental theories dealing with ionic conductivity are presented in Chapter 6.

The current theory for explaining the MAE considers both the structure of the glass and the coordination of the alkali ion. Greaves²² proposed the using modified random network model for glass structure. When small amounts of alkali are added (or any network modifying cation) to a glass, the alkali form microsegregates within the glass. Increasing the amount of alkali in the glasses above 16 mol % causes the percolation limit to be exceeded. The microsegregates regions begin to touch and form channels of alkali, therefore significantly increasing the ionic conductivity of the glass. When alkali are mixed within the same glass, these microsegregates regions contain both cations, therefore increasing the barrier for ionic migration.²² This theory of glass structure has become known as the dynamic structure of glass model (DSM). For more detail, refer to the work of Greaves.²²

Diffusion experiments show mixed alkali glasses contain two groups of ions, which are characterized by their mobility as fast or slow. It is proposed that each cation can only migrate down its own restricted pathway through the glass structure.⁶ This concept perceives the Anderson and Stuart approach (Chapter 6) as an over simplification. Anderson and Stuart⁹ assume that there are many empty sites for the ion to move into and the each movement is independent from that of the other alkali ions. The DSM of glasses negates both of the Anderson and Stuart assumptions. The model suggests that alkali ions in melts have specific sites. When the alkali are mixed, each alkali ion has its own respective sites and cannot migrate using sites for the other alkali ions, i.e. a sodium moves to a sodium site, a potassium moves to a potassium site, and a sodium cannot move to a potassium site. As the glass cools, these sites retract into smaller sites that are too small to allow the ion to move through the network. The activation energy for migration is the amount of energy required to restore this site to the appropriate size to accommodate the alkali ion. The work of Ngai,^{65,66} Funke^{20,21,65,66} and their co-workers disprove Anderson and Stuart's other assumption that each alkali movement is independent of all other ions. In binary alkali glasses, the most probable site for an ion moving from one site to the next site is for that ion to move back into its original site.

2.2 Alkali Germanate Anomaly

Glasses which do not behave like silicate glasses are considered anomalous. Adding alkali oxides to silica glasses results in a linear decrease in glass transition temperature and an increase in density and refractive index.⁶⁷ These property trends are related to the decrease in the connectivity of the network resulting from the presence of non-bridging oxygens. Some alkali germanate glasses exhibit maxima in density, refractive index, and glass transition temperature with increasing R₂O concentration. The trends in these properties have become known as the alkali germanate anomaly.⁶⁸⁻⁷⁰ The germanate anomaly has been extensively discussed in the literature.^{7,18,29-31,43,47,68-124} These extrema occur when approximately 15 to 20 mol% alkali oxide is added to the germania; the positions of the maxima are highly dependent upon cation identity.

A low alkali germanate anomaly is also found in the glass transition temperature (T_g). Alkali oxide additions as small as 1-5 mol% cause a decrease in T_g of >100 K, which is followed by an increase in T_g . T_g then passes through a maximum at ~15 to 20 mol % R_2O , after which it decreases.^{3,125} The low alkali germanate anomaly is particularly difficult to study because the glass transition temperature is greatly affected by both hydroxyl and alkali addition. Caution must be exercised when examining alkali germanate glasses with small amounts of alkali because the required melting temperatures are high and it is possible for large amount of alkali to evolve out of the melt, and unknown contamination in the batch materials.⁸³

There are two competing theories describing the structure of mixed alkali germanate glasses. Ivanov and Evstropiev,¹²⁶ and later Murthy and Ip,⁶⁸ developed the first and best known theory in the 1960's. This theory attributes the maximum in density to a coordination change between four and six coordinated germanium ions. The second theory by Henderson and Fleet,⁸⁵ developed in the 1990's, is based on Raman spectra and suggest that there is no coordination change in the glass structure. The germanate anomaly is a result of the development of three member rings of germania tetrahedra.

2.2.1 *Ivanov, Evstropiev, Murthy and Ip Theory*

Early theories concerning structural changes causing the germanate anomaly were based on infrared spectra which were interpreted as indicating that alkali germanate glasses with less than 15 to 20 mol % alkali oxide do not form non-bridging oxygens.¹⁰⁰ As alkali is added to the germanate glass, the fundamental absorption bands resulting from the Ge-O bond shift to higher wavenumber. The anomalous properties were attributed to a coordination change, similar to that proposed for the alkali borate glasses.^{3,67,69,70,75,87} GeO_2 crystals can contain germanium ions in both tetrahedra and octahedra.^{127,128} As a result, it was assumed that germanium can exist in 4-fold and 6-fold coordination sites in glasses. The theories state that additions of alkali oxide beyond the maxima in the density (~15 to 20 mol %) results in the six-coordinated germanium ions reverting back to four coordinated germanium ions. A lengthening of the Ge-O bond is observed in X-ray and neutron scattering⁷⁰ and EXAFS^{89,91,109} studies. Unfortunately,

theses techniques are unable to determine the actual coordination number of the germania ions. They can only indicate that it is greater than the four-coordinated germanium.

This theory assumes the addition of alkali oxide does not break up the network; there is an increase in the density and index because the alkali ions are packing into interstices in the network.^{3,68,70,71,87,125,127,129} The theory relies on two assumptions: (1) no non-bridging oxygen (NBO) form before 15 mol % alkali oxide addition, and (2) changes in coordination number of the germanium ions causes the anomalous properties. This theory has been the most widely accepted theory for the germanate anomaly.

2.2.2 *Henderson and Fleet Theory*

Henderson and Fleet proposed a different model for the alkali germanate anomaly.⁸⁵ They suggest that the germanium ions are always four coordinated in alkali germanate glasses and never transform into octahedral coordination. This structure is explained by the EXAFS data from Itie et al.⁹¹ and Raman data from the Henderson and Fleet study.⁸⁵ Itie et al. suggest that there is a reversible coordination change from four fold to six fold germanium only under pressure, and that six coordinated germanium does not exist in glasses at room temperature.⁹¹ Henderson and Fleet propose that the Raman absorption band shift that occurs with alkali oxide addition is not due to the formation of six-coordinated germanium, but instead due to the formation of 3-member rings and the elongation of the tetrahedral anion-cation bond.⁸⁵

2.2.3 *Current Theory*

The earlier theories of the germanate anomaly are oversimplifications. For example, with small additions of alkali, behavior of the T_g is very different from that of the density. There is an initial decrease of about 100 K with 1-2 mol% addition of alkali oxide. Shelby⁶⁷ suggests that this initial decrease is due to formation of NBO, which open the structure and allows room for the octahedra to form. The increase in T_g with additions of ~5-20 mol % alkali indicates an increase in connectivity, or at least a strengthening of the network.

The low alkali oxide germanate anomaly is also observed in Raman data from Henderson and Fleet.⁸⁴ Recently, Henderson shows that a Raman spectra cannot be

properly fit by assuming only a coordination change, but that there are two small bands, attributed to Q^3 and Q^2 species, that are needed to properly fit the spectra.⁸⁴

Since the historically accepted model for the alkali germanate structural models cannot explain the low alkali germanate anomaly, the model has been found to be unsatisfactory for explaining the data. The model states, with additions of alkali oxide greater than 20 mol %, the germanium ions revert back to their original tetrahedral coordination and the number of NBO increases. This behavior would result in a significant decrease in average bond length of Ge-O, however neutron diffraction studies⁷⁰ do not observe such a decrease in Ge-O bond length. The Ge-O bond length actually remains constant with high amounts of alkali oxide addition.⁸⁴

The early literature assume that the coordination change of germanium must be from four coordinated to six coordinated, based on crystalline forms of germania. While the neutron diffraction work by Hoppe et. al^{70,87,129} and Raman scattering work by Polsky et. al¹³⁰ definitively show that there is higher coordinated germanium ions, it was not until the recent O *K*-edge XANES work by Wang and Henderson^{116,117} that the germanium could conclusively be shown to exist as both four and five coordinated ions. Concentrations of alkali oxide greater than 30 mol % result in transformation of the five coordinated germanium ions back to four coordinated. Reanalysis of their 2002 Raman study⁸⁶ led Henderson and Wang to conclude that there are three stages to the germanate anomaly. First, with small additions of alkali oxide, the glass forms non-bridging oxygens along with increases in intermediate range order. The structure then forms five-coordinated germanium ions plus an NBO near the maximum in the germanate anomaly. Large amounts of alkali oxide (35 to 40 mol %) result in the transformation of some of the five-coordinated germanium ions, back to four-coordinated germanium ions and two NBO. Henderson suggests that the decrease in density is a result of the larger five-coordinated germanium ions forcing the glass network to expand. Unfortunately, Henderson and Wang did not examine glasses containing less than 5 mol % alkali oxide, so no correlation can be made between their Raman work and the minimum in the glass transition temperature.⁸⁴

In summary, some addition of alkali oxide to germania glasses results in property behavior unlike silicate glasses, the properties of the alkali germanate glasses are called

‘anomalous’. The exact mechanisms underlying this anomaly are unknown. The position of the germanate anomaly is cation dependent; this phenomena has yet to be explained by any model. It is known that the glass transition temperature is a good indicator of network connectivity, and with small amounts of alkali, the T_g is significantly decreased, indicating a weakening of the glass network. The minimum in T_g is followed by a maximum in T_g , therefore moderate amounts of alkali oxide in germanate glasses results in a strengthening of the glass network. Raman and NMR have confirmed the presence of non-bridging oxygen, and possible 3-member rings. The density and index of refraction exhibit maxima with alkali oxide additions between 15 and 20 mol %. As the radius of the alkali ion increases, the molar volume of the glass increases. The maximum in the density, index and T_g do not correlate with the maximum in the five-coordinated species.

2.3 References

1. J.O. Isard, "The Mixed Alkali Effect in Glass," *J. Non-Cryst. Solids*, **1** [3] 235-61 (1969).
2. C.T. Moynihan, A.J. Easteal, D.C. Tran, J.A. Wilder, and E.P. Donovan, "Heat Capacity and Structural Relaxation of Mixed-Alkali Glasses," *J. Am. Ceram. Soc.*, **59** [3-4] 137-40 (1976).
3. J.E. Shelby, "Thermal Expansion of Mixed-Alkali Germanate Glasses," *J. Appl. Phys.*, **46** [1] 193-6 (1975).
4. D.E. Day, "Mixed Alkali Glasses-Their Properties and Uses," *J. Non-Cryst. Solids*, **21** [3] 343-72 (1976).
5. O.V. Mazurin, "Glass in a Dielectric Field," pp. 5-55 in *Structure of Glass, Vol. 4, The Structure of Glass: Electrical Properties and Structure of Glass*. Edited by O. V. Mazurin. Consultants Bureau, New York, 1965.
6. M.D. Ingram, C.T. Imrie, and I. Konidakis, "Activation Volumes and Site Relaxation in Mixed Alkali Glasses," *J. Non-Cryst. Solids*, **352** [30-31] 3200-9 (2006).
7. S. Adams and J. Swenson, "Structure Conductivity Correlation in Reverse Monte Carlo Models of Single and Mixed Alkali Glasses," *Solid State Ionics*, **175** [1-4] 665-9 (2004).

8. R.M. Almedia and J.D. Mackenzie, "The Electrical Conductivity of Fluorozirconate and Chloro-Fluorozirconate Glasses," *J. Mater. Sci.*, **17** [9] 2533-8 (1982).
9. O.L. Anderson and D.A. Stuart, "Calculation of Activation Energy of Ionic Conductivity in Silica Glasses by Classical Methods," *J. Am. Ceram. Soc.*, **37** [12] 576-80 (1954).
10. F. Berkemeier, S. Voss, A.W. Imre, and H. Mehrer, "Molar Volume, Glass-Transition Temperature, and Ionic Conductivity of Na- and Rb- Borate Glasses in Comparison with Mixed Na-Rb Borate Glasses," *J. Non-Cryst. Solids*, **351** [52-54] 3816-25 (2005).
11. P.J. Bray and J.R. Hendrickson, "Dependence of the Mixed Alkali Effect on Ion Masses," *J. Non-Cryst. Solids*, **21** [2] 297-9 (1976).
12. A. Bunde, M.D. Ingram, and P. Maass, "The Dynamic Structure Model for Ion Transport in Glasses," *J. Non-Cryst. Solids*, **172-174** [Part 2] 1222-36 (1994).
13. A. Bunde, M.D. Ingram, and S. Russ, "A New Interpretation of the Dynamic Structure Model of Ion Transport in Molten and Solid Glasses," *Phys. Chem. Chem. Phys.*, **6** [13] 3663-8 (2004).
14. R.J. Charles, "The Mixed Alkali Effect in Glasses," *J. Am. Ceram. Soc.*, **48** [8] 432-4 (1965).
15. J.F. Cordaro and M. Tomozawa, "Mixed-Alkali Effect in Low-Alkali Germanate Glasses," *J. Am. Ceram. Soc.*, **65** [4] C50-C1 (1982).
16. J.F. Cordaro and M. Tomozawa, "Dependence Upon Alkali Concentration of the Electrical Conductivity in Sodium Silicate Glasses," *Phys. Chem. Glasses*, **27-28** [1] 27 (1984).
17. D.E. Day, "Review of Mechanical Relaxations in Mixed Alkali Silicate Glasses," pp. 39-47, *Amorphous Materials: Papers Presented to the Third International Conference on the Physics of Non-Crystalline Solids Held at Sheffield University, September, 1970*. Edited by R. W. Douglas and B. Ellis. Wiley-Interscience, New York, 1972.
18. A. Doi and D.E. Day, "Conduction Polarization in Sodium Germanate Glasses," *J. Appl. Phys.*, **52** [5] 3433-8 (1981).
19. M. Dubiel, B. Roling, and M. Futing, "AC Conductivity and Ion Transport in K⁺-for-Na⁺ Ion-Exchanged Glasses: Exchange Experiments Below and above the Glass Transition Temperature," *J. Non-Cryst. Solids*, **331** [1-3] 11-9 (2003).

20. K. Funke and R.D. Banhatti, "Modeling Frequency-Dependent Conductivities and Permittivities in the Framework of the Migration Concept," *Solid State Ionics*, **169** [1-4] 1-8 (2004).
21. K. Funke and R.D. Banhatti, "Translational and Localised Ionic Motion in Materials with Disordered Structures," *Solid State Sci.*, (article in press).
22. G.N. Greaves and K.L. Ngai, "Ionic Transport Properties in Oxide Glasses Derived from Atomic Structure," *J. Non-Cryst. Solids*, **172-174** [Part 2] 1378-88 (1994).
23. R. Green and K.B. Blodgett, "Electrically Conducting Glasses," *J. Am. Ceram. Soc.*, **31** [4] 89-100 (1948).
24. J. Habasaki, K.L. Ngai, Y. Hiwatari, and C.T. Moynihan, "Molecular Dynamics Simulations of the Dynamics of Ions in Single and Mixed Alkali Glasses " *J. Non-Cryst. Solids*, **349** 223-9 (2004).
25. Y.H. Han, N.J. Kreidl, and D.E. Day, "Alkali Diffusion and Electrical Conductivity in Sodium Borate Glasses," *J. Non-Cryst. Solids*, **30** [3] 241-52 (1979).
26. Y. Haven and B. Verkerk, "Diffusion and Electrical Conductivity of Sodium Ions in Sodium Silicate Glasses," *Phys. Chem. Glasses*, **6** [2] 38-45 (1965).
27. J.R. Hendrickson and P.J. Bray, "A Theory for the Mixed Alkali Effect in Glass, Part 1," *Phys. Chem. Glasses*, **13** [2] 43-9 (1972).
28. J.R. Hendrickson and P.J. Bray, "A Theory for the Mixed Alkali Effect in Glass, Part 2," *Phys. Chem. Glasses*, **13** [4] 107-15 (1972).
29. W.C. Huang and H. Jain, "Correlation between Local Structure and Electrical Response of Rb and (Rb, Ag) Germanate Glasses: DC Conductivity," *J. Non-Cryst. Solids*, **188** [3] 254-65 (1995).
30. W.C. Huang and H. Jain, "Local Structure and Electrical Response of Rb and (Rb, Ag) Germanate Glasses: Electrical Conductivity Relaxation," *J. Non-Cryst. Solids*, **212** [2-3] 117-25 (1997).
31. W.C. Huang, H. Jain, and G. Meitzner, "The Local Structure of Mixed Alkali Germanate Glasses by EXAFS," *J. Non-Cryst. Solids*, **255** [1] 103-11 (1999).
32. A.G. Hunt, "Mixed-Alkali Effect: Some New Results," *J. Non-Cryst. Solids*, **255** [1] 47-55 (1999).

33. C.C. Hunter and M.D. Ingram, "Na⁺ -Ion Conducting Glasses," *Solid State Ionics*, **14** [1] 31-40 (1984).
34. A.W. Imre, F. Berkemeier, H. Mehrer, Y. Gao, C. Cramer, and M.D. Ingram, "Transition from a Single-Ion to a Collective Diffusion Mechanism in Alkali Borate Glasses," *J. Non-Cryst. Solids*, **354** [2-9] 328-32 (2008).
35. A.W. Imre, S.V. Divinski, S. Voss, F. Berkemeier, and M. H., "A Revised View on the Mixed-Alkali Effect in Alkali Borate Glasses," *J. Non-Cryst. Solids*, **352** [8] 783-8 (2006).
36. A.W. Imre, S. Voss, and H. Mehrer, "Ionic Conduction, Diffusion and Glass Transition in 0.2[x Na₂O•(1-x) Rb₂O]•0.8 B₂O₃," *J. Non-Cryst. Solids*, **333** [3] 231-9 (2004).
37. M.D. Ingram, "Ionic Conductivity in Glass," *Phys. Chem. Glasses*, **28** [6] 215-34 (1987).
38. M.D. Ingram, "The Mixed Alkali Effect Revisited-a New Look at an Old Problem," *Glasstech. Ber. Glass Sci. Technol.*, **67** [6] 151-5 (1994).
39. M.D. Ingram, C.T. Moynihan, and A.V. Lesikar, "Ionic Conductivity and the Weak Electrolyte Theory of Glass," *J. Non-Cryst. Solids*, **38-39** [Part I] 371-6 (1980).
40. J.O. Isard, M. Jagla, and K. Mallick, "Simple Models for the Ionic Conduction Mechanism in Glasses," *J. Phys.*, **43** [C9] 387 (1982).
41. A.O. Ivanov, "Electrical Conductivity of Mixed Alkali Glasses of the Na₂O-K₂O-GeO₂ System," *Sov. Phys. Solid State (Engl. Transl.)*, **5** [9] 1933-7 (1964).
42. H. Jain, H.L. Downing, and N.L. Peterson, "The Mixed Alkali Effect in Lithium-Sodium Borate Glasses," *J. Non-Cryst. Solids*, **64** [3] 335-49 (1984).
43. H. Jain, W.C. Huang, E.I. Kamitsos, and Y.D. Yiannopoulos, "Significance of Intermediate Range Structure for Electrical Conduction in Alkali Germanate Glasses," *J. Non-Cryst. Solids*, **222** 361-8 (1997).
44. H. Jain and X. Lu, "Is There a Mixed Alkali Effect in the Low Temperature AC Conductivity of Glasses," *J. Non-Cryst. Solids*, **196** 285-90 (1996).
45. R. Kirchheim, "The Mixed Alkali Effect as a Consequence of Network Density and Site Energy Distribution," *J. Non-Cryst. Solids*, **272** [2-3] 85-102 (2000).
46. R. Kirchheim and D. Paulmann, "The Relevance of Site Energy Distribution for the Mixed Alkali Effect," *J. Non-Cryst. Solids*, **286** [3] 210-23 (2001).

47. Y.S. Krupkin and K.S. Evstrop'ev, "Properties and Structure of Multialkali Borogermanate Glasses," *Inorg. Mater.*, **1** [9] 1410-4 (1971).
48. J.C. Lapp and J.E. Shelby, "The Mixed Alkali Effect in Lithium-Sodium Aluminosilicate Glasses," *J. Non-Cryst. Solids*, **95-96** [Part 2] 889-96 (1987).
49. P. Maass, "Towards a Theory for the Mixed Alkali Effect in Glass," *J. Non-Cryst. Solids*, **255** [1] 34-46 (1999).
50. T. Minami, "Fast Ion Conducting Glass," *J. Non-Cryst. Solids*, **73** [1-4] 273-84 (1985).
51. R.A. Montani, "A Kinetic Model for the Mixed Alkali Effect on Ionic Conducting Glasses," *J. Non-Cryst. Solids*, **215** [2-3] 307-12 (1997).
52. L. Solymar and D. Walsh, *Electrical Properties of Materials*, 7th ed.; pp. 2-20. Oxford University Press, Oxford, 2004.
53. M. Tatsumisago, T. Minami, and M. Tanaka, "Properties of Highly Ionic Conducting Li₄SiOF-Li₃BO₃ Glasses Prepared by Rapid Quenching," *Glastech. Ber.*, **56K** 945-50 (1983).
54. R. Terai, "The Mixed Alkali Effect in the Na₂O-Cs₂O-SiO₂ Glasses," *J. Non-Cryst. Solids*, **18** [2] 121-35 (1971).
55. M.P. Thomas, "Electrical Conductivity and Tracer Diffusion in Sodium Germanate Glasses," *Solid State Ionics*, **14** [4] 297-307 (1984).
56. M. Tomozawa, "The Mixed Alkali Effect and Thermodynamic State of Glass," *Solid State Ionics*, **105** [1-4] 249-55 (1998).
57. M. Tomozawa, J.F. Cordaro, and M. Singh, "Applicability of Weak Electrolyte Theory to Glasses," *J. Non-Cryst. Solids*, **40** [1-3] 189-96 (1980).
58. M. Tomozawa and M. Yoshiyagawa, "AC Electrical Conductivity of Mixed Alkali Glasses," *Glastech. Ber.*, **56** [Part 2] 939-44 (1983).
59. J.-S. Wang, K.-M. Hon, K.-H. Yang, M.-C. Wang, and M.-H. Hon, "Mixed Alkali Effect on Calcium Aluminogermanate Glasses," *Ceram. Int.*, **23** [2] 153-7 (1997).
60. B.M. Wright and J.E. Shelby, "Phase Separation and the Mixed Alkali Effect," *Phys. Chem. Glasses*, **41** [4] 192-8 (2000).

61. A.K. Yakhkind, N.V. Ovcharenko, B.V. Tatarintsev, A.A. Kozmanyanyan, V.Y. Alaev, and A.K. Pogodaev, "Ion-Exchange Interaction between Germanate Glasses and Molten Alkali Nitrates and Refractive-Index Gradient Glasses," *Fiz. Khim. Stekla*, **6** [6] 720-5 (1980).
62. J. Zhang and D.L. Sidebottom, "Modeling the AC Conductivity Dispersion of Mixed Alkali Germanate Glasses," *J. Non-Cryst. Solids*, **288** [1-3] 18-29 (2001).
63. H.L. Tuller, "Amorphous Fast Ionic Conductors," pp. 51-88 in Vol. 199, *Science and Technology of Fast Ion Conductors*. Edited by H. L. Tuller and M. Balkanski. Plenum, New York, 1989.
64. R.L. Myuller, "Electrical Conductivity of Solid Ionic-Atomic Valent Substances. X. Electrical Conductivity of Glasses Containing Two Kinds of Alkali Ions," *Sov. Phys. Solid State (Engl. Transl.)*, **2** [6] 1219-23 (1960).
65. K.L. Ngai, "The Dynamics of Ions in Glasses: Importance of Ion-Ion Interactions," *J. Non-Cryst. Solids*, **323** [1-3] 120-6 (2003).
66. K.L. Ngai, Y. Wang, and C.T. Moynihan, "The Mixed Alkali Effect Revisited: The Importance of Ion-Ion Interactions," *J. Non-Cryst. Solids*, **307-310** 999-1011 (2002).
67. J.E. Shelby, *Introduction to Glass Science and Technology*; pp. 1-181. Royal Society of Chemistry, Cambridge, 1997.
68. M.K. Murthy and J. Ip, "Some Physical Properties of Alkali Germanate Glasses," *Nature (London)*, **201** [5] 285-6 (1964).
69. A.M. Efimov, "Infrared Spectra, Band Frequencies and Structure of Sodium Germanate Glasses," *Phys. Chem. Glasses*, **40** [4] 199-206 (1999).
70. U. Hoppe, R. Kranold, H.-J. Weber, and A.C. Hannon, "The Change of the Ge-O Coordination Number in Potassium Germanate Glasses Probed by Neutron Diffraction with High Real-Space Resolution," *J. Non-Cryst. Solids*, **248** [1] 1-10 (1999).
71. R.T. Amos and G.S. Henderson, "The Effects of Alkali Cation Mass and Radii on the Density of Alkali Germanate and Alkali Germano-Phosphate Glasses," *J. Non-Cryst. Solids*, **331** [1-3] 108-21 (2003).
72. C.B. Azzoni, D. Di Martino, A. Paleari, and R.M. Almedia, "Paramagnetic Sites in Alkali Germanate Glasses," *J. Non-Cryst. Solids*, **278** [1-3] 19-23 (2000).
73. A.D. Cox and P.W. McMillan, "An EXAFS Study of the Structure of Lithium Germanate Glasses," *J. Non-Cryst. Solids*, **44** [2-3] 257-64 (1981).

74. D. Di Martino, L.F. Santos, R.M. Almeida, and M.F. Montemor, "X-Ray Photoelectron Spectroscopy of Alkali Germanate Glasses," *Surf. Interface Anal.*, **34** [1] 324-7 (2002).
75. D. Di Martino, L.F. Santos, A.C. Marques, and R.M. Almeida, "Vibrational Spectra and Structure of Alkali Germanate Glasses," *J. Non-Cryst. Solids*, **293-295** 394-401 (2001).
76. V. Dimitrov and T. Komatsu, "Correlation of Optical Basicity and O1s Chemical Shift in XPS Spectra of Oxide Glasses," *Phys. Chem. Glasses*, **44** [5] 357-64 (2003).
77. A. Doi and D.E. Day, "Thermally Stimulated Polarization Current in Sodium Germanate Glass " *J. Mater. Sci.*, **15** [12] 3047-50 (1980).
78. T. Furukawa and W.B. White, "Raman Spectroscopic Investigation of the Structure and Crystallization of Binary Alkali Germanate Glasses," *J. Mater. Sci.*, **15** [7] 1648-62 (1980).
79. C. Garrault, B. Monnaye, and C. Bouaziz, "Lithium Germanates with the Formula $x\text{GeO}_2 \cdot y\text{Li}_2\text{O}$," *C. R. Seances Acad. Sci. Ser. C.*, **276** [5] 417-20 (1973).
80. I.A. Gee, R. Hussin, D. Holland, and C.F. McConville, "X-Ray Photoelectron Spectroscopy Study of the Germanate Anomaly in the $\text{Na}_2\text{O}-\text{GeO}_2$ System," *Phys. Chem. Glasses*, **41** [4] 175-81 (2000).
81. S. Giri, C. Gaebler, J. Helmus, M. Affatigato, S. Feller, and M. Kodama, "A General Study of Packing in Oxide Glass Systems Containing Alkali," *J. Non-Cryst. Solids*, **347** [1] 87-92 (2004).
82. V.V. Golubkov and I.G. Polyakova, "Structure and Structural Transformations of Lithium Germanate Glasses," *Fiz. Khim. Stekla*, **16** [4] 518-28 (1990).
83. M.M. Hall and J.E. Shelby, "Water Diffusion and Solubility in Alkali Germanate Melts," *Phys. Chem. Glasses*, **45** [4] 283-90 (2004).
84. G.S. Henderson, "The Germanate Anomaly: What Do We Know?," *J. Non-Cryst. Solids*, **353** [18-21] 1695-704 (2007).
85. G.S. Henderson and M.E. Fleet, "The Structure of Glass Along the $\text{Na}_2\text{O}-\text{GeO}_2$ Join," *J. Non-Cryst. Solids*, **134** [3] 259-69 (1991).
86. G.S. Henderson and H.M. Wang, "Germanium Coordination and the Germanate Anomaly," *Eur. J. Mineral.*, **14** [4] 733-44 (2002).

87. U. Hoppe, R. Kranold, H.-J. Weber, J. Neuefeind, and A.C. Hannon, "The Structure of Potassium Germanate Glasses - a Combined X-Ray and Neutron Scattering Study," *J. Non-Cryst. Solids*, **278** [1-3] 99-114 (2000).
88. H. Hosono and Y. Abe, "Temperature Dependence of Infrared Absorption Spectra of Hydroxyl Groups in Soda Germanate Glasses," *J. Am. Ceram. Soc.*, **72** [1] 44-8 (1989).
89. W.C. Huang, H. Jain, and G. Meitzner, "The Structure of Potassium Germanate Glasses by EXAFS," *J. Non-Cryst. Solids*, **196** 155-61 (1996).
90. R. Hussin, D. Holland, and R. Dupree, "Does Six-Coordinate Germanium Exist in Na₂O-GeO₂ Glasses? Oxygen-17 Nuclear Magnetic Resonance Measurements," *J. Non-Cryst. Solids*, **232-234** 440-5 (1998).
91. J.P. Itie, A. Polian, G. Calas, J. Petiau, A. Fontaine, and H. Tolentino, "Pressure-Induced Coordination Changes in Crystalline and Vitreous Germanium Dioxide," *Phys. Rev. Lett.*, **63** [4] 398-401 (1989).
92. G.L. Jin, Y. Liu, and J.N. Mundy, "Refractive Index and Density of Na-, Rb- and Mixed Na, Rb-Aluminogermanate Glasses," *J. Mater. Sci.*, **22** [10] 3672-8 (1982).
93. E.I. Kamitsos, Y.D. Yiannopoulos, C.P.E. Varsamis, and H. Jain, "Structure-Property Correlation in Glasses by Infrared Reflectance Spectroscopy," *J. Non-Cryst. Solids*, **222** [1] 59-68 (1997).
94. A. Karthikeyan and R.M. Almeida, "Structural Anomaly in Sodium Germanate Glasses by Molecular Dynamics Simulation," *J. Non-Cryst. Solids*, **281** [1-3] 152-61 (2001).
95. T.J. Kiczanski, C. Ma, E. Hammarsten, D. Wilkerson, M. Affatigato, and S. Feller, "A Study of Selected Physical Properties of Alkali Germanate Glasses over Wide Ranges of Composition," *J. Non-Cryst. Solids*, **272** [1] 57-66 (2000).
96. R. Kuchler, O. Kanert, S. Ruckstein, and H. Jain, "Correspondence between Nuclear Spin Relaxation and Ionic Conduction in Lithium Germanate Glasses," *J. Non-Cryst. Solids*, **128** [3] 328-32 (1991).
97. C.R. Kurkjian and R.W. Douglas, "The Viscosity of Glasses in the System Na₂O-GeO₂," *Phys. Chem. Glasses*, **1** [1] 19-25 (1960).
98. X. Lu, H. Jain, and W.C. Huang, "Structure of Potassium and Rubidium Germanate Glasses by X-Ray Photoelectron Spectroscopy," *Phys. Chem. Glasses*, **37** [5] 201-5 (1996).

99. N. Mochida, K. Sakai, and K. Kikuchi, "Raman Spectroscopic Study of the Structure of the Binary Alkali Germanate Glasses," *Yogyo Kyokaishi*, **92** [4] 164-72 (1984).
100. M.K. Murthy and E.M. Kirby, "Infra-Red Spectra of Alkali-Germanate Glasses," *Phys. Chem. Glasses*, **5** [5] 144-6 (1964).
101. M.K. Murthy and B. Scroggie, "Properties and Structure of Glasses in the System $M_2O-Al_2O_3-GeO_2$ ($M=Li, Na, K$)," *Phys. Chem. Glasses*, **6** [5] 162-7 (1965).
102. T. Nanba, J. Kieffer, and Y. Miura, "Molecular Dynamic Simulation on the Structure of Sodium Germanate Glasses," *J. Non-Cryst. Solids*, **277** [2-3] 188-206 (2000).
103. S.V. Nemilov, "Viscosity and Structure of Binary Germanate Glasses in the Softening Range," *Zh. Prikl. Khim. (Leningrad)*, **43** [12] 2602-10 (1970).
104. S.V. Nemilov, "Systematic Study of the Influence of Admixtures of Sodium Oxide on the Viscosity of Glassy Germanium Dioxide," *Zh. Prikl. Khim. (Leningrad)*, **45** [2] 256-62 (1972).
105. A. Osaka, K. Takahashi, and K. Ariyoshi, "The Elastic Constant and Molar Volume of Sodium and Potassium Germanate Glasses and the Germanate Anomaly," *J. Non-Cryst. Solids*, **70** [2] 243-52 (1985).
106. E.F. Riebling, "Structure of Molten Oxides. 2. A Density Study of Binary Germanates Containing $Li_2O, Na_2O, K_2O,$ and Rb_2O ," *J. Chem. Phys.*, **39** [11] 3022-30 (1963).
107. E.F. Riebling, "Nonideal Mixing in Binary GeO_2-SiO_2 Glasses," *J. Am. Ceram. Soc.*, **51** [7] 406-7 (1968).
108. J.A. Ruller, C.A. Shaw, and J.E. Shelby, "Properties and Morphology of Sodium Lead Germanate Glasses," *Phys. Chem. Glasses*, **33** [5] 161-6 (1992).
109. S. Sakka and K. Kamiya, "Structure of Alkali Germanate Glasses Studied by Spectroscopic Techniques," *J. Non-Cryst. Solids*, **49** [1-3] 103-16 (1982).
110. B.M.J. Smets and T.P.A. Lommen, "The Structure of Germanosilicate Glasses, Studied by X-Ray Photoelectron Spectroscopy," *J. Non-Cryst. Solids*, **46** [1] 21-32 (1981).
111. L.G. Soltay and G.S. Henderson, "Structural Differences between Lithium Silicate and Lithium Germanate Glasses by Raman Spectroscopy," *Phys. Chem. Glasses*, **46** [4] 381-4 (2005).

112. A.N. Trukhin, "Localized States in Germanate Glasses. Study of Luminescence.," *J. Non-Cryst. Solids*, **189** [3] 291-6 (1995).
113. V.A. Tyul'kin and N.I. Shalunenko, "Structure of Vitreous GeO₂ and The "Germanate Anomaly"," *Inorg. Mater.*, **7** [12] 1959-62 (1971).
114. H. Verweij and J.H.J.M. Buster, "The Structure of Lithium, Sodium and Potassium Germanate Glasses, Studied by Raman Scattering " *J. Non-Cryst. Solids*, **34** [1] 81-99 (1979).
115. N. Wada, M. Ichinotani, and K. Kojima, "Glass Composition Dependence of Luminescence Due to Ge²⁺ Center in Germanate Glasses," *J. Non-Cryst. Solids*, **352** [23-25] 2657-61 (2006).
116. H.M. Wang and G.S. Henderson, "Investigation of Coordination Number in Silicate and Germanate Glasses Using O K-Edge X-Ray Absorption Spectroscopy," *Chem. Geol.*, **213** [1-3] 17-30 (2004).
117. H.M. Wang and G.S. Henderson, "The Germanate Anomaly: Is the Presence of Five- or Six-Fold Ge Important?," *Phys. Chem. Glasses*, **46** [4] 337-80 (2005).
118. P.W. Wang, Y. Qi, and D.O. Henderson, "Oxygen Bonding in GeO₂ Glass," *J. Non-Cryst. Solids*, **224** [1] 31-5 (1998).
119. H.-J. Weber, "Bond Volumes in Crystals and Glasses and a Study of the Germanate Anomaly," *J. Non-Cryst. Solids*, **243** [2-3] 220-32 (1999).
120. A. Witkowska, B. Sikora, K. Trzebiatowski, and J. Rybicki, "Germanate Anomaly in Heavy Metal Oxide Glasses: An Exafs Analysis," *J. Non-Cryst. Solids*, **352** [40-41] (2006).
121. O.V. Yanush, V.O. Kabanov, G.O. Karapetyan, and I.A. Mukhitdinova, "Calculation of the Refractive Index and Density of Sodium Germanate Glasses," *Fiz. Khim. Stekla*, **10** [2] 230-5 (1984).
122. Y.D. Yiannopoulos, C.P.E. Varsamis, and E.I. Kamitsos, "Density of Alkali Germanate Glasses Related to Structure," *J. Non-Cryst. Solids*, **293-295** 244-9 (2001).
123. Y.D. Yiannopoulos, C.P.E. Varsamis, and E.I. Kamitsos, "Medium Range Order in Glass and the 'Germanate Anomaly' Effect," *Chem. Phys. Lett.*, **359** [3-4] 246-52 (2002).
124. C.D. Yin, H. Morikawa, F. Marumo, Y. Gohshi, Y.Z. Bai, and S. Fukushima, "Coordination Number of Ge Atoms in Na₂O-GeO₂ Glasses Studied by Chemical Shift Measurements," *J. Non-Cryst. Solids*, **69** [1] 97-103 (1984).

125. J.E. Shelby and J. Ruller, "Properties and Structure of Lithium Germanate Glasses," *Phys. Chem. Glasses*, **28** [6] 262-8 (1987).
126. K.S. Evstrop'ev and A.O. Ivanov, "Physicochemical Properties of Germanium Glasses," pp. 79-85 in Vol. 2, Proceedings of the VI International Congress on Glass. Plenum Press, Washington, D.C., 1962.
127. M.K. Murthy and J. Aguayo, "Studies in Germanium Oxide Systems: II, Phase Equilibria in the System $\text{Na}_2\text{O-GeO}_2$," *J. Am. Ceram. Soc.*, **47** [9] 444-7 (1964).
128. M. Catauro, F. de Gaetano, and A. Marotta, "Non-Isothermal Devitrification of Sodium Germanate Glasses," *Thermochim. Acta*, **404** [1-2] 55-61 (2003).
129. U. Hoppe, "Behavior of the Packing Densities of Alkali Germanate Glasses," *J. Non-Cryst. Solids*, **248** [1] 11-8 (1999).
130. C.H. Polysky, K.H. Smith, and G.H. Wolf, "Effect of Pressure on the Absolute Raman Scattering Cross Section of SiO_2 and GeO_2 Glasses," *J. Non-Cryst. Solids*, **248** [2-3] 159-68 (1999).

CHAPTER 3: EXPERIMENTAL PROCEDURES

This chapter presents the experimental procedures involved in the production of the glasses used for this study. Later chapters contain the appropriate experimental procedures to reproduce the experiments presented in each chapter.

3.1 Glass Batching

Glasses were batched using reagent grade carbonates and 99.99 % pure GeO_2 . The size of the melts ranged from 2.5 to 10 g depending on the glasses' crystallization behavior. Glasses were mixed by hand in a glass mortar and poured into a crucible. Three alkali germanate ternaries were studied: $\text{Na}_2\text{O}\cdot\text{K}_2\text{O}\cdot\text{GeO}_2$, $\text{Li}_2\text{O}\cdot\text{Cs}_2\text{O}\cdot\text{GeO}_2$ and $\text{K}_2\text{O}\cdot\text{Rb}_2\text{O}\cdot\text{GeO}_2$.

3.2 Glass Melting

Glasses were melted in a 90 Pt 10 Rh crucible in an electric furnace. Melting times and temperatures varied to minimize vaporization of the alkali. Melting temperatures ranged from 1100 to 1500°C and times ranged from 2 to 60 minutes. Glasses with ≤ 2 mol % alkali oxide, were melted at 1500 °C for 30 minutes, the furnace temperature was dropped to 1400 °C for an additional 30 min. Glasses with ≥ 5 mol % alkali oxide were melted at 1100 °C, melting times ranged from 2 to 15 minutes depending on the batch size, smaller batches were melted for shorter periods. Upon removal from the furnace, melts were quenched in one of three ways:

1. Placing the bottom of the crucible in water for a short time (this was the most common)
2. Air quenched by sitting the crucible on a refractory and allowing the crucible cool to room temperature
3. Pouring the glass into a steel mold with copper faced dies to form a disc

To assure that the melting conditions were not causing excessive alkali volatilization, the glass and crucible were weighed prior to melting and following melting to assure the final composition was within 1-2 % of the anticipated weight. This procedure could not be carried out for the glasses that were poured.

A TA Instruments[®] DSC 2910 Differential Scanning Calorimeter (DSC) with a ramp rate of 20 K/min was used to determine the glass transition temperature (T_g) for annealing. Further detail on using the DSC to obtain T_g is included in Chapters 4 and 6. Each glass was annealed by holding for half an hour at approximately 10 K below their T_g (unless the onset of crystallization was very close to the T_g , in which case the glass was annealed at 20 K below T_g) and then cooled at 5 K/min to room temperature. Glasses were stored in plastic boxes in a desiccator to minimize the surface reaction with water.

3.3 Cutting, Grinding and Polishing

Samples were made in two shapes. Samples with low enough viscosities to be poured did not require cutting. Samples that were cooled in a crucible were attached to an aluminum block using a thermal setting resin and cut into smaller pieces using a low speed diamond saw.

Samples were dry polished to avoid reaction with water. The highly reactive nature of the samples required that gloves be worn during grinding and polishing. Silicon carbide paper with grits of 240 and/or 320 were used to grind away the hydroxylated layer produced from cutting. To polish the samples, SiC paper of 400, 600, 800 and 1000 grits were used.

CHAPTER 4: GENERAL PROPERTIES

4.1 Introduction

The general properties discussed in this chapter are those that are most well defined in the literature for germanate glasses. The glass transition temperature (T_g) and density will be discussed for the binary alkali germanate glasses and for the $\text{Na}_2\text{O}\cdot\text{K}_2\text{O}\cdot\text{GeO}_2$ and $\text{Li}_2\text{O}\cdot\text{Cs}_2\text{O}\cdot 85 \text{ GeO}_2$ mixed alkali glasses. The data will be compared to those present in the literature where possible.

T_g and density both exhibit germanate anomalies. T_g also shows a mixed alkali effect as negative deviations from additivity. Since the germanate anomaly has a large effect on the properties of alkali germanate glasses, mixed alkali studies were performed at compositions containing 10 mol% alkali (when it is believed there are little to no non-bridging oxygens) and 15 mol % alkali (when non-bridging oxygen begin to form).

4.2 Literature Review

The Sci-Glass[®] database is a comprehensive database for glass property values. This database was used to collect the property values in the literature that are pertinent to the work presented in this and the following chapters. Since there are sometimes twenty or more papers dealing with a particular property for a single series of glasses, the names of the authors are not present on the figures. However, for the readers' interest, Appendix A will contain keys for all of the figures, with the symbol, author, and reference for each set of data presented.

4.2.1 *Glass Transition Temperature*

The glass transition temperature (T_g) is arguably the most essential property of glasses. The T_g must be known to properly anneal a glass. The glass transition temperature is defined as the temperature at which a material has a viscosity of $\approx 10^{11.3}$ Pa s. DSC measurements of T_g also provides characteristic information about the glass such as glass fragility, fictive temperature and the likelihood of crystallization. This section will present the fundamental theory behind the glass transition and an analysis of the literature values for the binary and mixed alkali germanate glasses.

The glass transition temperature is one of the most reported values for alkali germanate glasses. Since there are a larger number of studies,¹⁻¹⁹ Appendix A provides a key to each figure listing the authors and reference corresponding to each data point. It is important to note that the glass transition temperature of GeO₂ is highly dependent on hydroxyl content and trace alkali content.²⁰ Using the Sci-glass[®] data base the T_g of germania was found to range from 470 to 545 °C.²¹

The T_g values for x Li₂O•(100- x) GeO₂ glasses are shown in Figure 4-1. A minimum in the T_g occurs at 98 mol % GeO₂, followed by a maximum in T_g at 80 mol % GeO₂. These extrema are known as the low alkali and the high alkali germanate anomalies, respectively. Despite the large spread in the data, the maximum occurs at 80 mol % GeO₂ in all sets of data.

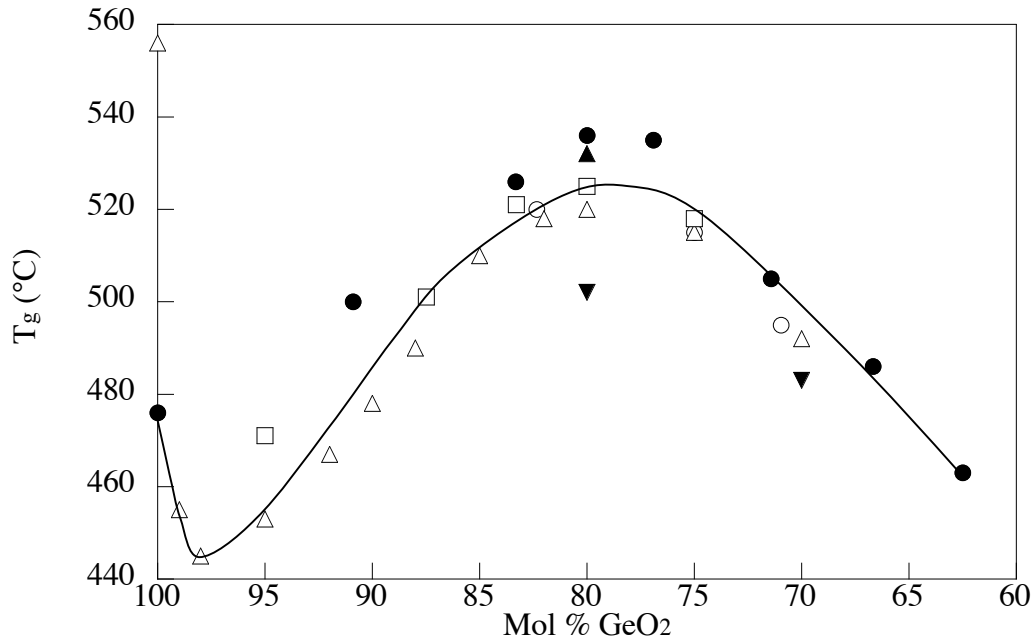


Figure 4-2. Glass transition temperature of Li₂O•GeO₂ glasses from the literature. Line added to aid the eye.

The most studied of the binary alkali germanate systems are the x Na₂O•(100- x) GeO₂ glasses. T_g values for these glasses are shown in Figures 4-2 and 4-3. Figure 4-2 shows the entire set of values available on the Sci-Glass database[®]. Glasses with high concentrations of alkali oxide are difficult to make and are prone to crystallization, which explains some of the scatter in the data for those glasses. Figure 4-3 shows the glass transition data for glasses containing 100 to 60 mol % GeO₂. A minimum in the T_g

occurs at 99 to 98 mol % GeO₂, followed by a maximum in T_g at ~83 mol % GeO₂. Unlike the x Li₂O•(100- x) GeO₂ glasses, the concentration of germania where all the T_g literature values reach a maximum varies among the studies over the range from 85 to 80 mol % GeO₂.

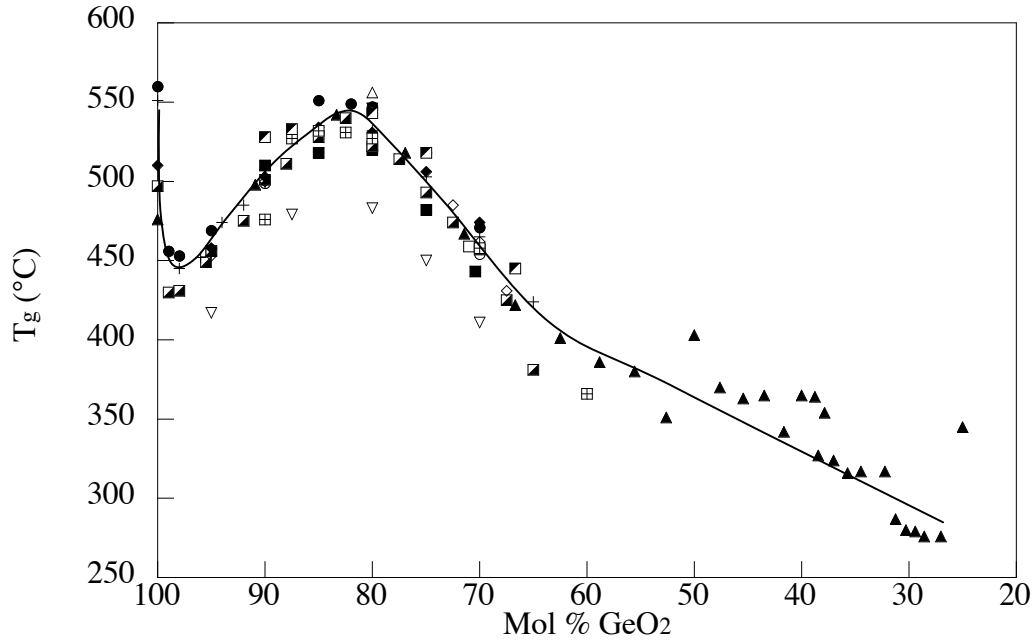


Figure 4-3. Glass transition temperature all of Na₂O•GeO₂ glasses from the literature. Line added to aid the eye.

The T_g values for x K₂O•(100- x) GeO₂ glasses are shown in Figures 4-4 and 4-5. Figure 4-4 shows the entire set of literature values. Figure 4-5 shows the glass transition data for glasses with 100 to 60 mol % GeO₂. The minimum in T_g, the low alkali germanate anomaly, occurs at 98 mol % GeO₂, followed by the high alkali germanate anomaly, the maximum in T_g, at ~84 mol % GeO₂. The position of the maximum ranges from 83 to 80 mol % GeO₂.

The T_g values for x Rb₂O•(100- x) GeO₂ glasses are shown in Figures 4-6 and 4-7. Figure 4-6 shows the entire set of literature values. Figure 4-7 shows the glass transition data for glasses with 100 to 60 mol % GeO₂. A minimum in the T_g occurs between 99 and 98 mol % GeO₂, followed by a maximum in T_g at ~84 mol % GeO₂. The maximum T_g ranges from 85 to 83 mol % GeO₂.

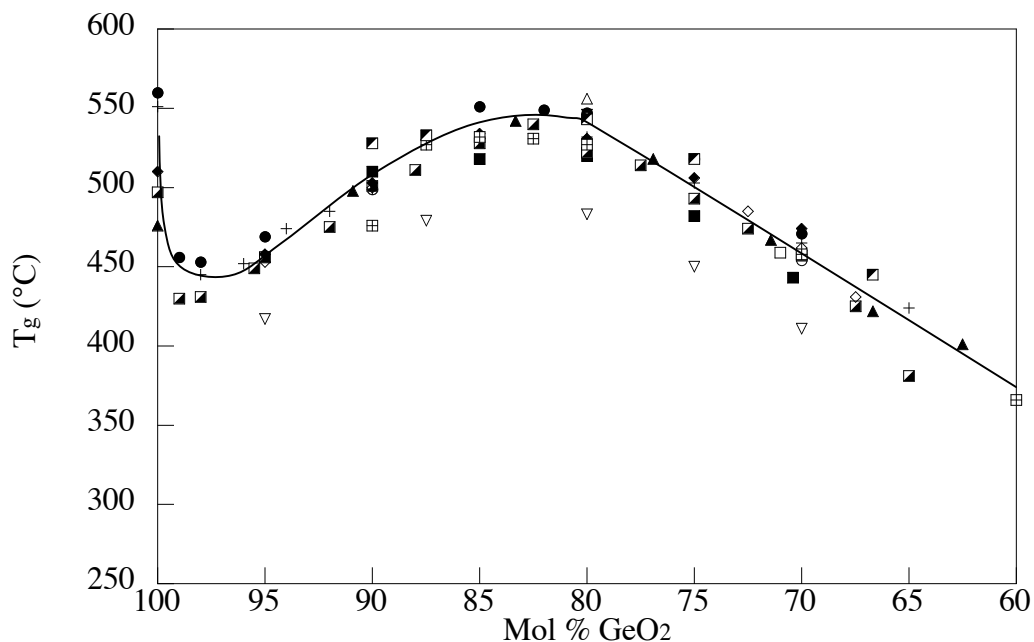


Figure 4-4. Glass transition temperature of $\text{Na}_2\text{O}\cdot\text{GeO}_2$ containing 60 to 100 mol % GeO_2 . Line added to aid the eye.

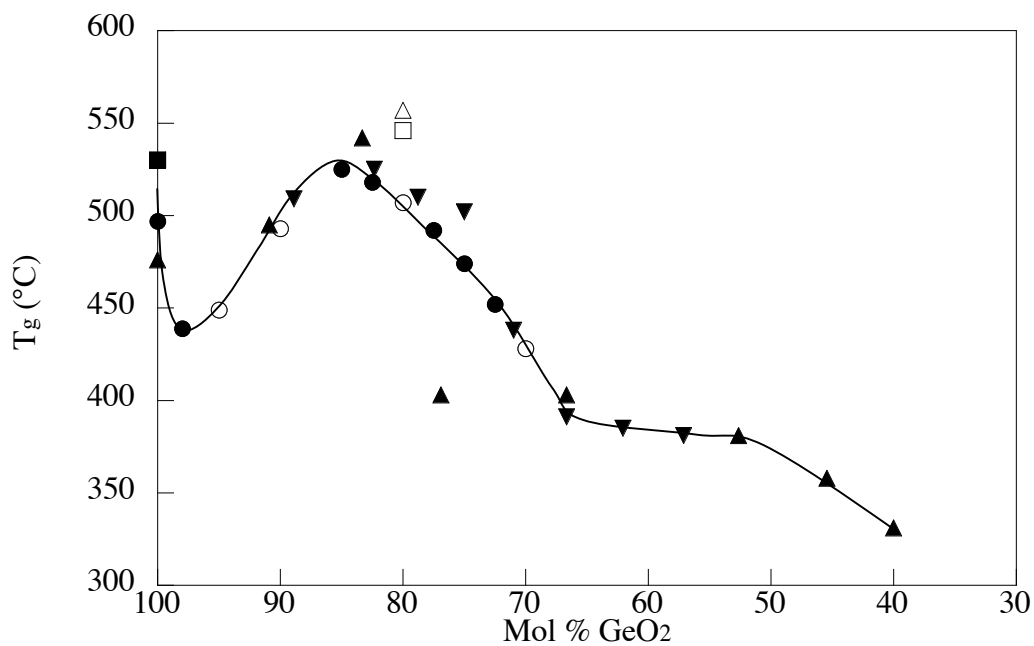


Figure 4-5. Glass transition temperature of $\text{K}_2\text{O}\cdot\text{GeO}_2$ glasses from the literature. Line added to aid the eye.

The $x \text{ Cs}_2\text{O}\cdot(100-x) \text{ GeO}_2$ glasses are the least studied alkali germanate binary system; T_g values for the glasses are shown in Figure 4-8. A minimum in the T_g occurs at 98 mol % GeO_2 , followed by a maximum in T_g at 85 mol % GeO_2 . Table 4-I lists the

mol % GeO₂ where the maxima and minima occur, and their corresponding value of T_g. In general, the low alkali germanate anomaly occurs at 99 to 98 mol % GeO₂ for all binary alkali germanate glasses. As the alkali ion becomes larger, the maximum shifts slightly to higher GeO₂ content.

Table 4-I. Maxima and Minima in T_g for the Binary Alkali Germanate Glasses

Glass	Minima Mol % GeO ₂	T _g (°C)	Maxima Mol % GeO ₂	T _g (°C)
Li ₂ O•GeO ₂	98	445	80	540
Na ₂ O•GeO ₂	98 to 99	425	80 to 85	550
K ₂ O•GeO ₂	98	440	80 to 83	525
Rb ₂ O•GeO ₂	98 to 99	450	83 to 85	525
Cs ₂ O•GeO ₂	98	455	85	550

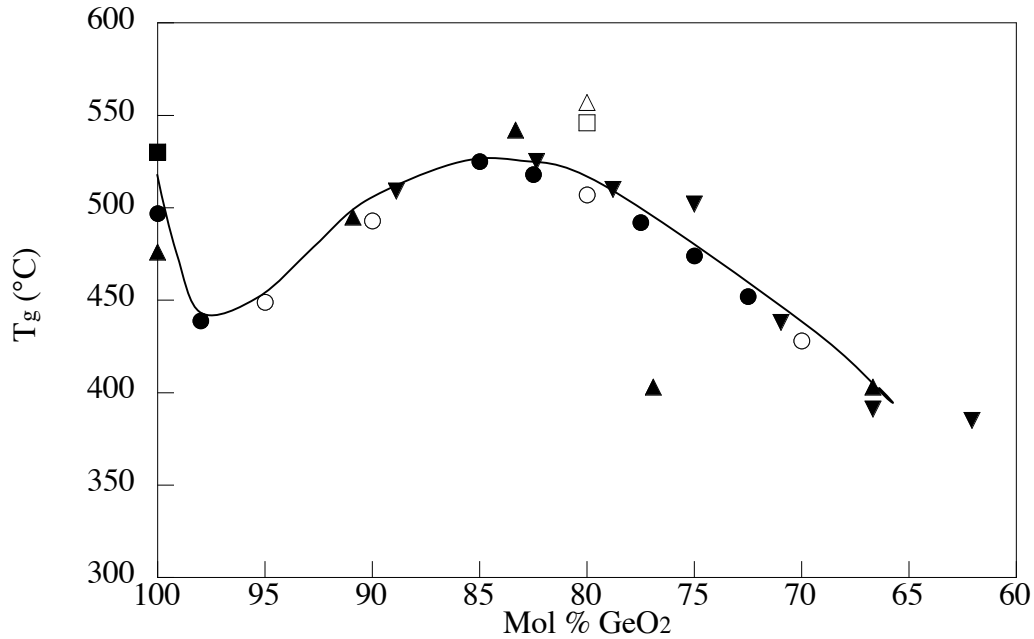


Figure 4-6. Glass transition temperature of K₂O•GeO₂ containing 60 to 100 mol % GeO₂. Line added to aid the eye.

It is worth mentioning that, while the data in Figures 4-2, 4-4 and 4-6 have a large amount of scatter for high concentrations of alkali oxide in the glasses, the break in the curve correlates quite well with the Henderson and Wang's work presented in Chapter 2. Henderson and Wang²² propose that the five-coordinated germanium revert back to four-coordinated and begin forming and additional NBO at approximately 30 mol % alkali

oxide addition. A second T_g study examining these high alkali germanate glasses would be useful in determining if this a true effect or just a result of experimental error.

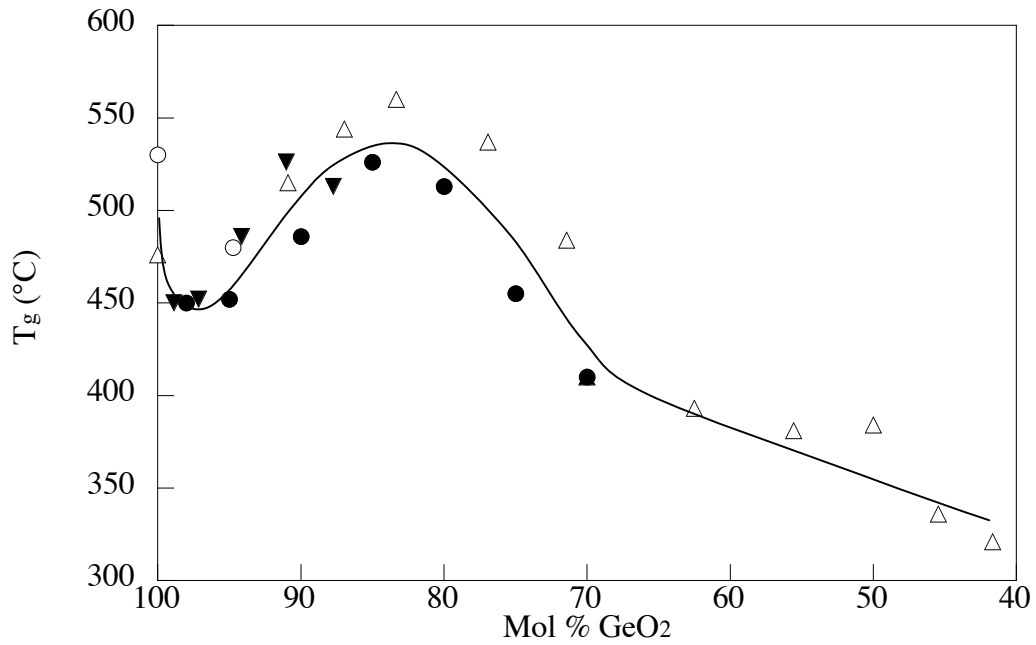


Figure 4-7. Glass transition temperature of $\text{Rb}_2\text{O}\cdot\text{GeO}_2$ glasses from the literature. Line added to aid the eye.

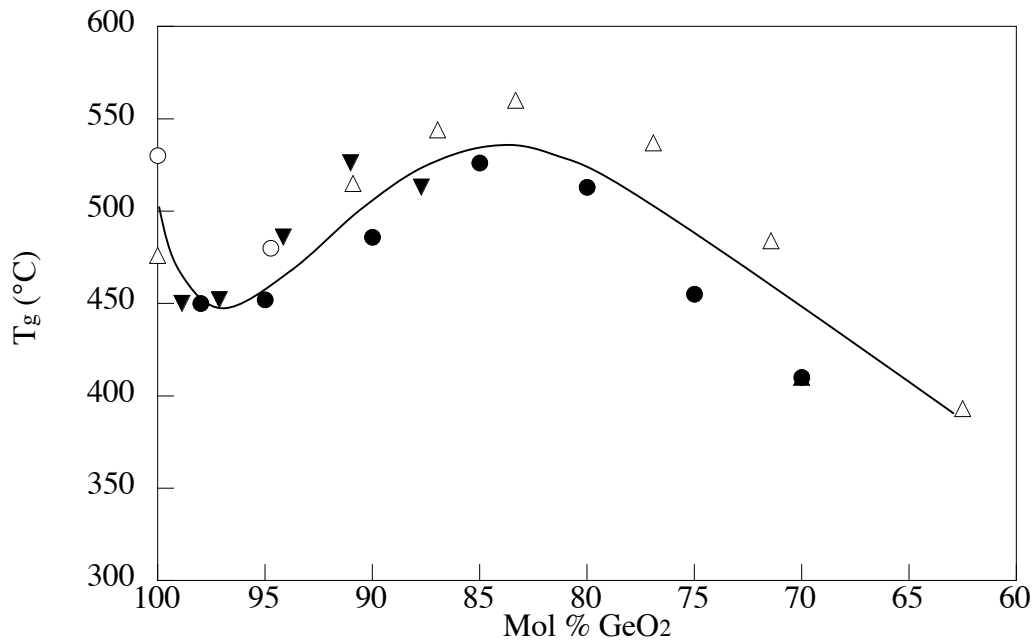


Figure 4-8. Glass transition temperature of $\text{Rb}_2\text{O}\cdot\text{GeO}_2$ containing 60 to 100 mol % GeO_2 . Line added to aid the eye.

Only one mixed alkali germanate ternary system has been studied. The T_g 's are shown in Figure 4-9 for glasses containing 80 mol % GeO_2 . There is good correlation between Marotta and Laudisio¹³ data, while Shelby's¹⁷ values are significantly lower. Shelby's samples were measured using a dilatometer, while Marotta and Laudisio used a DSC. The minimum in T_g occurs when the ratio of alkali oxide is 1:1. Figure 4-10 shows the T_g 's of mixed alkali glasses at four different concentrations of germania. The deviation from additivity increases with increasing alkali oxide concentration. The vertical shift in the T_g 's is a result of the germanate anomaly.

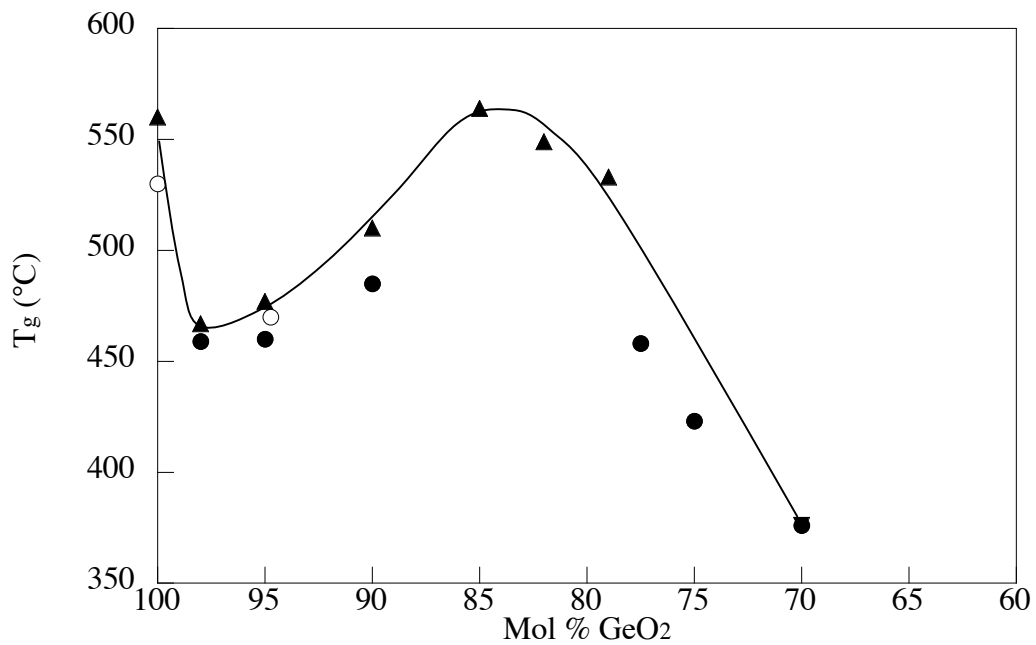


Figure 4-9. Glass transition temperature of $\text{Cs}_2\text{O}\cdot\text{GeO}_2$ glasses from the literature. Line added to aid the eye.

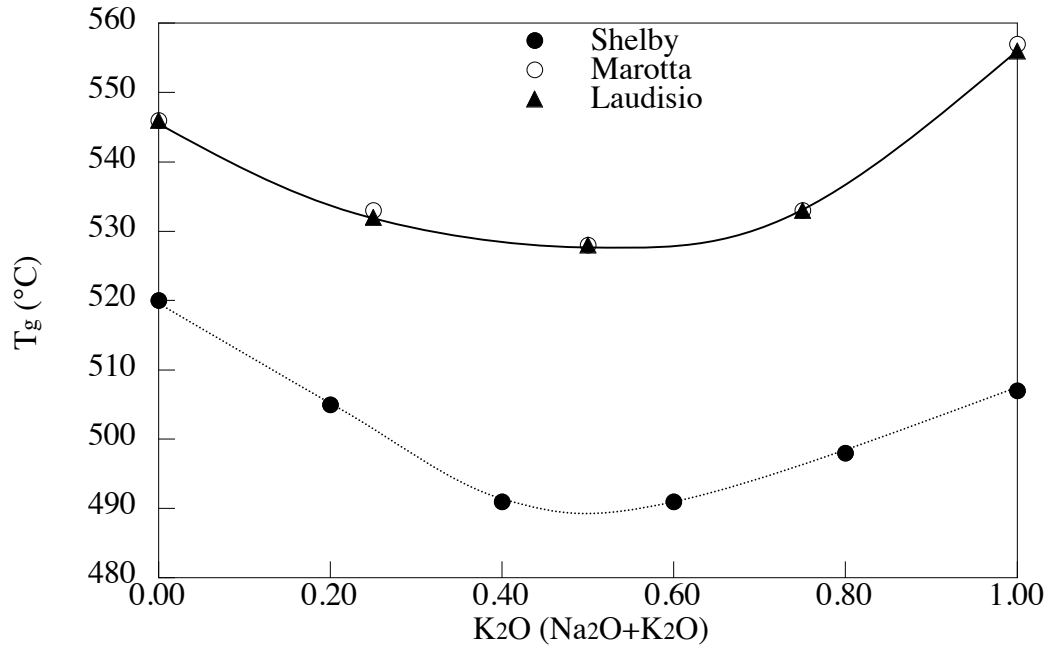


Figure 4-10. Glass transition temperatures of mixed alkali $\text{Na}_2\text{O}\cdot\text{K}_2\text{O}\cdot 80 \text{ GeO}_2$ glasses, from the literature. Lines added to aid the eye.

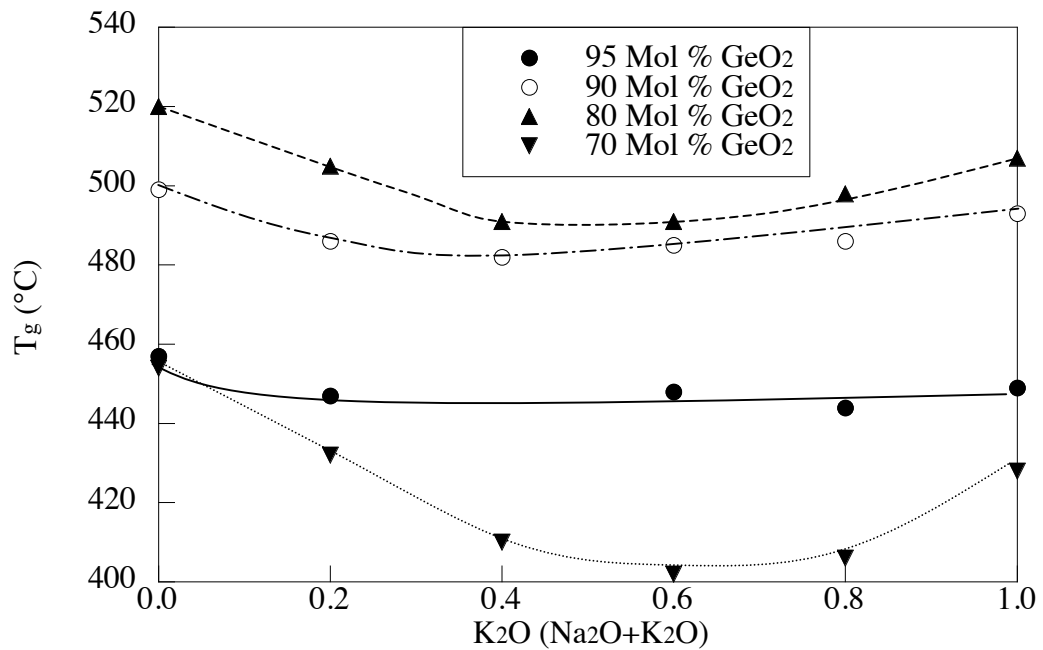


Figure 4-11. Glass transition temperatures of mixed alkali $\text{Na}_2\text{O}\cdot\text{K}_2\text{O}\cdot\text{GeO}_2$ glasses, from the Shelby. Lines added to aid the eye.

4.2.2 Density

Density is the second most reported value for the alkali germanate glasses.^{1,4,5,8,11,15,22-41} The behavior of the density was the basis for defining the germanate anomaly. The alkali germanate glasses show a maximum in density (or minimum in molar volume). In alkali silicate glasses, density increases linearly with increasing alkali concentration; the maximum in density that occurs in alkali germanate glasses is therefore considered anomalous.⁴² A key to the figures is provided in Appendix A.

Binary lithium germanate glasses exhibit a maximum density at approximately 80 mol % GeO₂, as shown in Figure 4-11. When the density values are converted to molar volumes, a minimum occurs at about 75 to 70 mol % GeO₂ (Figure 4-12). The maximum in density (Figure 4-13) for sodium germanate glasses occurs at ~ 84 mol % GeO₂ and the minimum in molar volume (Figure 4-14) occurs at 84 to 81 mol % GeO₂. The maximum in density and minimum in molar volume occur at 89 mol % GeO₂ for potassium germanate glasses, as shown in Figures 4-15 and 4-16, respectively. Density maximizes at 85 to 80 mol % GeO₂ for the rubidium germanate glasses, Figure 4-17. The minimum in molar volume occurs at 85 mol % GeO₂, Figure 4-18. Finally, for the cesium germanate glasses, the maximum occurs at 82 to 80 mol % GeO₂ and the minimum occurs at 95 mol % GeO₂ for density (Figure 4-19) and molar volume (Figure 4-20), respectively.

The values of density and molar volume for all the alkali germanate glasses are listed in Table 4-II. Figures 4-21 and 4-22 show the densities and molar volumes for all five binary alkali germanate glasses, respectively. Early literature discusses^{26,38} two anomalous behaviors for the density of alkali germanate glasses: the existence of maxima in density, and the non-systematic trend of the composition corresponding to the maxima with alkali density (Figure 4-21). If the densities are converted to molar volume, the second anomaly disappears, i.e. the minimum in molar volume shifts to larger R₂O contents with increasing cation mass, Figure 4-22.

Table 4-II. Approximate Maxima in Density and Minima in Molar Volume for Alkali Germanate Glasses

Glass	Mol % GeO ₂	Maxima in Density (g cm ⁻³)	Mol % GeO ₂	Minima in Molar Volume (cm ³ mol ⁻¹)
Li ₂ O•GeO ₂	80	4.13	70 to 75	21.5
Na ₂ O•GeO ₂	84	4.10	81 to 84	24.0
K ₂ O•GeO ₂	89	3.90	89	26.5
Rb ₂ O•GeO ₂	80 to 85	4.15	95	27.5
Cs ₂ O•GeO ₂	80 to 82	4.30	95	28.5

The maximum at approximately 15 to 20 mol % addition of alkali oxide is the only obvious anomaly in the density curves. Data for the rubidium and cesium germanate glasses, however show a break in the density curves at approximately 30 mol %, as shown in Figures 4-17 and 4-19. Glasses at these compositions are difficult to make. Since these data have not been confirmed by a second source, claiming this property is an artifact of a structural anomaly is questionable.

Only one set of data in the literature deals with the density of mixed alkali germanate glasses (Figure 4-23).³¹ As expected, there is little, if any deviation from additivity. There may be a small positive deviation from additivity for the glasses with 30 mol % alkali oxide.

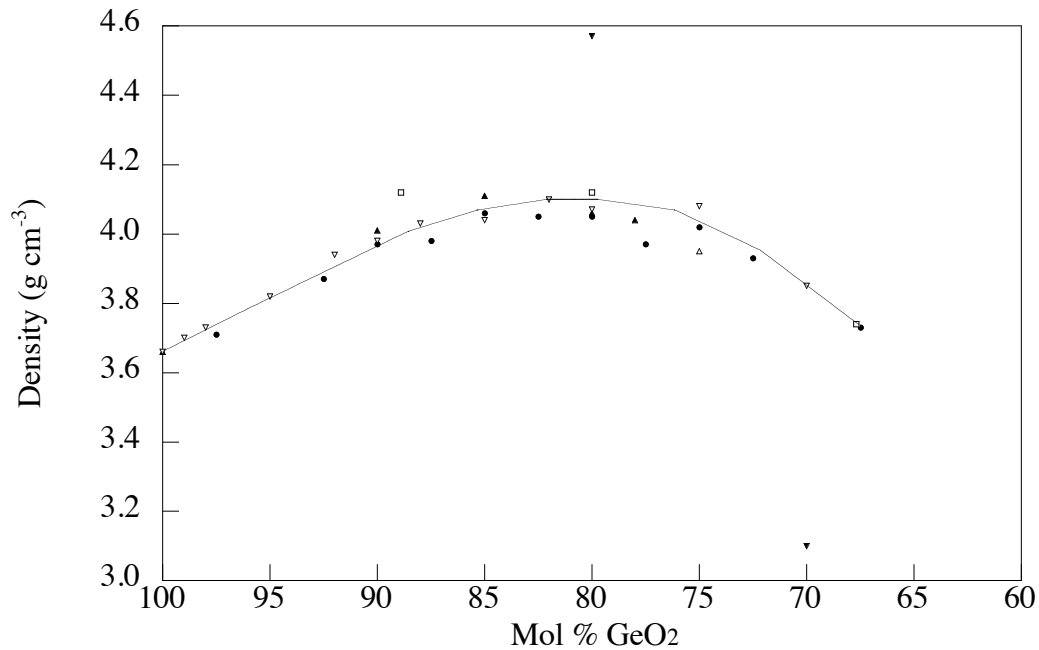


Figure 4-12. Density of Li₂O•GeO₂ glasses from the literature. Line added to aid the eye.

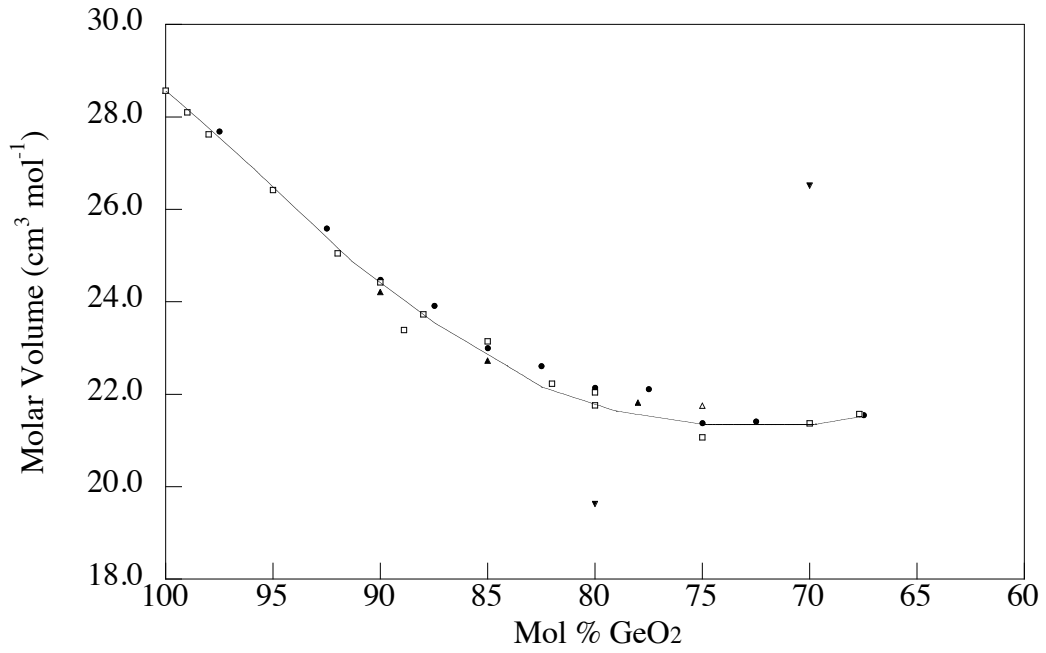


Figure 4-13. Molar volume of literature $\text{Li}_2\text{O}\cdot\text{GeO}_2$ glasses. Line added to aid the eye.

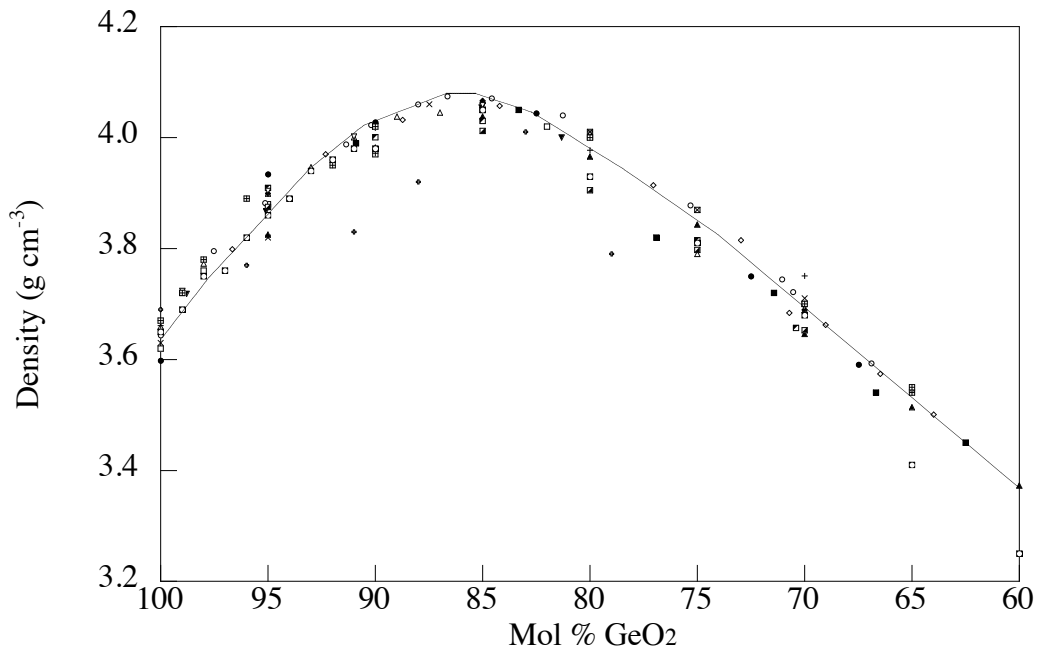


Figure 4-14. Density of $\text{Na}_2\text{O}\cdot\text{GeO}_2$ glasses from the literature. Line added to aid the eye.

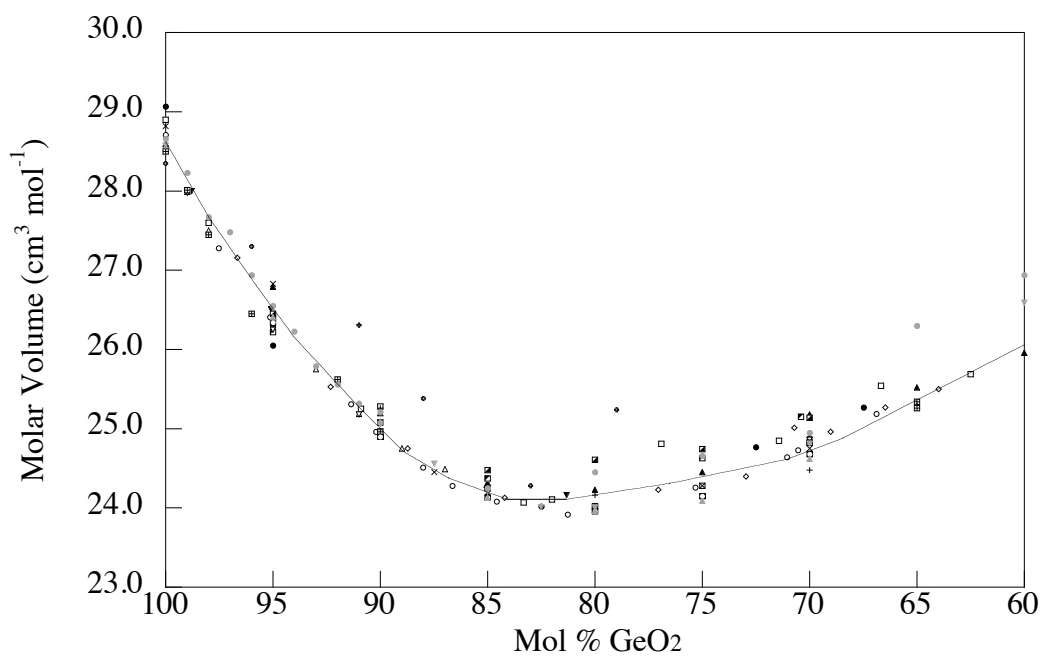


Figure 4-15. Molar volume of literature $\text{Na}_2\text{O}\cdot\text{GeO}_2$ glasses. Line added to aid the eye.

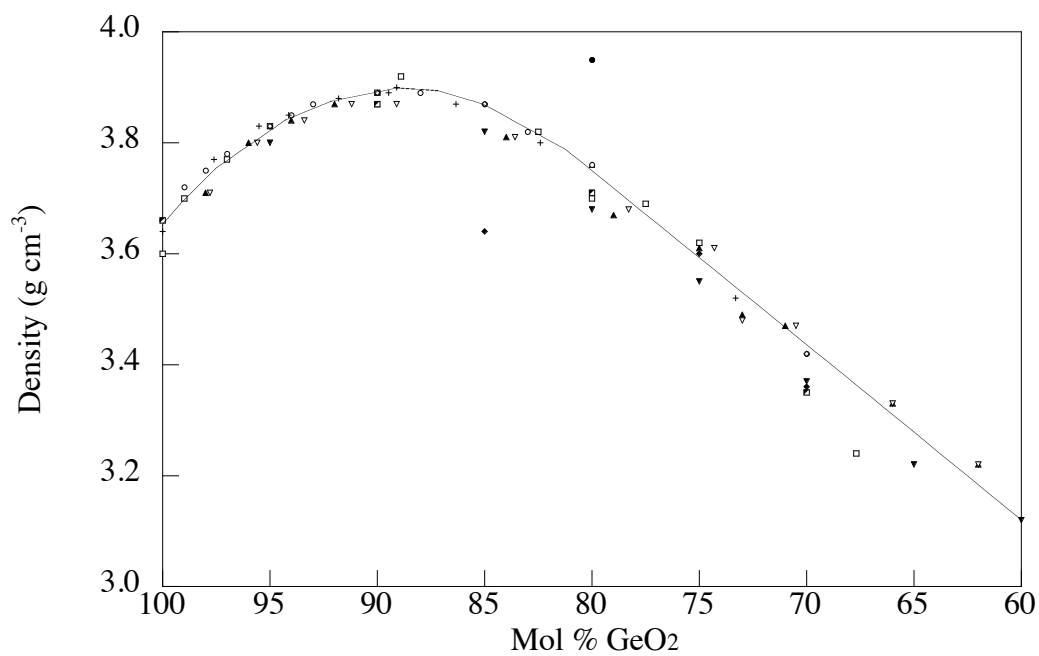


Figure 4-16. Density of $\text{K}_2\text{O}\cdot\text{GeO}_2$ glasses from the literature. Line added to aid the eye.

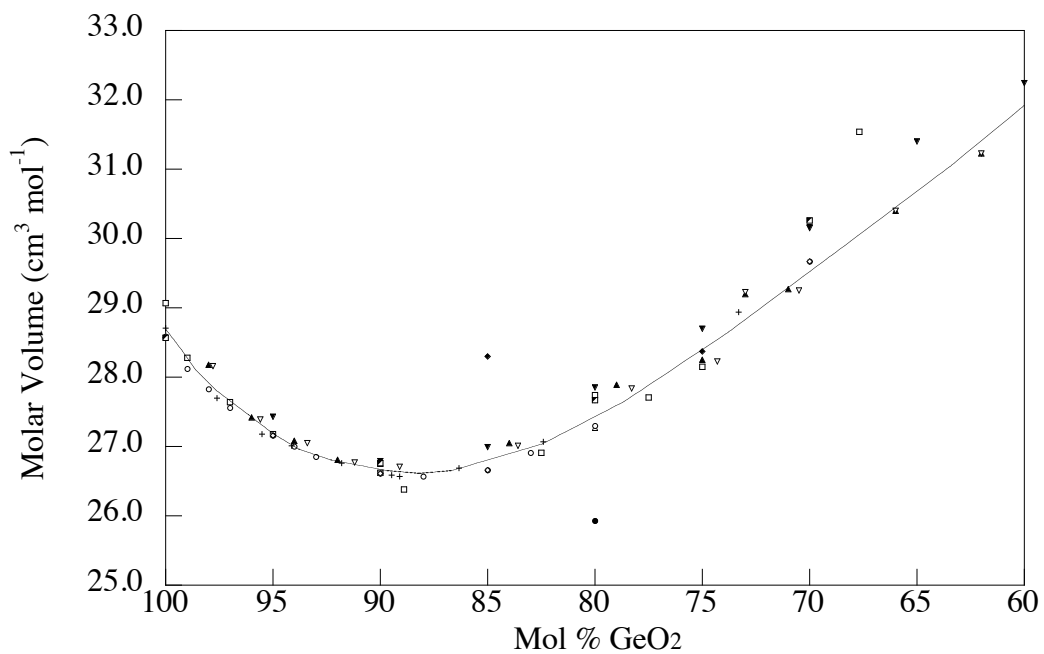


Figure 4-17. Molar volume of literature $K_2O \cdot GeO_2$ glasses. Line added to aid the eye.

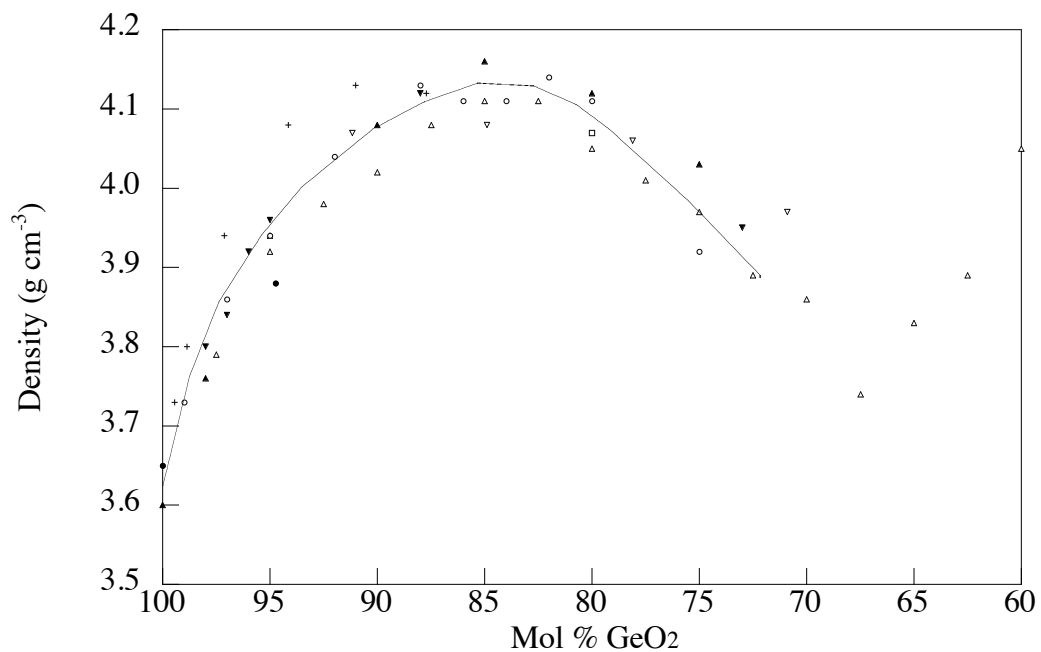


Figure 4-18. Density of $Rb_2O \cdot GeO_2$ glasses from the literature. Line added to aid the eye.

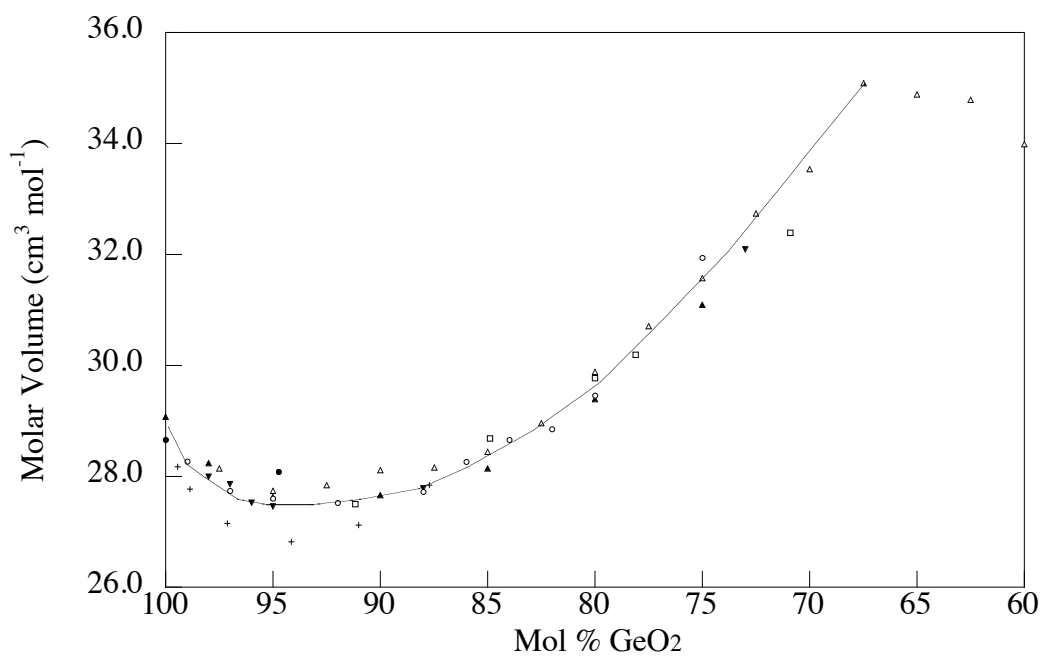


Figure 4-19. Molar volume of literature $\text{Rb}_2\text{O}\cdot\text{GeO}_2$ glasses. Line added to aid the eye.

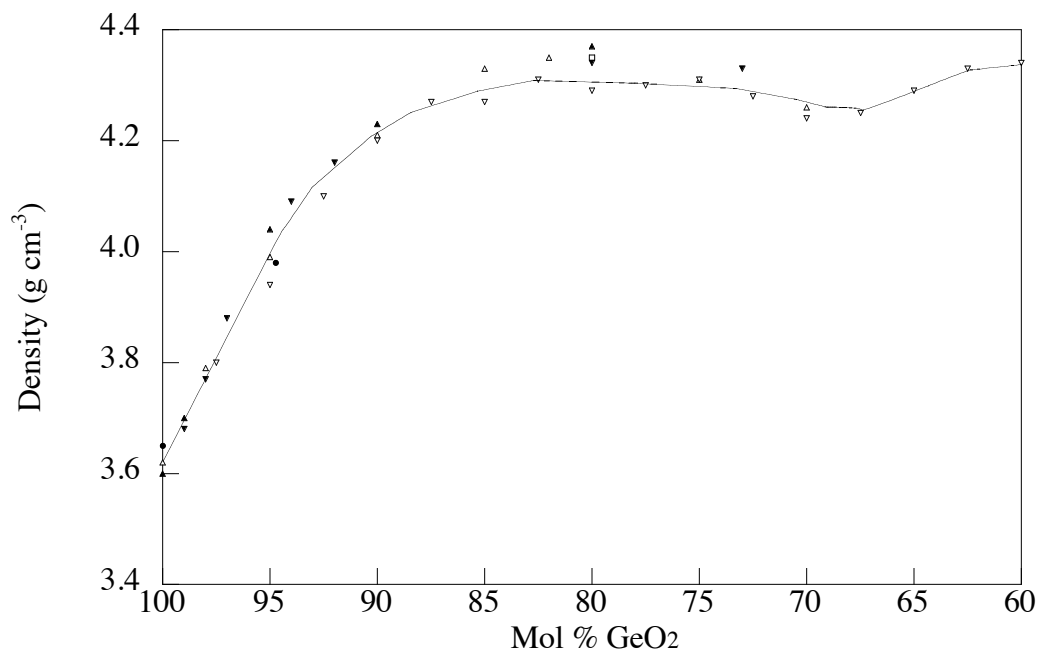


Figure 4-20. Density of $\text{Cs}_2\text{O}\cdot\text{GeO}_2$ glasses from the literature. Line added to aid the eye.

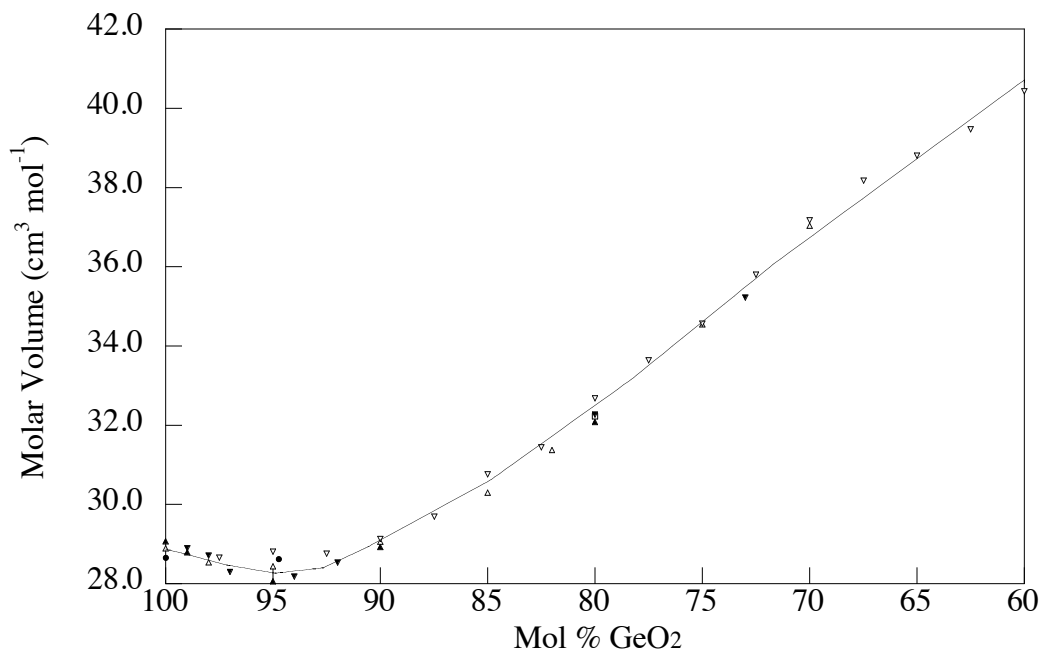


Figure 4-21. Molar volume of literature Cs₂O•GeO₂ glasses. Line added to aid the eye.

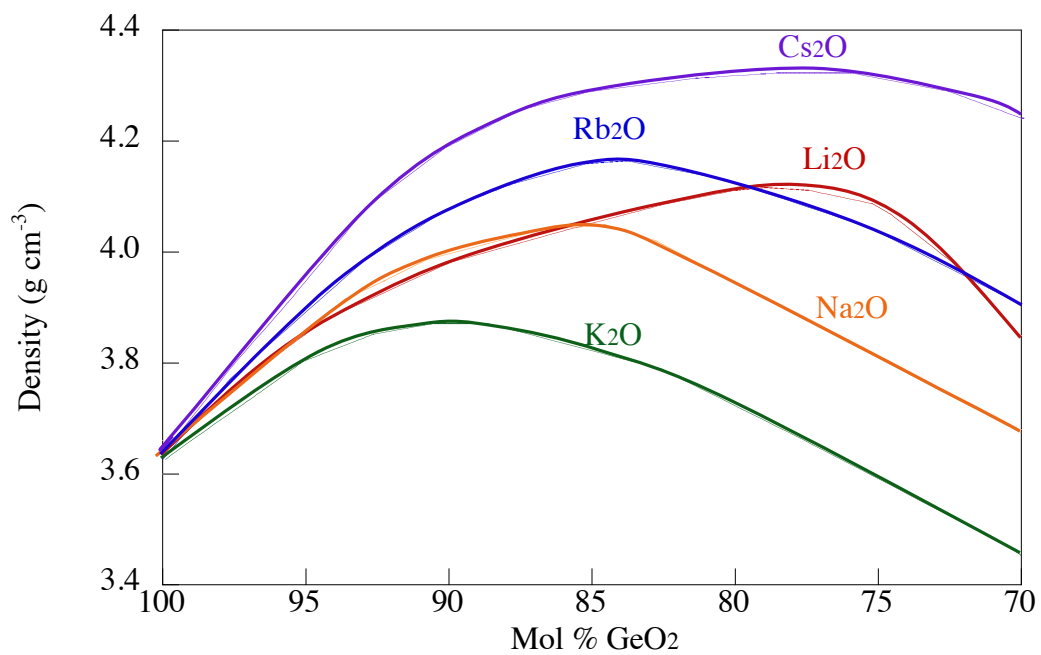


Figure 4-22. Density of R₂O•GeO₂ glasses.

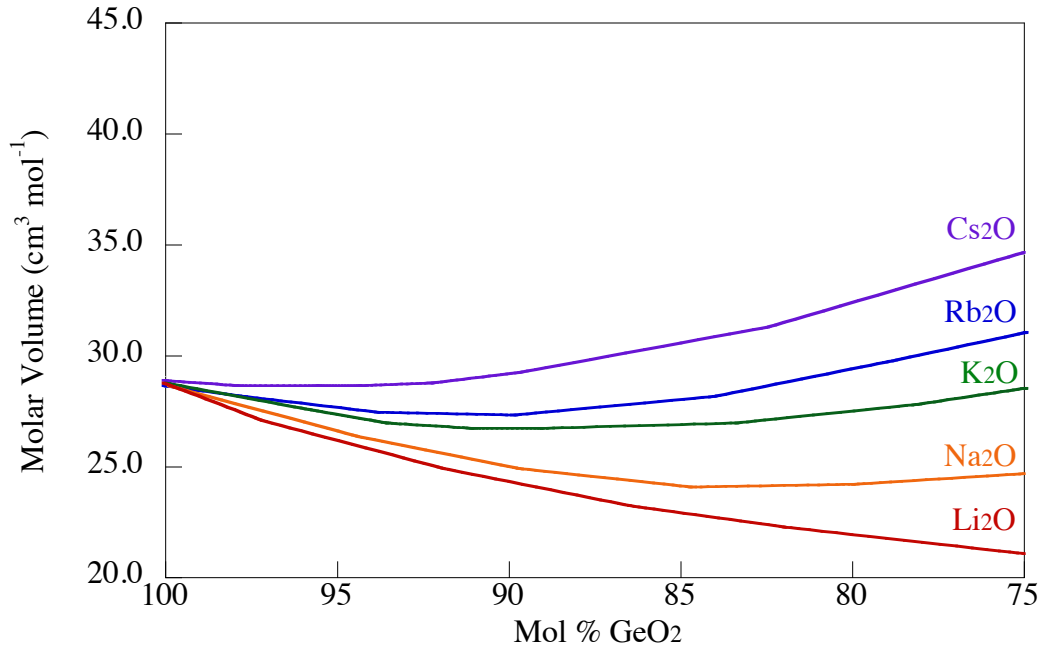


Figure 4-23. Molar volume of R₂O•GeO₂ glasses.

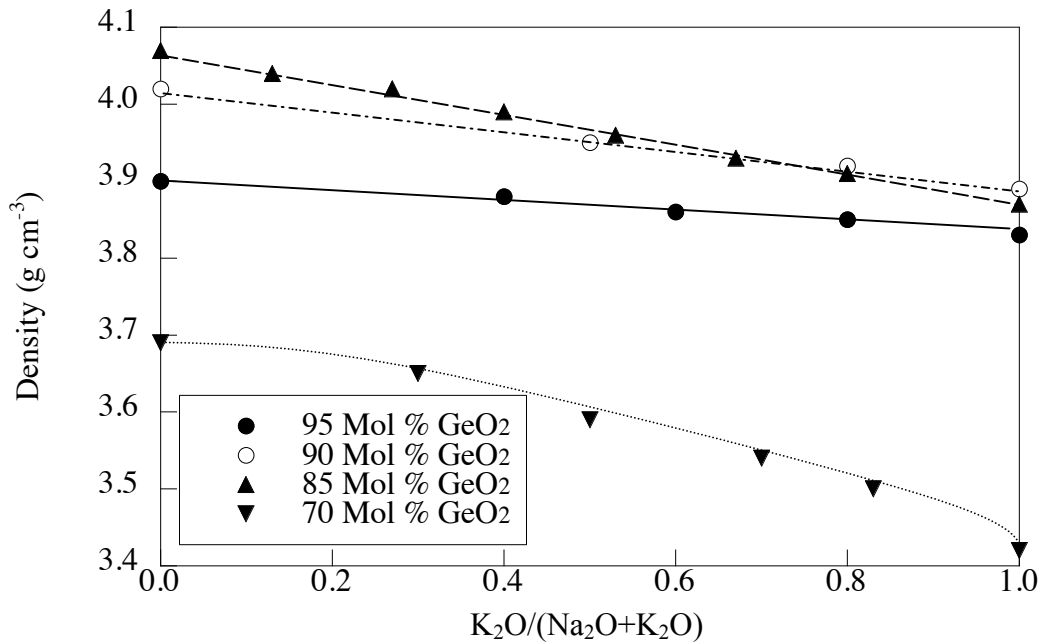


Figure 4-24. Density of mixed alkali Na₂O•K₂O•GeO₂ glasses from the literature. Lines added to aid the eye.

4.3 Experimental Procedure

4.3.1 Glass Transition Temperature

The glass transition temperature (T_g) was measured using differential scanning calorimetry (DSC). A TA Instruments[®] DSC 2910 Differential Scanning Calorimeter was used to perform all DSC measurements. TA Instruments[®] Universal Analysis software was used to analyze the DSC curves. T_g was found using the intercept method shown in Figure 4-24. The mass of the samples was measured for all experiments. Each spectrum was normalized for the mass. Aluminum pans were used for all experiments and the furnace cell was held under a flowing N_2 atmosphere.

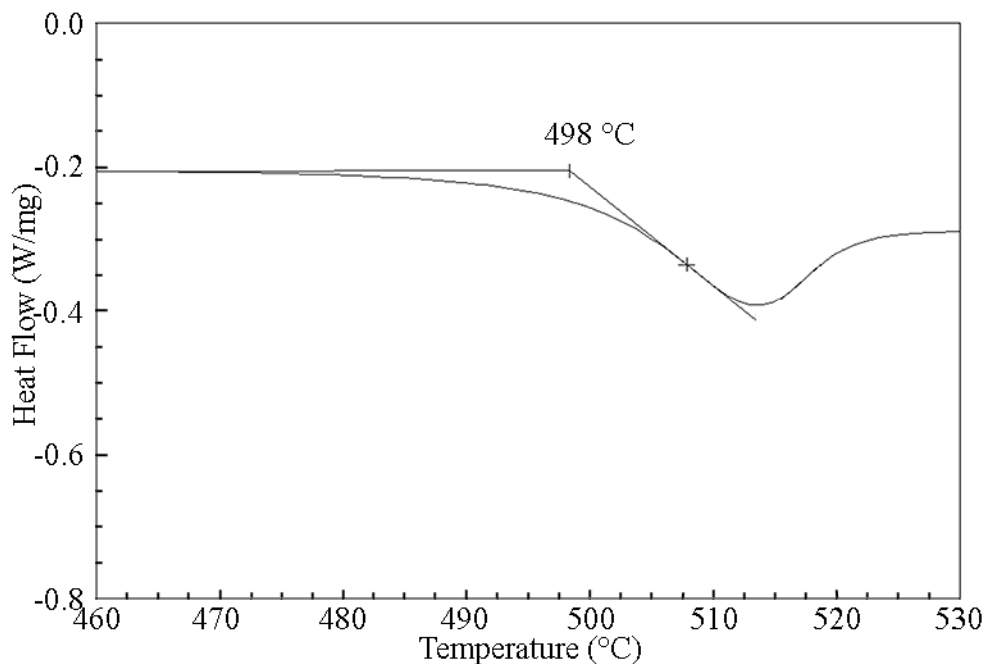


Figure 4-25. Glass transition temperature, found using the intercept method.

4.3.2 Density

Density (ρ) was measured using the Archimedes method, with kerosene as the immersion fluid. When possible, polished plates were used for the density measurement. If not available, samples with the least number of defects, such as cracks and bubbles were used. To insure the highest quality data and to eliminate sources of error, samples were measured five times each, in random order.

4.4 Results

4.4.1 Glass Transition Temperature

The glass transition temperature will first be discussed in the context of the mixed alkali effect. Data for the $\text{Na}_2\text{O}\cdot\text{K}_2\text{O}\cdot\text{GeO}_2$ glasses will be presented first, followed by that for the $\text{Li}_2\text{O}\cdot\text{Cs}_2\text{O}\cdot\text{GeO}_2$ glasses. Germania concentrations were either 85 mol % or 90 mol %. Following the mixed alkali results, results for glasses where the alkali oxide concentrations are held in a ratio of 1:1 and the germania content is varied will be presented. This part of the study examines the effect of cation identity on the germanate anomaly.

Substituting K_2O for Na_2O in alkali germanate glasses results in a negative deviation from additivity in T_g , i.e. the mixed alkali effect. Figures 4-25 and 4-26 show the glass transition temperatures for the mixed alkali sodium and potassium germanate glasses containing 90 mol % and 85 mol % GeO_2 , respectively. The negative deviations from additivity are shown in Figure 4-27. Glasses with more alkali exhibit a greater deviation from additivity. For the glasses containing 90 mol % GeO_2 , the greatest deviation from additivity occurs when the alkali oxides are in a ratio of 7:1 $\text{Na}_2\text{O}:\text{K}_2\text{O}$. When the alkali oxide content is increased to 15 mol %, the maximum in the deviation from additivity occurs when the alkali oxides are in a ratio of 1:7 $\text{Na}_2\text{O}:\text{K}_2\text{O}$.

There is also a negative deviation from additivity, when Li_2O is substituted for Cs_2O in alkali germanate glasses. Figures 4-28 and 4-29 show the T_g 's for the mixed alkali $\text{Li}_2\text{O}/\text{Cs}_2\text{O}$ germanate glasses containing 90 mol % and 85 mol % GeO_2 , respectively. The T_g 's for all of the mixed alkali glasses are listed in Table 4-III.

Table 4-III. Glass Transition Temperatures for $\text{Na}_2\text{O}\cdot\text{K}_2\text{O}\cdot\text{GeO}_2$ and $\text{Li}_2\text{O}\cdot\text{Cs}_2\text{O}\cdot\text{GeO}_2$ Glasses

Glasses 90 GeO_2	T_g ($^{\circ}\text{C}$)	Glasses 90 GeO_2	T_g ($^{\circ}\text{C}$)	Glasses 85 GeO_2	T_g ($^{\circ}\text{C}$)	Glasses 85 GeO_2	T_g ($^{\circ}\text{C}$)
10 Na_2O	515	10 Li_2O	498	15 Na_2O	543	15 Li_2O	510
7:1 $\text{Na}_2\text{O}:\text{K}_2\text{O}$	503	7:1 $\text{Li}_2\text{O}:\text{Cs}_2\text{O}$	500	7:1 $\text{Na}_2\text{O}:\text{K}_2\text{O}$	530	7:1 $\text{Li}_2\text{O}:\text{Cs}_2\text{O}$	513
3:1 $\text{Na}_2\text{O}:\text{K}_2\text{O}$	502	3:1 $\text{Li}_2\text{O}:\text{Cs}_2\text{O}$	492	3:1 $\text{Na}_2\text{O}:\text{K}_2\text{O}$	523	3:1 $\text{Li}_2\text{O}:\text{Cs}_2\text{O}$	505
1:1 $\text{Na}_2\text{O}:\text{K}_2\text{O}$	506	1:1 $\text{Li}_2\text{O}:\text{Cs}_2\text{O}$	491	1:1 $\text{Na}_2\text{O}:\text{K}_2\text{O}$	522	1:1 $\text{Li}_2\text{O}:\text{Cs}_2\text{O}$	497
1:3 $\text{Na}_2\text{O}:\text{K}_2\text{O}$	508	1:3 $\text{Li}_2\text{O}:\text{Cs}_2\text{O}$	495	1:3 $\text{Na}_2\text{O}:\text{K}_2\text{O}$	520	1:3 $\text{Li}_2\text{O}:\text{Cs}_2\text{O}$	512
1:7 $\text{Na}_2\text{O}:\text{K}_2\text{O}$	515	1:7 $\text{Li}_2\text{O}:\text{Cs}_2\text{O}$	507	1:7 $\text{Na}_2\text{O}:\text{K}_2\text{O}$	528	1:7 $\text{Li}_2\text{O}:\text{Cs}_2\text{O}$	517
10 K_2O	523	10 Cs_2O	513	15 K_2O	545	15 Cs_2O	542

The negative deviations from additivity are shown in Figure 4-30. Glasses containing more alkali exhibit a greater deviation from additivity. The greatest deviation from additivity occurs when the ratio of the alkali oxides is around 1:1 $\text{Li}_2\text{O}:\text{Cs}_2\text{O}$.

When the ratios of the alkali oxides are held constant at 1:1 and the germania concentration is decreased, the ternary alkali germanate glasses behave similarly to the binary alkali germanate glasses discussed earlier. Figure 4-31 shows the T_g 's for $x0.5 \text{Na}_2\text{O} \cdot x0.5 \text{K}_2\text{O} \cdot (100-x) \text{GeO}_2$ glasses. A minimum in the T_g occurs with an addition of 2 mol % of alkali oxide. The T_g maximizes when the alkali oxide concentration is 15 mol %. The T_g 's for $x0.5 \text{Li}_2\text{O} \cdot x0.5 \text{Cs}_2\text{O} \cdot (100-x) \text{GeO}_2$ glasses are shown in Figure 4-32. A minimum in T_g occurs for a 1 mol % addition of alkali oxide and a maximum in T_g occurs at 15 mol % alkali. This behavior is characteristic of the 'germanate anomaly' in alkali germanate glasses. Glass transition temperatures of these glasses are listed in Table 4-IV.

Table 4-IV. Glass Transition Temperatures for $0.5x \text{Na}_2\text{O} \cdot 0.5x \text{K}_2\text{O} \cdot (100-x) \text{GeO}_2$, $0.5x \text{Li}_2\text{O} \cdot 0.5x \text{Cs}_2\text{O} \cdot (100-x) \text{GeO}_2$ Glasses

Glasses 1:1 $\text{Na}_2\text{O}:\text{K}_2\text{O}$	T_g ($^{\circ}\text{C}$)	Glasses 1:1 $\text{Li}_2\text{O}:\text{Cs}_2\text{O}$	T_g ($^{\circ}\text{C}$)
99 GeO_2	442	99 GeO_2	442
98 GeO_2	436	98 GeO_2	444
97 GeO_2	437	97 GeO_2	-
95 GeO_2	463	95 GeO_2	468
90 GeO_2	506	90 GeO_2	491
85 GeO_2	522	85 GeO_2	497
83 GeO_2	500	83 GeO_2	496
79 GeO_2	-	79 GeO_2	482
75 GeO_2	-	75 GeO_2	482

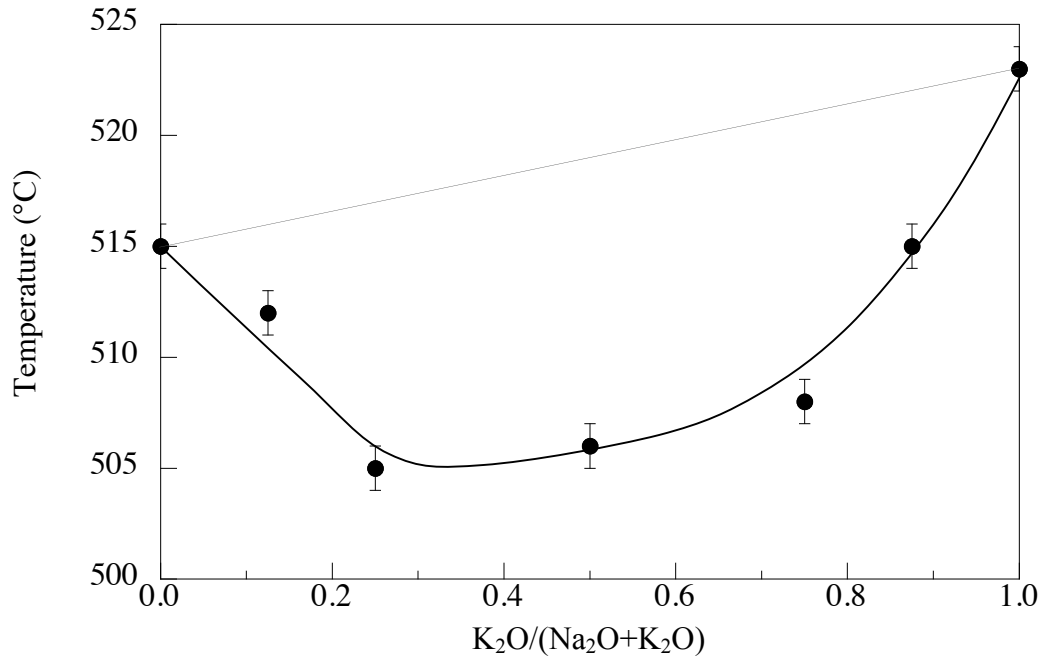


Figure 4-26. Glass transition temperatures for the glasses on the $Na_2O \cdot K_2O \cdot 90 GeO_2$ tie line. The faint line represents the T_g if it changed additively with composition. The bold line is added to aid the eye.

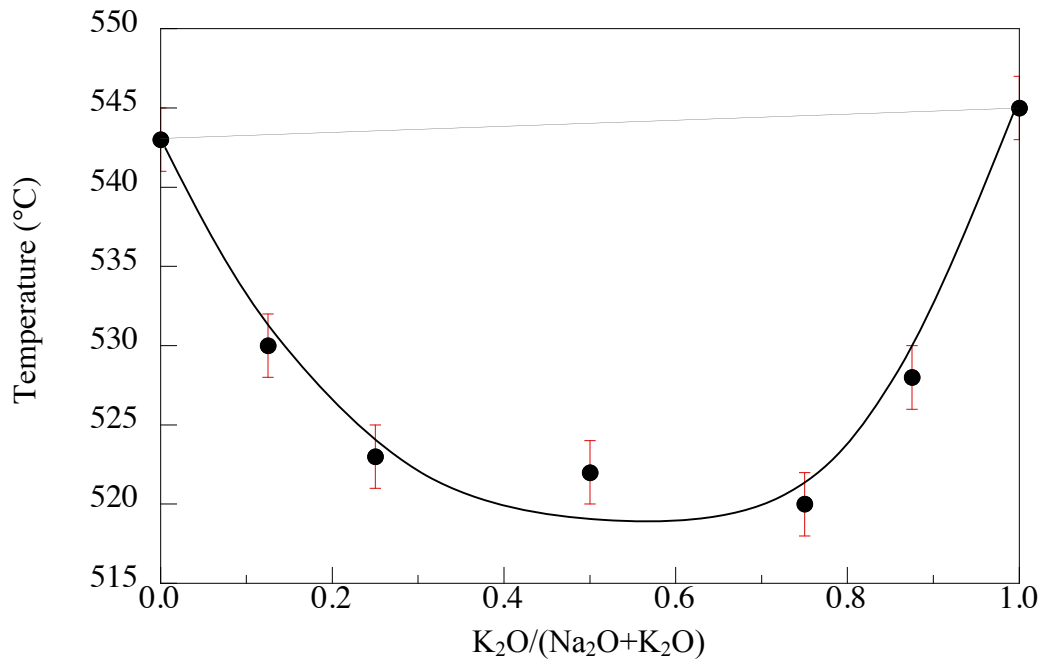


Figure 4-27. Glass transition temperatures for the glasses on the $Na_2O \cdot K_2O \cdot 85 GeO_2$ tie line. The faint line represents the T_g if they changed additively with composition. The bold line is added to aid the eye.

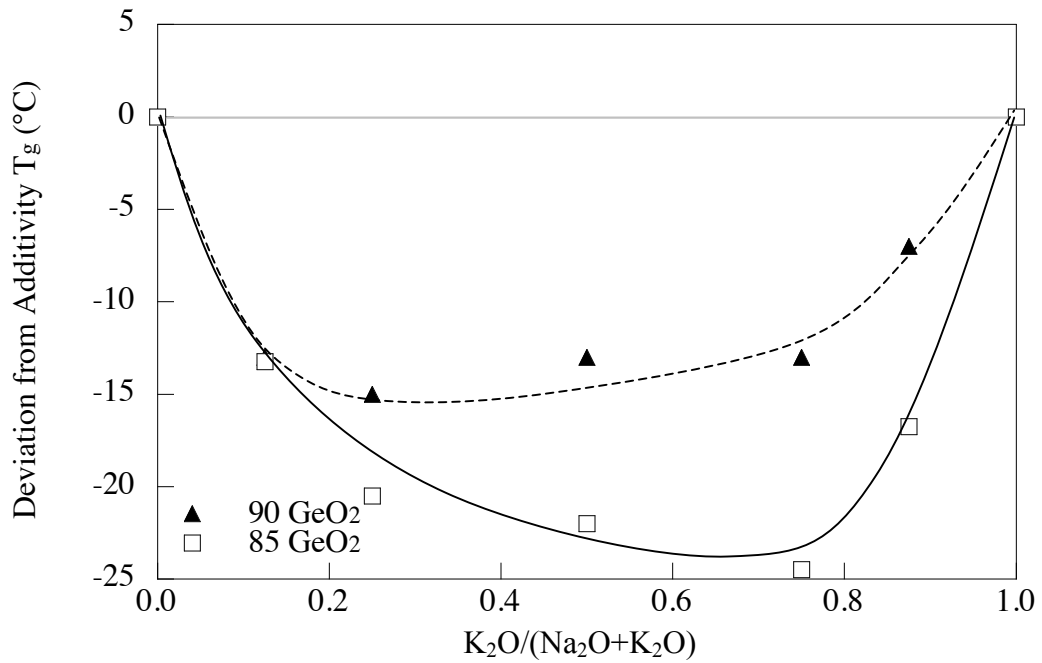


Figure 4-28. Deviation from additivity for the $Na_2O \cdot K_2O \cdot 90 GeO_2$ and $Na_2O \cdot K_2O \cdot 85 GeO_2$ glasses. The faint line represents the T_g if it changed additively with composition. The bold line is added to aid the eye.

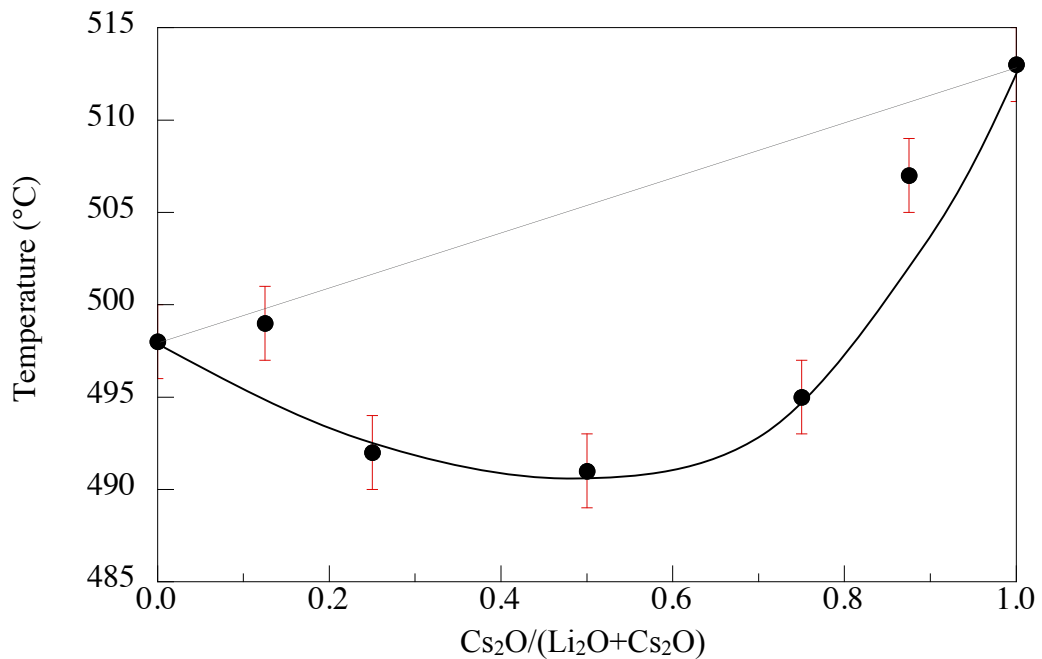


Figure 4-29. Glass transition temperatures for the glasses on the $Li_2O \cdot Cs_2O \cdot 90 GeO_2$ tie line. The faint line represents the T_g if they changed additively with composition. The bold line is added to aid the eye.

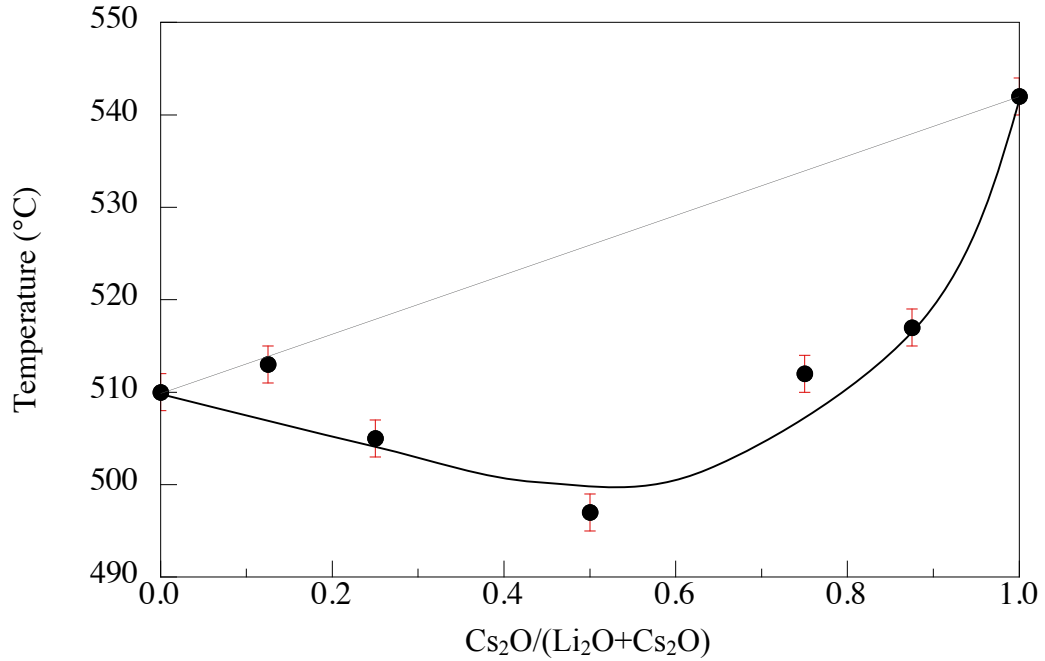


Figure 4-30. Glass transition temperatures for the glasses on the $\text{Li}_2\text{O}\cdot\text{Cs}_2\text{O}\cdot 85 \text{ GeO}_2$ tie line. The faint line represents the T_g if they changed additively with composition. The bold line is added to aid the eye.

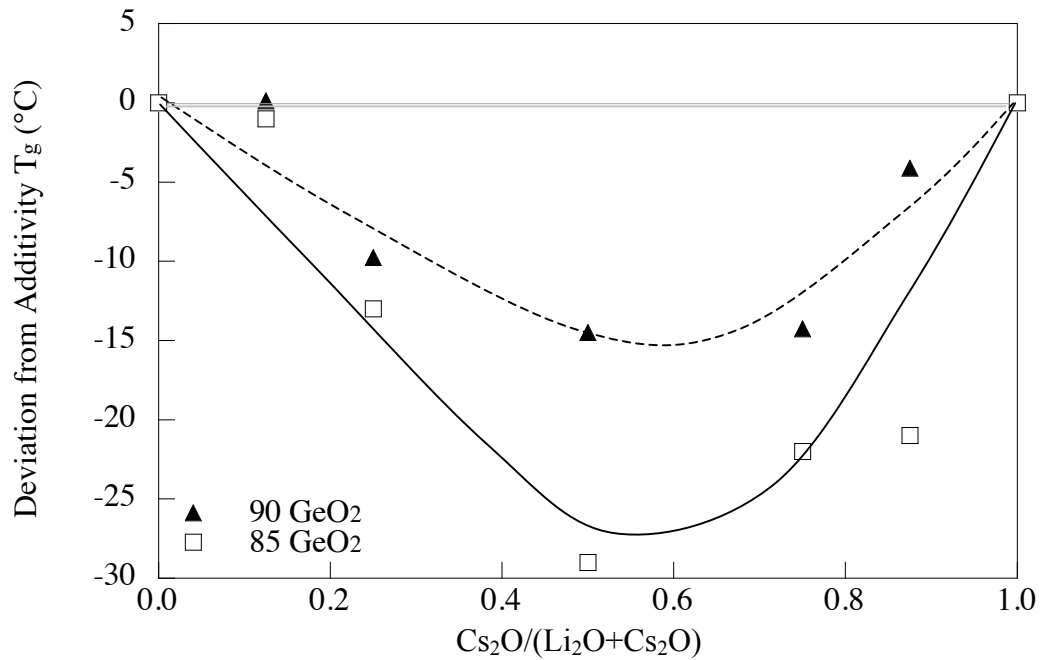


Figure 4-31. Deviation from additivity for the $\text{Li}_2\text{O}\cdot\text{Cs}_2\text{O}\cdot 90 \text{ GeO}_2$ and $\text{Li}_2\text{O}\cdot\text{Cs}_2\text{O}\cdot 85 \text{ GeO}_2$ glasses. The faint line represents the T_g if they changed additively with composition. The bold line is added to aid the eye.

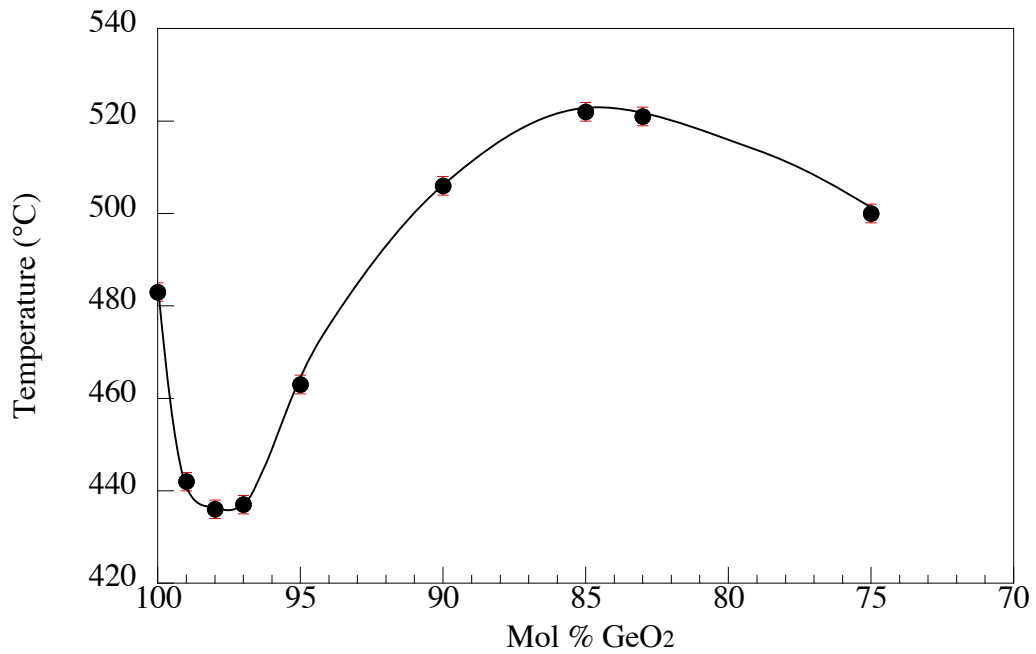


Figure 4-32. Germanate anomaly, shown for T_g data of the $\text{Na}_2\text{O}\cdot\text{K}_2\text{O}\cdot\text{GeO}_2$ system, down the 1:1 $\text{Na}_2\text{O}:\text{K}_2\text{O}$ line. Line added to aid the eye.

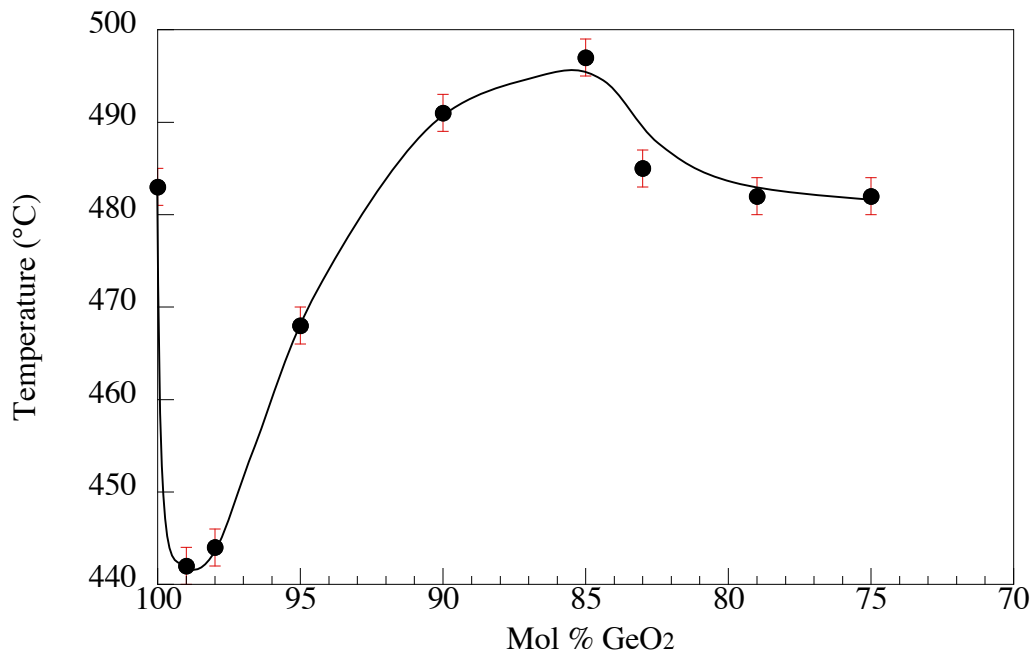


Figure 4-33. Germanate anomaly, shown for T_g data of the $\text{Li}_2\text{O}\cdot\text{Cs}_2\text{O}\cdot\text{GeO}_2$ system, down the 1:1 $\text{Li}_2\text{O}:\text{Cs}_2\text{O}$ line. Line added to aid the eye.

4.4.2 Density

Density does not usually show a significant response to mixing alkali oxides.⁴³ Figure 4-33 shows the densities of $x \text{Na}_2\text{O} \cdot (10-x) \text{K}_2\text{O} \cdot 90 \text{GeO}_2$ glasses. As sodium oxide is replaced by potassium oxide, the density decreases, following the additive line. Similarly, the molar volume increases as sodium oxide is replaced by potassium oxide, as shown in Figure 4-34. Density and molar volume are not affected by decreasing germania concentration from 90 to 85 mol %. Figures 4-35 and 4-36 show the densities and molar volumes, respectively, for $x \text{Na}_2\text{O} \cdot (15-x) \text{K}_2\text{O} \cdot 85 \text{GeO}_2$ glasses. Figure 4-37 shows the molar volume for glasses at both germania concentrations.

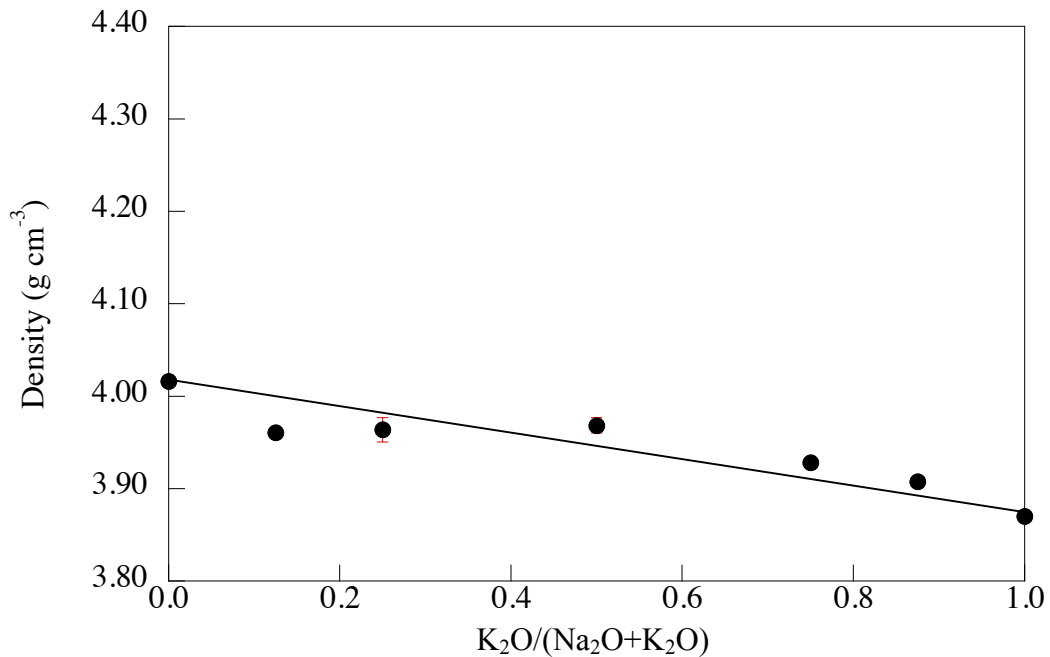


Figure 4-34. Densities of $x \text{Na}_2\text{O} \cdot (10-x) \text{K}_2\text{O} \cdot 90 \text{GeO}_2$ glasses. Line added to aid the eye.

The cation identity has a large effect on the density of mixed alkali germanate glasses. Figure 4-38 shows the density of $x \text{Li}_2\text{O} \cdot (10-x) \text{Cs}_2\text{O} \cdot 90 \text{GeO}_2$ glasses. As with the $x \text{Na}_2\text{O} \cdot (10-x) \text{K}_2\text{O} \cdot 90 \text{GeO}_2$ glasses, the molar volume increases as lithium oxide is replaced by cesium oxide, as shown in Figure 4-39. Figures 4-40 and 4-41 show the densities and molar volumes, respectively, for $x \text{Li}_2\text{O} \cdot (15-x) \text{Cs}_2\text{O} \cdot 85 \text{GeO}_2$ glasses. Figure 4-42 shows the molar volumes for glasses at each of the germania concentrations. Table 4-V lists the densities and molar volumes for all of the $x \text{Li}_2\text{O} \cdot (10-x) \text{Cs}_2\text{O} \cdot 90$

GeO₂ and x Na₂O•(10- x) K₂O•90 GeO₂ glasses and Table 4-VI lists the molar volumes for all of the x Li₂O•(15- x) Cs₂O•85 GeO₂ and x Na₂O•(15- x) K₂O•85 GeO₂ glasses.

Table 4-V. The Densities and Molar Volumes for x Li₂O•(10- x) Cs₂O•90 GeO₂ and x Na₂O•(10- x) K₂O•90 GeO₂ Glasses

Glasses	Density (g cm ⁻³)	Molar Volume (mol cm ⁻³)	Glasses	Density (g cm ⁻³)	Molar Volume (mol cm ⁻³)
10 Na ₂ O	4.02	24.93	10 Li ₂ O	-	-
7:1 Na ₂ O:K ₂ O	3.96	25.44	7:1 Li ₂ O:Cs ₂ O	3.97	25.27
3:1 Na ₂ O:K ₂ O	4.01	25.20	3:1 Li ₂ O:Cs ₂ O	4.05	25.51
1:1 Na ₂ O:K ₂ O	3.97	25.69	1:1 Li ₂ O:Cs ₂ O	4.10	26.77
1:3 Na ₂ O:K ₂ O	3.92	26.24	1:3 Li ₂ O:Cs ₂ O	4.15	27.94
1:7 Na ₂ O:K ₂ O	3.90	26.47	1:7 Li ₂ O:Cs ₂ O	4.21	28.32
10 K ₂ O	3.87	26.79	10 Cs ₂ O	4.19	29.21

Table 4-VI. The Densities and Molar Volumes for x Li₂O•(15- x) Cs₂O•85 GeO₂ and x Na₂O•(15- x) K₂O•85 GeO₂ Glasses

Glasses	Density (g cm ⁻³)	Molar Volume (mol cm ⁻³)	Glasses	Density (g cm ⁻³)	Molar Volume (mol cm ⁻³)
15 Na ₂ O	4.06	24.18	15 Li ₂ O	4.08	22.91
7:1 Na ₂ O:K ₂ O	4.02	24.56	7:1 Li ₂ O:Cs ₂ O	4.12	23.83
3:1 Na ₂ O:K ₂ O	4.01	24.82	3:1 Li ₂ O:Cs ₂ O	4.10	25.09
1:1 Na ₂ O:K ₂ O	4.00	25.16	1:1 Li ₂ O:Cs ₂ O	4.17	26.91
1:3 Na ₂ O:K ₂ O	3.89	26.16	1:3 Li ₂ O:Cs ₂ O	4.24	28.72
1:7 Na ₂ O:K ₂ O	3.86	26.53	1:7 Li ₂ O:Cs ₂ O	4.27	29.61
15 K ₂ O	3.83	26.89	15 Cs ₂ O	4.32	30.36

The mixed alkali effect has a strong effect on the densities and molar volumes of binary alkali germanate glasses. There is only one anomaly present in the density of binary alkali germanate glasses, unlike T_g where there are both low alkali and high alkali anomalies. The densities of the mixed alkali germanate glasses also exhibit a maximum, while the molar volumes exhibit a minimum. Table 4-VII lists the densities and the molar volumes for the mixed alkali germanate glasses, with varying germania concentration. The densities and molar volumes of the $0.5x$ Na₂O• $0.5x$ K₂O•(100- x) GeO₂ glasses are shown in Figures 4-43 and 4-44, respectively. The density passes through a maximum of 3.97 g cm⁻³ between 90 and 85 mol % GeO₂. Molar volume passes through a minimum of 25.35 mol cm⁻³ at 85 mol % GeO₂. The densities and molar volumes of the $0.5x$ Li₂O• $0.5x$ Cs₂O•(100- x) GeO₂ glasses are shown in Figures 4-

45 and 4-46, respectively. The density is a maximum of 4.18 g cm^{-3} at 83 mol % GeO_2 . Molar volume is a maximum of $26.83 \text{ mol cm}^{-3}$ at 90 mol % GeO_2 .

Table 4-VII. Densities and Molar Volumes of $0.5x \text{ Na}_2\text{O} \cdot 0.5x \text{ K}_2\text{O} \cdot (100-x) \text{ GeO}_2$, $0.5x \text{ Li}_2\text{O} \cdot 0.5x \text{ Cs}_2\text{O} \cdot (100-x) \text{ GeO}_2$ Glasses

Glasses 1:1 $\text{Na}_2\text{O}:\text{K}_2\text{O}$	Density (g cm^{-3})	Molar Volume (mol cm^{-3})	Glasses 1:1 $\text{Li}_2\text{O}:\text{Cs}_2\text{O}$	Density (g cm^{-3})	Molar Volume (mol cm^{-3})
99 GeO_2	3.71	28.11	99 GeO_2	3.73	28.15
98 GeO_2	3.75	27.73	98 GeO_2	3.76	28.09
97 GeO_2	-	-	95 GeO_2	3.94	27.22
95 GeO_2	3.83	26.98	90 GeO_2	4.09	26.83
90 GeO_2	3.97	25.69	85 GeO_2	4.17	26.91
85 GeO_2	3.97	25.35	83 GeO_2	4.18	27.13
83 GeO_2	3.93	25.44	79 GeO_2	4.15	27.77
			75 GeO_2	4.10	28.63

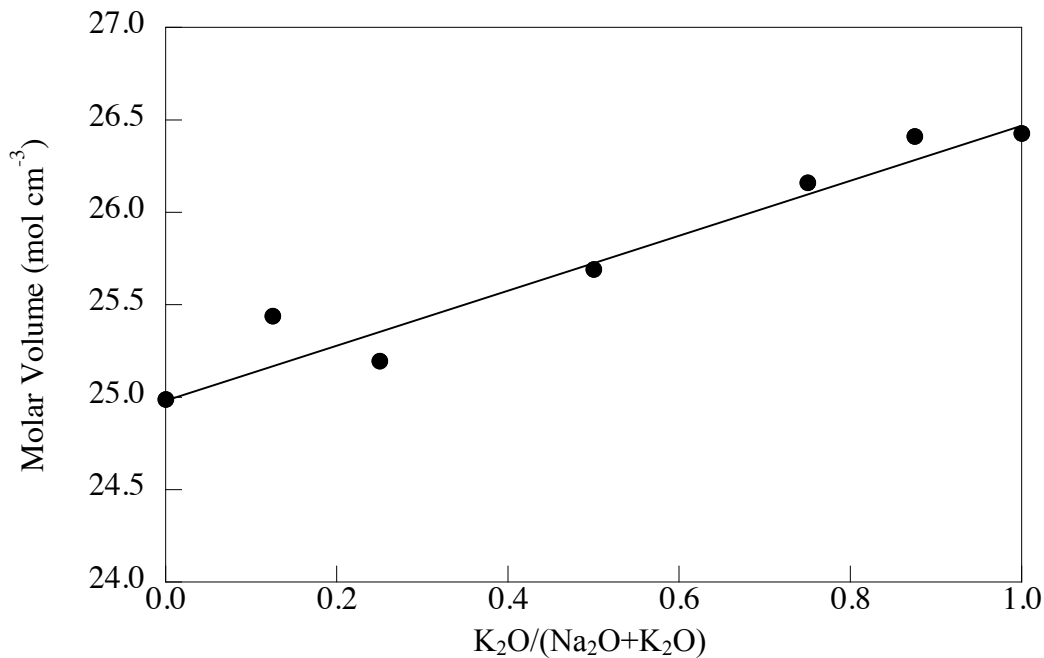


Figure 4-35. Molar volumes of $x \text{ Na}_2\text{O} \cdot (10-x) \text{ K}_2\text{O} \cdot 90 \text{ GeO}_2$ glasses. Line added to aid the eye.

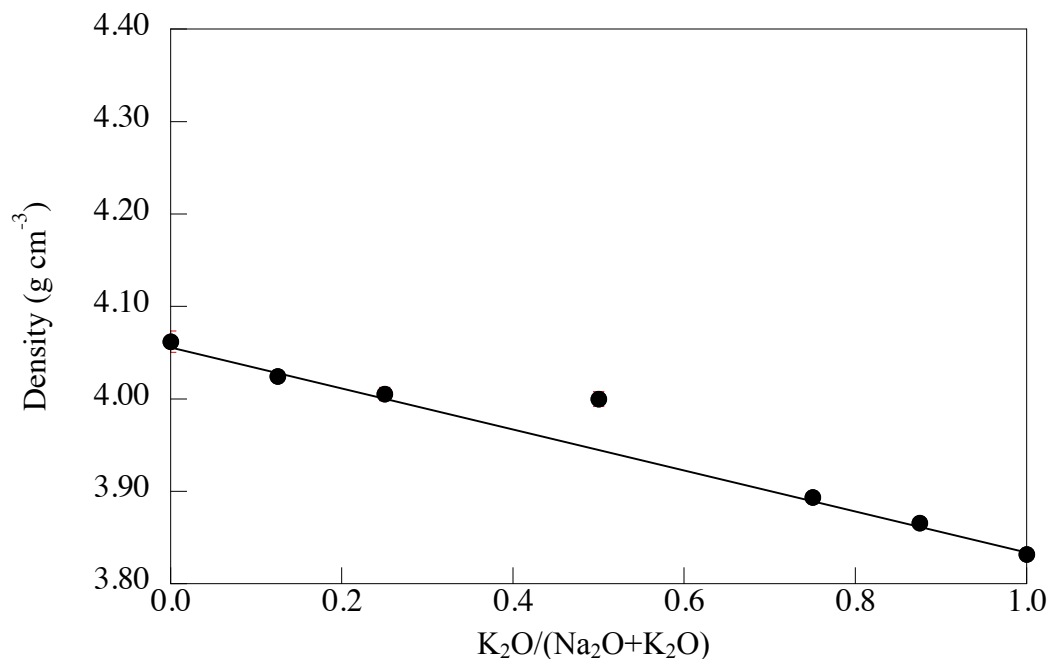


Figure 4-36. Densities of $x\ Na_2O \cdot (15-x)\ K_2O \cdot 85\ GeO_2$ glasses. Line added to aid the eye.

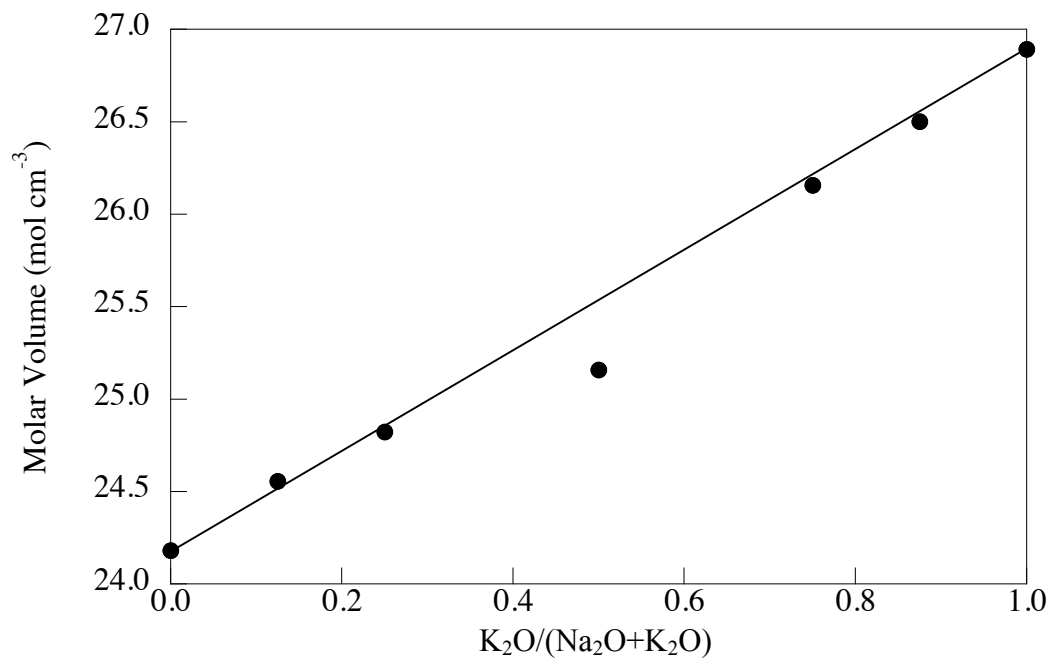


Figure 4-37. Molar volumes of $x\ Na_2O \cdot (15-x)\ K_2O \cdot 85\ GeO_2$ glasses. Line added to aid the eye.

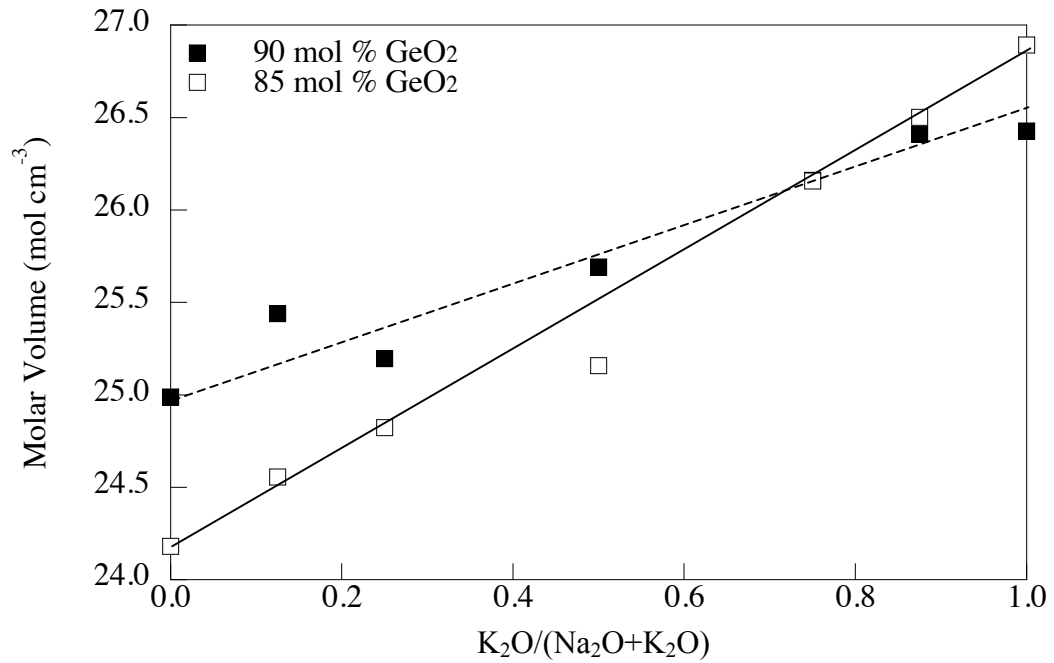


Figure 4-38. Comparison between the molar volumes of the $x \text{ Na}_2\text{O} \cdot (100-x-y) \text{ K}_2\text{O} \cdot y \text{ GeO}_2$, $y = 90$ and 85 mol %. Lines added to aid the eye.

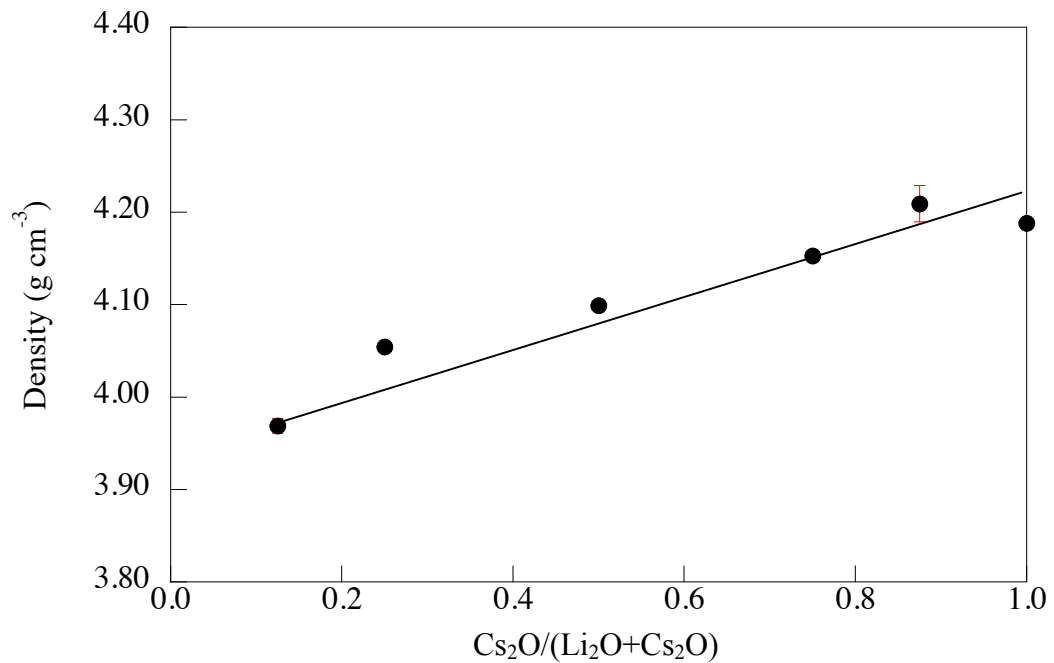


Figure 4-39. Densities of $x \text{ Li}_2\text{O} \cdot (10-x) \text{ Cs}_2\text{O} \cdot 90 \text{ GeO}_2$ glasses. Line added to aid the eye.

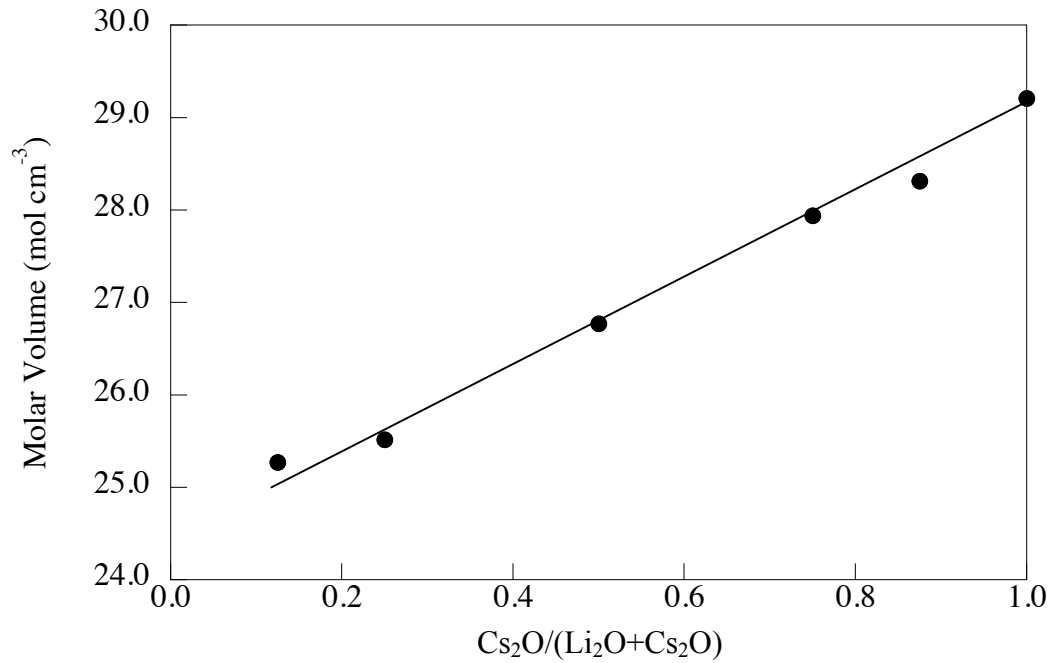


Figure 4-40. Molar volumes of $x \text{Li}_2\text{O} \cdot (10-x) \text{Cs}_2\text{O} \cdot 90 \text{GeO}_2$ glasses. Line added to aid the eye.

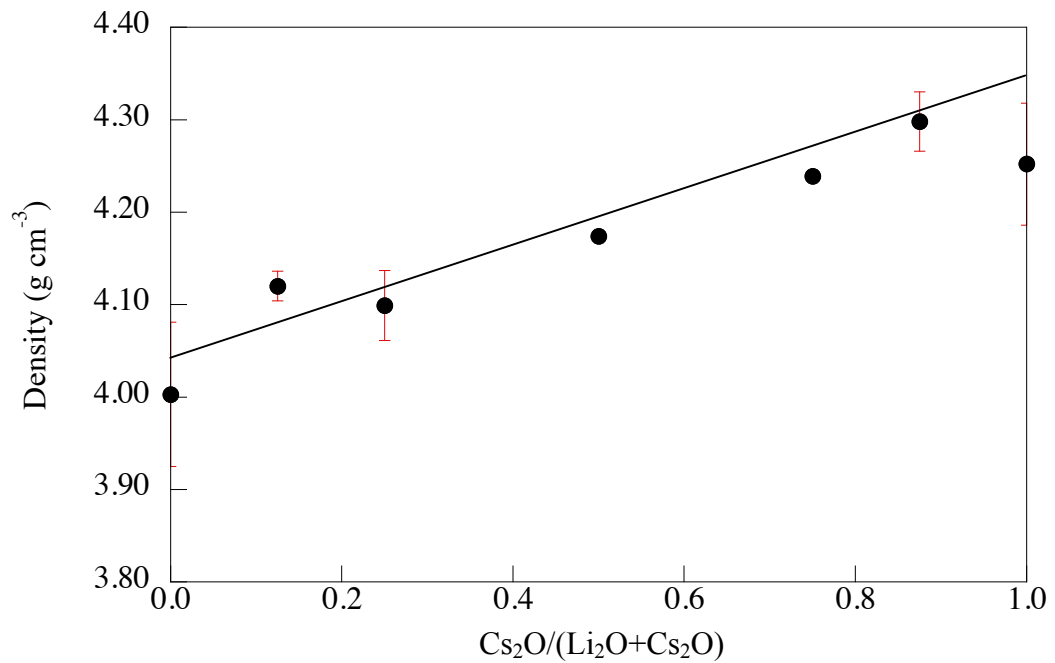


Figure 4-41. Densities of $x \text{Li}_2\text{O} \cdot (15-x) \text{Cs}_2\text{O} \cdot 85 \text{GeO}_2$ glasses. Line added to aid the eye.

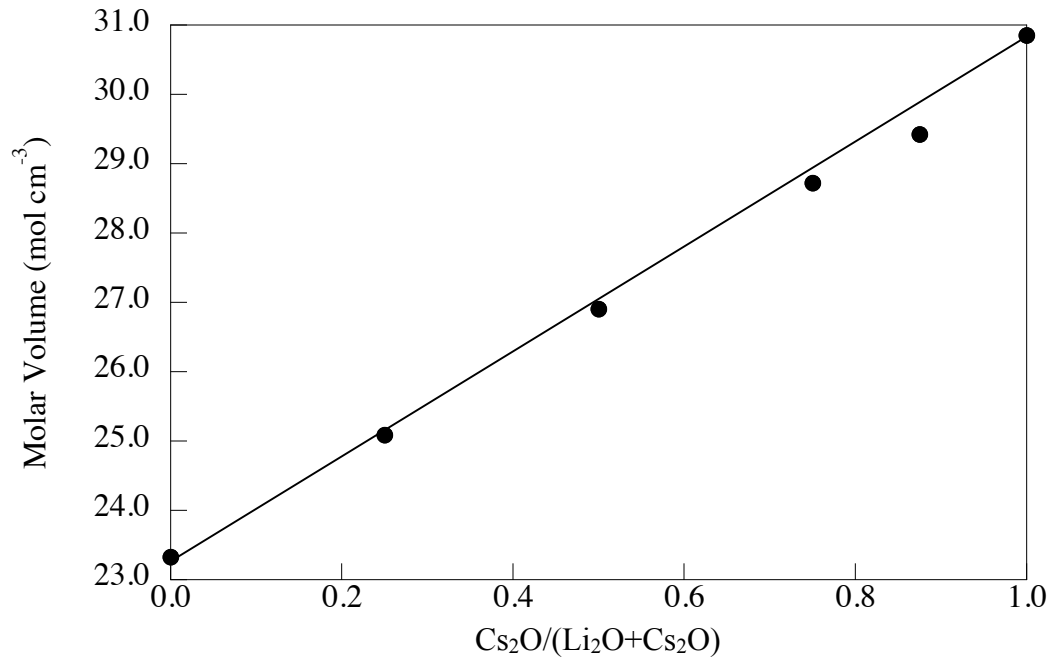


Figure 4-42. Molar volume of $x \text{Li}_2\text{O} \cdot (15-x) \text{Cs}_2\text{O} \cdot 85 \text{GeO}_2$ glasses. Line added to aid the eye.

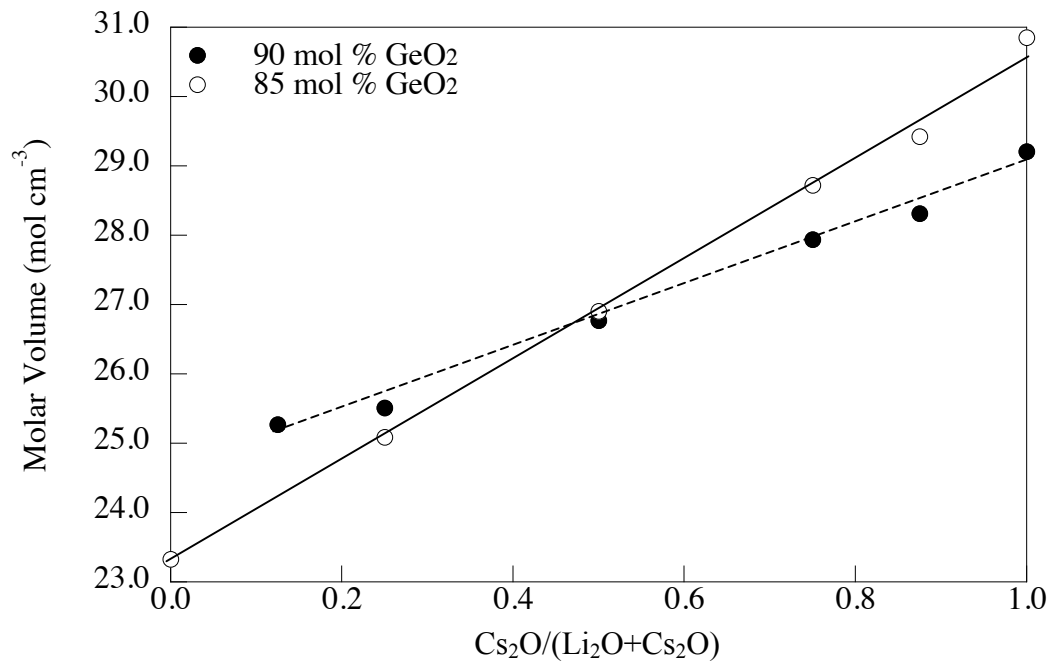


Figure 4-43. Comparison between the molar volume of the $x \text{Li}_2\text{O} \cdot (100-x-y) \text{Cs}_2\text{O} \cdot y \text{GeO}_2$, $y = 90$ and 85 mol %. Lines added to aid the eye.

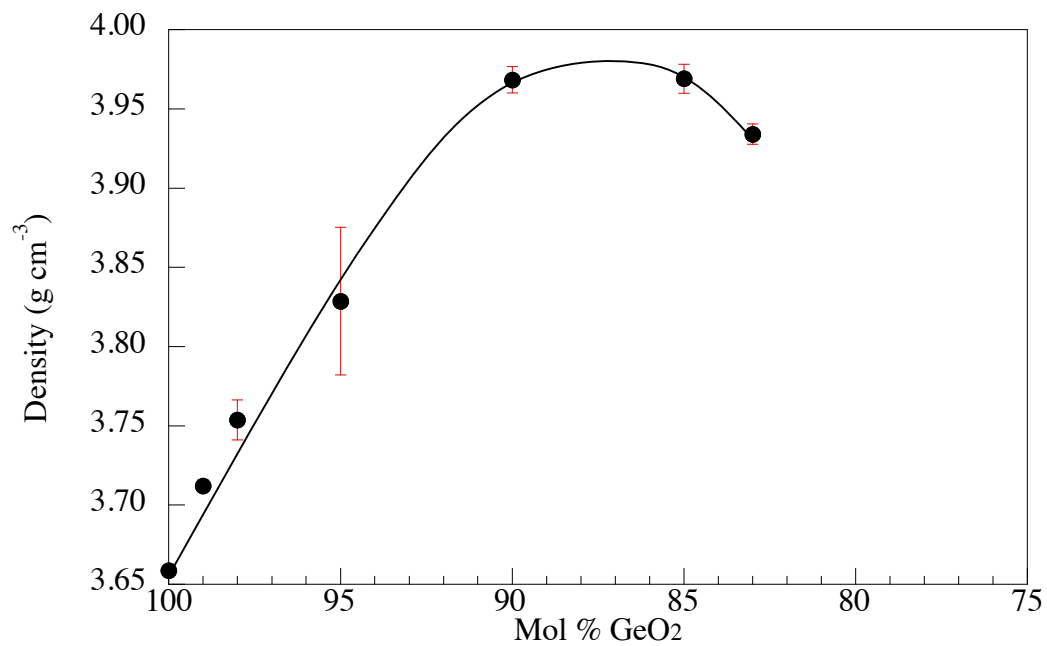


Figure 4-44. Densities of $0.5x \text{ Na}_2\text{O} \cdot 0.5x \text{ K}_2\text{O} \cdot (100-x) \text{ GeO}_2$. Line added to aid the eye.

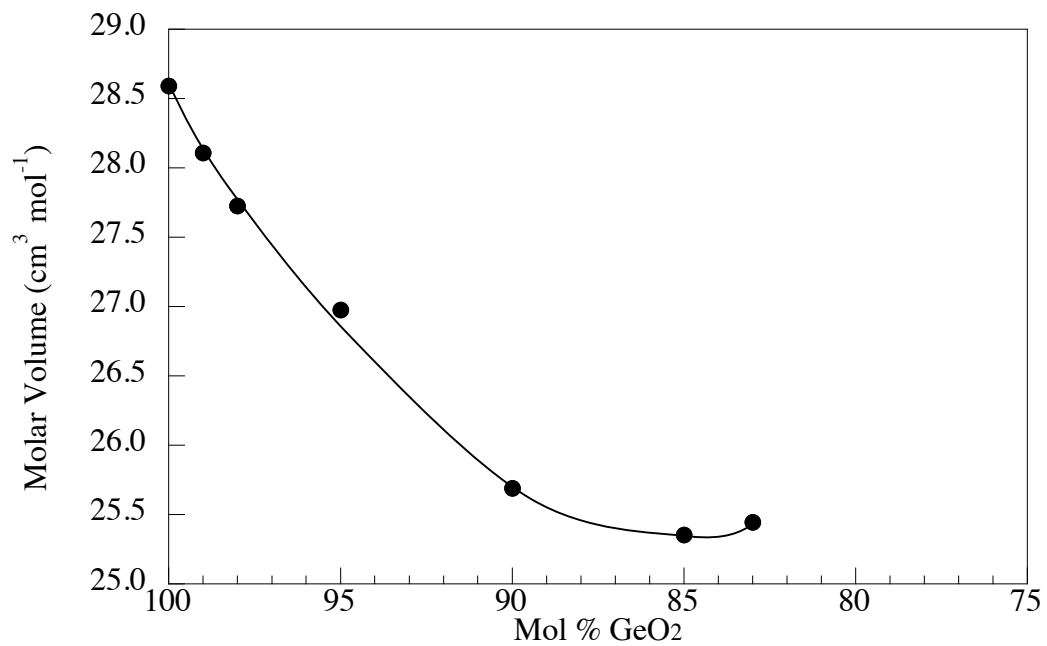


Figure 4-45. Molar volumes of $0.5x \text{ Na}_2\text{O} \cdot 0.5x \text{ K}_2\text{O} \cdot (100-x) \text{ GeO}_2$. Line added to aid the eye.

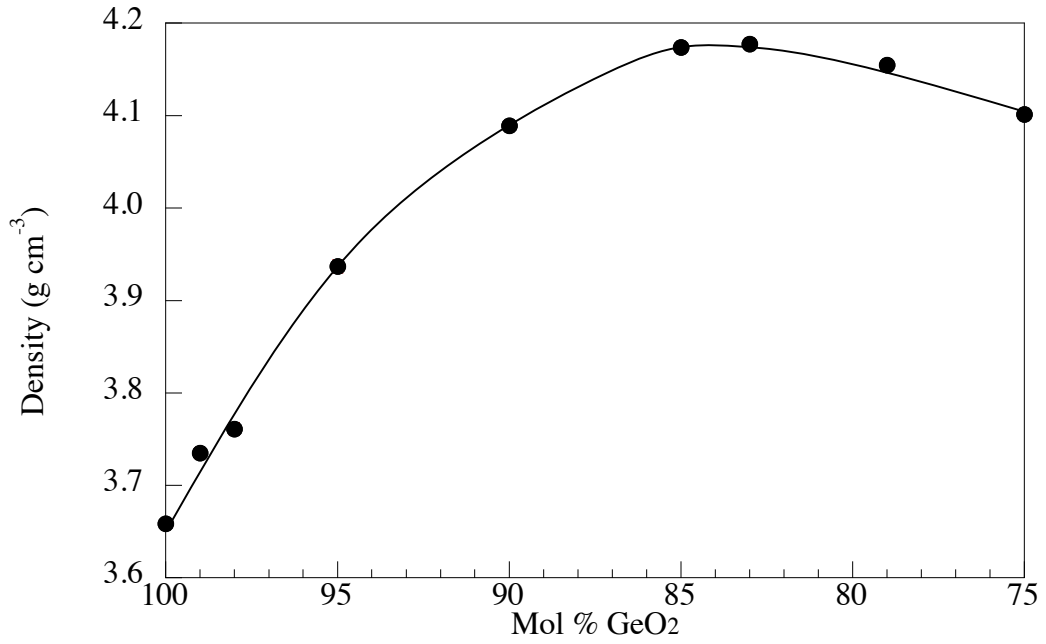


Figure 4-46. Densities of $0.5x \text{Li}_2\text{O} \cdot 0.5x \text{Cs}_2\text{O} \cdot (100-x) \text{GeO}_2$. Line added to aid the eye.

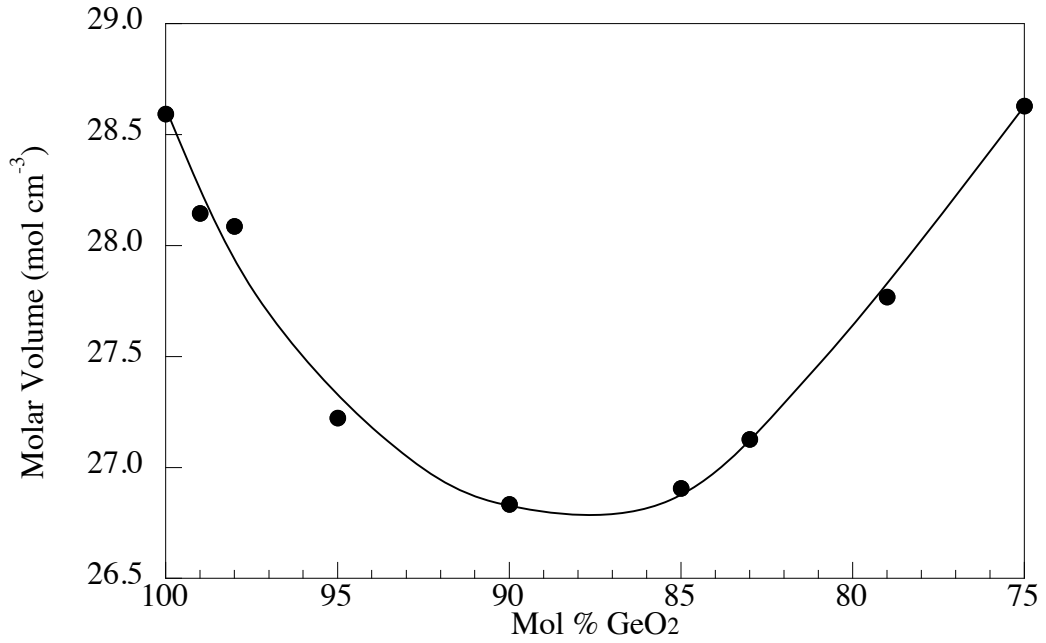


Figure 4-47. Molar volumes of $0.5x \text{Li}_2\text{O} \cdot 0.5x \text{Cs}_2\text{O} \cdot (100-x) \text{GeO}_2$. Line added to aid the eye.

4.5 Discussion

4.5.1 *Glass Transition Temperature*

The literature states that the deviation from additivity for T_g increases as the radius ratio of the cations increases. The radius ratio for $\text{Cs}^+:\text{Li}^+$ and $\text{K}^+:\text{Na}^+$ are 2.56 and 1.42, respectively, using Shannon and Prewitt's values.^{44,45} Figures 4-47 and 4-48 compare the deviations from additivity for the two different alkali pair at 90 and 85 mol % GeO_2 , respectively. As the amount of alkali in the glass increases, the deviation from additivity increases, as expected. Contrary to silicate and borate glasses, the deviation from additivity is independent of cation identity, as shown by the identical deviations from additivity for both glass systems.

The effect of cation identity on the low alkali germanate anomaly is minimal, as is shown in Figures 4-49 through 4-51. The minimum in T_g occurs at 1 mol % alkali oxide for the $\text{Li}_2\text{O}\cdot\text{Cs}_2\text{O}\cdot\text{GeO}_2$ glasses and 2 mol % for the $\text{Na}_2\text{O}\cdot\text{K}_2\text{O}\cdot\text{GeO}_2$ glasses. The T_g 's of the mixed alkali glasses are very similar to those of the binary glasses in their system at low alkali concentrations (Figures 4-50 and 4-51). The T_g 's for both glass systems (binary and ternary glasses) are very similar to each other until approximately 10 mol % addition of alkali oxide. Alkali oxide additions ≥ 10 mol % result in a difference in T_g of ≥ 15 °C. The maximum in T_g occurs at the same amount of alkali oxide for both systems, i.e. approximately 15 mol %.

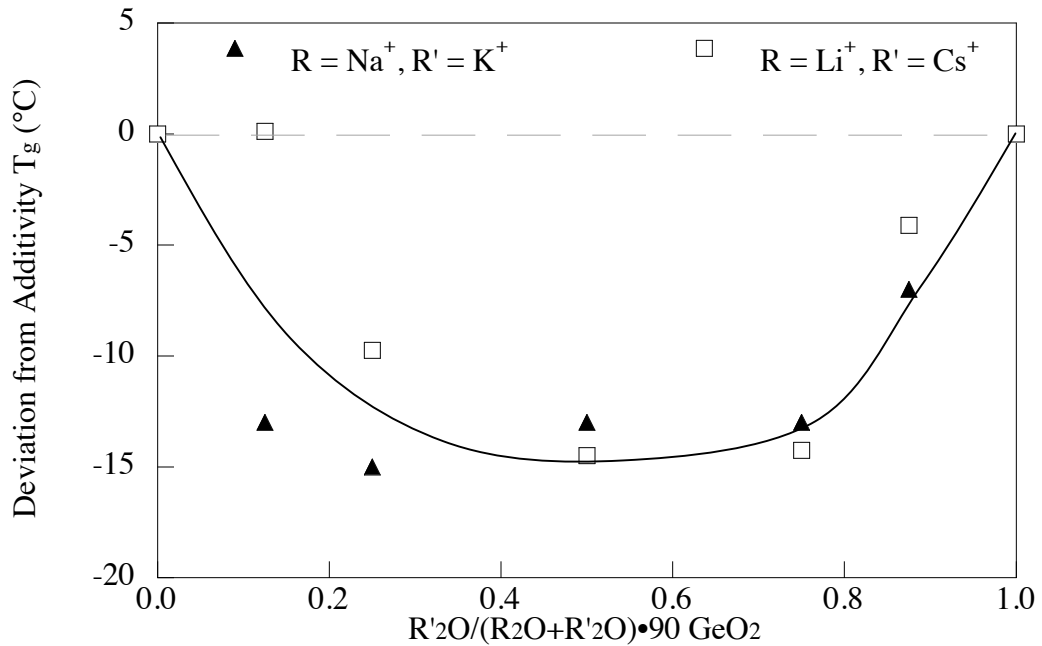


Figure 4-48. Comparison between the $\text{Na}_2\text{O}\cdot\text{K}_2\text{O}\cdot\text{GeO}_2$ and $\text{Li}_2\text{O}\cdot\text{Cs}_2\text{O}\cdot\text{GeO}_2$ glasses containing 90 mol% GeO_2 . The dotted line represents the T_g if they changed additively with composition. The bold line is added to aid the eye.

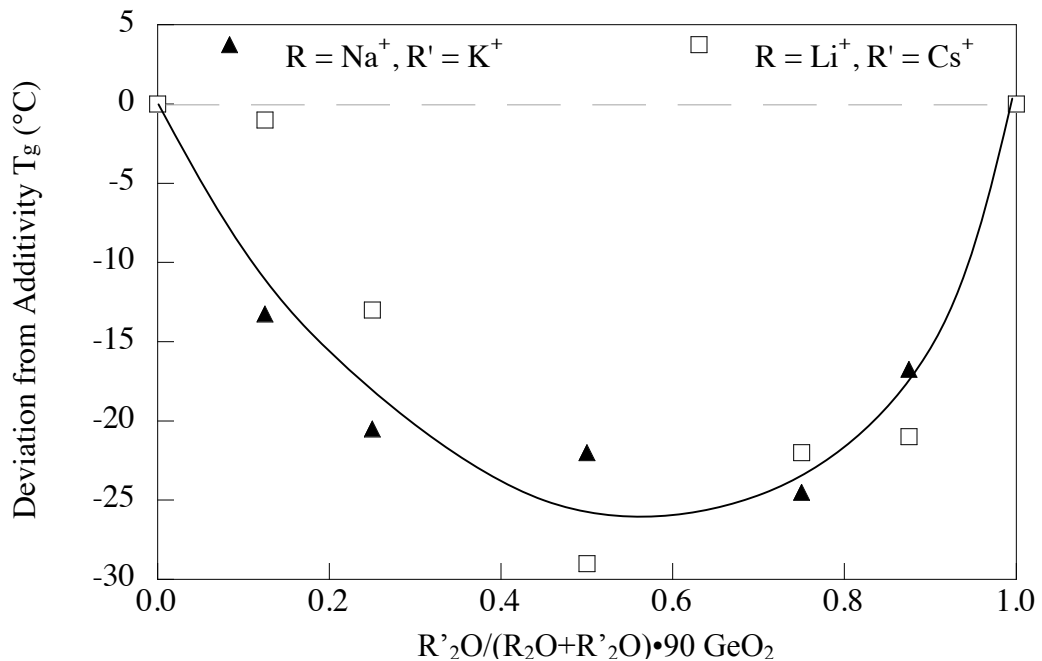


Figure 4-49. Comparison between the $\text{Na}_2\text{O}\cdot\text{K}_2\text{O}\cdot\text{GeO}_2$ and $\text{Li}_2\text{O}\cdot\text{Cs}_2\text{O}\cdot\text{GeO}_2$ glasses containing 85 mol % GeO_2 . The dotted line represents the T_g if they changed additively with composition. The bold line is added to aid the eye.

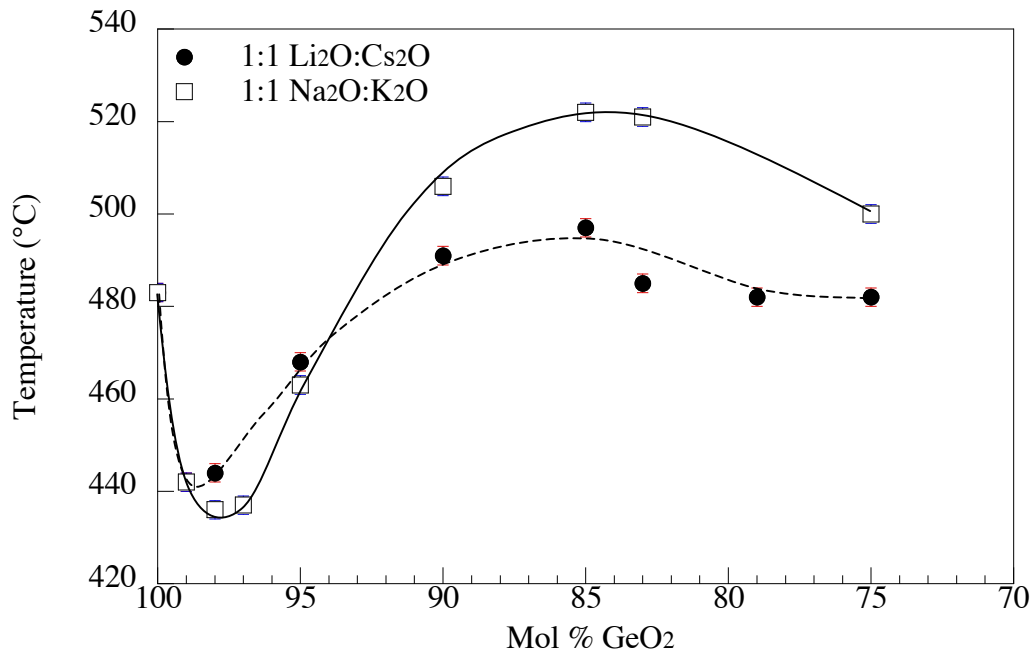


Figure 4-50. Comparison of the germanate anomaly for T_g data between the $\text{Li}_2\text{O}\cdot\text{Cs}_2\text{O}\cdot\text{GeO}_2$ and the $\text{Na}_2\text{O}\cdot\text{K}_2\text{O}\cdot\text{GeO}_2$ systems. Lines added to aid the eye.

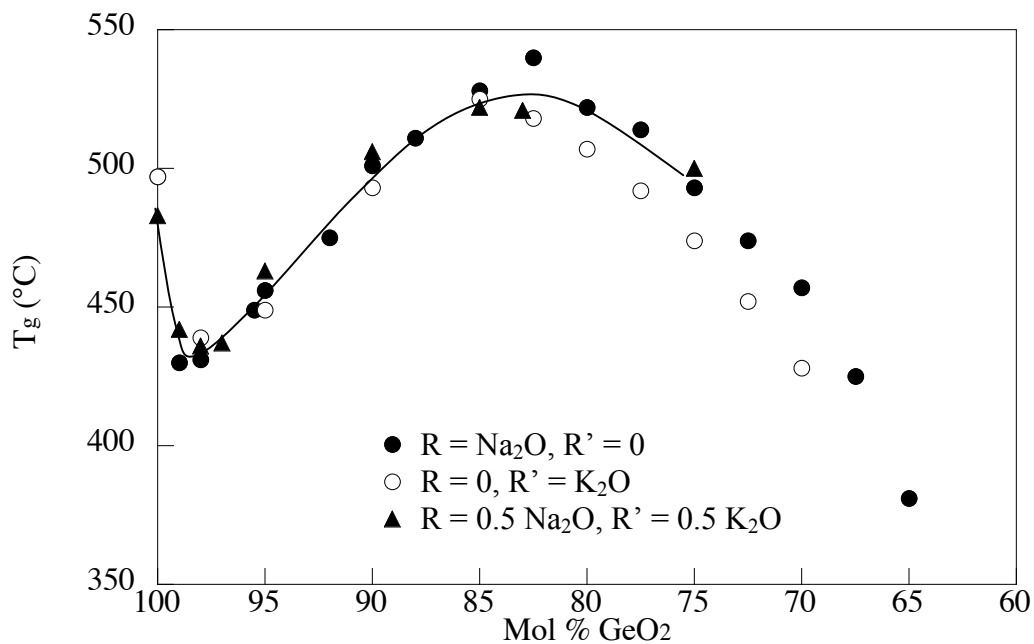


Figure 4-51. Glass transition temperature for the binary Na_2O and K_2O germanate glasses (from the literature¹⁷) and for the mixed alkali $\text{Na}_2\text{O}\cdot\text{K}_2\text{O}\cdot\text{GeO}_2$ glasses of this study. Line is added to accentuate the mixed alkali glasses.

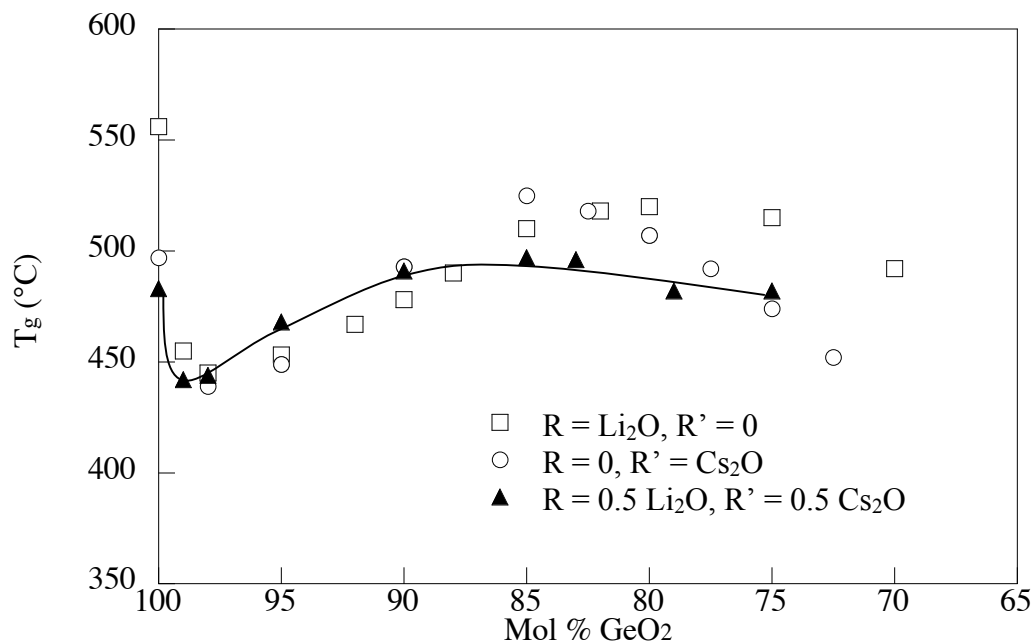


Figure 4-52. Glass transition temperature for the binary Li₂O and Cs₂O germanate glasses (from the literature^{5,17}) and for the mixed alkali Li₂O•Cs₂O•GeO₂ glasses of this study. Line is added to accentuate the mixed alkali glasses.

4.5.2 Density

Due to the large effect of the cation mass on density, the mixed alkali germanate glasses will be discussed on the basis of molar volume to account for the extremely large range of masses. The mixed alkali effect is not present in the densities of the alkali germanate glasses, which is consistent with the behavior in silicate glasses.⁴³ The greater the difference in the cation radius ratio, the greater the difference in molar volume, as the larger alkali ion is substituted for the smaller alkali ion. Figure 4-53 shows the molar volumes for the mixed alkali glasses containing 90 mol % GeO₂ and Figure 4-54 shows the molar volume for the mixed alkali glasses containing 85 mol % GeO₂.

As the total amount of alkali is increased in the mixed alkali glasses, the minimum typical of the germanate anomaly appears in the molar volume (Figure 4-55). The minimum occurs at 90 mol % GeO₂ in the Li₂O•Cs₂O•GeO₂ glass system and at 85 mol % GeO₂ for the Na₂O•K₂O•GeO₂ glass system. The larger the difference in the cation radius ratio, the smaller the effect of the germanate anomaly.

The densities of the mixed alkali glasses are compared to the binary alkali germanate glasses in Figures 4-55 and 4-56. The densities for both the Na₂O•K₂O•GeO₂

and the $\text{Li}_2\text{O}\cdot\text{Cs}_2\text{O}\cdot\text{GeO}_2$ mixed alkali glasses fall between their respective binary alkali germanate glasses.

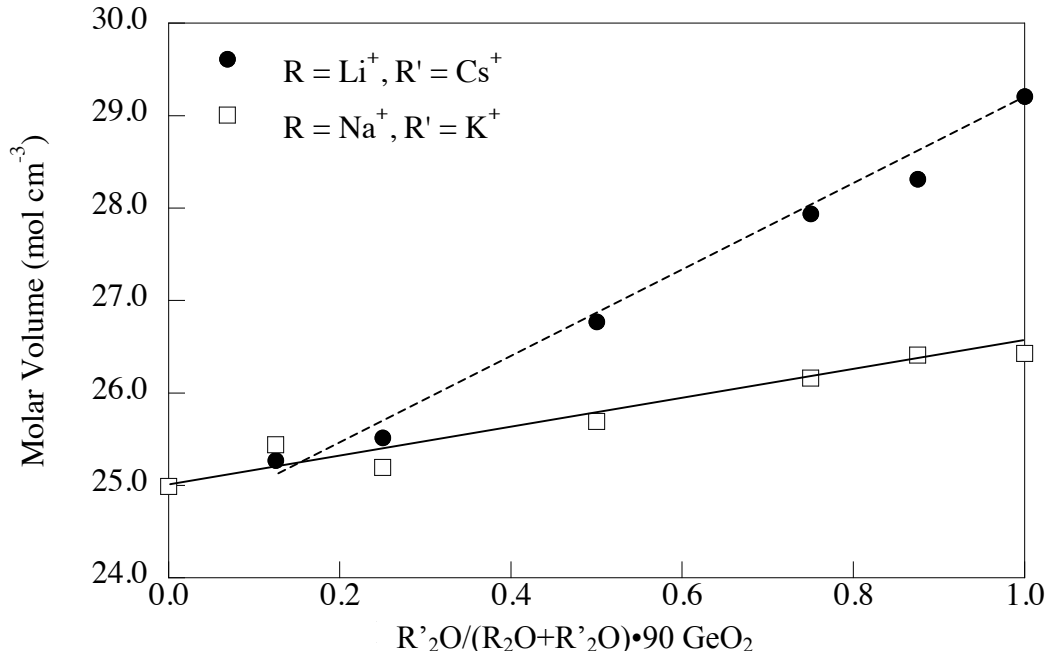


Figure 4-53. Comparison of the molar volume between the $\text{Na}_2\text{O}\cdot\text{K}_2\text{O}\cdot 90 \text{ GeO}_2$ and $\text{Li}_2\text{O}\cdot\text{Cs}_2\text{O}\cdot 90 \text{ GeO}_2$ systems. Line added to aid the eye.

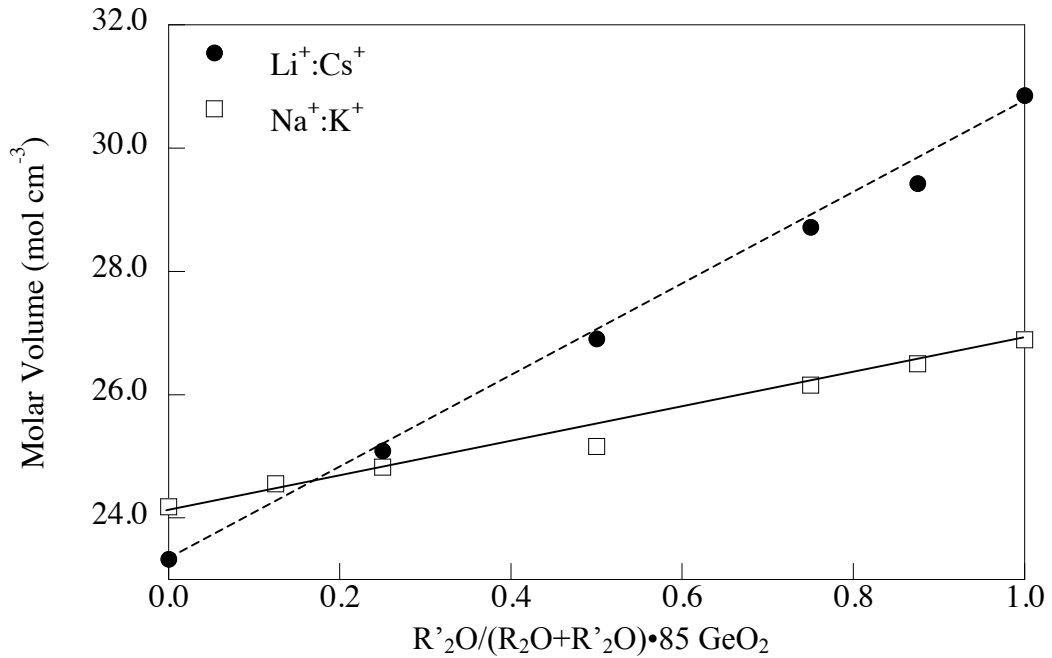


Figure 4-54. Comparison of the molar volume between the $\text{Na}_2\text{O}\cdot\text{K}_2\text{O}\cdot 85 \text{ GeO}_2$ and $\text{Li}_2\text{O}\cdot\text{Cs}_2\text{O}\cdot 85 \text{ GeO}_2$ systems. Line added to aid the eye.

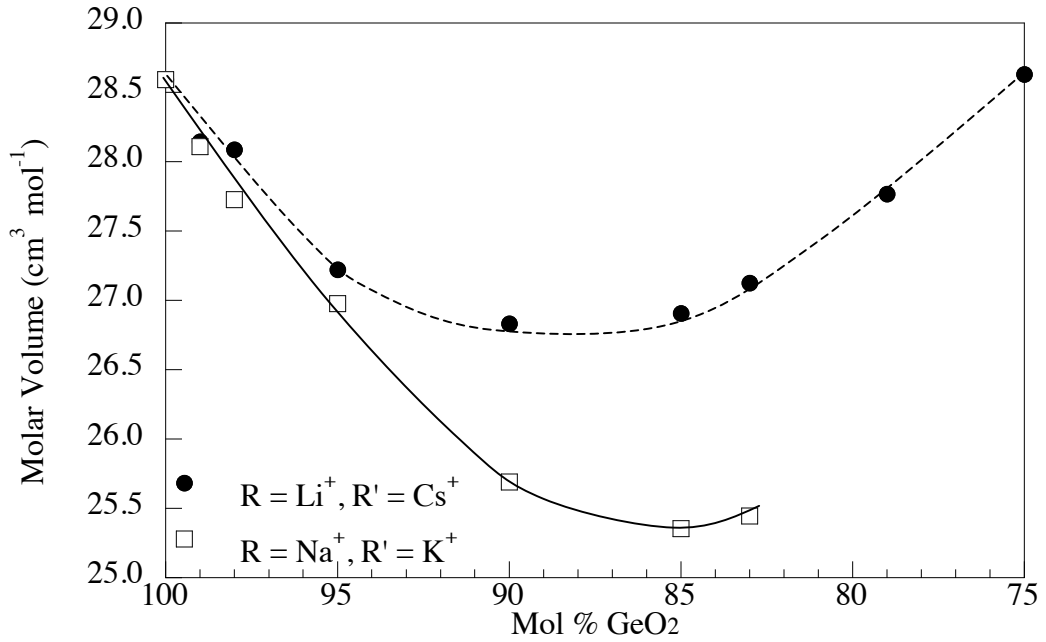


Figure 4-55. Comparison between the molar volume for the germanate anomaly. Lines added to accentuate the mixed alkali glasses.

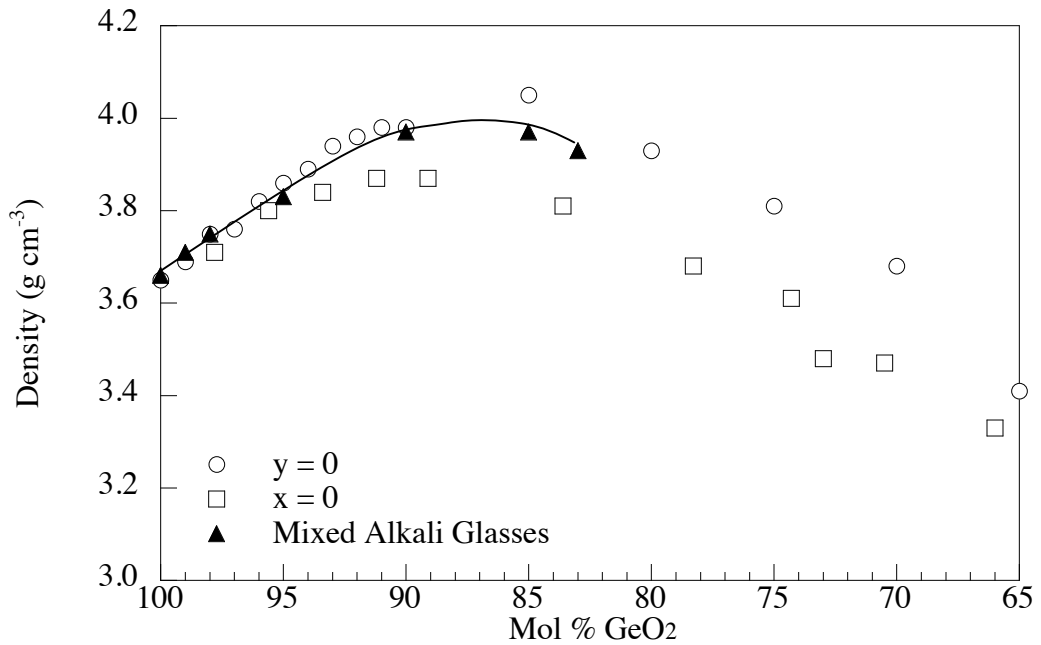


Figure 4-56. Literature values for density of the binary Na₂O and K₂O alkali-germanate glasses compared to the value for the Na₂O•K₂O•GeO₂ mixed alkali glasses. Line added to aid the eye.

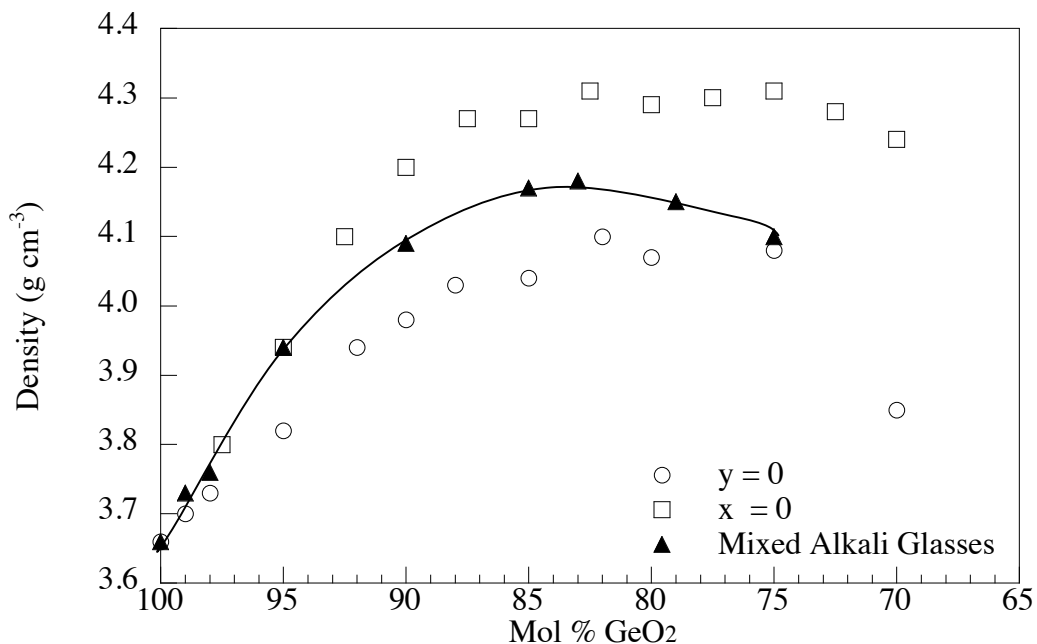


Figure 4-57. Literature values for density of the binary Li_2O and Cs_2O alkali-germanate glasses compared to the value for the $\text{Li}_2\text{O}\cdot\text{Cs}_2\text{O}\cdot\text{GeO}_2$ mixed alkali glasses. Line added to aid the eye.

4.6 Conclusion

Previous studies of mixed alkali glasses indicate that the deviation from additivity in T_g increases with increasing concentration of alkali oxides. This behavior is also found for the mixed alkali germanate glasses studied here. The current belief that the deviation from additivity also increases as the radius ratio increases does not hold true for the mixed alkali germanate glasses. The deviation from additivity was approximately the same for both the $\text{Na}_2\text{O}\cdot\text{K}_2\text{O}\cdot\text{GeO}_2$ and the $\text{Li}_2\text{O}\cdot\text{Cs}_2\text{O}\cdot\text{GeO}_2$ mixed alkali glasses.

The density and molar volumes behaved as anticipated. There was no mixed alkali effect for density or molar volume. The higher the concentration of alkali oxide in the germanate glasses, the greater the mixed alkali glasses differ in molar volume and density from their respective binary glasses. The densities of the mixed alkali glasses fall directly between the densities of the binary alkali germanate glasses. The cesium and lithium binary germanate glasses have the highest densities and are least affected by the germanate anomaly.

4.7 References

1. T.J. Kiczanski, C. Ma, E. Hammarsten, D. Wilkerson, M. Affatigato, and S. Feller, "A Study of Selected Physical Properties of Alkali Germanate Glasses over Wide Ranges of Composition," *J. Non-Cryst. Solids*, **272** [1] 57-66 (2000).
2. A. Marotta, A. Aronne, P. Pernice, and M. Catauro, "Glass Transition Temperature and Devitrification Behavior of Glasses in the Lithium Tetra Germanate-Sodium Tetra Germanate Composition Range " pp. 427-34 in Proceedings of the Second European Society of Glass Science and Technology Conference. Stazione Sperimentale del Vetro, Murano, Venice, Italy 1993.
3. N. Mochida and T. Sekiya, "Structure of Potassium Oxide-Germanium Dioxide Glasses Studied by Substitution by Stannic Oxide," *J. Ceram. Soc. Jpn.*, **94** [12] 1225-30 (1986).
4. K. Radhakirshnan and B.V.R. Chowdari, "Fast Ion Conduction in $\text{Li}_2\text{O-GeO}_2\text{-Nb}_2\text{O}_5$ Glasses," *Mater. Sci. Eng., B*, **14** [1] 17-22 (1992).
5. J.E. Shelby and J. Ruller, "Properties and Structure of Lithium Germanate Glasses," *Phys. Chem. Glasses*, **28** [6] 262-8 (1987).
6. A. Marotta, A. Aronne, P. Pernice, and M. Catauro, "Devitrification Behavior of Glasses in the Lead Tetragermanate-Lithium Tetragermanate Composition Range," *Mater. Chem. Phys.*, **42** [4] 247-52 (1995).
7. M. Catauro, F. de Gaetano, and A. Marotta, "Non-Isothermal Devitrification of Sodium Germanate Glasses," *Thermochim. Acta*, **404** [1-2] 55-61 (2003).
8. D. Di Martino, L.F. Santos, and R.M. Almeida, "Germanate Anomaly in Sodium and Cesium Binary Glass Systems: A Comparison," *Phys. Chem. Glasses*, **43C** 85-90 (2002).
9. P.K. Gangopadhyay, "Low Temperature Viscosity of Sodium Oxide-Germanium Dioxide Glasses," *Am. Ceram. Soc. Bull.*, **56** [11] 1008-11 (1977).
10. I.A. Gee, R. Hussin, D. Holland, and C.F. McConville, "X-Ray Photoelectron Spectroscopy Study of the Germanate Anomaly in the $\text{Na}_2\text{O-GeO}_2$ System," *Phys. Chem. Glasses*, **41** [4] 175-81 (2000).
11. T. Hanada, N. Soga, and M. Kunugi, "Physical Properties of Germanate Glasses in Sodium Oxide-Germanium Dioxide and Sodium Sulfide-Germanium Dioxide Systems. I. Elastic and Thermal Properties.," *Yogyo Kyokaishi*, **81** [11] 481-5 (1973).
12. K.A. Kostanyan and A.D. Akopyan, "Linear Coefficient of Thermal Expansion of Germanate Glasses," *Arm. Khim. Zh.*, **31** [2-3] 120 (1978).

13. G. Laudisio and M. Catauro, "Glass Transition Temperature and Devitrification Behavior of Glasses in the $\text{Na}_2\text{O} \cdot 4 \text{GeO}_2\text{-K}_2\text{O} \cdot 4 \text{GeO}_2$ Composition Range," *Mater. Chem. Phys.*, **51** [1] 54-8 (1997).
14. S.-K. Lee, M. Tatsumisago, and T. Minami, "Relation between Local Structure and Fragility of Sodium Germanate Glasses," *Phys. Chem. Glasses*, **36** [5] 225-7 (1995).
15. J.A. Ruller, C.A. Shaw, and J.E. Shelby, "Properties and Morphology of Sodium Lead Germanate Glasses," *Phys. Chem. Glasses*, **33** [5] 161-6 (1992).
16. J.E. Shelby, "Viscosity and Thermal Expansion of Alkali Germanate Glasses," *J. Am. Ceram. Soc.*, **57** [10] 436-9 (1974).
17. J.E. Shelby, "Thermal Expansion of Mixed-Alkali Germanate Glasses," *J. Appl. Phys.*, **46** [1] 193-6 (1975).
18. G. Laudisio and M. Catauro, "Bulk and Surface Crystallisation of Potassium Heptagermanate Glass," *Phys. Chem. Glasses*, **38** [5] 244-5 (1997).
19. K. Nassau and D.L. Chadwick, "Glass Formation in the System $\text{GeO}_2\text{-Bi}_2\text{O}_3\text{-Ti}_2\text{O}_5$," *J. Am. Ceram. Soc.*, **65** [4] 197-202 (1982).
20. M.M. Hall and J.E. Shelby, "Water Diffusion and Solubility in Alkali Germanate Melts," *Phys. Chem. Glasses*, **45** [4] 283-90 (2004).
21. Sciglass 6.5 [CD-ROM] ITC Inc., Newton, MA, 2005.
22. G.S. Henderson and H.M. Wang, "Germanium Coordination and the Germanate Anomaly," *Eur. J. Mineral.*, **14** [4] 733-44 (2002).
23. S. Sakka and K. Kamiya, "Structure of Alkali Germanate Glasses Studied by Spectroscopic Techniques," *J. Non-Cryst. Solids*, **49** [1-3] 103-16 (1982).
24. H. Verweij, J.H.J.M. Buster, and G.F. Remmers, "Refractive Index and Density of Lithium, Sodium, and Potassium Germanosilicate Glasses," *J. Mater. Sci.*, **14** [4] 931-40 (1979).
25. T. Yoshimura, J. Fukunaga, and I. Masayoshi, "Properties and Structure of Glasses in the Lithia-Boria-Germania System," *Yogyo Kyokaishi*, **79** [915] 428-34 (1971).
26. K.S. Evstrop'ev and A.O. Ivanov, "Physicochemical Properties of Germanium Glasses," pp. 79-85 in Vol. 2, Proceedings of the VI International Congress on Glass. Plenum Press, Washington, D.C., 1962.

27. J.N. Mundy and G.L. Gin, "Ionic Transport in Mixed Sodium Rubidium Aluminogermanate Glass," *Solid State Ionics*, **66** [1-2] 69-83 (1993).
28. J.E. Shelby, "Helium Migration in Alkali Germanate Glasses," *J. Appl. Phys.*, **50** [1] 276-9 (1979).
29. L.K. Shmatok and E.E. Shalamaiko, "Refractive Index and Density of Sodium Titanogermanate Glass," *Fiz. Khim. Stekla*, **12** [1] 81-5 (1986).
30. A.M. Efimov, E.K. Mazurina, V.A. Kharyuzov, and M.V. Proskuryakov, "Dependence of the Refractive Index and the Dielectric Constant on the Composition of Glasses in Silicate, Borate, and Germanate Systems with Group Ia-IIa Element Oxides," *Fiz. Khim. Stekla*, **2** [2] 151-6 (1976).
31. A.O. Ivanov, "Electrical Conductivity of Alkali Glasses of the Na₂O-K₂O GeO₂ System," *Fiz. Tverd. Tela (Leningrad)*, **5** [9] 2647-52 (1963).
32. M. Murthy and J. Aguayo, "Germanium Oxide Systems. II. Phase Equilibria in the System Na₂O-GeO₂," *J. Am. Ceram. Soc.*, **47** [9] 444-7 (1964).
33. G.S. Henderson and M.E. Fleet, "The Structure of Glass Along the Na₂O-GeO₂ Join," *J. Non-Cryst. Solids*, **134** [3] 259-69 (1991).
34. V.Y. Livshits and R.A. Nakhapetyan, "Moduli of Elasticity of Sodium Oxide-Aluminum Oxide Germanium Dioxide System Glasses," *Fiz. Khim. Stekla*, **12** [5] 663-6 (1986).
35. R.A. Secco and K.M. Ault, "Ionic Transport and Structure in High Pressure Na₂O:GeO₂ Glasses," *J. Non-Cryst. Solids*, **238** [3] 244-52 (1998).
36. K.A. Kostanyan and A.D. Akopyan, "Linear Coefficient of Thermal Expansion of Germanate Glasses," *Arm. Khim. Zh.*, **31** [2-3] 120-6 (1978).
37. A. Mayer and F. Trojer, "Coordination Behavior of Aluminum (3+) Ions in Melts and Glasses of the GeO₂-M₂O-Al₂O₃ System," *Glastech. Ber.*, **54** [9] 279-91 (1981).
38. M. Murthy and J. Ip, "Some Physical Properties of Alkali Germanate Glasses," *Nature (London)*, **201** [4916] 285-6 (1964).
39. K. Kamiya, S. Sakka, and T. Yoko, "Properties and Structure of Alkaline Earth Germanate Glasses," *Res. Rep. Fac. Eng. Mie Univ.*, **7** 107-119 (1982).
40. Y.S. Krupkin and K.S. Evstrop'ev, "Properties and Structure of Multialkali Borogermanate Glasses," *Inorg. Mater.*, **1** [9] 1410-4 (1971).

41. M.K. Murthy and J. Aguayo, "Studies in Germanium Oxide Systems: II, Phase Equilibria in the System Na₂O-GeO₂," *J. Am. Ceram. Soc.*, **47** [9] 444-7 (1964).
42. J.E. Shelby, *Introduction to Glass Science and Technology*; pp. 1-181. Royal Society of Chemistry, Cambridge, 1997.
43. D.E. Day, "Mixed Alkali Glasses-Their Properties and Uses," *J. Non-Cryst. Solids*, **21** [3] 343-72 (1976).
44. R.D. Shannon and C.T. Prewitt, "Effective Ionic Radii in Oxide and Fluorides," *Acta Crystallogr.*, **B25** [5] 925-46 (1969).
45. R.D. Shannon and C.T. Prewitt, "Effective Ionic Radii and Crystal Chemistry," *J. Inorg. Nucl. Chem.*, **32** [5] 1427-41 (1970).

CHAPTER 5: INFRARED SPECTRA

5.1 Introduction

Few studies investigating the infrared spectra of mixed alkali glasses exist.¹⁻¹⁴ These studies fall into two categories: those addressing the structural bands between 200 and 1200 cm^{-1} and those investigating the hydroxyl bands between 1500 and 4000 cm^{-1} . This study deals with the latter region. Infrared spectra were measured for glasses in the $\text{Li}_2\text{O}\cdot\text{Cs}_2\text{O}\cdot\text{GeO}_2$ and $\text{Na}_2\text{O}\cdot\text{K}_2\text{O}\cdot\text{GeO}_2$ systems and will be discussed in the context of the mixed alkali effect and the germanate anomaly.

5.2 Literature Review

An infrared spectrometer exposes a sample to a beam of light (usually 200 to 4000 cm^{-1}) and detects if this frequency is absorbed by the sample. Treating a molecule as two masses connected by a spring allows the molecule to be described mathematically as a harmonic oscillator. Differential equations can be written to describe the motion of each bond in a molecule. Each molecule has a limited number of distinct vibrational modes governed by quantum mechanics. Infrared light can couple with these vibrational modes. Since a real material is not perfect, these oscillations cause the springs to behave non-linearly. The oscillation becomes damped, and coupling occurs over a range of frequencies instead of one precise frequency. This thesis examines the bands caused by OH^- and overtones of the low frequency structural bands.¹⁵

Two studies have investigated the bands between 1500 and 4000 cm^{-1} .^{4,8} Hosono and Abe⁸ studied the effect of temperature on the infrared spectra of three sodium germanate glasses. Hall and Shelby⁴ studied water diffusion and solubility in sodium and potassium germanate melts. Hosono and Abe used analogy to the well characterized infrared absorption water bands of silicate glasses to assign the bands in the infrared spectra of alkali germanate glasses. Alkali silicate glasses have three bands associated with water.⁸ Band I is located at 3700 cm^{-1} and is attributed to the Si-OH interacting weakly with a bridging oxygen. Band II is located at approximately 2800 cm^{-1} and results from a Si-OH forming a strong hydrogen bond with a neighboring non-bridging oxygen. The final band at $\sim 2350 \text{ cm}^{-1}$ is assigned to a very strong hydrogen bond

forming between Si-OH and a nearby discrete silicate anion. Hosono and Abe found similar results between the silicate and germanate infrared spectra. In pure GeO₂ glasses, there is one absorption band at 3600 cm⁻¹ in the infrared spectrum. Larger alkali addition (> 22 mol %) to GeO₂ results in formation of two bands at 2800 and 2350 cm⁻¹. The most obvious difference between the infrared spectra of alkali silicate and alkali germanate glasses occurs with small additions of alkali to the glasses. Alkali concentrations of 5 mol % in germanate glasses results in a fourth band centered around 3300 cm⁻¹, which does not occur in silicates; Hosono and Abe call this “Band I’ ”. They attribute this band to Ge-OH interacting with oxygen’s in two coordination states and suggest the band at 3300 cm⁻¹ is a result of Ge-OH interacting weakly with a six coordinated bridging oxygen. Table 5-I lists the bands, their positions, and their vibrational assignments by Hosono and Abe.⁸

Table 5-I. Band Positions of the Infrared Absorption Water Bands of Germanate Glasses

Band	Position (cm ⁻¹)	Vibrational assignment by Hosono and Abe ⁸
I	3600	Ge-OH weakly interacting with bound 4-coordinated oxygen
I’	3300	Ge-OH weakly interacting with bound 6-coordinated oxygen
II	2800	Ge-OH strong hydrogen bond with a non-bridging oxygen
III	2350	Ge-OH very strong hydrogen forming with a germanate anion

Although, the work of Hall and Shelby focuses on the diffusion rate of hydroxyl in glasses, their work includes a substantial number of pre-water treated samples. They added to Hosono and Abe’s work by making seven different sodium germanate glasses. These additional glasses clearly show the development of the band at 3300 cm⁻¹. Spectra of glasses with 2 to 10 mol % sodium addition only exhibit Band I and I’. Spectra of glasses containing ≥ 15 mol % sodium have two new bands: one at about 2700 cm⁻¹ (Band II) and another at 2350 cm⁻¹ (Band III) which they attribute to the presence of neighboring non-bridging oxygens.

5.3 Experimental Procedures

Glasses were prepared as described in Chapter 3. Polished plates were placed into a Thermo-Nicolet® Avatar 380 FT-IR spectrometer. Spectra were collected from 1500 to 4000 cm⁻¹ and analyzed using EZ Omnic software (version 6.0a), by Thermo-Nicolet®. The background (transmission at 4000 cm⁻¹) for each sample was recorded

and subtracted from the spectra. The sample thickness was measured using calipers with an accuracy of ± 0.005 mm. After removing the background, spectra were divided by the sample thickness. The resolution of the instrument is ± 2 wavenumbers.

Some glasses were melted under high partial pressure of water vapor, to increase their hydroxyl content. Figure 5-1 shows a schematic of the furnace used in this study. Five gram batches were first melted in an electric furnace for 5 minutes (more detail is given in Chapter 3). The crucible was removed from the electric furnace and placed in the hot zone of the furnace, where it was held at 1050 °C for 15 minutes, under air saturated with water vapor. The water bath was maintained just below boiling at 98 °C during the experiment. Samples were removed from the furnace and cooled to room temperature by placing the crucible on a refractory brick. Samples were removed from the crucible and an infrared spectrum recorded.

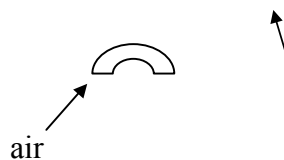


Figure 5-1. Schematic of water used to melt glasses under high vapor pressure of water.

5.4 Results

5.4.1 *Mixed Alkali Glasses*

The infrared spectra for x Li₂O•(10- x) Cs₂O• 90 GeO₂ glasses are shown in Figure 5-2. Glasses with a mixture of alkali ions have significantly more hydroxyl than glasses with only one alkali. Normalizing the spectra to the same scale makes differences in the spectra more obvious. Figure 5-3 shows the normalized infrared spectra for x Li₂O•(10- x) Cs₂O• 90 GeO₂ glasses. Band I shifts from 3440 cm⁻¹ for the binary 10 Li₂O•90 GeO₂ glasses to 3405 cm⁻¹ for binary 10 Cs₂O•90 GeO₂ glasses. Glasses with a 3:1 ratio of Li₂O:Cs₂O absorb at the largest wavenumbers, as shown in Figure 5-4, where a positive

deviation from additivity is obvious. Mixing the alkali ions also results in the increase in intensity of Band III (centered at about 2250 cm^{-1}). Atmospheric carbon dioxide absorption bands interfere with Band III, making it difficult to see more than an overall increase in absorption.

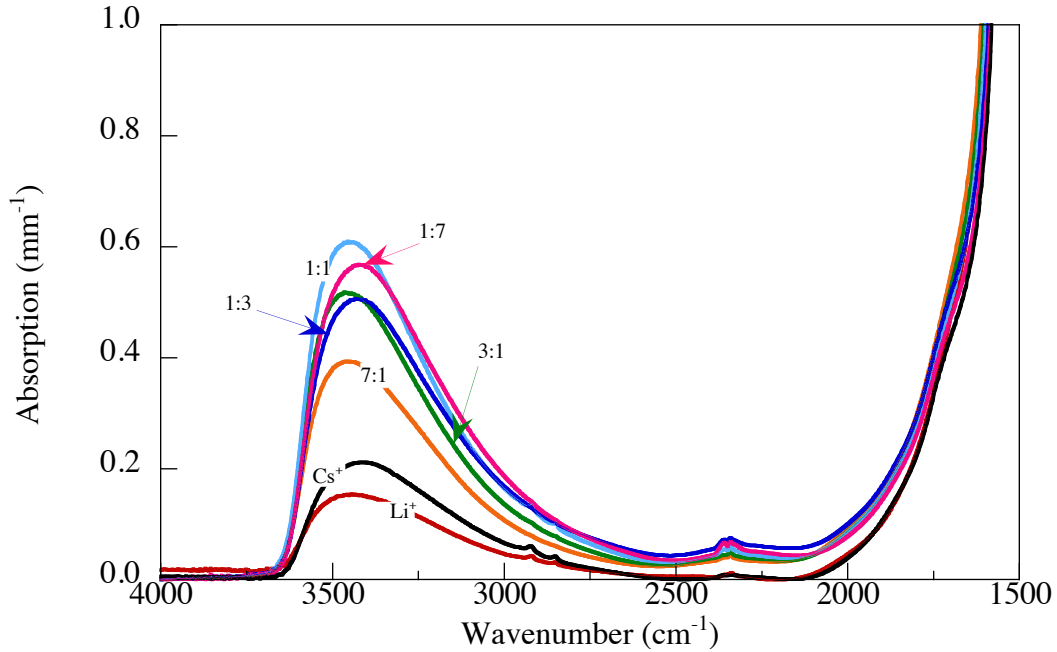


Figure 5-2. Infrared spectra for $x\text{ Li}_2\text{O}\cdot(10-x)\text{ Cs}_2\text{O}\cdot 90\text{ GeO}_2$ glasses. Labels are the ratio of $\text{Li}^+:\text{Cs}^+$.

Increasing the amount of alkali from 10 to 15 mol % in $x\text{ Li}_2\text{O}\cdot(15-x)\text{ Cs}_2\text{O}\cdot 85\text{ GeO}_2$ glasses results in dramatic changes in the infrared spectra. Spectra for these glasses are shown in Figure 5-5. The binary $\text{Cs}_2\text{O}\cdot\text{GeO}_2$ glass exhibits obvious absorptions due to Bands I, I', II and III. As the amount of cesium in the glass increases Bands II and III increase in intensity, as shown Figure 5-6. Band I shifts from 3415 cm^{-1} for the binary $15\text{ Li}_2\text{O}\cdot 85\text{ GeO}_2$ glasses to 3365 cm^{-1} for binary $15\text{ Cs}_2\text{O}\cdot 85\text{ GeO}_2$ glasses (Figure 5-7). The position of Band I is at a maximum frequency for glasses with a 3:1 ratio of $\text{Li}_2\text{O}:\text{Cs}_2\text{O}$, as shown in the Figure 5-6. A positive deviation from additivity in the position of this band for the mixed alkali glasses is shown in Figure 5-7.

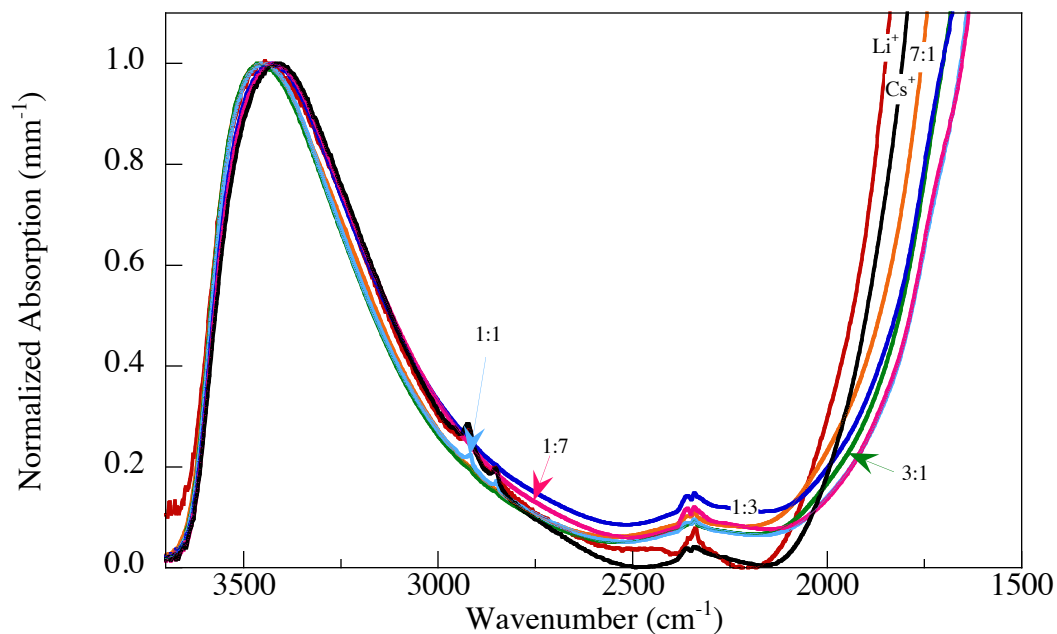


Figure 5-3. Normalized infrared spectra for $x \text{Li}_2\text{O} \cdot (10-x) \text{Cs}_2\text{O} \cdot 90 \text{GeO}_2$ glasses. Labels are the ratio of $\text{Li}^+:\text{Cs}^+$.

The infrared spectra for $x \text{Na}_2\text{O} \cdot (10-x) \text{K}_2\text{O} \cdot 90 \text{GeO}_2$ glasses are shown in Figure 5-8. Mixed alkali $x \text{Na}_2\text{O} \cdot (10-x) \text{K}_2\text{O} \cdot 90 \text{GeO}_2$ glasses have significantly more hydroxyl than the binary alkali glasses. Figure 5-9 shows the normalized infrared spectra for $x \text{Na}_2\text{O} \cdot (10-x) \text{K}_2\text{O} \cdot 90 \text{GeO}_2$ glasses. As the amount of K_2O increases, Band I broadens. The peak shift (Figure 5-10) is much smaller than for the $\text{Li}_2\text{O} \cdot \text{Cs}_2\text{O} \cdot \text{GeO}_2$ glass, ranging from 3450 cm^{-1} for the binary $10 \text{Na}_2\text{O} \cdot 90 \text{GeO}_2$ glass, to 3420 cm^{-1} for binary $10 \text{K}_2\text{O} \cdot 90 \text{GeO}_2$ glasses.

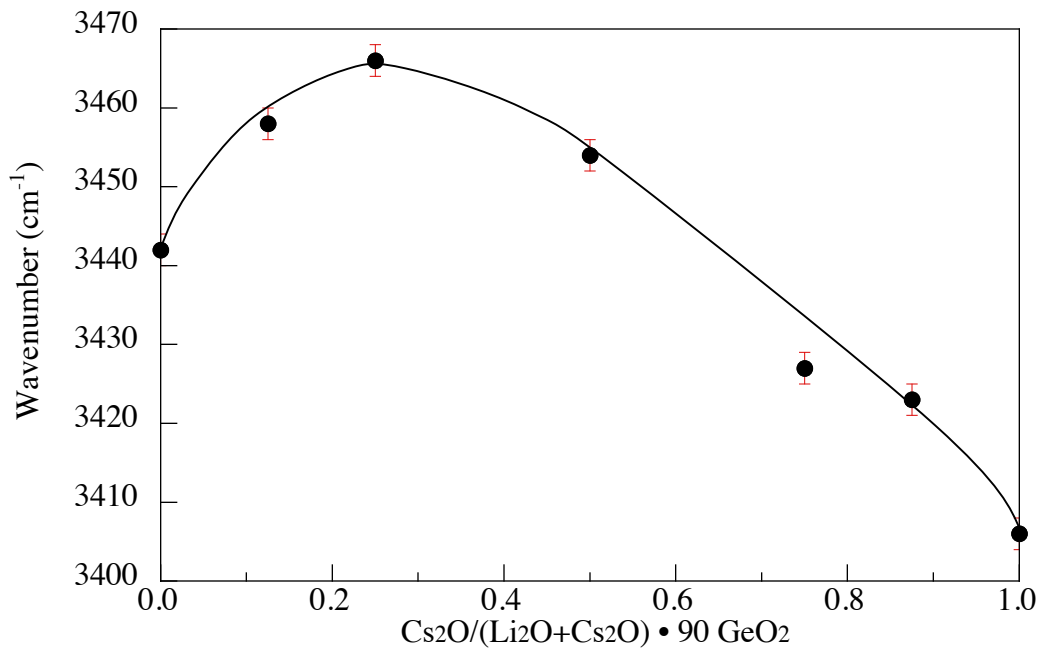


Figure 5-4. Peak position of Band I in the infrared spectra for $x \text{Li}_2\text{O} \cdot (10-x) \text{Cs}_2\text{O} \cdot 90 \text{GeO}_2$ glasses. Line drawn to aid the eye.

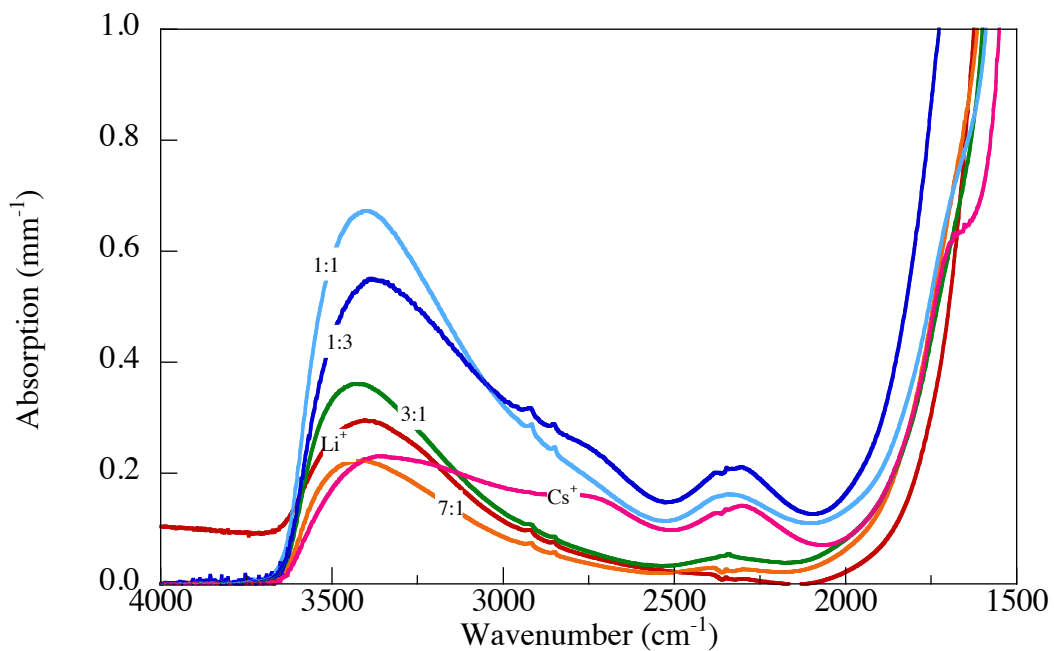


Figure 5-5. Infrared spectra for $x \text{Li}_2\text{O} \cdot (15-x) \text{Cs}_2\text{O} \cdot 85 \text{GeO}_2$ glasses. Labels are the ratio of $\text{Li}^+:\text{Cs}^+$.

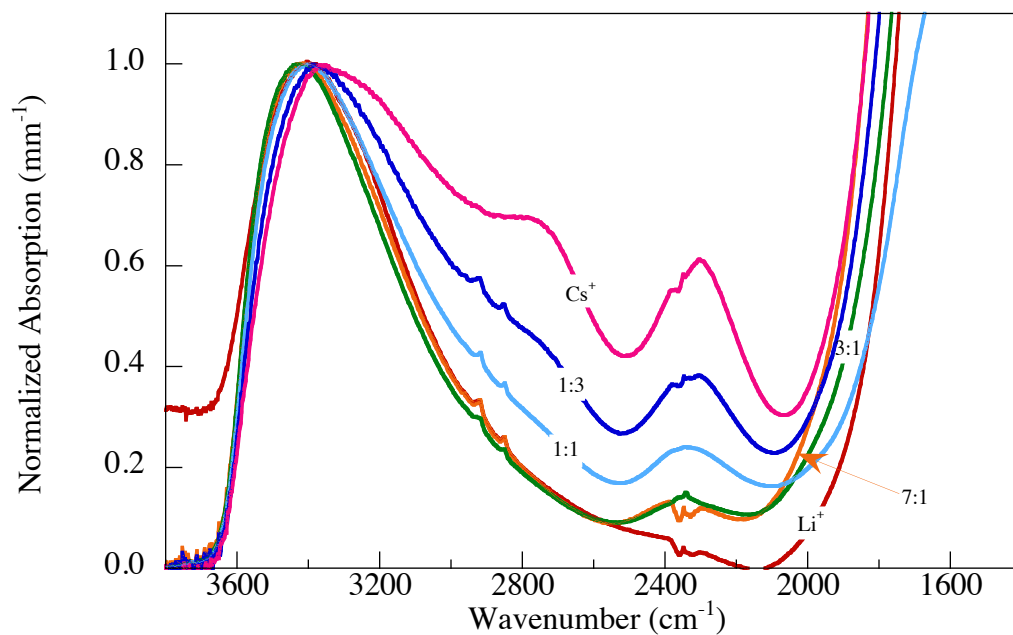


Figure 5-6. Normalized infrared spectra for $x \text{Li}_2\text{O} \cdot (15-x) \text{Cs}_2\text{O} \cdot 85 \text{GeO}_2$ glasses. Labels are the ratio of $\text{Li}^+:\text{Cs}^+$.

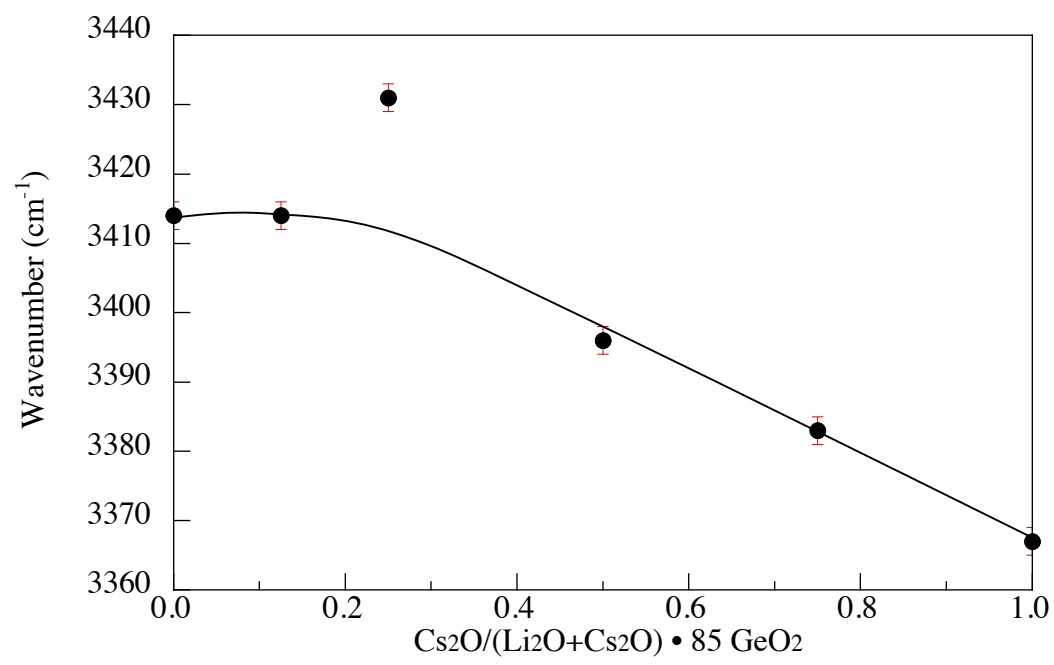


Figure 5-7. Peak position of Band I in the infrared spectra for $x \text{Li}_2\text{O} \cdot (15-x) \text{Cs}_2\text{O} \cdot 85 \text{GeO}_2$ glasses. Line drawn to aid the eye.

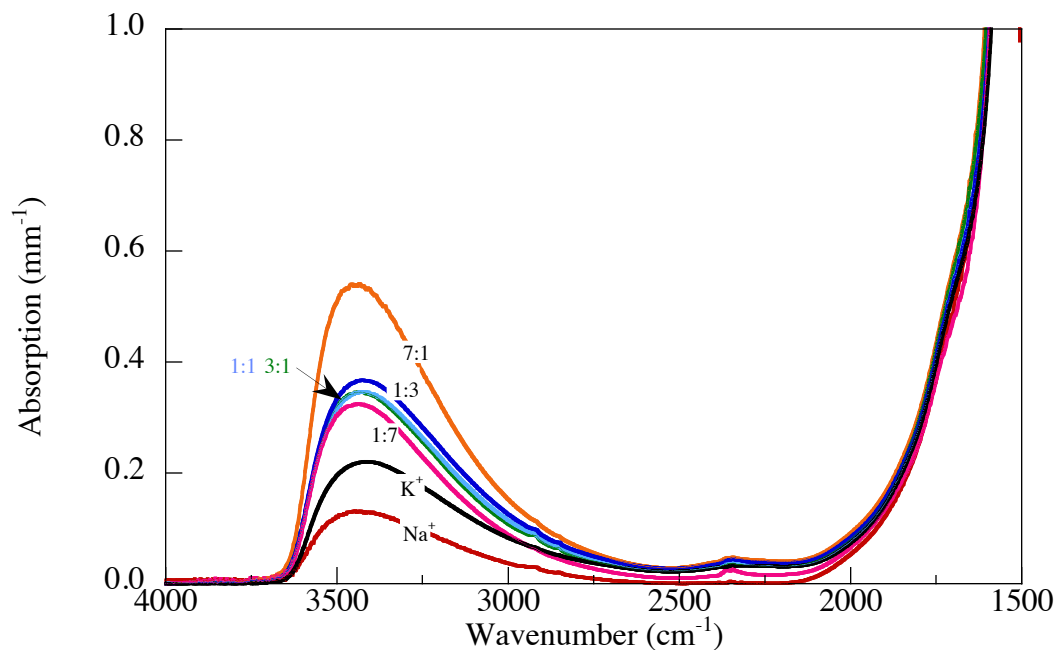


Figure 5-8. Infrared spectra for $x \text{Na}_2\text{O} \cdot (10-x) \text{K}_2\text{O} \cdot 90 \text{GeO}_2$ glasses. Labels are the ratio of $\text{Na}^+:\text{K}^+$.

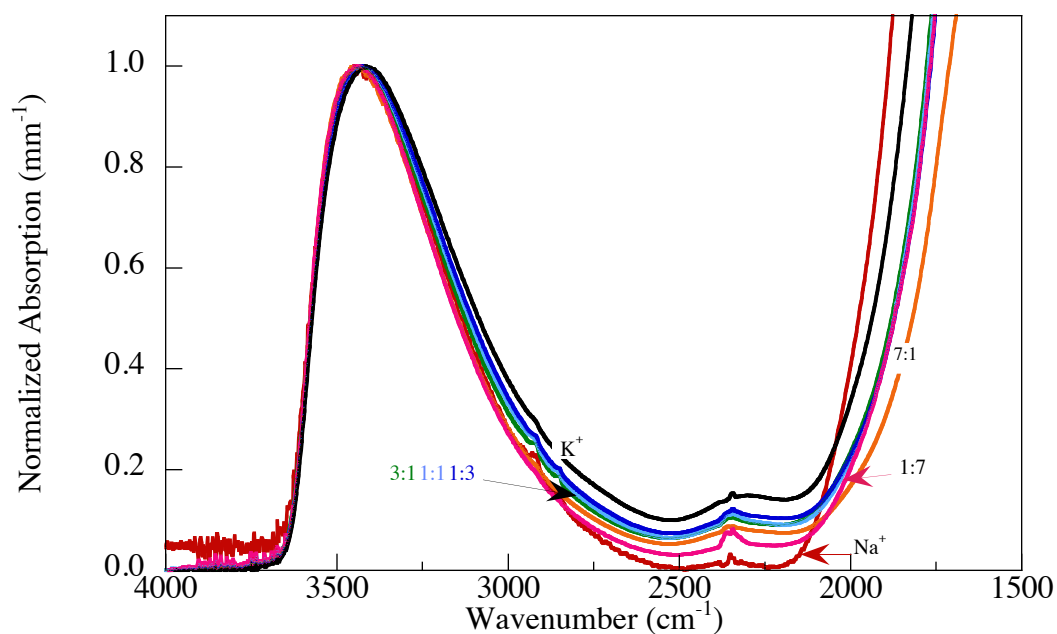


Figure 5-9. Normalized infrared spectra for $x \text{Na}_2\text{O} \cdot (10-x) \text{K}_2\text{O} \cdot 90 \text{GeO}_2$ glasses. Labels are the ratio of $\text{Na}^+:\text{K}^+$.

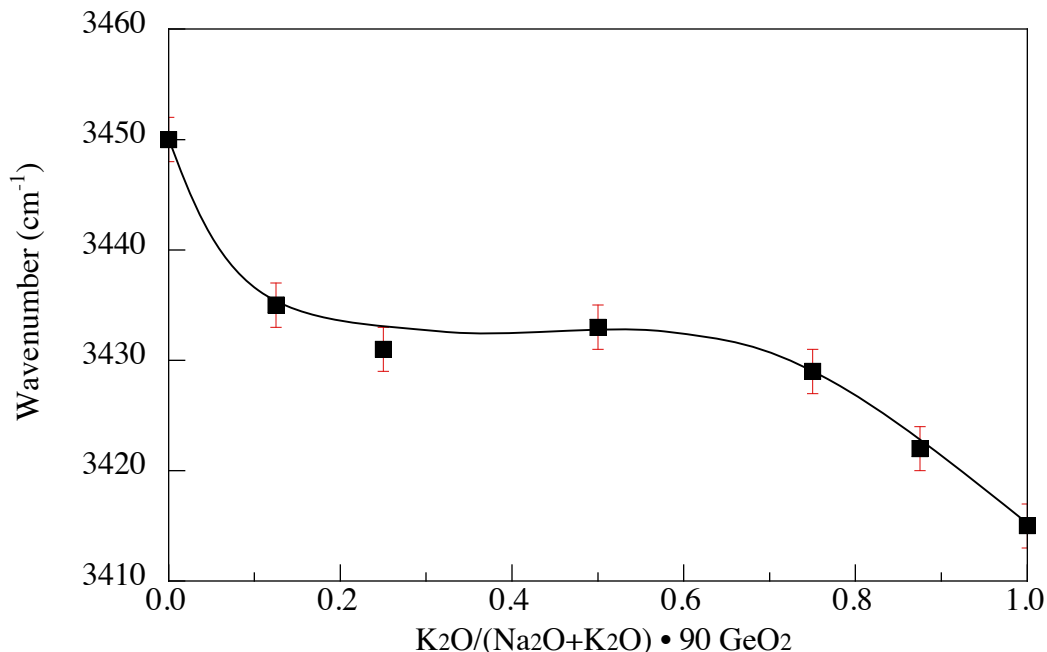


Figure 5-10. Peak position of Band I in the infrared spectra for x Na₂O•(10- x) K₂O•90 GeO₂ glasses. Line drawn to aid the eye.

Increasing the amount of alkali in the Na₂O•K₂O•GeO₂ glasses from 10 to 15 mol % results in an increase in intensity of Bands II and III in the infrared spectra. Spectra for x Na₂O•(15- x) K₂O• 85 GeO₂ glasses are shown in Figure 5-11. Binary K₂O•GeO₂ glasses and glasses with a 1:7 ratio of Na₂O:K₂O exhibit obvious Bands II and III. Figure 5-12 shows the normalized infrared spectra for x Na₂O•(15- x) K₂O•85 GeO₂ glasses. Band I shifts from 3400 cm⁻¹ for the binary 15 Na₂O•85 GeO₂ glasses to 3360 cm⁻¹ for binary 15 K₂O•85 GeO₂ glasses, Figure 5-13. Glasses with a ratio of 1:3 Na₂O:K₂O absorb at the highest wavenumbers (3455 cm⁻¹), while glasses with a ratio of 1:7 Na₂O:K₂O absorb at the lowest wavenumbers (3330 cm⁻¹). Band III is significantly affected by the alkali identity and ratio; it is more defined for the 15 K₂O•85 GeO₂ glasses than the 10 K₂O•90 GeO₂ glasses, however the absorption of Band II is strongest for the glasses with a ratio of 1:7 Na₂O:K₂O. Glasses with a ratios of 1:1 and 1:3 Na₂O:K₂O show spectra with minimal Band III's. Binary 15 Na₂O•85 GeO₂ glasses and glasses with more sodium than potassium all have similar absorptions for Band III.

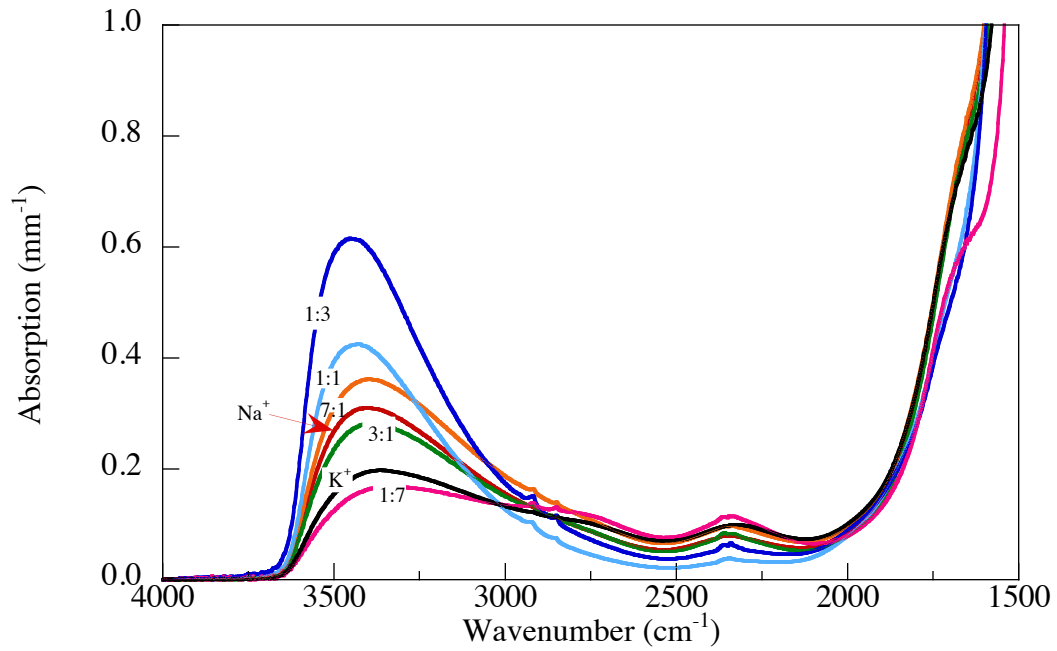


Figure 5-11. Infrared spectra for $x \text{Na}_2\text{O} \cdot (15-x) \text{K}_2\text{O} \cdot 85 \text{GeO}_2$ glasses. Labels are the ratio of $\text{Na}^+:\text{K}^+$.

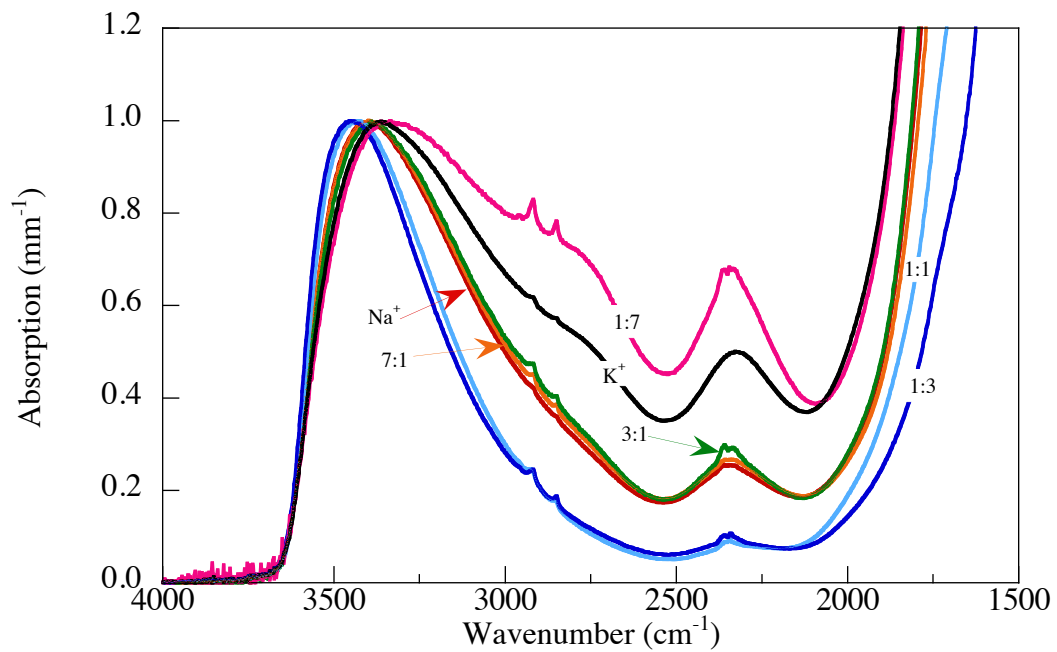


Figure 5-12. Normalized infrared spectra for $x \text{Na}_2\text{O} \cdot (15-x) \text{K}_2\text{O} \cdot 85 \text{GeO}_2$ glasses. Labels are the ratio of $\text{Na}^+:\text{K}^+$.

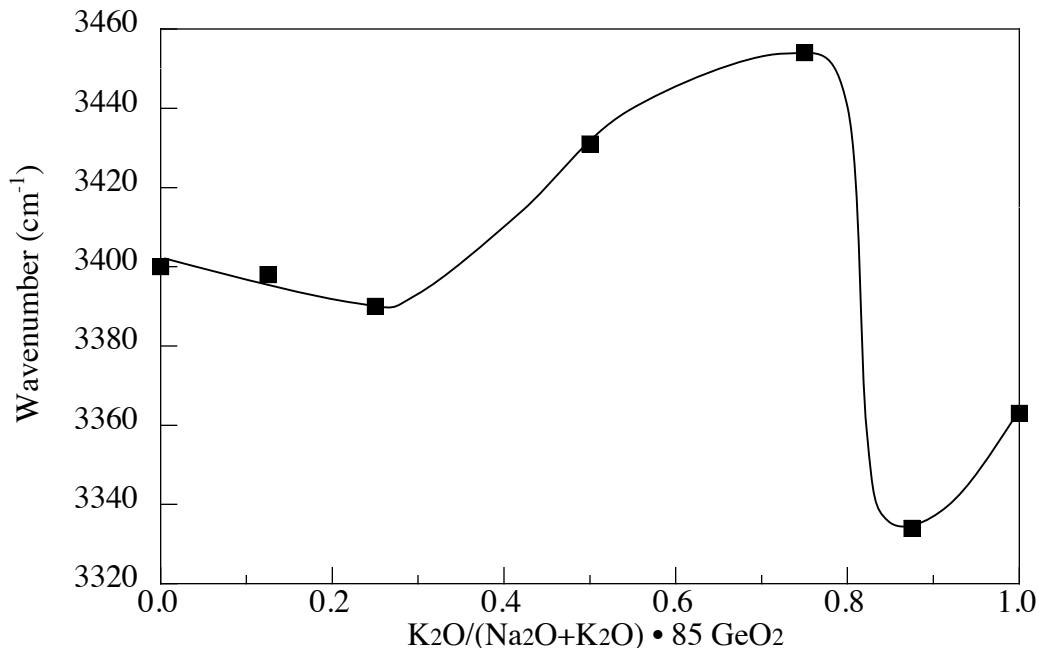


Figure 5-13. Position of Band I in the infrared spectra for $x \text{ Na}_2\text{O} \cdot (15-x) \text{ K}_2\text{O} \cdot 85 \text{ GeO}_2$ glasses. Line drawn to aid the eye, error bars smaller than data points.

5.4.2 Germanate Anomaly

Infrared spectra for $0.5x \text{ Li}_2\text{O} \cdot 0.5x \text{ Cs}_2\text{O} \cdot (100-x) \text{ GeO}_2$ and $0.5x \text{ Na}_2\text{O} \cdot 0.5x \text{ K}_2\text{O} \cdot (100-x) \text{ GeO}_2$ glasses are shown in Figures 5-14 and 5-15, respectively. The normalized spectra are shown in Figures 5-16 and 5-17 for $0.5x \text{ Li}_2\text{O} \cdot 0.5x \text{ Cs}_2\text{O} \cdot (100-x) \text{ GeO}_2$ and $0.5x \text{ Na}_2\text{O} \cdot 0.5x \text{ K}_2\text{O} \cdot (100-x) \text{ GeO}_2$ glasses, respectively. The infrared spectra of $0.5x \text{ Li}_2\text{O} \cdot 0.5x \text{ Cs}_2\text{O} \cdot (100-x) \text{ GeO}_2$ glasses with ≤ 10 mol % alkali exhibit only Bands I and I'. When the amount of alkali in the $0.5x \text{ Li}_2\text{O} \cdot 0.5x \text{ Cs}_2\text{O} \cdot (100-x) \text{ GeO}_2$ glasses is ≥ 15 mol %, Band II and III are present in the spectra. Infrared spectra for the $0.5x \text{ Na}_2\text{O} \cdot 0.5x \text{ K}_2\text{O} \cdot (100-x) \text{ GeO}_2$ glasses are similar to the $0.5x \text{ Li}_2\text{O} \cdot 0.5x \text{ Cs}_2\text{O} \cdot (100-x) \text{ GeO}_2$ glasses, however Bands II and III are not present until at least 17 mol % alkali is added. In both systems, the effect of alkali addition in the region near the multi-phonon edge is obvious, and is independent of the identity of the cations. When small amounts of alkali are added, ≤ 1 mol % alkali oxide, two bands appear at frequencies $< 2000 \text{ cm}^{-1}$. As the amount of alkali in the glass increases, these bands disappear into the multi-phonon edge which gradually moves to longer wavenumbers. The shift in the peak position at 3500 cm^{-1} is also independent of cation identity, as is shown in Figure 5-18.

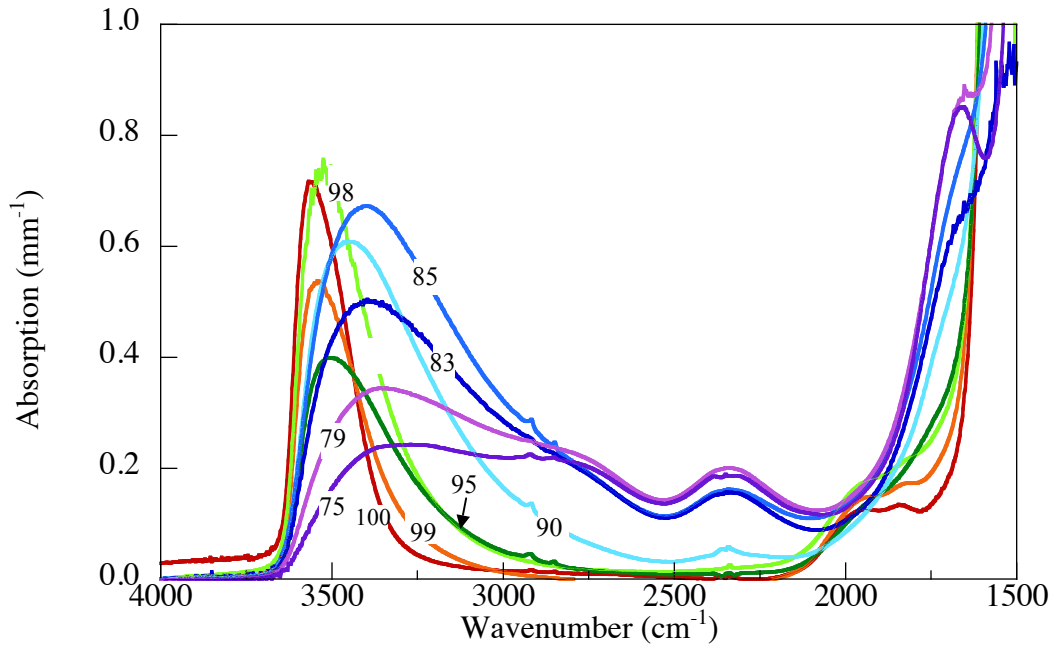


Figure 5-14. Infrared spectra for $0.5x \text{Li}_2\text{O} \cdot 0.5x \text{Cs}_2\text{O} \cdot (100-x) \text{GeO}_2$ glasses.

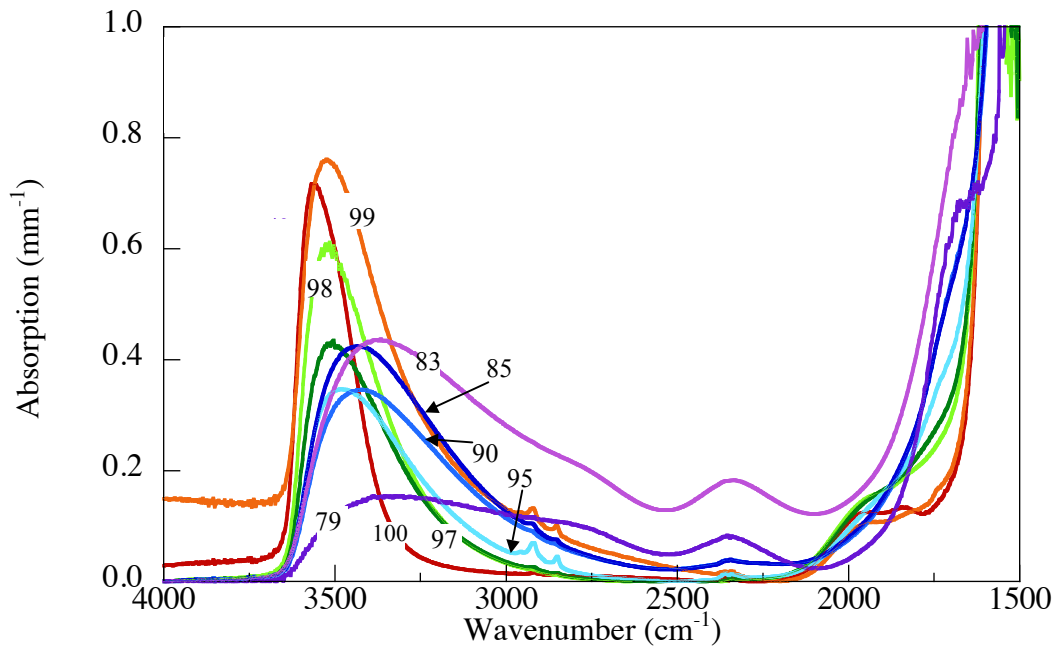


Figure 5-15. Infrared spectra for $0.5x \text{Na}_2\text{O} \cdot 0.5x \text{K}_2\text{O} \cdot (100-x) \text{GeO}_2$ glasses.

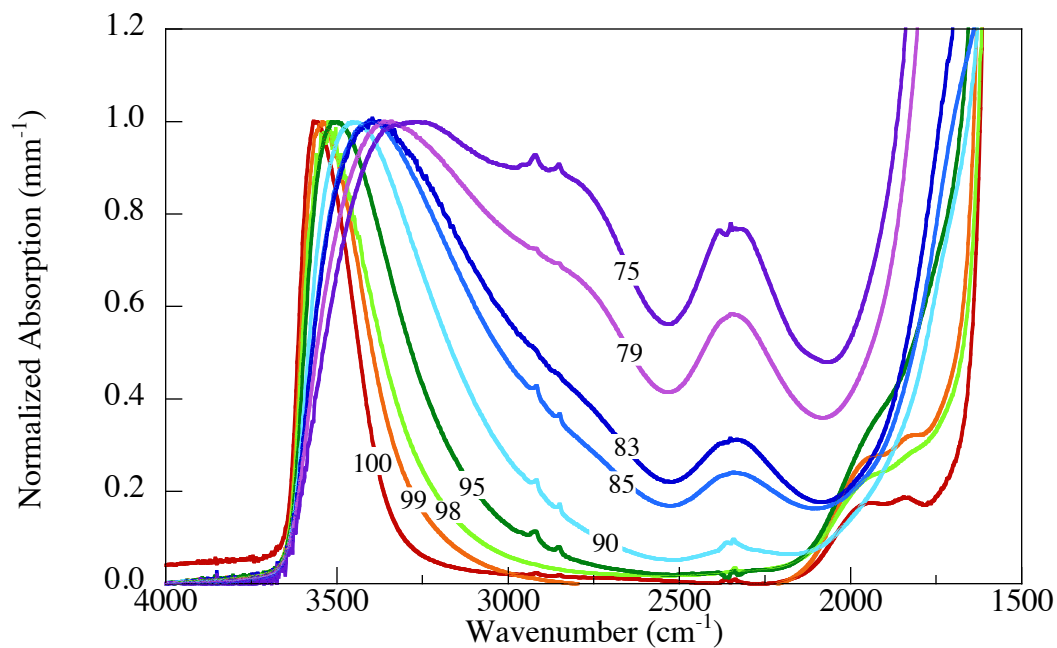


Figure 5-16. Normalized infrared spectra for $0.5x \text{Li}_2\text{O} \cdot 0.5x \text{Cs}_2\text{O} \cdot (100-x) \text{GeO}_2$ glasses.

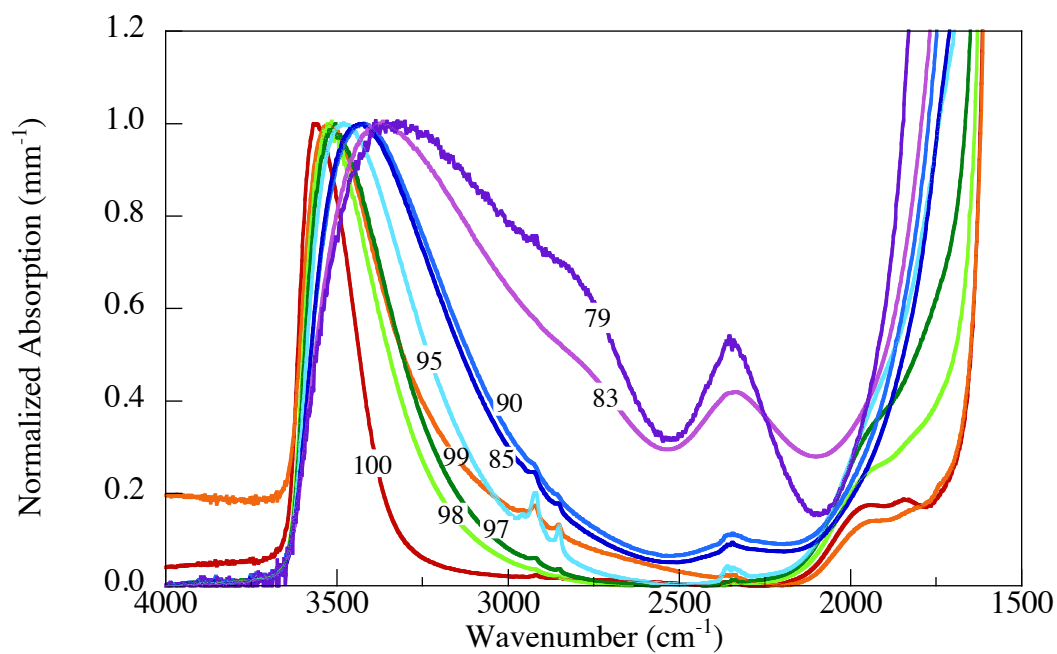


Figure 5-17. Normalized infrared spectra for $0.5x \text{Na}_2\text{O} \cdot 0.5x \text{K}_2\text{O} \cdot (100-x) \text{GeO}_2$ glasses.

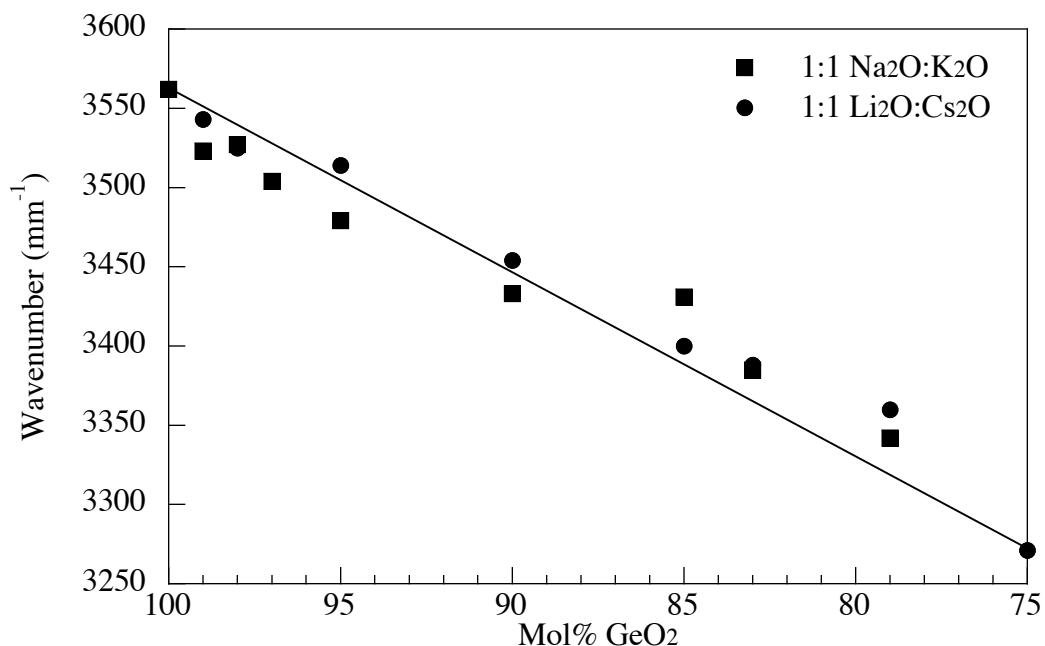


Figure 5-18. Position of Band I in the infrared spectra for $0.5x R_2O \cdot 0.5x R'_2O \cdot (100-x) GeO_2$ glasses. Line drawn to aid the eye, error bars generated from the accuracy of the instrument are smaller than data points.

5.5 Discussion

The infrared spectra will first be discussed with regard to cation identity, followed by alkali concentration, and finally band identification. The identity of the cation affects two areas of the infrared spectra. Figures 5-19 and 5-20 show a comparison between the two different cation pairs at 90 and 85 mol % GeO_2 , respectively. Glasses with Li_2O and Cs_2O behave similarly, with the position of Band I maximizing when Li_2O and Cs_2O are in a ratio of 3:1. The non-systematic shifting of the $Na_2O \cdot K_2O \cdot 85 GeO_2$ Band I could be a result of possible crystallite formation, resulting from the composition being near the edge of the glass forming region of the ternary system. Figure 5-21 shows the band position for the $Li_2O \cdot Cs_2O \cdot GeO_2$ glasses along the 90 and 85 mol % GeO_2 tie lines. The position of Band I in glasses containing Na_2O and K_2O vary over a large range of wavenumbers (Figure 5-22). Cation identity affects when the Bands II and III begin to appear in the spectra. In $Li_2O \cdot Cs_2O \cdot GeO_2$ glasses, Bands II and III are a major aspect of the infrared spectra in glasses with as little as 15 mol % alkali oxide. However, in the $Na_2O \cdot K_2O \cdot GeO_2$ glasses, these bands do not evolve until at least 17 mol % alkali.

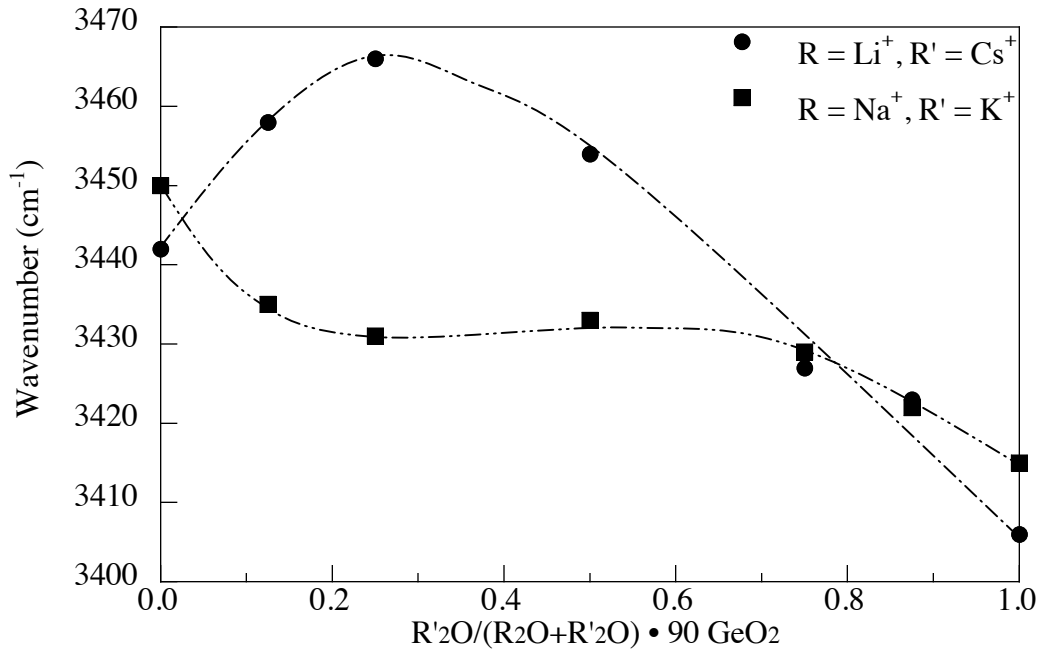


Figure 5-19. Position of Band I in the infrared spectra for $x \text{ R}_2\text{O} \cdot (10-x) \text{ R}'_2\text{O} \cdot 90 \text{ GeO}_2$ glasses. Line drawn to aid the eye, error bars smaller than data points.

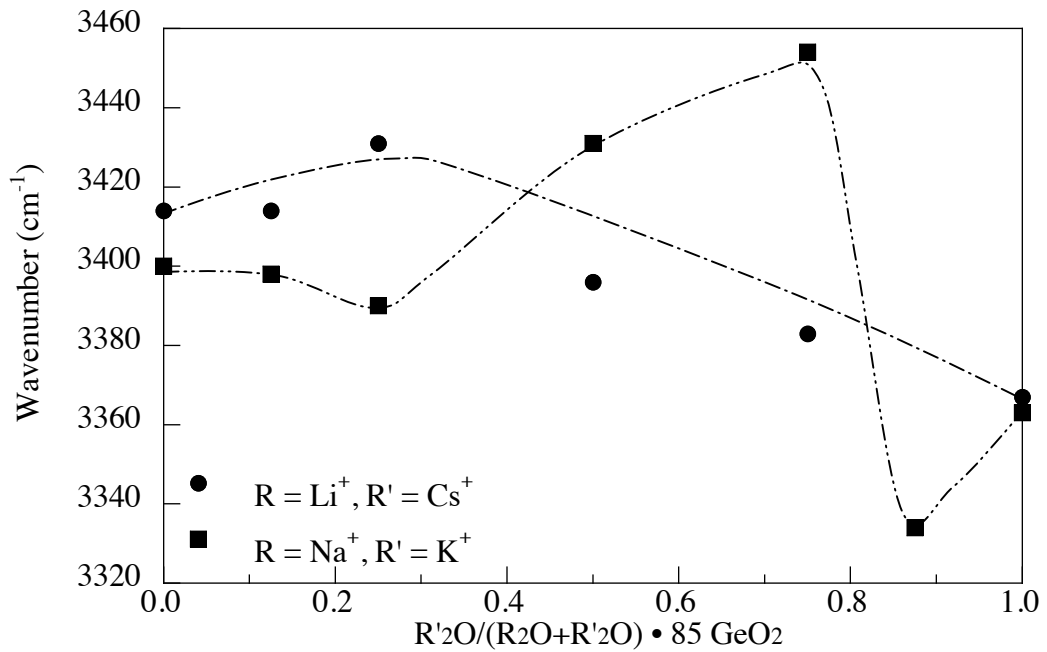


Figure 5-20. Position of Peak I in the infrared spectra for $x \text{ R}_2\text{O} \cdot (15-x) \text{ R}'_2\text{O} \cdot 85 \text{ GeO}_2$ glasses. Line drawn to aid the eye, error bars smaller than data points.

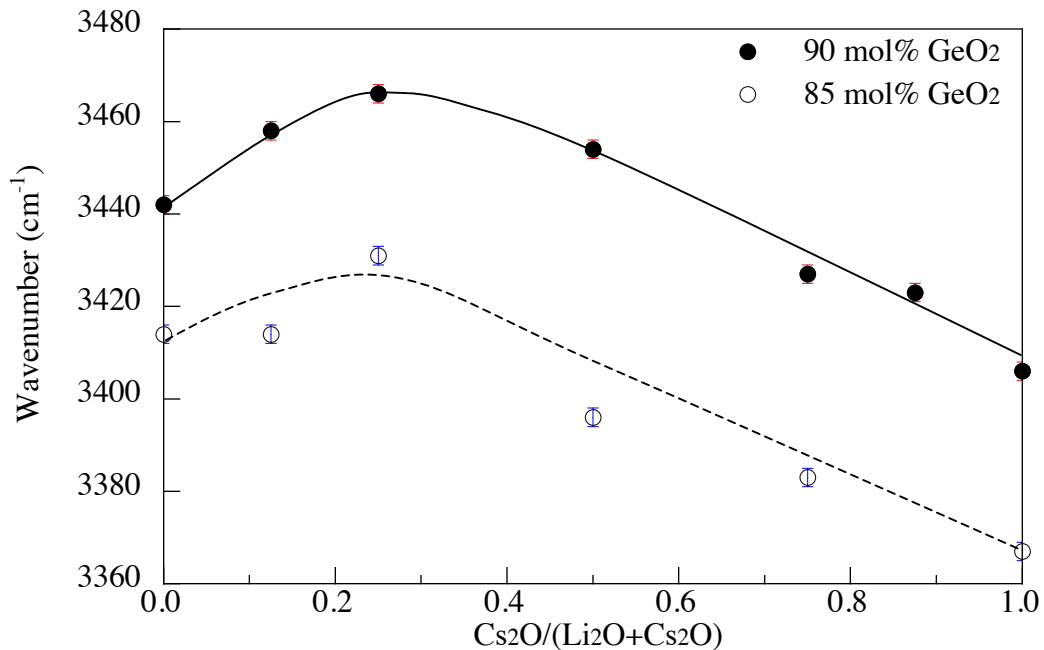


Figure 5-21. Position of Band I in the infrared spectra for $x \text{Li}_2\text{O} \cdot y \cdot x \text{Cs}_2\text{O} \cdot (100-x-y) \text{GeO}_2$ glasses, where $y = 10$ or 15 . Lines drawn to aid the eye.

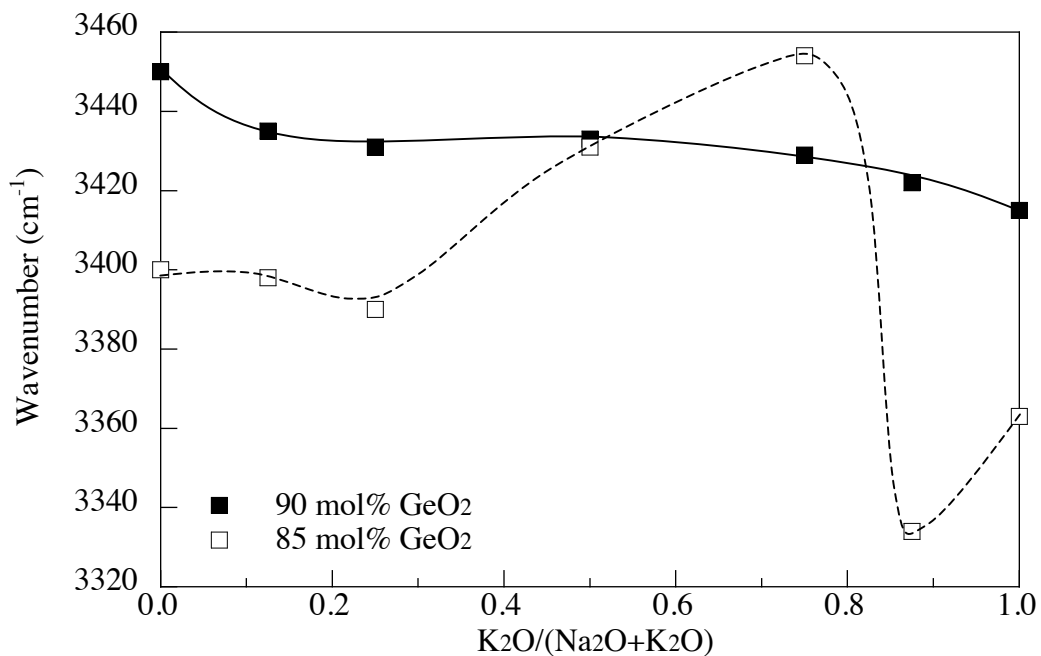


Figure 5-22. Position of Band I in the infrared spectra for $x \text{Na}_2\text{O} \cdot y \cdot x \text{K}_2\text{O} \cdot (100-x-y) \text{GeO}_2$ glasses, where $y = 10$ or 15 . Lines drawn to aid the eye, error bars smaller than data points.

Currently, the infrared spectra bands of the germanate glasses in the range of 4000 to 1500 cm^{-1} have been assigned by analogy with the band position of silicate glasses. An experiment was performed in order to confirm that these bands are actually a result of the presence of water in the glass and not a result of the glass structure. The glass with the most pronounced bands ($8.5 \text{ Li}_2\text{O} \cdot 8.5 \text{ Cs}_2\text{O} \cdot 83 \text{ GeO}_2$) was melted following the experimental procedures in section 5.3. The results of this experiment are shown in Figure 5-23. It is obvious from the spectra that Bands I, I', II and III are a result of water in the glass, because they increase when the amount of water in the glass is increased. Figure 5-24 shows the normalized infrared spectra by dividing by the sample thickness. The peaks lie exactly on top of one another, revealing that bands in each of the spectra are a due to the same mechanism. An interesting effect of the water treatment on the infrared spectra of the glass is found in the shifting of the multi-phonon edge to lower wavenumber, resulting in a clearly defined shoulder band, which is an overtone of the structural bands.⁹

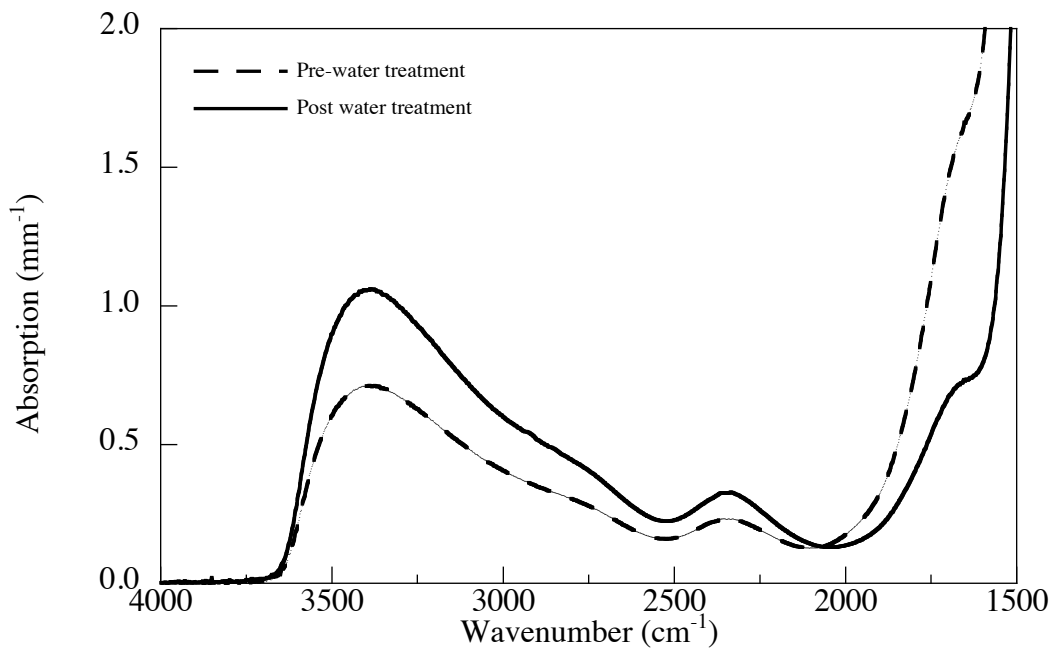


Figure 5-23. Infrared spectra for $8.5 \text{ Li}_2\text{O} \cdot 8.5 \text{ Cs}_2\text{O} \cdot 83 \text{ GeO}_2$ glasses prior and following treatment in a water furnace.

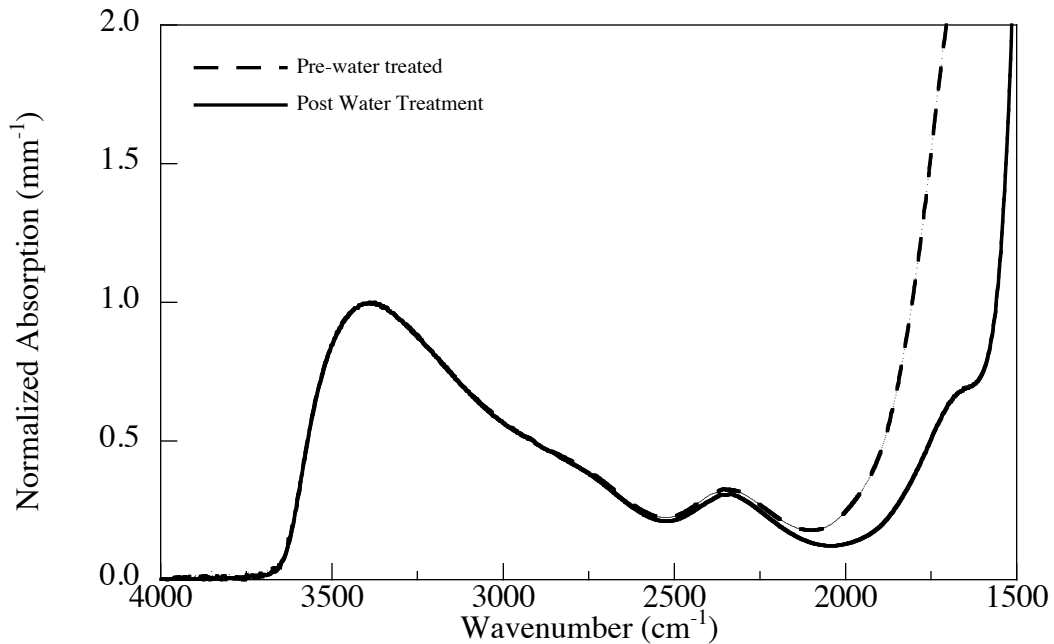


Figure 5-24. Normalized infrared spectra for 8.5 $\text{Li}_2\text{O}\cdot 8.5 \text{Cs}_2\text{O}\cdot 83 \text{GeO}_2$ glasses prior and following treatment in a water furnace.

5.6 Conclusion

Mixed alkali germanate glasses have similar infrared spectra curves to silicate glasses. This study confirms that the bands at approximately 3600 cm^{-1} , 3300 cm^{-1} , 2800 cm^{-1} and 2350 cm^{-1} are a result of water in the glasses. It is believed that these bands result from similar mechanisms as in silicate glasses. The band at 3400 cm^{-1} is attributed to Ge-OH interacting weakly with bridging oxygen. When the alkali concentration is between 1 and 90 mol %, the band shifts toward 3400 cm^{-1} due to growth of a Band I' at 3300 cm^{-1} resulting from the Ge-OH interacting weakly with bridging oxygen associated with five-fold coordinated germania. The development of the Bands II and III, at about 2800 and 2350 cm^{-1} , are a direct result of non-bridging oxygen formation. The band near the multi-phonon edge is an overtone of a low frequency structural band.

5.7 References

1. D. Di Martino, L.F. Santos, A.C. Marques, and R.M. Almeida, "Vibrational Spectra and Structure of Alkali Germanate Glasses," *J. Non-Cryst. Solids*, **293-295** 394-401 (2001).

2. A.M. Efimov, "Infrared Spectra, Band Frequencies and Structure of Sodium Germanate Glasses," *Phys. Chem. Glasses*, **40** [4] 199-206 (1999).
3. T. Furukawa and W.B. White, "Raman Spectroscopic Investigation of the Structure and Crystallization of Binary Alkali Germanate Glasses," *J. Mater. Sci.*, **15** [7] 1648-62 (1980).
4. M.M. Hall and J.E. Shelby, "Water Diffusion and Solubility in Alkali Germanate Melts," *Phys. Chem. Glasses*, **45** [4] 283-90 (2004).
5. G.S. Henderson, "The Germanate Anomaly: What Do We Know?," *J. Non-Cryst. Solids*, **353** [18-21] 1695-704 (2007).
6. G.S. Henderson and M.E. Fleet, "The Structure of Glass Along the Na₂O-GeO₂ Join," *J. Non-Cryst. Solids*, **134** [3] 259-69 (1991).
7. G.S. Henderson and H.M. Wang, "Germanium Coordination and the Germanate Anomaly," *Eur. J. Mineral.*, **14** [4] 733-44 (2002).
8. H. Hosono and Y. Abe, "Temperature Dependence of Infrared Absorption Spectra of Hydroxyl Groups in Soda Germanate Glasses," *J. Am. Ceram. Soc.*, **72** [1] 44-8 (1989).
9. E.I. Kamitsos, Y.D. Yiannopoulos, C.P.E. Varsamis, and H. Jain, "Structure-Property Correlation in Glasses by Infrared Reflectance Spectroscopy," *J. Non-Cryst. Solids*, **222** [1] 59-68 (1997).
10. N. Mochida, K. Sakai, and K. Kikuchi, "Raman Spectroscopic Study of the Structure of the Binary Alkali Germanate Glasses," *Yogyo Kyokaishi*, **92** [4] 164-72 (1984).
11. M.K. Murthy and E.M. Kirby, "Infra-Red Spectra of Alkali-Germanate Glasses," *Phys. Chem. Glasses*, **5** [5] 144-6 (1964).
12. L.G. Soltay and G.S. Henderson, "Structural Differences between Lithium Silicate and Lithium Germanate Glasses by Raman Spectroscopy," *Phys. Chem. Glasses*, **46** [4] 381-4 (2005).
13. H. Verweij and J.H.J.M. Buster, "The Structure of Lithium, Sodium and Potassium Germanate Glasses, Studied by Raman Scattering " *J. Non-Cryst. Solids*, **34** [1] 81-99 (1979).
14. H.M. Wang and G.S. Henderson, "The Germanate Anomaly: Is the Presence of Five- or Six-Fold Ge Important?," *Phys. Chem. Glasses*, **46** [4] 337-80 (2005).

15. B. Bendow, "Infrared and Raman Spectroscopy of Glass," pp. 33-79 in *Experimental Techniques of Glass Science*. Edited by C. J. Simmons and O. H. El-Bayoumi. American Ceramic Society, Westerville, OH, 1993.

CHAPTER 6: ELECTRICAL CONDUCTIVITY

6.1 Introduction

Most inorganic glasses are ionic conductors. As the temperature of a glass increases, the ions in the glass have enhanced mobility. Applying an electric field to the glass causes movement of these cations. Understanding the way charge moves through a glass can be very useful for determining the structure of the glass. For example, a glass with an open network and/or small ions (such as Li^+) will allow cations to move easily throughout the network, resulting in a higher electrical conductivity. Mixing two types of mobile ions results in a decrease in the electrical conductivity; this phenomena is called the mixed alkali, or mixed mobile ion effect.

This chapter reports two studies designed to increase our understanding of the mixed alkali effect and electrical conductivity behavior of alkali germanate glasses. The first study presented in this chapter involves a series of DC electrical conductivity measurements performed on two of the mixed alkali ternary systems, $\text{Li}_2\text{O}\cdot\text{Cs}_2\text{O}\cdot\text{GeO}_2$ and $\text{Na}_2\text{O}\cdot\text{K}_2\text{O}\cdot\text{GeO}_2$. The study examines the effect of mixing two different alkali ions on the electrical conductivity. Germania concentration was held constant at two different values, 90 and 85 mol %, while the alkali ions were added in differing ratios across this tie line. These two amounts of germania are structurally significant. Glasses containing 90 mol% GeO_2 are thought to contain two different coordination states of germanium, while the 85 mol% tie line is important because this is approximately where the system begins to lose connectivity, due to the formation of non-bridging oxygen, and begins to behave more like silicate glasses.

The second study examines the three alkali oxide germanate ternary systems $\text{Li}_2\text{O}\cdot\text{Cs}_2\text{O}\cdot\text{GeO}_2$, $\text{Na}_2\text{O}\cdot\text{K}_2\text{O}\cdot\text{GeO}_2$, and $\text{K}_2\text{O}\cdot\text{Rb}_2\text{O}\cdot\text{GeO}_2$. The size difference between the alkali ions is greatest for the $\text{Li}_2\text{O}\cdot\text{Cs}_2\text{O}\cdot\text{GeO}_2$ glasses, and is least for the $\text{K}_2\text{O}\cdot\text{Rb}_2\text{O}\cdot\text{GeO}_2$ glasses. The alkali oxides contents were held constant in a ratio of 1:1, while the GeO_2 concentration was varied from 100 to 70 mol % to examine the effect of cation identity on the electrical conductivity. Two additional tie lines are examined in the $\text{Li}_2\text{O}\cdot\text{Cs}_2\text{O}\cdot\text{GeO}_2$ system to study the influence of the mixed alkali effect on the germanate anomaly.

6.2 Literature Review

The literature review in this chapter includes a review of ionic conductivity in glasses, where the basic mechanisms will be discussed, along with brief summaries of some of the most relevant theories on ionic conductivity in glasses. Following the review of ionic conductivity, there is a brief discussion of the mixed mobile ion effect in the context of ionic conductivity. Since the mixed mobile ion effect is closely related to ionic mobility, this material is presented in Chapter 2, where the mixed mobile ion effect is reviewed—please refer to Chapter 2 for more detail on this subject. The final section of the literature review summarizes previous electrical conductivity studies on alkali germanate glasses.

6.2.1 Ionic Conductivity in Glasses

An enormous amount of work has been performed on ionic conductivity in glasses.¹⁻⁵⁸ In oxide glasses (SiO_2 , B_2O_3 , GeO_2 and most P_2O_5 glasses), electrical conduction is a result of the migration of cations through the glass structure, i.e. ionic conduction is directly linked to the mobility of ions in the network. Alkali ions are among the most mobile ions in glasses. The smaller alkali ions, lithium and sodium, are highly mobile. The larger ions, potassium, rubidium and cesium, yield low electrical conductivities compared to the smaller alkali ions. The Shannon and Prewitt radii of these ions are listed in Table 6-I, and shown in Figure 6-1. Three mechanisms for ion transport have been proposed and will be discussed in this section: classical methods, weak electrolyte theory, and the defect hypotheses. The contemporary work of Ngai and Funke are discussed in Chapter 2, and will only be mentioned briefly here.

Table 6-I. Cation Ratios, Radius Values Taken from Shannon and Prewitt

Cation	Coordination Number*	Radius (pm)
Li^+	4 – 6	66.5
Na^+	6	102
K^+	6-8	145
Rb^+	6-8	155
Cs^+	6	170

*If more than one coordination number, and average of the lengths was used

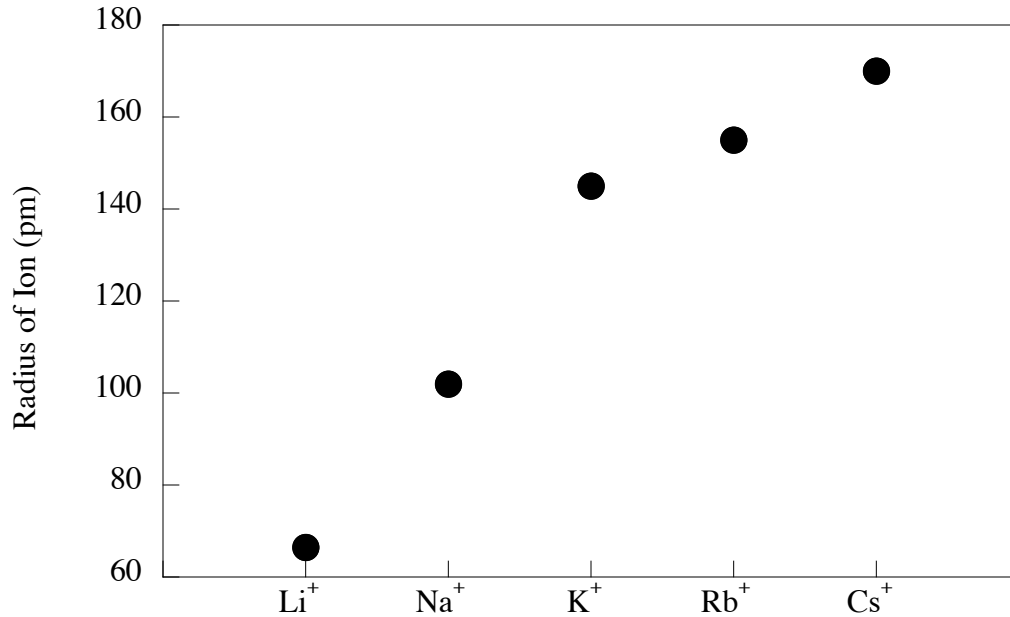


Figure 6-1. Shannon and Prewitt ionic radii of alkali ions.

6.2.1.1 Classical Model

Anderson and Stuart proposed the foundational work on ionic conductivity of glasses in 1954.³ Their approach is based on classical ionic crystal and elastic theories. They make two important assumptions. First, the ions move independently of one another, and second, there are a large number of empty sites through which the mobile ions can move. The calculations of Anderson and Stuart are based a single model for the activation energy for the cation to migrate through alkali silicate glasses. The basic bonding of glasses is assumed to be covalent for the network components (SiO₂, B₂O₃, GeO₂, etc.), while the bonding of the network modifier (Na⁺, K⁺, Ca⁺⁺, etc.) to the structure is ionic. Since ionic bonds are much weaker than covalent bonds, the modifying ions can be removed from these sites in the structure at relatively low temperatures and can migrate, leading to ionic conductivity in glasses. As the temperature of the glass increases, conductivity increases. At temperatures above T_g, the network ions can also break free and contribute to the conductivity.³

To calculate ionic conductivity in glasses, Anderson and Stuart³ first assume that the amount of strain energy generated in a glassy network resulting from the enlargement of a doorway to radius, r_D , to allow an ion of radius, r , to pass, is approximated by the

elastic energy required to dilate a spherical cavity from radius r to radius r_D . They begin with Frenkel's equation describing the total energy for dilation in a liquid

$$E_s = 8\pi Gr_D(r - r_D)^2, \quad (6-1)$$

where E_s is the strain energy, G is the shear energy, r_D is the radius of the doorway and r is the radius of the migrating ion. Anderson and Stuart³ propose a modification of the factor 8π to 4π to compensate for the difference between the denser packing of a close-packed liquid and the more open structure of a glass. Frankel's equation (6-1) becomes

$$E_s = 4\pi Gr_D(r - r_D)^2. \quad (6-2)$$

McElfresh and Howitt⁶⁰ later proposed that the geometry of Equation 6-2 be adjusted to treat the doorway as a short cylinder, or

$$E_s = \frac{\pi G(r - r_D)^2 l}{2}, \quad (6-3)$$

where l is the jump distance.

After considering the total strain energy (E_s) caused by moving an ion through the glass network, one must also consider the amount of energy required to break the bond between the ion and the neighboring non-bridging oxygen. Anderson and Stuart³ begin with ionic crystal theory, where the chemical binding energy consist of four terms,

$$E_b = E_c + E_r + E_p + E_v, \quad (6-4)$$

E_b , E_c , E_r , E_p , and E_v , are the energies of binding, coulombic, repulsive, polarization and van der Waal, respectively. The E_v term is zero for all ions having a dipole moment equal to zero, and E_p is negligible compared to the other energy terms. If the net forces are required to balance to zero, then the interatomic spacing is equal to the radius sum. Using ionic crystal theory, E_c is proportional to $(r + r_0)^{-1}$ and E_r is proportional to $(r + r_0)^{-m}$, where Anderson and Stuart state m is equal to about 9 or 10, and r_0 is equal to the radius of the O^{2-} ion. Using these assumptions, Equation 6-4 becomes

$$E_b = -(1 - 1/m)E_c. \quad (6-5)$$

Performing a series of mathematical manipulations to Equation (6-5) results in the following approximation for the electrostatic potential,

$$\Delta E_b \approx \frac{zz_0 e^2}{(r + r_0)} - \frac{zz_0 e^2}{\lambda/2}. \quad (6-6)$$

Assuming a jump distance equal to the lattice constant (λ) for cristobalite, $\lambda = 7$ a.u., neglecting the small and rapidly changing repulsive potential, and applying Pauling's value for the radius of oxygen ($r_0 = 1.4$ a.u.) results in

$$\Delta E_b \approx -\beta E_b. \quad (6-7)$$

where β is the finite displacement factor and equal to $\frac{2.1-r}{3.5}$; therefore, for silicate glasses the change in the binding energy can be written as

$$\Delta E_b = -\frac{\beta}{\gamma} E_b, \quad (6-8)$$

where γ accounts for the deformability of the oxygen atom.[◇]

Anderson and Stuart's theory thus reduces to

$$E_A = E_b + E_s, \quad (6-9)$$

where E_A is the total energy required to move an ion through the system. Ingram²² summarizes their work concisely, saying the total amount of energy required for ionic migration is the sum of energy required to overcome the electrostatic forces, combined with the amount of energy required to open up 'doorways' in the structure large enough for the ions to pass. Figure 6-2 illustrates the potential wells that must be overcome by the mobile ion to move from its original site to the next.^{22,33}

—

[◇] Anderson and Stuart note that the value of γ is determined by experiment and always found to be equal to the dielectric constant.

Figure 6-2. Illustration showing the shear energy and the electrostatic barriers for ionic conduction, taken with permission from Ingram.²²

6.2.1.2 Weak Electrolyte Theory

The weak electrolyte theory expresses ionic conductivity as a product of the concentration of mobile ions and the mobility of the conducting ion,

$$\sigma = n^* z e u \quad (6-10)$$

where σ is the electrical conductivity, n^* is the number of mobile ions per unit volume, z is the charge of the mobile ion, e is the electronic charge, and u is the mobility of the ions.^{22,25} If the mobile ions in a glass, such as Na^+ , were all equally mobile then glasses would behave similar to strong electrolytes, e.g. salt dissolved in water.²⁵ However, since glasses act as weak electrolytes, n^* is less than the stoichiometric concentration of the ions.²² Ravaine and Souquet^{53,54} developed the first model correlating ionic conductivity and the thermodynamic activation energy. Tomozawa^{48,52} later developed an approach using simple Arrhenius theory of electronic dissociation to account for low amounts of alkali oxides. These two different approaches to the weak electrolyte theory in glasses are discussed below.

6.2.1.2.1 Ravaine-Souquet Model

Ravaine and Souquet^{53,54} observed that, when the log of conductivity is plotted versus the log of the activity of the alkali ion, there is a linear relationship. They developed the following empirical relationship,

$$\sigma = \text{const}(a_{\text{Na}_2\text{O}}) \quad (6-11)$$

where σ is the electrical conductivity and $a_{\text{Na}_2\text{O}}$ is the activity of the alkali ion, in this example, sodium. They proposed the following explanation for this behavior. There is an equilibrium state in glass where,



Using conventional thermodynamics, they show that:

$$\mu_{\text{Na}_2\text{O}} = \mu_{\text{Na}_2\text{O}}^o + RT \ln a_{\text{Na}_2\text{O}} \quad (6-13)$$

$$\mu_{\text{Na}_2\text{O}} = \mu_{\text{Na}_2\text{O}}^o + RT \left[\text{Na}^+ \right] \left[\text{ONa}^- \right] \quad (6-14)$$

$$\mu_{\text{Na}_2\text{O}} = \mu_{\text{Na}_2\text{O}}^o + RT \left[\text{Na}^+ \right]^2 \quad (6-15)$$

They assume constant activity coefficients and charge neutrality, and combining Equations 6-11, 6-13, and 6-15, yield,

$$\sigma = \text{const}[M^+]. \quad (6-16)$$

Equation 6-15 is important because it implies that the mobility of the ion is completely dependent upon the concentration of the mobile species and is independent of all other components of the glass composition. Isard applies this theory to the activation energy and, using Equation 6-12, suggests,

$$E_A(\sigma) = \frac{\Delta H}{2} + E_m, \quad (6-17)$$

where, ΔH is the enthalpy of the reaction (Equation 6-12) and E_m is the ‘true’ activation energy. This theory is useful in explaining the atypical (i.e. the non-silicate like behavior) of electrical conductivity such as the mixed alkali effect, the mixed glass former effect, and the increased conductivity in the presence of halides.²²

Martin and Angell³³ compare the Anderson and Stuart model and the weak electrolyte model and suggest that there is very little difference between the two models. Essentially, the Anderson and Stuart model assumes a fixed number of sites with an energy barrier to the exchange of ions between sites and an electrostatic work term, which allows the ion to move through the neighboring ‘doorway’. As the amount of alkali oxide in the system increases, the average site separation decreases, resulting in a decrease in the columbic energy (Equation 6-4), and, as the temperature increases, the amount of work required to move the ion through the ‘doorway’ decreases because the rigidity of the network decreases (Equation 6-3). The weak electrolyte model suggests there are two types of sites, which requires thermal energy to populate high-energy sites. Assuming the simplest case, where the energy required for the ion to pass through the ‘doorway’ is constant (i.e. constant mobility), the effect of composition is to decrease the energy between the mobile and immobile ion sites.

Martin and Angell show that the work of populating the higher energy mobile sites is electrostatic in nature. An energy diagram similar to Figure 6-2 can be drawn for the weak electrolyte model. The major difference is the lack of the ridge in Figure 6-2 caused by the electrostatic energy term (E_s). Martin and Angell state that at higher temperatures, the thermal energy that populates the high energy sites in the weak

electrolyte model also causes the E_b term of the Anderson and Stuart model to increase in energy, and essentially results in one energy barrier instead of two, therefore behaving like the weak electrolyte model.³³

6.2.1.2.2 Tomozawa Theory

Tomozawa^{52,55} approaches the weak electrolyte theory from a different angle than Ravaine and Souguet. His theory begins with the weak electrolyte theory developed for solutions and focuses on electrical conductivity of glasses with small amounts of alkali oxide. Using the simple Arrhenius theory of electrolytic dissociation (K),

$$K = \frac{\alpha^2 c}{1 - \alpha} \cong \alpha^2 c = \left(\frac{\Lambda}{\Lambda_0} \right)^2 c, \quad (6-18)$$

where, α is the fraction of single alkali ions dissociated, c is the molar concentration of single alkali ions (mol cm^{-3}) and Λ is the molar conductivity. Taking logarithms of Equation 6-18 and rearranging results in,

$$\log \Lambda = -\frac{1}{2} \log c + \frac{1}{2} \log(\Lambda_0^2 K). \quad (6-19)$$

If the weak electrolyte theory is applicable in glasses, a plot of Equation 6-19 will have a slope of $-\frac{1}{2}$. Tomozawa shows that the solutions approach to weak electrolyte theory is applicable to glasses when the alkali ions are at low concentrations and/or the temperature of the system is high. The weak electrolyte theory assumes that the mobility of the ion is constant with increasing concentration. Since alkali disrupt the network and increasing the concentration of alkali oxide allows the ions to become more mobile, this theory breaks down for concentrations of alkali oxides greater than 1 mol %.⁶ Imre et al.²⁰ in a series of recent work^{20,21,56-58} applied Tomozawa's weak electrolyte theory and claim that using this theory eliminates the mixed alkali effect in glasses with low concentrations of alkali.

6.2.1.3 Defect Hypotheses

The final theory used to describe electrical conductivity in glasses is the defect hypotheses; this approach begins by looking at ionic conductivity in crystals. There are three types of migration defects discussed in ionic conduction in crystals: vacancies, interstitials and interstitialcies. Vacancies are cations or anions missing from their sites

in the lattice. Interstitials occur when a cation or anion sits on a site that does not usually contain an atom. Interstices and vacancies can move throughout a crystal. When a pair of interstices move simultaneously, this is called interstitialcy (the pair can be called interstitials, interstitial pairs or interstitialcies).²² Two different methods have been established for examining electrical conductivity using defects, the Haven-Verkerk⁶¹ approach, and the Moynihan-Ingram-Lesikar theory.⁶² The defect method provided the initial work for Ngai^{37,63} and Funke,^{64,65} who later developed the theory of ionic diffusion used today (Chapter 2).

6.2.1.3.1 Haven-Verkerk Approach

Since glasses do not have a regularly repeating network, using a defect model can become quite precarious when defining interstitials and vacancies. Haven and Verkerk define interstitial sites as the sites corresponding to an energy level higher than the average energy of the migrating ion. They define a vacancy as an unoccupied site that has the same energy as the average energy of the site occupied by the migrating ion. The Haven-Verkerk⁶¹ approach begins by describing particle A , which has a single charge e , that can jump in a crystal at distance d , with a probability of $\nu \text{ sec}^{-1}$, in each of z directions leading to the diffusion coefficients (D_A) for particle A ,

$$D_A = (z/6)\nu d^2 . \quad (6-20)$$

They address ionic conductivity by calculating σ_A , which is the ionic conductivity contributed by a certain number of A particles per cm^{-3} , N :

$$\sigma_A = \frac{z\nu Ne^2 d^2}{6kT} . \quad (6-21)$$

Using Equations 6-20 and 6-21, the diffusion coefficient for self-diffusion (D_{calc}) can be calculated using the Nernst-Einstein equation,

$$D_{calc} = \frac{\sigma kT}{Ne^2} . \quad (6-22)$$

Haven and Verkerk⁶¹ argue that an interstitial defect cannot occur in a glass. They believe the only defects generated in glasses are the vacancy or an interstitialcy. To account for the non-random distribution of diffusing particles, Haven and Verkerk⁶¹ developed a correlation factor, f , to account for the increased probability that an ion moving forward

in the network will return to its original site instead of continuing its forward migration. This factor is closely related to the random walk diffusion theory,

$$f = 1 + 2 \sum_{j=1}^{\infty} \cos \theta_{i,i+j}, \quad (6-23)$$

where, $\cos \theta_{i,i+j}$ is the average of the cosine of the angle θ between the direction of step number, i of the atom and step number $(i+j)$, following i , of the same atom. This factor is not needed in the ionic conductivity because the increased probability of an ion to jump in one direction is counter balanced by the probability that it will jump in the other direction. Taking this into consideration, they developed the relation,

$$\frac{D_A}{\sigma_A} = \frac{fkT}{Ne^2}. \quad (6-24)$$

This relation can be reduced further to

$$\frac{D_A}{D_{Calc}} = f = H_R. \quad (6-25)$$

The correlation factor has now become known as the Haven ratio (H_R) and is used by Haven and Verkerk to describe the mixture of vacancy and interstitial processes in conductivity.⁶¹ It has also been used to describe many of the phenomena that occur in the electrical conductivity of glasses, such as phase separation and preferential pathways for conduction.²² However, the reproducibility of the measured Haven ratio, within the same composition,⁶⁶ is lacking. As a result, the concept of defect migration is open for further development.

The most notable concept proposed by Haven and Verkerk is the idea that the ions migrate through the glass structure in interstitial pairs. This concept was further developed and supported by Ingram and will be discussed in the following section.²²

6.2.1.3.2 Moynihan-Ingram-Lesikar Theory

Moynihan and Lesikar,⁶⁷ and later Moynihan and Ingram,⁶⁸ approach ionic conductivity in glasses as interstitial defects migrating through the glass network, building on the work of Haven. They show the two major types of defects in the glasses are vacancy and interstitialcies, implying that the ions move through the glass as pairs of alkali ions. Instead of assuming that these interstitials are 'free' with constant mobility

(like in the Ravaine-Souquet model), this theory suggests that an ion's mobility is dependent upon other ions with less mobility acting as 'stepping stones' to migration.

6.2.2 Mixed Mobile Ion Effects on Conductivity

The mixed mobile ion effect is discussed in detail in Chapter 2 and will be discussed only briefly here. Mixing alkali ions results in a negative deviation from additivity for the electrical conductivity and a positive deviation from additivity for the activation energy.^{8,26,69} The greater the difference in size between the alkali ions, the greater the deviation from additivity.^{8,26,69} Figure 6-3 shows a comparison of the radius ratios for all possible alkali pairs. The radii ratio can be divided into 3 groups. Group I has the largest size difference, with alkali ion R' being roughly 2 to 2.5 times larger than the alkali ion R (radii ratios of 2.18 to 2.56). Group II ions have R' approximately 1.5 times larger than the R (radii ratios of 1.42 to 1.67). Group III ions are near the same size, with radii ratios of 1.07 to 1.17. This thesis examines one ternary system from each group, i.e. lithium-cesium-germanate glasses which have the greatest difference between the radii of the alkali, potassium-rubidium-germanate glasses are closest in size, and sodium-potassium-germanate glasses, which are from Group II and are the most studied mixed alkali germanate glasses.

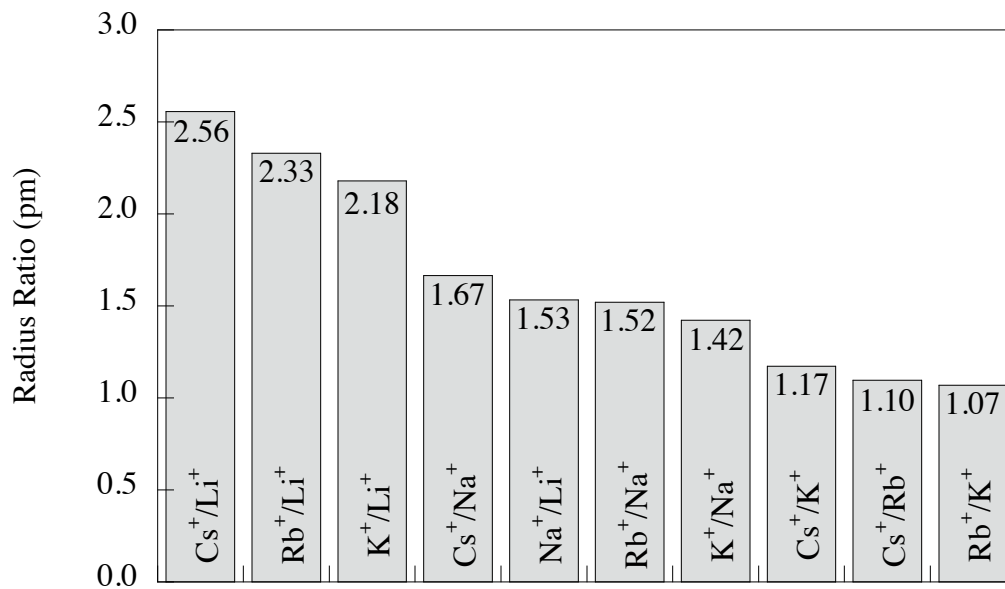


Figure 6-3. Radii ratio for the larger ion to the smaller ion, numerical values shown at top of bar.

6.2.3 Germanate Anomaly

A number of studies examining the electrical conductivity of alkali germanate glasses exist in the literature.^{9,10,17,28-30,43,47,51,58,70-83} The germanate anomaly is obvious in the electrical conductivity behavior of alkali germanate glasses. Larger additions of alkali oxide (~15 mol %) result in electrical conductivities with modest differences due to cation identity. At small additions of alkali oxide, however, the electrical conductivity is very dependent on alkali identity, which is very different from the behavior of silicate glasses. The smaller alkali ions, Li^+ and Na^+ , cause an initial increase in conductivity of 2 to 3 orders of magnitude when as little as 2 mol % alkali oxide is added. Addition of small amounts of the larger ions, K^+ , Rb^+ and Cs^+ , does not increase in conductivity and may actually decrease the electrical conductivity. For more detail on the germanate anomaly, refer to Chapter 2. The relatively small amount of literature on the electrical conductivity of alkali germanate glasses allows a thorough review of the existing work. Only one of these conductivity studies, Ivanov's⁸⁴ study of $x \text{Na}_2\text{O} \cdot y \text{K}_2\text{O} \cdot (100-x-y) \text{GeO}_2$ glasses, directly relates to the primary work reported in this thesis.

This section will discuss the binary alkali germanate glasses, beginning with lithium and following with each progressively larger alkali ion. Ivanov's $x \text{Na}_2\text{O} \cdot y \text{K}_2\text{O} \cdot (100-x-y) \text{GeO}_2$ study will be discussed later in Section 6.5. The data presented are found in the glass literature. In the case of the $\text{Cs}_2\text{O} \cdot \text{GeO}_2$ system the author could not find any study with values for electrical conductivity, so only Shelby's unpublished data are shown.

Three sets of data for the electrical conductivity of $\text{Li}_2\text{O} \cdot \text{GeO}_2$ glasses exist in the literature. Each set shows an initial increase in electrical conductivity of 2 to 3 orders of magnitude, as shown in Figure 6-4. As the amount of Li_2O in the glass increases, the electrical conductivity increases, with exception to the final point by Karnet for 25 mol% Li_2O , where he reported a 2 order of magnitude decrease in conductivity relative to a glass with 7 mol % Li_2O . There is a broad range of electrical conductivities for 100 % GeO_2 in the literature, which range from $6.92 \text{ E-}09$ to $2.04 \text{ E-}10 \text{ S cm}^{-1}$, the figures in this section use the intermediate value of $9.41 \text{ E-}10 \text{ S cm}^{-1}$.

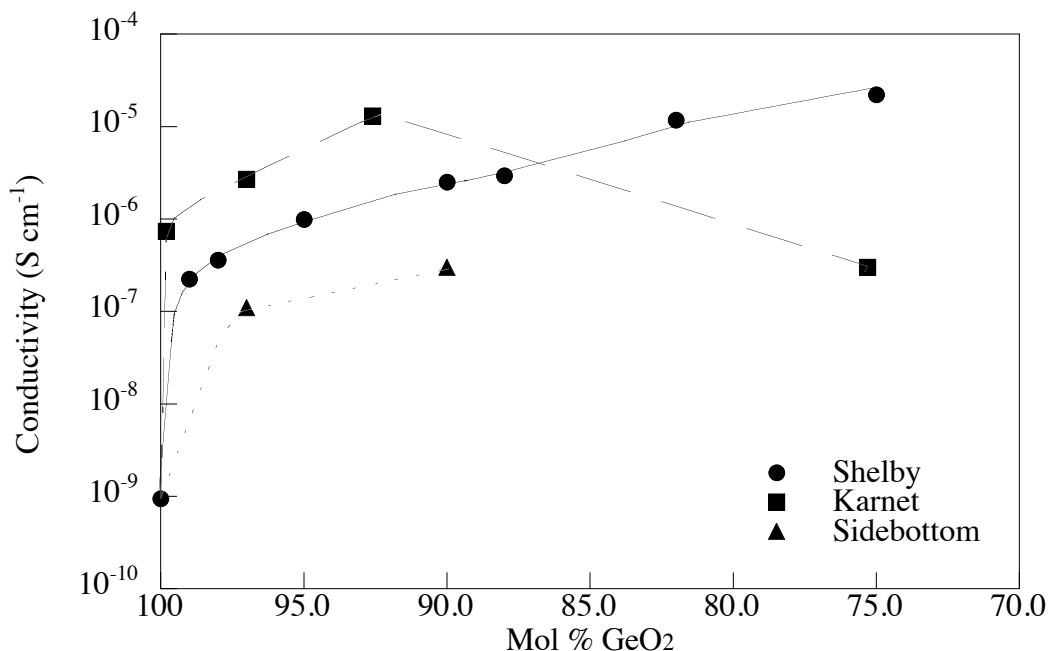


Figure 6-4. Literature values for the DC electrical conductivity, at 300 °C, of $\text{Li}_2\text{O}\cdot\text{GeO}_2$ glasses.

The calculation for error bars for the activation energies is discussed in detail in Section 6.3.3. There is an initial larger decrease in activation energy with a small addition (1-3 mol %) of Li_2O . When the alkali oxide addition is greater than 3 mol % Li_2O , the rate of activation energy decrease with increasing alkali oxide addition slows.

There is no identifiable trend in the value of the pre-exponential factors. Anderson and Stuart³ assume that this pre-exponential is independent of composition. The data shown in Figure 6-6 demonstrate that this is not the case and that the pre-exponential term can vary orders of magnitude with composition. Nowick, Lee and Jain³⁹ suggest that the pre-exponential for most ionic conductors is ≈ 10 and that there are three different regions for the pre-exponential term. The first region is observed when all the charge carriers are free and the pre-exponential is ≈ 10 . The second region occurs when the ions are bound at specific defect sites, and only a small number of ions are free to move, resulting in the number of charge carriers being much lower than the concentration of charge carriers, which results in the pre-exponential being surprisingly low. This mechanism is temperature independent. The third and final category occurs when almost all of the ions are trapped at specific defect sites. Only when the ions are released can they contribute to the electrical conductivity. The number of ions released increases

exponentially with temperature. When these conditions are present, the pre-exponential will be much greater than predicted. For more details refer directly to the work of Nowick, Lee and Jain.³⁹

For the $\text{Li}_2\text{O}\cdot\text{GeO}_2$ system, most pre-exponentials fall within an order of magnitude of the calculated value of ≈ 10 . However, the values from Karnet's work are almost 2 orders of magnitude greater, implying that the charge carriers are moving by a different mechanism than in the other studies.

The literature values for the $\text{Na}_2\text{O}\cdot\text{GeO}_2$ binary glasses are more consistent than those for the glasses in $\text{Li}_2\text{O}\cdot\text{GeO}_2$ binary. Figure 6-7 shows the literature values for the electrical conductivity of $\text{Na}_2\text{O}\cdot\text{GeO}_2$ glasses. With exception of the data from Sidebottom, a few points from Secco, and one value from Ivanov, the data trend similarly. First, the addition of 1 mol% Na_2O causes the conductivity to increase almost two orders of magnitude. With increasing amounts of Na_2O , the electrical conductivity remains almost constant until 10 mol %, after which the electrical conductivity increases linearly with increasing alkali oxide (approximately an order of magnitude for each 5 mol % addition.)

The activation energy for conductivity behaves differently for the $\text{Na}_2\text{O}\cdot\text{GeO}_2$ glasses than for the $\text{Li}_2\text{O}\cdot\text{GeO}_2$ glasses (Figure 6-8). Instead of an initial decrease, the activation energy remains constant until about 10 mol % Na_2O alkali oxide addition, then decreases significantly as the amount of alkali oxide increases. Again, as with the $\text{Li}_2\text{O}\cdot\text{GeO}_2$ glasses there is no clear trend in the pre-exponential values, Figure 6-9. There are a number of random spikes in the pre-exponential factor which are not explained by the authors.

The conductivity of the glasses containing alkali ions the size of potassium or greater initially decreases. Figure 6-10 shows the electrical conductivity for $\text{K}_2\text{O}\cdot\text{GeO}_2$ glasses. In these glasses, the conductivity decreases by 0.5 to 1 order of magnitude when the amount of alkali oxide is less than 15 mol %. A minimum in conductivity occurs at about 6 mol % K_2O . When the amount of K_2O in the glass is 15 to 25 mol %, the conductivity increases rapidly by about 4 orders of magnitude. Additions of K_2O greater than 25 mol % result in only a small additional increase in conductivity.

The activation energy for conductivity behaves as expected when the conductivity decreases. The activation energy for $\text{K}_2\text{O}\cdot\text{GeO}_2$ glasses (Figure 6-11) increases sharply when K_2O is added and remains high until 10 mol % K_2O is added. When the amount of K_2O is greater than 10 mol%, the activation energy decreases linearly with increasing alkali oxide.

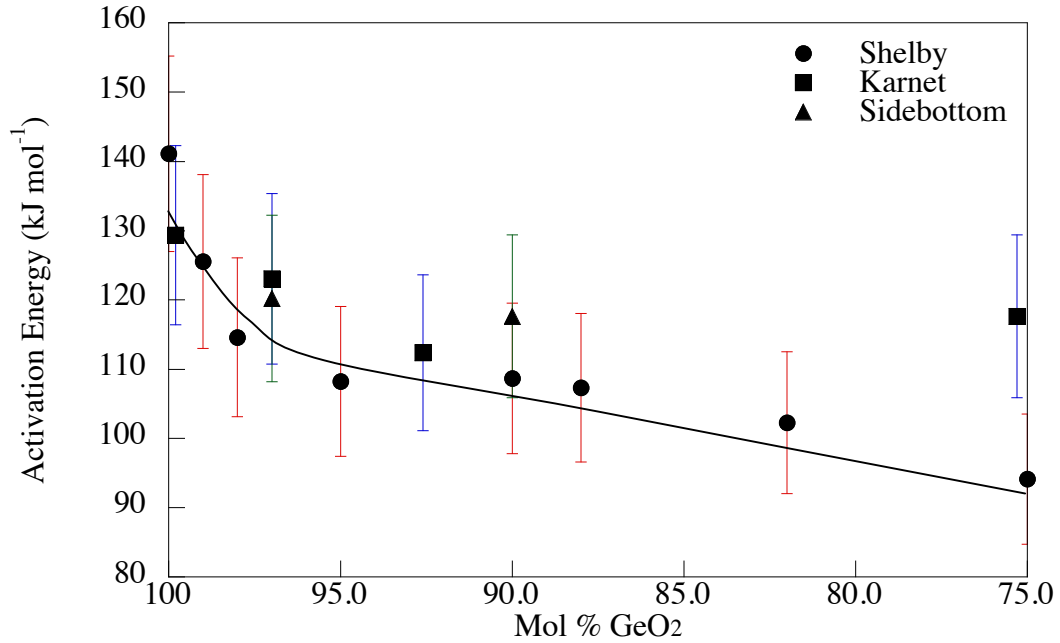


Figure 6-5. Activation energy for DC conductivity of $\text{Li}_2\text{O}\cdot\text{GeO}_2$ glasses.

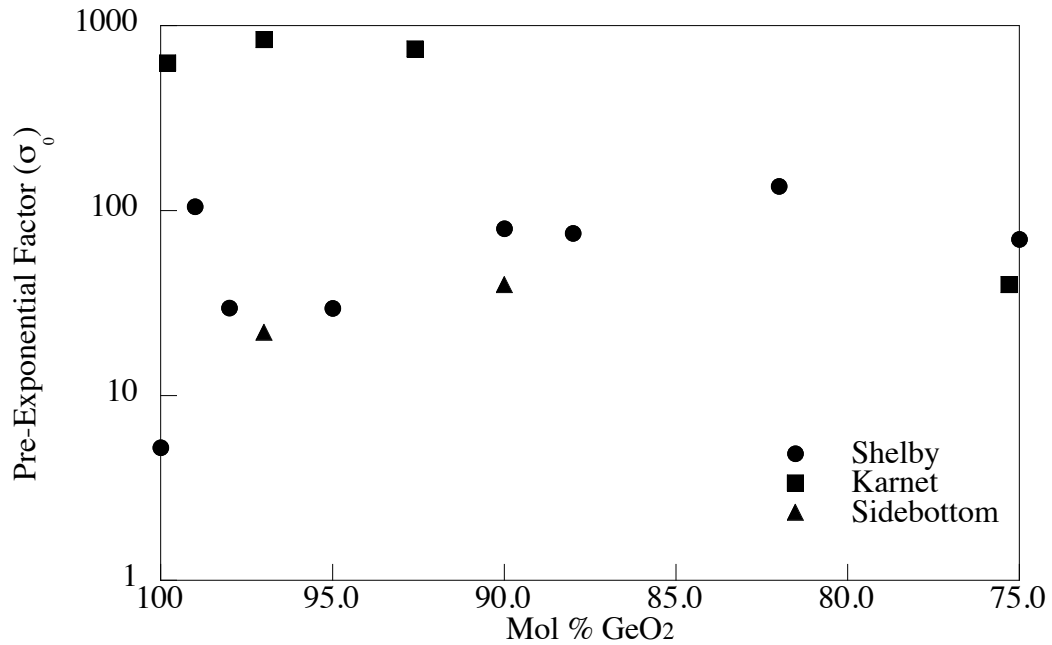


Figure 6-6. Pre-exponential factors for $\text{Li}_2\text{O}\cdot\text{GeO}_2$ glasses.

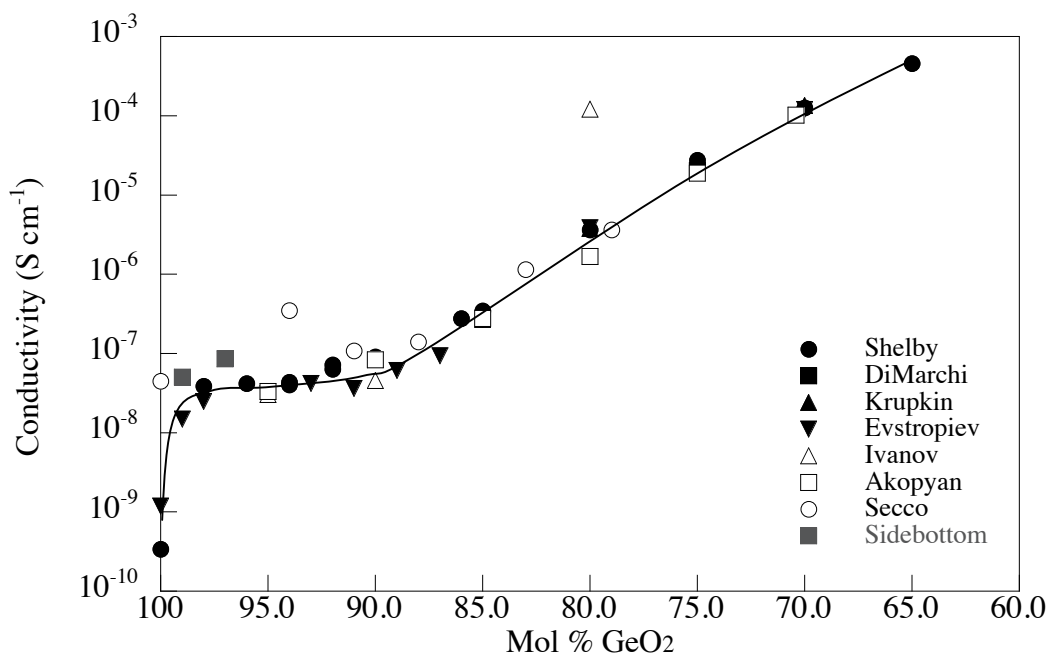


Figure 6-7. Literature values for the DC electrical conductivity, at 300 °C, of Na₂O•GeO₂ glasses.

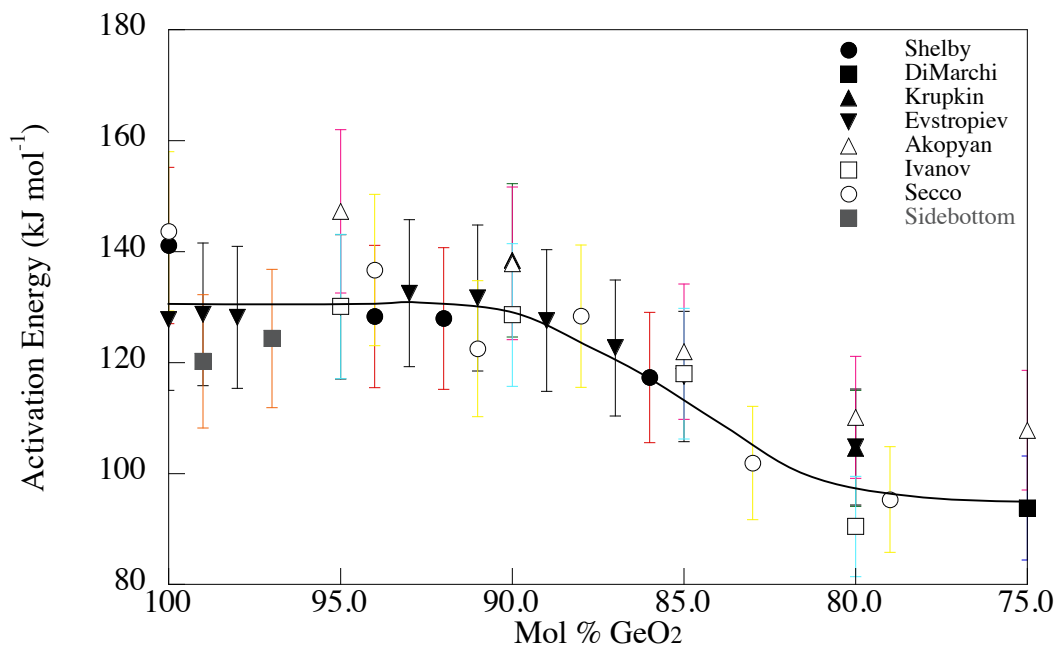


Figure 6-8. Activation energy for DC conductivity of Na₂O•GeO₂ glasses.

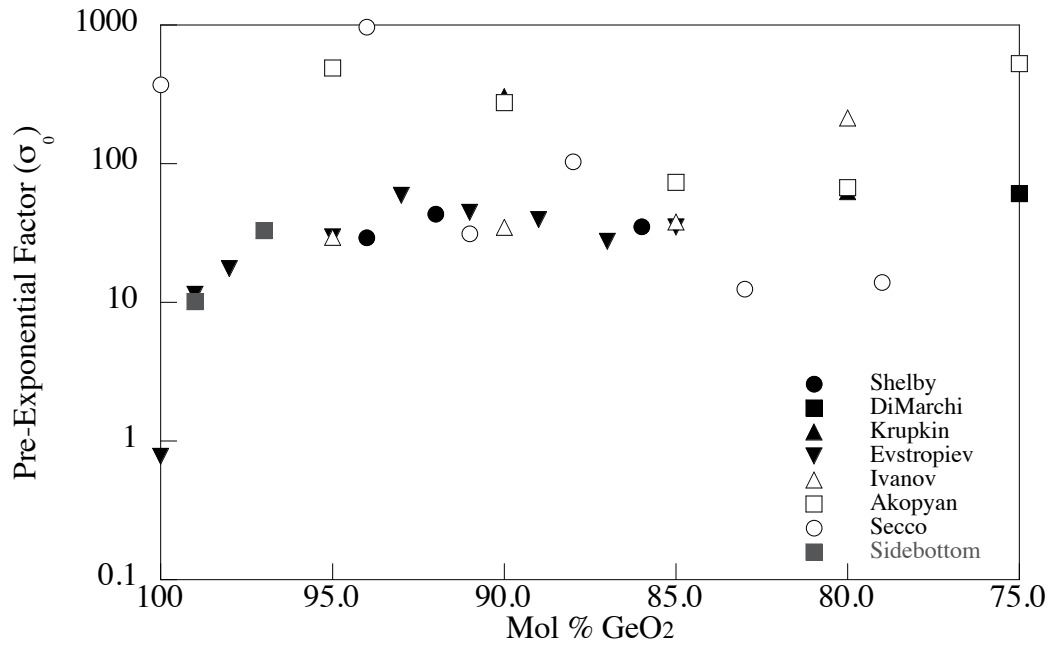


Figure 6-9. Pre-exponential factors for $\text{Na}_2\text{O}\cdot\text{GeO}_2$ glasses.

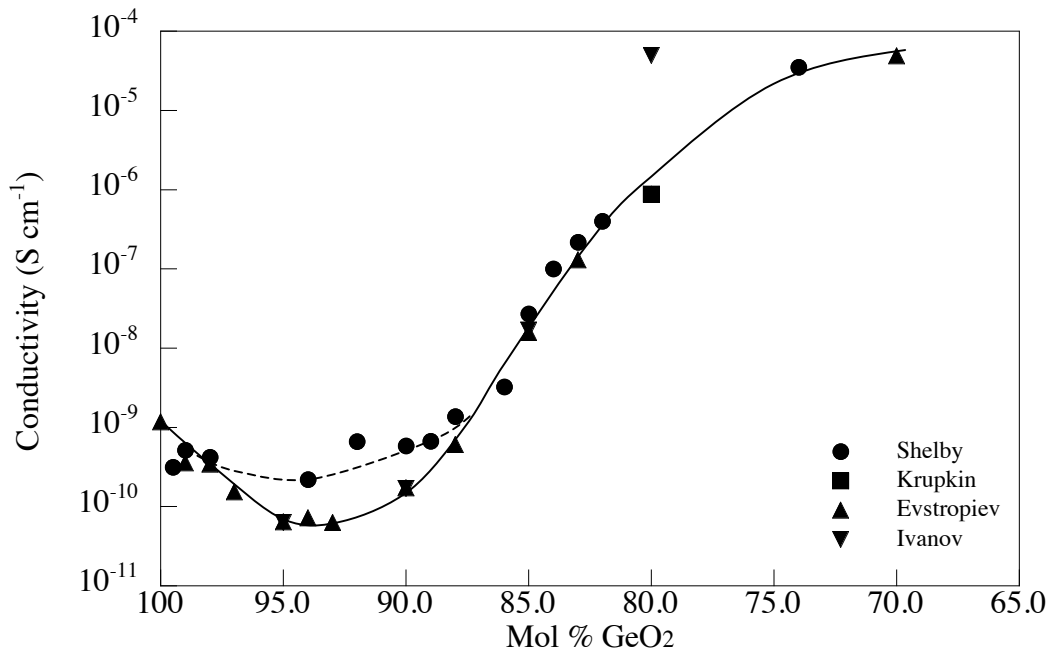


Figure 6-10. Literature values for the DC electrical conductivity, at 300 °C, of $\text{K}_2\text{O}\cdot\text{GeO}_2$ glasses.

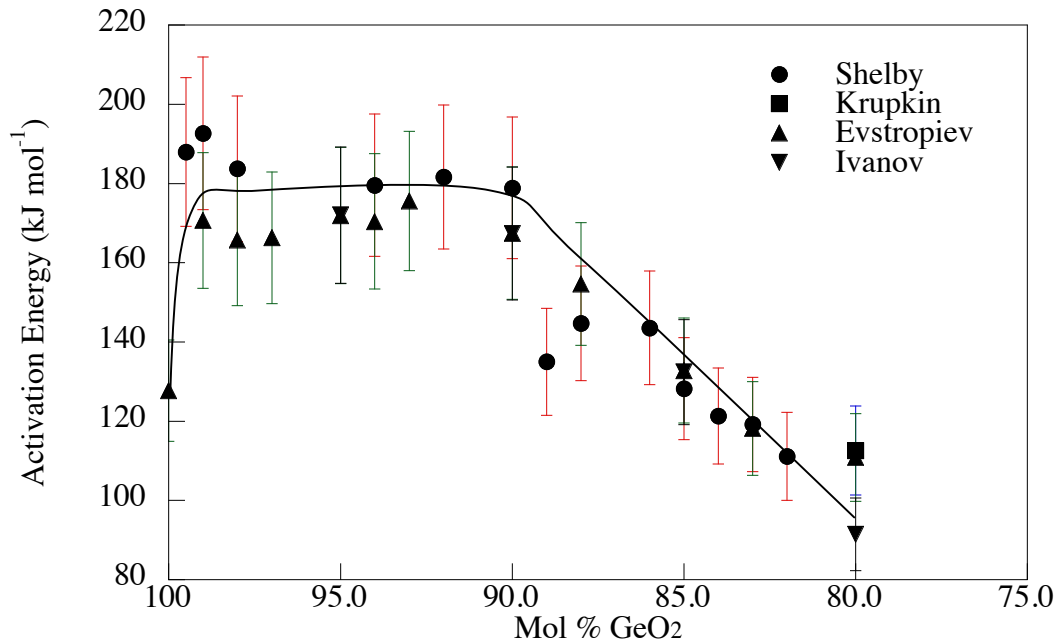


Figure 6-11. Activation energy for DC conductivity of $K_2O \cdot GeO_2$ glasses.

Unlike the behavior for the two smaller alkali ions, the pre-exponential of the $K_2O \cdot GeO_2$ glasses is obviously greater than 10; in some cases, it is as great as three orders of magnitude higher, as shown in Figure 6-12. Using the theory of Nowick, et al., this behavior would suggest that there is a different mechanism of conductivity in glasses with less than 10 mol % K_2O . Their work suggests that conductivity values with such high pre-exponentials are thermally activated. Shelby's values are significantly larger than those of Evstropiev. Evstropiev's values were taken from data measured at 200 to 400 °C, whereas Shelby's data were collected between 300 and 450 °C. If the mechanism of conductivity increases with temperature exponentially, as Nowick et al. suggest, then it is reasonable to conclude that increase in conductivity is a result of the increase in temperature at which the conductivity was measured.

The electrical conductivity of the $Rb_2O \cdot GeO_2$ and $Cs_2O \cdot GeO_2$ glasses is similar and will be discussed concurrently. Figure 6-13 shows the electrical conductivity for $Rb_2O \cdot GeO_2$ glasses. There is an initial sharp decrease in electrical conductivity with very small additions of Rb_2O , followed by an increase of about 5 orders of magnitude with further Rb_2O additions. A similar trend is shown in Figure 6-14, for $Cs_2O \cdot GeO_2$ glasses.

The activation energy behavior for the two different alkali oxide containing glasses is very similar. There is a sharp increase with a small addition of Rb_2O as shown in Figure 6-15. The activation energy for the $\text{Rb}_2\text{O}\cdot\text{GeO}_2$ glass gradually decreases in until 12 mol % Rb_2O addition, where a sharp decrease in activation energy occurs, followed by a gradual decrease. The $\text{Cs}_2\text{O}\cdot\text{GeO}_2$ glasses exhibit similar behavior, but with less abrupt change in activation energy, as shown in Figure 6-16.

The pre-exponential factors for the $\text{Rb}_2\text{O}\cdot\text{GeO}_2$ glasses (Figure 6-17) have the largest range of values of all the alkali oxides. Some of the low alkali oxide containing glasses have pre-exponential factors $> 10^4$. The $\text{Cs}_2\text{O}\cdot\text{GeO}_2$ glasses (Figure 6-18) exhibit a different behavior. The pre-exponential is very large for the glass with 2 mol % Cs_2O , while the values for glasses with Cs_2O concentration > 5 mol %, are in the normal range.

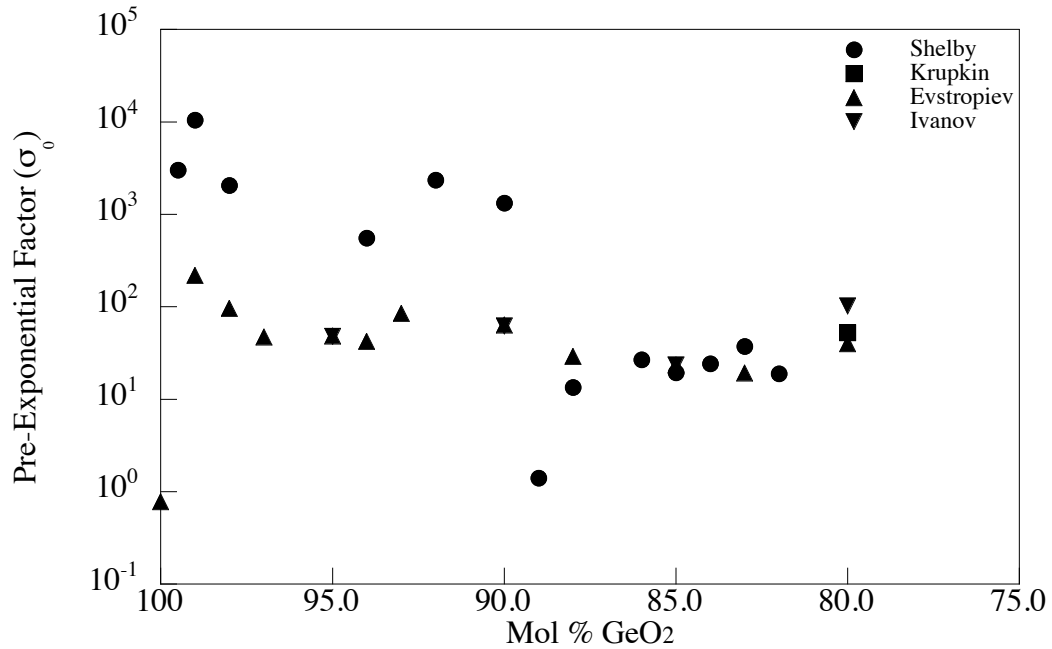


Figure 6-12. Pre-exponential factors for $\text{K}_2\text{O}\cdot\text{GeO}_2$ glasses.

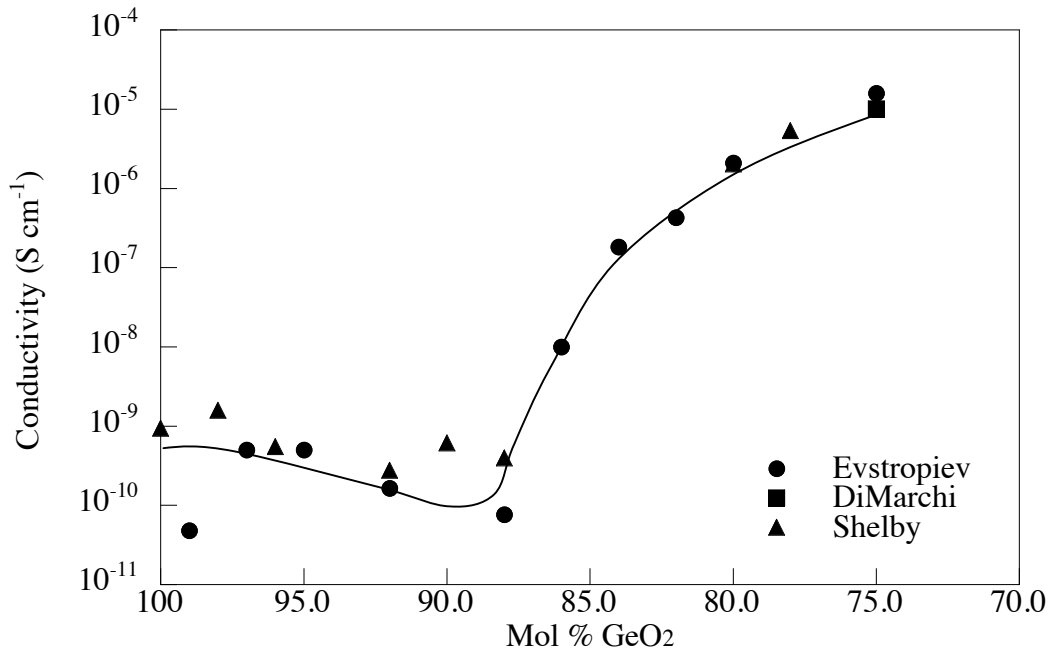


Figure 6-13. Literature values for the DC electrical conductivity, at 300 °C, of $\text{Rb}_2\text{O}\cdot\text{GeO}_2$ glasses.

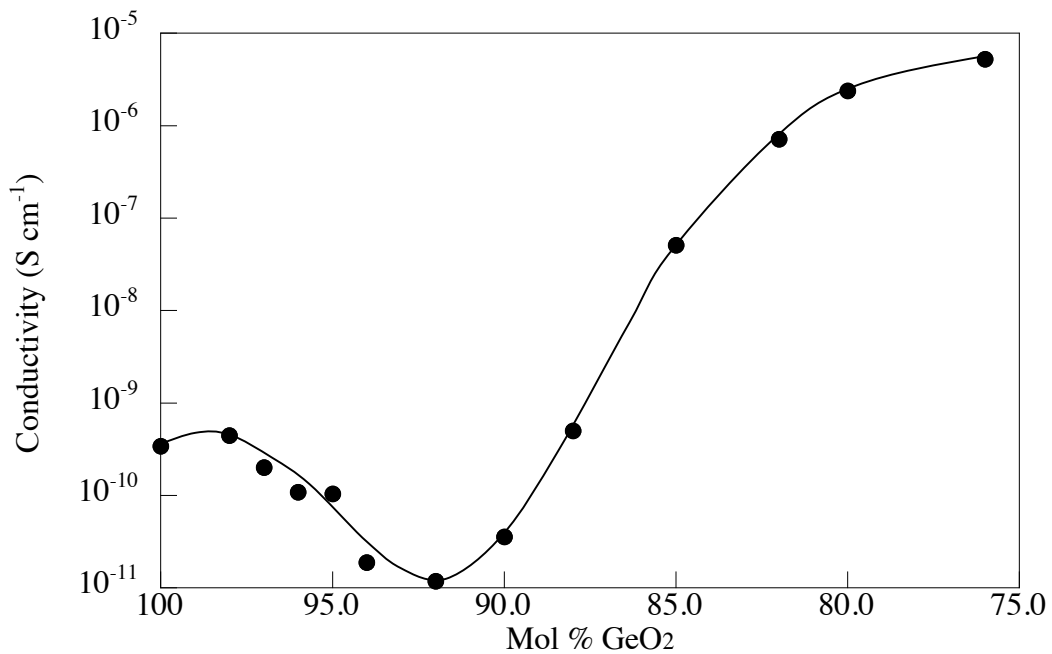


Figure 6-14. Unpublished DC electrical conductivity at 300 °C, provided by J.E. Shelby, for $\text{Cs}_2\text{O}\cdot\text{GeO}_2$ glasses.

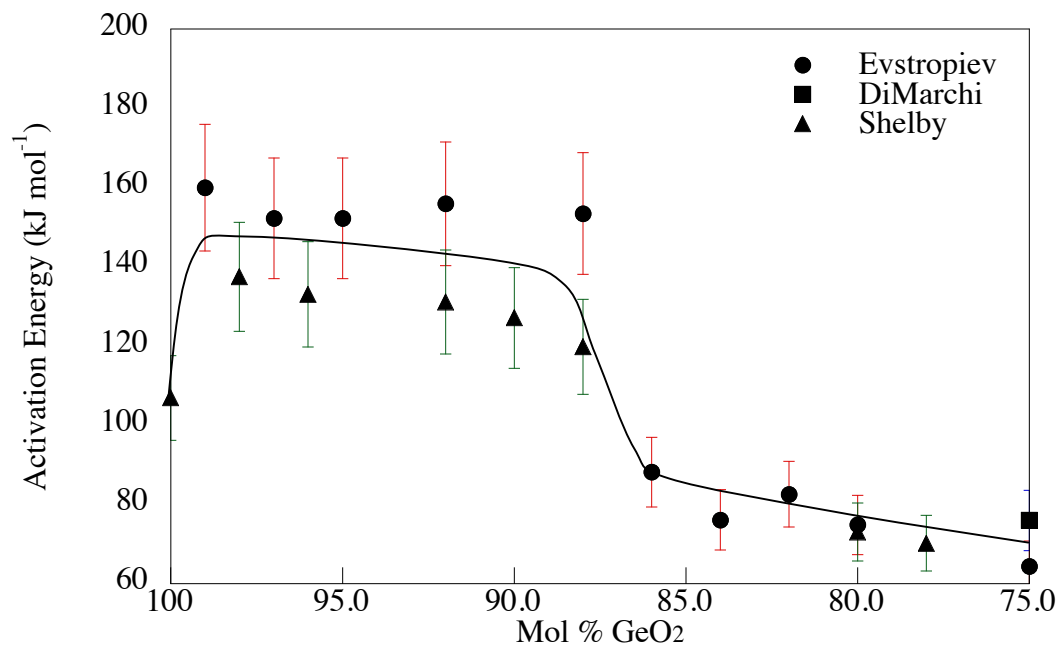


Figure 6-15. Activation energy for DC conductivity of Rb₂O•GeO₂ glasses.

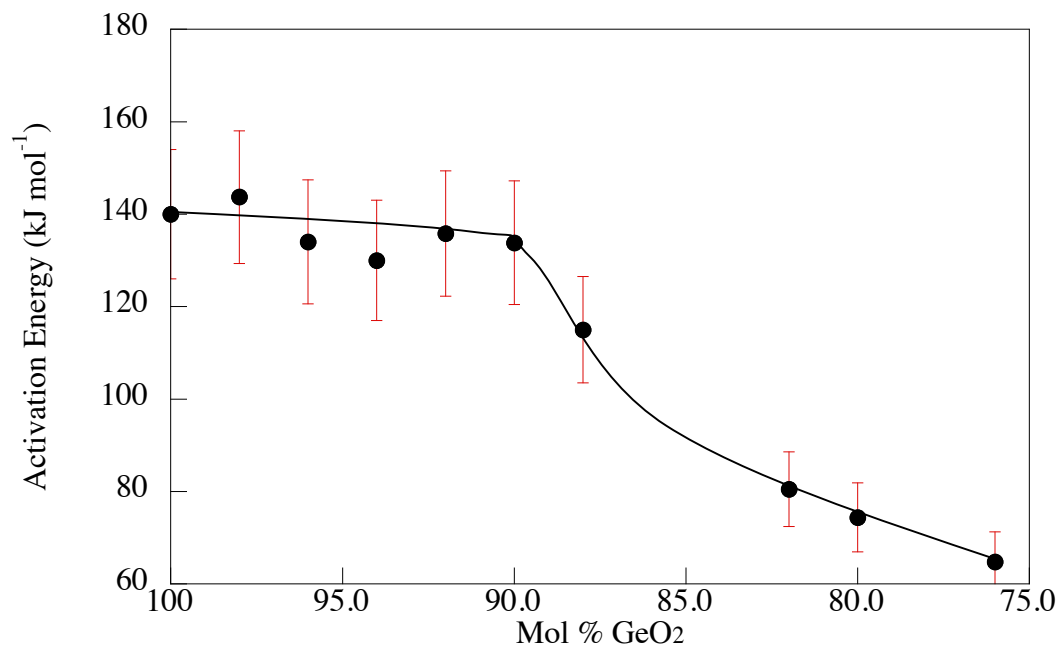


Figure 6-16. Activation energy for DC conductivity of Cs₂O•GeO₂ glasses.

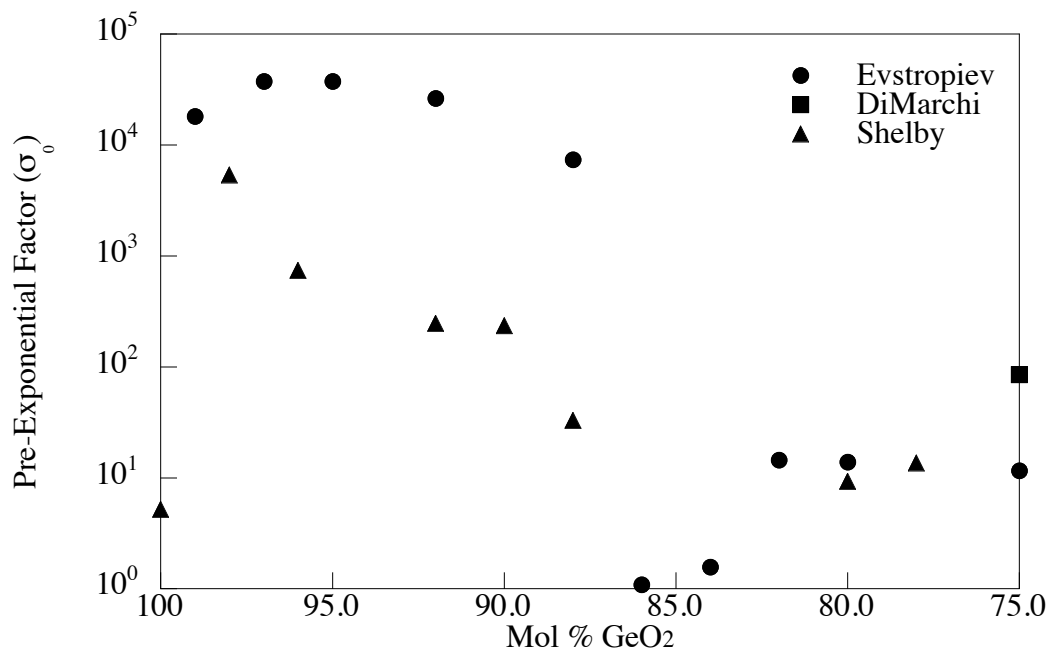


Figure 6-17. Pre-exponential factors for Rb₂O•GeO₂ glasses.

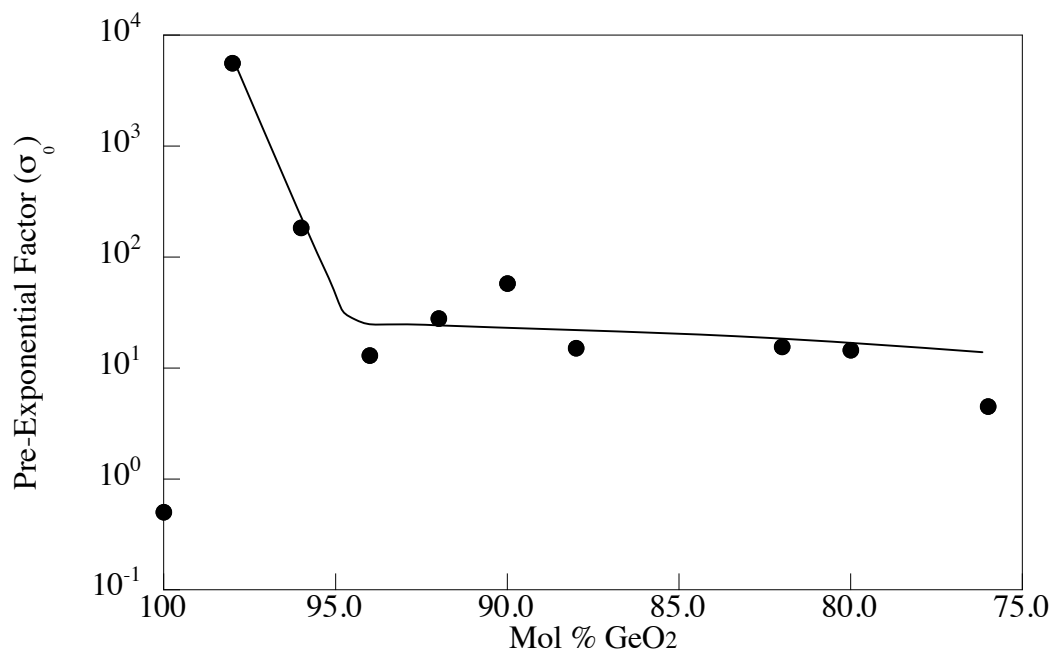


Figure 6-18. Pre-exponential factors for Cs₂O•GeO₂ glasses.

The curves for electrical conductivity and from these figures' activation energies for all of the alkali ions are shown in Figures 6-19 and 6-20, respectively. The electrical conductivity behavior for the smaller alkali ions (Li⁺, Na⁺) is quite different from that of

the larger alkali ions (K^+ , Rb^+ , Cs^+). The glasses with lithium exhibit a sharp increase in conductivity with less than 2 mol % alkali oxide, followed by a very gradual increase in conductivity. The glasses containing sodium have an increase similar to the lithium germanate glasses, however the conductivity remains constant from about 2 to 7 mol % addition, then begins to increase significantly. The glasses with the larger alkali initially decrease in conductivity, a minimum occurs at 5 to 10 mol % addition of alkali oxide, followed by increasing conductivity with increasing alkali oxide content beyond 10 mol %. Similar electrical behavior occurs at higher alkali oxide concentrations regardless of the alkali identity.

Activation energies for all of the binary glasses can be discussed in a similar manner. The activation energy for glasses containing the larger alkali ions initially increases, has a plateau region, and then decreases. The smaller alkali (Li^+ , Na^+) ions act differently. There is a continuous decrease in the activation energy for the lithium and sodium germanate glasses. Lithium germanate glasses initially decrease in activation energy and then only slightly decrease with additions beyond 2 mol %.

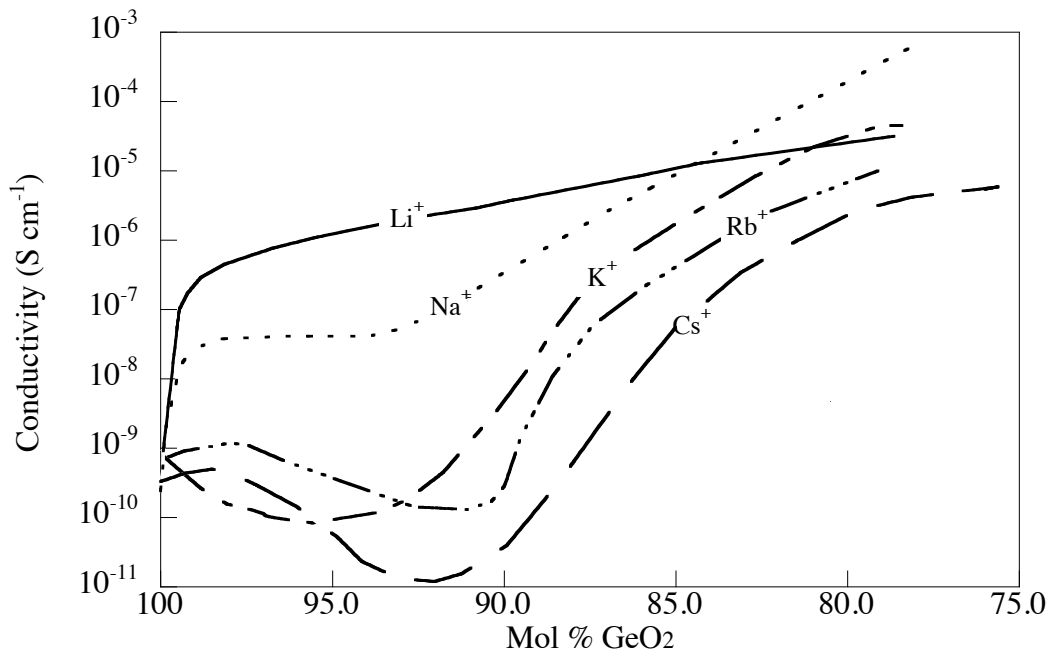


Figure 6-19. Literature values for the DC electrical conductivity, at 300 °C, of $R_2O \cdot GeO_2$ glasses.

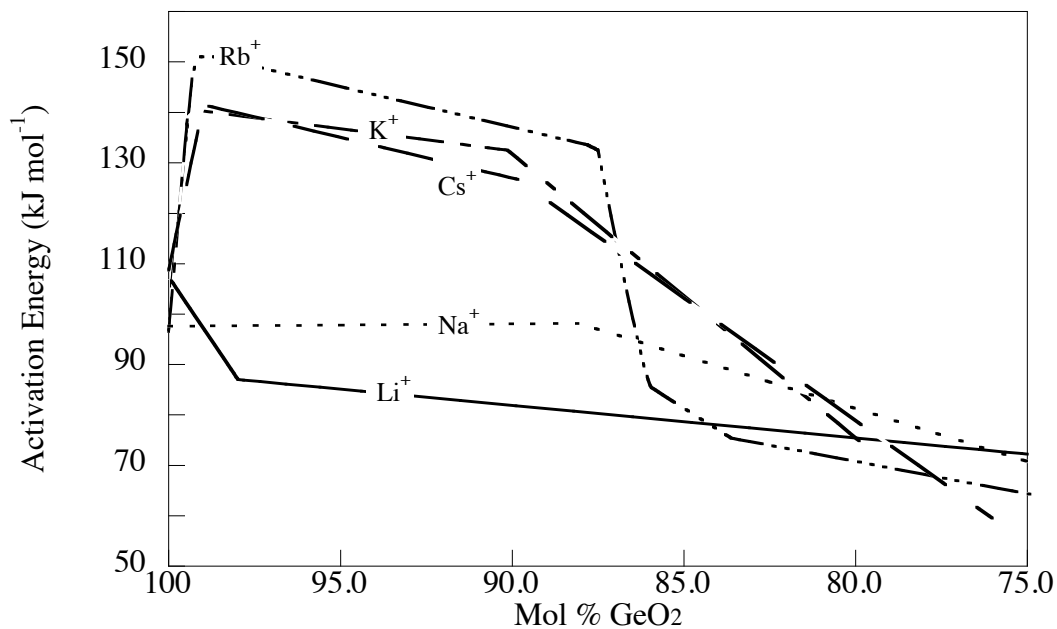


Figure 6-20. Activation energies for electrical conductivity, from the literature, for binary alkali-germanate glasses.

6.3 Experimental Procedures

6.3.1 Sample Preparation

Optically polished samples (Chapter 3) were sputtered on all sides with a AuPd alloy. A guard ring was placed on one side of each sample, masking the area under the ring from the metallic coating (Figure 6-21). One of three rings was used, with electrode areas of 0.113 cm², 0.261 cm², or 0.785 cm². Samples ranged in thickness from about 0.5 mm to 2.5 mm.



Figure 6-21. Illustration of the samples used in the DC conductivity experiments.

6.3.2 *Electrical Conductivity Measurements*

Electrical conductivity measurements were performed using a three-probe DC approach, which is shown in Figure 6-22. The sample is placed against a piece of Pt foil on a Macor® ceramic disk. The inner electrode is placed in the center of the ring, as shown in Figure 6-22. The outer electrode is placed outside the ring. A thermocouple sits directly above the sample. The sample holder is placed in a tube furnace. The atmosphere in the furnace is ambient. The circuit diagram is shown in Figure 6-23.

Electrical conductivity measurements are performed by heating the furnace to the temperature where the sample first begins to conduct at the measurement level. The furnace is held at this temperature for 30 minutes to allow the glass to reach the temperature of the furnace. The temperature of the furnace is then increased in 10 K increments, with 10 minute intervals between measurements.



Figure 6-22. Illustration of the DC conductivity apparatus used in this thesis.



Figure 6-23. Illustration of the circuit used in the DC conductivity apparatus.

The electrical conductivity can be calculated using the following formulas.

$$R = \frac{R_{Ref}(V_B - V_D)}{V_D}, \quad (6-26)$$

where R is the resistance, R_{Ref} is the reference resistance, V_B is the voltage of the battery (~ 9 V in this case), and V_D is the voltage drop across the reference resistor. To calculate the resistivity (ρ) from the resistance use,

$$\rho = R \left(\frac{A}{L} \right), \quad (6-27)$$

where A is,

$$A = \pi(r_2^2) \quad (6-28)$$

Conductivity is the inverse of the resistance $1/\rho$. To further analyze the data, the conductivity values are plotted as log conductivity versus $1000/T$ (in absolute temperature), and an exponential fit is applied to the data. The exponential fits the following equation⁶⁹

$$\sigma = \sigma_0 \exp\left(\frac{-E}{RT}\right), \quad (6-29)$$

where σ_0 is the pre-exponential factor, R is the gas constant in kJ/mol, E is the activation energy for conductivity and T is the absolute temperature. The conductivity can then be calculated for any reference temperature, for comparison of different glasses. Reference temperatures of 300 °C and T_g are used here.

6.3.3 Comparing to NIST Standards

The National Bureau of Standards and Testing (NIST) provides standard glass 624 for electrical conductivity measurements. Figure 6-24 shows the electrical

conductivity measurements for NIST 624 with apparatus used in this thesis, compared to the data supplied by NIST.

Accuracy of activation energies for conductivity is overestimated in much of the glass literature. An estimate of the accuracy of activation energies measured in ideal conditions can be calculated. If electrical conductivity measurements were made using a NIST certified Type K[Ⓜ] thermocouple and the instrument measuring electrical conductivity is as accurate as that used at NIST, this idealized experimental apparatus would yield a minimum error in conductivity at 300 °C of ± 0.37 %. If the furnace uses a Type B, R, or S thermocouple, then the minimum error at 300 °C increases to ± 1.30 %. If the furnace maintains temperature at ± 5 K, the minimum error is ± 1.84 %. These errors are only from one source of error, i.e. the best temperature capabilities of the apparatus. If all the sources of error (e.g. corroded electrodes, variations in sample thickness, samples with defects, etc.) over the entire set is taken into consideration, the activation energies should be reported in the literature with much greater error bars. The variance in the literature is actually much closer to ± 5 %, which is used here.

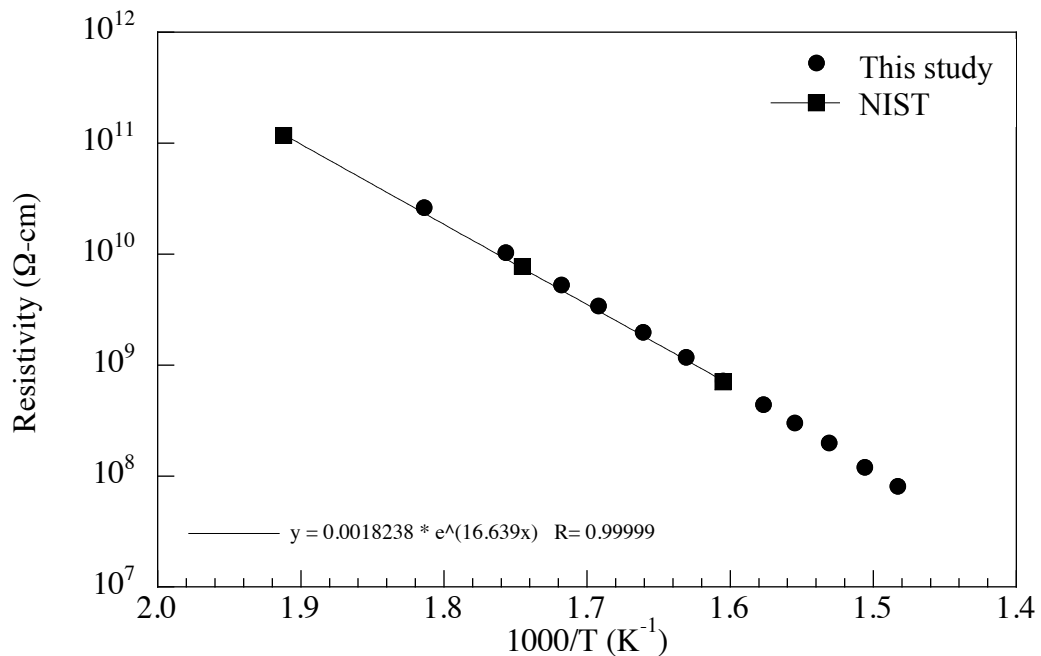


Figure 6-24. NIST standard 624 and the values measured using the equipment used in this study. The points are larger than the error bars.

[Ⓜ] <http://www.cstl.nist.gov/div836/836.05/thermometry/calibrations/uncertainty.htm>

6.4 Results

6.4.1 *Mixed Alkali Germanate Glasses*

The results of the effect of mixing alkali ions on the electrical conductivity will be presented first, followed by the effect of GeO_2 content on the conductivity. The $\text{Li}_2\text{O}\cdot\text{Cs}_2\text{O}\cdot\text{GeO}_2$ system will be discussed before the $\text{Na}_2\text{O}\cdot\text{K}_2\text{O}\cdot\text{GeO}_2$ system.

The DC conductivity data for $x \text{Li}_2\text{O}\cdot(10-x) \text{Cs}_2\text{O}\cdot 90 \text{GeO}_2$ glasses is presented in Figure 6-25. As cesium replaces lithium in the network, there is a clear shift of the curve to higher temperature. Inspection of the slopes in Figure 6-25 shows the mixed alkali glasses have slightly different slopes. As the number of cesium ions in the glass increases, the slope becomes steeper, with the examples of the binary cesium germanate glass.

Electrical conductivity values of the glasses at their glass transition temperature and at $300\text{ }^\circ\text{C}$ are shown in Figure 6-26. As the temperature of the glass approaches the T_g , the conductivity of the glass increases. The effect of temperature on conductivity is greater for the glasses with more cesium ions. The conductivity of the binary cesium germanate glasses increases about 3.5 orders of magnitude from $300\text{ }^\circ\text{C}$ to T_g , whereas the conductivity of the lithium germanate glasses increases about 2 orders of magnitude from $300\text{ }^\circ\text{C}$ to T_g . Figure 6-27 shows the logarithmic of the deviation from additivity in conductivity for both the conductivity at $300\text{ }^\circ\text{C}$ and at T_g . There is no appreciable difference between the deviation from additivity of the conductivity at either temperature. The greatest deviation from additivity occurs when the $\text{Li}_2\text{O}:\text{Cs}_2\text{O}$ ratio is 1:7.

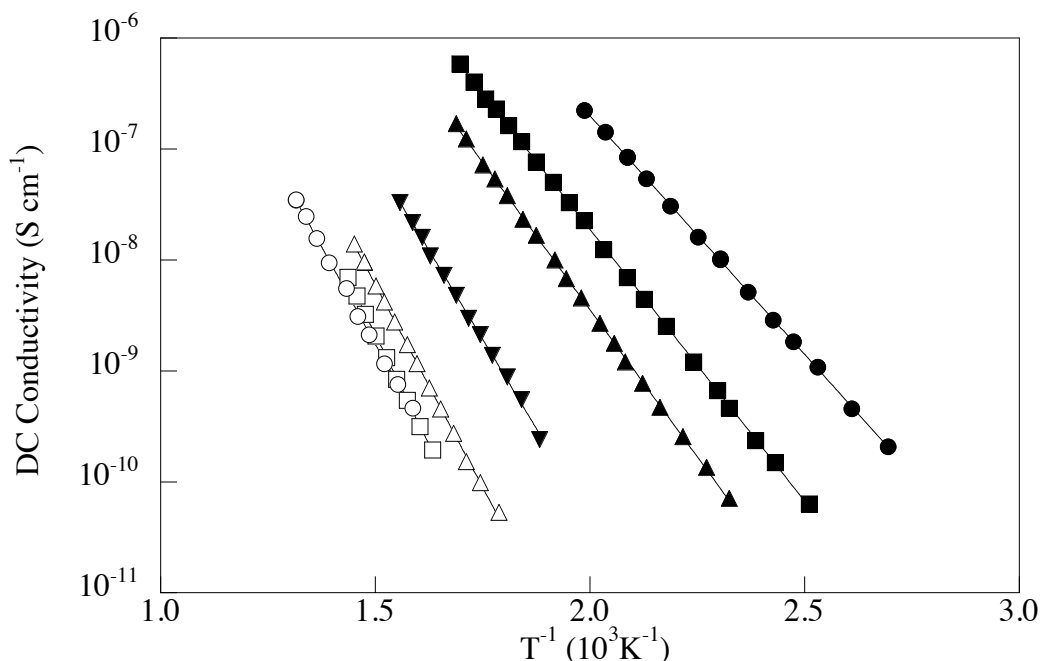


Figure 6-25. DC conductivity for the $x \text{Li}_2\text{O} \cdot (10-x) \text{Cs}_2\text{O} \cdot 90 \text{GeO}_2$ mixed alkali glasses. Lines are an exponential fit. (● = 10 $\text{Li}_2\text{O} \cdot 90 \text{GeO}_2$, ■ = 7:1 $\text{Li}_2\text{O}:\text{Cs}_2\text{O} \cdot 90 \text{GeO}_2$, ▲ = 3:1 $\text{Li}_2\text{O}:\text{Cs}_2\text{O} \cdot 90 \text{GeO}_2$, ▼ = 1:1 $\text{Li}_2\text{O}:\text{Cs}_2\text{O} \cdot 90 \text{GeO}_2$, △ = 1:3 $\text{Li}_2\text{O}:\text{Cs}_2\text{O} \cdot 90 \text{GeO}_2$, □ = 1:7 $\text{Li}_2\text{O}:\text{Cs}_2\text{O} \cdot 90 \text{GeO}_2$, ○ = 10 $\text{Cs}_2\text{O} \cdot 90 \text{GeO}_2$)

Activation energy for conductivity was calculated from the values obtained from the exponential fit to the data shown in Figure 6-25. Introducing cesium ions into the glass causes an almost linear increase in the activation energy (Figure 6-28) from the 10 $\text{Li}_2\text{O} \cdot \text{GeO}_2$ glass to the 1:7 $\text{Li}_2\text{O}:\text{Cs}_2\text{O} \cdot 90 \text{GeO}_2$ glass, however there is a sharp decrease in the activation energy for the binary 10 $\text{Cs}_2\text{O} \cdot \text{GeO}_2$ glass, resulting in a positive deviation from additivity, shown in Figure 6-29. The pre-exponential factor ranges from 59 to 1700, as shown in Figure 6-30. All of the pre-exponential factors of the mixed $\text{Li}_2\text{O}:\text{Cs}_2\text{O} \cdot 90 \text{GeO}_2$ glasses are at least an order of magnitude greater than 10. The conductivity values at both T_g and 300 °C, activation energies and pre-exponential factors are listed in Table 6-II.

Table 6-II. Electrical Conductivity Properties for the $\text{Li}_2\text{O}\cdot\text{Cs}_2\text{O}\cdot 90 \text{ GeO}_2$ Glasses

Glass Composition 90 Mol% GeO_2	T_g	σ_0	E_{act} (kJ mol^{-1})	σ (S cm^{-1}) 300 °C	σ (S cm^{-1}) T_g
10 Li_2O	498	58.74	134	2.50 E-06	2.12 E-4
7:1 $\text{Li}_2\text{O}:\text{Cs}_2\text{O}$	500	1700	151	3.38 E-07	2.99 E-5
3:1 $\text{Li}_2\text{O}:\text{Cs}_2\text{O}$	492	835.8	142	8.09 E-08	1.70 E-5
1:1 $\text{Li}_2\text{O}:\text{Cs}_2\text{O}$	491	324.9	123	2.09 E-09	1.31 E-6
1:3 $\text{Li}_2\text{O}:\text{Cs}_2\text{O}$	495	146.8	102	9.24 E-11	1.80 E-7
1:7 $\text{Li}_2\text{O}:\text{Cs}_2\text{O}$	507	120.9	93.9	2.45 E-11	1.15 E-7
10 Cs_2O	513	80.06	82.4	3.34 E-11	1.16 E-7

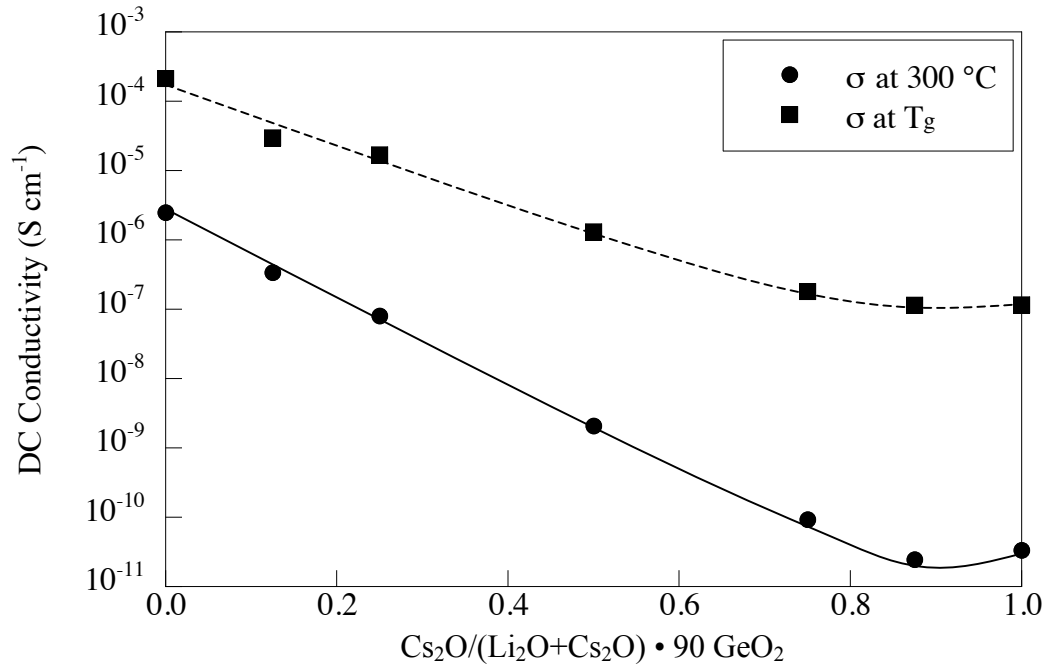


Figure 6-26. DC conductivity for $x \text{ Li}_2\text{O}\cdot(10-x) \text{ Cs}_2\text{O}\cdot 90 \text{ GeO}_2$ glasses at the glass transition temperature (T_g) and at 300 °C. Lines are added as a guide to the eye.

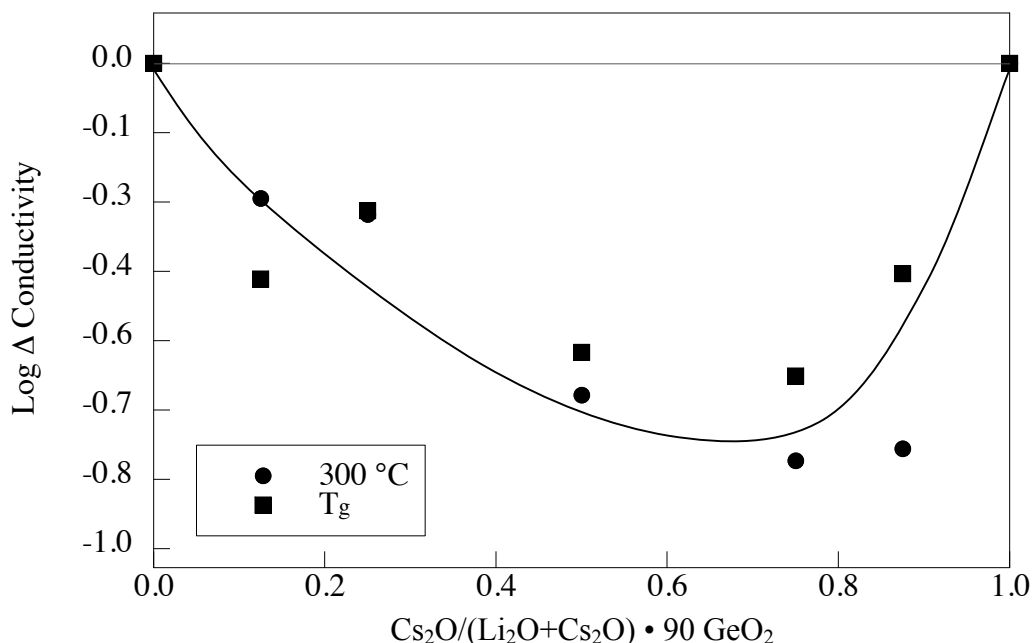


Figure 6-27. Log plot of the deviation from additivity for the DC electrical conductivity of $x \text{Li}_2\text{O} \cdot (10-x) \text{Cs}_2\text{O} \cdot 90 \text{GeO}_2$ glasses at the glass transition temperature (T_g) and 300 °C. Line is added as a guide to the eye.

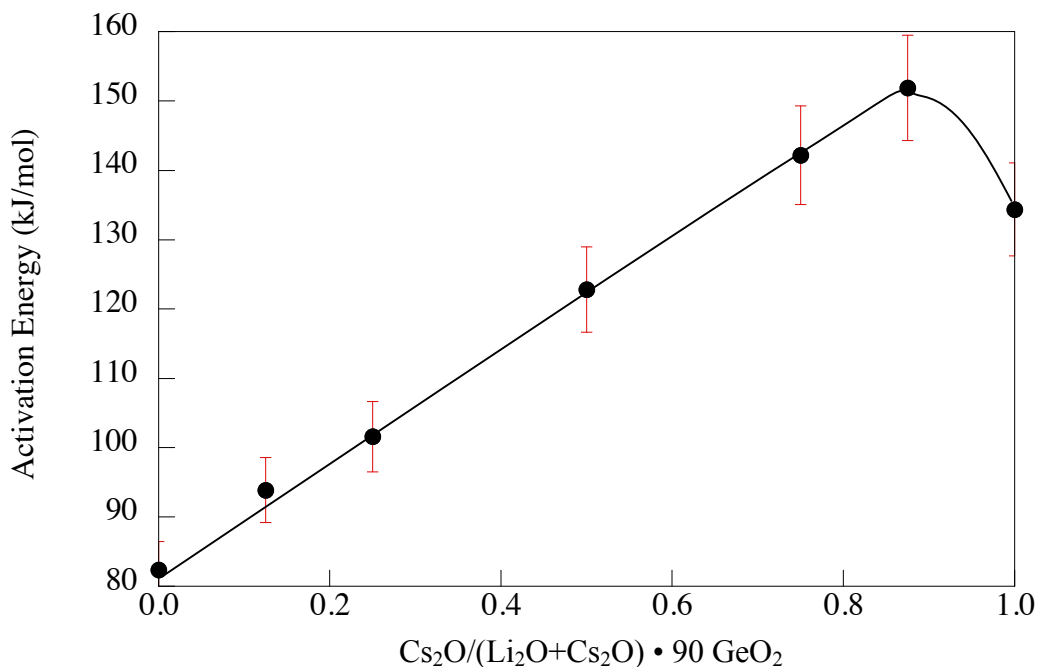


Figure 6-28. Activation energy for DC conductivity of the mixed alkali $x \text{Li}_2\text{O} \cdot (10-x) \text{Cs}_2\text{O} \cdot 90 \text{GeO}_2$ glasses. Line is added as a guide to the eye.

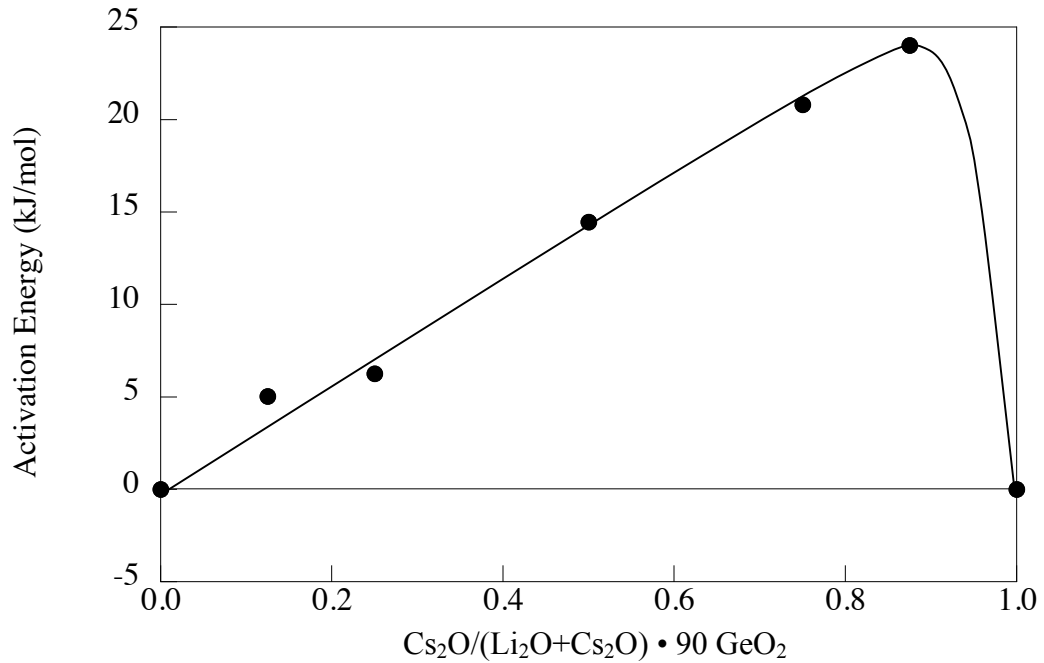


Figure 6-29. Deviation from additivity of the activation energy for DC conductivity for the mixed alkali $x \text{Li}_2\text{O} \cdot (10-x) \text{Cs}_2\text{O} \cdot 90 \text{GeO}_2$ glasses. Line is added as a guide to the eye.

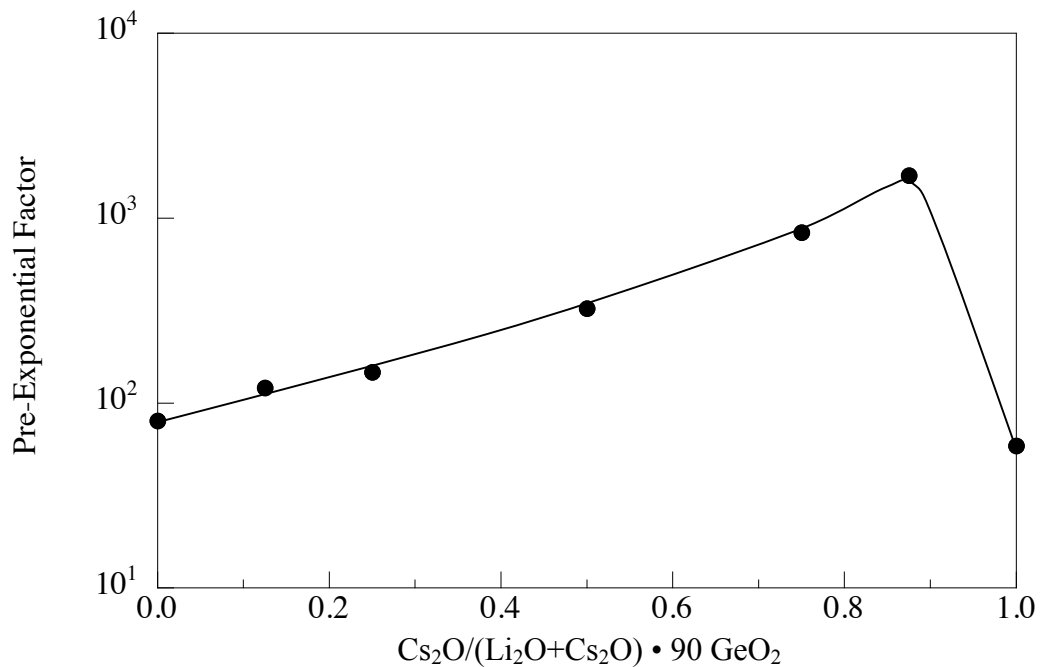


Figure 6-30. Pre-exponential factor (σ_0) of the Arrhenius equation for the mixed alkali $x \text{Li}_2\text{O} \cdot (10-x) \text{Cs}_2\text{O} \cdot 90 \text{GeO}_2$ glasses. Line is added as a guide to the eye.

The DC conductivity curves for $x\text{Li}_2\text{O}\cdot(15-x)\text{Cs}_2\text{O}\cdot 85\text{ GeO}_2$ glasses are shown in Figure 6-31. As cesium replaces lithium in the network, the curve shifts to higher temperature. Since large enough samples to measure conductivity could not be made for $15\text{ Cs}_2\text{O}\cdot 85\text{ GeO}_2$ and $15\text{ Li}_2\text{O}\cdot 85\text{ GeO}_2$ glasses, due to crystallization, numbers were interpolated from curves for the binary glasses measured on the same instrument. Figure 6-32 shows the conductivity of the glasses at both $300\text{ }^\circ\text{C}$ and T_g . The negative deviation from additivity for the electrical conductivity at $300\text{ }^\circ\text{C}$ for $x\text{ Li}_2\text{O}\cdot(15-x)\text{ Cs}_2\text{O}\cdot 85\text{ GeO}_2$ glasses is shown in Figure 6-33. The maximum deviation occurs when the alkali are in a ratio of 1:3 $\text{Li}_2\text{O}:\text{Cs}_2\text{O}$.

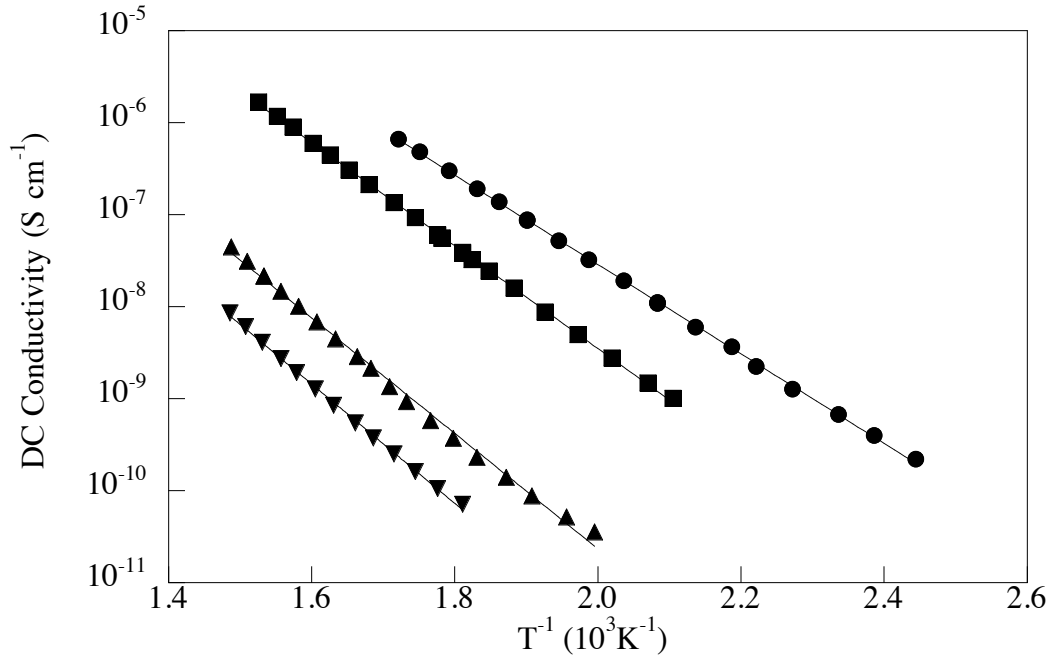


Figure 6-31. DC electrical conductivity for $x\text{ Li}_2\text{O}\cdot(15-x)\text{ Cs}_2\text{O}\cdot 85\text{ GeO}_2$ glasses. Lines are an exponential fit. (\bullet = 7:1 $\text{Li}_2\text{O}:\text{Cs}_2\text{O}\cdot 85\text{ GeO}_2$, \blacksquare = 3:1 $\text{Li}_2\text{O}:\text{Cs}_2\text{O}\cdot 85\text{ GeO}_2$, \blacktriangle = 1:1 $\text{Li}_2\text{O}:\text{Cs}_2\text{O}\cdot 85\text{ GeO}_2$, \blacktriangledown = 1:3 $\text{Li}_2\text{O}:\text{Cs}_2\text{O}\cdot 85\text{ GeO}_2$)

Activation energy for conductivity of $x\text{ Li}_2\text{O}\cdot(15-x)\text{ Cs}_2\text{O}\cdot 85\text{ GeO}_2$ glasses is shown in Figure 6-34. There is a maximum in activation energy when the alkali ratio is between 0.5 and 0.75. Since the electrical conductivities for the binary glasses are calculated the deviation from additivity at T_g for the activation energy is not available. The pre-exponential factors are shown in Figure 6-35. All pre-exponentials are an order of magnitude higher than the expected value of 10, except for the 1:3 $\text{Li}_2\text{O}:\text{Cs}_2\text{O}$ glasses.

Table 6-III lists the values of the pre-exponential, the activation energies and the conductivities at both T_g and 300 °C

Table 6-III. Electrical Conductivity Properties for $\text{Li}_2\text{O}\cdot\text{Cs}_2\text{O}\cdot 85 \text{ GeO}_2$ Glasses

Glass Composition 85 Mol% GeO_2	T_g	σ_0	E_{act} (kJ mol^{-1})	σ (S cm^{-1}) 300 °C	σ (S cm^{-1}) T_g
15 Li_2O	510	-	$\sim 80^*$	7.30 E-06	-
7:1 $\text{Li}_2\text{O}:\text{Cs}_2\text{O}$	513	151.3	92.6	5.12 E-07	1.07 E-4
3:1 $\text{Li}_2\text{O}:\text{Cs}_2\text{O}$	505	541.6	107	9.76 E-08	3.60 E-5
1:1 $\text{Li}_2\text{O}:\text{Cs}_2\text{O}$	497	450.4	128	9.17 E-10	3.98 E-7
1:3 $\text{Li}_2\text{O}:\text{Cs}_2\text{O}$	512	66.85	128	1.52 E-10	2.12 E-7
1:7 $\text{Li}_2\text{O}:\text{Cs}_2\text{O}$	517	-	-	-	-
15 Cs_2O	542	-	$\sim 90^*$	5.12 E-08	-

*Estimate from literature values in Section 6-2

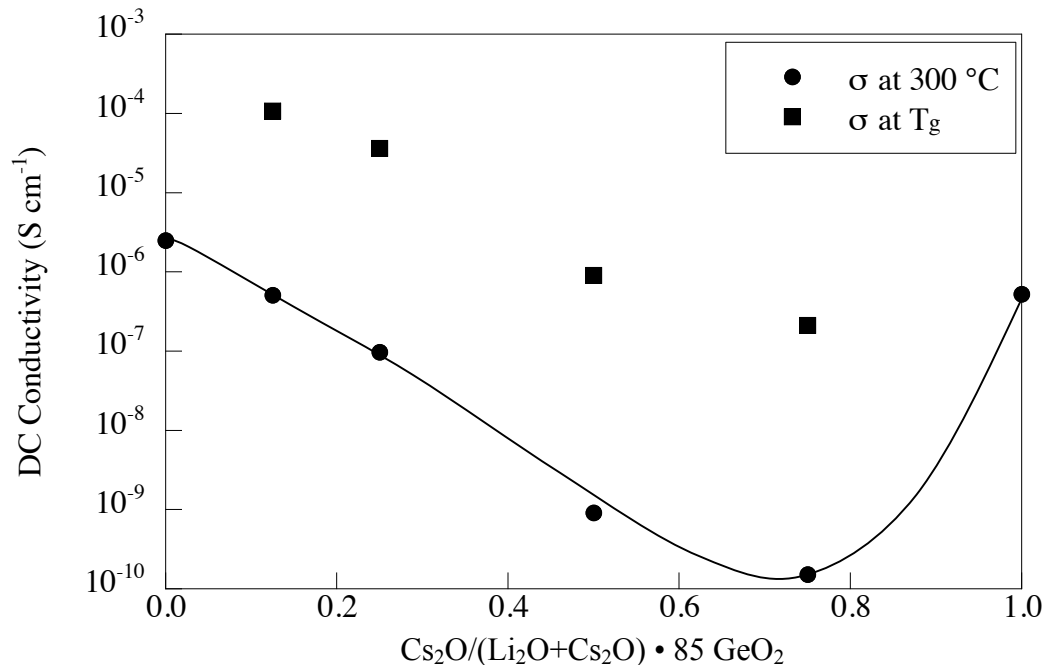


Figure 6-32. Values for DC electrical conductivity at the glass transition temperature and T_g for $x \text{ Li}_2\text{O}\cdot(15-x) \text{ Cs}_2\text{O}\cdot 85 \text{ GeO}_2$ glasses. Line is added as a guide to the eye.

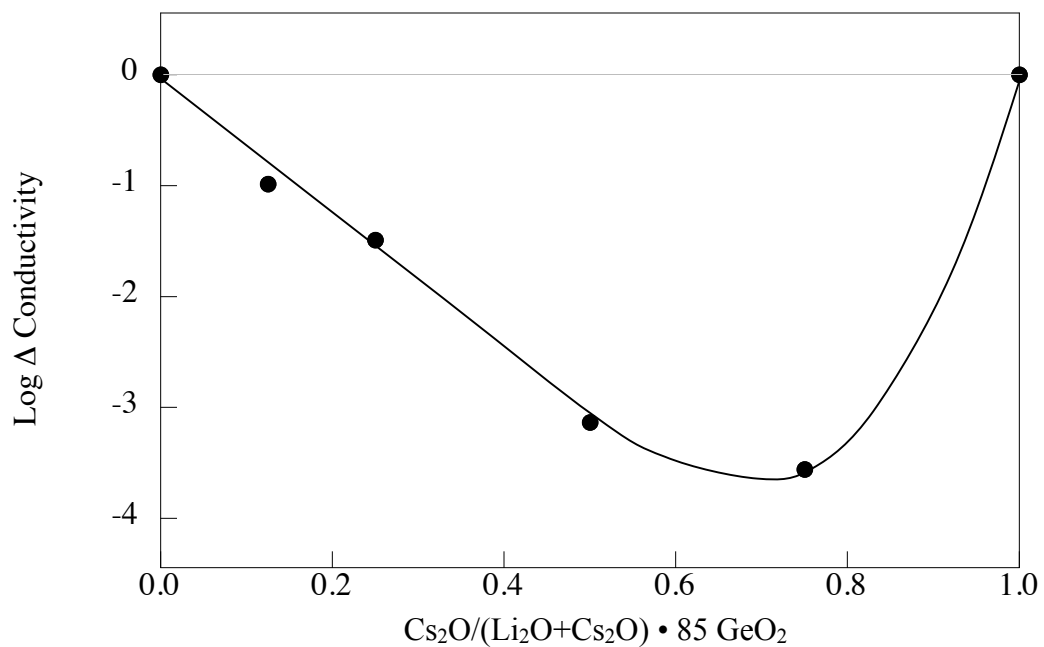


Figure 6-33. The deviation from additivity for the Log of the DC electrical conductivity at 300°C for $x\text{Li}_2\text{O}\cdot 15-x\text{Cs}_2\text{O}\cdot 85 \text{ GeO}_2$ glasses. Line is added as a guide to the eye.

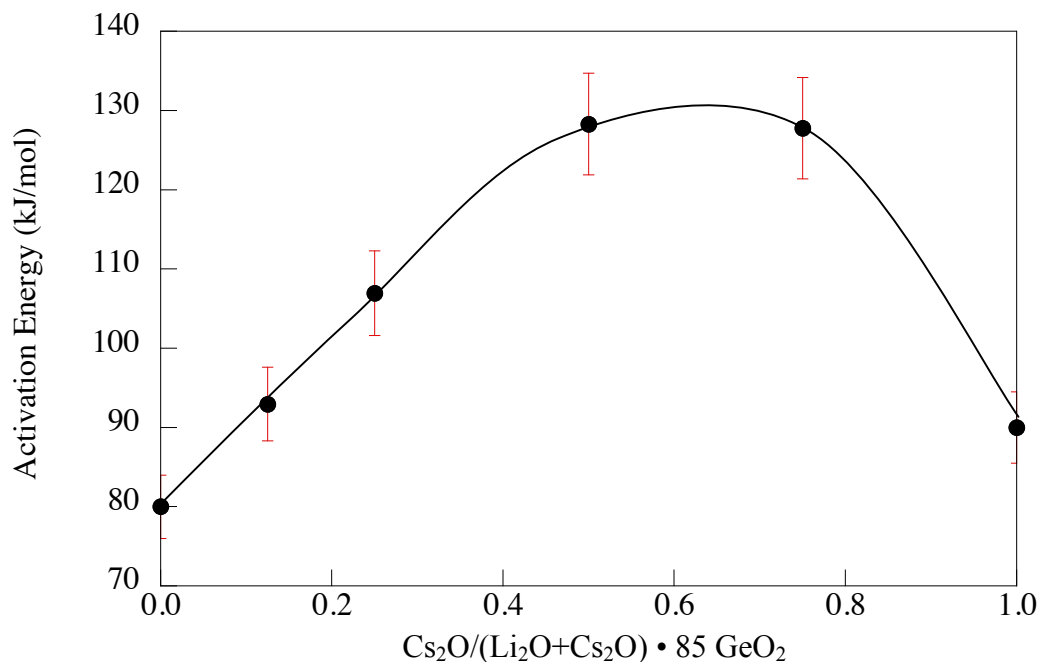


Figure 6-34. Activation energy for crystallization for $x \text{ Li}_2\text{O}\cdot (15-x) \text{ Cs}_2\text{O}\cdot 85 \text{ GeO}_2$ glasses. Line is added as a guide to the eye.

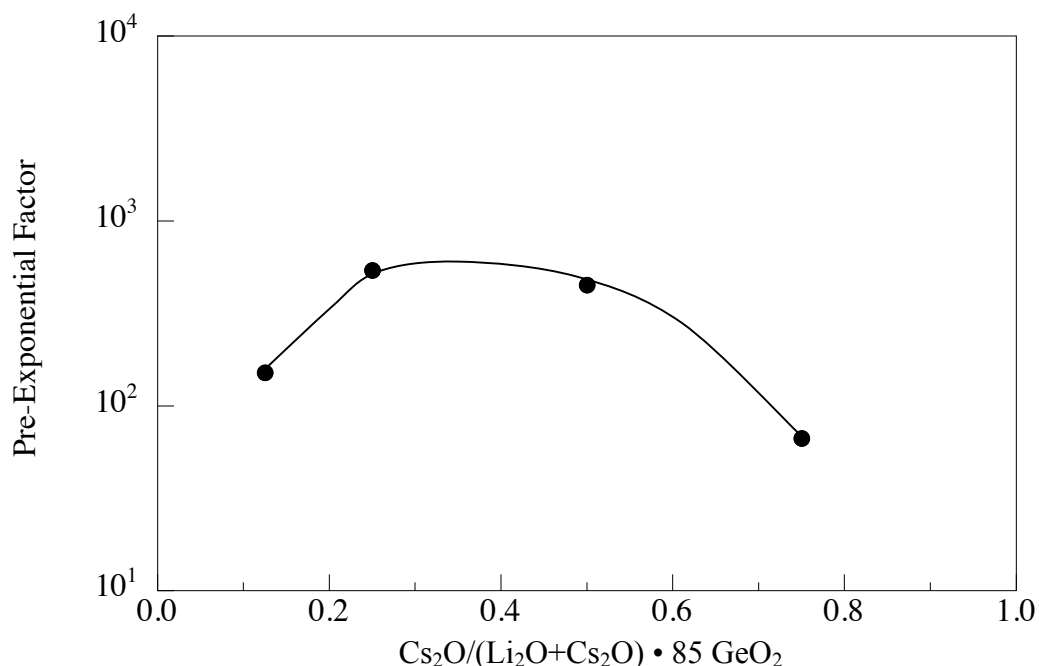


Figure 6-35. Pre-exponential factors (σ_0) for $x \text{Li}_2\text{O} \cdot (15-x) \text{Cs}_2\text{O} \cdot 85 \text{GeO}_2$ glasses. Line is added as a guide to the eye.

The DC conductivity/temperature curves for $x \text{Na}_2\text{O} \cdot 10-x \text{K}_2\text{O} \cdot 90 \text{GeO}_2$ glasses are shown in Figure 6-36. Figure 6-37 shows the electrical conductivity for $x \text{Na}_2\text{O} \cdot (10-x) \text{K}_2\text{O} \cdot 90 \text{GeO}_2$ glasses at both T_g and 300°C . The differences between the log of the measured conductivity and the log of the additive conductivity are shown in Figure 6-38. When the conductivity is measured at 300°C , there is clearly a minimum in conductivity when the alkali oxide ratio is 1:7 $\text{Na}_2\text{O}:\text{K}_2\text{O}$. The minimum shifts to an alkali oxide ratio of 0.6, when conductivity is measured at T_g .

The activation energy for conductivity of $x \text{Na}_2\text{O} \cdot (10-x) \text{K}_2\text{O} \cdot 90 \text{GeO}_2$ glasses maximizes when the alkali oxides is in a ratio of 1:7 $\text{Na}_2\text{O}:\text{K}_2\text{O}$, shown in Figure 6-39. The positive deviation from additivity is shown in Figure 6-40, where the maximum occurs when the alkali oxides are in a ratio of 1:7 $\text{Na}_2\text{O}:\text{K}_2\text{O}$. Figure 6-41 shows the pre-exponential factors, where all of the pre-exponentials are close to or more than an order of magnitude greater than 10. Table 6-IV lists the values of the pre-exponential, the activation energies and the conductivities at both T_g and 300°C .

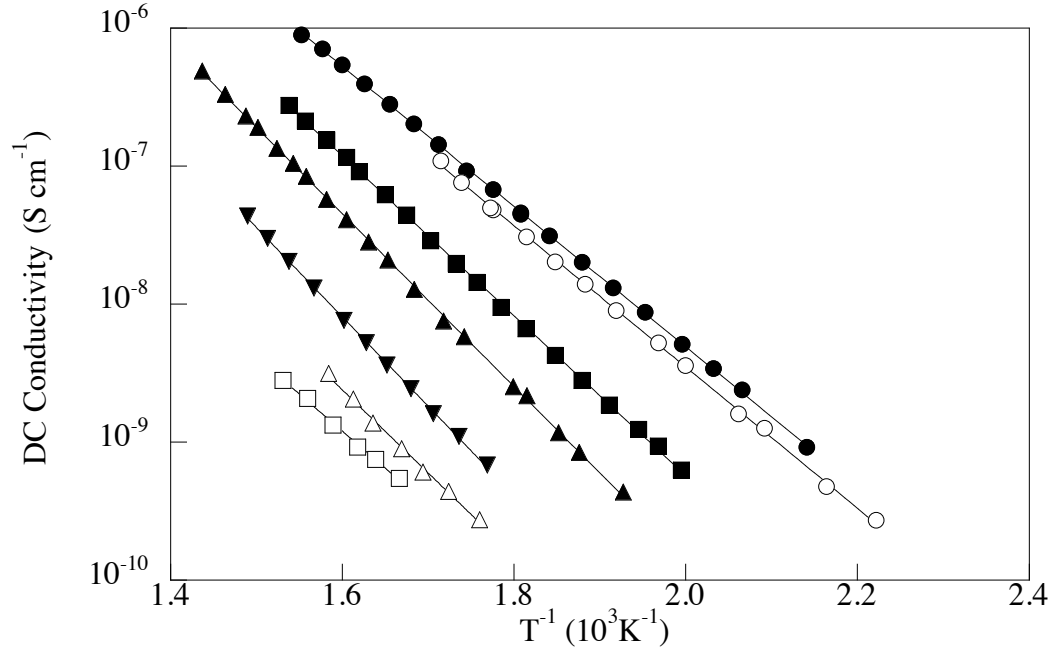


Figure 6-36. DC electrical conductivity values for $x \text{ Na}_2\text{O} \cdot (10-x) \text{ K}_2\text{O} \cdot 90 \text{ GeO}_2$ glasses. Lines are an exponential fit. (● = 10 $\text{Na}_2\text{O} \cdot 90 \text{ GeO}_2$, ■ = 7:1 $\text{Na}_2\text{O}:\text{K}_2\text{O} \cdot 90 \text{ GeO}_2$, ▲ = 3:1 $\text{Na}_2\text{O}:\text{K}_2\text{O} \cdot 90 \text{ GeO}_2$, ▼ = 1:1 $\text{Na}_2\text{O}:\text{K}_2\text{O} \cdot 90 \text{ GeO}_2$, △ = 1:3 $\text{Na}_2\text{O}:\text{K}_2\text{O} \cdot 90 \text{ GeO}_2$, □ = 1:7 $\text{Na}_2\text{O}:\text{K}_2\text{O} \cdot 90 \text{ GeO}_2$, ○ = 10 $\text{K}_2\text{O} \cdot 90 \text{ GeO}_2$)

Table 6-IV. Electrical Conductivity Properties for the $\text{Na}_2\text{O} \cdot \text{K}_2\text{O} \cdot 90 \text{ GeO}_2$ Glasses

Glass Composition 90 Mol% GeO_2	T_g	σ_0	E_{act} (kJ mol^{-1})	σ (S cm^{-1}) 300 °C	σ (S cm^{-1}) T_g
10 Na_2O	515	71.52	97.3	9.75 E-08	2.55 E-5
7:1 $\text{Na}_2\text{O}:\text{K}_2\text{O}$	503	222.3	99.5	1.72 E-08	1.15 E-5
3:1 $\text{Na}_2\text{O}:\text{K}_2\text{O}$	502	474.6	102	5.61 E-09	3.95 E-6
1:1 $\text{Na}_2\text{O}:\text{K}_2\text{O}$	506	184.5	106	9.36 E-10	9.07 E-7
1:3 $\text{Na}_2\text{O}:\text{K}_2\text{O}$	508	509.5	110	2.48 E-10	4.47 E-7
1:7 $\text{Na}_2\text{O}:\text{K}_2\text{O}$	515	803.5	112	1.38 E-10	4.19 E-7
10 K_2O	523	41.52	115	1.48 E-09	1.25 E-6

The DC electrical conductivity curves for $x \text{ Na}_2\text{O} \cdot (15-x) \text{ K}_2\text{O} \cdot 85 \text{ GeO}_2$ glasses are shown in Figure 6-42. Calculated electrical conductivities at T_g and 300 °C are shown in Figure 6-43. A minimum in electrical conductivity occurs when the alkali oxides are in a ratio of 1:1 $\text{Na}_2\text{O}:\text{K}_2\text{O}$. Figure 6-44 shows the log deviation from additivity for conductivity of T_g and 300 °C.

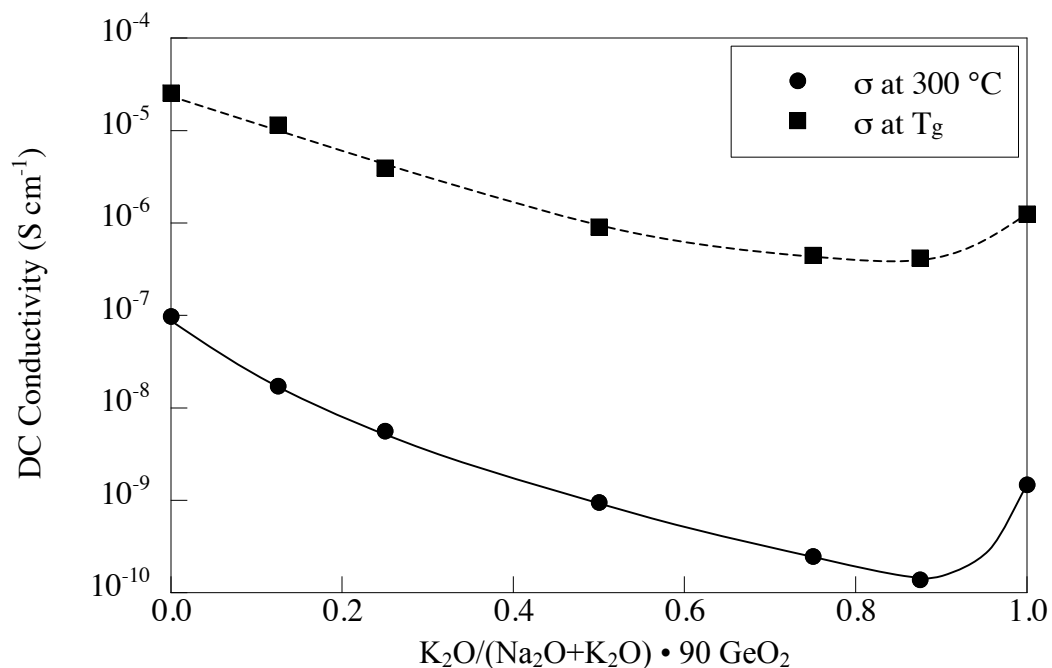


Figure 6-37. DC conductivity for $x Na_2O \cdot (10-x) K_2O \cdot 90 GeO_2$ glasses at the glass transition temperature (T_g) and at 300 °C. Lines added as an aid to the eye.

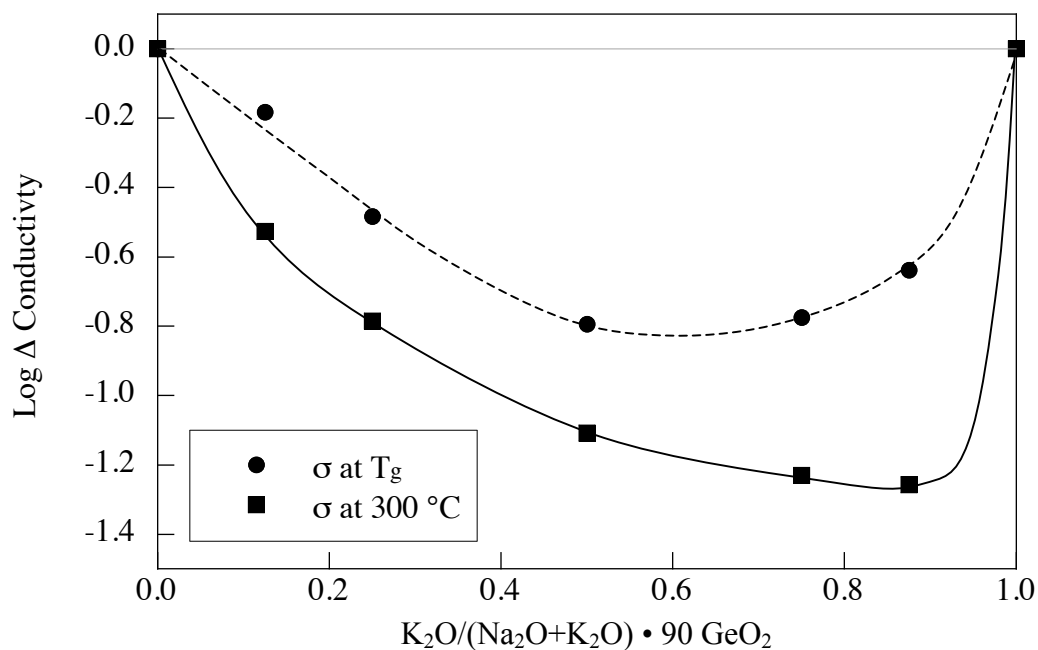


Figure 6-38. Log of the deviation from additivity for the DC electrical conductivity for $x Na_2O \cdot (10-x) K_2O \cdot 90 GeO_2$ glasses at the glass transition temperature (T_g) and 300 °C. Lines added as an aid to the eye.

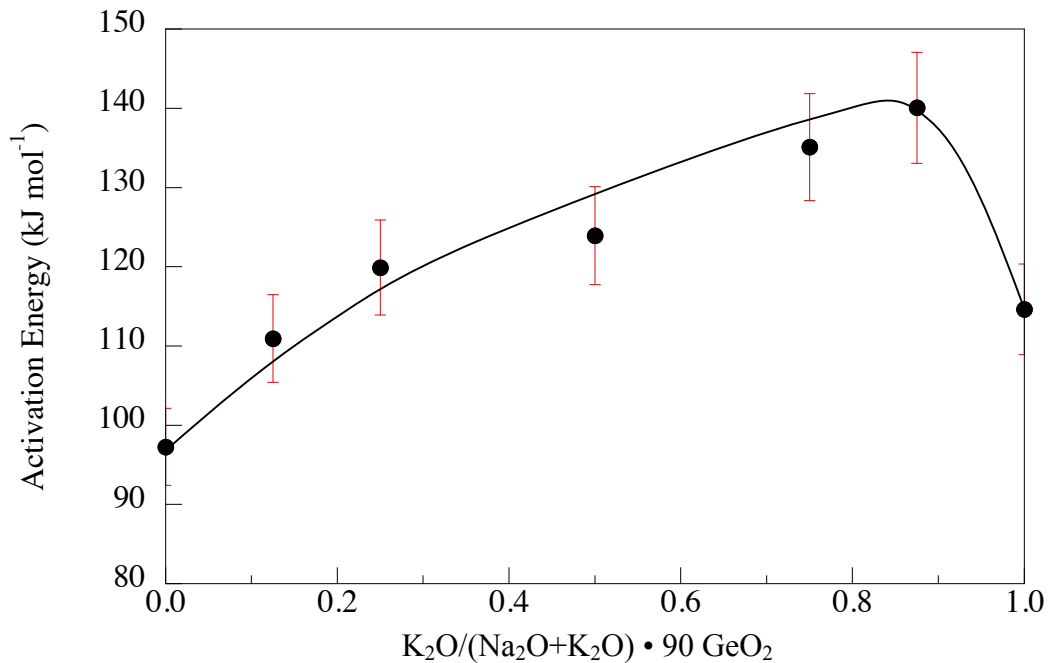


Figure 6-39. Activation energy for DC conductivity of the mixed alkali $x Na_2O \cdot (10-x) K_2O \cdot 90 GeO_2$ glasses. Line added as an aid to the eye.

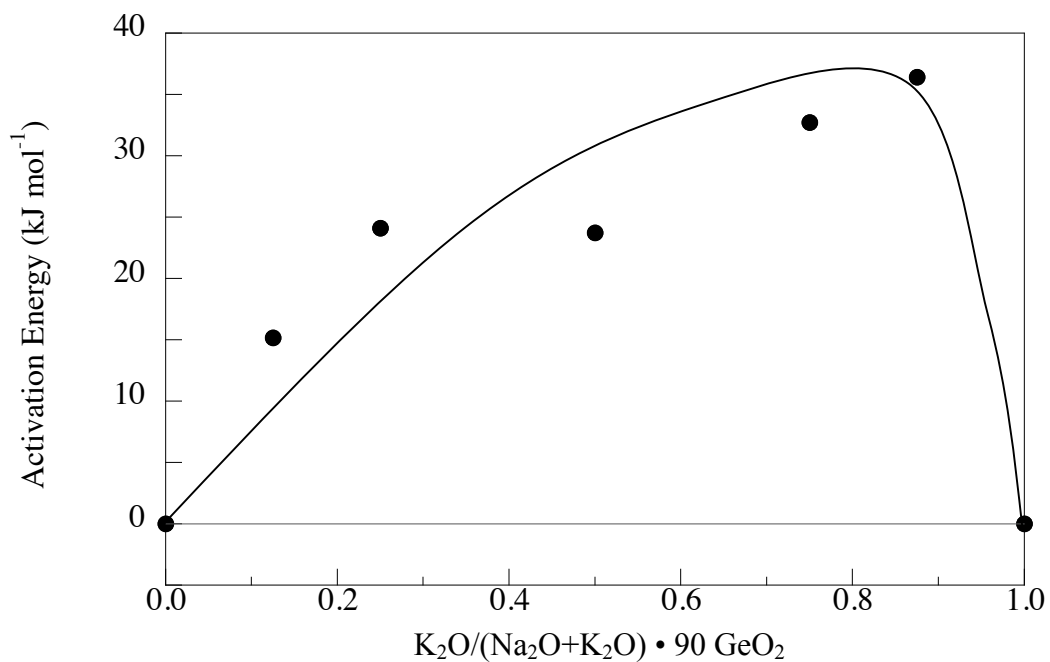


Figure 6-40. Deviation from additivity of the activation energy for DC conductivity for the mixed alkali $x Na_2O \cdot (10-x) K_2O \cdot 90 GeO_2$ glasses. Line added as an aid to the eye.

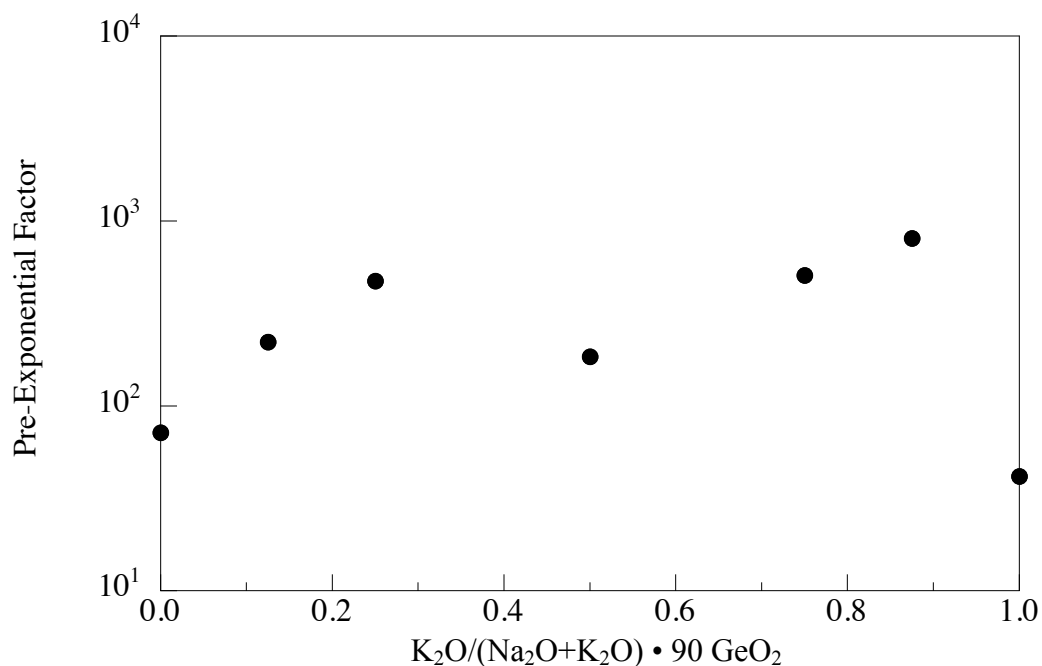


Figure 6-41. Pre-exponential (σ_0) factors for x Na₂O•(10- x) K₂O•90 GeO₂ glasses

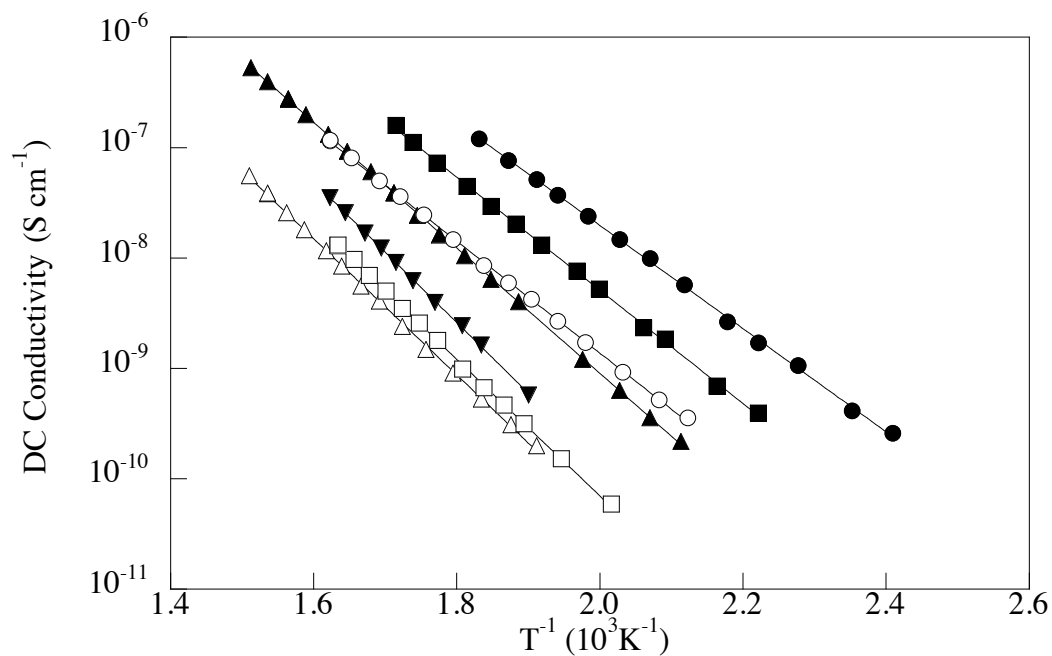


Figure 6-42. DC electrical conductivity values for x Na₂O•(15- x) K₂O•85 GeO₂ glasses. Lines are an exponential fit. (● = 15 Na₂O•85 GeO₂, ■ = 7:1 Na₂O:K₂O•85 GeO₂, ▲ = 3:1 Na₂O:K₂O•85 GeO₂, ▼ = 1:1 Na₂O:K₂O•85 GeO₂, △ = 1:3 Na₂O:K₂O•85 GeO₂, □ = 1:7 Na₂O:K₂O•85 GeO₂, ○ = 15 K₂O•85 GeO₂)

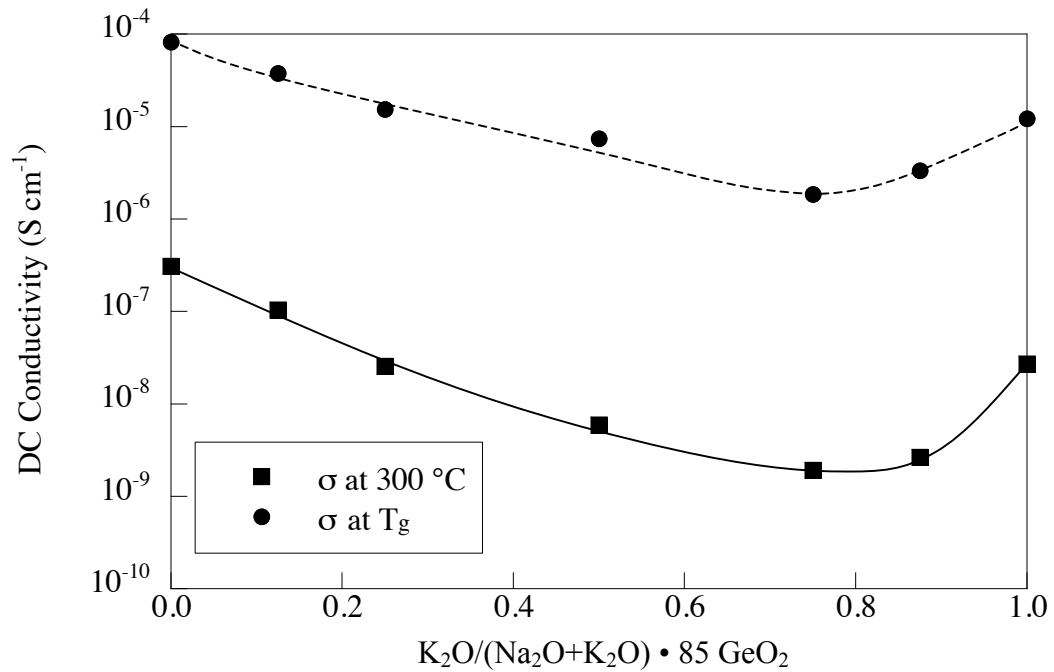


Figure 6-43. DC conductivity for $x \text{ Na}_2\text{O} \cdot (15-x) \text{ K}_2\text{O} \cdot 85 \text{ GeO}_2$ glasses at the glass transition temperature (T_g) and at 300 °C. Lines added as aid to the eye.

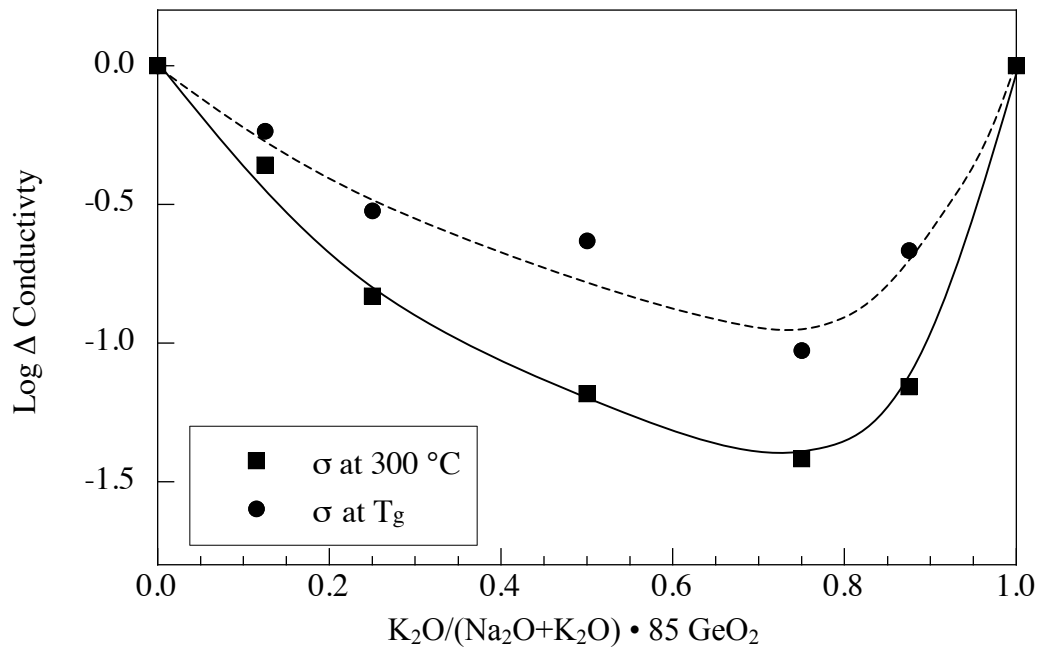


Figure 6-44. Log of the deviation from additivity for the DC electrical conductivity $x \text{ Na}_2\text{O} \cdot (15-x) \text{ K}_2\text{O} \cdot 85 \text{ GeO}_2$ glasses at the glass transition temperature (T_g) and 300 °C. Lines added as aid to the eye.

Activation energy for $x \text{ Na}_2\text{O} \cdot (15-x) \text{ K}_2\text{O} \cdot 85 \text{ GeO}_2$ glasses passes through a maximum when the ratio of the alkali ions is 1:1 $\text{Na}_2\text{O}:\text{K}_2\text{O}$, as in Figure 6-45 and 6-46. The pre-exponential factors are shown in Figure 6-47. The pre-exponential factor of the binary 15 $\text{K}_2\text{O} \cdot 85 \text{ GeO}_2$ glass is around the expected value of 10. The other glasses in the $x \text{ Na}_2\text{O} \cdot (15-x) \text{ K}_2\text{O} \cdot 85 \text{ GeO}_2$ series have pre-exponentials 1 to 1.5 orders of magnitude higher than the anticipated value of 10. Table 6-V lists the values of the pre-exponential, the activation energies and the conductivities at both T_g and 300 °C.

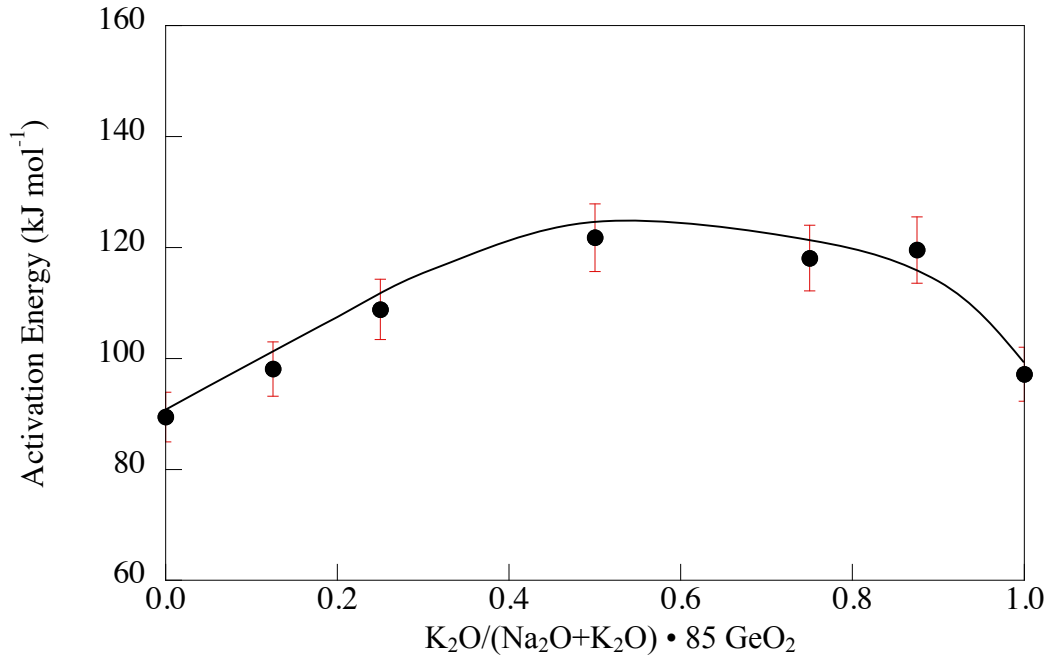


Figure 6-45. Activation energy for DC conductivity of the mixed alkali $x \text{ Na}_2\text{O} \cdot (15-x) \text{ K}_2\text{O} \cdot 85 \text{ GeO}_2$ glasses. Line added as aid to the eye.

Table 6-V. Electrical Conductivity Properties for the $\text{Na}_2\text{O} \cdot \text{K}_2\text{O} \cdot 85 \text{ GeO}_2$ Glasses

Glass Composition 85 Mol% GeO_2	T_g	σ_0	E_{act} (kJ mol ⁻¹)	σ (S cm ⁻¹) 300 °C	σ (S cm ⁻¹) T_g
15 Na_2O	543	43.70	89.47	3.07 E-7	8.23 E-5
7:1 $\text{Na}_2\text{O}:\text{K}_2\text{O}$	530	90.13	98.10	1.04 E-7	3.76 E-5
3:1 $\text{Na}_2\text{O}:\text{K}_2\text{O}$	523	211.5	108.9	2.55 E-8	1.53 E-5
1:1 $\text{Na}_2\text{O}:\text{K}_2\text{O}$	522	738.8	121.8	5.90 E-9	7.40 E-6
1:3 $\text{Na}_2\text{O}:\text{K}_2\text{O}$	520	110.3	118.1	1.91 E-9	1.85 E-6
1:7 $\text{Na}_2\text{O}:\text{K}_2\text{O}$	528	207.8	119.6	2.64 E-9	3.33 E-6
15 K_2O	545	19.45	97.18	2.71 E-8	1.22 E-5

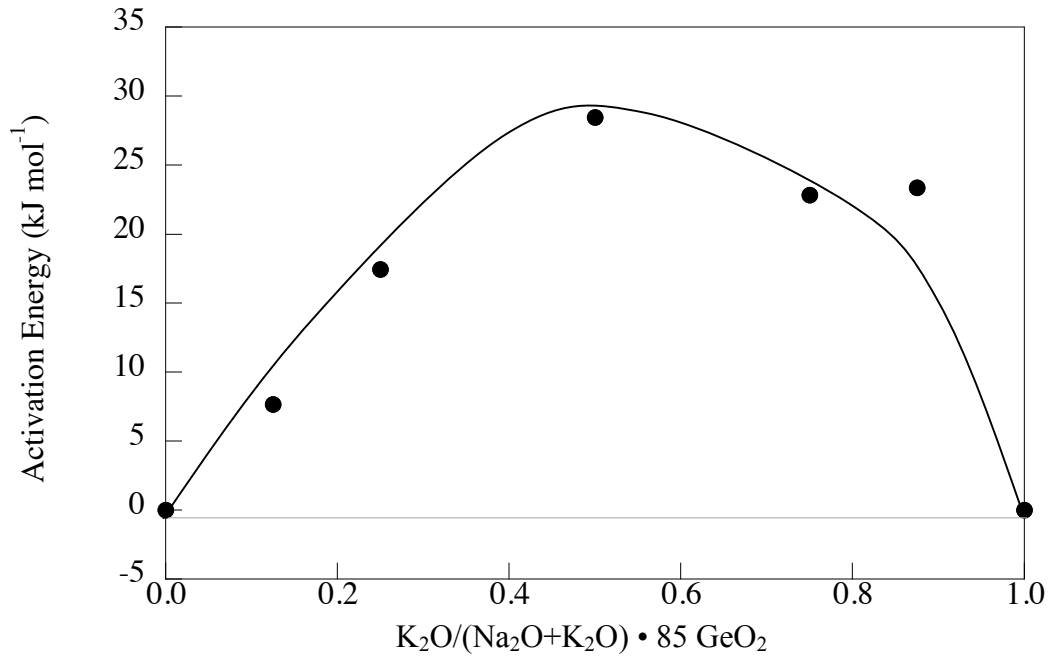


Figure 6-46. Deviation from additivity of the activation energy for DC conductivity for the mixed alkali $x Na_2O \cdot (15-x) K_2O \cdot 85 GeO_2$ glasses. Line added as aid to the eye.

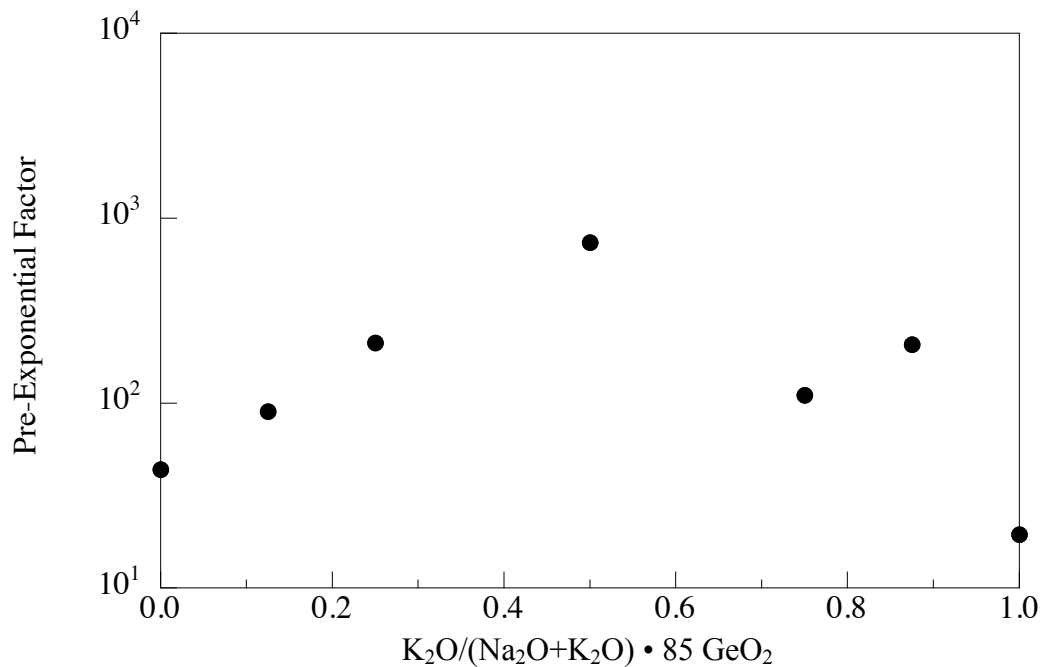


Figure 6-47. Pre-exponential (σ_0) factors for $x Na_2O \cdot (15-x) K_2O \cdot 85 GeO_2$ glasses.

6.4.2 Germanate Anomaly

Three different alkali germanate ternary systems were studied to examine the effect of alkali radius ratios on conductivity. Results for the $\text{Li}_2\text{O}\cdot\text{Cs}_2\text{O}\cdot\text{GeO}_2$ system will be presented; first these alkali ions have the greatest difference in radii of any alkali pair. The effect of decreasing germania concentration on three lines of constant alkali ratio was studied. Results will be presented for the 1:1 $\text{Li}_2\text{O}\cdot\text{Cs}_2\text{O}$ line, the 3:1 $\text{Li}_2\text{O}\cdot\text{Cs}_2\text{O}$, and the 1:3 $\text{Li}_2\text{O}\cdot\text{Cs}_2\text{O}$ line. The second system, $\text{Na}_2\text{O}\cdot\text{K}_2\text{O}\cdot\text{GeO}_2$, has a moderate difference in alkali ionic radii. The final system has the closest ionic radii of all the alkali pairs $\text{K}_2\text{O}\cdot\text{Rb}_2\text{O}\cdot\text{GeO}_2$.

DC conductivity data for $0.5x \text{Li}_2\text{O}\cdot 0.5x \text{Cs}_2\text{O}\cdot(100-x) \text{GeO}_2$ glasses are shown in Figure 6-48. Figure 6-49 shows the effect of increasing alkali oxide concentration on the conductivity at T_g and 300°C . A maximum in conductivity occurs with 2 mol% addition of alkali oxide, after which the conductivity decreases. The conductivity at T_g is approximately 2.25 orders of magnitude higher than that at 300°C . Increasing alkali oxide concentration results in an increase in activation energy as shown in Figure 6-50. The pre-exponential (Figure 6-51) for small additions of alkali oxide (1 to 2 mol %) increases 2 orders of magnitude, after which continuing to increase alkali oxide results in the pre-exponential dropping into the hundreds. Table 6-VI lists the values of the pre-exponential, the activation energies and the conductivities at both T_g and 300°C .

The electrical conductivity behavior for the 3:1 $\text{Li}_2\text{O}:\text{Cs}_2\text{O}$ glasses and the 1:3 $\text{Li}_2\text{O}:\text{Cs}_2\text{O}$ glasses will be discussed together. The DC conductivity curves are shown in Figures 6-52 and 6-53 for 3:1 $\text{Li}_2\text{O}:\text{Cs}_2\text{O}$ glasses and 1:3 $\text{Li}_2\text{O}:\text{Cs}_2\text{O}$ glasses, respectively. The glasses with 3:1 $\text{Li}_2\text{O}:\text{Cs}_2\text{O}$ initially increase in conductivity with alkali oxide addition up to 5 mol % addition, with a relatively constant conductivity after that. The conductivity of glasses with 1:3 $\text{Li}_2\text{O}:\text{Cs}_2\text{O}$ pass through a maximum for a 2 mol % addition, followed by a minimum in conductivity at approximately 10 mol % alkali oxide.

Table 6-VI. Electrical Conductivity Properties for $0.5x \text{Li}_2\text{O} \cdot 0.5x \text{Cs}_2\text{O} \cdot (100-x) \text{GeO}_2$ Glasses

1:1 $\text{Li}_2\text{O}:\text{Cs}_2\text{O}$ Mol% GeO_2	T_g	σ_0	E_{act} (kJ mol^{-1})	σ (S cm^{-1}) 300 °C	σ (S cm^{-1}) T_g
100	482	5.217	107	9.41 E-10	2.19 E-07
99	442	414.3	113	1.99 E-08	2.22 E-06
98	444	1178	116	2.89 E-08	3.89 E-06
95	468	165.2	112	9.86 E-09	1.90 E-06
90	491	103.0	117	2.19 E-09	1.02 E-06
85	497	84.30	120	9.34 E-10	5.35 E-07
83	496	395.9	128	8.88 E-10	7.41 E-07
79	482	196.7	124	1.01 E-09	5.16 E-07

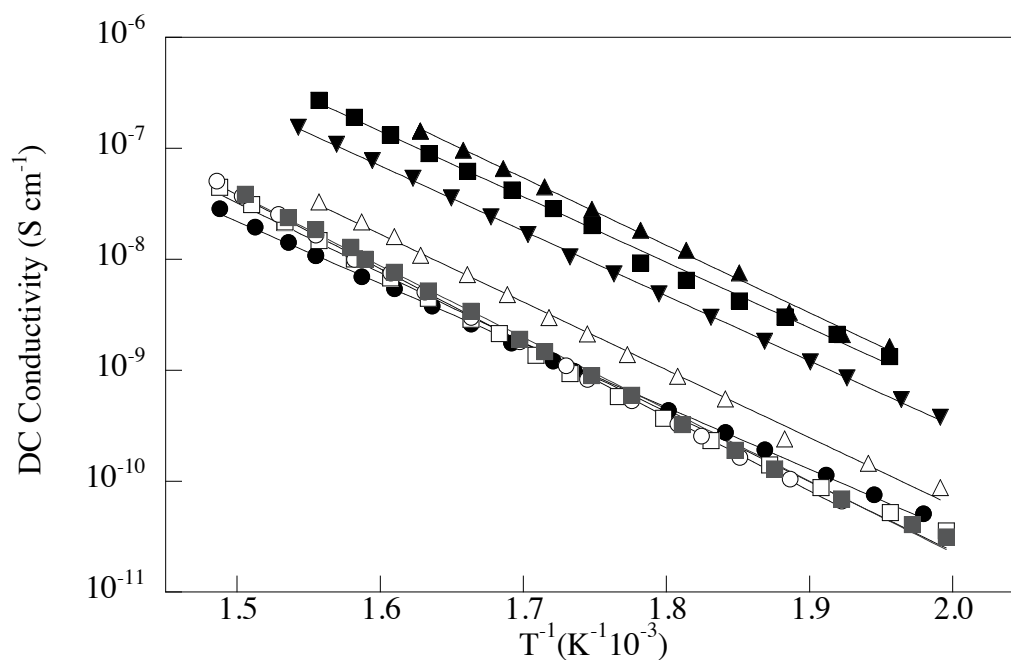


Figure 6-48. DC electrical conductivity values for $0.5x \text{Li}_2\text{O} \cdot 0.5x \text{Cs}_2\text{O} \cdot (100-x) \text{GeO}_2$ glasses. Lines are an exponential fit. (\bullet = 100 GeO_2 , \blacksquare = 99 GeO_2 , \blacktriangle = 98 GeO_2 , \blacktriangledown = 95 GeO_2 , \triangle = 90 GeO_2 , \square = 85 GeO_2 , \circ = 83 GeO_2 , \blacksquare = 79 GeO_2).

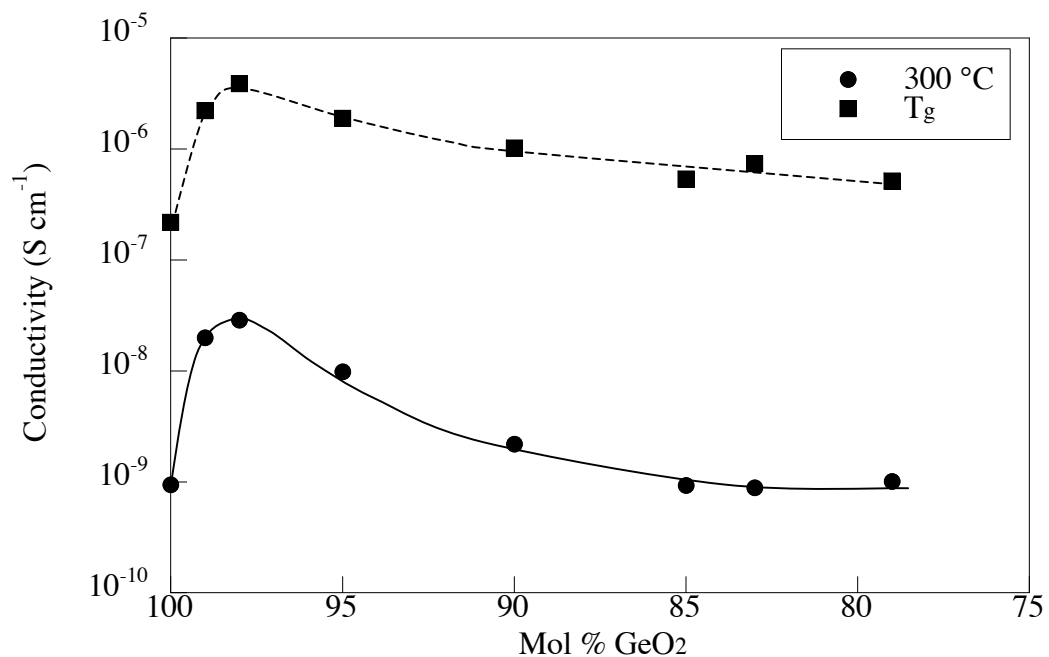


Figure 6-49. DC conductivity for 0.5x Li₂O•0.5x Cs₂O•(100-x) GeO₂ glasses at the glass transition temperature (T_g) and at 300 °C. Lines added as aid to the eye.

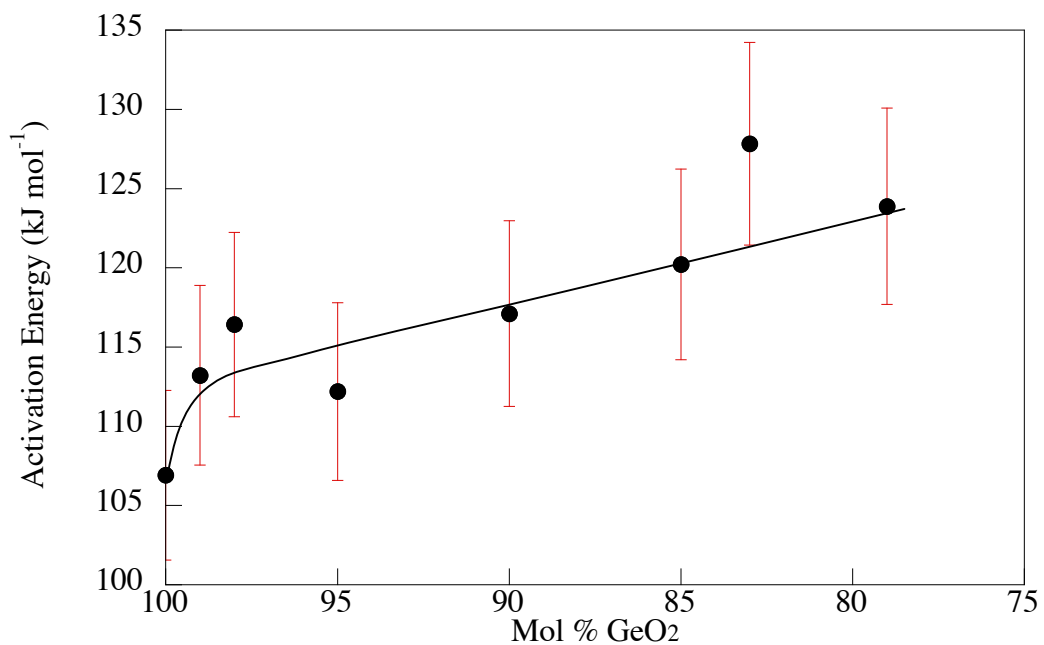


Figure 6-50. Activation energy for 0.5x Li₂O•0.5x Cs₂O•(100-x) GeO₂ glasses. Line added as aid to the eye.

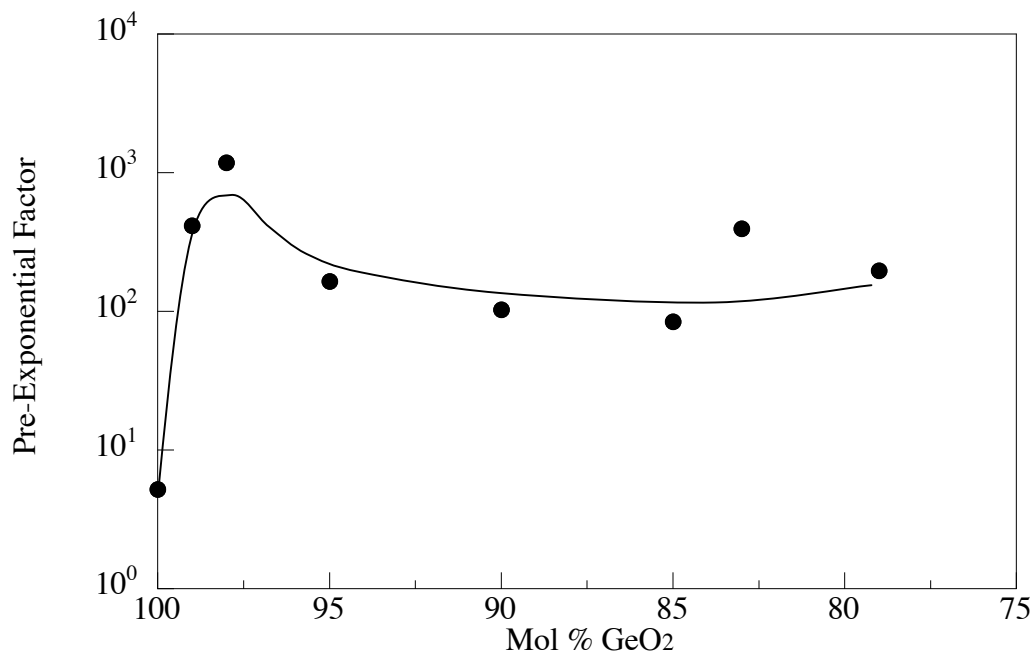


Figure 6-51. Pre-exponential (σ_0) factors for $0.5x \text{Li}_2\text{O} \cdot 0.5x \text{Cs}_2\text{O} \cdot (100-x) \text{GeO}_2$ glasses. Line added as aid to the eye.

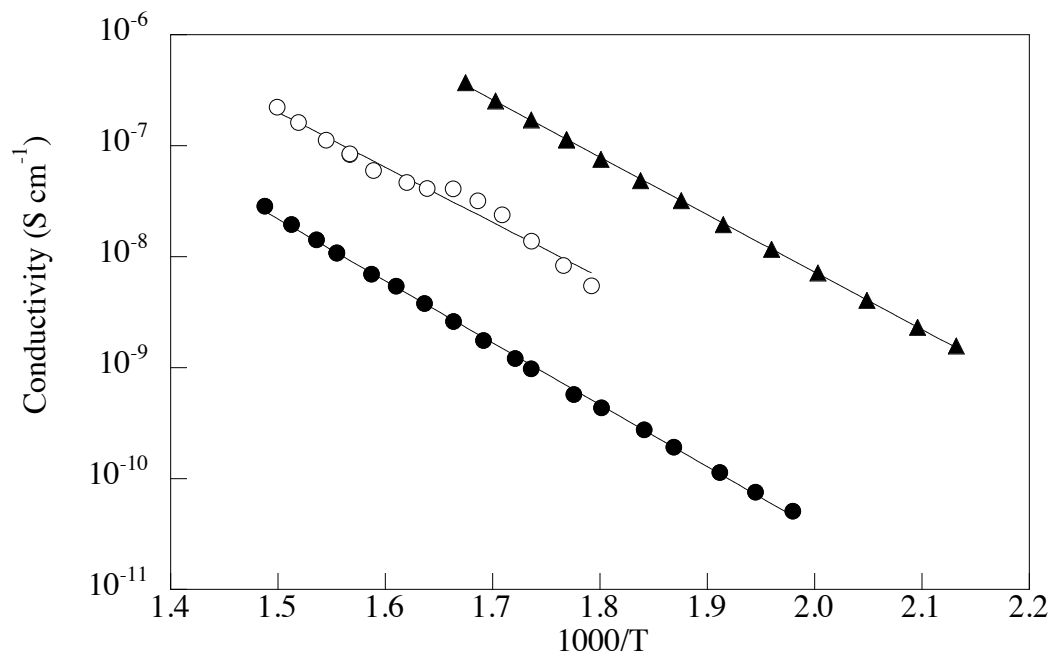


Figure 6-52. DC electrical conductivity values for $0.75x \text{Li}_2\text{O} \cdot 0.25x \text{Cs}_2\text{O} \cdot (100-x) \text{GeO}_2$ glasses. Lines are an exponential fit. (● = 100 GeO₂, ○ = 98 GeO₂, ▲ = 95 GeO₂)

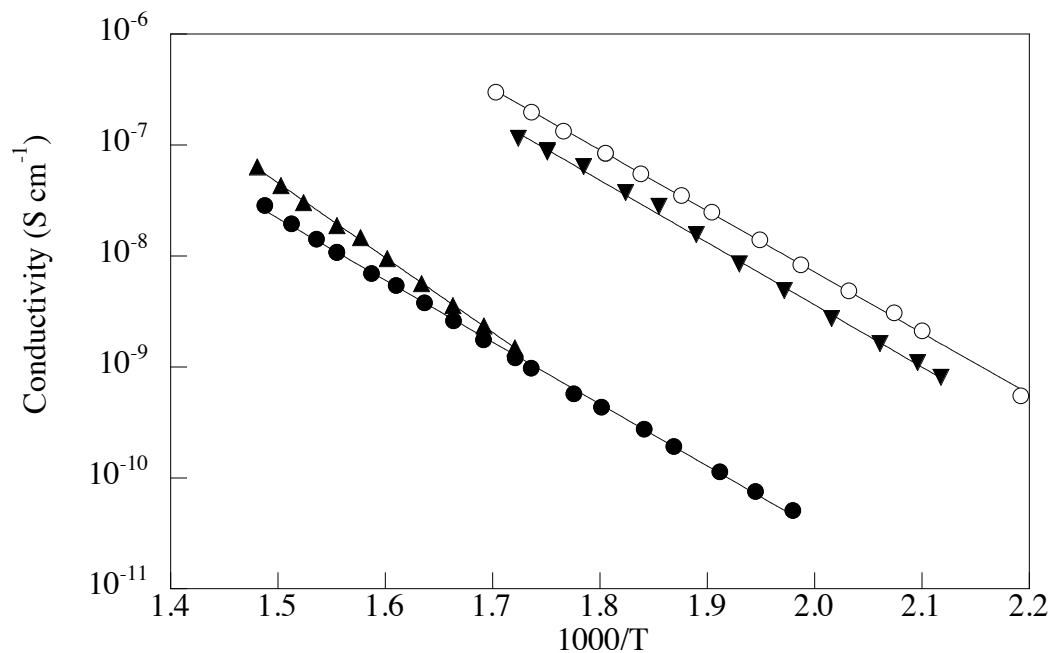


Figure 6-53. DC electrical conductivity values for $0.25x \text{Li}_2\text{O} \cdot 0.75x \text{Cs}_2\text{O} \cdot (100-x) \text{GeO}_2$ glasses. Lines are an exponential fit. (\bullet = 100 GeO₂, \circ = 98 GeO₂, \blacktriangle = 95 GeO₂, \blacktriangledown = 80 GeO₂)

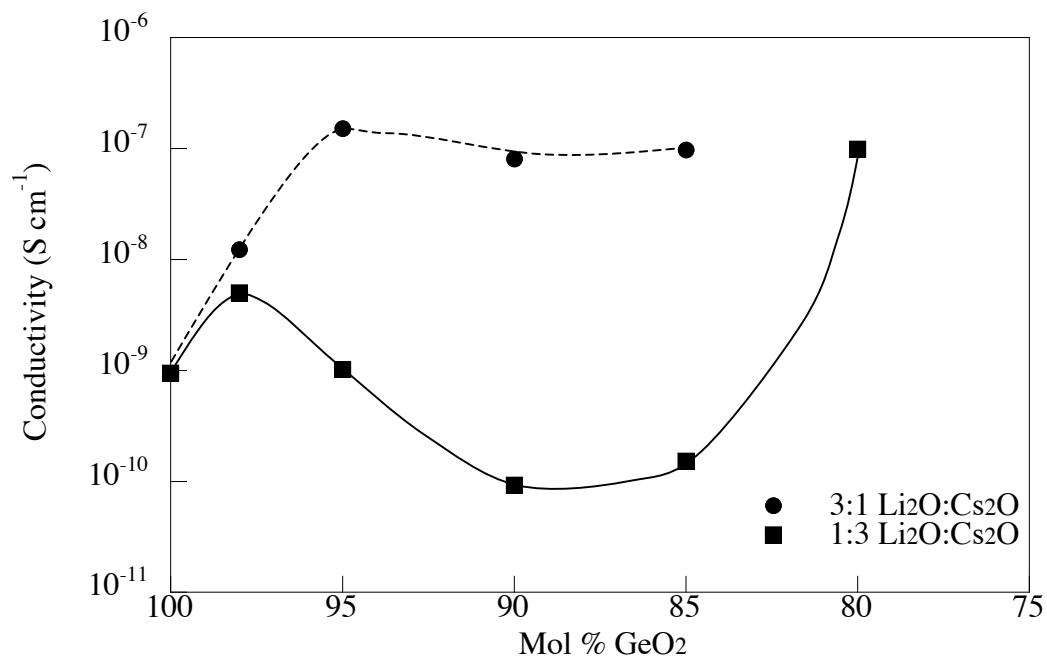


Figure 6-54. DC conductivity for $0.75x \text{Li}_2\text{O} \cdot 0.25x \text{Cs}_2\text{O} \cdot (100-x) \text{GeO}_2$ and $0.25x \text{Li}_2\text{O} \cdot 0.75x \text{Cs}_2\text{O} \cdot (100-x) \text{GeO}_2$ glasses at 300 °C. Lines added to aid the eye.

The activation energies for the 3:1 Li₂O:Cs₂O and the 1:3 Li₂O:Cs₂O glasses are shown in Figure 6-55. A 2 mol % addition of alkali oxide results in a decrease in the activation energy in both systems. Continuing to increase the alkali oxide concentration causes a steady increase in the activation energy of the 3:1 Li₂O:Cs₂O glasses. The 1:3 Li₂O:Cs₂O glasses exhibit a maximum in activation energy for glasses with 5 to 15 mol % alkali oxide. The pre-exponential factors (Figure 5-56) for the glasses with an alkali oxide ratio of 1:3 Li₂O:Cs₂O range from 1 to 2 orders of magnitude about the germania value, and the expected value of 10. Tables 6-VII and 6-VIII lists the values of the pre-exponential, the activation energies and the conductivities at both T_g and 300 °C for the 3:1 Li₂O:Cs₂O and 1:3 Li₂O:Cs₂O glasses, respectively.

Table 6-VII. Electrical Conductivity Properties for 0.75x Li₂O•0.25x Cs₂O•(100-x) GeO₂ Glasses.

3:1 Li ₂ O:Cs ₂ O Mol% GeO ₂	σ_0	E _{act} (kJ mol ⁻¹)	σ (S cm ⁻¹) 300 °C	σ (S cm ⁻¹) T _g
100	5.217	107	9.41 E-10	2.20 E-07
98	5.556	95.0	1.23 E-08	7.01 E-07
95	62.1	99.1	1.52 E-07	1.45 E-05
90	146.8	102	8.09 E-08	1.71 E-05
85	541.6	107	9.76 E-08	3.60 E-05

Table 6-VIII. Electrical Conductivity Properties for 0.25x Li₂O•0.75x Cs₂O•(100-x) GeO₂ Glasses.

1:3 Li ₂ O:Cs ₂ O Mol% GeO ₂	σ_0	E _{act} (kJ mol ⁻¹)	σ (S cm ⁻¹) 300 °C	σ (S cm ⁻¹) T _g
100	5.217	107	9.41 E-10	2.20 E-07
98	47.12	109	5.02 E-09	5.05 E-07
95	580.3	129	1.02 E-09	3.45 E-07
90	835.8	142	9.24 E-11	1.80 E-07
85	66.85	128	1.52 E-10	2.12 E-07
80	609.0	107	9.83 E-08	2.75 E-05

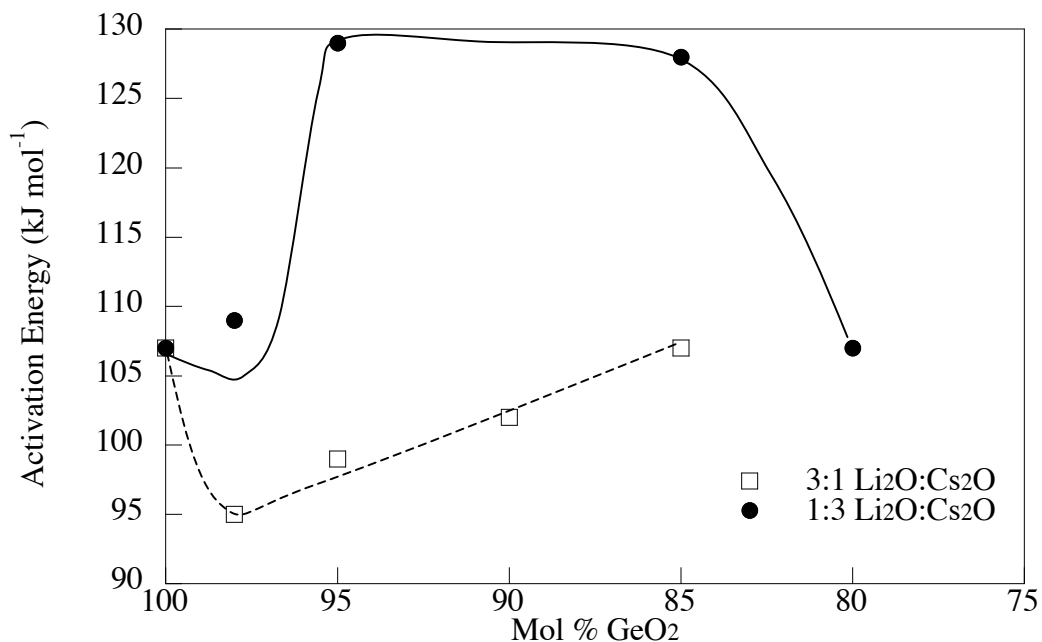


Figure 6-55. Activation energies for DC conductivity for $0.75x \text{Li}_2\text{O} \cdot 0.25x \text{Cs}_2\text{O} \cdot (100-x) \text{GeO}_2$ and $0.25x \text{Li}_2\text{O} \cdot 0.75x \text{Cs}_2\text{O} \cdot (100-x) \text{GeO}_2$ glasses. Lines added as aid to the eye.

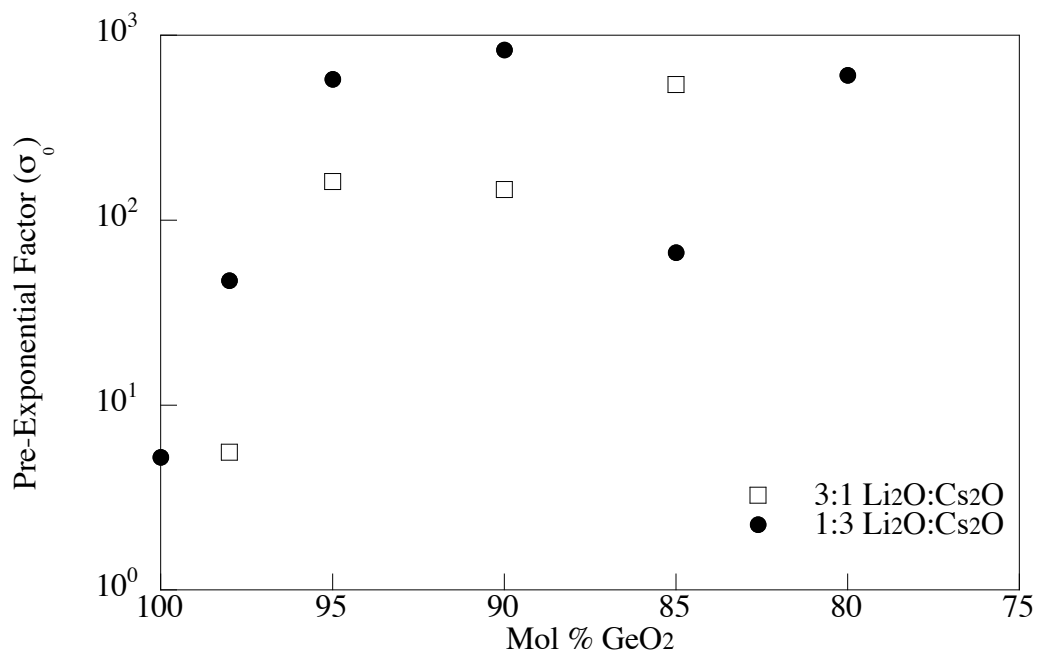


Figure 6-56. Pre-exponential (σ_0) factors for $0.75x \text{Li}_2\text{O} \cdot 0.25x \text{Cs}_2\text{O} \cdot (100-x) \text{GeO}_2$ and $0.25x \text{Li}_2\text{O} \cdot 0.75x \text{Cs}_2\text{O} \cdot (100-x) \text{GeO}_2$ glasses.

The DC electrical conductivity data for $0.5x \text{ Na}_2\text{O} \cdot 0.5x \text{ K}_2\text{O} \cdot (100-x) \text{ GeO}_2$ glasses are shown in Figure 6-57. Figure 6-58 shows the electrical conductivity for $0.5x \text{ Na}_2\text{O} \cdot 0.5x \text{ K}_2\text{O} \cdot (100-x) \text{ GeO}_2$ glasses at both the T_g and 300°C . Adding 2 mol % or less alkali oxide to the glass results in an increase in conductivity of 1 to 1.5 orders of magnitude. Alkali oxide additions greater than 2 mol % result in a decrease in conductivity. A minimum in conductivity occurs at 15 mol % alkali oxide.

Activation energies for $0.5x \text{ Na}_2\text{O} \cdot 0.5x \text{ K}_2\text{O} \cdot (100-x) \text{ GeO}_2$ glasses are shown in Figure 6-59. Alkali oxide additions ≤ 2 mol % result in a decrease in the activation energy. Addition of alkali oxide > 2 mol % result in an increase in the activation energy for conductivity. The pre-exponential of $0.5x \text{ Na}_2\text{O} \cdot 0.5x \text{ K}_2\text{O} \cdot (100-x) \text{ GeO}_2$ glasses increases about one order of magnitude with any addition of alkali oxide into the glass and remains about 100 until 17 mol% alkali oxide where it increases into the thousands, as shown in Figure 6-60. Table 6-IX lists the values of the pre-exponential, the activation energies and the conductivities at both T_g and 300°C .

Table 6-IX. Electrical Conductivity Properties for $0.5x \text{ Na}_2\text{O} \cdot 0.5x \text{ K}_2\text{O} \cdot (100-x) \text{ GeO}_2$ Glasses

1:1 $\text{Na}_2\text{O}:\text{K}_2\text{O}$ Mol% GeO_2	T_g	σ_0	E_{act} (kJ mol^{-1})	σ (S cm^{-1}) at 300°C	σ (S cm^{-1}) T_g
100	482	5.217	107	9.41 E-10	2.19 E-07
99	442	65.29	105	1.80 E-08	1.42 E-06
98	436	81.39	102	4.17 E-08	2.51 E-06
97	437	202.6	115	6.53 E-09	6.69 E-07
95	463	28.31	113	1.50 E-09	3.18 E-07
90	506	215.3	125	9.20 E-10	9.29 E-07
85	522	92.91	123	6.30 E-10	8.24 E-07
83	500	2095	126	6.50 E-09	1.03 E-05

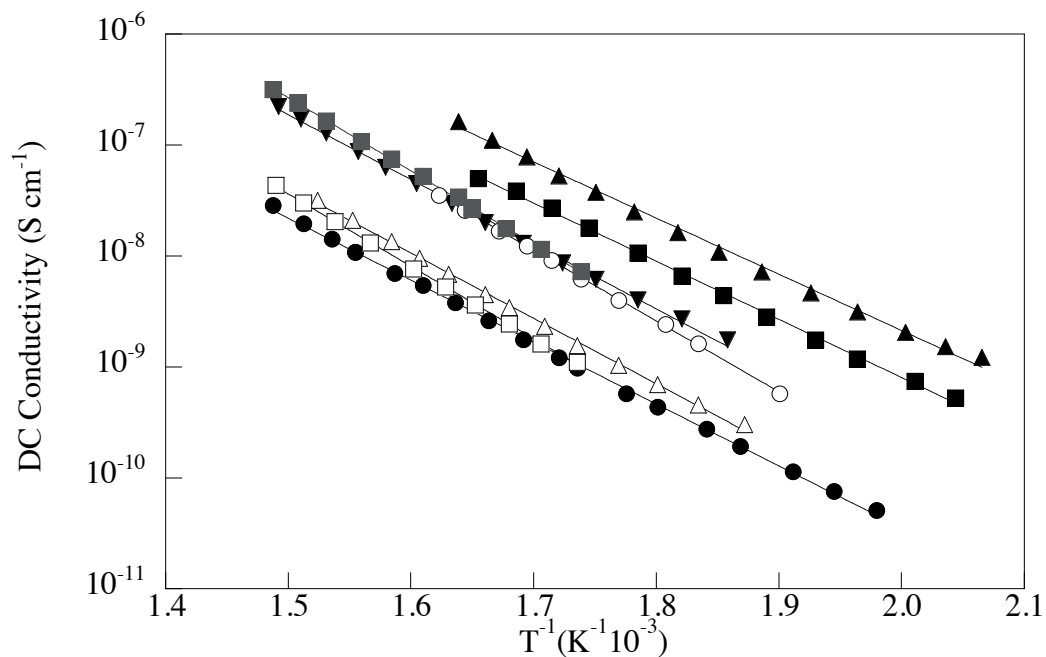


Figure 6-57. DC electrical conductivity values for $0.5x \text{ Na}_2\text{O} \cdot 0.5x \text{ K}_2\text{O} \cdot (100-x) \text{ GeO}_2$ glasses. Lines are an exponential fit. (\bullet = 100 GeO₂, \blacksquare = 99 GeO₂, \blacktriangle = 98 GeO₂, \blacktriangledown = 97 GeO₂, \triangle = 95 GeO₂, \square = 90 GeO₂, \circ = 85 GeO₂, \blacksquare = 83 GeO₂)

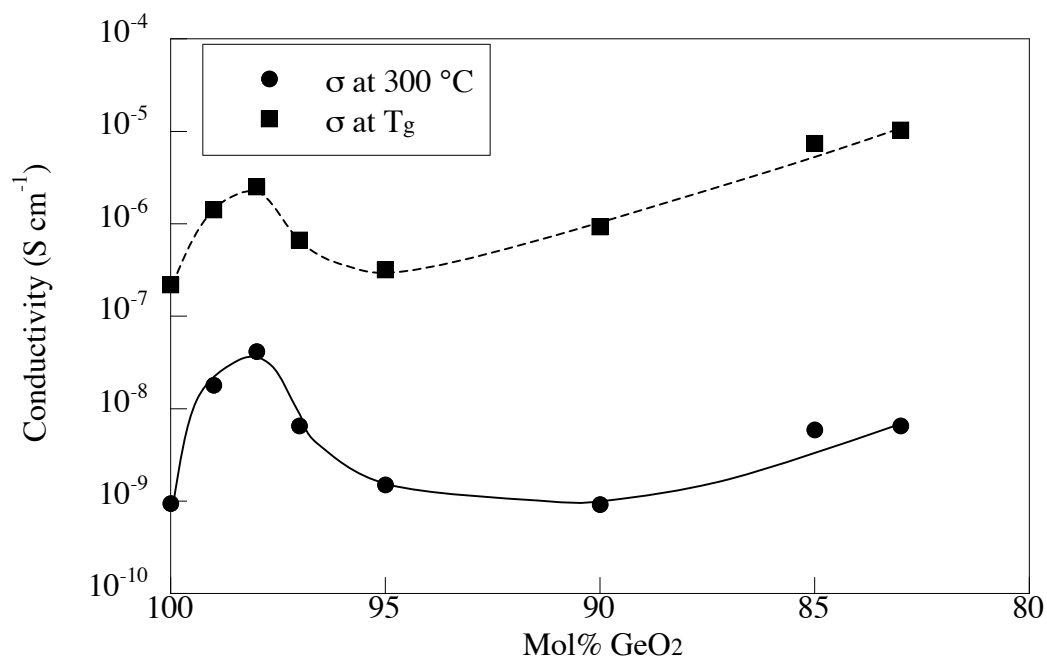


Figure 6-58. DC conductivity for $0.5x \text{ Na}_2\text{O} \cdot 0.5x \text{ K}_2\text{O} \cdot (100-x) \text{ GeO}_2$ glasses at the glass transition temperature (T_g) and at 300 °C. Lines added as aid to the eye.

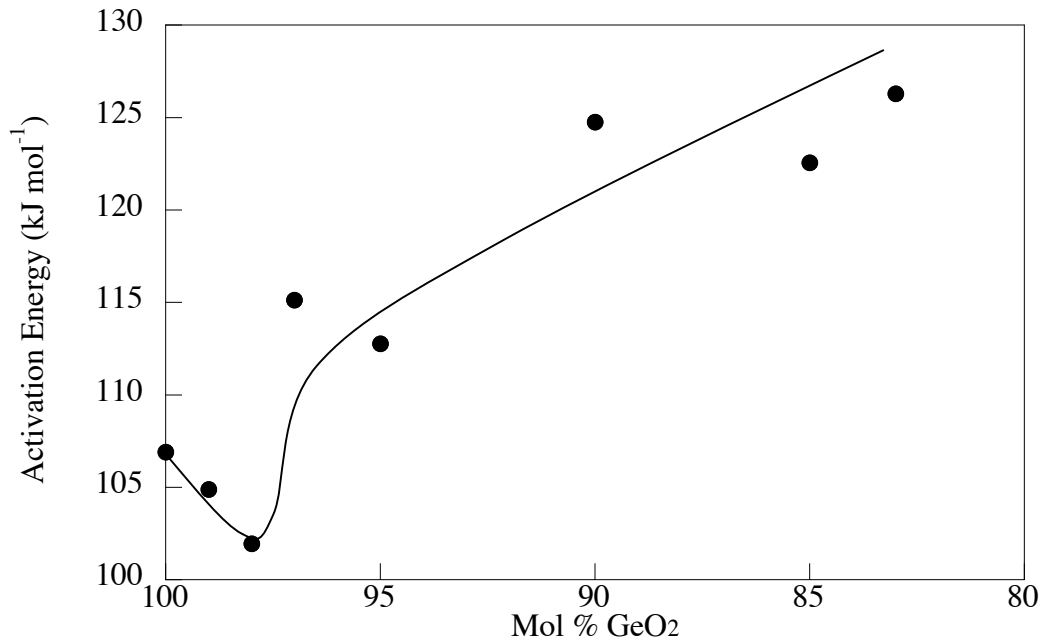


Figure 6-59. Activation energy for $0.5x \text{Na}_2\text{O} \cdot 0.5x \text{K}_2\text{O} \cdot (100-x) \text{GeO}_2$ glasses. Line added as aid to the eye.

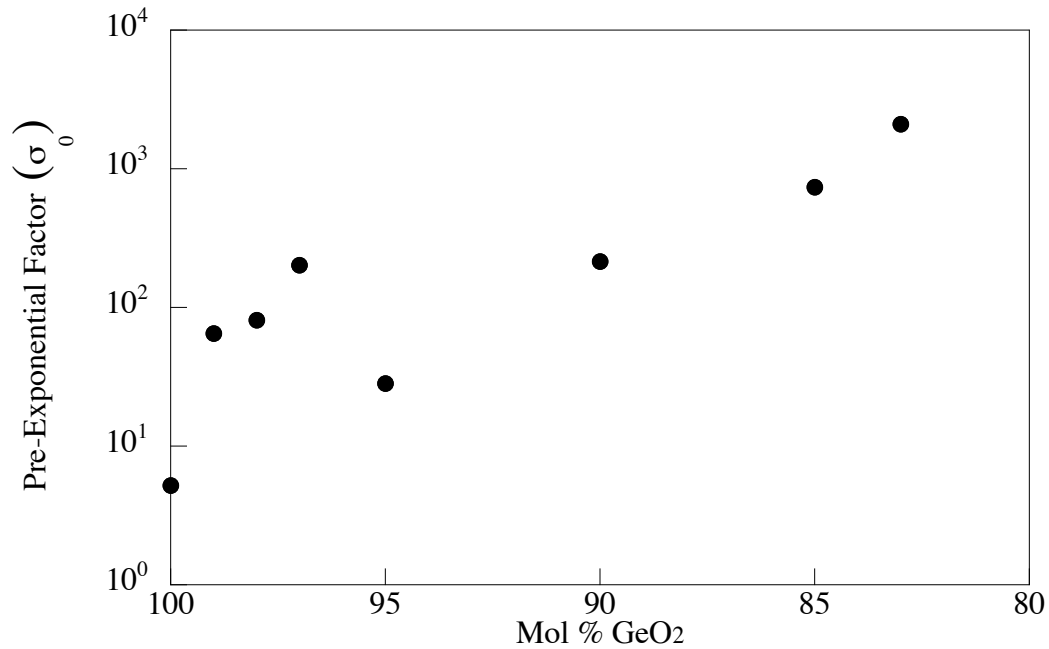


Figure 6-60. Pre-exponential (σ_0) factors for $0.5x \text{Na}_2\text{O} \cdot 0.5x \text{K}_2\text{O} \cdot (100-x) \text{GeO}_2$ glasses.

The electrical conductivity data for $0.5x \text{K}_2\text{O} \cdot 0.5x \text{Rb}_2\text{O} \cdot (100-x) \text{GeO}_2$ are shown in Figure 6-61. The conductivities at 300 °C and T_g are shown in Figure 6-62. At 300 °C, the conductivity decreases with increasing alkali oxide until 15 mol % alkali oxide is

added, then the electrical conductivity increase 4 orders of magnitude between 10 mol % and 15 mol % alkali oxide addition. The conductivity at T_g behaves differently, with a minimum occurring at 95 mol %, and all conductivities lying within one order of magnitude.

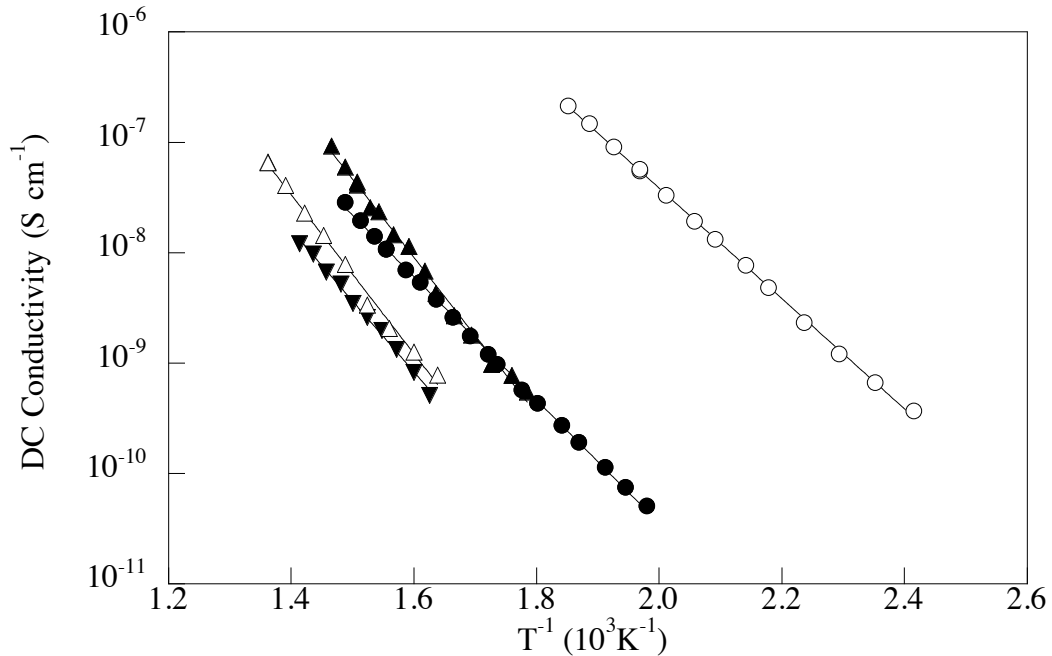


Figure 6-61. DC electrical conductivity values for $0.5x \text{ K}_2\text{O} \cdot 0.5x \text{ Rb}_2\text{O} \cdot (100-x) \text{ GeO}_2$ glasses. Lines are an exponential fit ($\bullet = 100 \text{ GeO}_2$, $\blacktriangle = 98 \text{ GeO}_2$, $\triangle = 95 \text{ GeO}_2$, $\blacktriangledown = 90 \text{ GeO}_2$, $\circ = 85 \text{ GeO}_2$).

Activation energies for conductivity are shown in Figure 6-63. Addition of alkali oxide results in an ‘M’ shaped curve with maxima occurring at 2 and 10 mol % alkali oxide. The pre-exponential factors are shown in Figure 6-64. A small amount of alkali oxide (2 mol %) causes the pre-exponential to increase almost 5 orders of magnitude, with 5 mol % alkali oxide addition the pre-exponential drops back to an expected value. Alkali oxide additions greater than 5 mol % resulting in a pre-exponential around 1000. Table 6-X lists the values of the pre-exponential, the activation energies and the conductivities at both T_g and 300 °C.

Table 6-X. Electrical Conductivity Properties for $0.5x \text{K}_2\text{O} \cdot 0.5x \text{Rb}_2\text{O} \cdot (100-x) \text{GeO}_2$ Glasses.

1:1 $\text{K}_2\text{O}:\text{Rb}_2\text{O}$ Mol% GeO_2	σ_0	E_{act} (kJ mol^{-1})	σ (S cm^{-1}) 300 °C	σ (S cm^{-1}) T_g
100	5.217	107	9.41 E-10	2.19 E-07
98	7516	143	7.21 E-10	3.48 E-07
95	5.941	117	1.18 E-10	3.55 E-08
90	966.0	143	9.06 E-11	4.78 E-07
85	514.0	96.9	7.53 E-07	1.39 E-06

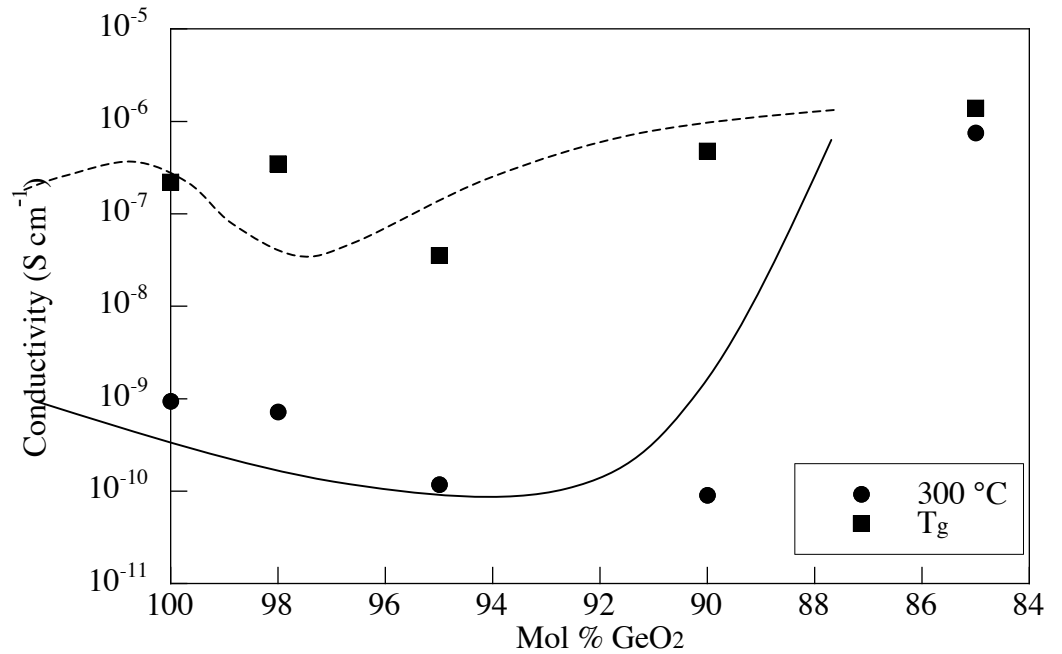


Figure 6-62. DC conductivity for $0.5x \text{K}_2\text{O} \cdot 0.5x \text{Rb}_2\text{O} \cdot (100-x) \text{GeO}_2$ glasses at the glass transition temperature (T_g) and at 300 °C. Lines added as aid to the eye.

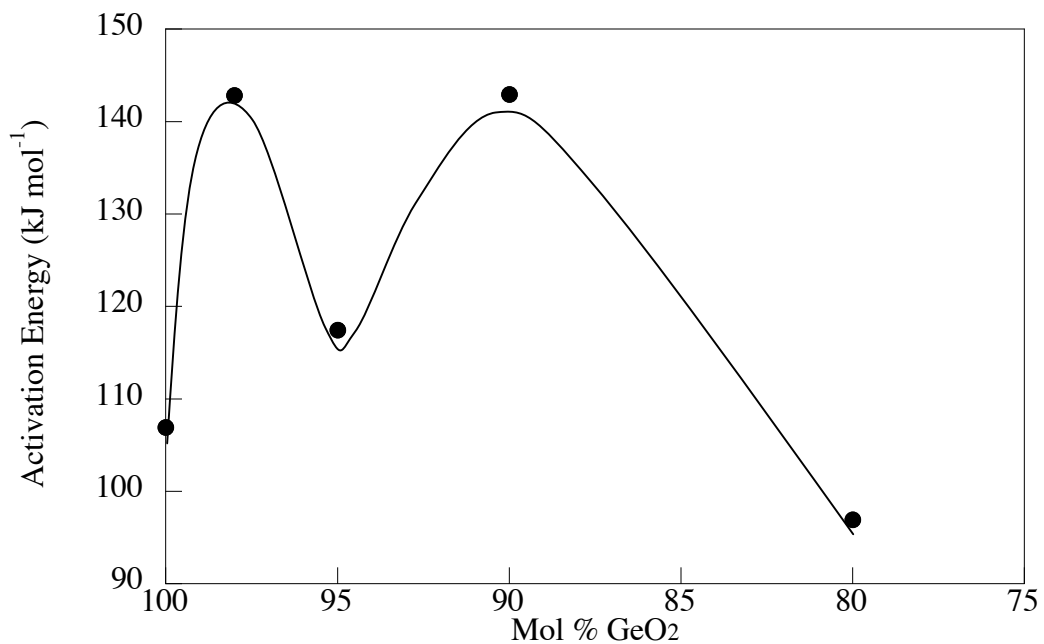


Figure 6-63. Activation energy for $0.5x \text{K}_2\text{O} \cdot 0.5x \text{Rb}_2\text{O} \cdot (100-x) \text{GeO}_2$ glasses. Line added as aid to the eye.

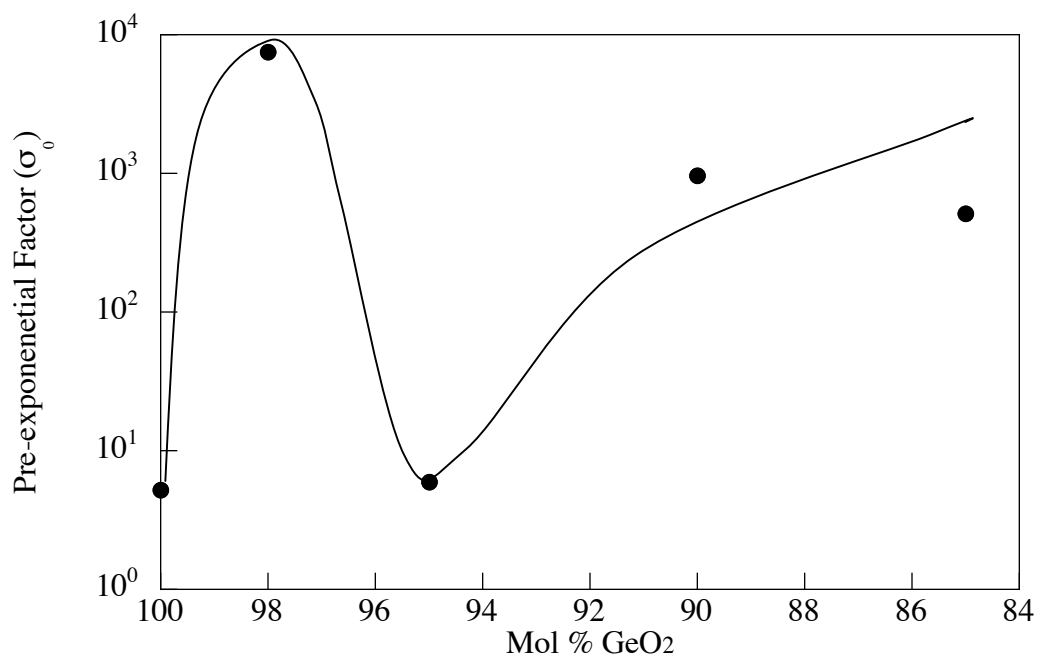


Figure 6-64. Pre-exponential (σ_0) factors for $0.5x \text{K}_2\text{O} \cdot 0.5x \text{Rb}_2\text{O} \cdot (100-x) \text{GeO}_2$ glasses. Line added as aid to the eye.

6.5 Discussion

6.5.1 *Mixed Alkali Effect*

This section will first compare the 90 mol % line to the 85 mol % line for the $x \text{Li}_2\text{O} \cdot y \text{Cs}_2\text{O} \cdot (100-x-y) \text{GeO}_2$ and $x \text{Na}_2\text{O} \cdot y \text{K}_2\text{O} \cdot (100-x-y) \text{GeO}_2$ glasses, followed by a discussion of the effect of the cation identity on conductivity. For simplicity, unless otherwise noted, all electrical conductivities discussed were measured at 300 °C. The results will be discussed in the context of the electrical conductivities, activation energies, pre-exponential factors and comparisons to the literature.

6.5.1.1 Electrical Conductivity

Comparing the electrical conductivity of the $x \text{Li}_2\text{O} \cdot 10-x \text{Cs}_2\text{O} \cdot 90 \text{GeO}_2$ glasses to $x \text{Li}_2\text{O} \cdot 15-x \text{Cs}_2\text{O} \cdot 85 \text{GeO}_2$ glasses (Figure 6-65) shows similar conductivities for glasses with more Li_2O than Cs_2O . As the Cs_2O content increases, the conductivities start to behave differently. The largest difference occurs for the binary $\text{Cs}_2\text{O} \cdot \text{GeO}_2$ glasses, where the conductivity of the 15 $\text{Cs}_2\text{O} \cdot 85 \text{GeO}_2$ glass is 4 orders of magnitude greater than that of the 10 $\text{Cs}_2\text{O} \cdot 90 \text{GeO}_2$ glass. Figure 6-66 shows the difference additivity and the actual conductivity. The glasses containing 10 mol % alkali oxide exhibit a deviation from additivity of no more than 0.8 orders of magnitude, where the glasses with 15 mol % alkali oxide exhibit a maximum deviation almost 2.5 orders of magnitude. This behavior is expected, as glasses with more alkali oxide have more charge carriers.^{66,69,84} The minimum occurs on the Cs_2O rich side of the compositional series.

Comparison of the electrical conductivity of the $x \text{Na}_2\text{O} \cdot (10-x) \text{K}_2\text{O} \cdot 90 \text{GeO}_2$ glasses with that of $x \text{Na}_2\text{O} \cdot (15-x) \text{K}_2\text{O} \cdot 85 \text{GeO}_2$ glasses shows behavior similar to the $\text{Li}_2\text{O} \cdot \text{Cs}_2\text{O} \cdot \text{GeO}_2$ glasses. The greatest deviation in additivity occurs in the glasses with 15 mol % alkali oxide, where there is a deviation of approximately 2 orders of magnitude when the $\text{Na}_2\text{O}:\text{K}_2\text{O}$ ratio is 1:1 (Figure 6-68). The glasses containing only 10 mol % alkali oxide have a maximum deviation of only 1.2 orders of magnitude, with a minimum in conductivity for a $\text{Na}_2\text{O}:\text{K}_2\text{O}$ ratio of 1:7.

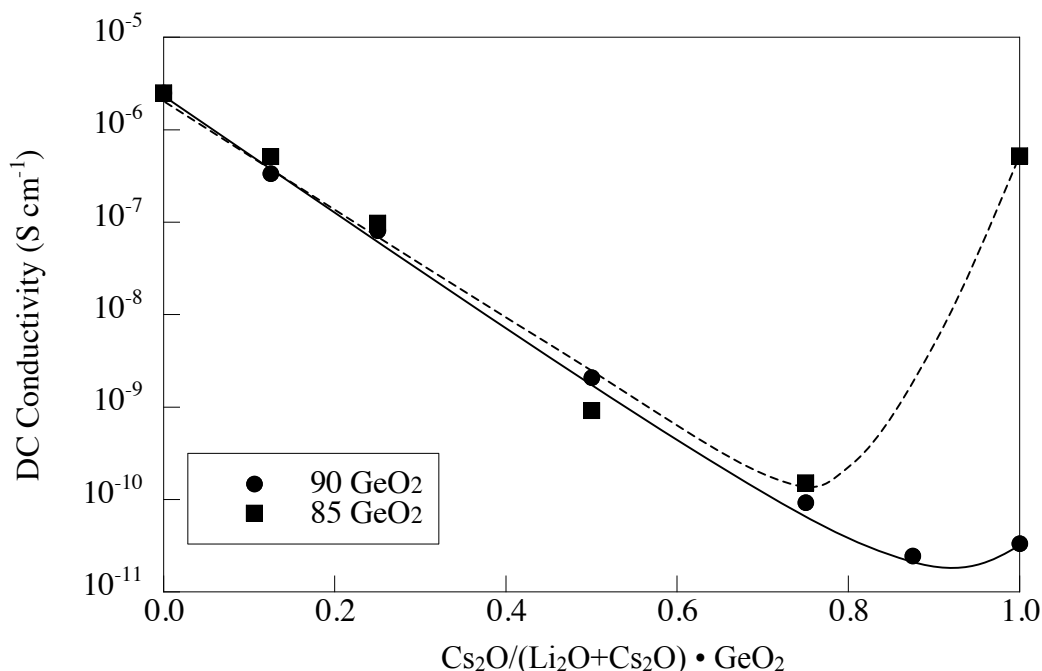


Figure 6-65. Comparison of the DC conductivity at 300 °C for $\text{Li}_2\text{O} \cdot \text{Cs}_2\text{O} \cdot \text{GeO}_2$ glasses with 90 and 85 mol % GeO_2 . Lines added as aid to the eye.

Comparison of the effect of the cation identity on electrical conductivity yields surprising results. Figure 6-69 shows the deviation from additivity of the log of the electrical conductivity for glasses with 90 mol % GeO_2 . Note that the glasses with Li_2O and Cs_2O (a larger size difference between ions) have a smaller deviation from additivity than the glasses with Na_2O and K_2O (a smaller difference between ionic radii). In silicate glasses, it is well established that, the greater the difference in alkali sizes, the greater the deviation from additivity.⁸ The deviation from conductivity is less ‘anomalous’ for glasses containing 15 mol % alkali oxide (Figure 6-70). Where the $\text{Li}_2\text{O}/\text{Cs}_2\text{O}$ glasses show a two order of magnitude greater deviation from additivity than the $\text{Na}_2\text{O}/\text{K}_2\text{O}$ glasses. It is important to recall, that the structure of the germanate glasses differs at these two different concentrations of germania. Glasses containing 90 mol % GeO_2 contain both four-coordinated and five-coordinated germanium with few NBO (Chapter 2). When the concentration of germania reaches 85 mol %, however, non-bridging oxygen begin to form in significant quantities.

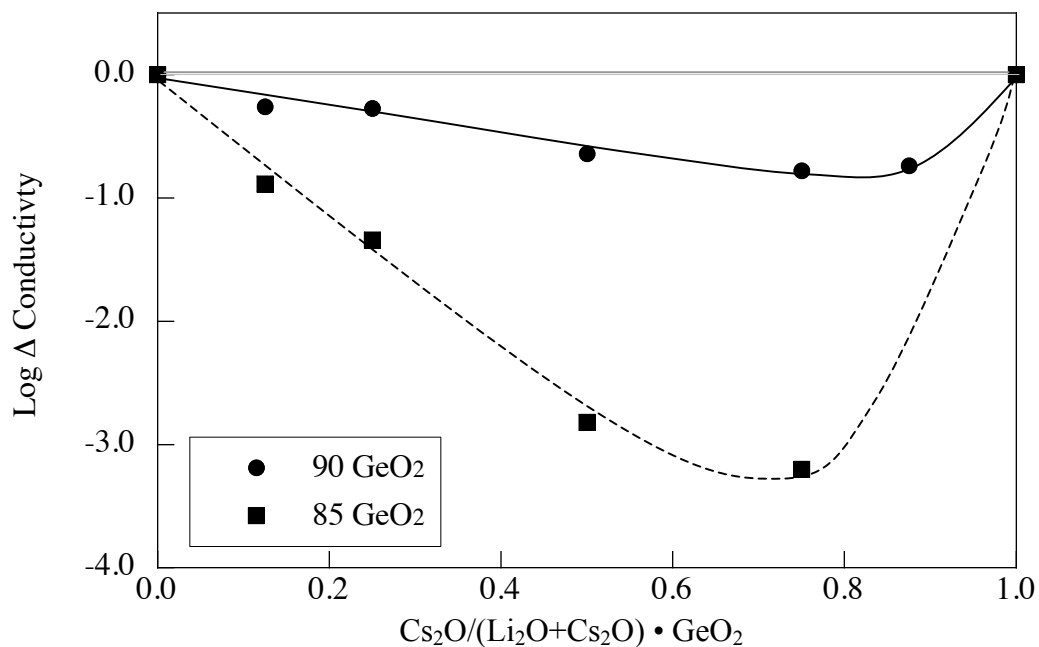


Figure 6-66. Difference between the log of the conductivity at 300 °C and the log of the additive line for $\text{Li}_2\text{O}\cdot\text{Cs}_2\text{O}\cdot\text{GeO}_2$ glasses with 90 and 85 mol % GeO_2 . Lines added as an aid to the eye.

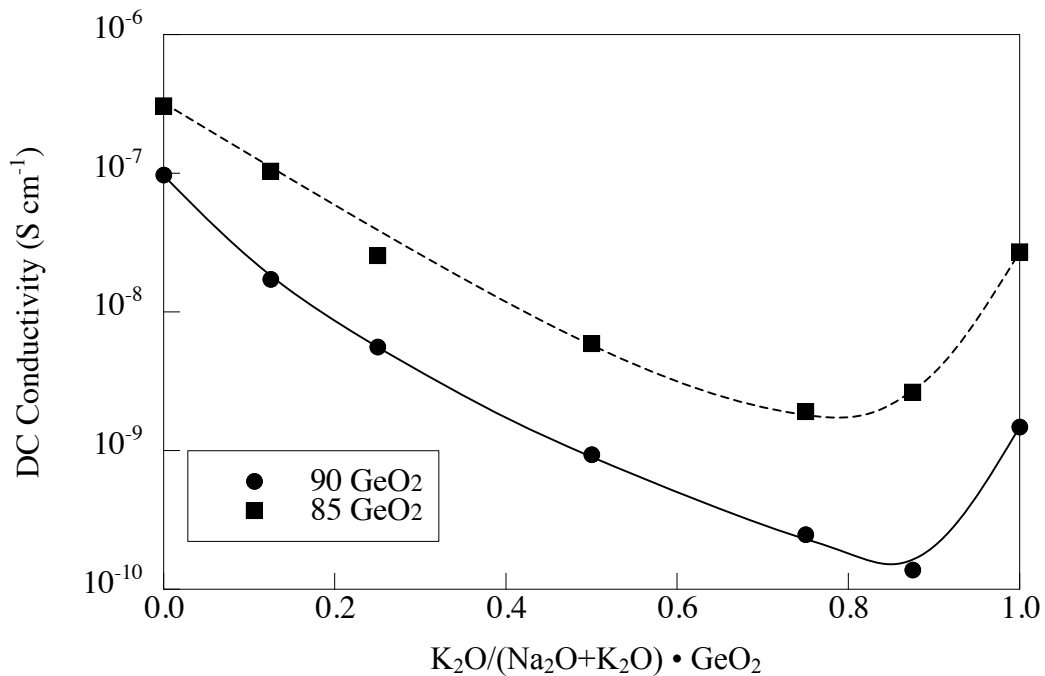


Figure 6-67. Comparison of the DC conductivity at 300 °C for $\text{Na}_2\text{O}\cdot\text{K}_2\text{O}\cdot\text{GeO}_2$ glasses with 90 and 85 mol % GeO_2 . Lines added as aid to the eye.

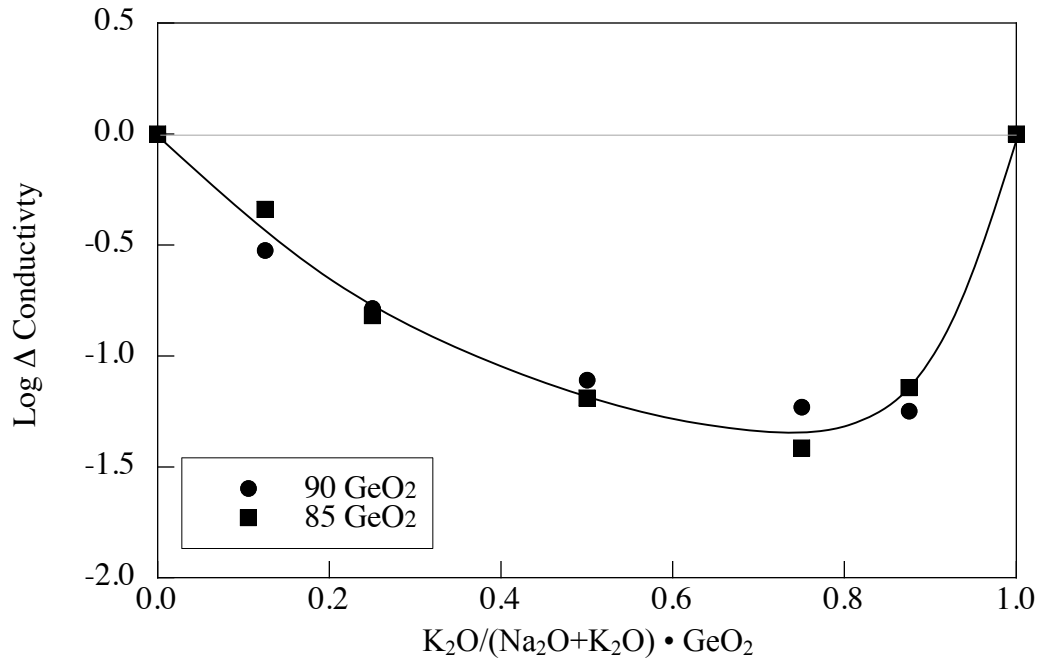


Figure 6-68. Difference between the log of the conductivity at 300 °C and the log of the additive line for $Na_2O \cdot K_2O \cdot GeO_2$ glasses with 90 and 85 mol % GeO_2 . Line added as an aid to the eye.

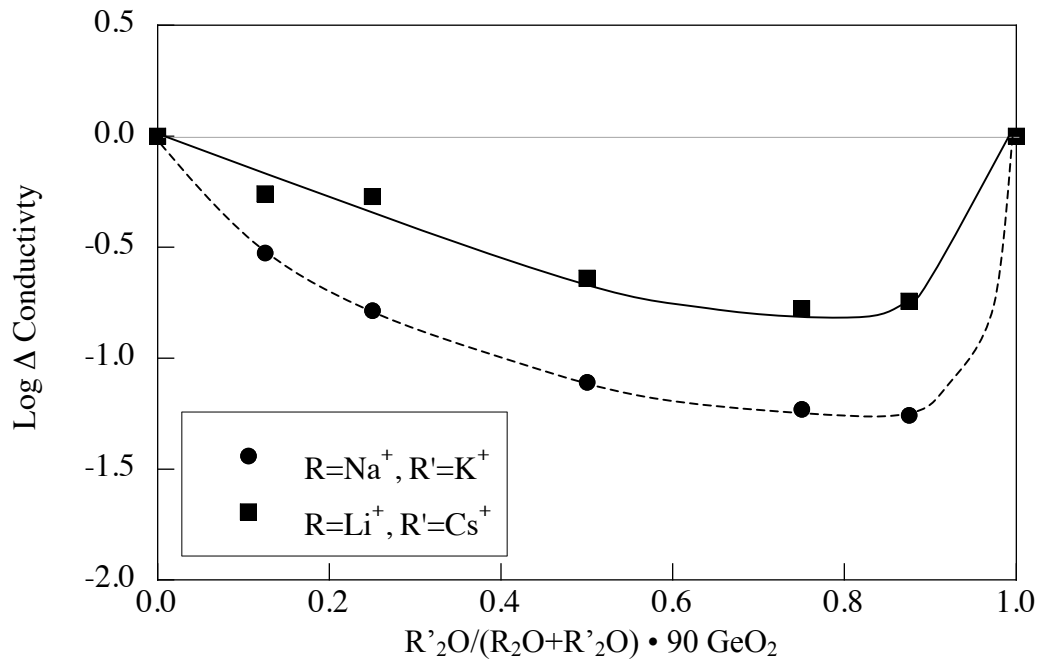


Figure 6-69. Difference between the log of the conductivity at 300 °C and the log of the additive line for mixed alkali glasses with 90 mol % GeO_2 . Lines added as an aid to the eye.

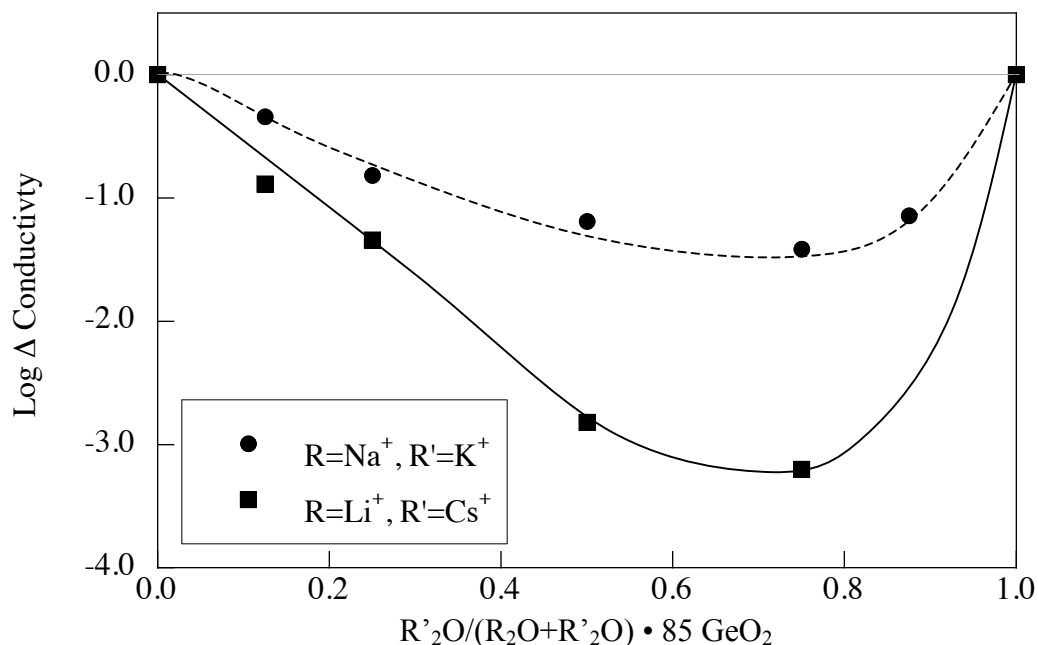


Figure 6-70. Difference between the log of the conductivity at 300 °C and the log of the additive line for mixed alkali glasses with 85 mol % GeO₂. Lines added as an aid to the eye.

6.5.1.2 Activation Energy

Glasses containing 10 mol % alkali oxide exhibit maxima in activation energy when the alkali oxides are in a ratio 1:7 R₂O:R'₂O, where R' is the larger alkali. This effect is independent of cation identity (Figures 6-71 and 6-72). The addition of a small amount of a smaller alkali ion to a glass primarily containing the larger alkali ion results in an increase of approximately 13 to 17 % in the activation energy. A larger deviation occurs for the glasses where the alkali ions are closer in size (Na₂O•K₂O•GeO₂). When the alkali oxide concentration in the glass is 15 mol %, the activation energies are smaller and the maximum shifts toward a larger fraction of the smaller alkali ion. The overall activation energy for electrical conductivity is ~ 13 % higher for the Na₂O•K₂O•GeO₂ glasses than for the Li₂O•Cs₂O•GeO₂ glasses.

Activation energies are higher for alkali oxide additions of 10 mol % than for 15 mol %. In this composition region, the glass contains few NBO. Mixing of alkali ions causes the activation energy to increase as the concentration of the larger ion increases. Glasses containing 15 mol % alkali oxide are near the maximum in the germanate anomaly, where it is believed that significant numbers of non-bridging oxygens are

present. Increases in concentration of non-bridging oxygen in silicate glasses cause a decrease in activation energy which suggest that alkali association with non-bridging oxygens are more mobile than those associated with 5-fold coordinated of germanium.

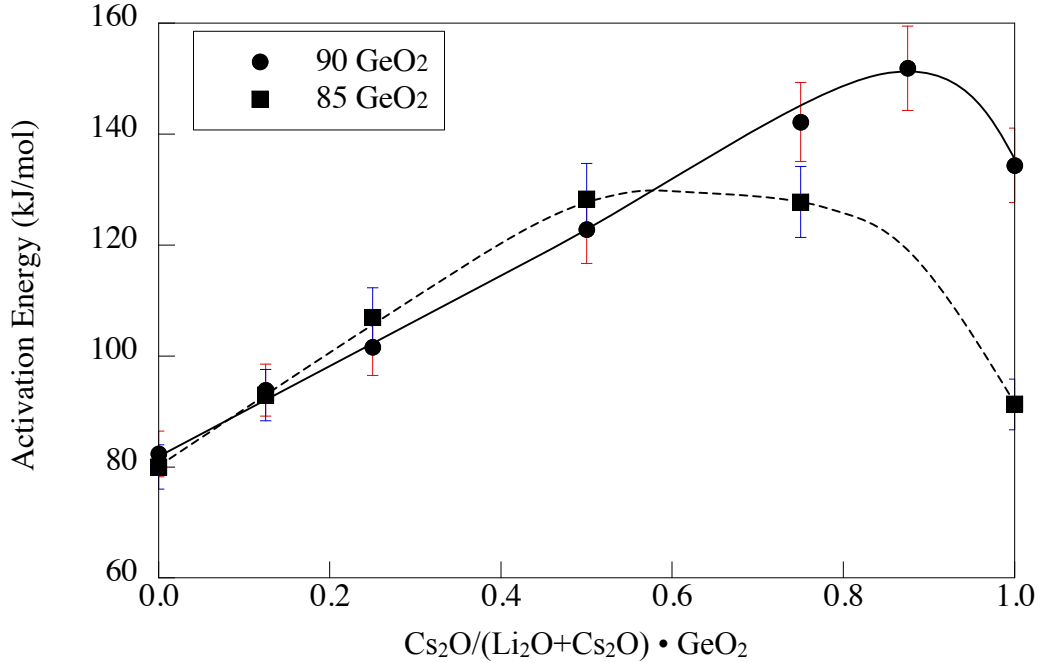


Figure 6-71. Comparison between activation energies of $\text{Li}_2\text{O} \cdot \text{Cs}_2\text{O} \cdot \text{GeO}_2$ glasses, with 90 and 85 mol % GeO_2 . Lines are added as an aid to the eye.

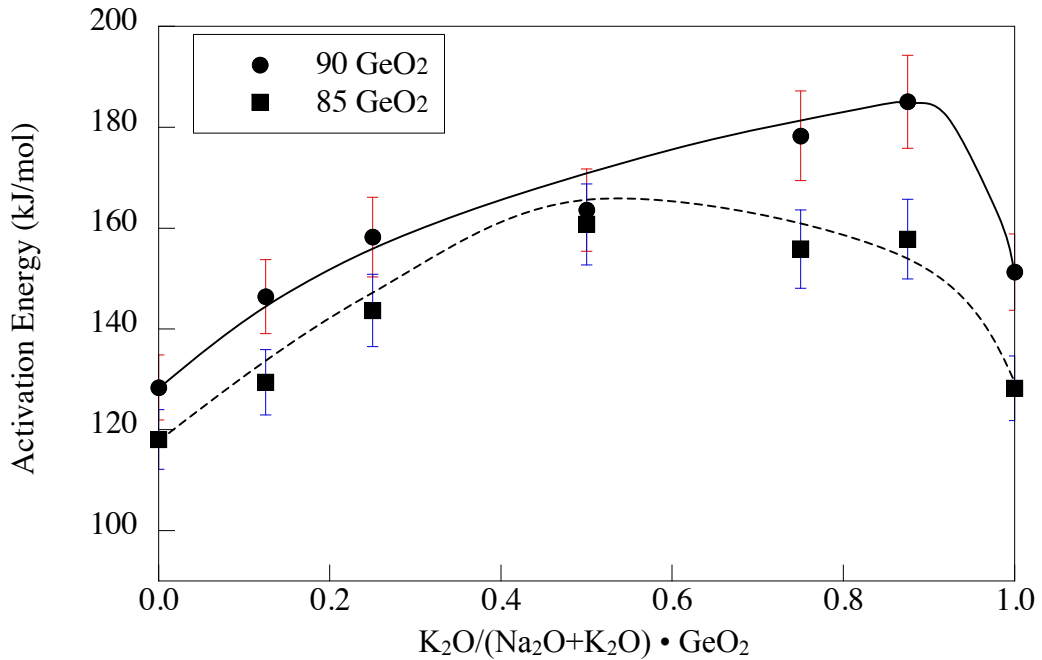


Figure 6-72. Comparison between activation energies of $\text{Na}_2\text{O} \cdot \text{K}_2\text{O} \cdot \text{GeO}_2$ glasses, with 90 and 85 mol % GeO_2 . Lines are added as an aid to the eye.

6.5.1.3 Pre-Exponential Factor

The pre-exponential factors for all but three of the glasses are approximately 1 to 2 orders of magnitude greater than 10, which is the value predicted by Nowick et al. for glasses. For discussion purposes, this value will be referred to as $\sigma_{0\text{ref}}$. The pre-exponential factor for the mixed alkali glasses on the 90 and 85 mol % GeO_2 lines are shown in Figure 6-73. Only binary K_2O or Cs_2O glasses have a pre-exponential factor of approximately 10.

As discussed in Section 6.2, Nowick et al. discuss three levels of value of the pre-exponential (σ_0). When $\sigma_0 \approx \sigma_{0\text{ref}}$, they suggest that all the charge carriers are free. When $\sigma_0 \gg \sigma_{0\text{ref}}$, Nowick et al. suggest that most of the charge carriers are bound at traps and the charge carrier must be released from the trap contribute to conductivity. As the temperature increases the number of charge carries increases exponentially. The activation energy for conduction in these glasses can be written as

$$E = \Delta H + H_m, \quad (6-27)$$

where ΔH is the contribution to the activation energy of the ion traps and H_m is the migration enthalpy. Using this approach to the pre-exponential factor leads to the conclusion that, in mixed alkali germanate glasses, the alkali ions do not migrate freely through the glass as in other glass systems. Lapp and Shelby³⁰ studied the mixed alkali effect in lithium sodium aluminosilicate glasses, where the number of non-bridging oxygen is minimized when the $\text{Al}_2\text{O}_3/\text{R}_2\text{O}$ to ratio is maintained at 1.1. They report that σ_0 is 2 to 3 order of magnitude greater than $\sigma_{0\text{ref}}$. In their glasses the increase in σ_0 is not related to non-bridging oxygen formation. A similar effect may occur here, such that the role of the alkali ions in the coordination change of the germanium could create traps for a portion of the alkali ions.

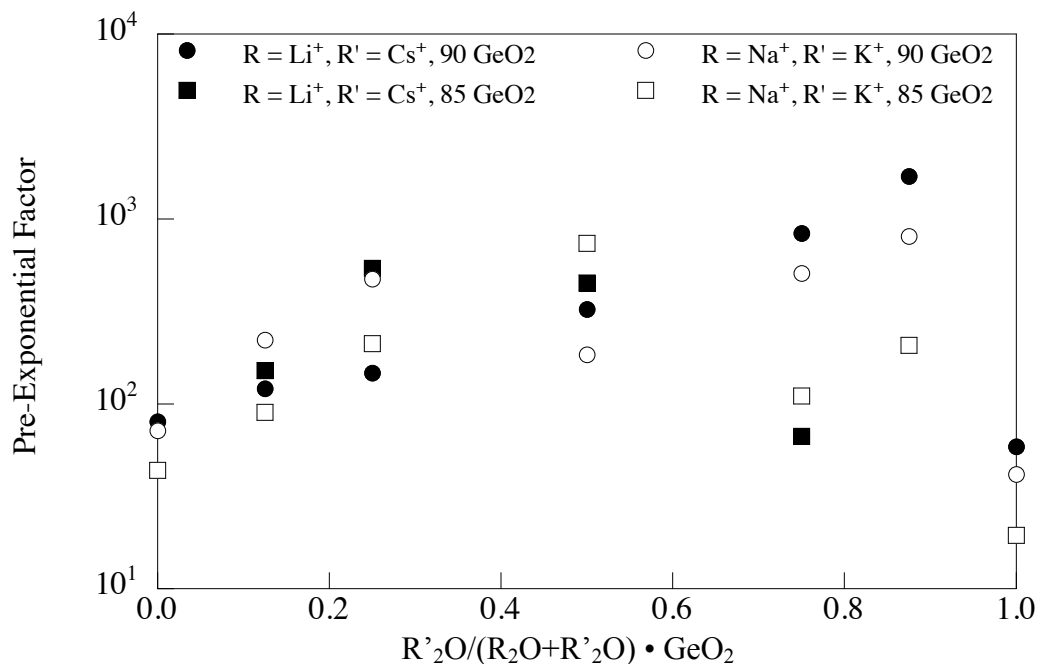


Figure 6-73. Pre-exponential factor for all mixed alkali germanate glasses.

6.5.1.4 Comparison to Literature

The only literature data which the results of this study can be compared to is that of Ivanov.⁸⁴ Figures 6-74 and 6-75 show the DC conductivity at 300 °C for glasses containing 90 mol % GeO₂ and 85 mol % GeO₂, respectively. The primary difference between Ivanov's results and those of this study occur for the 10 mol % alkali additions, where the binary Na₂O, and K₂O glasses do not have the same conductivities as found here. The conductivities of the mixed alkali glasses, however, are essentially identical.

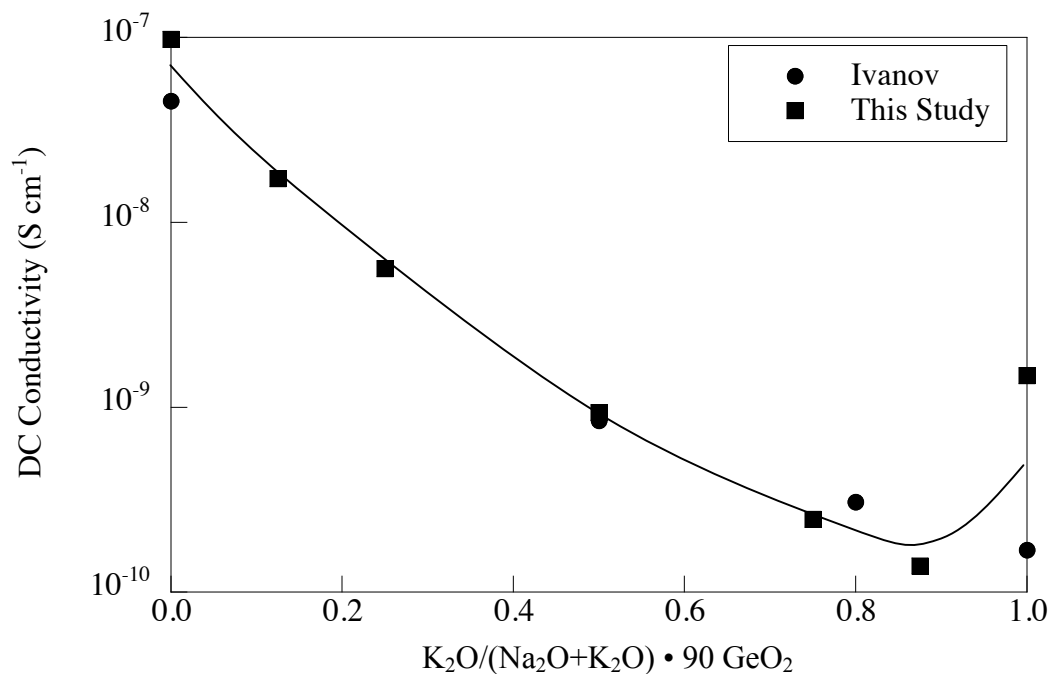


Figure 6-74. Comparison between the literature values and this study for the DC conductivity at 300 °C for $Na_2O \cdot K_2O \cdot 90 GeO_2$. Lines added as aid to the eye.

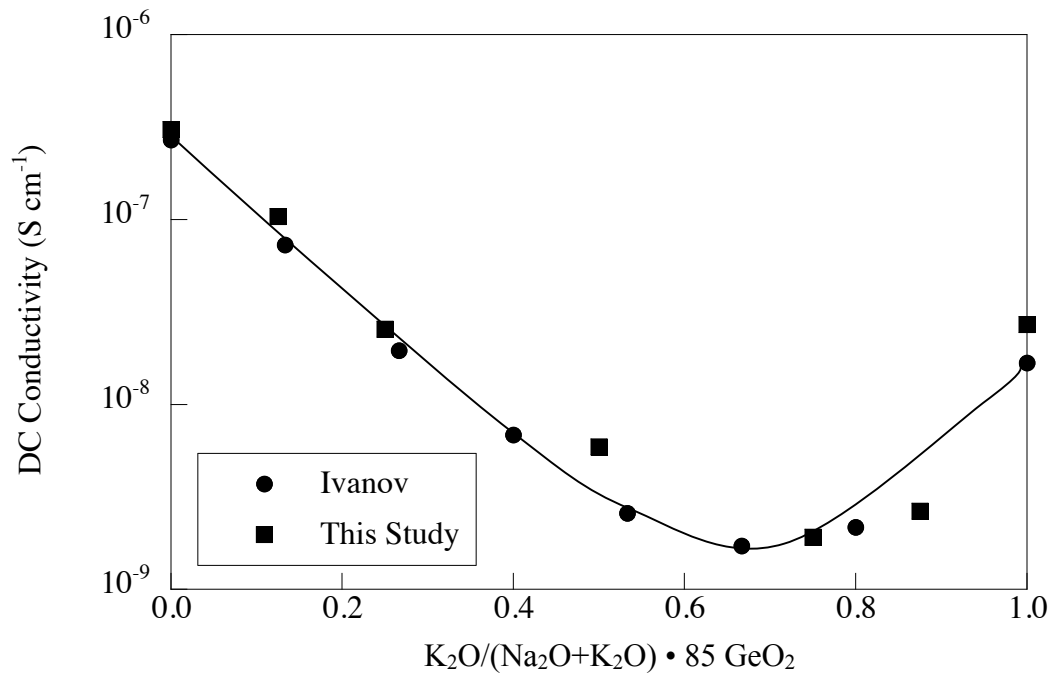


Figure 6-75. Comparison between the literature values and this study for the DC conductivity at 300 °C for $Na_2O \cdot K_2O \cdot 85 GeO_2$, lines added as aid to the eye.

6.5.2 Germanate Anomaly

The effect of varying GeO_2 concentration on the electrical conductivity of mixed alkali glasses will be discussed in three sections governed by the radius ratio of the cations. The electrical conductivity and activation energy of conduction for all mixed alkali glasses will be compared to the binary glasses. Since the largest difference between alkali should yield the greatest deviations from additivity^{8,26,69} $\text{Li}_2\text{O}:\text{Cs}_2\text{O}\cdot\text{GeO}_2$ glasses were examined along three different alkali ratios (3:1, 1:1, and 1:3 $\text{Li}_2\text{O}:\text{Cs}_2\text{O}$) to observe both the germanate anomaly and the mixed alkali effect.

6.5.2.1 Alkali Ions with a Radius Ratio of About 1

Potassium and rubidium are the two alkali ions closest in size⁸⁵ and have a radius ratio of 1.07 $\text{K}^+:\text{Rb}^+$. Figure 6-76 shows the electrical conductivity values at 300 °C for the binary $\text{K}_2\text{O}\cdot\text{GeO}_2$ and $\text{Rb}_2\text{O}\cdot\text{GeO}_2$ glasses, and the mixed alkali glasses with a 1:1 ratio of $\text{K}_2\text{O}:\text{Rb}_2\text{O}$. All three curves lie within half an order of magnitude of each other. The mixed alkali glasses have a slightly lower conductivity than the binary alkali germanate glasses. Potassium germanate glasses with low concentrations of alkali oxide are slightly less conductive than the rubidium germanate glasses.

The activation energies for the three glasses are shown in Figure 6-77. The activation energies are about the same for the potassium and rubidium germanate glasses. Small additions of alkali oxide cause activation energy for the mixed alkali glasses to initially increase, followed by a minimum at 5 mol % addition of alkali oxide. The activation energy for conductivity of the mixed alkali glasses is always lower than that of the binary glasses, implying it is easier to move the ions through the glass.

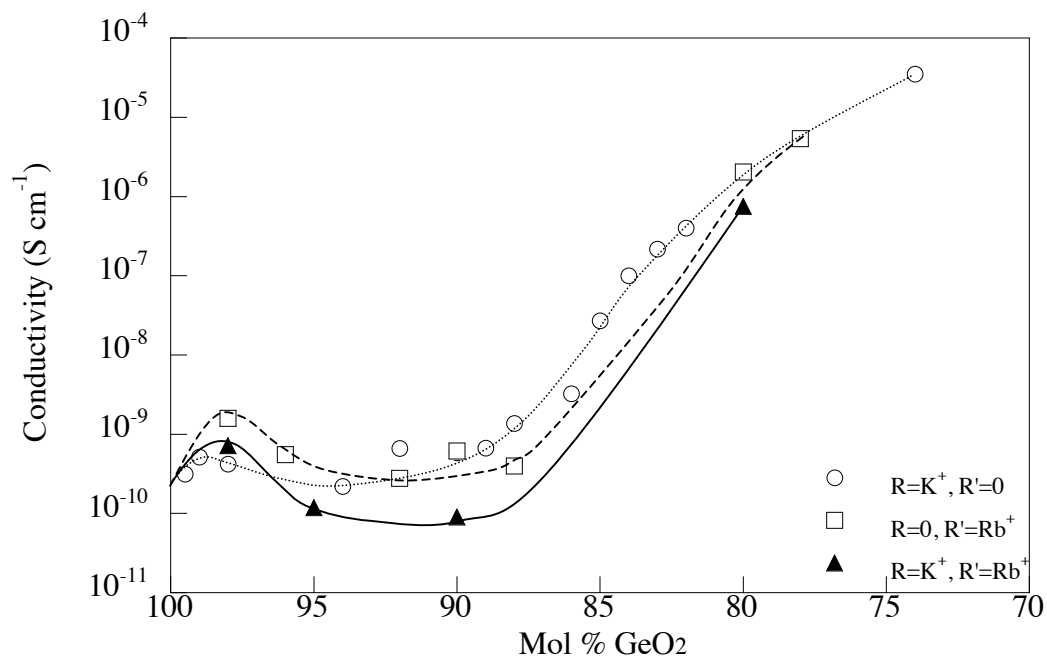


Figure 6-76. DC conductivity for $0.5x \text{K}_2\text{O} \cdot 0.5x \text{Rb}_2\text{O} \cdot (100-x) \text{GeO}_2$, $x \text{K}_2\text{O} \cdot (100-x) \text{GeO}_2$ and $x \text{Rb}_2\text{O} \cdot (100-x) \text{GeO}_2$ glasses at 300 °C. Lines added to aid the eye.

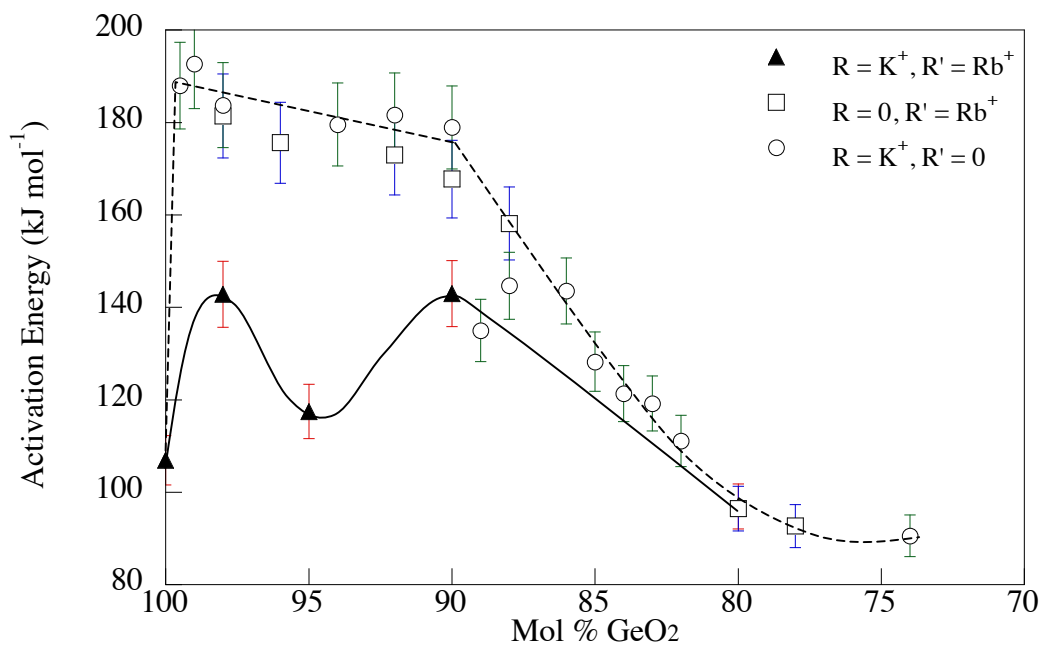


Figure 6-77. Comparison between activation energies of $\text{K}_2\text{O} \cdot \text{GeO}_2$, $\text{Rb}_2\text{O} \cdot \text{GeO}_2$ and $\text{K}_2\text{O} \cdot \text{Rb}_2\text{O} \cdot \text{GeO}_2$ glasses. Lines are added as an aid to the eye.

6.5.2.2 Alkali Ions with a Radius Ratio of about 1.5

The electrical conductivity curves for $x0.5 \text{ Na}_2\text{O} \cdot x0.5 \text{ K}_2\text{O} \cdot (100-x) \text{ GeO}_2$ glasses (Figure 6-78) are very different from the $x\text{K}_2\text{O} \cdot y \text{ Rb}_2\text{O} \cdot (100-x-y) \text{ GeO}_2$ glasses. In this case, the binary alkali germanate glasses have very different electrical conductivities. The conductivity of sodium germanate glasses initially increases (≤ 2 mol % alkali oxide), followed by a region where the electrical conductivity remains constant with alkali oxide concentration of $2 > x > 7$ mol % after which the conductivity increases. Binary $\text{K}_2\text{O} \cdot \text{GeO}_2$ glasses do not exhibit an initial increase in electrical conductivity. The conductivity remains relatively constant until about 10 mol % K_2O , after which conductivity increases with increasing K_2O concentration. The electrical conductivities of the binary sodium and binary potassium glasses are about the same for glasses containing ~ 20 mol % alkali oxide. The electrical conductivity behavior of the mixed alkali glasses is surprising. Many reputable glass scientists^{8,26,69} claim that the mixed alkali effect always results in a negative deviation from additivity. However, germanates do not follow this rule if the radius ratio of the migrating ions is > 1.5 . Examination of Figure 6-78 shows that the electrical conductivity of the mixed alkali glass for small additions of alkali oxide (< 2 mol %) is approximately the same as that of the binary $\text{Na}_2\text{O} \cdot \text{GeO}_2$ glass. A mixed alkali glass with the same conductivity as one of the end member glasses yields a positive deviation from additivity. This work is not the first to show this anomaly in the electrical conductivity. Ivanov⁸⁴ also reported a positive deviation from additivity for his $x \text{ Na}_2\text{O} \cdot y \text{ K}_2\text{O} \cdot (100-x-y) \text{ GeO}_2$ glasses with 5 mol % alkali oxide (Figure 6-79).

The activation energies of the glasses are shown in Figure 6-80. End member glasses behave as expected. The mixed alkali glasses containing > 10 mol % exhibit a simultaneous increase in conductivity and activation energy. This behavior can be attributed to the larger scatter in the pre-exponential factor of these glasses. The activation energy remains constant when the conductivity remains constant. As the glass become more conductive, the activation energy decreases.

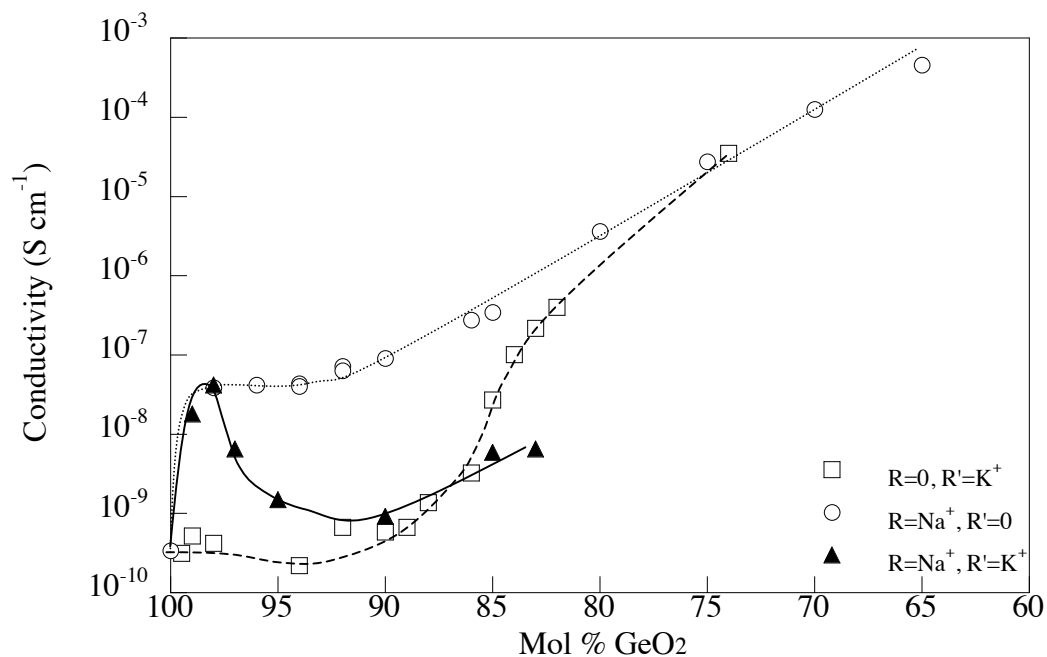


Figure 6-78. DC conductivity for $0.5x \text{Na}_2\text{O} \cdot 0.5x \text{K}_2\text{O} \cdot (100-x) \text{GeO}_2$, $x \text{Na}_2\text{O} \cdot (100-x) \text{GeO}_2$ and $x \text{K}_2\text{O} \cdot (100-x) \text{GeO}_2$ glasses at 300 °C. Lines added to aid the eye.

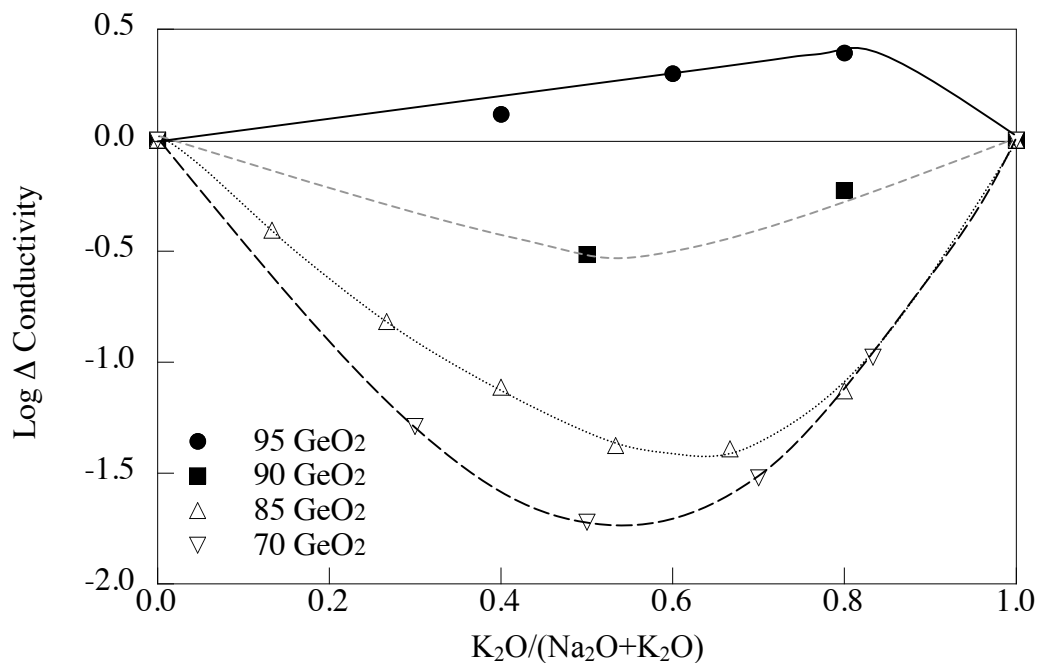


Figure 6-79. Difference between the log of the conductivity at 300 °C and the log of the additive line for mixed alkali glasses for all $\text{Na}_2\text{O} \cdot \text{K}_2\text{O} \cdot \text{GeO}_2$ glasses. Lines added as an aid to the eye, data from Ivanov.⁸⁴

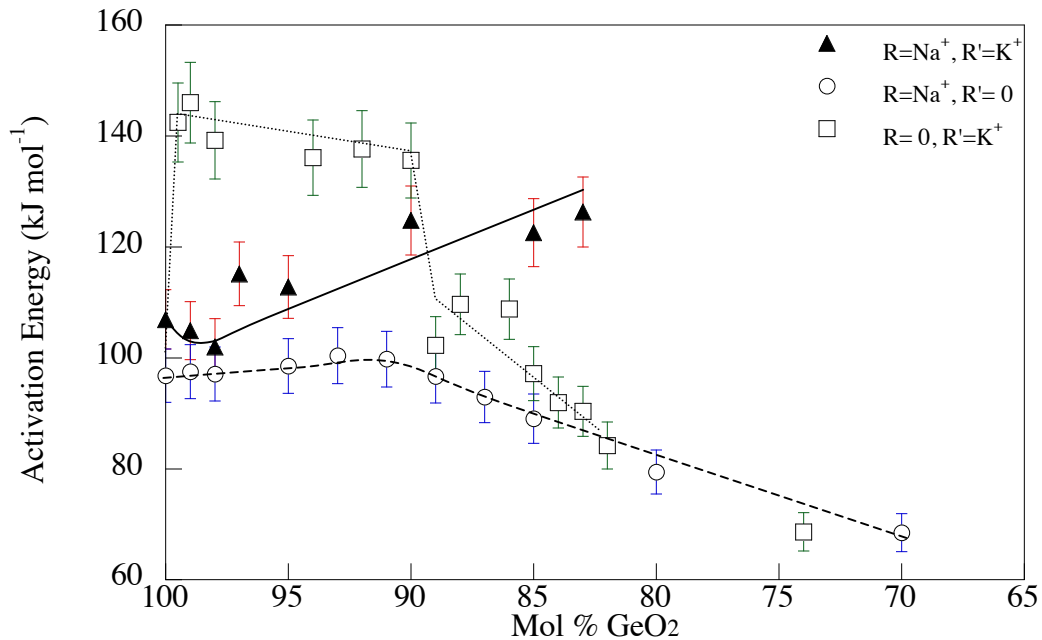


Figure 6-80. Comparison between activation energies of $\text{Na}_2\text{O}\cdot\text{GeO}_2$, $\text{K}_2\text{O}\cdot\text{GeO}_2$ and $\text{Na}_2\text{O}\cdot\text{K}_2\text{O}\cdot\text{GeO}_2$ glasses. Lines are added as an aid to the eye.

6.5.2.3 Alkali Ions with a Radius Ratio of 2 to 2.5

Mixed alkali $0.5x \text{Li}_2\text{O}\cdot 0.5x \text{Cs}_2\text{O}\cdot (100-x) \text{GeO}_2$ glasses behave similarly to $0.5x \text{Na}_2\text{O}\cdot 0.5x \text{K}_2\text{O}\cdot (100-x) \text{GeO}_2$ glasses. As the size difference between the two alkali increases, the anomalous behavior becomes more pronounced. Figure 6-81 shows the electrical conductivities of the binary $\text{Li}_2\text{O}\cdot\text{GeO}_2$ and $\text{Cs}_2\text{O}\cdot\text{GeO}_2$ glasses (Shelby⁴³) and mixed alkali 1:1 $\text{Li}_2\text{O}:\text{Cs}_2\text{O}\cdot\text{GeO}_2$ glasses. Alkali oxide addition ≤ 2 mol % result in an increase in the electrical conductivity of both the $\text{Li}_2\text{O}\cdot\text{GeO}_2$ and the 1:1 $\text{Li}_2\text{O}:\text{Cs}_2\text{O}\cdot\text{GeO}_2$ glasses. Continuing to increase the alkali oxide concentration beyond 2 mol % in the 1:1 $\text{Li}_2\text{O}:\text{Cs}_2\text{O}\cdot\text{GeO}_2$ glasses causes the conductivity to decrease. Mixing the Li_2O and Cs_2O alkali ions yields conductivities between those of the binary glasses until approximately 13 mol % addition of alkali oxide, after which $\text{Li}_2\text{O}:\text{Cs}_2\text{O}\cdot\text{GeO}_2$ glasses with > 13 mol % alkali oxide have conductivities 2 to 3 orders of magnitude less than the binary glasses.

Activation energies for this binary and 1:1 $\text{Li}_2\text{O}:\text{Cs}_2\text{O}\cdot\text{GeO}_2$ glasses are shown in Figure 6-82. The activation energy for the binary glasses behavior expected, i.e. the electrical conductivity and activation energy are inversely related. The mixed alkali glasses however, have unusual activation energies as will be discussed later.

Mixed alkali $x \text{Li}_2\text{O} \cdot (1-x) \text{Cs}_2\text{O} \cdot (100-2x) \text{GeO}_2$ glasses with two ratios of Li_2O and Cs_2O were made to observe the mixed alkali effect on the germanate anomaly. Figure 6-83 shows the electrical conductivity curves, at 300 °C, for glasses with ratios of 1:1, 3:1 and 1:3 $\text{Li}_2\text{O}:\text{Cs}_2\text{O}$. The conductivity of the 3:1 mixed alkali glasses remains constant with addition of alkali oxide > 5 mol %, yielding conductivities two orders of magnitude lower than those of the binary $\text{Li}_2\text{O} \cdot \text{GeO}_2$ glasses. When there is more Cs_2O in the glass than Li_2O the electrical conductivity initially increases, and then decreases rapidly passing through a minimum around 15 to 20 mol % R_2O . The $0.5x \text{Li}_2\text{O} \cdot 0.5x \text{Cs}_2\text{O} \cdot (100-x) \text{GeO}_2$ glasses exhibit a max in conductivity at ≈ 2 mol % R_2O followed by a continual decrease in conductivity with addition of R_2O .

The large initial increases in conductivity for the 1:1 and 1:3 $\text{Li}_2\text{O}:\text{Cs}_2\text{O}$ glasses, containing 2 mol % alkali result in a positive deviation from additivity (Figure 6-84). When small amounts of lithium oxide are added to cesium germanate glasses, the structure of the glass allows the conductivity to increase significantly from that of the binary glass. This is not surprising in this system, due to the large difference in size between the lithium and the cesium ion and the high molar volume of the binary cesium germanate. This positive deviation is also present in the mixed alkali sodium-potassium germanate glasses, where the mobile ions and the molar volumes are much closer in size; therefore the effect is more likely a result of a structural change that occurs when small amounts of alkali are added to the germania glass. Examining the molar volume data for these glasses (Figure 4-55) shows when small amounts of alkali oxide are added to the germanate glasses; the molar volume is approximately the same (within $0.5 \text{ cm}^3 \text{ mol}^{-1}$) for all glasses regardless of the cation identity. In contrast, alkali oxide concentration exceeding 5 mol % in the binary alkali germanate glasses results in molar volume ranges spanning over $2.5 \text{ cm}^3 \text{ mol}^{-1}$. Adding small amounts of mixed alkali oxides (≤ 5 mol %) to germanate glasses results in glasses where the structure allows ions of different radii to move through the glass network at similar rates.

Activation energies for the mixed alkali $\text{Li}_2\text{O}\cdot\text{Cs}_2\text{O}\cdot\text{GeO}_2$ glasses are shown in Figure 6-85. The electrical conductivities and activation energies for the 1:1, 3:1 and 1:3 $\text{Li}_2\text{O}\cdot\text{Cs}_2\text{O}\cdot\text{GeO}_2$ glasses are shown in Figures 6-86 through 6-88, respectively. Glasses with a ratio of 1:1 $\text{Li}_2\text{O}:\text{Cs}_2\text{O}$ exhibit odd behavior when the alkali oxide addition is < 2 mol %, in that the activation energy increases with increasing conductivity. The pre-exponential factors for the mixed alkali glasses with varying GeO_2 concentration are shown in Figure 6-89. All of the mixed alkali glasses except one, the 3:1 $\text{Li}_2\text{O}:\text{Cs}_2\text{O}\cdot 98$ GeO_2 glass, have pre-exponentials one to two orders of magnitude greater than 10. There are no other trends in the pre-exponential except they are higher than expected.

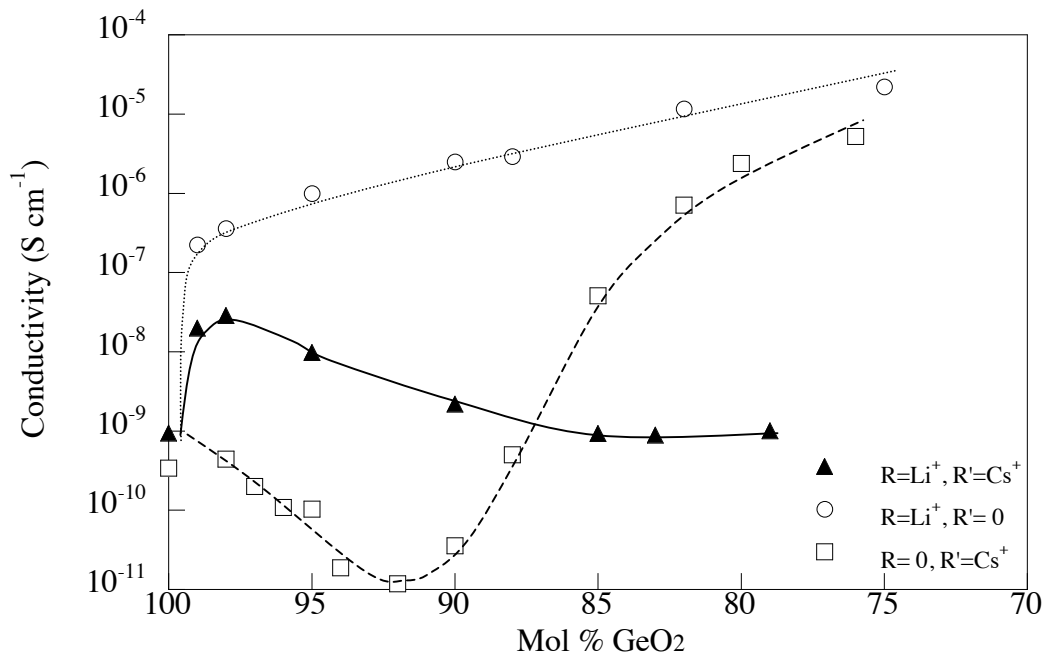


Figure 6-81. DC conductivity for $0.5x \text{Li}_2\text{O}\cdot 0.5x \text{Cs}_2\text{O}\cdot (100-x) \text{GeO}_2$, $x \text{Li}_2\text{O}\cdot (100-x) \text{GeO}_2$ and $x \text{Cs}_2\text{O}\cdot (100-x) \text{GeO}_2$ glasses at 300 °C. Lines added to aid the eye.

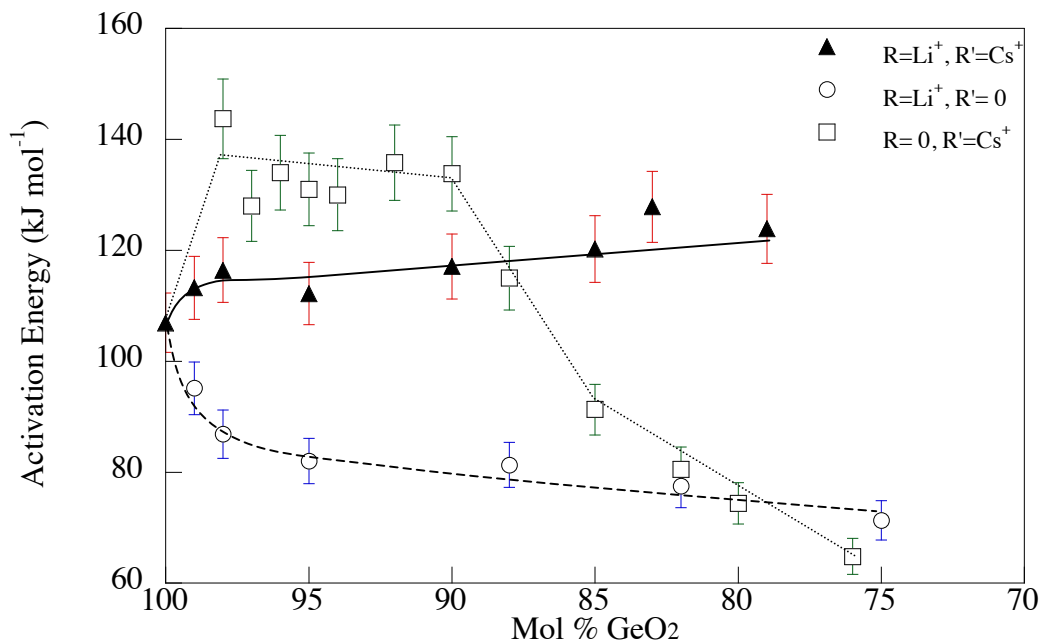


Figure 6-82. Comparison between activation energies of Li₂O•GeO₂, Cs₂O•GeO₂ and Li₂O•Cs₂O•GeO₂ glasses. Lines are added as an aid to the eye.

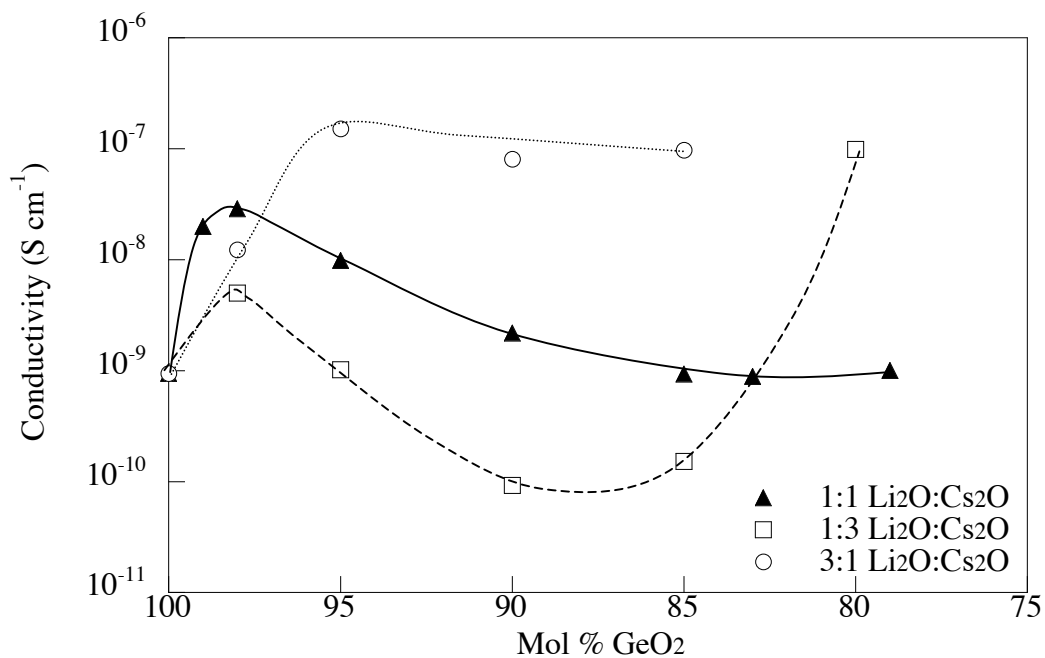


Figure 6-83. DC conductivity for 0.75x Li₂O•0.25x Cs₂O•(100-x) GeO₂, 0.5x Li₂O•0.5x Cs₂O•(100-x) GeO₂ and 0.25x Li₂O•0.75x Cs₂O•(100-x) GeO₂ glasses at 300 °C. Lines added to aid the eye.

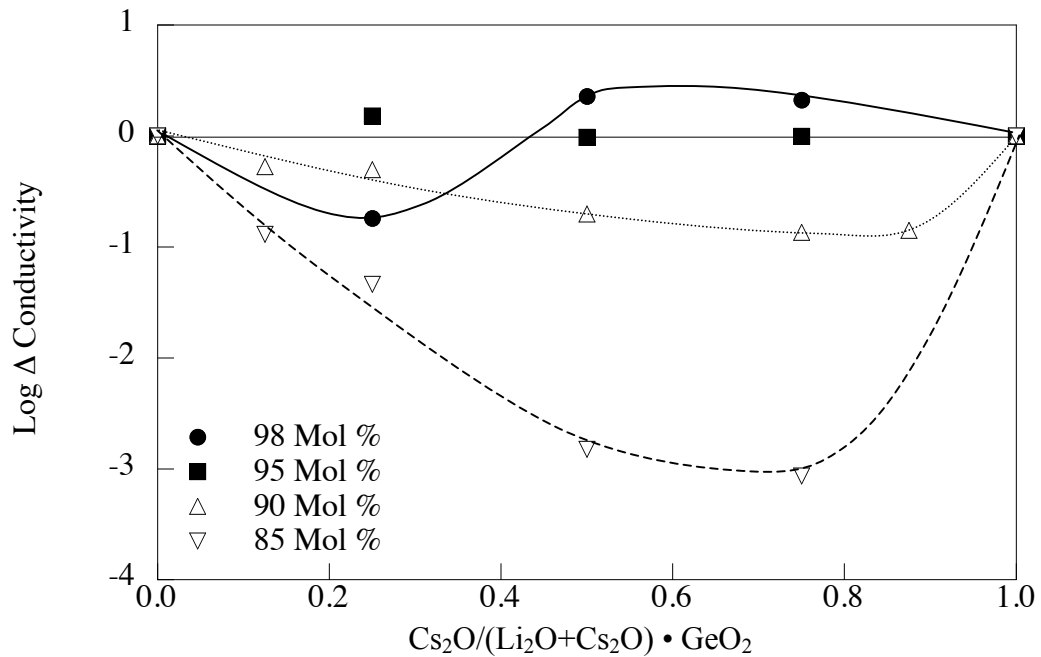


Figure 6-84. Difference between the log of the conductivity at 300 °C and the log of the additive line for mixed alkali glasses for all $\text{Li}_2\text{O}\cdot\text{Cs}_2\text{O}\cdot\text{GeO}_2$ glasses. Lines added as an aid to the eye.

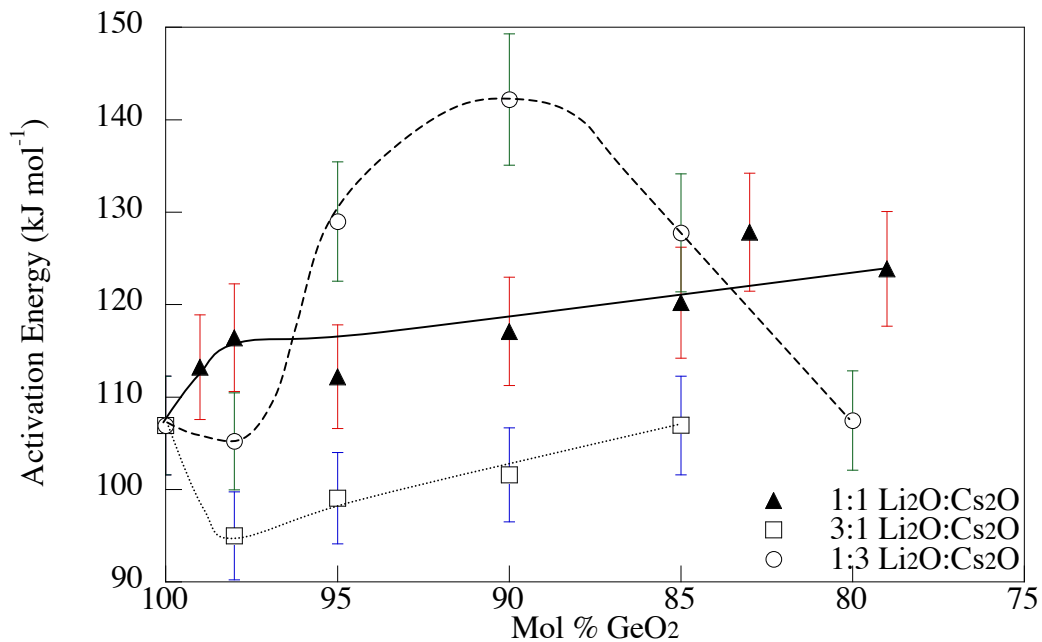


Figure 6-85. Comparison between activation energies of $\text{Li}_2\text{O}\cdot\text{Cs}_2\text{O}\cdot\text{GeO}_2$ glasses, with varying ratios of alkali. Lines are added as an aid to the eye.

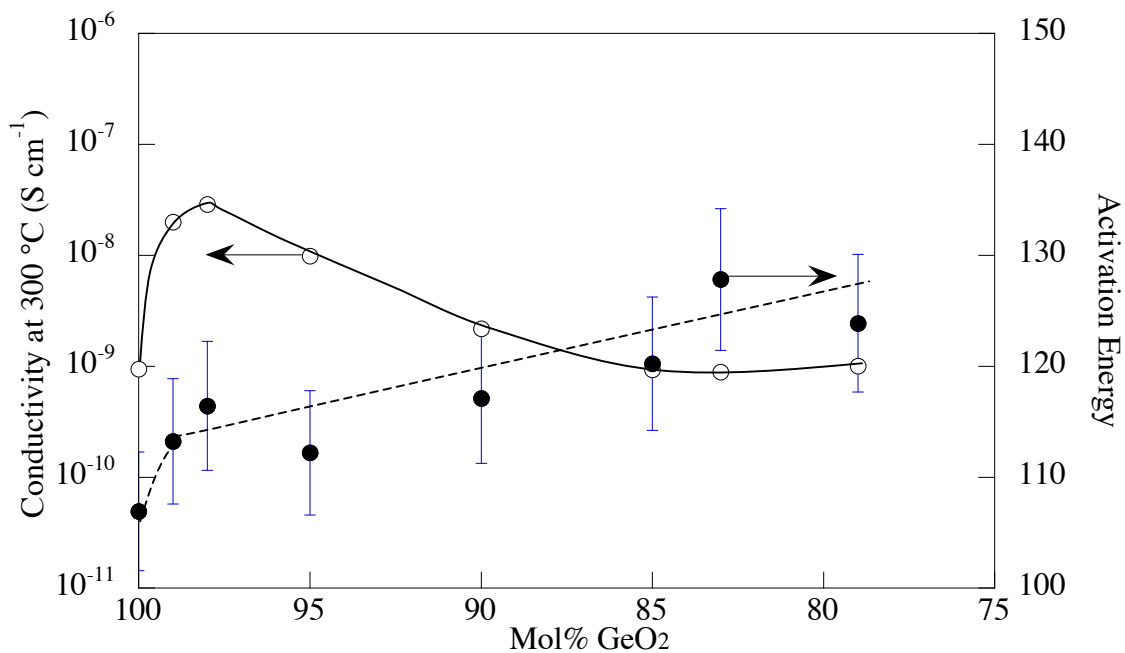


Figure 6-86. Comparison between the conductivity at 300 °C and the activation energy of conduction for 1:1 Li₂O:Cs₂O•GeO₂ glasses. Lines are added as an aid to the eye.

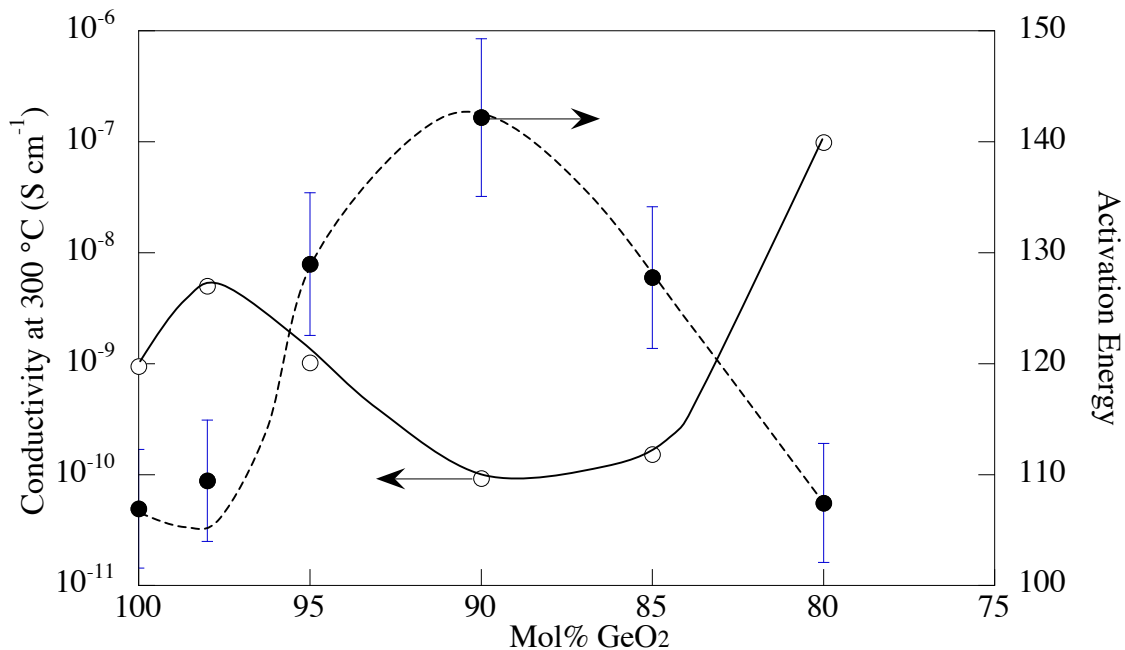


Figure 6-87. Comparison between the conductivity at 300 °C and the activation energy of conduction for 1:3 Li₂O:Cs₂O•GeO₂ glasses. Lines are added as an aid to the eye.

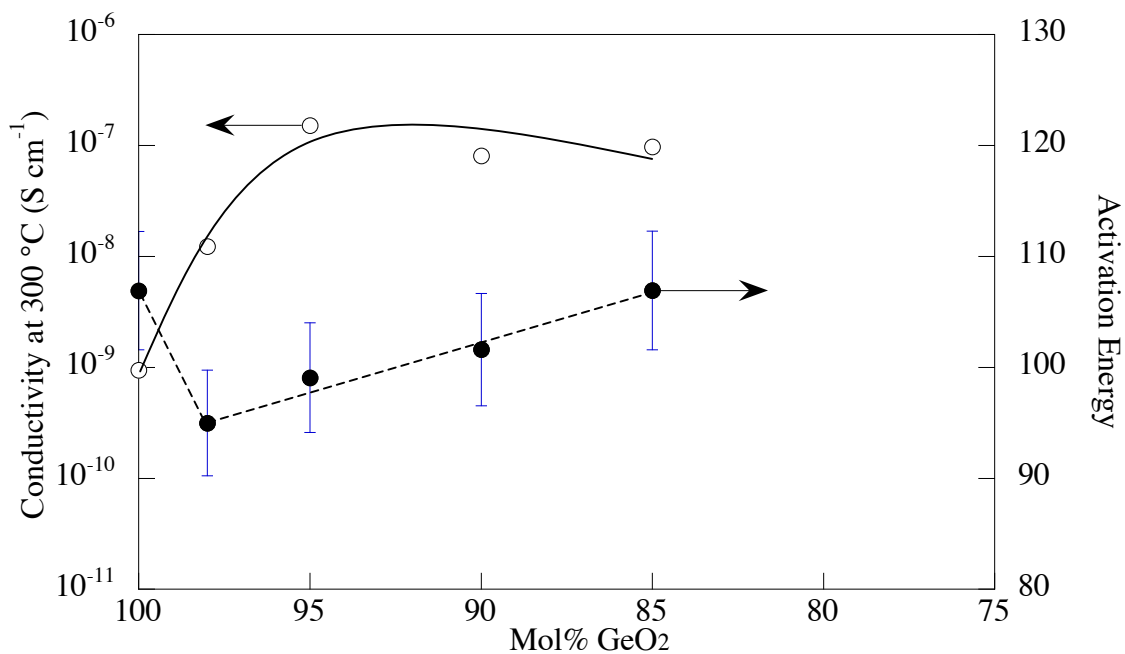


Figure 6-88. Comparison between the conductivity at 300 °C and the activation energy of conduction for 3:1 Li₂O:Cs₂O•GeO₂ glasses. Lines are added as an aid to the eye.

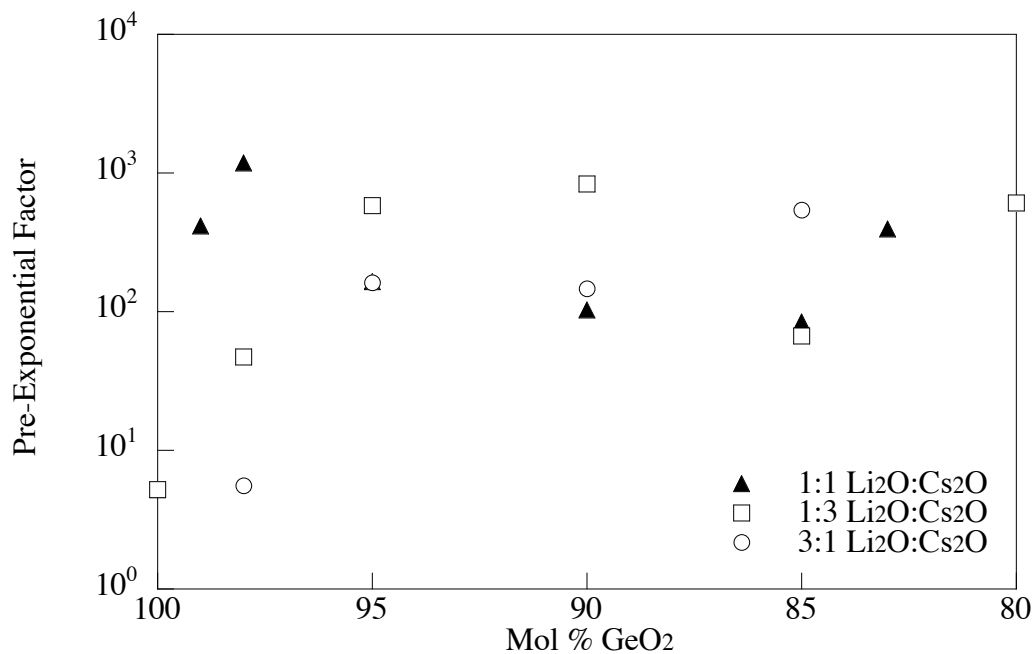


Figure 6-89. Pre-exponential (σ_0) factors for x Li₂O• y Cs₂O•(100- x - y) GeO₂ glasses.

6.5.2.4 The Effect of the Radii Ratio

Electrical conductivities for glasses with an alkali oxide ratio of 1:1, in all three ternary systems are shown in Figure 6-90. The $0.5x \text{ K}_2\text{O} \cdot 0.5x \text{ Rb}_2\text{O} \cdot (100-x) \text{ GeO}_2$ glasses with large amounts of alkali oxide are surprisingly conductive, with conductivities approximately 3 orders of magnitude higher than the $0.5x \text{ Li}_2\text{O} \cdot 0.5x \text{ Cs}_2\text{O} \cdot (100-x) \text{ GeO}_2$. The $0.5x \text{ Na}_2\text{O} \cdot 0.5x \text{ K}_2\text{O} \cdot (100-x) \text{ GeO}_2$ glasses with small amounts of alkali oxide (≤ 2 mol %) initially behave like the $0.5x \text{ Li}_2\text{O} \cdot 0.5x \text{ Cs}_2\text{O} \cdot (100-x) \text{ GeO}_2$, with an increase in conductivity. Intermediate amounts of alkali oxide in the glass ($2 < x \leq 10$ mol %) results in the electrical conductivity falling between the other two systems until the amount of alkali oxide is ≥ 15 mol%, after which the conductivity is similar to that of the $0.5x \text{ K}_2\text{O} \cdot 0.5x \text{ Rb}_2\text{O} \cdot (100-x) \text{ GeO}_2$ glasses.

Activation energies for the three systems are shown in Figure 6-91. The $0.5x \text{ Li}_2\text{O} \cdot 0.5x \text{ Cs}_2\text{O} \cdot (100-x) \text{ GeO}_2$ glasses have the smallest range of activation energies, approximately 10 kJ mol^{-1} . As the radius ratio approaches 1, the range in the activation energies increases, with a range of over 150 kJ mol^{-1} for the $0.5x \text{ K}_2\text{O} \cdot 0.5x \text{ Rb}_2\text{O} \cdot (100-x) \text{ GeO}_2$ glasses.

The pre-exponential factors behave in a similar manner to the activation energies (Figure 6-92). The pre-exponentials of the $0.5x \text{ Li}_2\text{O} \cdot 0.5x \text{ Cs}_2\text{O} \cdot (100-x) \text{ GeO}_2$ glasses range over one order of magnitude. As the ions become closer in size the range of the pre-exponential factors increase. For $0.5x \text{ K}_2\text{O} \cdot 0.5x \text{ Rb}_2\text{O} \cdot (100-x) \text{ GeO}_2$ glasses, the pre-exponential factors span four orders of magnitude. The large spread in the values of the pre-exponential factor, coupled with the abrupt changes in activation energy, suggest that the electrical conductivity behavior of alkali germanate glasses is a result of different mechanisms of electrical conduction.

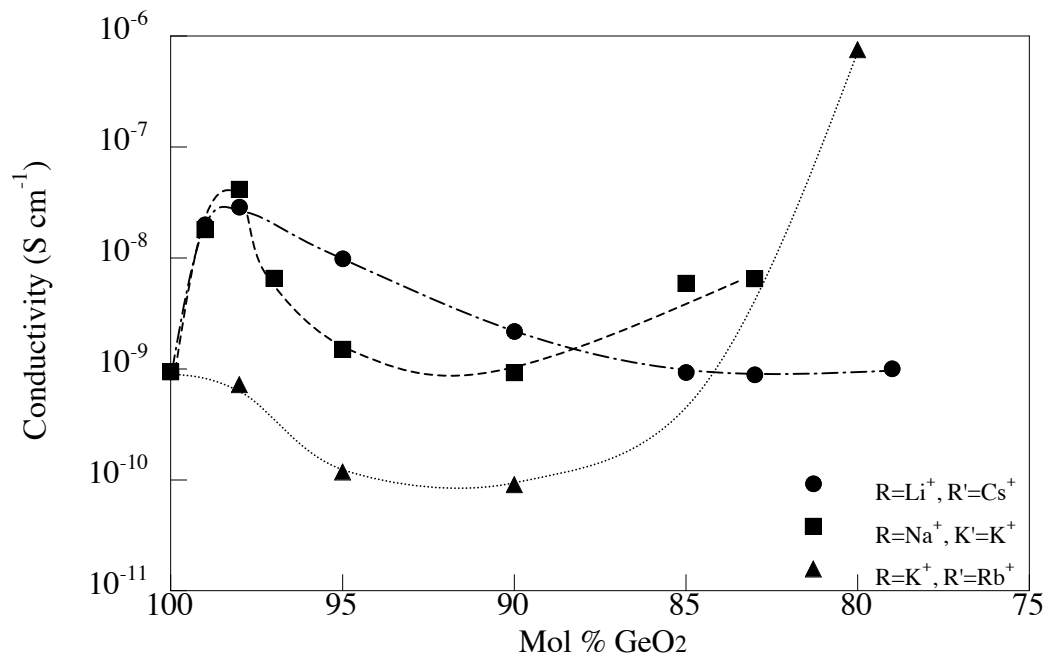


Figure 6-90. DC conductivity for $0.5x \text{Li}_2\text{O} \cdot 0.5x \text{Cs}_2\text{O} \cdot (100-x) \text{GeO}_2$, $x \text{Li}_2\text{O} \cdot (100-x) \text{GeO}_2$ and $x \text{Cs}_2\text{O} \cdot (100-x) \text{GeO}_2$ glasses at 300 °C. Lines added to aid the eye.

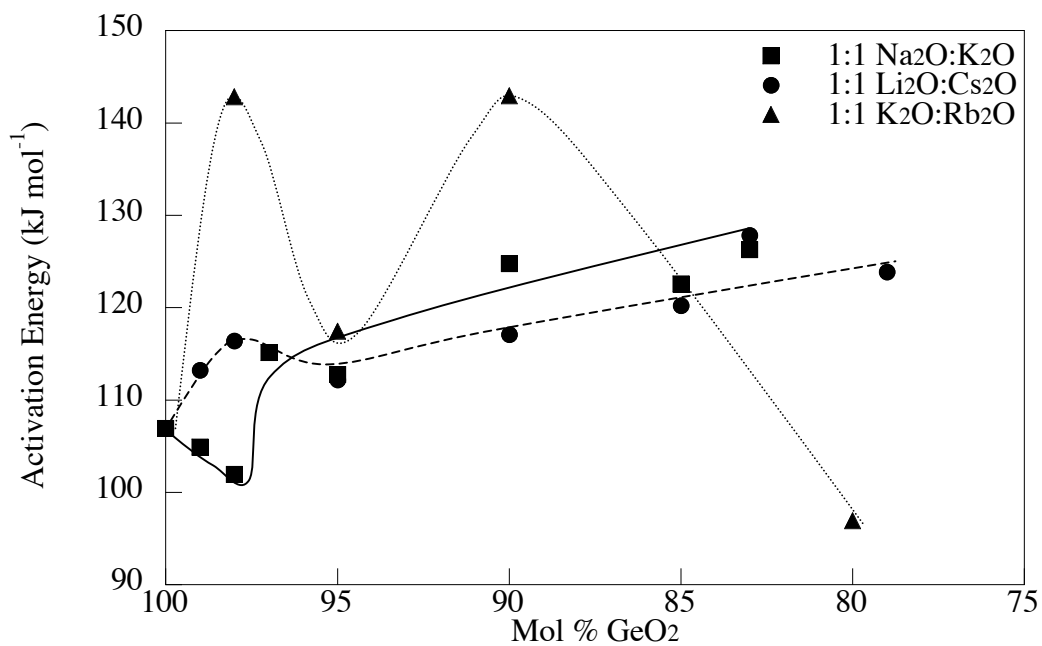


Figure 6-91. Activation energy for $0.5x \text{K}_2\text{O} \cdot 0.5x \text{Rb}_2\text{O} \cdot (100-x) \text{GeO}_2$ glasses. Line added as aid to the eye.

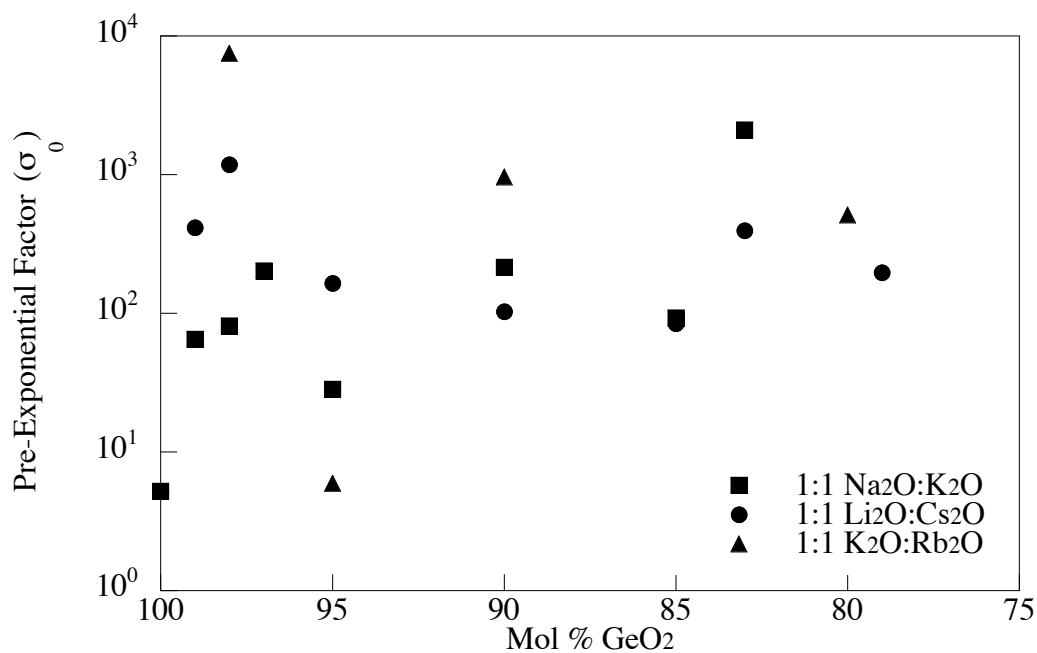


Figure 6-92. Pre-exponential (σ_0) factor for $x R_2O \cdot y R'_2O \cdot (100-x-y) GeO_2$ glasses.

6.6 Conclusions

The electrical conductivity of mixed alkali germanate glasses is different from that of other systems studied to date. The literature review indicates that binary alkali germanate glasses exhibit two types of behaviors. Glasses containing the smaller Li^+ and Na^+ ions exhibit larger initial increases in conductivity, where those containing larger ions (K^+ , Rb^+ , Cs^+) initially decrease in conductivity and only begin to increase in conductivity after the addition of approximately 10 mol % alkali oxide. When alkali ions are mixed a few unexpected behaviors emerge.

Complex behavior is observed for the mixed alkali germanate glasses, as summarized below.

(1) In the $x Li_2O \cdot y Cs_2O \cdot (100-x-y) GeO_2$ glasses, glasses containing ≥ 10 mol % alkali oxide exhibit negative deviations from additivity, which increase with increasing alkali oxide. Alkali germanate glasses exhibit unique conductivity behavior when the alkali content is < 5 mol % alkali oxide; glasses with 2 mol % alkali exhibit a positive deviation from additivity and glasses containing 5 mol% alkali oxide behave additively. Ivanov observed similar results in $x Na_2O \cdot y K_2O \cdot (100-x-y) GeO_2$ glasses.

(2) It has been stated for many years that a larger difference between cation radii results in a larger deviation from additivity for mixed alkali glasses. This study shows

there is at least one exception to this rule. If mixed alkali germanate glasses contain 10 mol % alkali oxide, the greatest deviation from additivity occurs for the ions with the closest radius ratio. This behavior is probably due to structural changes in the glass.

(3) The low alkali oxide and high alkali oxide germanate anomalies are present in the data for all of the mixed alkali glasses.

(4) Mixed alkali glasses with more of one cation ($R > R'$ or $R' > R$) exhibit electrical conductivity curves with the same shape as those of the binary glass of the majority cation. Figure 6-83 shows the conductivities for the $0.75x \text{ Li}_2\text{O} \cdot 0.25x \text{ Cs}_2\text{O} \cdot (100-x) \text{ GeO}_2$, $0.5x \text{ Li}_2\text{O} \cdot 0.5x \text{ Cs}_2\text{O} \cdot (100-x) \text{ GeO}_2$ and $0.25x \text{ Li}_2\text{O} \cdot 0.75x \text{ Cs}_2\text{O} \cdot (100-x) \text{ GeO}_2$ glasses at 300 °C. The curves for the glasses with more lithium than cesium resemble the binary $\text{Li}_2\text{O} \cdot \text{GeO}_2$ glasses. The curves for the glasses with more cesium than lithium resemble the binary $\text{Cs}_2\text{O} \cdot \text{GeO}_2$ glasses.

The findings of this study reiterate the caution needed when assuming models for transport phenomena based on silicate glasses. Silicate glasses do not undergo changes in network coordination. In some cases they are also phase separated, which prevents observation of the effect of small amounts of the smaller alkali on conductivity.²

6.7 References

1. H.L. Tuller, "Amorphous Fast Ionic Conductors," pp. 51-88 in Vol. 199; *Science and Technology of Fast Ion Conductors*. Edited by H. L. Tuller and M. Balkanski. Plenum, New York, 1989.
2. S. Adams and J. Swenson, "Structure Conductivity Correlation in Reverse Monte Carlo Models of Single and Mixed Alkali Glasses," *Solid State Ionics*, **175** [1-4] 665-9 (2004).
3. O.L. Anderson and D.A. Stuart, "Calculation of Activation Energy of Ionic Conductivity in Silica Glasses by Classical Methods," *J. Am. Ceram. Soc.*, **37** [12] 576-80 (1954).
4. P.J. Bray and J.R. Hendrickson, "Dependence of the Mixed Alkali Effect on Ion Masses," *J. Non-Cryst. Solids*, **21** [2] 297-9 (1976).
5. A. Bunde, M.D. Ingram, and P. Maass, "The Dynamic Structure Model for Ion Transport in Glasses," *J. Non-Cryst. Solids*, **172-174** [Part 2] 1222-36 (1994).
6. J.F. Cordaro and M. Tomozawa, "Mixed-Alkali Effect in Low-Alkali Germanate Glasses," *J. Am. Ceram. Soc.*, **65** [4] C50-C1 (1982).

7. D.E. Day, "Review of Mechanical Relaxations in Mixed Alkali Silicate Glasses," pp. 39-47 in *Amorphous Materials: Papers Presented to the Third International Conference on the Physics of Non-Crystalline Solids Held at Sheffield University, September, 1970*. Edited by R. W. Douglas and B. Ellis. Wiley-Interscience, New York, 1972.
8. D.E. Day, "Mixed Alkali Glasses-Their Properties and Uses," *J. Non-Cryst. Solids*, **21** [3] 343-72 (1976).
9. A. Doi and D.E. Day, "Thermally Stimulated Polarization Current in Sodium Germanate Glass " *J. Mater. Sci.*, **15** [12] 3047-50 (1980).
10. A. Doi and D.E. Day, "Conduction Polarization in Sodium Germanate Glasses," *J. Appl. Phys.*, **52** [5] 3433-8 (1981).
11. M. Dubiel, B. Roling, and M. Futing, "AC Conductivity and Ion Transport in K⁺-for-Na⁺ Ion-Exchanged Glasses: Exchange Experiments Below and above the Glass Transition Temperature," *J. Non-Cryst. Solids*, **331** [1-3] 11-9 (2003).
12. R. Green and K.B. Blodgett, "Electrically Conducting Glasses," *J. Am. Ceram. Soc.*, **31** [4] 89-100 (1948).
13. J. Habasaki, K.L. Ngai, Y. Hiwatari, and C.T. Moynihan, "Molecular Dynamics Simulations of the Dynamics of Ions in Single and Mixed Alkali Glasses " *J. Non-Cryst. Solids*, **349** 223-9 (2004).
14. Y.H. Han, N.J. Kreidl, and D.E. Day, "Alkali Diffusion and Electrical Conductivity in Sodium Borate Glasses," *J. Non-Cryst. Solids*, **30** [3] 241-52 (1979).
15. I.M. Hodge, K.L. Ngai, and C.T. Moynihan, "Comments on the Electrical Modulus Function," *J. Non-Cryst. Solids*, **351** [2] 104-15 (2005).
16. W.C. Huang and H. Jain, "Correlation between Local Structure and Electrical Response of Rb and (Rb, Ag) Germanate Glasses: DC Conductivity," *J. Non-Cryst. Solids*, **188** [3] 254-65 (1995).
17. W.C. Huang and H. Jain, "Local Structure and Electrical Response of Rb and (Rb, Ag) Germanate Glasses: Electrical Conductivity Relaxation," *J. Non-Cryst. Solids*, **212** [2-3] 117-25 (1997).
18. A.G. Hunt, "Mixed-Alkali Effect: Some New Results," *J. Non-Cryst. Solids*, **255** [1] 47-55 (1999).

19. C.C. Hunter and M.D. Ingram, "Na⁺-Ion Conducting Glasses," *Solid State Ionics*, **14** [1] 31-40 (1984).
20. A.W. Imre, S.V. Divinski, S. Voss, F. Berkemeier, and M. H., "A Revised View on the Mixed-Alkali Effect in Alkali Borate Glasses," *J. Non-Cryst. Solids*, **352** [8] 783-8 (2006).
21. A.W. Imre, S. Voss, and H. Mehrer, "Ionic Conduction, Diffusion and Glass Transition in 0.2[x Na₂O•(1-x) Rb₂O]•0.8 B₂O₃," *J. Non-Cryst. Solids*, **333** [3] 231-9 (2004).
22. M.D. Ingram, "Ionic Conductivity in Glass," *Phys. Chem. Glasses*, **28** [6] 215-34 (1987).
23. M.D. Ingram, "The Mixed Alkali Effect Revisited-a New Look at an Old Problem," *Glasstech. Ber. Glass Sci. Technol.*, **67** [6] 151-5 (1994).
24. M.D. Ingram, C.T. Imrie, and I. Konidakis, "Activation Volumes and Site Relaxation in Mixed Alkali Glasses," *J. Non-Cryst. Solids*, **352** [30-31] 3200-9 (2006).
25. M.D. Ingram, C.T. Moynihan, and A.V. Lesikar, "Ionic Conductivity and the Weak Electrolyte Theory of Glass," *J. Non-Cryst. Solids*, **38-39** [Part I] 371-6 (1980).
26. J.O. Isard, "The Mixed Alkali Effect in Glass," *J. Non-Cryst. Solids*, **1** [3] 235-61 (1969).
27. H. Jain, H.L. Downing, and N.L. Peterson, "The Mixed Alkali Effect in Lithium-Sodium Borate Glasses," *J. Non-Cryst. Solids*, **64** [3] 335-49 (1984).
28. H. Jain, W.C. Huang, E.I. Kamitsos, and Y.D. Yiannopoulos, "Significance of Intermediate Range Structure for Electrical Conduction in Alkali Germanate Glasses," *J. Non-Cryst. Solids*, **222** 361-8 (1997).
29. H. Jain and X. Lu, "Is There a Mixed Alkali Effect in the Low Temperature AC Conductivity of Glasses," *J. Non-Cryst. Solids*, **196** 285-90 (1996).
30. J.C. Lapp and J.E. Shelby, "The Mixed Alkali Effect in Lithium-Sodium Aluminosilicate Glasses," *J. Non-Cryst. Solids*, **95-96** [Part 2] 889-96 (1987).
31. C. Leon, A. Rivera, A. Varez, J. Sanz, J. Santamaria, C.T. Moynihan, and K.L. Ngai, "Crossover of Near-Constant Loss to Ion Hopping Relaxation in Ionically Conducting Materials: Experimental Evidences and Theoretical Interpretation," *J. Non-Cryst. Solids*, **305** [1-3] 88-95 (2002).

32. P. Maass, "Towards a Theory for the Mixed Alkali Effect in Glass," *J. Non-Cryst. Solids*, **255** [1] 34-46 (1999).
33. S.W. Martin and C.A. Angell, "DC and AC Conductivity in Wide Composition Range $\text{Li}_2\text{O-P}_2\text{O}_5$ Glasses," *J. Non-Cryst. Solids*, **83** [1-2] 185-207 (1986).
34. R.A. Montani, "A Kinetic Model for the Mixed Alkali Effect on Ionic Conducting Glasses," *J. Non-Cryst. Solids*, **215** [2-3] 307-12 (1997).
35. M.K. Murthy and J. Ip, "Some Physical Properties of Alkali Germanate Glasses," *Nature (London)*, **201** [5] 285-6 (1964).
36. M.L.F. Nascimento, E.d. Nascimento, and S. Watanabe, "'Universal' Curve of Ionic Conductivities in Binary Alkali Germanate Glasses," *Mater. Chem. Phys.*, **96** [1] 55-8 (2006).
37. K.L. Ngai, Y. Wang, and C.T. Moynihan, "The Mixed Alkali Effect Revisited: The Importance of Ion-Ion Interactions," *J. Non-Cryst. Solids*, **307-310** 999-1011 (2002).
38. A.S. Nowick and B.S. Berry, *Anelastic Relaxation in Crystalline Solids*; p. 677. Academic Press, New York, 1972.
39. A.S. Nowick, W.-K. Lee, and H. Jain, "Survey and Interpretation of Pre-Exponential of Conductivity," *Solid State Ionics*, **28-30** [Part 1] 89-94 (1988).
40. E.F. Riebling, "Nonideal Mixing in Binary $\text{GeO}_2\text{-SiO}_2$ Glasses," *J. Am. Ceram. Soc.*, **51** [7] 406-7 (1968).
41. B. Roling and M.D. Ingram, "Mixed Alkaline-Earth Effects in Ion Conducting Glasses," *J. Non-Cryst. Solids*, **265** [1-2] 113-9 (265).
42. G.B. Rouse, J.M. Gordon, and W.M. Risen, "The Mixed Alkali Effect: Theoretical Considerations " *J. Non-Cryst. Solids*, **33** [1] 83-94 (1979).
43. J.E. Shelby and J. Ruller, "Properties and Structure of Lithium Germanate Glasses," *Phys. Chem. Glasses*, **28** [6] 262-8 (1987).
44. D.L. Sidebottom, "Evidence for Site Memory Effects in the Ionic Relaxation of $(\text{Li}_2\text{O})_x(\text{Na}_2\text{O})_y(\text{GeO}_2)_{1-x-y}$ Glasses," *J. Non-Cryst. Solids*, **255** [1] 67-77 (1999).
45. L. Solymar and D. Walsh, *Electrical Properties of Materials*, 7th ed.; pp. 2-20. Oxford University Press, Oxford, 2004.
46. R. Terai, "The Mixed Alkali Effect in the $\text{Na}_2\text{O-Cs}_2\text{O-SiO}_2$ Glasses," *J. Non-Cryst. Solids*, **18** [2] 121-35 (1971).

47. M.P. Thomas, "Electrical Conductivity and Tracer Diffusion in Sodium Germanate Glasses," *Solid State Ionics*, **14** [4] 297-307 (1984).
48. M. Tomozawa, "The Mixed Alkali Effect and Thermodynamic State of Glass," *Solid State Ionics*, **105** [1-4] 249-55 (1998).
49. M. Tomozawa and M. Yoshiyagawa, "AC Electrical Conductivity of Mixed Alkali Glasses," *Glastech. Ber.*, **56** [Part 2] 939-44 (1983).
50. J.-S. Wang, K.-M. Hon, K.-H. Yang, M.-C. Wang, and M.-H. Hon, "Mixed Alkali Effect on Calcium Aluminogermanate Glasses," *Ceram. Int.*, **23** [2] 153-7 (1997).
51. J. Zhang and D.L. Sidebottom, "Modeling the AC Conductivity Dispersion of Mixed Alkali Germinate Glasses," *J. Non-Cryst. Solids*, **288** [1-3] 18-29 (2001).
52. J.F. Cordaro and M. Tomozawa, "Dependence Upon Alkali Concentration of the Electrical Conductivity in Sodium Silicate Glasses," *Phys. Chem. Glasses*, **27-28** [1] 27 (1984).
53. D. Ravaine and J.L. Souquet, "A Thermodynamic Approach to Ionic Conductivity in Oxide Glasses. Part 1. Correlation of the Ionic Conductivity with the Chemical Potential of Alkali Oxide in Oxide Glasses.," *Phys. Chem. Glasses*, **18** [2] 27 (1977).
54. D. Ravaine and J.L. Souquet, "A Thermodynamic Approach to Ionic Conductivity in Oxide Glasses. Part 2. A Statistical Model for the Variations of the Chemical Potential of the Constituents in Binary Alkali Oxide Glasses.," *Phys. Chem. Glasses*, **19** [5] 115 (1978).
55. M. Tomozawa, J.F. Cordaro, and M. Singh, "Applicability of Weak Electrolyte Theory to Glasses," *J. Non-Cryst. Solids*, **40** [1-3] 189-96 (1980).
56. F. Berkemeier, S. Voss, A.W. Imre, and H. Mehrer, "Molar Volume, Glass-Transition Temperature, and Ionic Conductivity of Na- and Rb- Borate Glasses in Comparison with Mixed Na-Rb Borate Glasses," *J. Non-Cryst. Solids*, **351** [52-54] 3816-25 (2005).
57. A.W. Imre, F. Berkemeier, H. Mehrer, Y. Gao, C. Cramer, and M.D. Ingram, "Transition from a Single-Ion to a Collective Diffusion Mechanism in Alkali Borate Glasses," *J. Non-Cryst. Solids*, **354** [2-9] 328-32 (2008).
58. S. Voss, "Words a Universal Behavior of Ion Dynamics in Na- and Rb-Oxide Glasses," *Solid State Ionics*, **176** [15-16] 1383-91 (2005).

59. R.D. Shannon and C.T. Prewitt, "Effective Ionic Radii in Oxide and Fluorides," *Acta Crystallogr.*, **B25** [5] 925-46 (1969).
60. D.K. McElfresh and D.G. Howitt, "Activation Enthalpy for Diffusion in Glass," *J. Am. Ceram. Soc.*, **69** [10] C-237-C-8 (1986).
61. Y. Haven and B. Verkerk, "Diffusion and Electrical Conductivity of Sodium Ions in Sodium Silicate Glasses," *Phys. Chem. Glasses*, **6** [2] 38-45 (1965).
62. Vol. 20; *Handbuch D. Physik*; pp. 246-349. Edited by A.B. Lidiard. S. Flugge. Springer-Verlag, Berlin, 1957.
63. K.L. Ngai, "The Dynamics of Ions in Glasses: Importance of Ion-Ion Interactions," *J. Non-Cryst. Solids*, **323** [1-3] 120-6 (2003).
64. K. Funke and R.D. Banhatti, "Modeling Frequency-Dependent Conductivities and Permittivities in the Framework of the Migration Concept," *Solid State Ionics*, **169** [1-4] 1-8 (2004).
65. K. Funke and R.D. Banhatti, "Translational and Localised Ionic Motion in Materials with Disordered Structures," *Solid State Sci.*, 1-14 (Article in Press).
66. J.E. Shelby, *Introduction to Glass Science and Technology*; pp. 1-181. The Royal Society of Chemistry, Cambridge, 1997.
67. C.T. Moynihan and A.V. Lesikar, "Weak-Electrolyte Models for the Mixed-Alkali Effect in Glass," *J. Am. Ceram. Soc.*, **64** [1] 40 (1981).
68. C.T. Moynihan and M.D. Ingram, "Mobile-Ion Concentrations and Mixed-Alkali Effects in B-Alumina Solid Electrolytes," *Solid State Ionics*, **6** [4] 303-10 (1982).
69. O.V. Mazurin, "Glass in a Dielectric Field," pp. 5-55 in *Structure of Glass, Vol. 4, The Structure of Glass: Electrical Properties and Structure of Glass*. Edited by O. V. Mazurin. Consultants Bureau, New York, 1965.
70. G. De Marchi, P. Mazzoldi, and A. Miotello, "Ionic Conductivity in Glass Network," *J. Non-Cryst. Solids*, **123** [1-3] 231-4 (1990).
71. K.S. Evstrop'ev and A.O. Ivanov, "Physicochemical Properties of Germanium Glasses," pp. 79-85 in Vol. 2, *Proceedings of the VI International Congress on Glass*. Plenum Press, Washington, D.C., 1962.
72. V.V. Golubkov and I.G. Polyakova, "Structure and Structural Transformations of Lithium Germanate Glasses," *Fiz. Khim. Stekla*, **16** [4] 518-28 (1990).

73. H. Jain and S. Kirshnaswami, "Composition Dependence of Frequency Power Law of Ionic Conductivity of Glasses," *Solid State Ionics*, **105** [1-4] 129-37 (1998).
74. H. Jain, S. Krishnaswami, and O. Kanert, "'Jellyfish' Fluctuations of Atoms in Solids," *J. Non-Cryst. Solids*, **307-310** 1017-23 (2002).
75. H. Jain and J.N. Mundy, "Analysis of AC Conductivity of Glasses by a Power Law Relationship," *J. Non-Cryst. Solids*, **91** [3] 315-23 (1987).
76. G.L. Jin, Y. Liu, and J.N. Mundy, "Refractive Index and Density of Na-, Rb- and Mixed Na, Rb-Aluminogermanate Glasses," *J. Mater. Sci.*, **22** [10] 3672-8 (1982).
77. K.A. Kostanyan and A.D. Akopyan, "Linear Coefficient of Thermal Expansion of Germanate Glasses," *Arm. Khim. Zh.*, **31** [2-3] 120 (1978).
78. Y.S. Krupkin and T.P. Dgebuadze, "Dielectric Properties of Glasses in M_2O - GeO_2 and M_2O - B_2O_3 - GeO_2 Systems," *Neorg. Mater.*, **5** [8] 1478 (1969).
79. Y.S. Krupkin and K.S. Evstrop'ev, "Properties and Structure of Multialkali Borogermanate Glasses," *Inorg. Mater.*, **1** [9] 1410-4 (1971).
80. R. Kuchler, O. Kanert, S. Ruckstein, and H. Jain, "Correspondence between Nuclear Spin Relaxation and Ionic Conduction in Lithium Germanate Glasses," *J. Non-Cryst. Solids*, **128** [3] 328-32 (1991).
81. T. Minami, N. Fujikawa, and M. Tanaka, "Electric Conduction and Dielectric Relaxation in Na_2O - GeO_2 Glasses," *Yogyo Kyokaishi*, **85** [8] 26-30 (1977).
82. R.A. Secco and K.M. Ault, "Ionic Transport and Structure in High Pressure $Na_2O:GeO_2$ Glasses," *J. Non-Cryst. Solids*, **238** [3] 244-52 (1998).
83. A.K. Yakhkind, N.V. Ovcharenko, B.V. Tatarintsev, A.A. Kozmanyanyan, V.Y. Alaev, and A.K. Pogodaev, "Ion-Exchange Interaction between Germanate Glasses and Molten Alkali Nitrates and Refractive-Index Gradient Glasses," *Fiz. Khim. Stekla*, **6** [6] 720-5 (1980).
84. A.O. Ivanov, "Electrical Conductivity of Mixed Alkali Glasses of the Na_2O - K_2O - GeO_2 System," *Sov. Phys. Solid State (Engl. Transl.)*, **5** [9] 1933-7 (1964).
85. R.D. Shannon and C.T. Prewitt, "Effective Ionic Radii and Crystal Chemistry," *J. Inorg. Nucl. Chem.*, **32** [5] 1427-41 (1970).

CHAPTER 7: CRYSTALLIZATION

7.1 Introduction

Only a few studies¹⁻⁶ have examined the crystallization behavior of binary alkali germanate glasses. These studies are restricted to the smaller alkali ions lithium, sodium and potassium. The crystallization behavior of mixed alkali glasses is not well understood. Only two of the ten mixed alkali germanate systems have been studied.^{3,4} Laudisio and Catauro have examined the $x \text{ Na}_2\text{O} \cdot (20-x) \text{ K}_2\text{O} \cdot 80 \text{ GeO}_2$ and $x \text{ Li}_2\text{O} \cdot (20-x) \text{ K}_2\text{O} \cdot 80 \text{ GeO}_2$ ternaries.³⁻⁴ This thesis will present new data for glasses in the $x \text{ Li}_2\text{O} \cdot (15-x) \text{ Cs}_2\text{O} \cdot 85 \text{ GeO}_2$ ternary.

Crystallization in glass requires the formation of a nuclei followed by the growth of a crystal. Each distinct glass composition has unique nucleation and growth temperatures, determined by the kinetic and thermodynamic properties of the glass. Nuclei are formed during thermal processing of the glass, usually achieved during a heat treatment in the glass transition region. Fragile glasses can form nuclei in the short amount of time it takes to remove the glass from a furnace and quench it; at the other extreme are glasses that requires a long heat treatment time at a precise temperature to grow nuclei. A more detailed explanation of crystallization will be presented in the literature review of this chapter.

In this study, a Kissinger experiment is used to determine the activation energies of crystallization for the mixed alkali glasses on the 85 mol % GeO_2 tie-line. A study investigating the effect of particle size on bulk and/or surface crystallization was performed using a DSC. The results are confirmed using scanning electron microscopy (SEM). High temperature x-ray diffraction (HTXRD) is used to determine crystal phases.

7.2 Literature Review

7.2.1 *Crystallization Kinetics*

Crystallization kinetics in glass can be studied using a differential thermal analyzer (DTA) or a DSC in one of two ways: isothermally or non-isothermally. The

isothermal approach involves holding the temperature of the sample constant and measuring the exothermic reaction over time. The fundamental theory behind isothermal crystallization studies was developed by Johnson and Mehl,⁷ and Avrami,⁸⁻¹⁰ and is commonly call the JMA approach. In a non-isothermal study, the heating rate is varied (2 K/min to 30 K/min), and the exothermic reaction is measured over a temperature range. Since Kissinger^{11,12} developed much of the theory behind non-isothermal crystallization, this method is commonly referred to as the Kissinger approach. In this section, the underlying assumptions and derivations for both the JMA and Kissinger approaches will be discussed.

The crystallization of a melt has two stages. The formation of nuclei is the first step of crystallization^{13,14} and can be either homogenous—within the melt, or heterogeneous—at a pre-existing surface. Crystals then grow on these nuclei.^{14,15} The presence of nuclei does not mean the glass will behave as if it is crystalline.¹⁴ These nuclei are small and few, and are essentially just defects in the glass. If the thermodynamics and kinetics allow, these nuclei serve as the foundation for crystal growth. This section will briefly cover the necessary requirements in the glass system to result in nucleation and growth of crystals. A discussion of the basic kinetics and thermodynamics of nucleation and crystal growth in glasses will follow the discussion of isothermal and non-isothermal crystallization kinetics.

7.2.1.1 Isothermal Crystallization Kinetics

The expression describing isothermal crystallization kinetics is shown in Equation 7-1. This Equation describes crystallization as a result of the volume percent crystallized, x , over time, t , as a function of the crystal growth rate, u , and the frequency of nuclei per unit volume, I_v ,

$$x = 1 - \exp \left[-g \int_0^t I_v \left(\int_{t'}^t u d\tau \right)^m dt' \right]. \quad (7-1)$$

The geometric factor g depends on the shape of the growing crystal, while m is an integer that is dependent upon the mechanism of growth. One of two mechanisms, interface-controlled or diffusion-controlled, dominates the crystallization process. Interface-

controlled diffusion[◇] results in m being an integer 1, 2, or 3. The integer corresponds to the dimensionality of crystal growth i.e., 1 is one-dimensional, etc. Diffusion-controlled growth,[‡] where the growth rate decreases according to $t^{-1/2}$, is indicated by m values of 1/2, 1 and 3/2 for one-, two-, and three-dimensional growth, respectively.¹⁶

The Johnson-Mehl-Avrami (JMA) approach assumes the simplest case for crystallization kinetics, where the reaction is isokinetic.^{^7,9} Equation 7-1 becomes

$$x = 1 - \exp\left[-(Kt)^n\right], \quad (7-2)$$

where K is the overall reaction rate and defined by Equation 7-3, t is time, and $n = m+1$. n is also known as the Avrami parameter. The reaction rate, K , is given by

$$K = K_o \exp\left(-\frac{E}{RT}\right) \quad (7-3)$$

The overall reaction rate is dependent on the effective activation energy, E , the gas constant, R , and the temperature, T . K_o is the frequency factor or the pre-exponential factor.¹⁶

An important specific case of isothermal crystallization occurs when the nucleation frequency and growth rate are independent of time. Equation 7-1 then becomes

$$x = 1 - \exp(-g' I_v u^m t^n), \quad (7-4)$$

where all constants are as previously defined in section 7.2.1.1 and g' is the new shape factor. By comparing Equation 7-2 to 7-4, it can be seen that $K^n \propto I_v u^m$, which is important because it shows mathematically that the temperature dependence of the effective overall reaction rate, K , is Arrhenian in nature when the temperature dependences of I_v and u are Arrhenian in nature.

Nucleation and growth rates that are independent of time do not occur in most real systems. In most real cases, the temperature dependence of nucleation frequency is not Arrhenian in nature. The growth rate of crystals is not Arrhenian over a broad range of temperatures. However, over the small range of temperatures, for example the range of

[◇] Interface diffusion is crystal growth that is independent of time.

[‡] Diffusion controlled growth is crystal growth that is time dependent.

^{^◇} Isokinetic is when the rate of nucleation and growth remain constant throughout the reaction.

temperatures over which a crystallization peak occurs in a DSC or DTA, u and I_v may be described by the following zeroth-order approximations:¹⁶

$$I_v \approx I_{v0} \exp\left(-\frac{E_N}{RT}\right) \quad (7-5)$$

and

$$u \approx u_0 \exp\left(-\frac{E_G}{RT}\right). \quad (7-6)$$

The new terms in these Equations, E_N and E_G , are defined as the effective activation energy for nucleation and the effective activation energy for growth, respectively.

To obtain an expression for the overall effective activation energy for isothermal crystallization, where the nucleation and growth rates are independent of time, Equations 7-2 through 7-6 can be combined to yield

$$E \approx \frac{E_N + mE_G}{n}. \quad (7-7)$$

If the nucleation frequency is negligible over the experimental temperature range, then $E \approx E_G$. The application of Equations 7-1 through 7-7 to other special cases such as bulk crystallization and grain boundary crystallization are presented in detail in the work of Johnson and Mehl⁷ and Avrami.⁸⁻¹⁰

7.2.1.2 Non-Isothermal Crystallization Kinetics

While isothermal crystallization studies are accurate and based on sound mathematics, these studies are extremely time consuming. Consequently, many studies have been performed to develop a faster method using non-isothermal crystallization methods that are as accurate as the JMA approach.^{11,12,17-27} Yinnon and Uhlmann,¹⁶ in their 1982 review article, compare the similarities and differences between the most highly developed approaches. Since, in this thesis, the Kissinger^{11,12} method has been employed, further discussion will be focused on his derivation. For more details on other approaches, please refer to Yinnon and Uhlmann.¹⁶ In summary, a non-isothermal crystallization study involves DSC or DTA experiments, where the heating rate (ϕ) is varied, resulting in the following equation,

$$T = T_0 + \phi t, \quad (7-8)$$

where T is the temperature and T_0 is the starting temperature. The desired outcome of this approach is to find two parameters, which, when plotted, result in a straight line and yield the activation energy of the reaction.

In the following derivation, Kissinger, shows that the kinetic constants can be calculated by performing series of DTA experiments with different heating rates.¹¹ Varying the heating rate causes the maximum point of the exothermic peak (T_p) to shift to higher temperatures and is an effect of the glasses intrinsic thermal properties. A linear dependence is observed between $\phi/(T^P)^2$ and $1/T^P$.

Beginning with the JMA Equation (7-2) and the Arrhenius Equation (7-3),

$$x = 1 - \exp[-(Kt)^n], \quad (7-2)$$

and,

$$K = K_0 \exp\left(\frac{-E}{RT}\right), \quad (7-3)$$

one must differentiate Equation 7-2 with respect to time to describe the reaction when temperature is changing with time,

$$\frac{dx}{dt} = 0 - \exp[-(Kt)^n] * -nK^{n-1}t^n \frac{dK}{dt} - \exp[-(Kt)^n] * -nK^n t^{n-1} \quad (7-9)$$

Simplifying Equation 7-9 results in Equation 7-10:

$$\frac{dx}{dt} = \exp[-(Kt)^n] nK^n t^{n-1} \left(\frac{t}{K} \frac{dK}{dt} + 1\right) \quad (7-10)$$

Rearranging Equation 7-2 and substituting it into Equation 7-10 yields Equations 7-11 and 7-12, respectively:

$$\exp[-(Kt)^n] = (1 - x) \quad (7-11)$$

$$\frac{dx}{dt} = (1 - x) nK^n t^{n-1} \left(\frac{t}{K} \frac{dK}{dt} + 1\right) \quad (7-12)$$

The derivative of K with respect to time is obtained from Equations 7-8 and 7-3.

Performing the following mathematical manipulation, $\frac{dK}{dt} = \frac{dK}{dT} \frac{dT}{dt}$, yields:

$$\frac{dK}{dT} = \frac{-K_0 E}{RT^2} \exp\left(\frac{-E}{RT}\right), \quad (7-13)$$

$$\frac{dT}{dt} = \phi \quad (7-14)$$

and thus,

$$\frac{dK}{dt} = \frac{-K_0 E \phi}{RT^2} \exp\left(\frac{-E}{RT}\right). \quad (7-15)$$

Letting $a = \frac{-E\phi}{RT^2}$ and substituting it into Equation 7-15 yields,

$$\frac{dK}{dt} = aK. \quad (7-16)$$

Substituting Equation 7-16 into Equation 7-12 results in,

$$\frac{dx}{dt} = (1-x)nK^n t^{n-1}(at+1). \quad (7-17)$$

If the initial temperature T_0 is much smaller than T , the term $at = \frac{E}{RT}$. When $\frac{E}{RT} \ll 1$

Equation 7-17 becomes

$$\frac{dx}{dt} = (1-x)nK^n t^{n-1} \quad (7-18)$$

Time can be represented in terms of temperature as in Equation 7-8 or x as in Equation 7-19:

$$t = \frac{[-\ln(1-x)]^{1/n}}{K} \quad (7-19)$$

Substituting Equation 7-19 into Equation 7-18,

$$\frac{dx}{dt} = (1-x)K^n \frac{[-\ln(1-x)]^{(n-1)/n}}{K}. \quad (7-20)$$

Substituting in Equation 7-3 and assuming that near the maximum in the crystallization reaction rate $[-\ln(1-x)]^{(n-1)/n}$ is a constant (denoted as A), yields:

$$\frac{dx}{dt} = A(1-x)K_0 \exp\left(\frac{-E}{RT}\right). \quad (7-21)$$

Taking the second derivative of Equation 7-21 with respect to time and assuming the maximum rate of crystallization occurs at the peak of the exotherm at time t^P (x^P) and temperature T^P , allows the second derivative to be set equal to zero:

$$\frac{d^2x}{dt^2} = AK_0 \left(\frac{E}{R(T^P)^2} - \frac{AK_0}{\phi} e^{\frac{-E}{RT^P}} \right) \phi (1-x^P) e^{\frac{-E}{RT^P}} = 0. \quad (7-22)$$

Rearranging Equation 7-22 and taking the natural log of each side results in the Kissinger equation,

$$\frac{d \ln \left[\frac{\phi}{(T^P)^2} \right]}{d \frac{1}{T^P}} = -\frac{E}{R} \quad (7-23)$$

In the form of Equation 7-23, $\ln[\phi/(T^P)^2]$ versus $1/T^P$ yields a straight line where the activation energy for crystallization can be calculated from the slope, as shown in Figure 7-1.

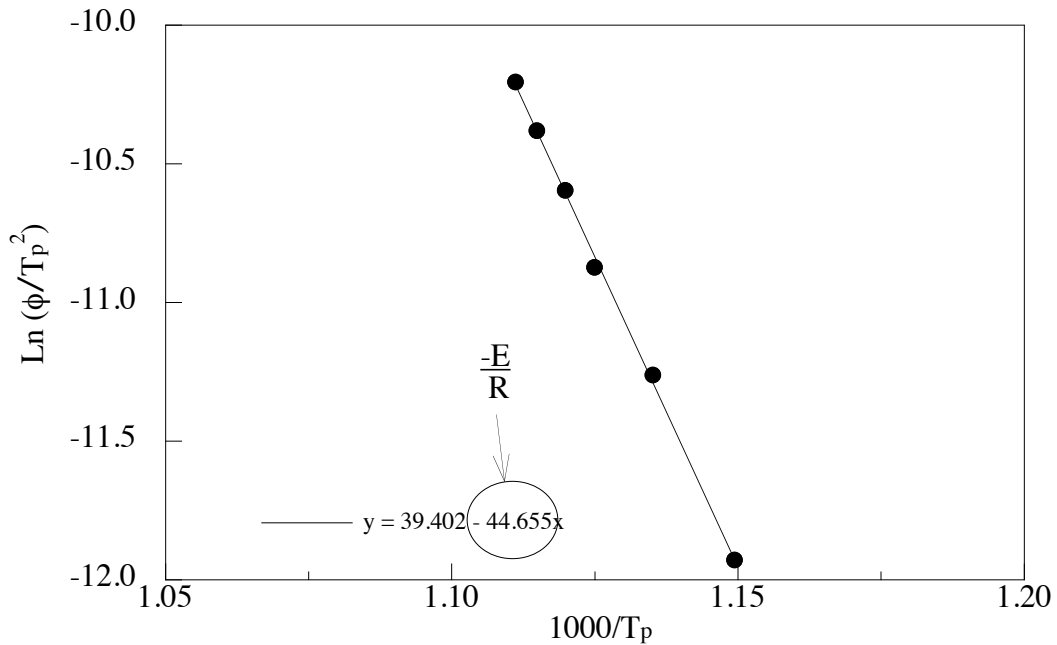


Figure 7-1. Example Kissinger plot for a mixed alkali germanate glass. Line is a linear fit.

7.2.1.3 Nucleation

All classical liquids, regardless of their chemical composition, will theoretically form glasses, i.e. the kinetic theory of glasses is applicable to all materials. A supercooled material will form if the cooling rate and the crystallization kinetic constants are favorable to glass formation.^{28,29} The following section will address the effect of nucleation on crystallization and give a brief review of nucleation theory. More detail

concerning the basic assumptions and derivations of nucleation in glasses can be found in the review articles by Uhlmann²⁹ and James.³⁰

A crystalline solid has a lower free energy than a compound of the same composition in the glassy state. Glasses theoretically could transform into crystalline phases at temperatures below T_g if the correct thermodynamic and kinetic conditions are met.^{29,30} The first requirement for crystallization is the formation of nuclei of the new crystalline phase. Homogenous crystal nucleation, I , of a single component glass has a steady state rate given

$$I = A \exp \left[- \frac{(W^* + \Delta G_D)}{kT} \right] \quad (7-24)$$

where W^* is the Gibbs free energy to form a critical nucleus, G_D is the kinetic barrier to nucleation, k is Boltzmann's constant, and T is absolute temperature. The pre-exponential factor, A , is a function of the volume, V , the crystal-melt interfacial free energy, γ , and constants k and h , where h is Planck's constant, yielding:

$$A = 2n_v V^{1/3} \left(\frac{kT}{h} \right) \left(\frac{\gamma}{kT} \right)^{1/2} . \quad (7-25)$$

The derivation of this equation can be found in many locations.^{28,31-35} In other words, W^* is the thermodynamic barrier to nucleation involving the change in the free energy of the system when a nucleus is formed, and G_D is the kinetic barrier and describes the systems ability to rearrange the mass to allow the growth of a crystal out of the liquid. Over the temperature range used for nucleation measurements, A is assumed to be constant,³⁰ resulting in Equation 7-25 becoming

$$A = n_v \left(\frac{kT}{h} \right) . \quad (7-26)$$

Closer examination (specifically, the case of a spherical particle with a radius of r) of the thermodynamic barrier to nucleation, W^* , will expose the complexity of the nucleation process.

$$W^* = \frac{4}{3} \pi r^2 \Delta G_v + 4 \pi r^2 \gamma \quad (7-27)$$

This equation contains two competing terms. The first term, $\frac{4}{3} \pi r^2 \Delta G_v$, describes the decrease in volume free energy that occurs because the crystalline state has a lower free

energy than the glassy state. The second term, $4\pi r^2\gamma$, describes the increase in surface energy resulting from the formation of the new surface between the crystal and the glass. It follows that every nucleus formed results in both a decrease in free energy and an increase in surface energy. Since nuclei are small, the surface energy term will dominate in the beginning of the nucleation processes, resulting in a very small value of W^* . As the radius of the crystal begins to increase, the value of W^* will become large and result in an unstable particle, but if this particle can continue to grow, the volume free energy term will begin to dominate and decrease W^* and lead to a large stable particle on which a crystal can later grow.

The other barrier to nucleation[‡] is the kinetic term, ΔG_D . The kinetics of the reaction can be approached in terms of the effective diffusion coefficient, D ,

$$D = \left(\frac{kT\lambda^2}{h} \right) \exp\left(\frac{-\Delta G_D}{kT} \right) \quad (7-28)$$

where λ is the atomic jump distance. The effective diffusion coefficient is sometimes assumed to be related to the viscosity of the melt, η , through the Stokes-Einstein relation

$$D = \frac{kT}{3\pi\lambda\eta}. \quad (7-29)$$

In other words, a glass with a low viscosity will have a higher effective diffusion coefficient and will therefore be easier to crystallize.

To apply the effective diffusion coefficient to the original expression for nucleation, Equation 7-24, we can use the relationship between Equation 7-28 and Equation 7-29,

$$\exp\left(\frac{-\Delta G_D}{kT} \right) = \frac{hD}{kT\lambda^2} = \frac{h}{3\pi\lambda^3\eta}, \quad (7-30)$$

and substitute Equations 7-26 and 7-30 into Equation 7-24 to yield:

$$I = \left(\frac{n_v kT}{3\pi\lambda^3\eta} \right) \exp\left(\frac{-W^*}{kT} \right). \quad (7-31)$$

The equations for heterogeneous nucleation, as shown by James,³⁰ describe the nucleation that occurs at the surface of a foreign material, such as the crucible wall, or a nucleating agent. The nucleation rate is then

[‡] in this specific case homogenous nucleation

$$I_{het} = A_{het} \exp \left[\frac{-(W_{het}^* + \Delta G_D)}{kT} \right] \quad (7-32)$$

where the subscript ‘*het*’ refers to the specific case of heterogeneous nucleation and where W_{het}^* is a function of the contact angle between the crystal nucleus and the substrate. A_{het} can be written similarly to Equation 7-26

$$A_{het} = n_s \left(\frac{kT}{h} \right), \quad (7-33)$$

where n_s is the number of formula units of the melt in contact with to substrate per unit area.

Equations 7-30 and 7-31 can be used to predict the shape of a glass nucleation curve; an illustration of the nucleation curve is shown in Figure 7-2. As you cool the glass from T_m , there is a region where the ΔG_v is very small and the very small nucleus is not stable. Since the critical radius (r^*) of the nucleus required for crystal growth is much larger than the size of the nuclei in this region, the glass is essentially nuclei free, this is called the metastable zone of undercooling. The equation for the critical radius is

$$r^* = \frac{-2\gamma}{\Delta G_v}. \quad (7-34)$$

As the glass is further cooled, the free energy, ΔG_v , becomes larger, therefore decreasing the critical radius of the nuclei and allowing stable nuclei to form. The extent of the metastable zone of undercooling can range from less than a degree to hundreds of degrees.¹⁴ As the temperature continues to decrease, the nucleation rate increases because the thermodynamic barrier decreases with increasing temperature. The nucleation rate continues to increase until the viscosity of the glass becomes too high[◇] and the kinetics become too slow and begin to dominate the nucleation process, after which point nucleation ceases.

[◇] viscosity increases with increasing temperature

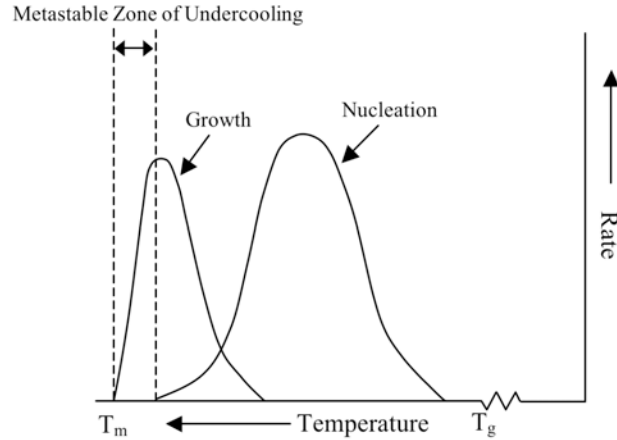


Figure 7-2. Illustration showing the effect of temperature on the rate of nucleation and crystal growth in glasses.

7.2.1.4 Crystal Growth

Arguments concerning crystal growth are similar to those for nucleation. There are many growth equations in the literature, however, most are unique to the system being studied.²⁹⁻³⁸ A general form of the nucleation equation is

$$U = a_0 v \exp\left(\frac{-\Delta E}{kT}\right) \left[1 - \exp\left(\frac{\Delta G}{kT}\right)\right], \quad (7-35)$$

where a_0 is the interatomic separation distance, v is the vibrational frequency, and ΔE and ΔG are the kinetic and thermodynamic barriers to crystal growth, respectively. Using Equations 7-28 and 7-29, along with the same mathematics shown in the nucleation section, Equation 7-35 becomes

$$U = \left(\frac{kT}{3\pi a_0^2 \eta}\right) \left[1 - \exp\left(\frac{\Delta G}{kT}\right)\right]. \quad (7-36)$$

The Gibbs free energy can be written in terms of the heat of fusion (ΔH_f)³⁹ using the following approximation of Gibbs free energy

$$\Delta G = -\Delta H_f \frac{(T_m - T)}{T_m}. \quad (7-37)$$

There is no temperature region where growth is unstable, therefore as long as a nucleus is present, crystal growth can begin immediately below T_m , as illustrated in Figure 7-2. Glasses that crystallize heterogeneously are very likely to begin immediate crystallization

upon cooling from T_m because the nucleation site is present in the melt or on the surface of the glass. Growth eventually slows due to the decrease in viscosity as the melt cools.¹⁴

7.2.2 Previous Work

7.2.2.1 Devitrification of Binary and Ternary Alkali Germanate Glasses

The most pertinent literature to this study is found in the three studies by Pernice and Catauro and co-workers who have extensively studied the devitrification of binary lithium tetra-germanate glasses.^{4,6,40} In addition to the lithium germanate system, Vergano and Uhlmann⁴¹ examined the crystallization of vitreous GeO_2 . There is no literature dealing with crystallization in the cesium germanate binary or in the lithium-cesium germanate ternary systems. However, a few studies concerned with other alkali ions (sodium and/or potassium) in germanate glasses are present in the literature.^{1-3,5} A small amount of work on the binary phase diagrams, performed by Murthy, Angelone and Ip,^{42,43} will be presented in the following section.

Vergano and Uhlmann found that GeO_2 crystallizes heterogeneously, with no need for seeding to initiate crystallization.⁴¹ When Li_2O is added to germania, in amounts as small as 5 mol %, the crystallization is altered from heterogeneous surface crystallization to homogeneous crystallization in the bulk of the glass. Lithia germanate glasses with 12 mol% or less alkali oxide devitrify into $\text{Li}_2\text{Ge}_7\text{O}_{15}$ and crystalline GeO_2 , as predicted by the phase diagram, shown in Figure 7-3.⁴²⁻⁴⁶ The DTA curves show two distinct crystallization peaks, one at about 575 °C and the other around 600 °C. Pernice⁶ suggests that this is a three step process: (1) at 555 °C, metastable crystals grow, (2) At 622 °C, the metastable crystals convert into $\text{Li}_2\text{Ge}_7\text{O}_{15}$ crystals, (3) at 819 °C, the $\text{Li}_2\text{Ge}_7\text{O}_{15}$ crystals act as nucleating sites for GeO_2 crystal formation. His argument is based XRD patterns, where peaks due to the low temperature phase are barely identifiable under the amorphous hump, while a clear pattern occurs for the high temperature phase.⁶ Laudisio and Catauro studied the mixed lithium and potassium tetra-germanate glasses. Phase identification, using XRD data, shows that compositions with 0 to 25 % of the alkali being the potassium ion, crystallize into compounds of lithia-germania. When the ratio of Li_2O to K_2O is 1:1 or if this melt contains more of the larger potassium ion, the crystallized compounds are no longer lithium-germanium oxides, but

are potassium-germanium oxides, with no trace of compounds containing the smaller ion.³ This finding differs from results for the $x \text{Na}_2\text{O} \cdot (20-x) \text{K}_2\text{O} \cdot 80 \text{GeO}_2$ system, where the K^+ and Na^+ ions are close in size, resulting in the formation of solid solutions when the alkali ions are mixed.³

7.2.2.2 Phase Diagrams

The phase diagrams for the $\text{Li}_2\text{O} \cdot \text{GeO}_2$ and $\text{Cs}_2\text{O} \cdot \text{GeO}_2$ binaries, developed by Murthy,^{42,43} are shown below in Figures 7-3 and 7-4, respectively. This study is keeping the mol% GeO_2 constant at 85 mol%. Since the phase diagrams are shown in wt% the equivalent mol% are calculated to be about 95 wt% GeO_2 for the $\text{Li}_2\text{O} \cdot \text{GeO}_2$ system, and about 67 wt% GeO_2 for the $\text{Cs}_2\text{O} \cdot \text{GeO}_2$ system; these compositions are marked in Figures 7-3 and 7-4 at their approximate locations with an ☆ symbol.

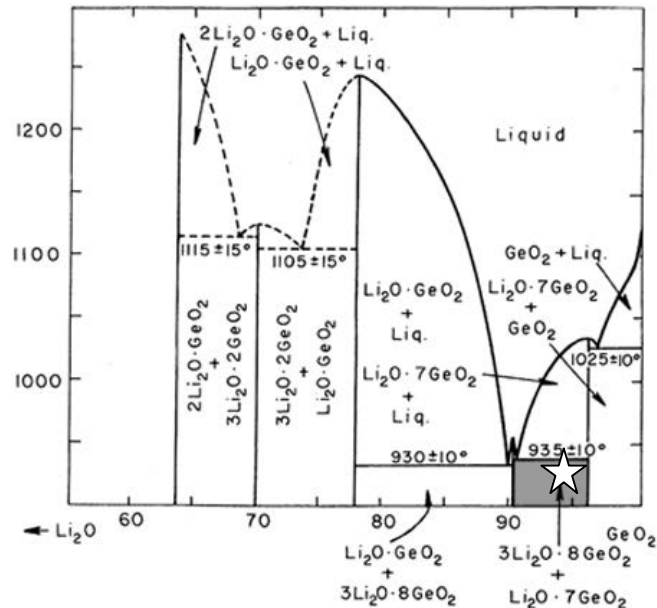


Figure 7-3. Phase diagram for $\text{Li}_2\text{O} \cdot \text{GeO}_2$, taken from Murthy (1971).⁴²

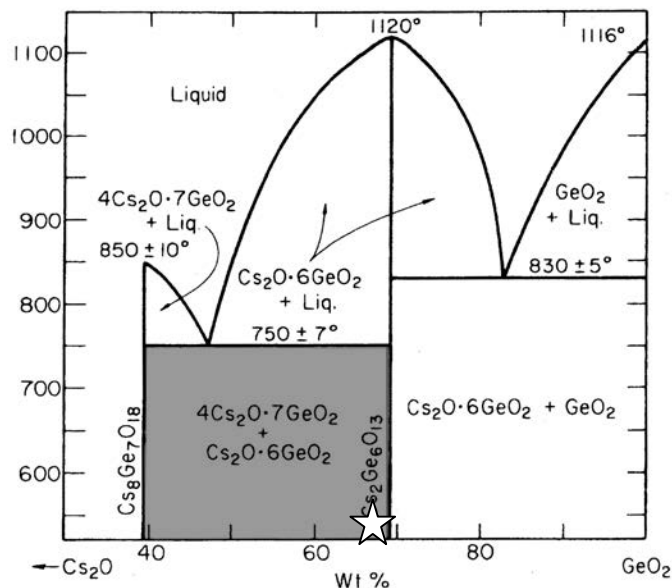


Figure 7-4. Phase diagram for $\text{Cs}_2\text{O}\cdot\text{GeO}_2$, taken from Murthy (1964).⁴³

7.3 Experimental Procedure

7.3.1 Sample Preparation

Glass samples were crushed with glass mortar and pestles. The crushed glass was sifted through sieves ranging from 20 to 270 mesh. To confirm that the samples were initially glass, XRD was performed on samples of two different particle sizes (500 to 850 μm and $< 53 \mu\text{m}$).

7.3.2 Differential Scanning Calorimetry

A TA Instruments[®] DSC 2910 Differential Scanning Calorimeter was used to perform all DSC runs. TA Instruments[®] Universal Analysis software was used to analyze the DSC curves. T_g and T_x were found using the intercept method shown in Figure 7-5. T_g was measured seven times, the maximum variance of the T_g is $\pm 2 \text{ }^\circ\text{C}$. Aluminum pans were used for all measurements with a maximum temperature under 600 $^\circ\text{C}$ and platinum pans were used for measurements with a maximum temperature $> 600 \text{ }^\circ\text{C}$. Measurements were made under a flowing N_2 atmosphere.

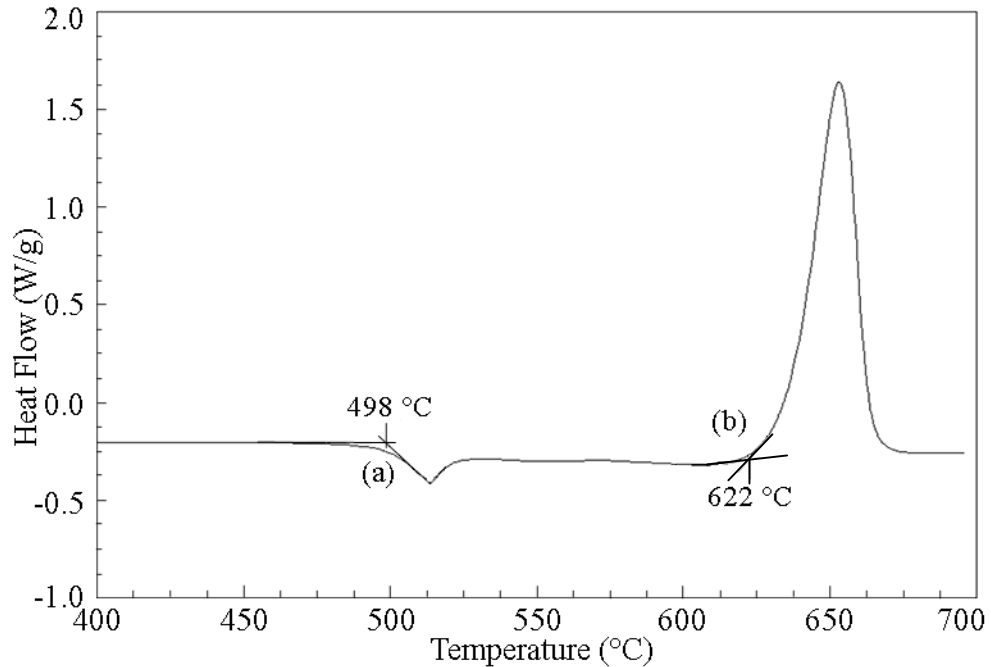


Figure 7-5. Glass transition temperature (a) and onset of crystallization (b), found using the intercept method.

7.3.2.1 Kissinger Study

Six different ramp rates were used to study the effect of heating rate on crystallization: 5, 10, 15, 20, 25, and 30 K/min. Sample sizes ranged from 7 to 12 mg. A particle size range of 63 to 75 μm was used in the study.

7.3.2.2 Particle Size Study

Seven different particle size ranges were used to study the effect of particle size on crystallization behavior. The particle sizes are listed in Table 7-I, along with their U.S. sieve size number. Sample sizes ranged from 7 to 12 mg. The ramp rate was held constant at 20 K/min. Particle sizes were confirmed by measuring the diameters of sieved glasses particles using scanning electron microscopy.

Table 7-I. Table Showing the Different Particle Size Ranges Used in the DSC Experiment

Particle Size Range (μm)	US Sieve Number of Smaller Particle Sieve	US Sieve Number of Larger Particle Sieve
500-850	20	35
425-500	35	40
250-500	40	60
150-250	60	100
106-150	100	140
63-75	200	230
< 53	270	-

7.3.3 X-Ray Diffraction

X-ray diffraction studies were performed using high temperature x-ray diffraction (HTXRD), with a cobalt X-ray and a Bragg-Brentano detector. The scan range was 5 to 75 $^{\circ}2\theta$. The scan rate was 5 $^{\circ}2\theta/\text{minute}$. The sample chamber was filled with N_2 and the sample holder was polycrystalline alumina in the corundum phase. An initial room temperature scan was recorded, then the furnace was ramped at 0.33 K/sec (20 K/min) to the composition's unique T_x , found using the DSC. The sample was held at the crystallization temperature for 24 scans totaling a time of 336 minutes (5.6 hours), then cooled to 50 $^{\circ}\text{C}$, where a final scan was taken to eliminate the shift in the peak positions that occur due to thermal expansion. The peaks were identified with powder diffraction file (pdf) cards using Jade 6.0 software.

7.3.4 Environmental Scanning Electron Microscopy

Each composition studied was heat treated according to the times listed in Table 7-II. Following heat treatment, each sample was sliced, ground and epoxy mounted on its edge, to examine the interior and edge of the sample. The epoxy mounted samples were polished with 320, 600, 800 and 1000 SiC paper, and 15, 6 and 1 μm diamond paste. Following polishing, the samples were sputter coated with a 200 to 300 \AA coating of Au-Pd. Samples were examined in a Phillips Environmental Scanning Electron Microscope (ESEM), under high vacuum, with an accelerating potential of 20 keV.

Table 7-II. Heat Treatment Times and Temperatures for All Glasses

Composition	Heat Treatment Time (min)	Heat Treatment Temperature (°C)
15 Li ₂ O•85 GeO ₂	30	540
15 Li ₂ O•85 GeO ₂	15	635
7:1 Li ₂ O:Cs ₂ O•85 GeO ₂	15	540
3:1 Li ₂ O:Cs ₂ O•85 GeO ₂	15	540
1:1 Li ₂ O:Cs ₂ O•85 GeO ₂	15	605
1:3 Li ₂ O:Cs ₂ O•85 GeO ₂	15	510
1:7 Li ₂ O:Cs ₂ O•85 GeO ₂	15	485
15 Cs ₂ O•85 GeO ₂	15	580

7.4 Results

7.4.1 DSC Studies

7.4.1.1 Kissinger Study

The binary alkali-germanate glasses will be discussed first, beginning with the lithium-germanate binary. Figure 7-6 shows the DSC curves for the glasses containing 15 mol% Li₂O. The glass transition temperature (T_g) shifts from 504 °C when the ramp rate is 5 K/min to 514 °C when the ramp rate is 30 K/min. The shift in T_g decreases as the ramp rate increases. There are two crystallization peaks present below 700 °C. The onset of crystallization (T_x) of the low temperature peak occurs from 551 to 573 °C for ramp rates 5 and 30 K/min, respectively. The onset of crystallization for the high temperature peak ranges from 616 to 648 °C, again for the ramp rates 5 and 30 K/min, respectively. The peak crystallization temperature (T_p) for peak one ranges from 605 to 639 °C and 616 to 648 °C for peak two, with ramp rates 5 and 30 K/min respectively. Table 7-III list the shift in T_g , T_x , and T_p for the 15 Li₂O•85 GeO₂ glass. The effect of ramp rate on these values is shown in Figure 7-7.

Table 7-III. T_g , T_x , and T_p Values for 15 Li₂O•85 GeO₂ Glasses

Ramp Rate (K/min)	T_g (°C)	T_x (°C)-I	T_p (°C)-I	T_x (°C)-II	T_p (°C)-II
5	504	551	557	605	616
10	506	558	566	616	629
15	509	563	569	624	636
20	512	568	574	629	641
25	512	571	576	634	645
30	514	573	579	639	648

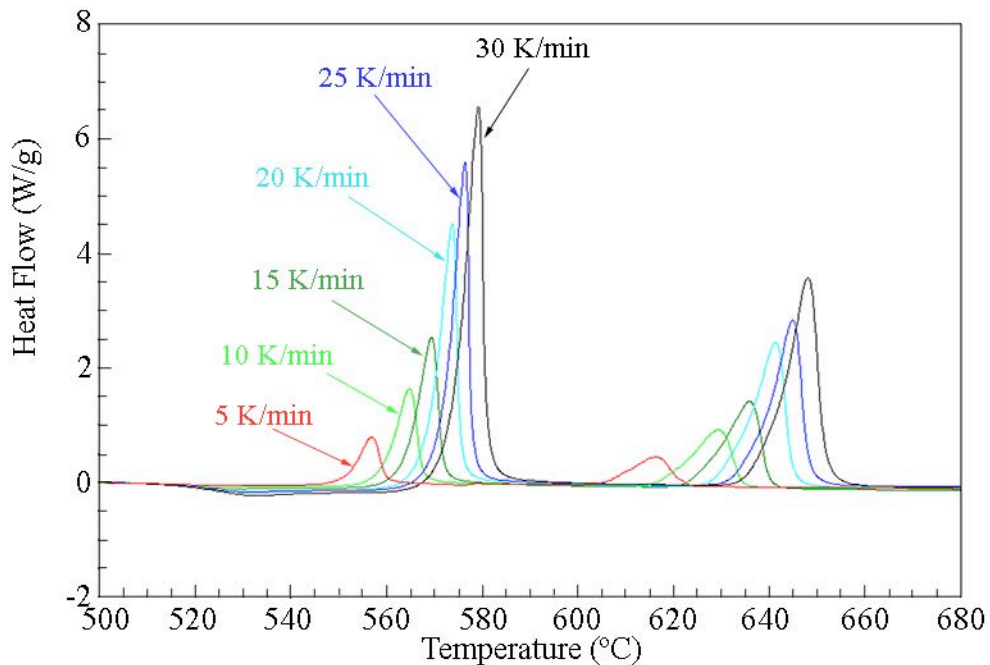


Figure 7-6. DSC curves with ramp rates ranging from 5 to 30 K/min curve for 15 $\text{Li}_2\text{O}\cdot 85 \text{ GeO}_2$ glasses.

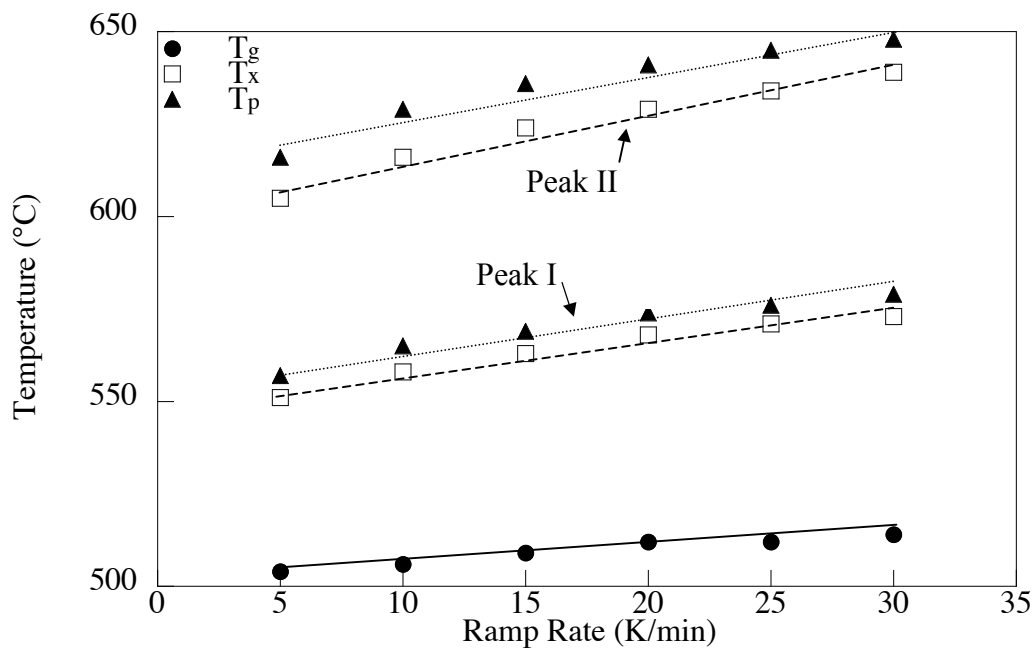


Figure 7-7. T_g , T_x , and T_p values for 15 $\text{Li}_2\text{O}\cdot 85 \text{ GeO}_2$ glasses as a result of varying ramp rate. Lines added to aid the eye.

A Kissinger plot for both the low temperature crystalline phase and the high temperature crystalline phase of the 15 $\text{Li}_2\text{O}\cdot 85 \text{ GeO}_2$ glasses is shown in Figure 7-8.

The activation energy of crystallization of the low temperature phase is 472 kJ/mol. The difference between T_p and T_g ($T_p - T_g$) can be used as an indication of glass forming ability. A large value for $T_p - T_g$ is characteristic of a strong glass. The $T_p - T_g$ for 15 $\text{Li}_2\text{O} \cdot 85 \text{ GeO}_2$ ranges from 53 to 65 K.

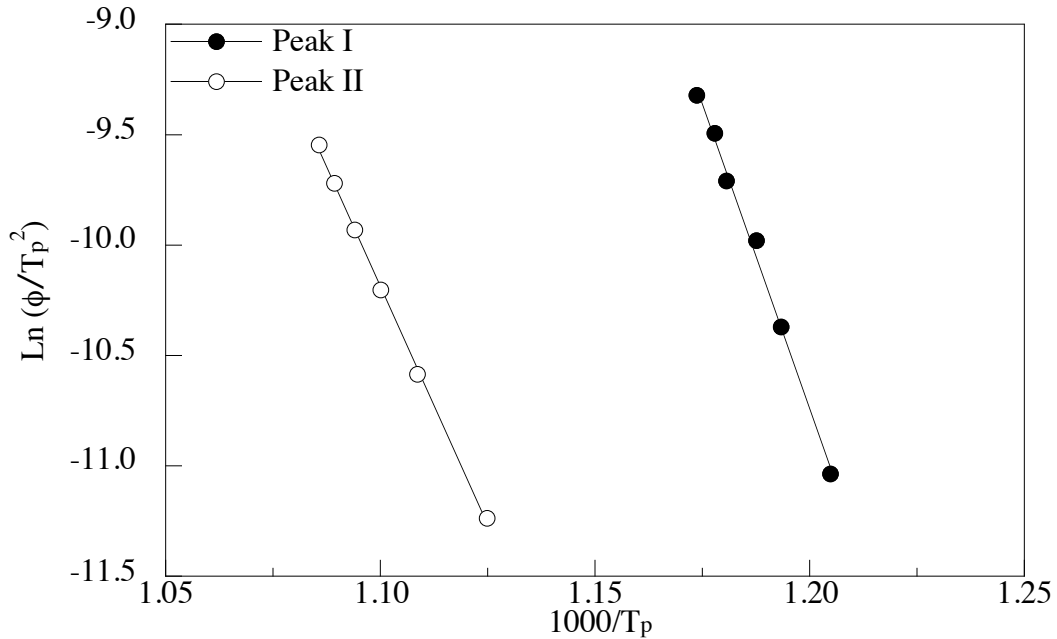


Figure 7-8. Kissinger plot for 15 $\text{Li}_2\text{O} \cdot 85 \text{ GeO}_2$ glass. Lines are linear fits.

The DSC curves for glasses containing 15 mol% Cs_2O have only one peak at temperatures below 700 °C, as shown in Figure 7-9. The peak is broad in comparison to the 15 $\text{Li}_2\text{O} \cdot 85 \text{ GeO}_2$ glass. The T_g shifts from 527 °C when the ramp rate is 5 K/min to 552 °C when the ramp rate is 30 K/min. T_x is undetectable for the 5 K/min ramp rate, as the crystallization peak appears to begin immediately following the T_g . Ramp rates of 10 K/min and higher show a shift in the T_x from 594 °C for the 10 K/min ramp rate to 613 °C for the 30 K/min rate. T_p shifts from 597 to 627 °C for ramp rates 5 and 30 K/min, respectively. Table 7-IV lists the values of T_g , T_x , and T_p for the 15 $\text{Cs}_2\text{O} \cdot 85 \text{ GeO}_2$ glass. The shifts of T_g , T_x and T_p to higher temperature are shown in Figure 7-10.

Table 7-IV. T_g , T_x , and T_p Values for 15 $\text{Cs}_2\text{O}\cdot 85 \text{GeO}_2$ Glasses

Ramp Rate (K/min)	T_g ($^{\circ}\text{C}$)	T_x ($^{\circ}\text{C}$)	T_p ($^{\circ}\text{C}$)
5	527	-	597
10	545	594	608
15	549	600	616
20	550	606	620
25	551	609	624
30	552	613	627

Using the values of T_p , a Kissinger plot for the 15 $\text{Cs}_2\text{O}\cdot 85 \text{GeO}_2$ glasses is shown in Figure 7-11. The activation energy of crystallization is 371 kJ/mol. The difference between T_p and T_g ranges from 63 to 75 K.

The mixed alkali glasses will be discussed in the order of increasing mol% Cs_2O . Each glass composition has unique crystallization behavior; differences are obvious in the shape of the crystallization peaks, and the temperature of T_x and T_p . As Cs_2O concentration increases, the formability of the glass decreases and analysis becomes less obvious.

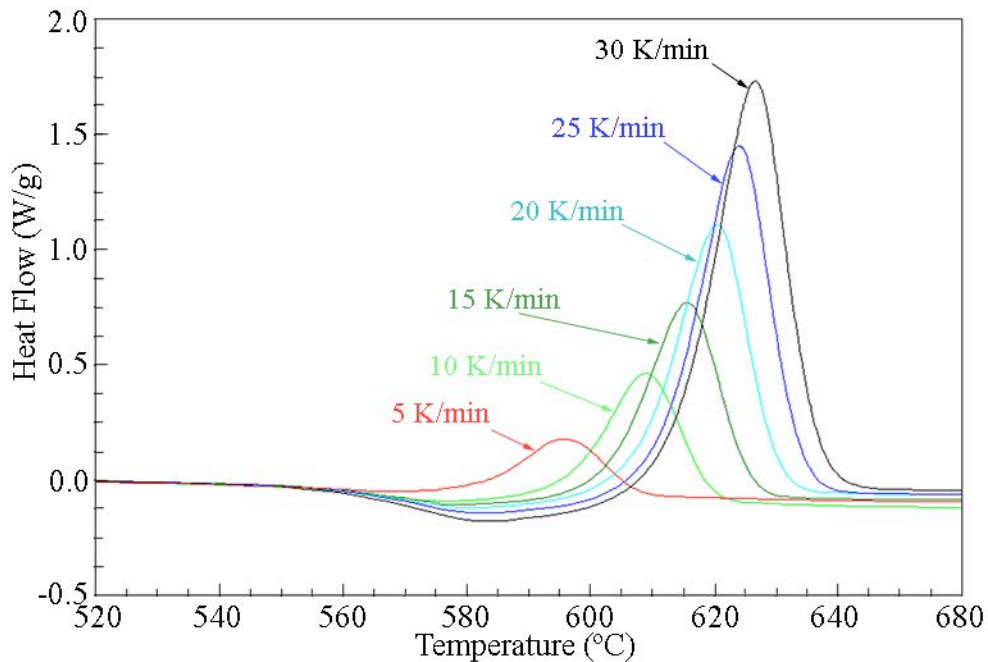


Figure 7-9. DSC curves with ramp rates ranging from 5 to 30 K/min curve for 15 $\text{Cs}_2\text{O}\cdot 85 \text{GeO}_2$ glasses.

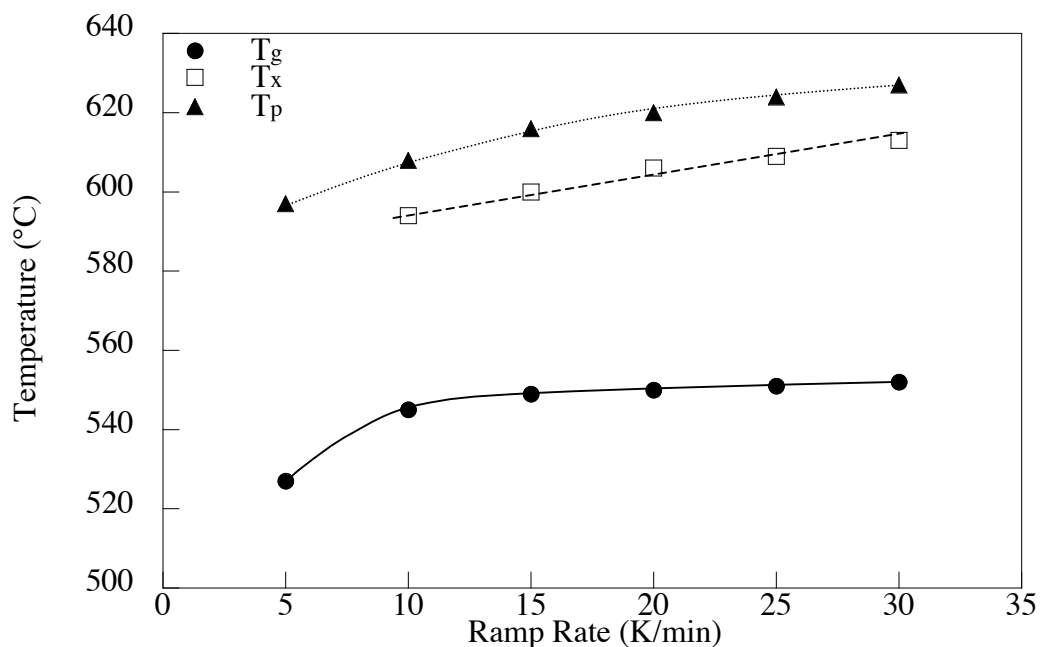


Figure 7-10. T_g , T_x , and T_p values for 15 $\text{Cs}_2\text{O}\cdot 85 \text{GeO}_2$ glasses as a result of varying ramp rate. Lines added to aid the eye.

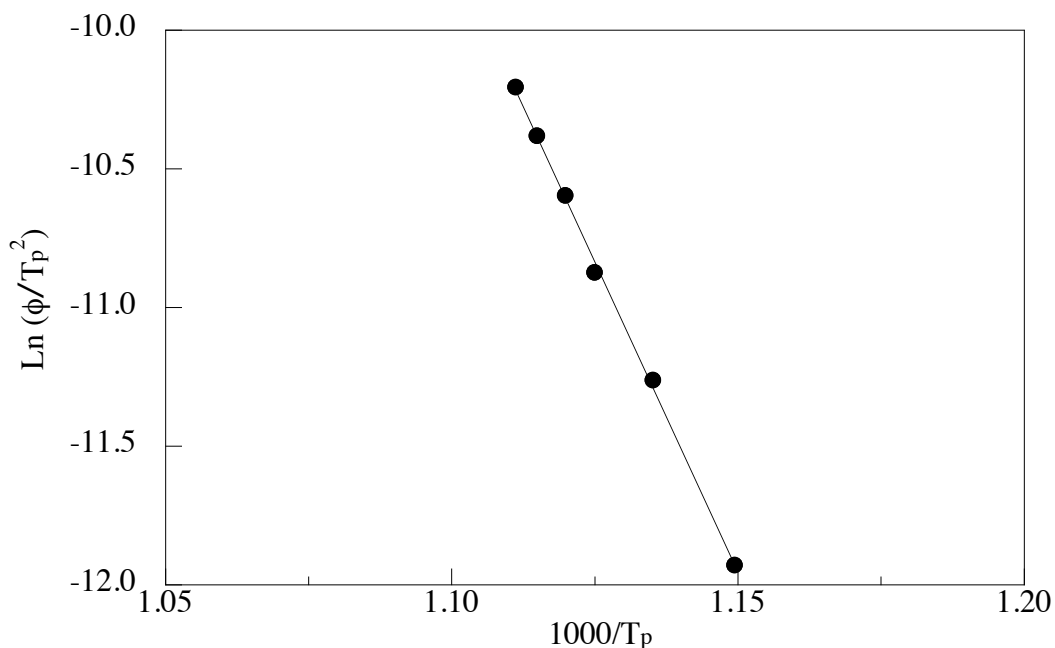


Figure 7-11. Kissinger plot for 15 $\text{Cs}_2\text{O}\cdot 85 \text{GeO}_2$ glass. Line is a linear fit.

The DSC curves for glasses containing a ratio of 7:1 $\text{Li}_2\text{O}:\text{Cs}_2\text{O}$ have one narrow peak at temperatures below 700 °C, as shown in Figure 7-12. The peak is extremely

narrow and leans towards higher temperature. Curves of this shape are characteristic of strong exothermic reactions that cause the sample chamber to overheat, therefore causing the temperature of the cell to be greater than the temperature of the furnace is ramping. The peak height becomes greater with a faster ramp rate. T_g shifts smoothly from 502 °C when the ramp rate is 5 K/min to 516 °C when the ramp rate is 30 K/min. T_x is 550 °C for the 5 K/min ramp rate and shifts to 569 °C for the 30 K/min rate. T_p shifts from 555 to 580 °C for ramp rates 5 and 30 K/min, respectively. Table 7-V lists T_g , T_x , and T_p for the 7:1 $\text{Li}_2\text{O}:\text{Cs}_2\text{O}\cdot 85 \text{ GeO}_2$ glass. The shift of T_g , T_x and T_p to higher temperatures is shown in Figure 7-13.

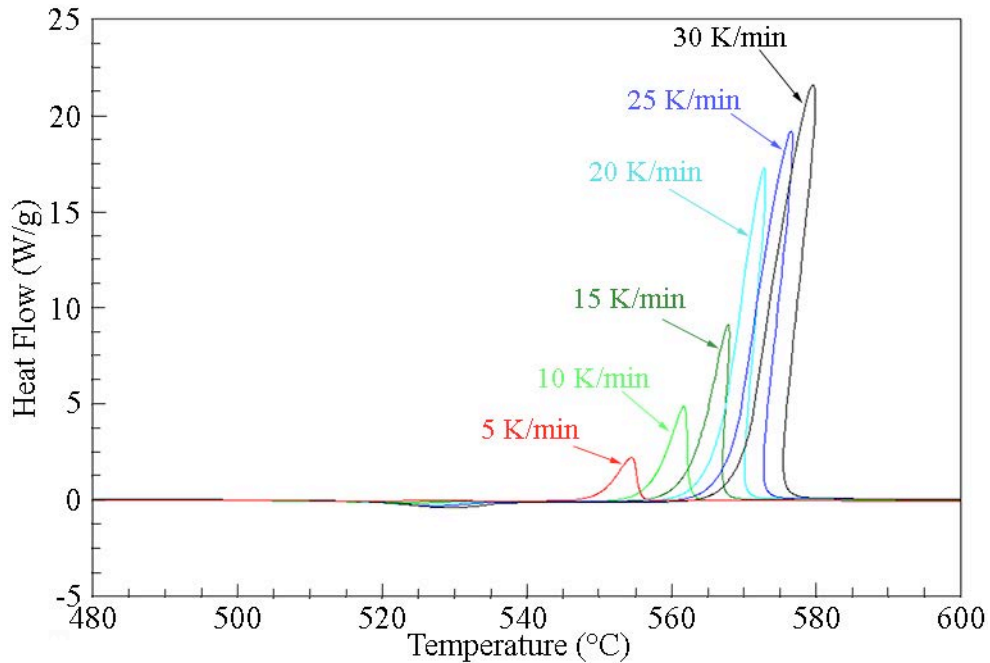


Figure 7-12. DSC curves with ramp rates ranging from 5 to 30 K/min curve for 7:1 $\text{Li}_2\text{O}:\text{Cs}_2\text{O}\cdot 85 \text{ GeO}_2$ glasses.

Table 7-V. T_g , T_x , and T_p Values for 7:1 $\text{Li}_2\text{O}:\text{Cs}_2\text{O}\cdot 85 \text{ GeO}_2$ Glasses

Ramp Rate (K/min)	T_g (°C)	T_x (°C)	T_p (°C)
5	502	550	555
10	507	556	562
15	510	561	568
20	512	566	573
25	514	568	577
30	516	569	580

Figure 7-14 shows the Kissinger plot for the 7:1 $\text{Li}_2\text{O}:\text{Cs}_2\text{O}\cdot 85 \text{ GeO}_2$ glass. The activation energy of crystallization is 395 kJ/mol. The difference between T_p and T_g for all of the glasses fall between 53 and 61 K.

Figure 7-15 shows the DSC curves for glasses with an alkali ratio of 3:1 $\text{Li}_2\text{O}:\text{Cs}_2\text{O}$. The spectra show one broad peak at temperatures below 700 °C. The T_g shifts linearly from 495 °C when the ramp rate is 5 K/min to 508 °C when the ramp rate is 30 K/min. The T_x is 559 °C for the 5 K/min ramp rate and shifts to 569 °C for the 30 K/min rate. The T_p shifts from 557 to 579 °C for ramp rates 5 and 30 K/min, respectively. Table 7-VI lists the values of T_g , T_x , and T_p for the 3:1 $\text{Li}_2\text{O}:\text{Cs}_2\text{O}\cdot 85 \text{ GeO}_2$ glass. The shift of T_g , T_x and T_p to higher temperature is shown in Figure 7-16.

The activation energy for crystallization of the 3:1 $\text{Li}_2\text{O}:\text{Cs}_2\text{O}\cdot 85 \text{ GeO}_2$ glass is 459 kJ/mol. Activation energy was calculated using the Kissinger method, which is shown below in Figure 7-17. The T_p minus T_g values ranged from 62 to 71 K.

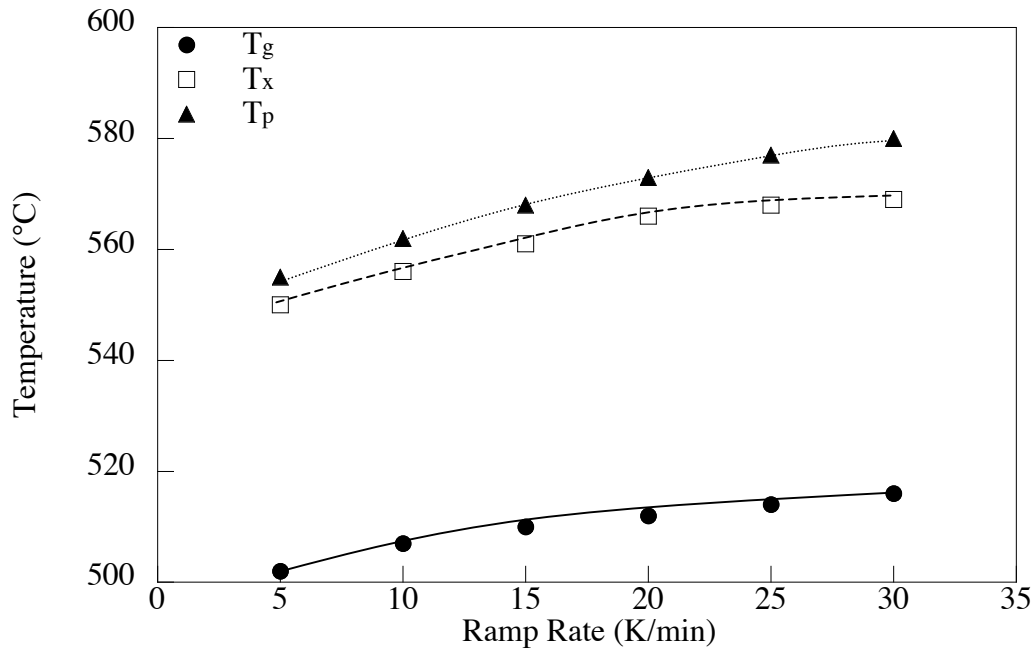


Figure 7-13. T_g , T_x , and T_p values for 7:1 $\text{Li}_2\text{O}:\text{Cs}_2\text{O}\cdot 85 \text{ GeO}_2$ glasses as a result of varying ramp rate. Lines added to aid the eye.

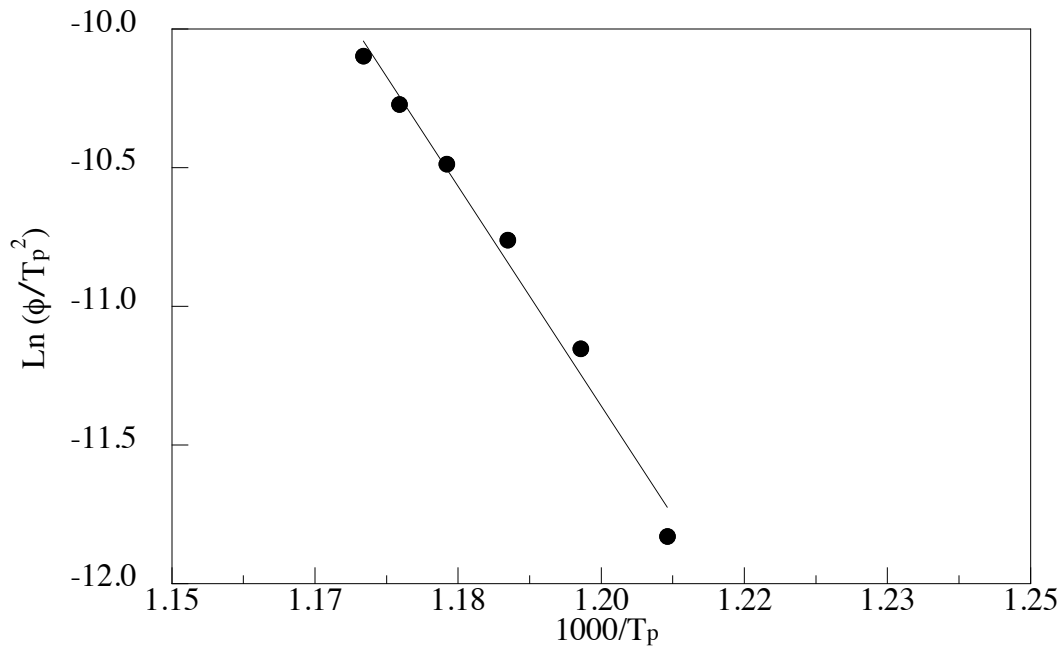


Figure 7-14. Kissinger plot for 7:1 Li₂O:Cs₂O•85 GeO₂ glass. Line is a linear fit.

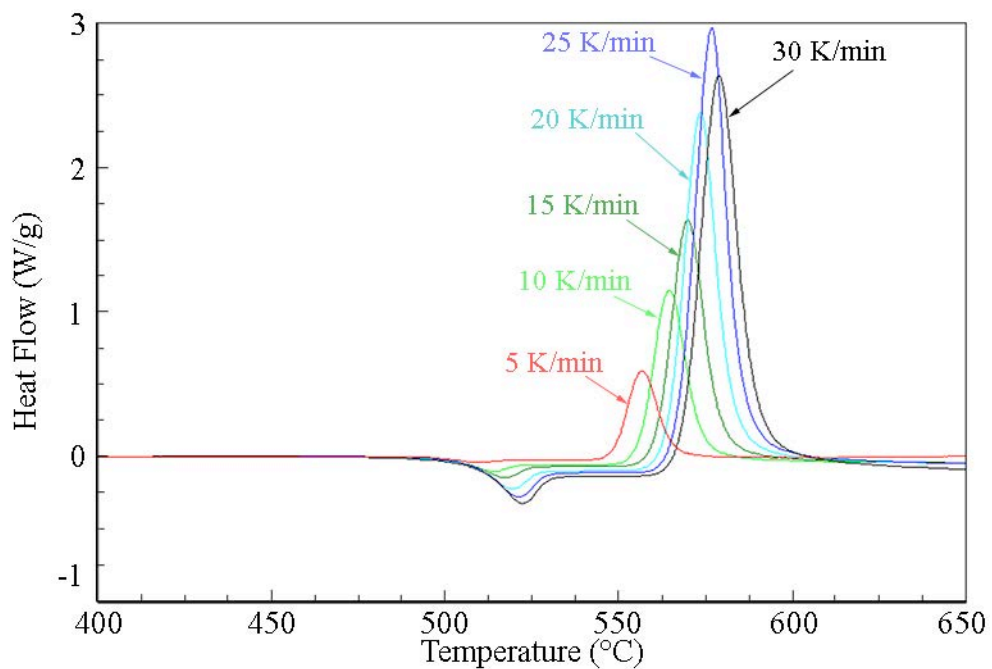


Figure 7-15. DSC curves with ramp rates ranging from 5 to 30 K/min curve for 3:1 Li₂O:Cs₂O•85 GeO₂ glasses.

Table 7- VI. T_g , T_x , and T_p Values for 3:1 $\text{Li}_2\text{O}:\text{Cs}_2\text{O}\cdot 85 \text{ GeO}_2$ Glasses

Ramp Rate (K/min)	T_g ($^{\circ}\text{C}$)	T_x ($^{\circ}\text{C}$)	T_p ($^{\circ}\text{C}$)
5	495	549	557
10	499	556	565
15	502	561	570
20	505	564	574
25	507	567	577
30	508	569	579

Glasses with alkali in one to one ratio are the best glass formers of all the glasses studied in this section. Figure 7-18 shows the DSC curves for glasses with a ratio of 1:1 $\text{Li}_2\text{O}:\text{Cs}_2\text{O}$. The spectra show one broad peak, at temperatures below 700°C , more than 100 K above the T_g . The T_g shifts linearly from 489°C when the ramp rate is 5 K/min to 501°C when the ramp rate is 30 K/min. T_x and T_p shift from 605 to 638°C for ramp rates 5 and 30 K/min, and 621°C for the 5 K/min ramp rate and shifts to 657°C for the 30 K/min rate, respectively. T_x and T_p shift for ramp rates of 5 through 20 K/min, with very little change in T_x or T_p beyond 20 K/min. Table 7-VII lists the values of T_g , T_x , and T_p , they are shown in Figure 7-19.

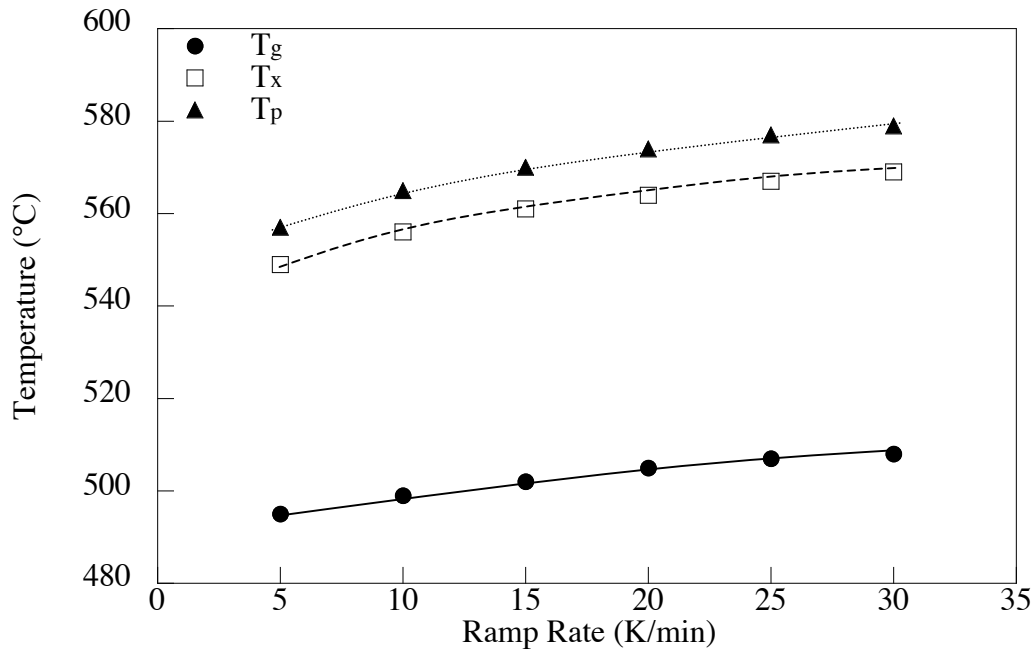


Figure 7-16. T_g , T_x , and T_p values for 3:1 $\text{Li}_2\text{O}:\text{Cs}_2\text{O}\cdot 85 \text{ GeO}_2$ glasses as a result of varying ramp rate. Lines added to aid the eye.

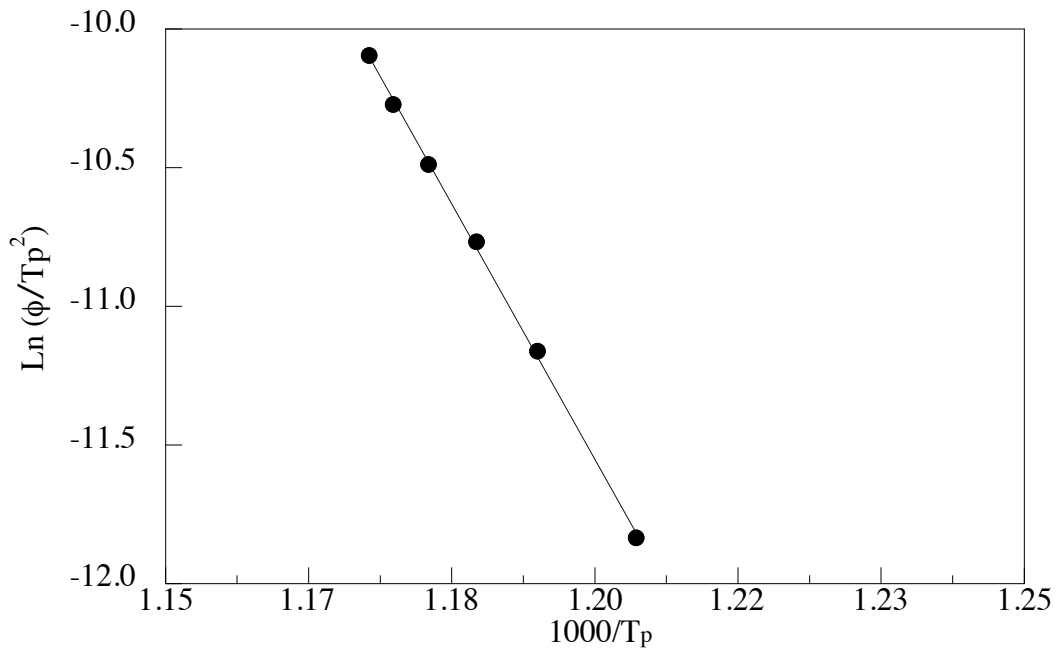


Figure 7-17. Kissinger plot for 3:1 Li₂O:Cs₂O•85 GeO₂ glass. Line is a linear fit.

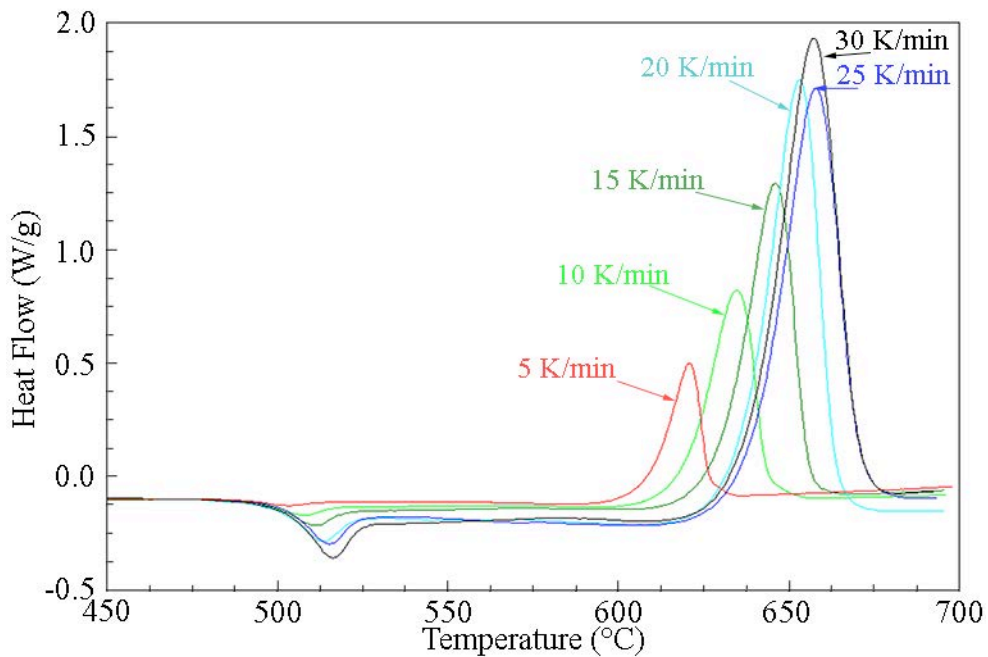


Figure 7-18. DSC curves with ramp rates ranging from 5 to 30 K/min curve for 1:1 Li₂O:Cs₂O•85 GeO₂ glasses.

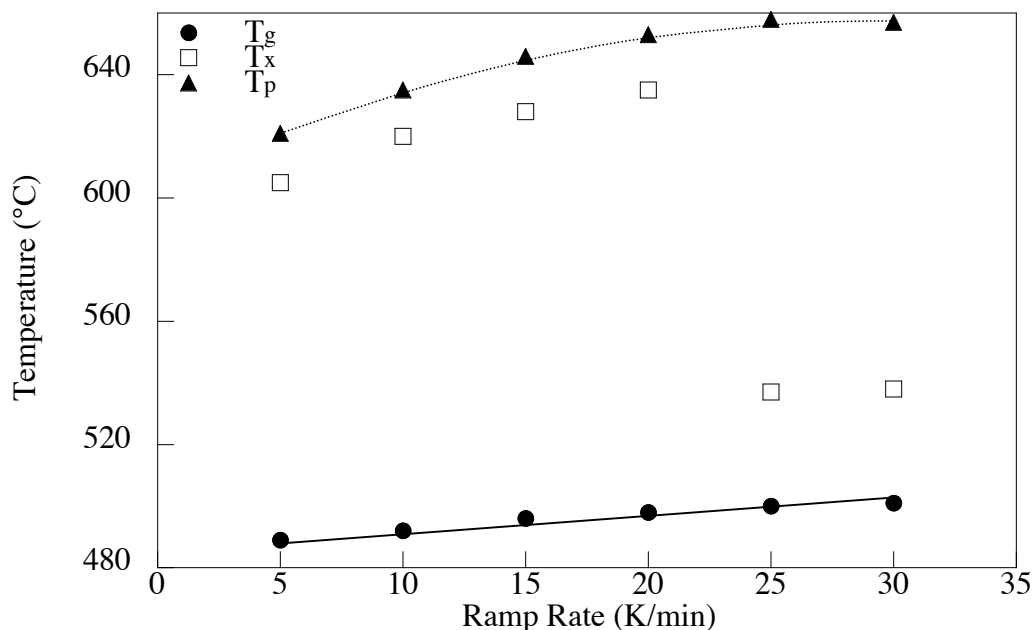


Figure 7-19. T_g , T_x , and T_p values for 1:1 $\text{Li}_2\text{O}:\text{Cs}_2\text{O}\cdot 85 \text{ GeO}_2$ glasses as a result of varying ramp rate. Lines added to aid the eye.

Table 7-VII. T_g , T_x , and T_p Values for 1:1 $\text{Li}_2\text{O}:\text{Cs}_2\text{O}\cdot 85 \text{ GeO}_2$ Glasses

Ramp Rate (K/min)	T_g (°C)	T_x (°C)	T_p (°C)
5	489	605	621
10	492	620	635
15	496	628	646
20	498	635	653
25	500	637	658
30	501	638	657

The activation energy for crystallization is 281 kJ/mol, calculated from Figure 7-20. The difference between T_p and T_g ranged from 132 to 158 K making it the best glass former on the $x \text{ Li}_2\text{O}:(15-x) \text{ Cs}_2\text{O}\cdot 85 \text{ GeO}_2$ tie line.

Glasses containing a greater concentration of Cs_2O than Li_2O have more complicated crystallization curves. Figure 7-21 shows the DSC curves for glasses with a ratio of 1:3 $\text{Li}_2\text{O}:\text{Cs}_2\text{O}$. The curves contain two peaks at temperatures below 700 °C. When the ramp rate is slow (5 and 10 K/min), these two peaks blend into a simple peak. When the ramp rate is fast, the peaks clearly separate into two distinct broad peaks. The T_g shifts from 501 °C when the ramp rate is 5 K/min to 515 °C when the ramp rate is 30 K/min. T_x for peak I shifts from 520 to 561 °C for ramp rates 5 and 30 K/min,

respectively. T_x for peak II shifts from 570 °C for the 10 K/min ramp rate to 605 °C for the 30 K/min rate. The onset of crystallization begins in the glass transition region for the sample when using a ramp rate of 5 K/min, so a T_x could not be measured. T_p for peak I shift from 547 to 576 K/min for the 5 and 30 K/min ramp rates, respectively. T_p for peak II shifts from 561 to 617 °C for ramp rates of 5 to 30 K/min, respectively. Table 7-VIII lists the values of T_g , T_x , and T_p for the 1:3 $\text{Li}_2\text{O}:\text{Cs}_2\text{O}\cdot 85 \text{ GeO}_2$ glass. T_g , T_x and T_p trend for all five series and are shown in Figure 7-22.

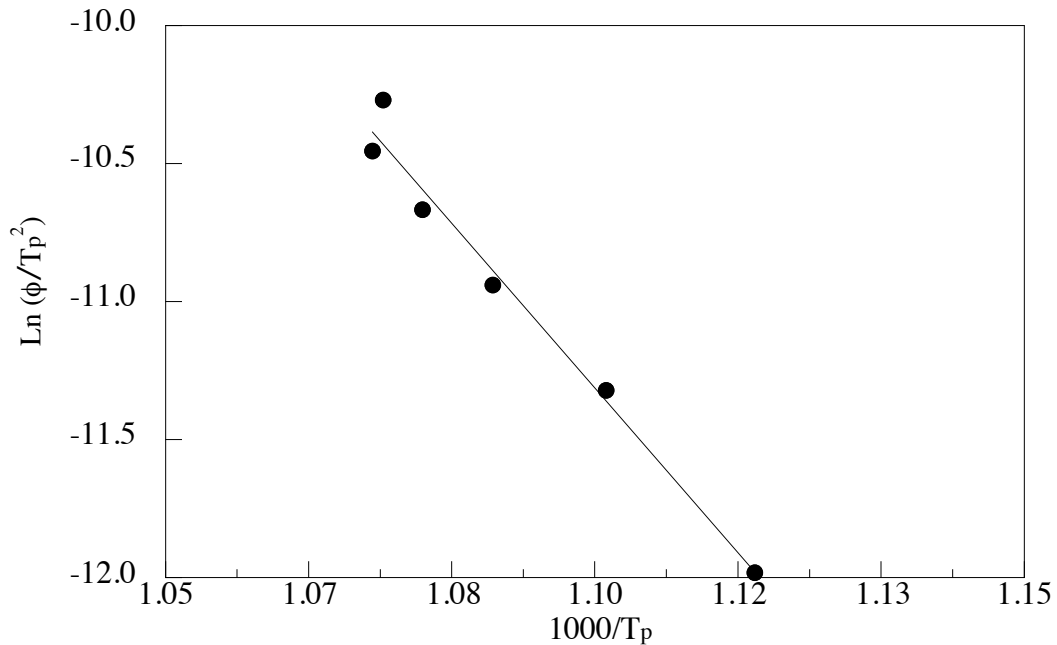


Figure 7-20. Kissinger plot for 1:1 $\text{Li}_2\text{O}:\text{Cs}_2\text{O}\cdot 85 \text{ GeO}_2$ glass. Line is a linear fit.

The Kissinger data shown in Figure 7-23 shows the Kissinger plots for both peak I and peak II. The activation energy for the low temperature peak (peak I) is calculated to be 347 kJ/mol. The maximum difference between T_p and T_g is 61 K and the minimum difference is 46 K.

Table 7-VIII. T_g , T_x , and T_p Values for 1:3 $\text{Li}_2\text{O}:\text{Cs}_2\text{O}\cdot 85 \text{ GeO}_2$ Glasses

Ramp Rate (K/min)	T_g (°C)	T_x (°C)-I	T_p (°C)-I	T_x (°C)-II	T_p (°C)-II
5	501	520	547	-	561
10	506	538	557	570	577
15	509	545	563	580	588
20	511	547	568	587	599
25	512	558	572	597	608
30	515	561	576	605	617

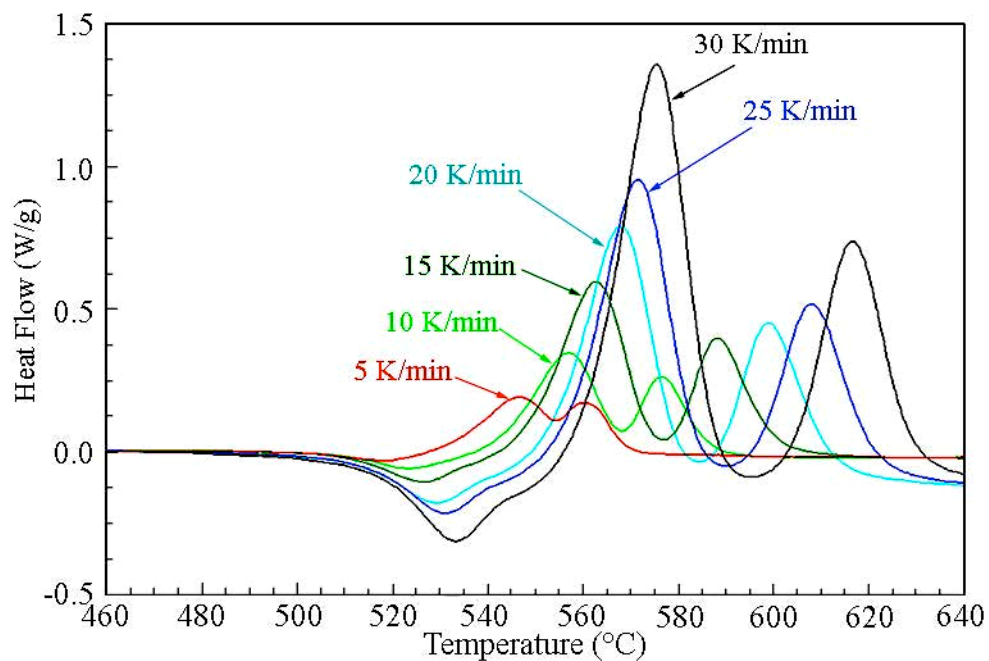


Figure 7-21. DSC curves with ramp rates ranging from 5 to 30 K/min curve for 1:3 $\text{Li}_2\text{O}:\text{Cs}_2\text{O}\cdot 85 \text{ GeO}_2$ glasses.

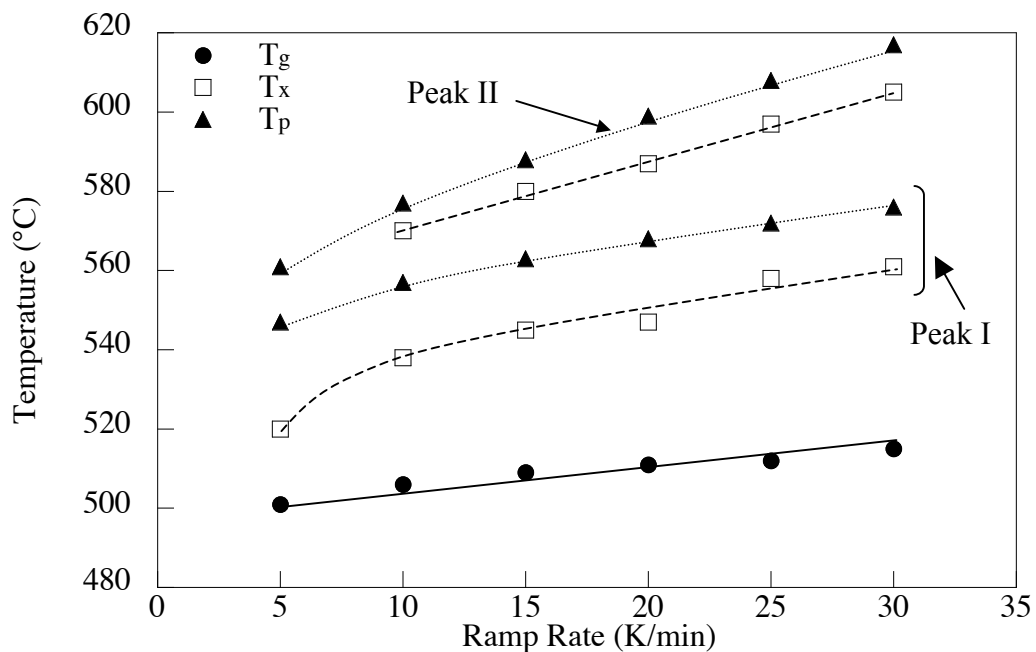


Figure 7-22. T_g , T_x , and T_p values for 1:3 $\text{Li}_2\text{O}:\text{Cs}_2\text{O}\cdot 85 \text{ GeO}_2$ glasses as a result of varying ramp rate. Lines added to aid the eye.

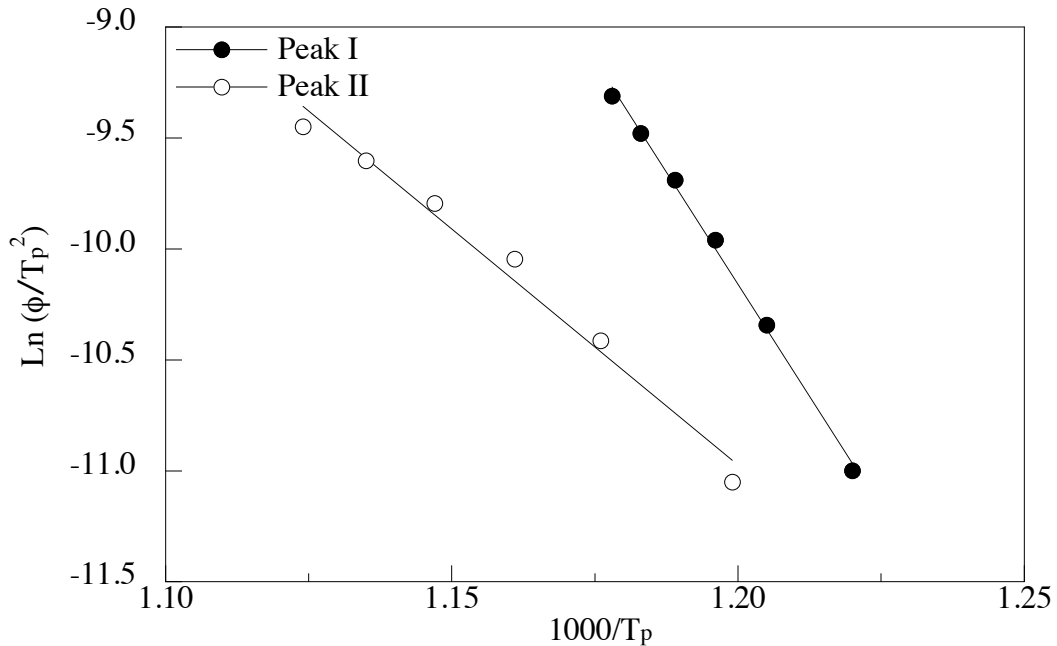


Figure 7-23. Kissinger plot for 1:3 $\text{Li}_2\text{O}:\text{Cs}_2\text{O}\cdot 85 \text{ GeO}_2$ glass. Lines are a linear fit.

Glasses with a 1:7 ratio of $\text{Li}_2\text{O}:\text{Cs}_2\text{O}$ are very hard to form, crystallizing readily during cooling. To make a glass, the melt must be quenched quickly. The tendency for these glasses to crystallize is shown through the immediate crystallization peak following the T_g (Figure 7-24). The T_g shifts from 493 °C when the ramp rate is 5 K/min to 517 °C when the ramp rate is 30 K/min. The spectra show one large crystallization band with three major peaks at temperatures below 700 °C. T_x could not be calculated because the onset of crystallization begins within the glass transition region for all ramp rates. When the ramp rate is slow (5, 10 and 15 K/min), the crystallization peak occurs at a lower temperature. When the ramp rate is fast, the peaks within the band shift to higher temperatures, which explains the discontinuity in the T_p data shown in Figure 7-25. Table 7-IX lists the values of T_g and T_p for the 1:7 $\text{Li}_2\text{O}:\text{Cs}_2\text{O}\cdot 85 \text{ GeO}_2$ glass. T_g and T_p values are shown in Figure 7-25.

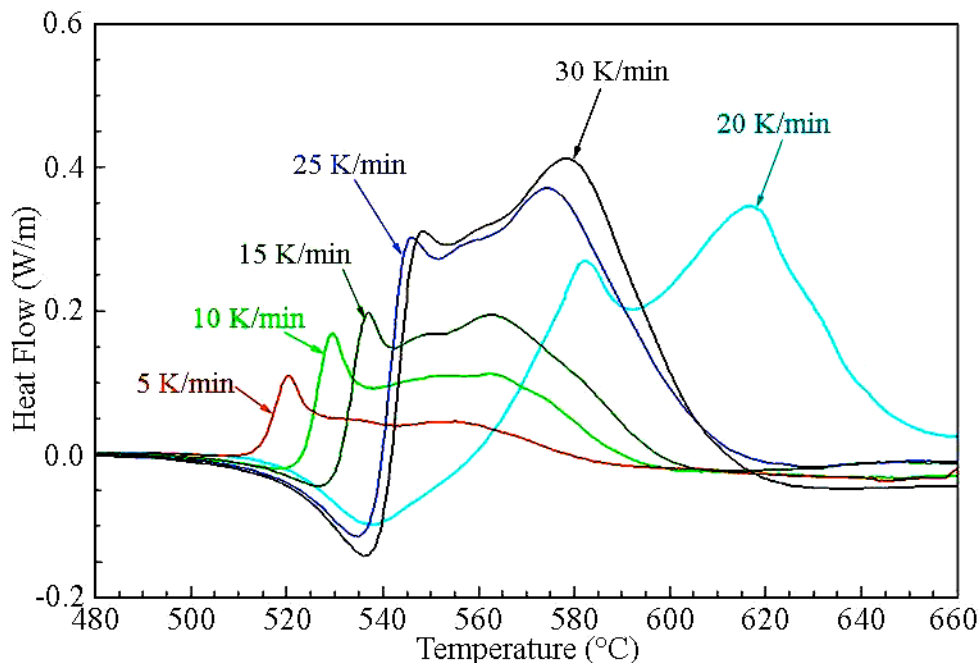


Figure 7-24. DSC curves with ramp rates ranging from 5 to 30 K/min curve for 1:7 $\text{Li}_2\text{O}:\text{Cs}_2\text{O}\cdot 85 \text{GeO}_2$ glasses.

Table 7-IX. T_g , T_x , and T_p Values for 1:7 $\text{Li}_2\text{O}:\text{Cs}_2\text{O}\cdot 85 \text{GeO}_2$ Glasses

Ramp Rate (K/min)	T_g (°C)	T_x (°C)	T_p (°C)
5	493	-	520
10	497	-	529
15	506	-	537
20	509	-	568
25	516	-	574
30	517	-	578

The data shown in Figure 7-26 were used to calculate the activation energy. The activation energy for this glass is only a rough estimate due to the large discontinuities between the slow and fast ramp rates. The best estimate for the activation energy is 333 kJ/mol, but it is almost surely greater than that, because the slope of the fit is compromised by the discontinuity. The maximum difference between T_p and T_g is 75 K and the minimum difference is 63 K.

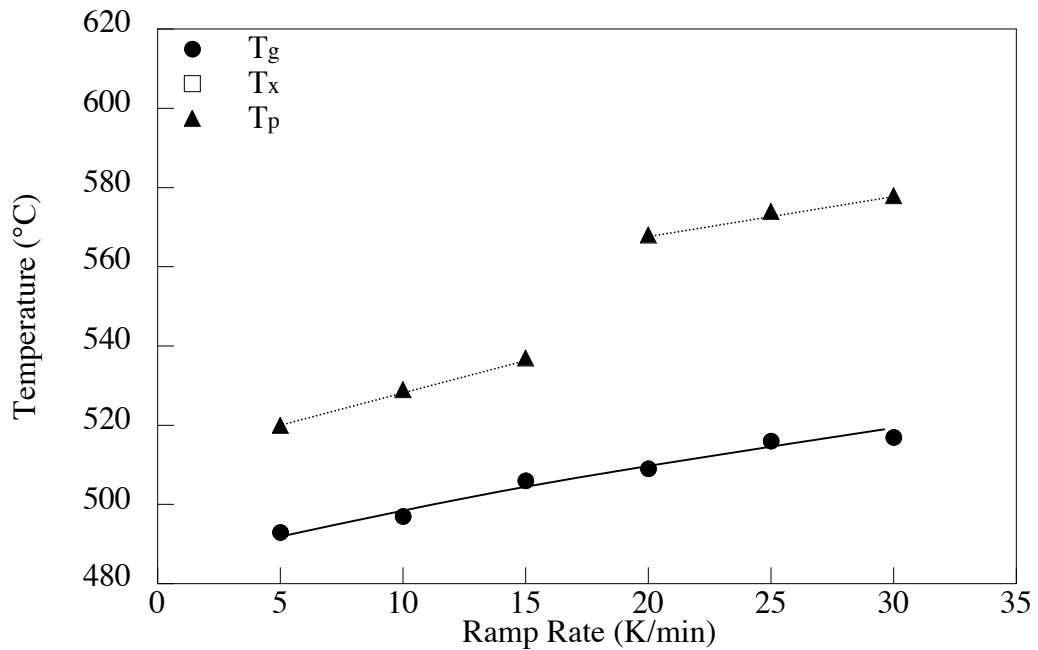


Figure 7-25. T_g , T_x , and T_p values for 1:7 $\text{Li}_2\text{O}:\text{Cs}_2\text{O}\cdot 85 \text{GeO}_2$ glasses as a result of varying ramp rate. Lines added to aid the eye.

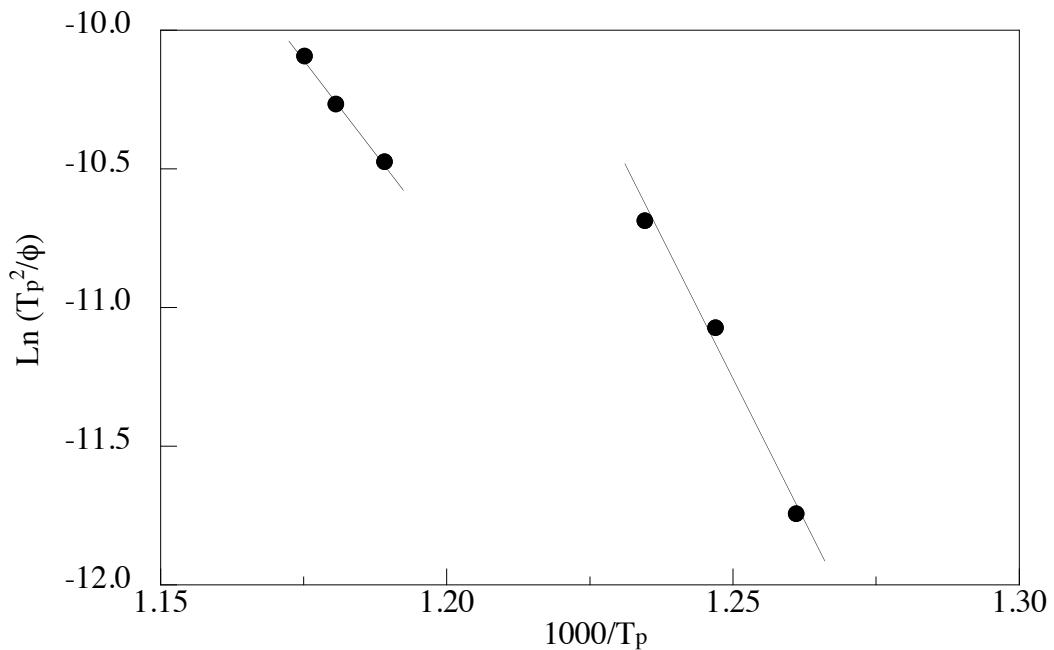


Figure 7-26. Kissinger plot for 1:7 $\text{Li}_2\text{O}:\text{Cs}_2\text{O}\cdot 85 \text{GeO}_2$ glass. Line is a linear fit.

7.4.1.2 Particle Size Study

Results of the particle size study will be presented in the same order as the previous results. First, the 15 Li₂O•85 GeO₂ data will be addressed, followed by the 15 Cs₂O•85 GeO₂ and concluding with the data for the mixed alkali glasses.

The DSC curves for the 15 Li₂O•85 GeO₂ glass show two crystallization peaks when the particle size is smaller than 250 μm. The low temperature phase is not affected by the particle size as shown in Figure 7-27 where T_x is constant at 566.7 ± 2.3 °C and T_p is constant at 574.1 ± 1.3 °C. The T_x for the high temperature phase is 627.9 ± 1.6 °C, however the curve evolves from one peak into two distinct peaks as the particle size is increased from 250 to 800 μm. T_p of peak II for glasses with particle sizes < 250 μm is 640.5 ± 0.5 °C. The values of T_x, T_p and T_g are listed in Table 7-X. It is also worth mentioning that the T_g of the glass does not change with particle size; the T_g obtained from the seven DSC curves is 510.7 ± 1.4 °C.

Table 7-X. T_g, T_x, and T_p Values for Different Particle Sizes of 15 Li₂O•85 GeO₂ Glasses

Particle Size (μm)	T _g (°C)	T _x (°C)-I	T _p (°C)-I	T _x (°C)-II	T _p (°C)-II
500-800	512	568	574	627	632/641
425-500	509	565	573	628	640
250-425	509	564	573	626	637
150-250	510	566	574	629	640
106-150	511	566	573	626	640
63-75	512	571	576	629	641
< 53	512	567	576	630	641

The shape of the DSC curves for the 15 Cs₂O•85 GeO₂ changes noticeably with varying particle size, as shown in Figure 7-28. Again, when the particle size is below 250 μm, there is only one peak in the curve. Unlike the 15 Li₂O•85 GeO₂ glass, however, the T_x and T_p shift to lower temperature with decreasing particle size, where T_x shifts from 604 °C for particles < 56 μm and 618 °C for particle sizes 150 to 250 μm and T_p shifts from 619 to 631 °C for the < 56 μm and 150 to 250 μm particle sizes, respectively. The T_g of the 15 Cs₂O•85 GeO₂ has a larger standard deviation than the 15 Li₂O•85 GeO₂, glass and is 543.4 ± 7.3 °C. This variation is at least partially due to the

T_x beginning in the glass transition region of the curve. The values of T_x , T_p and T_g are listed in Table 7-XI.

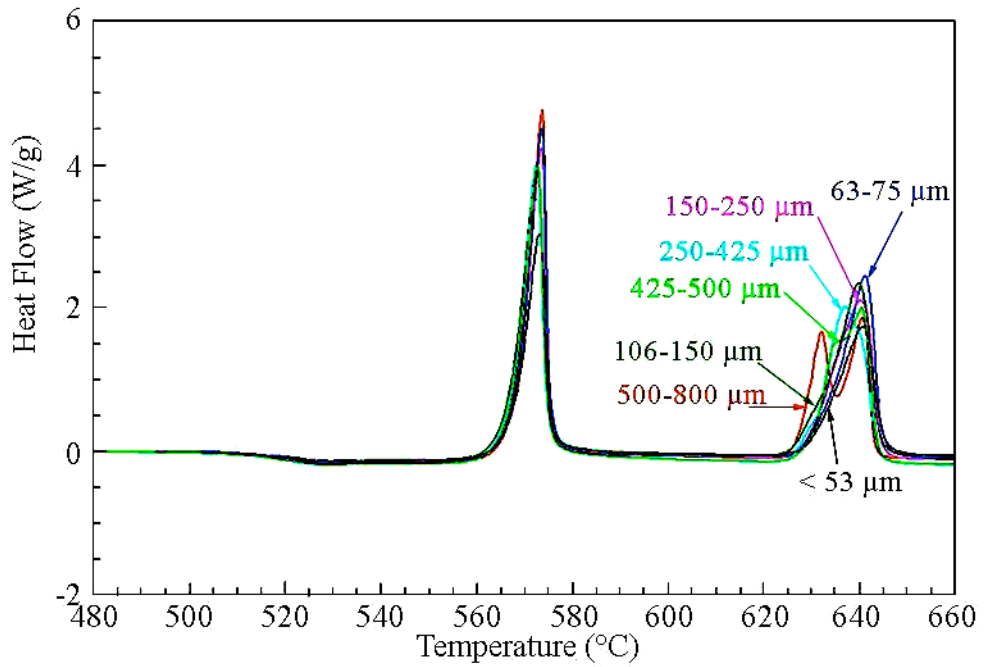


Figure 7-27. DSC curves of glasses with different particle sizes for 15 $\text{Li}_2\text{O}\cdot 85 \text{ GeO}_2$ glasses.

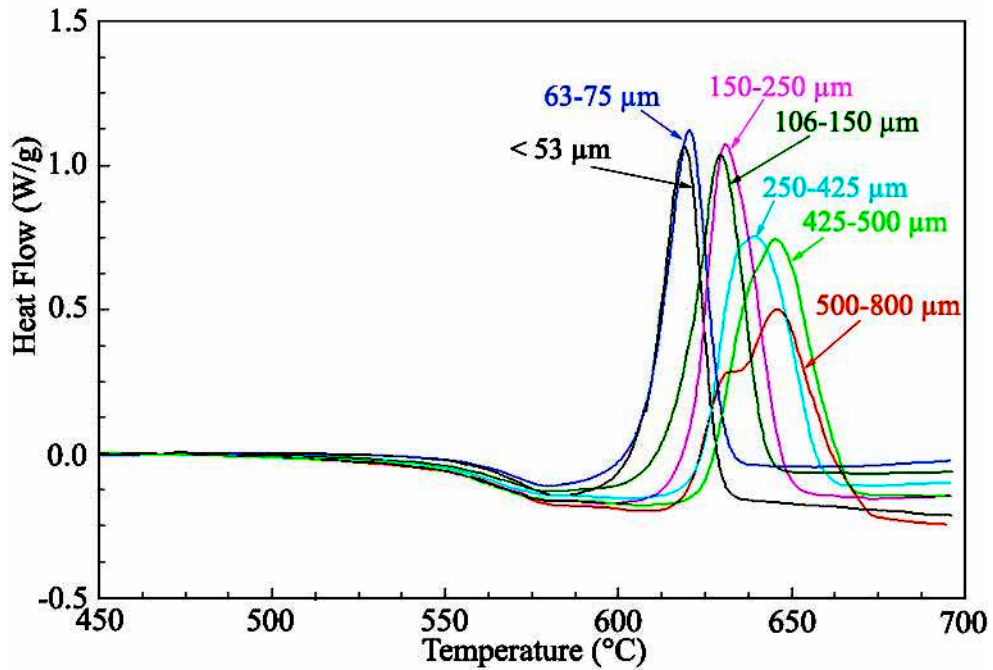


Figure 7-28. DSC curves of glasses with different particle sizes for 15 $\text{Cs}_2\text{O}\cdot 85 \text{ GeO}_2$ glasses.

Table 7-XI. T_g , T_x , and T_p Values for Different Particle Sizes of 15 Cs₂O•85 GeO₂ Glasses

Particle Size (μm)	T_g (°C)	T_x (°C)-I	T_p (°C)-I
500-800	550	618	646
425-500	536	625	645
250-425	540	623	639
150-250	536	618	631
106-150	539	613	630
63-75	550	606	620
< 53	553	604	619

The shapes of the DSC curves for the 7:1 Li₂O:Cs₂O•85 GeO₂ glass and the 3:1 Li₂O:Cs₂O•85 GeO₂ glass will be discussed simultaneously. The curves for the 7:1 Li₂O:Cs₂O•85 GeO₂ glass are shown in Figure 7-29 and for the 3:1 Li₂O:Cs₂O•85 GeO₂ glass in Figure 7-30. The T_x for both glasses is the same value of 565 ± 2 °C (specifically T_x is 565.3 ± 0.6 °C for the 7:1 Li₂O:Cs₂O glass and 565.0 ± 1.0 °C for the 3:1 Li₂O:Cs₂O glass). There was no effect on the crystallization curves due to particles size, as shown by the fact that the glasses with a particle size of < 53 μm and a particle size of 500 to 800 μm have the same T_x and T_p . The only difference between the two compositions is the T_g , which is 512 ± 0.0 °C for the 7:1 Li₂O:Cs₂O glass and 505 ± 0.0 °C for the 3:1 Li₂O:Cs₂O glass. The values of T_x , T_p and T_g are listed in Table 7-XII for the 7:1 Li₂O:Cs₂O glass and Table 7-XIII for the 3:1 Li₂O:Cs₂O glass.

Table 7-XII. T_g , T_x , and T_p Values for Different Particle Sizes of 7:1 Li₂O:Cs₂O•85 GeO₂ Glasses

Particle Size (μm)	T_g (°C)	T_x (°C)	T_p (°C)
500-800	512	565	573
63-75	512	566	573
< 53	512	565	571

Table 7-XIII. T_g , T_x , and T_p Values for Different Particle Sizes of 3:1 Li₂O:Cs₂O•85 GeO₂ Glasses

Particle Size (μm)	T_g (°C)	T_x (°C)	T_p (°C)
500-800	505	566	572
63-75	505	564	574
< 53	505	565	574

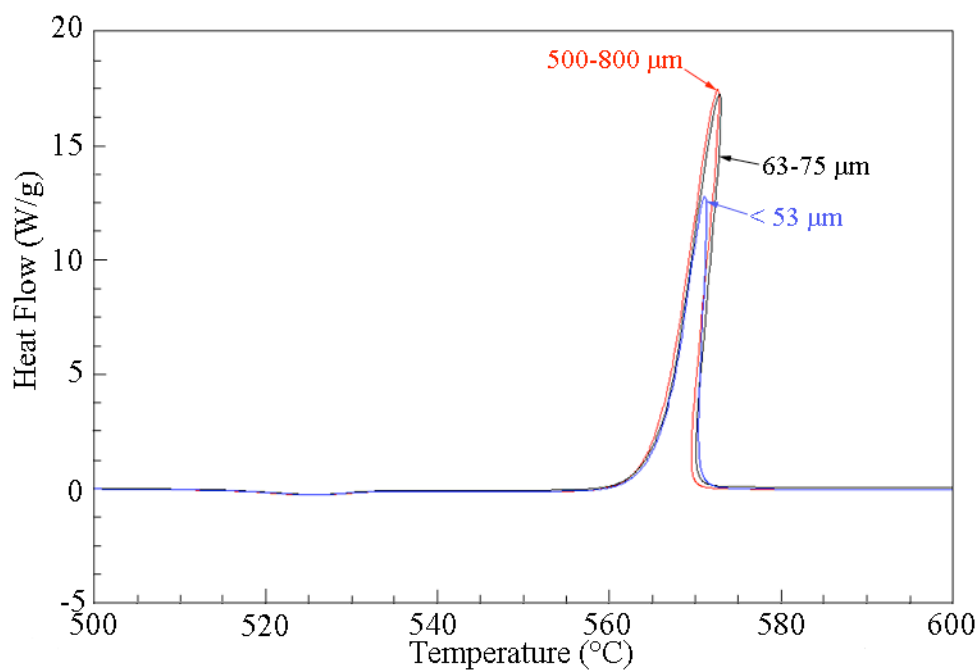


Figure 7-29. DSC curves of glasses with different particle sizes for 7:1 $\text{Li}_2\text{O}:\text{Cs}_2\text{O}\cdot 85 \text{GeO}_2$ glasses.

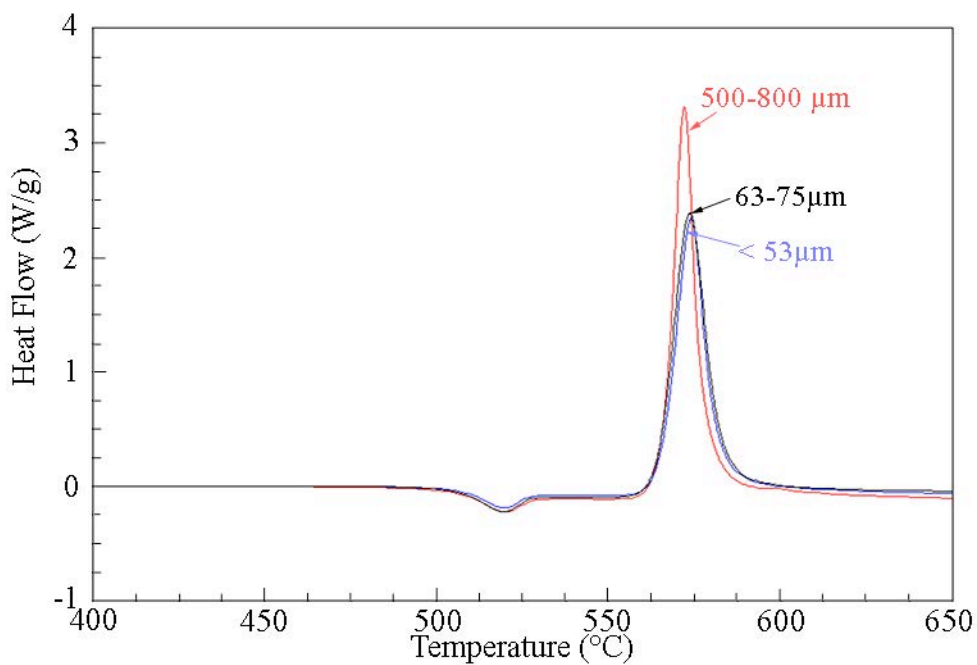


Figure 7-30. DSC curves of glasses with different particle sizes for 3:1 $\text{Li}_2\text{O}:\text{Cs}_2\text{O}\cdot 85 \text{GeO}_2$ glasses.

The crystallization curves for the 1:1 $\text{Li}_2\text{O}:\text{Cs}_2\text{O}\cdot 85 \text{ GeO}_2$ glass are shown in Figure 7-31. When the particle size is below $425 \mu\text{m}$ there is only one peak, and the T_x and T_p shift to higher temperatures with increasing particle sizes. T_x shifts from 631°C for particles $< 56 \mu\text{m}$ to 643°C for particle sizes 106 to $150 \mu\text{m}$ and then decreases back to 638°C for 250 to $425 \mu\text{m}$. T_p is 653°C and constant for the two smallest particle sizes, then shifts to 660°C for the 250 to $425 \mu\text{m}$ particle sizes. The T_g remains constant at $496.6 \pm 1.4^\circ\text{C}$. The values of T_x , T_p and T_g are listed in Table 7-XIV.

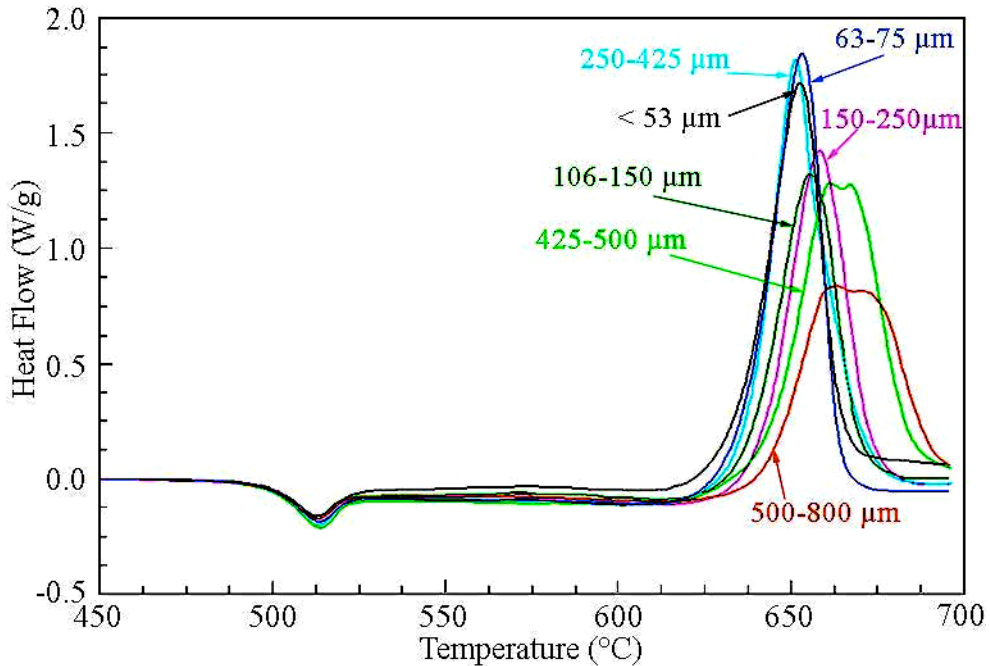


Figure 7-31. DSC curves of glasses with different particle sizes for 1:1 $\text{Li}_2\text{O}:\text{Cs}_2\text{O}\cdot 85 \text{ GeO}_2$ glasses.

Table 7-XIV. T_g , T_x , and T_p Values for Different Particle Sizes of 1:1 $\text{Li}_2\text{O}:\text{Cs}_2\text{O}\cdot 85 \text{ GeO}_2$ Glasses

Particle Size (μm)	T_g ($^\circ\text{C}$)	T_x ($^\circ\text{C}$)	T_p ($^\circ\text{C}$)
500-800	497	642	663
425-500	498	644	661
250-425	496	638	660
150-250	497	640	658
106-150	496	643	655
63-75	498	635	653
< 53	494	631	653

Unlike the previously discussed glass, where one peak developed into two peaks with increasing particle size, the spectra of the smaller particle size 1:3 Li₂O:Cs₂O•85 GeO₂ glasses contain two distinct peaks which merge into a single broad band as the particle size increases, as shown in Figure 7-32. As observed for the previously discussed glasses, as the particle size increases, the T_x increases. When the particle size is < 53 μm, the T_x is difficult to distinguish from the glass transition region, T_x is 545 for this particle size. The T_x shifts to 570 °C for the largest particle size range of 500 to 800 μm. T_p for the low temperature peak (I) shifts from 563 °C for the < 53 μm particle size to 610 °C for the particle size range 500 to 800 μm. The high temperature peak (II) has a T_p of 600 °C for the < 53 μm particles and shifts to 595 °C for the 106 to 150 μm particles. The onset of crystallization for peak II is only distinguishable for the two smallest particle sizes where T_x is estimated to be 590 °C and 587 °C for particle ranges < 53 μm, and 63 to 75 μm, respectively. The T_g for this glass is 510.0 ± 1.4 °C. T_g, T_x and T_p are listed in Table 7-XV.

Table 7-XV. T_g, T_x, and T_p Values for Different Particle Sizes of 1:3 Li₂O:Cs₂O•85 GeO₂ Glasses

Particle Size (μm)	T _g (°C)	T _x (°C)-I	T _p (°C)-I	T _x (°C)-II	T _p (°C)-II
500-800	512	570	610	-	-
425-500	508	559	599	-	-
250-425	510	555	593	-	-
150-250	509	554	578	-	-
106-150	509	551	569	-	595
63-75	511	547	568	587	599
< 53	511	545	563	590	600

The DSC curves for the 1:7 Li₂O:Cs₂O•85 GeO₂ glasses are very different for each different particle size. T_x begins in the glass transition region for each glass so it cannot be determined from Figure 7-33. Many peaks occur after T_g; each particle size has a different peak that results in T_p. Therefore there is no trend in T_p, and the temperatures over which T_p occurs range from 568 to 589 °C. The T_g is 511.6 ± 2.1 °C. T_g and T_p are listed in Table 7-XVI.

Table 7-XVI. T_g , T_x , and T_p Values for Different Particle Sizes of 1:7 $\text{Li}_2\text{O}:\text{Cs}_2\text{O}\cdot 85$ GeO_2 Glasses

Particle Size (μm)	T_g ($^\circ\text{C}$)	T_x ($^\circ\text{C}$)	T_p ($^\circ\text{C}$)
500-800	512	-	576
425-500	512	-	589
250-425	513	-	583
150-250	509	-	581
106-150	511	-	570
63-75	509	-	568
< 53	512	-	568

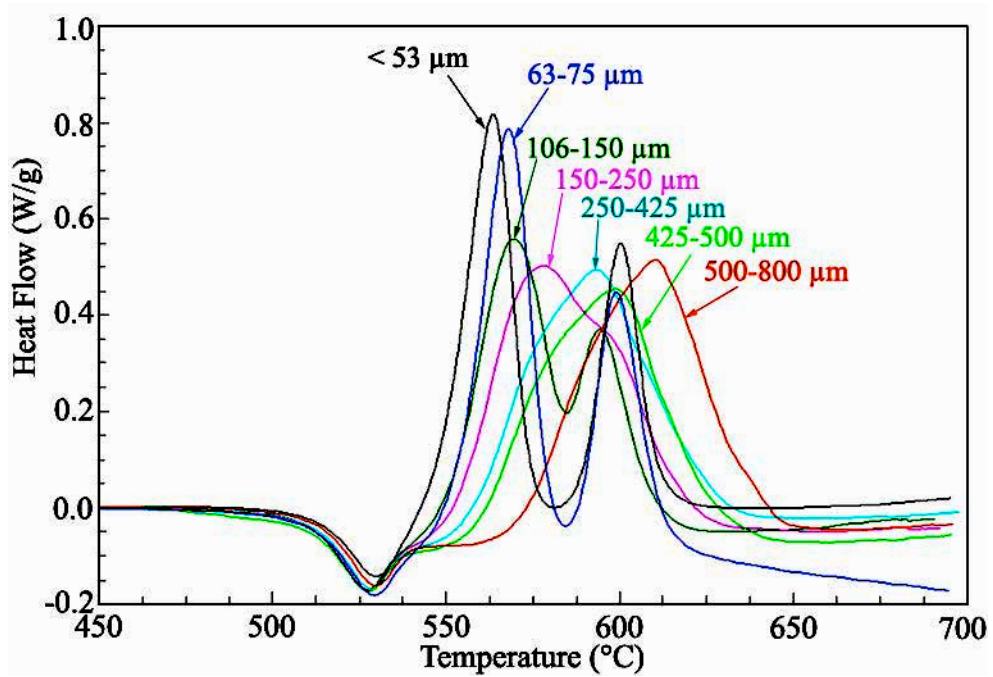


Figure 7-32. DSC curves of glasses with different particle sizes for 1:3 $\text{Li}_2\text{O}:\text{Cs}_2\text{O}\cdot 85$ GeO_2 glasses.

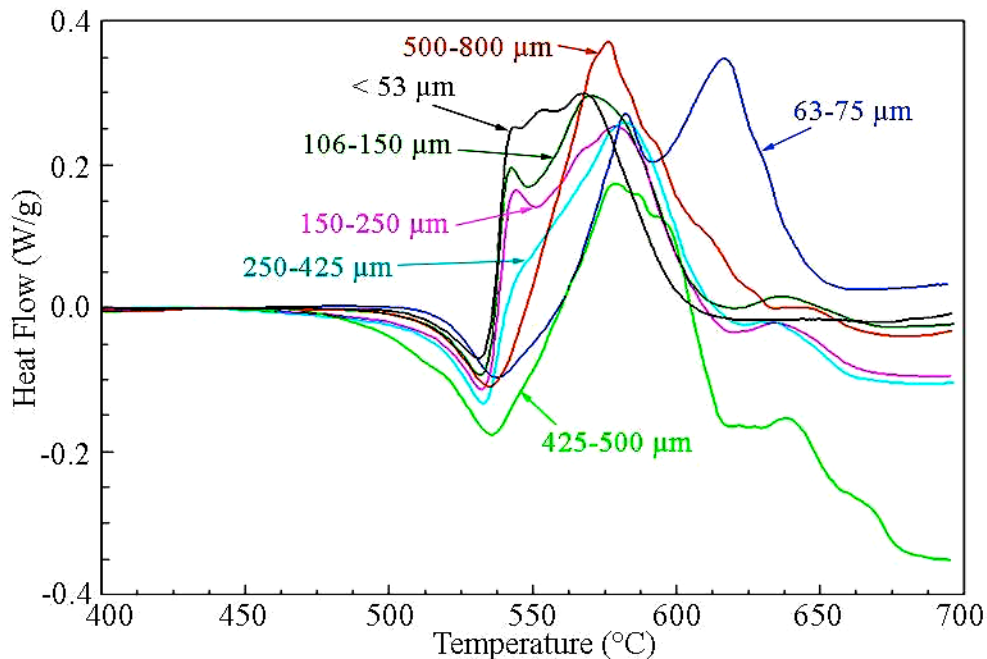


Figure 7-33. DSC curves of glasses with different particle sizes for 1:7 $\text{Li}_2\text{O}:\text{Cs}_2\text{O}\cdot 85$ GeO_2 glasses.

7.4.2 High Temperature X-Ray Diffraction

7.4.2.1 Binary Glasses

High temperature X-ray diffraction (HTXRD) was used to identify the phases formed during crystallization. Figure 7-34 shows the diffraction patterns for the formation of the phase causing the low temperature crystallization peak of the 15 $\text{Li}_2\text{O}\cdot 85$ GeO_2 glass. The first curve just shows the amorphous hump of the glass. The heat treatment temperature required to result only in the low temperature phase is 550 °C, just below the onset of crystallization temperature found using the DSC experiments. Each scan represents an additional 15 minutes of isothermal heat treatment. The experiment was performed for 24 scans (5.6 hours). For clarity only a third of the curves are shown, i.e. 30 minutes elapses between each scan in Figure 7-34. After 90 minutes, there is no further change in the number of peaks in the pattern, only narrowing of each peak with increasing heat treatment time. The identity of the crystalline phases, their powder diffraction file (pdf) number, crystal system, and space group are listed in Table 7-XVII and shown in Figure 7-35, with each peak identified with the corresponding phase. According to the phase diagram (Figure 7-3), the crystalline phases present at this

composition should be $\text{Li}_2\text{Ge}_7\text{O}_{15}$ and $\text{Li}_6\text{Ge}_8\text{O}_{19}$. The peak at $31.5^\circ 2\theta$ is due to chromium contamination in the furnace, from previous, unrelated experiments. This was confirmed by repeating the experiment, scanning from 28 to $33^\circ 2\theta$, no peak appeared at $31.5^\circ 2\theta$.

Table 7-XVII. Crystal Phases Resulting from the Low and High Temperature Heat Treatments of $15 \text{Li}_2\text{O} \cdot 85 \text{GeO}_2$ Glass

Symbol	Phase	Name	pdf Number	Crystal System	Space Group
●	$\text{Li}_2\text{Ge}_4\text{O}_9$	Lithium Germanium Oxide	00-037-1363	Orthorhombic	Pcca
■	$\text{Li}_2\text{Ge}_7\text{O}_{15}$	Lithium Heptagermanate	00-049-0523	Orthorhombic	Pbcn

The HTXRD patterns for an isothermal treatment at 645°C , corresponding to the high temperature crystallization peak are shown in Figure 7-36. The higher heat treatment did not result in any new phases forming. The only difference from the treatment at 550°C is a narrowing of the diffractions peaks (Figure 7-37), indicating crystal growth. Analysis of the XRD pattern shows two lithium germanate phases, $\text{Li}_2\text{Ge}_7\text{O}_{15}$ and $\text{Li}_2\text{Ge}_4\text{O}_9$. The first phase, $\text{Li}_2\text{Ge}_7\text{O}_{15}$, agrees with the phase diagram shown in Figure 7-3; the later phase $\text{Li}_2\text{Ge}_4\text{O}_9$, is not present on the phase diagram. At this temperature, the diffraction pattern does not develop slowly. The peaks that form during the first 30 minutes continue unchanged throughout the entire 336 min (5.6 hours). Comparison between the low and high temperature diffraction patterns are shown in Figure 7-38.

The HTXRD patterns for the $15 \text{Cs}_2\text{O} \cdot 85 \text{GeO}_2$ glass is shown in Figure 7-39. The DSC curve shows only one peak, so only one heat treatment temperature was used. The crystallization temperature for the HTXRD experiment was 590°C . Analysis of the XRD pattern shows two cesium germanate phases, $\text{Cs}_2\text{Ge}_6\text{O}_{13}$, and $\text{Cs}_4\text{Ge}_{11}\text{O}_{24}$, shown in Figure 7-40. The phase diagram in Figure 7-4 predicts a composition of $15 \text{Cs}_2\text{O} \cdot 85 \text{GeO}_2$ should form crystalline phases of $\text{Cs}_2\text{Ge}_6\text{O}_{13}$ and $\text{Cs}_8\text{Ge}_7\text{O}_{18}$. Unfortunately, there is no pattern in the pdf library for the later phase. Table 7-XVIII lists the crystal information for this composition.

Table 7-XVIII. Crystal Phases Resulting from the Low Temperature Heat Treatment of $15 \text{Cs}_2\text{O} \cdot 85 \text{GeO}_2$ Glass

Symbol	Phase	Name	pdf Number	Crystal System	Space Group
□	$\text{Cs}_4\text{Ge}_{11}\text{O}_{24}$	Cesium Germanium Oxide	00-020-0277	Cubic	-
○	$\text{Cs}_2\text{Ge}_6\text{O}_{13}$	Cesium Germanium Oxide [‡]	00-024-0251	Unknown	-

[‡] Quality of the pattern in the PDF database is doubtful

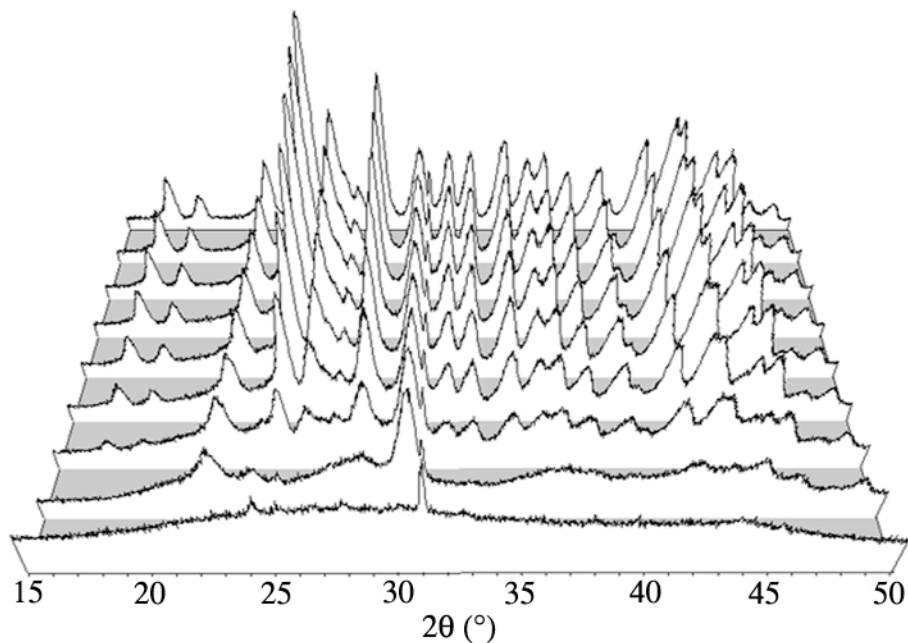


Figure 7-34. HTXRD scans for isothermal heat treatment at 550 °C for the 15 $\text{Li}_2\text{O}\cdot 85 \text{GeO}_2$ glass.

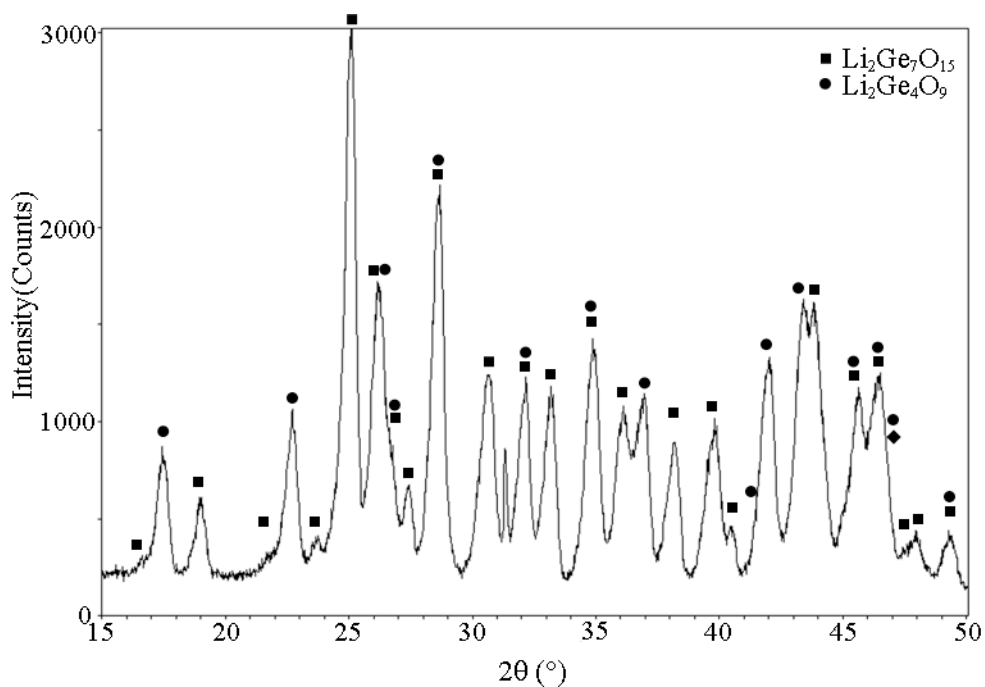


Figure 7-35. Diffraction pattern of the room temperature crystals, following the HTXRD experiment and heat treatment at 550 °C, for the 15 $\text{Li}_2\text{O}\cdot 85 \text{GeO}_2$ glass.

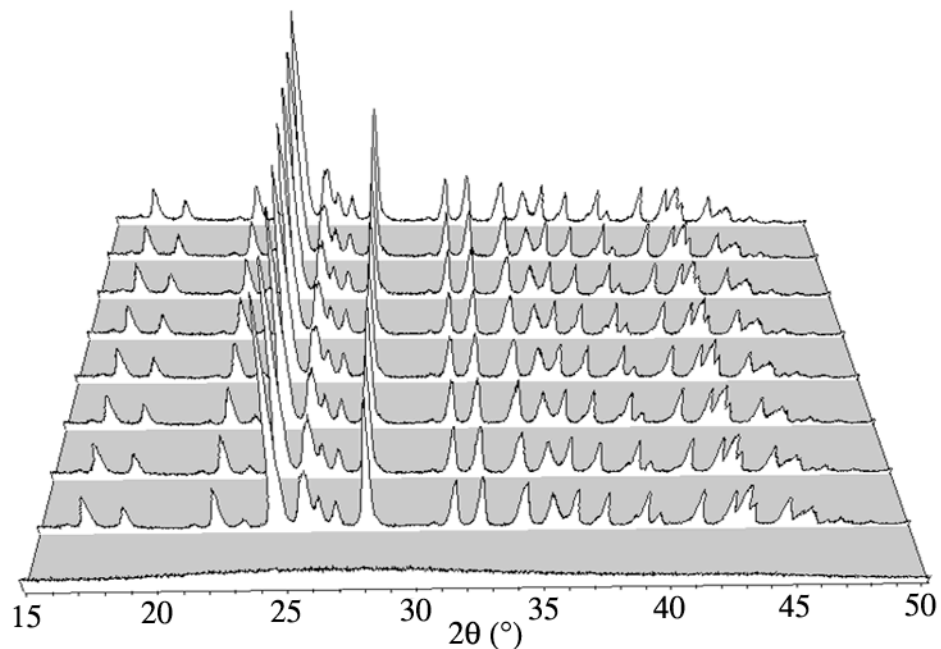


Figure 7-36. HTXRD scans for isothermal heat treatment at 645 °C for the 15 Li₂O•85 GeO₂ glass.

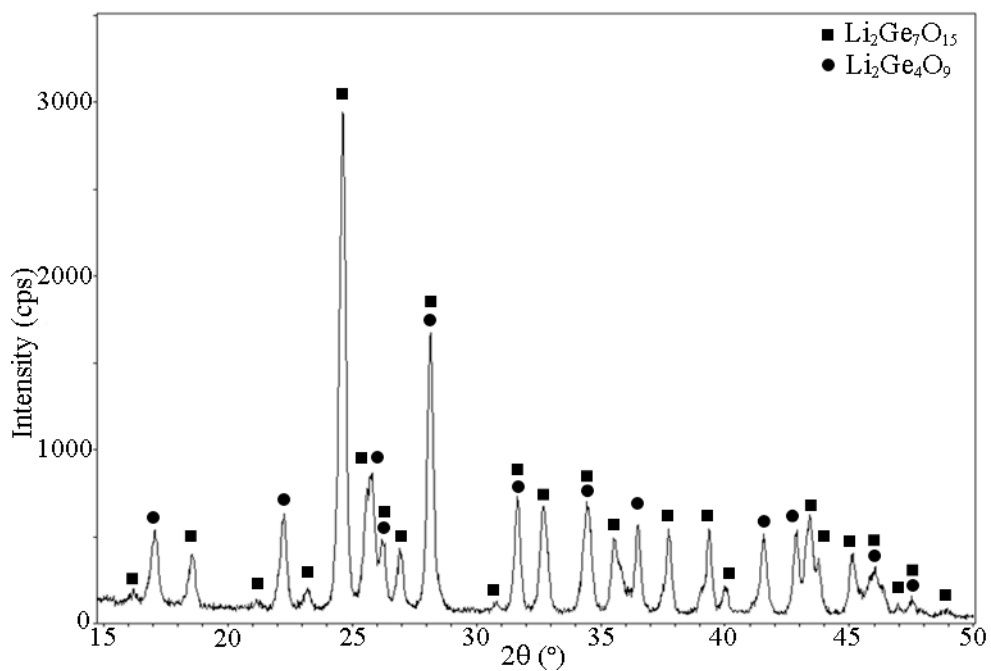


Figure 7-37. Diffraction pattern of the room temperature crystals, following the HTXRD experiment and heat treatment at 645 °C, for the 15 Li₂O•85 GeO₂ glass.

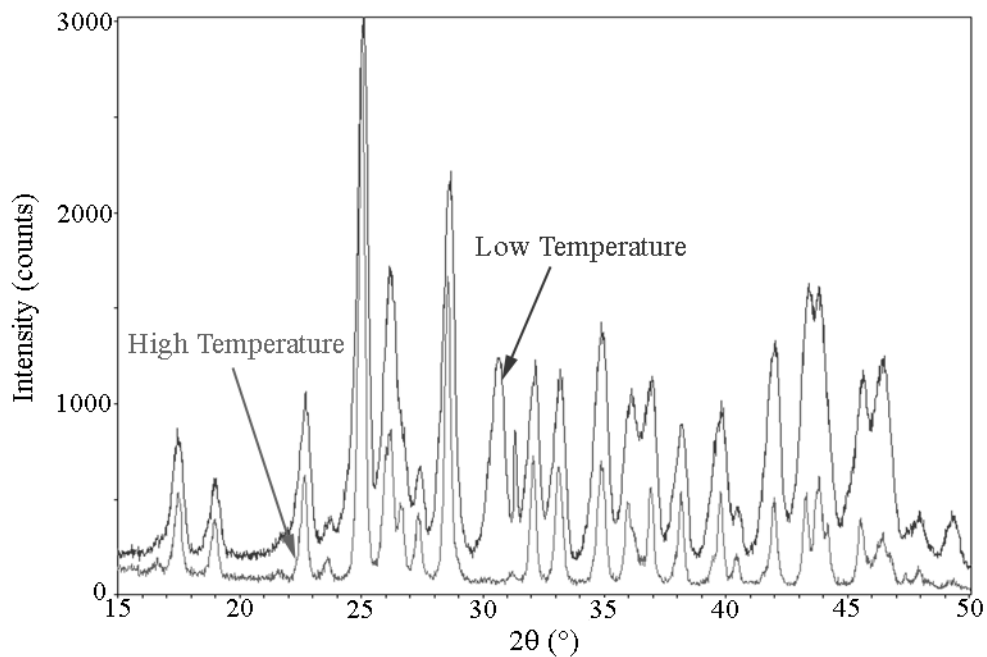


Figure 7-38. Diffraction patterns of 15 Li₂O•85 GeO₂ glass powder, following HTXRD with isothermal heat treatments at 550 °C and 645 °C.

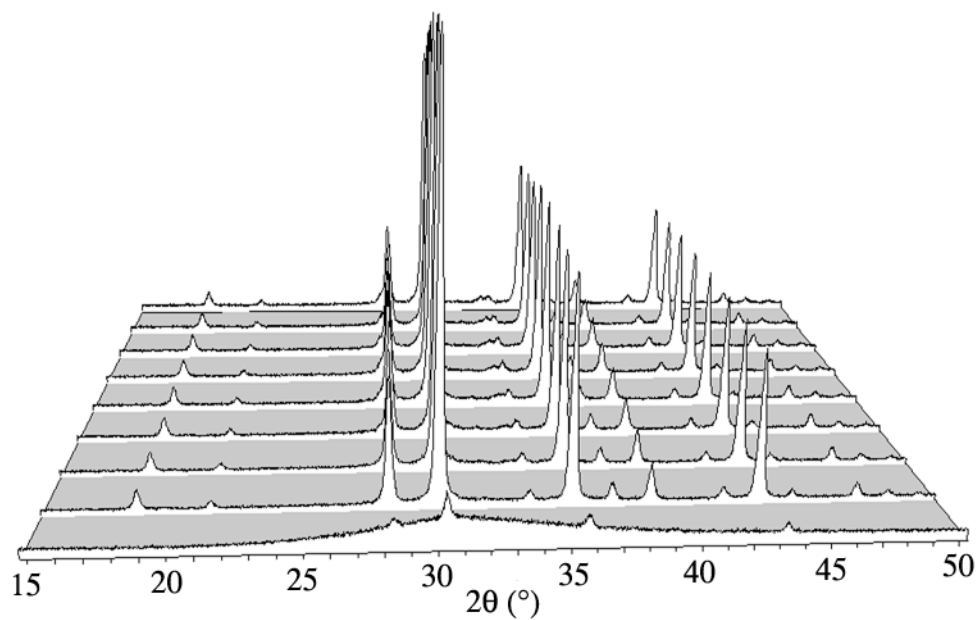


Figure 7-39. HTXRD scans for isothermal heat treatment at 590 °C for the 15 Cs₂O•85 GeO₂ glass.

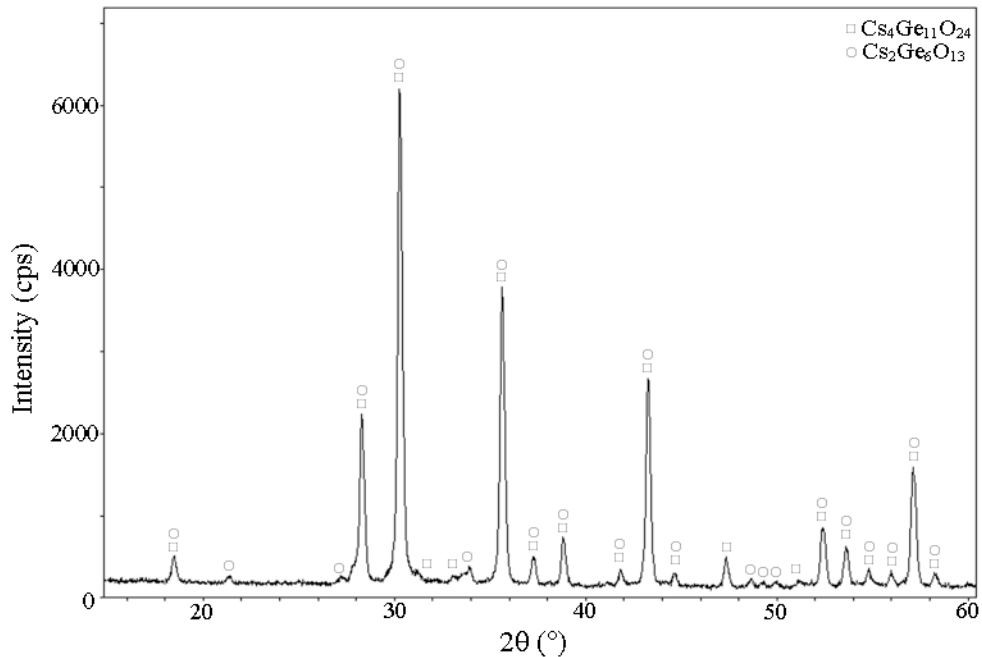


Figure 7-40. Diffraction pattern of the room temperature crystals, following the HTXRD experiment and heat treatment at 590 °C, for the 15 Cs₂O•85 GeO₂ glass.

7.4.2.2 Mixed Alkali Glasses

The behavior of the 7:1 Li₂O:Cs₂O•85 GeO₂ and 3:1 Li₂O:Cs₂O•85 GeO₂ glasses are similar and will be discussed concurrently in this section. The DSC curves for both glasses show one crystallization peak at the same temperature, so only one heat treatment temperature was used. The crystallization temperature for these HTXRD experiments was 550 °C for both glasses. Figure 7-41 shows the HTXRD pattern for 7:1 Li₂O:Cs₂O•85 GeO₂, while the final scan at 50 °C is shown in Figure 7-42. The 3:1 Li₂O:Cs₂O•85 GeO₂ glass has a similar HTXRD patterns, as shown in Figures 7-43 and 7-44. Analysis of the XRD patterns does not lead conclusively to any known crystal. The similarities in the two patterns can be seen in Figure 7-45 where the two diffraction patterns are overlaid. The most outstanding difference between the two patterns is the narrowing of some of the broad bands into more defined peaks. To show the difference between this pattern and those of the binary phases, all three patterns are shown in Figure 7-46.

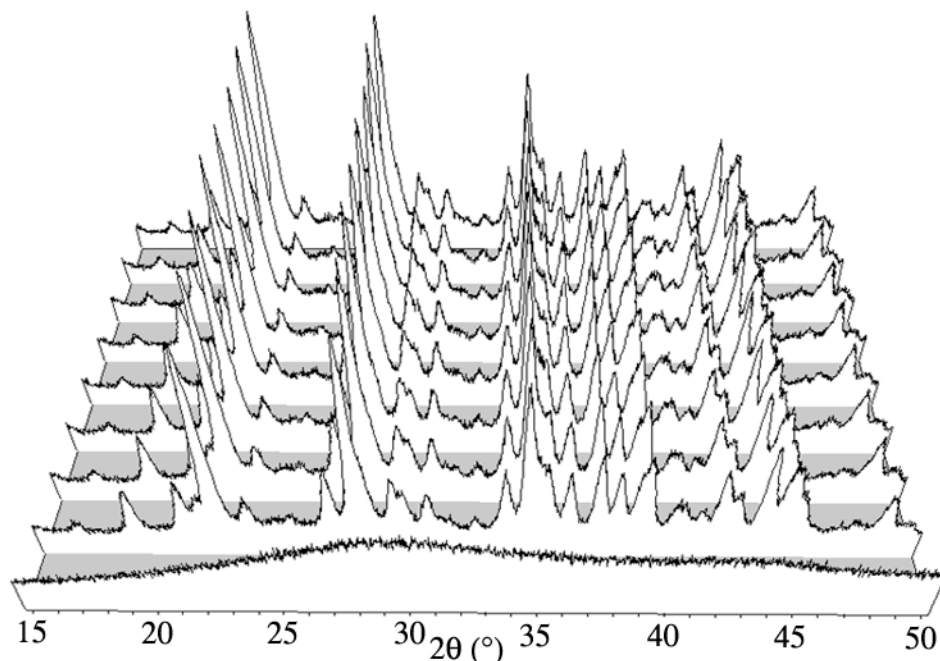


Figure 7-41. HTXRD scans for isothermal heat treatment at 590 °C for the 7:1 $\text{Li}_2\text{O}:\text{Cs}_2\text{O}\cdot 85 \text{ GeO}_2$ glass.

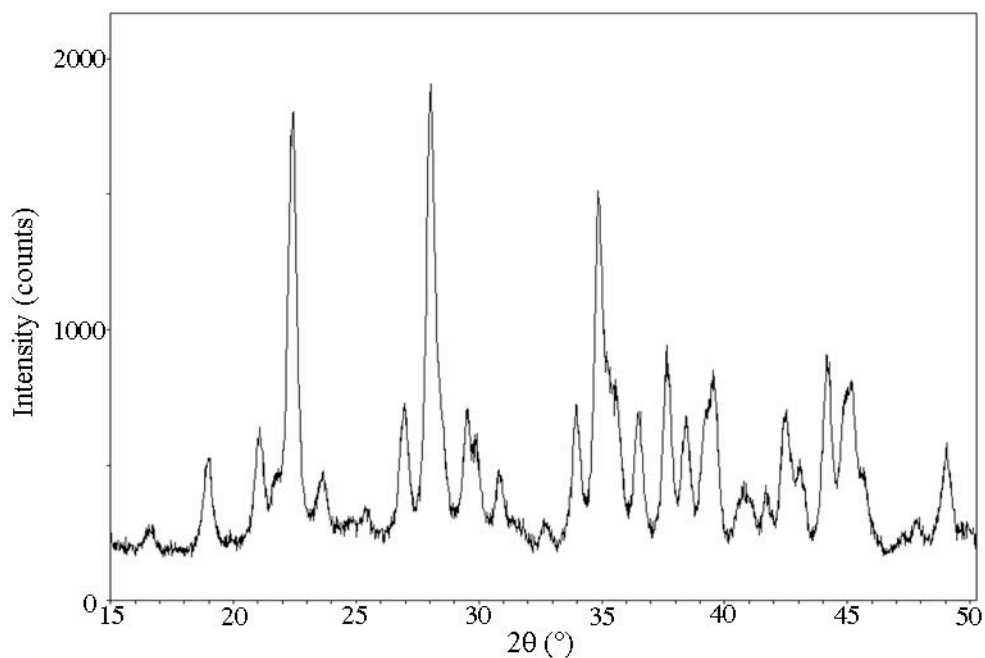


Figure 7-42. Diffraction pattern of the room temperature crystals, following the HTXRD experiment and heat treatment at 550 °C, for the 7:1 $\text{Li}_2\text{O}:\text{Cs}_2\text{O}\cdot 85 \text{ GeO}_2$ glass.

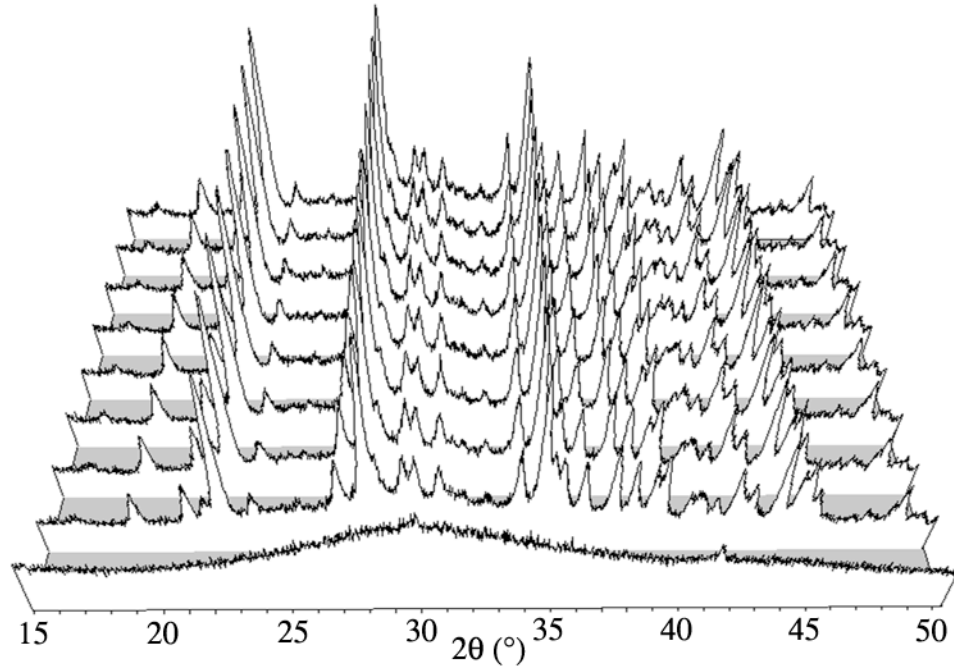


Figure 7-43. HTXRD scans for isothermal heat treatment at 550 °C for the 3:1 $\text{Li}_2\text{O}:\text{Cs}_2\text{O}\cdot 85 \text{ GeO}_2$ glass.

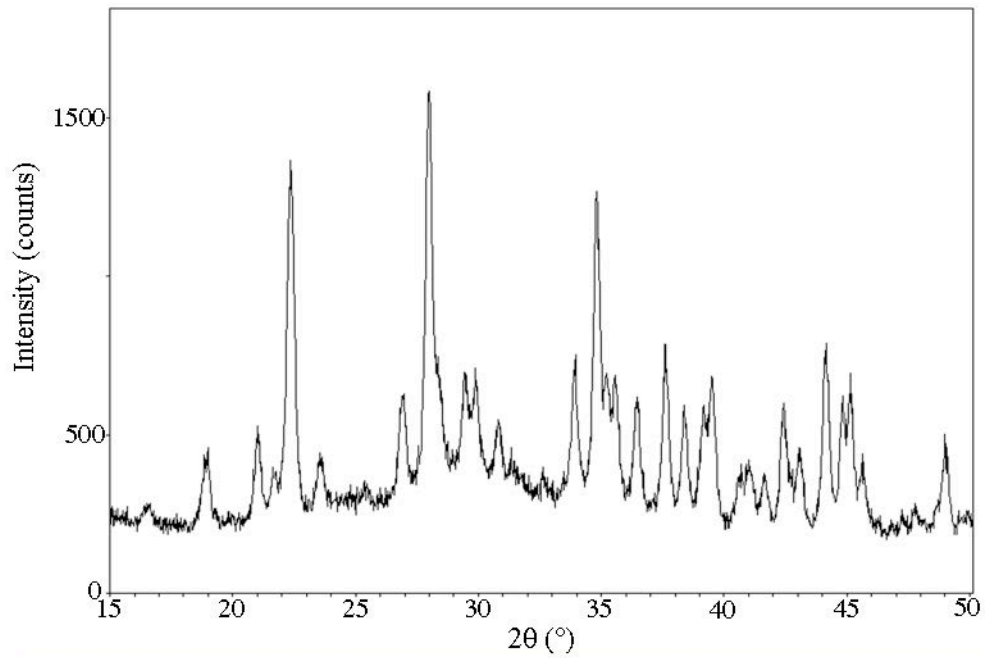


Figure 7-44. Diffraction pattern of the room temperature crystals, following the HTXRD experiment and heat treatment at 550 °C, for the 3:1 $\text{Li}_2\text{O}:\text{Cs}_2\text{O}\cdot 85 \text{ GeO}_2$ glass.

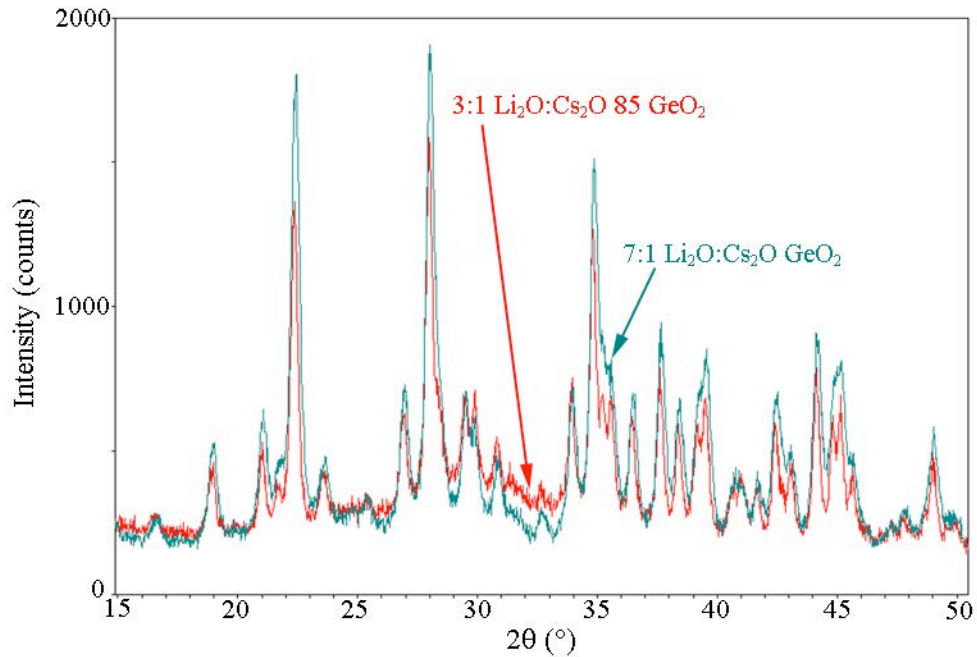


Figure 7-45. Comparison between diffraction patterns of 7:1 Li₂O:Cs₂O•85 GeO₂ and 3:1 Li₂O:Cs₂O•85 GeO₂, following isothermal heat treatment at 550 °C.

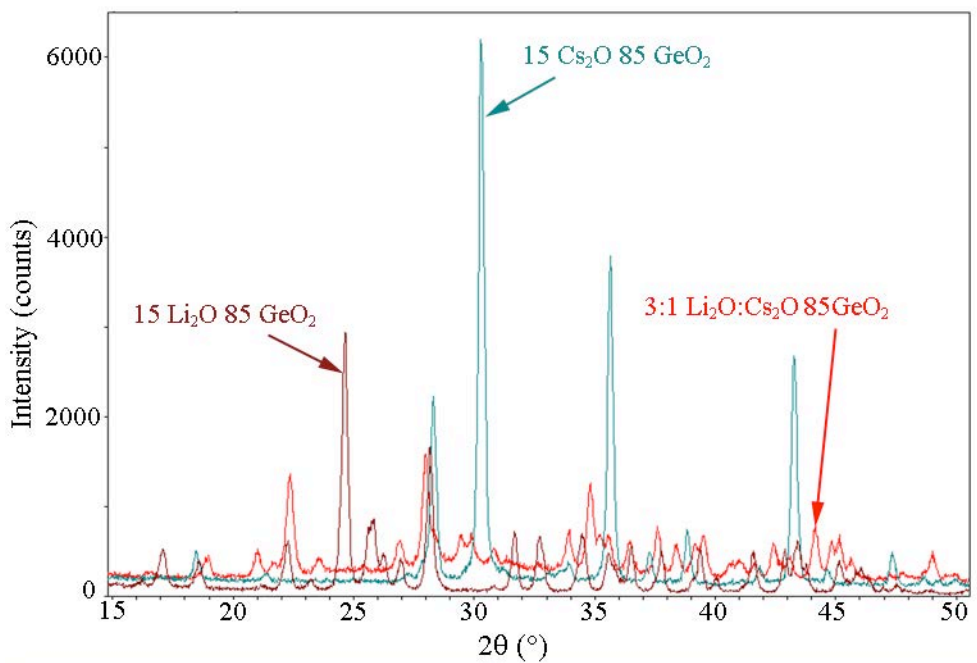


Figure 7-46. Comparison between the diffraction patterns of the crystallized binary glasses and 3:1 Li₂O:Cs₂O 85 GeO₂ glasses, following isothermal heat treatment.

The remaining mixed alkali glasses, 1:1 $\text{Li}_2\text{O}:\text{Cs}_2\text{O}\cdot 85 \text{ GeO}_2$ and 1:3 $\text{Li}_2\text{O}:\text{Cs}_2\text{O}\cdot 85 \text{ GeO}_2$, and 1:7 $\text{Li}_2\text{O}:\text{Cs}_2\text{O}\cdot 85 \text{ GeO}_2$ glasses behave similarly, and therefore, they will be discussed together. While the DSC curves for all of these glasses contain multiple crystallization peaks, the peaks are so close together that a return to the base line is not achieved, implying both bulk and surface crystallization, so only one heat treatment temperature for each glass was used. The treatment temperature for the HTXRD was 605 °C for 1:1 $\text{Li}_2\text{O}:\text{Cs}_2\text{O}\cdot 85 \text{ GeO}_2$ glass, 520 °C for 1:3 $\text{Li}_2\text{O}:\text{Cs}_2\text{O}\cdot 85 \text{ GeO}_2$ glass and 495 °C for 1:7 $\text{Li}_2\text{O}:\text{Cs}_2\text{O}\cdot 85 \text{ GeO}_2$ glass. Figure 7-47 shows the HTXRD pattern for the 1:1 $\text{Li}_2\text{O}:\text{Cs}_2\text{O}\cdot 85 \text{ GeO}_2$ glass. Analysis of the XRD pattern (Figure 7-48) shows the four phases present are a blend of the binary lithium germanate and cesium germanate crystals identified in the previous section on the binary glasses. The crystal data for this system is listed in Tables 7-17 and 7-18. As the composition becomes richer in cesium oxide, the lithium phases become less visible in the pattern. The 1:3 $\text{Li}_2\text{O}:\text{Cs}_2\text{O}\cdot 85 \text{ GeO}_2$ glass (Figure 7-49) forms three phases: a new lithium phase ($\text{Li}_4\text{Ge}_5\text{O}_{12}$) and the same two cesium germanate phases, as shown in Figure 7-50. The 1:7 $\text{Li}_2\text{O}:\text{Cs}_2\text{O}\cdot 85 \text{ GeO}_2$ (Figure 7-51) glass yields crystals of just the $\text{Cs}_2\text{Ge}_6\text{O}_{13}$ and $\text{Cs}_4\text{Ge}_{11}\text{O}_{24}$ compositions (Figure 7-52).

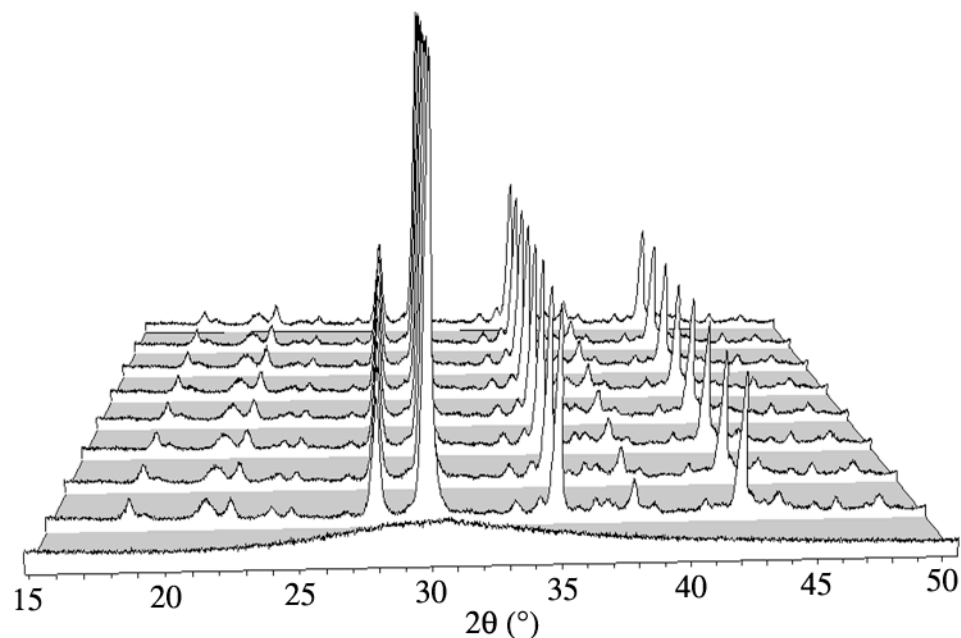


Figure 7-47. HTXRD scans for isothermal heat treatment at 605 °C for the 1:1 $\text{Li}_2\text{O}:\text{Cs}_2\text{O}\cdot 85 \text{ GeO}_2$ glass.

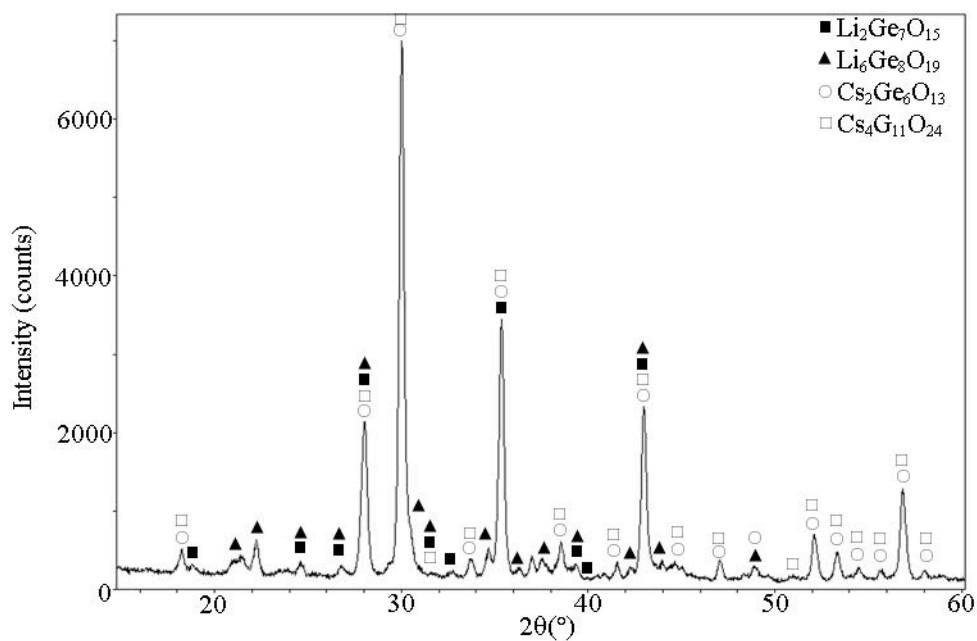


Figure 7-48. Diffraction pattern of the room temperature crystals, following the HTXRD experiment and heat treatment at 605 °C, for the 1:1 $\text{Li}_2\text{O}:\text{Cs}_2\text{O}\cdot 85 \text{ GeO}_2$ glass.

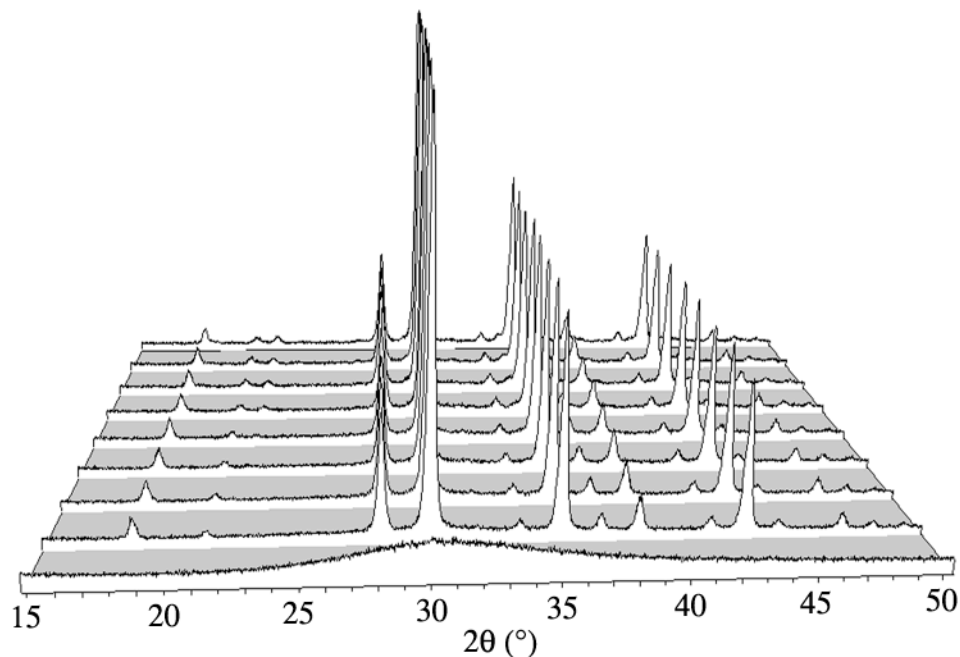


Figure 7-49. HTXRD scans for isothermal heat treatment at 520 °C for the 1:3 $\text{Li}_2\text{O}:\text{Cs}_2\text{O}\cdot 85 \text{ GeO}_2$ glass.

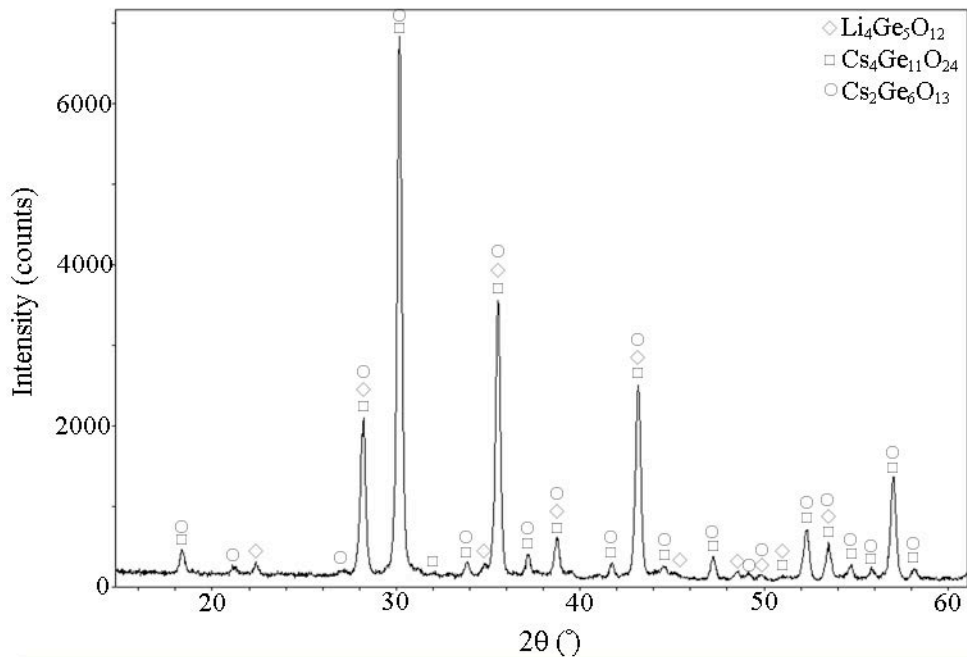


Figure 7-50. Diffraction pattern of the room temperature crystals, following the HTXRD experiment and heat treatment at 520 °C, for the 1:3 $\text{Li}_2\text{O}:\text{Cs}_2\text{O}\cdot 85 \text{ GeO}_2$ glass.

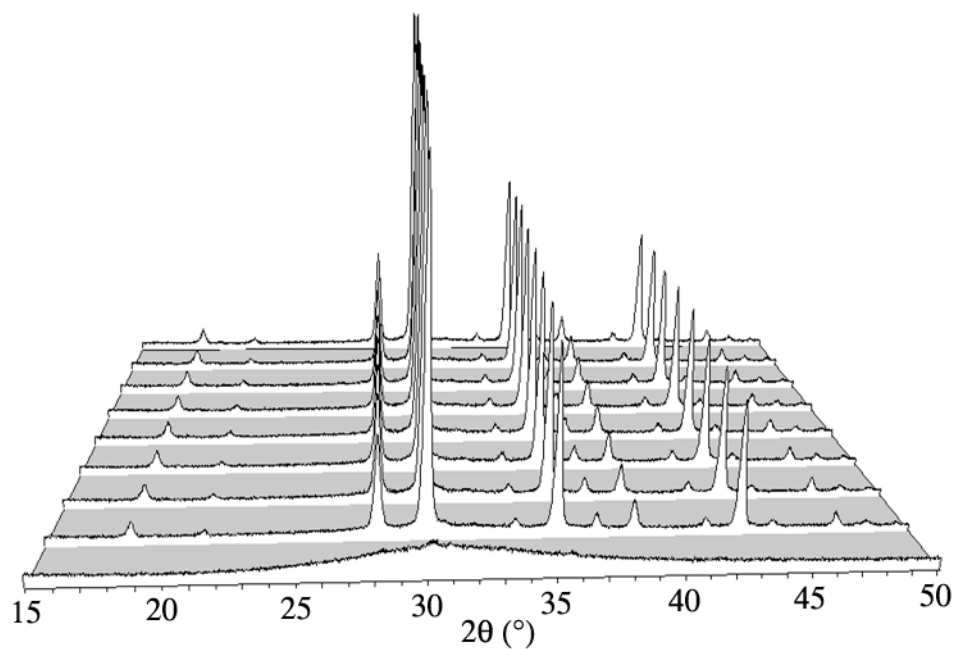


Figure 7-51. HTXRD scans for isothermal heat treatment at 495 °C for the 1:7 $\text{Li}_2\text{O}:\text{Cs}_2\text{O}\cdot 85 \text{ GeO}_2$ glass.

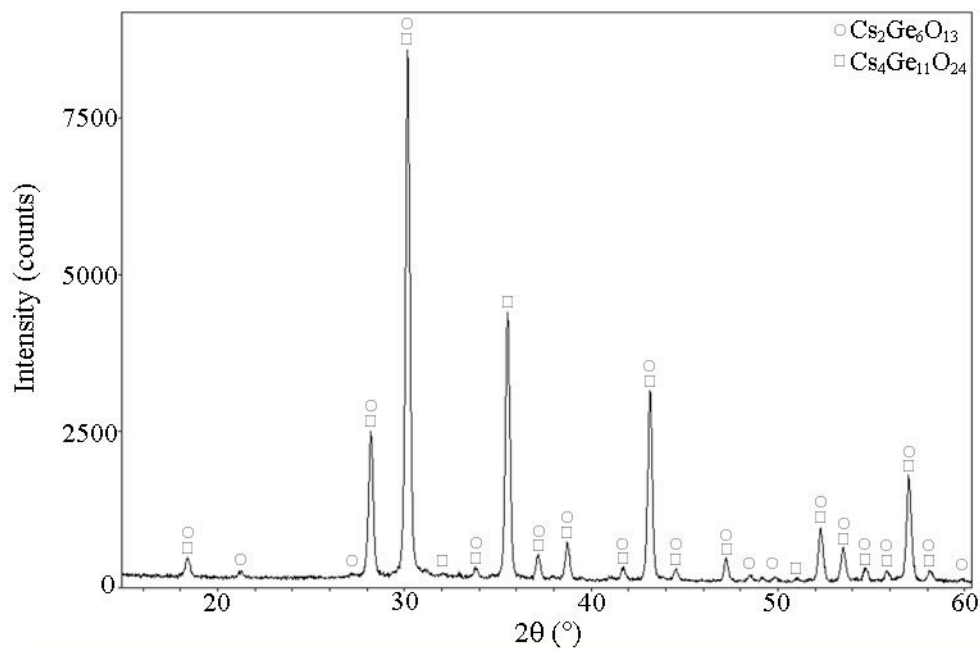


Figure 7-52. Diffraction pattern of the room temperature crystals, following the HTXRD experiment and heat treatment at 495 °C, for the 1:7 $\text{Li}_2\text{O}:\text{Cs}_2\text{O}\cdot 85 \text{ GeO}_2$ glass.

7.5 Discussion

7.5.1 Kissinger Study

The DSC curves for each glass composition at a heating rate of 20 K/min exhibit different crystallization peak position and glass transitions as shown in Figure 7-53. There is no simple correlation between the T_g and T_p , shown in Figure 7-54. The glass transition temperature yields the expected mixed alkali effect, with a minimum occurring when the alkali ratio is 1:1. There is no identifiable trend in the peak crystallization temperature. Glasses with the highest amounts of lithia exhibited the largest exothermal peaks. Comparing the shape of the DSC curve to the crystal formed for each composition does not add insight into the shape of the DSC curve. Each glass exhibits its own unique crystallization reaction, which is reasonable due to the complexity of nucleation and growth behavior discussed in sections 7.2.1.3-7.2.1.4.

The activation energy for crystallization of the glasses is shown in Figure 7-55 as a function of composition. If there is more than one crystallization peak, the activation energy for the lowest temperature peak is shown. There is no obvious trend along the line; therefore, a mixed alkali effect does not occur in the activation energy for crystallization of $x \text{Li}_2\text{O} \cdot (15-x) \text{Cs}_2\text{O} \cdot 85 \text{GeO}_2$ glasses. The activation energies occur in two groups on this line. Glasses with more Li_2O than Cs_2O have distinctly higher activation energy of crystallization than glasses where the ratio of Li_2O to Cs_2O is equal or which contain more Cs_2O than Li_2O . The T_g , T_p , and activation energies are listed in Table 7-XIX.

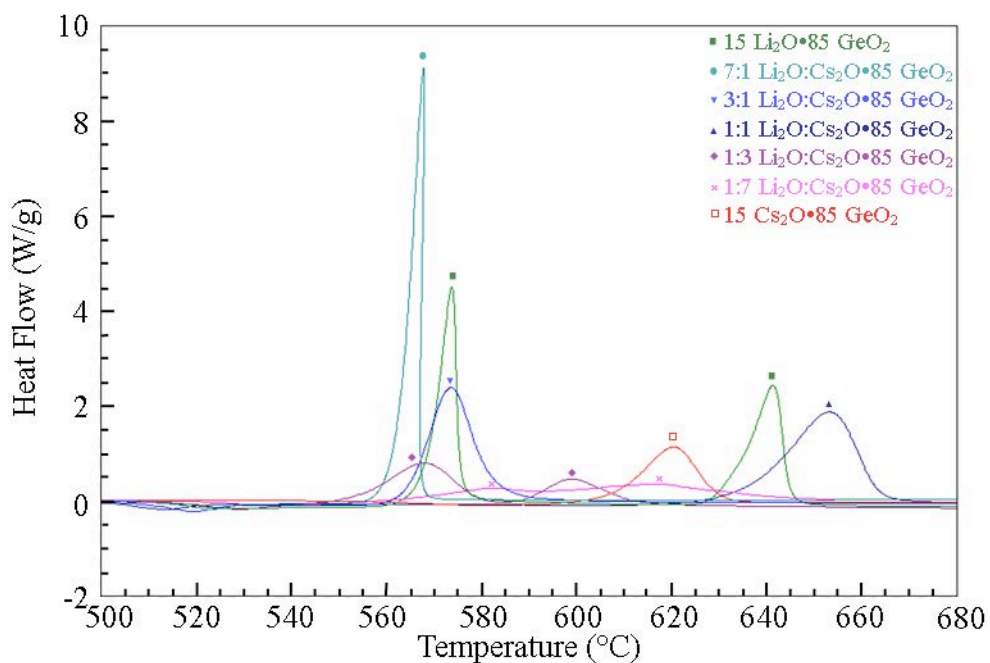


Figure 7-53. DSC curves for glasses on the $x \text{Li}_2\text{O} \cdot (15-x) \text{Cs}_2\text{O} \cdot 85 \text{GeO}_2$ line, with a 20 K/min heating rate.

Table 7-XIX. Peak Crystallization Temperature and Activation Energies for Crystallization for All $x \text{Li}_2\text{O} \cdot (15-x) \text{Cs}_2\text{O} \cdot 85 \text{GeO}_2$ Glasses (20 K/min, 63 to 75 μm)

Glass	T_g ($^{\circ}\text{C}$)	T_p ($^{\circ}\text{C}$)	Activation E (kJ/mol)
15 $\text{Li}_2\text{O} \cdot 85\text{GeO}_2$	512	576	472
7:1 $\text{Li}_2\text{O} \cdot \text{Cs}_2\text{O} \cdot 85 \text{GeO}_2$	512	573	395
3:1 $\text{Li}_2\text{O} \cdot \text{Cs}_2\text{O} \cdot 85 \text{GeO}_2$	505	574	459
1:1 $\text{Li}_2\text{O} \cdot \text{Cs}_2\text{O} \cdot 85 \text{GeO}_2$	498	635	281
1:3 $\text{Li}_2\text{O} \cdot \text{Cs}_2\text{O} \cdot 85 \text{GeO}_2$	511	568	347
1:7 $\text{Li}_2\text{O} \cdot \text{Cs}_2\text{O} \cdot 85 \text{GeO}_2$	509	568	333
15 $\text{Cs}_2\text{O} \cdot 85 \text{GeO}_2$	550	620	371

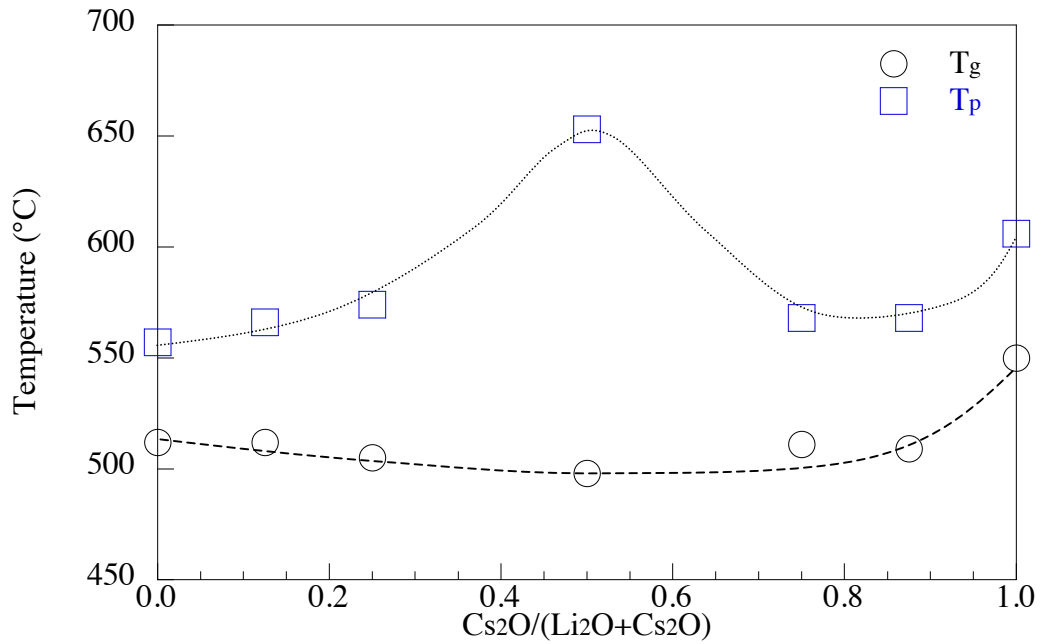


Figure 7-54. T_g and T_p for all glasses along $x \text{Li}_2\text{O} \cdot (15-x) \text{Cs}_2\text{O} \cdot 85 \text{GeO}_2$, with a 20 K/min heating rate. Lines added to aid the eye.

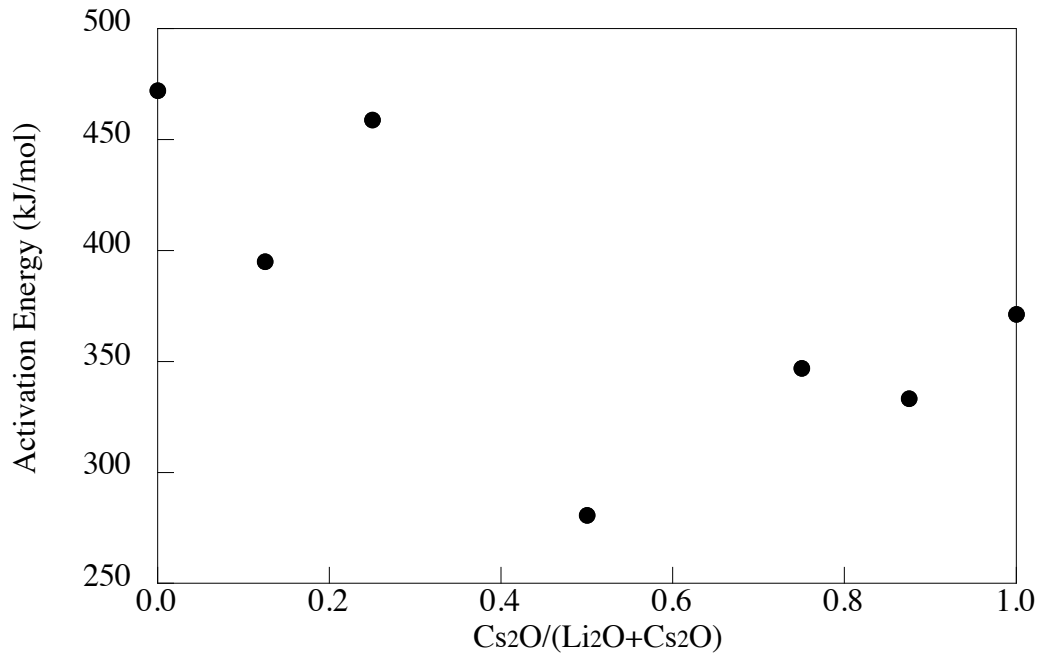


Figure 7-55. Activation energy of crystallization for $x \text{Li}_2\text{O} \cdot (15-x) \text{Cs}_2\text{O} \cdot 85 \text{GeO}_2$ glasses.

7.5.2 *Effect of Particle Size*

Changing the particle size of the samples used in the DSC did not change the glass transition temperature of the glasses. However, changing the particle size did result in some peaks evolving from one peak into doublets, or the merging of two peaks into a single peak. A good example of this is shown in Figure 7-27. In many cases, evolution of a single peak into two separate peaks when the heating rate is changed results from the presence of both surface and bulk crystallization in the glass. If the resolution of these peaks is a function of particle size, then the glass must be able to crystallize by growth of both bulk and surface nuclei.¹⁴ Since many of the glasses studied here develop (all but the 7:1 and 3:1 $\text{Li}_2\text{O}:\text{Cs}_2\text{O}\cdot 85 \text{ GeO}_2$ compositions) both surface and bulk phases, scanning electron microscopy (SEM) images were taken of all of the glasses following crystallization.

The 15 $\text{Li}_2\text{O}\cdot\text{GeO}_2$ glasses form the same two phases for both the low temperature and high temperature heat treatments. The low temperature heat treatment, Figure 7-56, results in two distinct phases. Crystallization also results in formation of obvious voids in the samples, since crystals are denser than glass of the equivalent composition, growth of those crystals depletes the surrounding glass of much of the network former and the structure develops voids. The lighter colored phase is $\text{Li}_2\text{Ge}_7\text{O}_{14}$. The second phase is $\text{Li}_2\text{Ge}_4\text{O}_9$, which appears darker in the micrograph due to the higher relative concentration of lithium ions. The crystals formed at the lower heat treatment temperature are very small, on the order of 100 to 200 nm. As a result, the crystallized sample is transparent. Since the crystals are too small to scatter visible light. High temperature heat treatment results in growth of these two phases, as shown in Figure 7-57 (a) and (b). The crystals are no longer invisible to the human eye, and the sample appears white.

The particle size DSC study of the 7:1 and 3:1 $\text{Li}_2\text{O}:\text{Cs}_2\text{O}\cdot 85 \text{ GeO}_2$ glasses suggests that only one phase forms, which is confirmed by the XRD data. A potential surface phase is indicated by the light gray edge and a bulk phase (the darker interior) phase seen in Figure 7-58. This surface phase appears to be residual glass with a high concentration of cesium. Figure 7-59 shows an ESEM image of the crystallized 3:1

$\text{Li}_2\text{O}:\text{Cs}_2\text{O}\cdot 85 \text{ GeO}_2$ glass. The bright gray edge is obvious in the image and careful observation shows the beginning formation of lines similar to the ones in Figure 7-58.

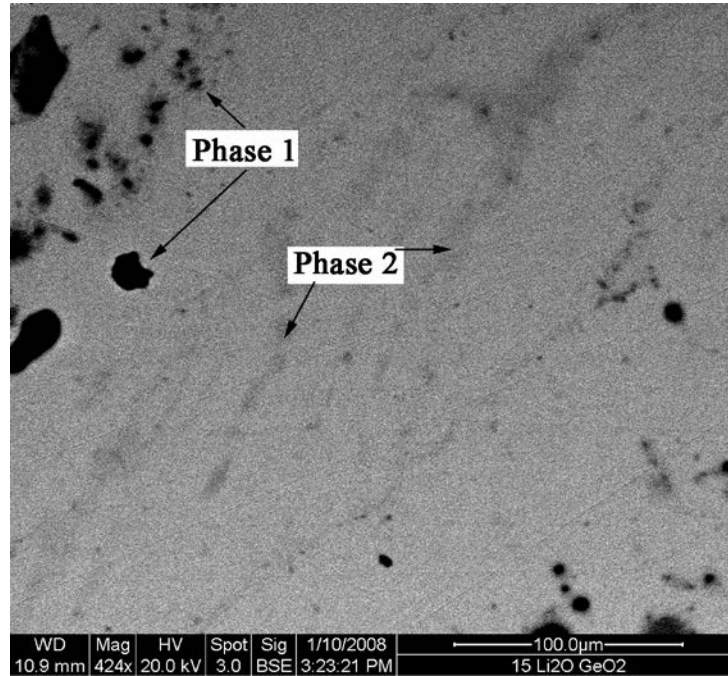


Figure 7-56. ESEM image, in backscatter electron mode, of crystals formed in 15 $\text{Li}_2\text{O}\cdot 85 \text{ GeO}_2$ glass after the low temperature heat treatment (485 °C).

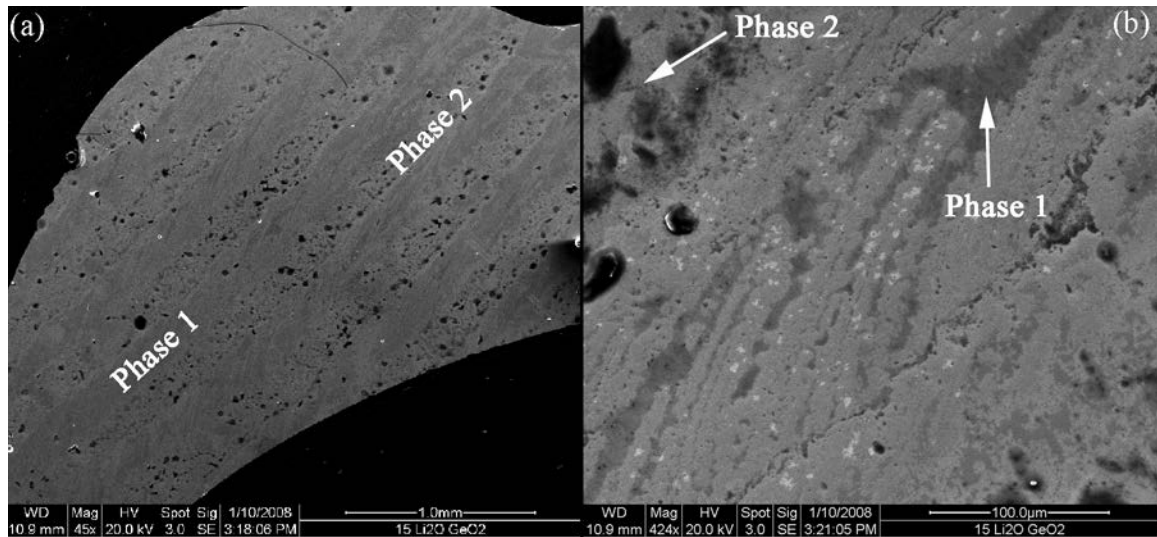


Figure 7-57. ESEM image of crystals formed in 15 $\text{Li}_2\text{O}\cdot 85 \text{ GeO}_2$ glass after the high temperature heat treatment (635 °C) (a) is a low magnification image showing both phases, (b) is a higher magnification showing the detailed morphology of both phases.

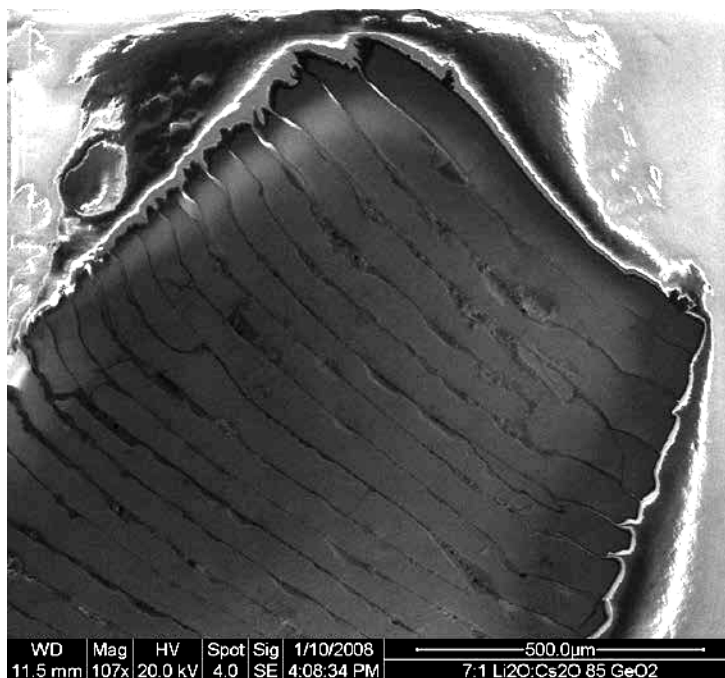


Figure 7-58. ESEM image of crystals formed in 7:1 $\text{Li}_2\text{O}:\text{Cs}_2\text{O}\cdot 85 \text{GeO}_2$ glass.

The particle size study for 1:1 $\text{Li}_2\text{O}:\text{Cs}_2\text{O}\cdot 85 \text{GeO}_2$ glasses shows two peaks that merge with increasing particle size, implying both surface and bulk crystallization. Glasses with the composition 1:1 $\text{Li}_2\text{O}:\text{Cs}_2\text{O}\cdot 85 \text{GeO}_2$ have the most complex and numerous crystals of all. Figure 7-59 (a-d) shows the large variety of crystals formed, as many as six different phases are present.

The particle size studies for 1:3 and 1:7 $\text{Li}_2\text{O}:\text{Cs}_2\text{O}\cdot 85 \text{GeO}_2$ glasses are difficult to interpret. The DSC curves for varying particle sizes of the 15 $\text{Cs}_2\text{O}\cdot 85 \text{GeO}_2$ glasses show that both surface and bulk crystals should be present. XRD data shows that the 1:3, 1:7 $\text{Li}_2\text{O}:\text{Cs}_2\text{O}\cdot 85 \text{GeO}_2$ and 15 $\text{Cs}_2\text{O}\cdot 85 \text{GeO}_2$ glasses predominantly contain the same two major crystalline phases, but the ESEM images reveal very different crystal morphologies. The 1:3 $\text{Li}_2\text{O}:\text{Cs}_2\text{O}\cdot 85 \text{GeO}_2$ crystals are predominantly in the bulk of the glass with a very small layer at the surface, as shown in Figure 7-61. The 1:7 $\text{Li}_2\text{O}:\text{Cs}_2\text{O}\cdot 85 \text{GeO}_2$ samples have the opposite morphology (Figure 7-62), with a thick surface layer and very fine crystals in the bulk of the glass. The binary 15 $\text{Cs}_2\text{O}\cdot 85 \text{GeO}_2$ glass, shown in Figure 7-62, has similar amounts of surface and bulk crystals.

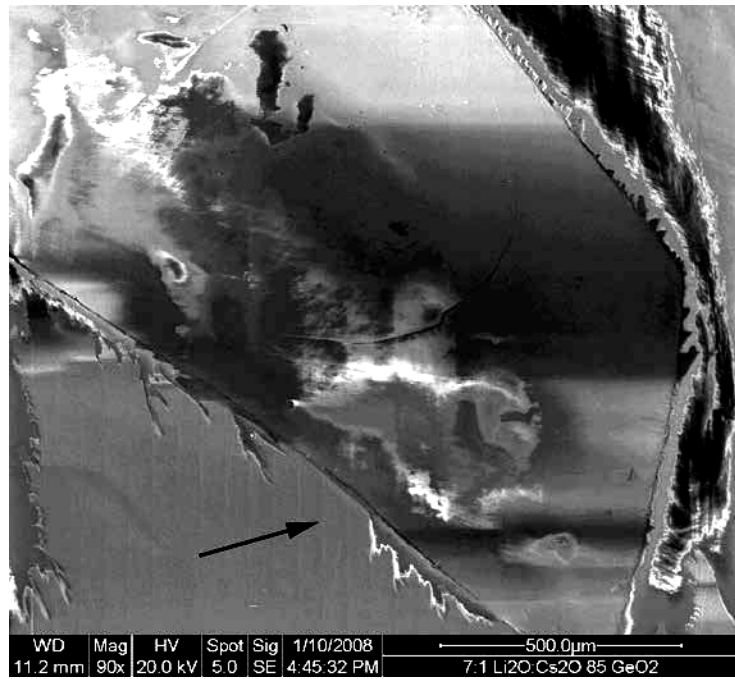


Figure 7-59. ESEM image of crystals formed in 3:1 $\text{Li}_2\text{O}:\text{Cs}_2\text{O}\cdot 85 \text{ GeO}_2$ glass.

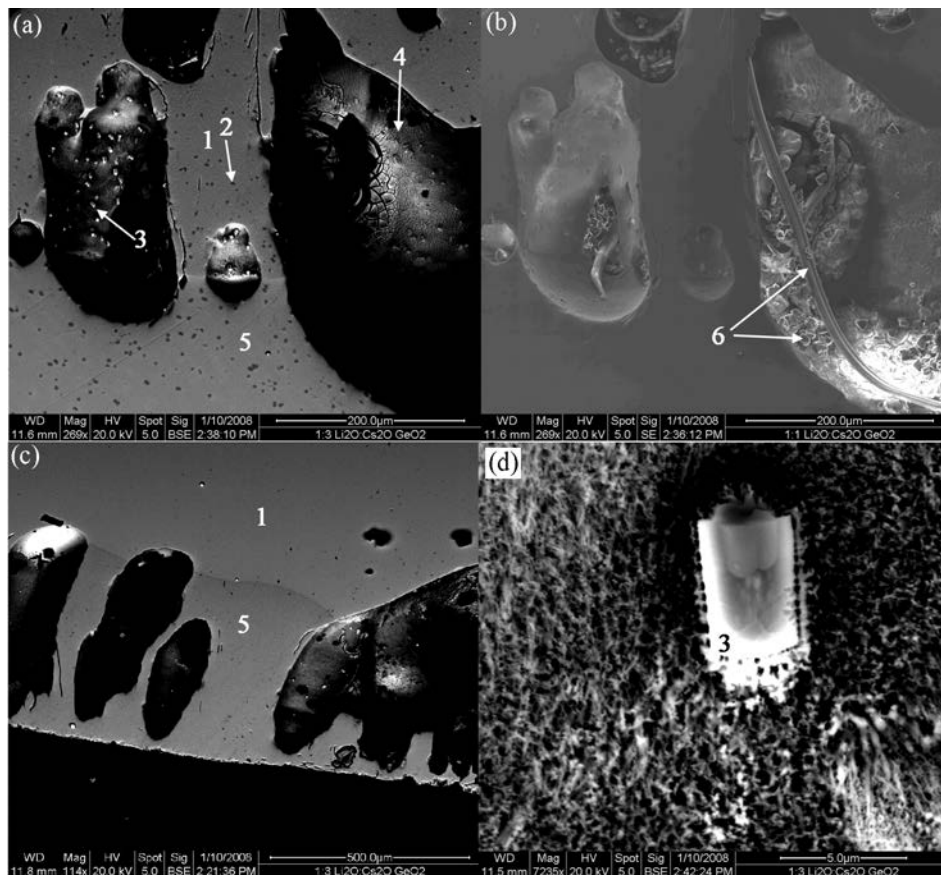


Figure 7-60. ESEM image of crystals formed in 1:1 $\text{Li}_2\text{O}:\text{Cs}_2\text{O}\cdot 85 \text{ GeO}_2$ glass.

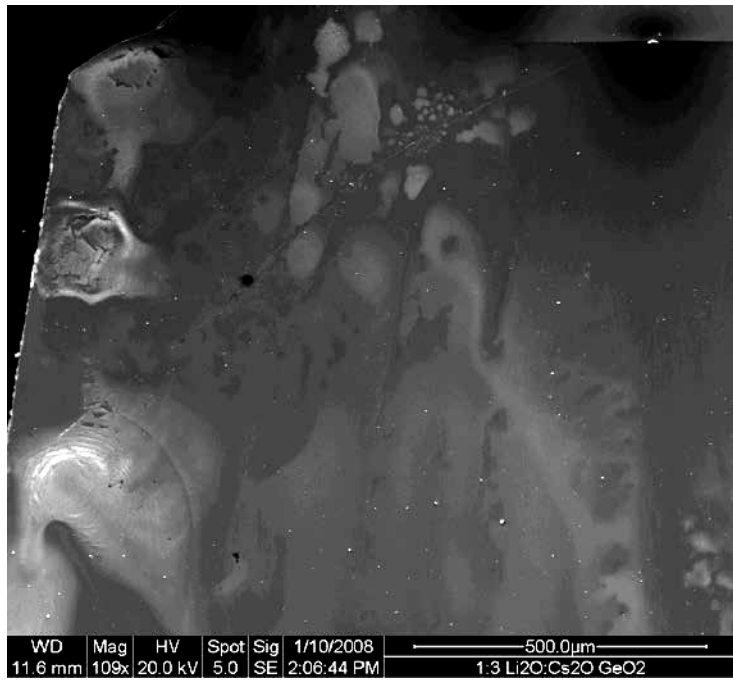


Figure 7-61. ESEM image of crystals formed in 1:3 $\text{Li}_2\text{O}:\text{Cs}_2\text{O}\cdot 85 \text{ GeO}_2$ glass.

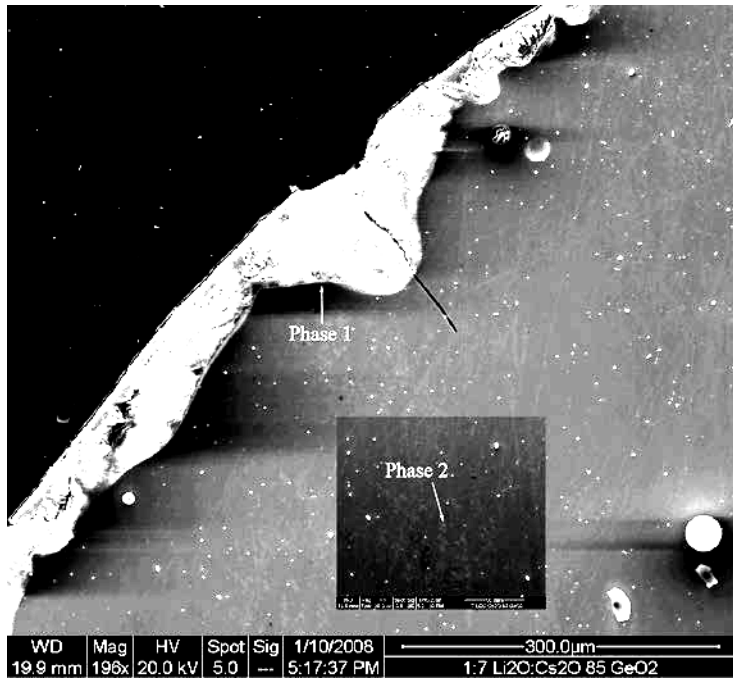


Figure 7-62. ESEM image of crystals formed in 1:7 $\text{Li}_2\text{O}:\text{Cs}_2\text{O}\cdot 85 \text{ GeO}_2$ glass.

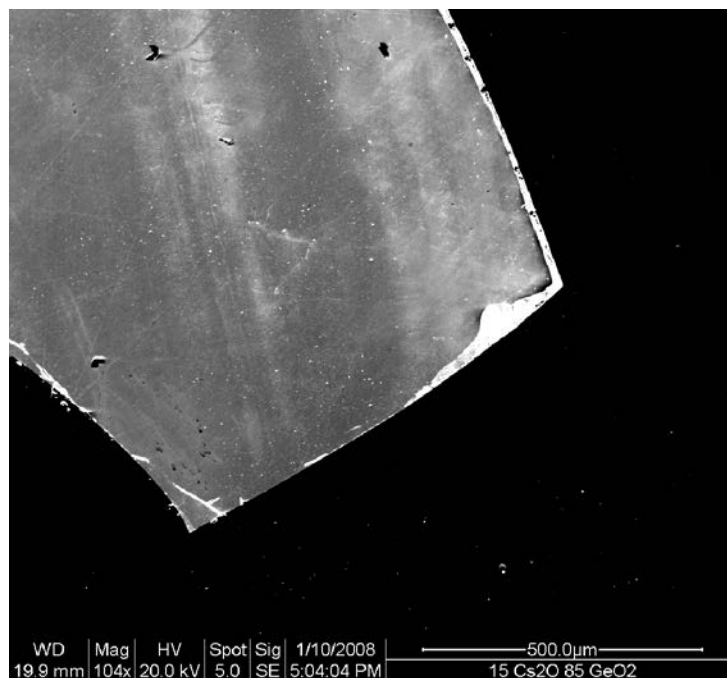


Figure 7-63. ESEM image of crystals formed in 15 Cs₂O•85 GeO₂ glass.

7.5.3 X-ray Diffraction

The DSC crystallization curves for the binary 15 Li₂O•85 GeO₂ glass suggest that two different crystal phases are formed, one corresponding to each of the crystallization peaks. This however is not the case. The crystals formed at the low temperature heat treatment are very small. The initial DSC sample produced when the experiment ended at 600 °C (prior to the second crystallization peak) is transparent. The DSC sample was ground into a fine powder and XRD was performed to identify the phase. The crystallites are so small and at such a low concentration that the X-ray pattern appears to be that of an amorphous sample. ESEM images (Figure 7-56) confirm the presence of crystals. A longer heat treatment time at 550 °C allows the crystals to grow larger, as shown in the HTXRD study, where the growth of the low temperature phase eventually results in a crystal pattern. At the higher heat treatment temperature, the crystallites are much larger and are the same phase, as confirmed by the diffraction patterns. To confirm these XRD results, a second high temperature study was performed to replicate the heat treatment the glasses received in the DSC. The temperature of the glass powder was increased at a rate of 20 K/min. A small scan range of 28 to 33 °2θ, and fast scan rate (5 °2θ/min) was used to eliminate a dwell time at any particular temperature while the diffraction measurement

was performed, decreasing the diffraction measurement time from 15 minutes to 1 minute and reasonably recreating the conditions of the DSC experiment. This study confirmed that the unidentifiable peaks at 30.0 to 31.5 °2θ resulted from contamination.

Adding a small amount of Cs₂O into the Li₂O•85 GeO₂ glass results in the formation of a phase that has not been identified. Figure 7-64 shows all seven XRD patterns. Examination of the patterns (Figure 7-46) show that the most intense peaks from the cesium germanium oxide and lithium germanate oxide binary crystals are non-existent, implying that the new crystalline phase is not a solid solution of the two crystals.

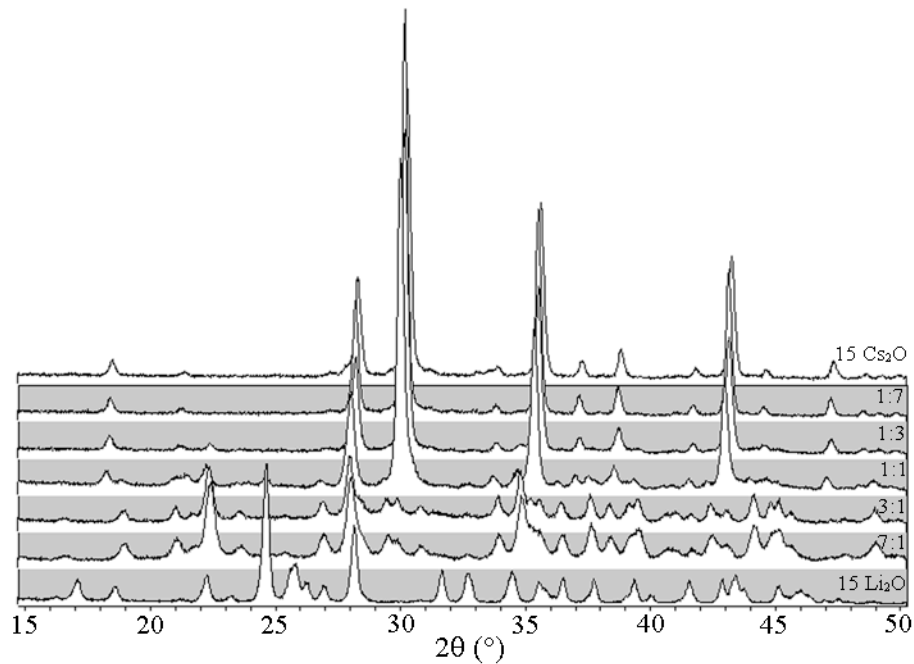


Figure 7-64. X-ray diffraction patterns for all seven $x \text{Li}_2\text{O} \cdot (15-x) \text{Cs}_2\text{O} \cdot 85 \text{GeO}_2$ compositions following isothermal heat treatment.

Once the glass contains a 1:1 ratio of Li₂O:Cs₂O or more Cs₂O, the dominant crystalline phases are binary cesium germanate phases. Figure 7-65 shows the diffraction patterns for the 1:1, 1:3, 1:7 Li₂O:Cs₂O•85 GeO₂ and 15 Cs₂O•85 GeO₂ glasses. Analysis of the 1:1 Li₂O:Cs₂O•85 GeO₂ pattern reveals a small amount of binary lithium germanate crystals, which decrease in concentration as the amount of lithia in the glass is reduced. These results are confirmed by the ESEM images.

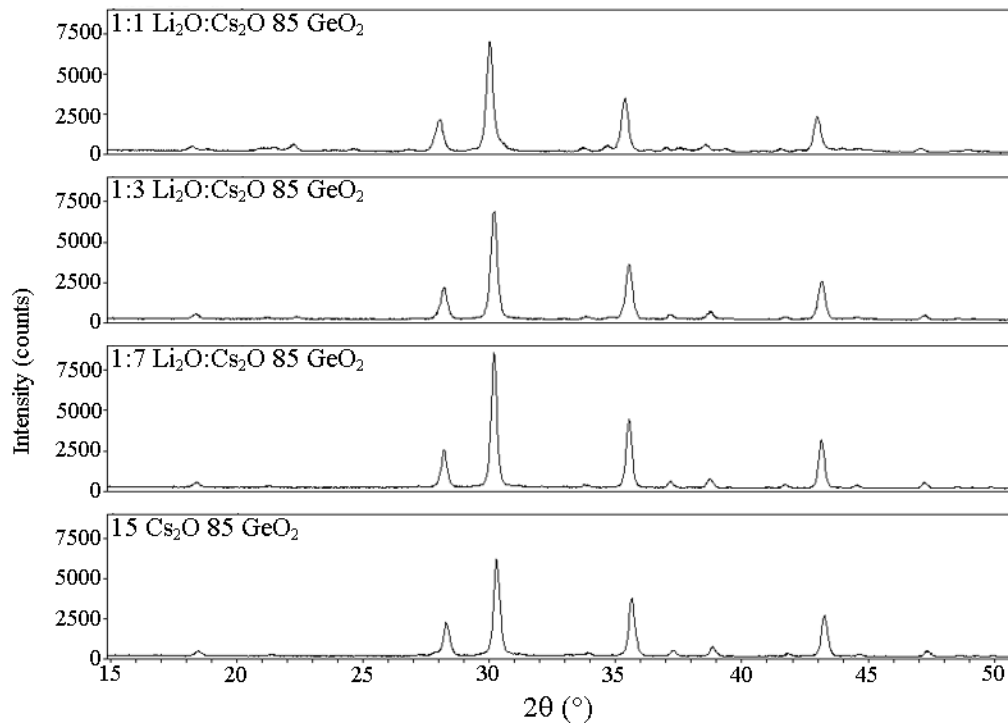


Figure 7-65. X-ray diffraction patterns for glasses where the predominate crystal phases are binary cesium germanium oxides.

7.5.4 Comparison to Literature Data

Only one study in the literature relates directly to this study. Pernice and co-authors studied the non-isothermal devitrification of lithium germanate glasses, containing 80 mol% GeO_2 .⁶ The current study agrees with the work of Pernice et al. Revisiting the phase diagram (Figure 7-3) shows that the binary lithium germania composition studied in this chapter lies in the lithium tetragermanate phase field. The same phases should have formed in both studies; XRD confirmed the existence of $\text{Li}_2\text{Ge}_7\text{O}_{15}$ and $\text{Li}_2\text{Ge}_4\text{O}_9$ crystals in both studies. Similarly, both studies found that the formation of the low temperature phase resulted in an amorphous XRD pattern.

The two studies concerning the crystallization of mixed alkali germanate glasses can be compared to this study. Laudisio and Catauro³ found sodium and potassium ions are close enough in size that a solid solution forms in the $\text{Na}_2\text{O}\cdot\text{K}_2\text{O}\cdot 4 \text{ GeO}_2$ system. This result was not found in the $\text{Li}_2\text{O}\cdot\text{K}_2\text{O}\cdot 4 \text{ GeO}_2$ system.⁴ In that case, instead of forming a solid solution upon crystallization, these glasses form only lithium compounds

when the amount of lithium is greater than potassium in the glass. When the Li_2O and K_2O are in a ratio of 1:1, or when the glass contains more K_2O , then only potassium germanium oxides form. This finding is similar to the results found in this study, where lithium germanium oxides formed when the concentration of lithia was greater than cesia, but when the concentration of Cs_2O and Li_2O are equal or the glass contains more Cs_2O than Li_2O , the cesium germanates dominated.

7.6 Conclusion

This is the first study examining the crystallization behavior of $x \text{Li}_2\text{O} \cdot (15-x) \text{Cs}_2\text{O} \cdot 85 \text{GeO}_2$ glasses. There is no preexisting phase diagram for the system. When the Li_2O and Cs_2O are mixed in a ratio of 1:1 or contain more Cs_2O than Li_2O , all the phases can be identified. The samples consist of mixtures of crystals of binary phases. However, when small amounts of cesium oxide are added to the binary $15 \text{Li}_2\text{O} \cdot 85 \text{GeO}_2$ glasses, a new phase that has yet to be identified forms. This result is the same in both the 7:1 $\text{Li}_2\text{O}:\text{Cs}_2\text{O} \cdot 85 \text{GeO}_2$ and the 3:1 $\text{Li}_2\text{O}:\text{Cs}_2\text{O} \cdot 85 \text{GeO}_2$ glasses. This is shown through the XRD pattern, the ESEM images, similar crystallization curves (both the Kissinger study and the particle size study), and the similar activation energy for crystallization. Similarly, glasses with a greater amount of Li_2O to Cs_2O have similar activation energies.

7.7 References

1. A. Aronne, M. Catauro, P. Pernice, and A. Marotta, "Gel Synthesis and Crystallisation of Sodium Tetragermanate Glass Powders," *Phys. Chem. Glasses*, **35** [4] 160-3 (1994).
2. M. Catauro, F. de Gaetano, and A. Marotta, "Non-Isothermal Devitrification of Sodium Germanate Glasses," *Thermochim. Acta*, **404** [1-2] 55-61 (2003).
3. G. Laudisio and M. Catauro, "Glass Transition Temperature and Devitrification Behavior of Glasses in the $\text{Na}_2\text{O} \cdot 4 \text{GeO}_2$ - $\text{K}_2\text{O} \cdot 4 \text{GeO}_2$ Composition Range," *Mater. Chem. Phys.*, **51** [1] 54-8 (1997).
4. G. Laudisio and M. Catauro, "Glass Transition Temperature and Crystallisation of Glasses in the $\text{Li}_2\text{O} \cdot 4 \text{GeO}_2$ - $\text{K}_2\text{O} \cdot 4 \text{GeO}_2$ Composition Range," *J. Eur. Ceram. Soc.*, **18** [4] 359-62 (1998).

5. M.K. Murthy and J. Aguayo, "Studies in Germanium Oxide Systems: II, Phase Equilibria in the System $\text{Na}_2\text{O-GeO}_2$," *J. Am. Ceram. Soc.*, **47** [9] 444-7 (1964).
6. P. Pernice, A. Aronne, and A. Marotta, "The Non-Isothermal Devitrification of Lithium Tetragermanate Glass," *Mater. Chem. Phys.*, **30** [3] 195-8 (1992).
7. W.A. Johnson and R.F. Mehl, "Reaction Kinetics in Processes of Nucleation and Growth," *Tans. Am. Inst. Min., Metall. Pet. Eng.*, **135** 416-58 (1939).
8. M. Avrami, "Kinetics of Phase Change 1: General Theory," *J. Chem. Phys.*, **7** [12] 1103-12 (1939).
9. M. Avrami, "Kinetics of Phase Change 2: Transformation-Time Relations for Random Distribution of Nuclei," *J. Chem. Phys.*, **8** [2] 212-24 (1940).
10. M. Avrami, "Granulation, Phase Change, and Microstructure: Kinetics of Phase Change 3," *J. Chem. Phys.*, **9** [2] 177-84 (1941).
11. H.E. Kissinger, "Variation of Peak Temperature with Heating Rate in Differential Thermal Analysis," *J. Res. Natl. Bur. Stand. (U. S.)*, **57** [4] 217-21 (1956).
12. H.E. Kissinger, "Reaction Kinetics in Differential Thermal Analysis," *Anal. Chem.*, **29** [11] 1702-6 (1957).
13. S.D. Stookey, "Ceramics Made by Nucleation of Glass," pp. 1-4 in Symposium on Nucleation and Crystallization in Glasses and Melts. Edited by M. K. Reser, G. Smith, and H. Insley. American Ceramic Society, Columbus, OH, 1962.
14. J.E. Shelby, *Introduction to Glass Science and Technology*; pp. 1-181. Royal Society of Chemistry, Cambridge, 1997.
15. A.K. Varshneya, *Fundamentals of Inorganic Glasses*; pp. 1-50. Academic Press, Boston, 1994.
16. H. Yinnon and D.R. Uhlmann, "Applications of Thermoanalytical Techniques to the Study of Crystallization Kinetics in Glass-Forming Liquids, Part I: Theory," *J. Non-Cryst. Solids*, **54** [3] 253-75 (1983).
17. J.A. Augis and J.E. Bennett, "Calculation of the Avrami Parameters for Heterogeneous Solid State Reactions Using a Modification of the Kissinger Method," *J. Therm. Anal.*, **13** [2] 283-92 (1978).
18. N.P. Bansal and R.H. Doremus, "Determination of Reaction Kinetic Parameters from Variable Temperature DSC or DTA," *J. Therm. Anal.*, **29** [1] 115-9 (1984).

19. P.F. James, "Kinetics of Crystal Nucleation in Silicate Glasses," *J. Non-Cryst. Solids*, **73** [1-3] 517-40 (1985).
20. K. Matusita and S. Sakka, "Kinetic Study of the Crystallisation of Glass by Differential Scanning Calorimetry," *Phys. Chem. Glasses*, **20** [4] 81-4 (1979).
21. K. Matusita, S. Sakka, and Y. Matsui, "Determination of the Activation Energy for Crystal Growth by Differential Thermal Analysis," *J. Mater. Sci.*, **10** [6] 1975 (1975).
22. P. Murray and J. White, "Kinetics of the Thermal Decomposition of Clays," *Trans. J. Br. Ceram. Soc.*, **48** 187-206 (1949).
23. P. Murray and J. White, "Kinetics of the Thermal Decomposition of Clay, Part II: Isothermal Decomposition of Clay Minerals " *Trans. J. Br. Ceram. Soc.*, **54** 151-88 (1955).
24. P. Murray and J. White, "Kinetics of the Thermal Dehydration of Clays, Part III: Kinetic Analysis of Mixtures of the Clay Minerals," *Trans. J. Br. Ceram. Soc.*, **54** 189-203 (1955).
25. P. Murray and J. White, "Kinetics of the Thermal Dehydration of Clays, Part IV: Interpretation of the Differential Thermal Analysis of the Clay Minerals," *Trans. J. Br. Ceram. Soc.*, **54** 204-38 (1955).
26. J. Sestak, "The Applicability of DTA to the Study of Crystallization Kinetics of Glasses," *Phys. Chem. Glasses*, **15** [6] 137-40 (1974).
27. G.L. Smith, G.F. Neilson, and M.C. Weinberg, "Crystal Nucleation in Lithium Borate Glass," *Phys. Chem. Glasses*, **28** [6] 257-61 (1987).
28. D. Turnbull, "Kinetic and Molecular Constitutive Criteria for Glass Formation," p. 75 in Symposium on Nucleation and Crystallization in Glasses and Melts. Edited by M. K. Reser, G. Smith, and H. Insley. American Ceramic Society, Columbus, OH, 1962.
29. D.R. Uhlmann, "Crystallization and Melting in Glass Forming Systems," pp. 172-97 in Vol. 4, *Kinetics of Reactions in Ionic Systems*. Edited by T. J. Gray and V. D. Frechette. Plenum Press, New York, NY 1969.
30. P.F. James, "Nucleation in Glass-Forming Systems-a Review," pp. 1-48 in *Advances in Ceramics, Vol. 4, Nucleation and Crystallization in Glasses*. Edited by J. H. Simmons, D. R. Uhlmann, and G. H. Beall. American Ceramic Society, Columbus, OH, 1982.

31. W.B. Hillig, "Theory of Crystal Growth in Undercooled Pure Liquids," *J. Chem. Phys.*, **24** [4] 914 (1956).
32. W.B. Hillig, "A Theoretical and Experimental Investigation of Nucleation Leading to Uniform Crystallization of Glass," pp. 77-90 in Symposium on Nucleation and Crystallization in Glasses and Melts. Edited by M. K. Reser, G. Smith, and H. Insley. American Ceramic Society, Columbus, OH, 1962.
33. W.B. Hillig, "A Derivation of Classical Two-Dimensional Nucleation Kinetics and the Associated Crystal Growth Laws," *Acta Metallurgica*, **14** [12] 1868-9 (1966).
34. D. Kashchiev, "Solution of the Non-Steady State Problem in Nucleation Kinetics," *Surf. Sci.*, **14** [1] 209-20 (1969).
35. D. Turnbull and J.C. Fisher, "Rate of Nucleation in Condensed Systems," *J. Chem. Phys.*, **17** [1] 71-3 (1949).
36. K.A. Jackson, D.R. Uhlmann, and J.D. Hunt, "On the Nature of Crystal Growth from the Melt," *J. Cryst. Growth*, **1** [1] 1-36 (1967).
37. D.R. Uhlmann, "Crystal Growth in Glass-Forming Systems: A Ten-Year Perspective," pp. 80-124 in Advances in Ceramics, Vol. 4, *Nucleation and Crystallization in Glasses*. Edited by J. H. Simmons, D. R. Uhlmann, and G. H. Beall. American Ceramic Society, Columbus, OH, 1982.
38. F.E. Wagstaff, "Crystallization and Melting Kinetics of Cristobalite," *J. Am. Ceram. Soc.*, **52** [12] 650-4 (1969).
39. D.R. Gaskell, *Introduction to the Thermodynamics of Materials*, 4th ed.; p. 601. Taylor & Francis, New York, 2003.
40. A. Marotta, A. Aronne, P. Pernice, and M. Catauro, "Devitrification Behavior of Glasses in the Lead Tetragermanate-Lithium Tetragermanate Composition Range," *Mater. Chem. Phys.*, **42** [4] 247-52 (1995).
41. P.J. Vergano and D.R. Uhlmann, "Crystallisation Kinetics of Germanium Dioxide: The Effect of Stoichiometry on Kinetics," *Phys. Chem. Glasses*, **11** [2] 30-8 (1970).
42. M.K. Murthy and L. Angelone, "Germanium Oxide Systems. 5. Phase Equilibria in the System Cesium Oxide-Germanium Oxide," *J. Am. Ceram. Soc.*, **54** [3] 173 (1971).
43. M.K. Murthy, M. Krishna, and J. Ip, "Germanium Oxide Systems: 1. Phase Equilibria in the System $\text{Li}_2\text{O-GeO}_2$," *J. Am. Ceram. Soc.*, **47** [7] 330 (1964).

44. P.P. Budnikov, S.G. Tresvyatskii, and R.I. Baikova, "Diagrams of State for the GeO₂-Li₂O System," *Dokl. Bulg. Akad. Nauk*, **99** 761 (1954).
45. C. Garrault, B. Monnaye, and C. Bouaziz, "Lithium Germanates with the Formula x GeO₂• y Li₂O," *C. R. Seances Acad. Sci. Ser. C.*, **276** [5] 417-20 (1973).
46. R. Schwarz, "The Chemistry of Germanium, 1," *Ber. Dtsch. Keram. Ges.*, **62** 2477-83 (1929).

CHAPTER 8: CONCLUSIONS

The properties of mixed alkali germanate glasses have been extensively studied. While many of the results were expected, there are a few unanticipated results that will be highlighted here.

(1) Additions of ≤ 5 mol % alkali oxide result in similar molar volumes between the $\text{Li}_2\text{O}\cdot\text{Cs}_2\text{O}\cdot\text{GeO}_2$ glasses and the $\text{Na}_2\text{O}\cdot\text{K}_2\text{O}\cdot\text{GeO}_2$ glasses.

(2) The long assumed idea that when two mobile ions are mixed in a glass, the larger the radius ratio of the two cations, the greater the deviation from additivity does not hold true for the glass transition temperatures of mixed alkali germanate glasses. $\text{Li}_2\text{O}\cdot\text{Cs}_2\text{O}\cdot\text{GeO}_2$ glasses have approximately the same negative deviation from additivity as the $\text{Na}_2\text{O}\cdot\text{K}_2\text{O}\cdot\text{GeO}_2$ glasses.

(3) A positive deviation from additivity in conductivity is observed in glasses with ≤ 5 mol % alkali oxide. As the amount of alkali oxide is increased beyond 5 mol % the deviation from additivity becomes negative and increases with increasing concentration of alkali oxide.

(4) The greatest deviation from additivity in conductivity is observed when the radius ratio of the alkali is close to 1.

This study has shown properties, which respond with only slightest disruption to the connectivity of the glass network, i.e. the glass transition temperature and electrical conductivity. There exists both a low alkali germanate anomaly and a high germanate anomaly. Both the glass transition temperature and the DC electrical conductivity show minima occurring at approximately 2 mol % addition of alkali oxide. Therefore, it can be concluded that small additions of alkali oxide weaken the bonding of the network. The most likely cause of the disruption is the formation of non-bridging oxygen.

The literature has stated the cause of the high alkali germanate anomaly is a result instead of a non-bridging oxygen from the presence of alkali results in an increase in coordination of the germanium ion. The lack of non-bridging oxygens results in a strong glass network, which exhibits properties such as a maximum in the glass transition temperature and density and a minimum in the electrical conductivity. The alkali concentration leading to a maximum or minimum is not the same for every property and

is greatly effected by the cation identity. The mystery surrounding the alkali germanate is far from being solved. However, this study has contributed property data that will be required for modelers to properly describe the system.

APPENDIX A

Table A-I. Authors, Symbols and References for T_g of $\text{Li}_2\text{O}\cdot\text{GeO}_2$ Glasses (Figure 4-1).

Author	Symbol	Reference
Kiczinski	●	J. Non Cryst. Solids, 272 [1] 57 (2000)
Mochida	○	J. Cerm. Soc. Jpn. 94 [12]1225 (1986)
Marotta	▲	Proc. 2 nd Int. Conf. Fundamentals of Glass Science and Technology, Venice, 1993, 427
Radhakrishnan	▼	Mater. Sci. Eng. B14 [1] 17 (1992)
Shelby	△	Phys. Chem. Glasses 28 [6] 262 (1987)
Marotta-2	□	Phys. Chem. Glasses 37 [4] 134 (1996)

Table A-II. Authors, Symbols and References for T_g of $\text{Na}_2\text{O}\cdot\text{GeO}_2$ Glasses (Figures 4-2 and 4-3).

Author	Symbol	Reference
Di Martino	●	Phys. Chem. Glasses 43C 85 (2002)
Shelby	○	J. Am. Ceram. Soc. 57 [10] 436 (1974)
Kiczinski	▲	J. Non Cryst. Solids, 272 [1] 57 (2000)
Marotta	▼	Proc. 2 nd Int. Conf. Fundamentals of Glass Science and Technology, Venice, 1993, 427
Laudisio	△	Mater. Chem. Phys. 51 [1] 54 (1997)
Mundy	□	Solid State Ionics 21 [4] 305 (1986)
Akopyan	■	Arm. Khim. Zh. 31 [2-3] 120 (1978)
Shelby-2	▣	J. Appl. Phys. 46 [1] 193 (1975)
Ruller	+	Phy. Chem. Glasses 33 [5] 161 (1992)
Gangopadhyay	◇	Am. Ceram. Soc. Bull. 56 [11] 1008 (1977)
Lee	◆	Phy. Chem. Glasses 36 [5] 225 (1995)
Hanada	▽	J. Ceram. Soc. Jpn. 81 [11] 481 (1973)
Marotta-2	⊕	Proc. XVIII th Inter. Congr. On Glass CD-ROM San Francisco, 1998, p. D5, 116
Gee	⊞	Phys. Chem. Glasses 41 [4] 175 (2000)
Catauro	▣	Thermochim. Acta 404 55 (2003)

Table A-III. Authors, Symbols and References for T_g of $\text{K}_2\text{O}\cdot\text{GeO}_2$ Glasses (Figures 4-4 and 4-5).

Author	Symbol	Reference
Shelby	●	J. Am. Ceram. Soc. 57 [10] 436 (1974)
Shelby-2	○	J. Appl. Phys. 46 [1] 193 (1975)
Kiczinski	▲	J. Non Cryst. Solids, 272 [1] 57 (2000)
Mochida	▼	J. Cerm. Soc. Jpn. 94 [12]1225 (1986)
Marotta	△	Proc. XVIII th Inter. Congr. On Glass CD-ROM San Francisco, 1998, p. D5, 116
Laudisio	□	Phy. Chem. Glasses 38 [5] 244 (1997)
Hall	■	Phy. Chem. Glasses 45 [4] 283 (2004)

Table A-IV. Authors, Symbols and References for T_g of $Rb_2O \cdot GeO_2$ Glasses (Figures 4-6 and 4-7).

Author	Symbol	Reference
Shelby	●	J. Am. Ceram. Soc. 57 [10] 436 (1974)
Nassau	○	J. Am. Ceram. Soc. 65 [4] 197 (1982)
Shelby-2	▲	J. Appl. Phys. 46 [1] 193 (1975)
Huang	▼	J. Non Cryst. Solids, 255 [1] 103 (1999)
Kiczinski	△	J. Non Cryst. Solids, 272 [1] 57 (2000)

Table A-V. Authors, Symbols and References for T_g of $Cs_2O \cdot GeO_2$ Glasses Figure 4-8.

Author	Symbol	Reference
Shelby	●	J. Am. Ceram. Soc. 57 [10] 436 (1974)
Nassau	○	J. Am. Ceram. Soc. 65 [4] 197 (1982)
Di Martino	▲	Phys. Chem. Glasses 43C 85 (2002)
Shelby-2	▼	J. Appl. Phys. 46 [1] 193 (1975)

Table A-VI. Authors, Symbols and References for Density of $Li_2O \cdot GeO_2$ Glasses (Figures 4-11 and 4-12).

Author	Symbol	Reference
Henderson	●	Eur. J. Mineral. 14 [4] 733 (2002)
Verweij	□	J. Mater. Sci. 14 [4] 931 (1979)
Sakka	▲	J. Non Cryst. Solids 49 [1-3] 103 (1982)
Radhakrishnan	▼	Mater. Sci. Eng. B14 [1] 17 (1992)
Yoshimira	△	Yogyo Kyokaishi 79 [915] 428 (1971)
Shelby	▽	Phys. Chem. Glasses 28 [6] 262 (1987)

Table A-VII. Authors, Symbols and References for Density of $Na_2O \cdot GeO_2$ Glasses (Figures 4-13 and 4-14).

Author	Symbol	Reference
Di Martino	□	Phys. Chem. Glasses 43C 85 (2002)
Shelby	●	J. Appl. Phys. 50 [1] 276 (1979)
Henderson	▲	Eur. J. Mineral. 14 [4] 733 (2002)
Evstrop'ev	△	Advances in Glass Technology, Plenum Press, NY 1962, vol. 2, p.79
Kiczinski	■	J. Non Cryst. Solids, 272 [1] 57 (2000)
Mundy	▼	Solid State Ionics 21 [4] 305 (1986)
Shmatok	▽	Fizika i Khimiya Stkla 12 [1] 81 (1986)
Efimov	○	Fizika i Khimiya Stkla 2 [2] 151 (1976)
Ivanov	◆	Fizika Tverdogo Tella 9 [5] 2647 (1963)
Sakka	+	J. Non Cryst. Solids 49 [1-3] 103 (1982)
Murthy	◇	J. Am. Ceram. Soc. 47 [9] 444 (1964)
Hanada	▽	J. Ceram. Soc. Jpn. 81 [11] 481 (1973)
Livshits	▣	Fizika i Khimiya Stkla 2 [2] 151 (1976)
Henderson-2	◻	J. Non Cryst. Solids 134 [3] 259 (1991)
Secco	⊕	J. Non Cryst. Solids 238 [3] 244 (1998)
Ruller	⊞	Phy. Chem. Glasses 33 [5] 161 (1992)
Akopyan	▣	Arm. Khim. Zh. 31 [2-3] 120 (1978)

Table A-VIII. Authors, Symbols and References for Density of $K_2O \cdot GeO_2$ Glasses (Figure 4-15 and 4-16).

Author	Symbol	Reference
Mayer	●	Glastech. Ber. 54 [9] 279 (1981)
Shelby	□	J. Appl. Phys. 50 [1] 276 (1979)
Murthy	▲	J. Am. Ceram. Soc. 47 [9] 444 (1964)
Henderson	▼	Eur. J. Mineral. 14 [4] 733 (2002)
Krupkin	△	Negro. Mater. 7 [9] 1591 (1971)
Verweij	□	J. Mater. Sci. 14 [4] 931 (1979)
Evstrop'ev	○	Advances in Glass Technology, Plenum Press, NY 1962, vol. 2, p.79
Efimov	+	Fizika i Khimiya Stkla 2 [2] 151 (1976)
Sakka	◆	J. Non Cryst. Solids 49 [1-3] 103 (1982)
Ivanov	◇	Fizika Tverdogo Tella 5 [9] 2647 (1963)
Kamiya	■	Res. Rep. Fac. Eng. Mie. 7 107 (1982)
Murthy	▽	Nature 201 [4916] 285 (1964)

Table A-IX. Authors, Symbols and References for Density of $Rb_2O \cdot GeO_2$ Glasses (Figures 4-17 and 4-18).

Author	Symbol	Reference
Nassau	●	J. Am. Ceram. 65 [4] 197 (1982)
Mayer	□	Glastech. Ber. 54 [9] 279 (1981)
Shelby	▲	J. Appl. Phys. 46 [1] 193 (1975)
Murthy	▼	Nature 201 [4916] 285 (1964)
Henderson	△	Eur. J. Mineral. 14 [4] 733 (2002)
Mundy	▽	Solid State Ionics 21 [4] 305 (1986)
Evstrop'ev	○	Advances in Glass Technology, Plenum Press, NY 1962, vol. 2, p.79
Huang	+	J. Non Cryst. Solids, 255 [1] 103 (1999)

Table A-X. Authors, Symbols and References for Density of $Cs_2O \cdot GeO_2$ Glasses (Figures 4-19 and 4-20).

Author	Symbol	Reference
Nassau	●	J. Am. Ceram. 65 [4] 197 (1982)
Mayer	□	Glastech. Ber. 54 [9] 279 (1981)
Shelby	▲	J. Appl. Phys. 46 [1] 193 (1975)
Murthy	▼	Nature 201 [4916] 285 (1964)
Di Martino	△	Phys. Chem. Glasses 43C 85 (2002)
Henderson	▽	Eur. J. Mineral. 14 [4] 733 (2002)

APPENDIX A

Table A-XI. Authors, Symbols and References for T_g of $\text{Li}_2\text{O}\cdot\text{GeO}_2$ Glasses (Figure 4-1).

Author	Symbol	Reference
Kiczinski	●	J. Non Cryst. Solids, 272 [1] 57 (2000)
Mochida	○	J. Cerm. Soc. Jpn. 94 [12]1225 (1986)
Marotta	▲	Proc. 2 nd Int. Conf. Fundamentals of Glass Science and Technology, Venice, 1993, 427
Radhakrishnan	▼	Mater. Sci. Eng. B14 [1] 17 (1992)
Shelby	△	Phys. Chem. Glasses 28 [6] 262 (1987)
Marotta-2	□	Phys. Chem. Glasses 37 [4] 134 (1996)

Table A-XII. Authors, Symbols and References for T_g of $\text{Na}_2\text{O}\cdot\text{GeO}_2$ Glasses (Figures 4-2 and 4-3).

Author	Symbol	Reference
Di Martino	●	Phys. Chem. Glasses 43C 85 (2002)
Shelby	○	J. Am. Ceram. Soc. 57 [10] 436 (1974)
Kiczinski	▲	J. Non Cryst. Solids, 272 [1] 57 (2000)
Marotta	▼	Proc. 2 nd Int. Conf. Fundamentals of Glass Science and Technology, Venice, 1993, 427
Laudisio	△	Mater. Chem. Phys. 51 [1] 54 (1997)
Mundy	□	Solid State Ionics 21 [4] 305 (1986)
Akopyan	■	Arm. Khim. Zh. 31 [2-3] 120 (1978)
Shelby-2	◻	J. Appl. Phys. 46 [1] 193 (1975)
Ruller	+	Phy. Chem. Glasses 33 [5] 161 (1992)
Gangopadhyay	◇	Am. Ceram. Soc. Bull. 56 [11] 1008 (1977)
Lee	◆	Phy. Chem. Glasses 36 [5] 225 (1995)
Hanada	▽	J. Ceram. Soc. Jpn. 81 [11] 481 (1973)
Marotta-2	⊕	Proc. XVIII th Inter. Congr. On Glass CD-ROM San Francisco, 1998, p. D5, 116
Gee	⊞	Phys. Chem. Glasses 41 [4] 175 (2000)
Catauro	◼	Thermochim. Acta 404 55 (2003)

Table A-XIII. Authors, Symbols and References for T_g of $\text{K}_2\text{O}\cdot\text{GeO}_2$ Glasses (Figures 4-4 and 4-5).

Author	Symbol	Reference
Shelby	●	J. Am. Ceram. Soc. 57 [10] 436 (1974)
Shelby-2	○	J. Appl. Phys. 46 [1] 193 (1975)
Kiczinski	▲	J. Non Cryst. Solids, 272 [1] 57 (2000)
Mochida	▼	J. Cerm. Soc. Jpn. 94 [12]1225 (1986)
Marotta	△	Proc. XVIII th Inter. Congr. On Glass CD-ROM San Francisco, 1998, p. D5, 116
Laudisio	□	Phy. Chem. Glasses 38 [5] 244 (1997)
Hall	■	Phy. Chem. Glasses 45 [4] 283 (2004)

Table A-XIV. Authors, Symbols and References for T_g of $Rb_2O \cdot GeO_2$ Glasses (Figures 4-6 and 4-7).

Author	Symbol	Reference
Shelby	●	J. Am. Ceram. Soc. 57 [10] 436 (1974)
Nassau	○	J. Am. Ceram. Soc. 65 [4] 197 (1982)
Shelby-2	▲	J. Appl. Phys. 46 [1] 193 (1975)
Huang	▼	J. Non Cryst. Solids, 255 [1] 103 (1999)
Kiczinski	△	J. Non Cryst. Solids, 272 [1] 57 (2000)

Table A-XV. Authors, Symbols and References for T_g of $Cs_2O \cdot GeO_2$ Glasses Figure 4-8.

Author	Symbol	Reference
Shelby	●	J. Am. Ceram. Soc. 57 [10] 436 (1974)
Nassau	○	J. Am. Ceram. Soc. 65 [4] 197 (1982)
Di Martino	▲	Phys. Chem. Glasses 43C 85 (2002)
Shelby-2	▼	J. Appl. Phys. 46 [1] 193 (1975)

Table A-XVI. Authors, Symbols and References for Density of $Li_2O \cdot GeO_2$ Glasses (Figures 4-11 and 4-12).

Author	Symbol	Reference
Henderson	●	Eur. J. Mineral. 14 [4] 733 (2002)
Verweij	□	J. Mater. Sci. 14 [4] 931 (1979)
Sakka	▲	J. Non Cryst. Solids 49 [1-3] 103 (1982)
Radhakrishnan	▼	Mater. Sci. Eng. B14 [1] 17 (1992)
Yoshimira	△	Yogyo Kyokaishi 79 [915] 428 (1971)
Shelby	▽	Phys. Chem. Glasses 28 [6] 262 (1987)

Table A-XVII. Authors, Symbols and References for Density of $Na_2O \cdot GeO_2$ Glasses (Figures 4-13 and 4-14).

Author	Symbol	Reference
Di Martino	□	Phys. Chem. Glasses 43C 85 (2002)
Shelby	●	J. Appl. Phys. 50 [1] 276 (1979)
Henderson	▲	Eur. J. Mineral. 14 [4] 733 (2002)
Evstrop'ev	△	Advances in Glass Technology, Plenum Press, NY 1962, vol. 2, p.79
Kiczinski	■	J. Non Cryst. Solids, 272 [1] 57 (2000)
Mundy	▼	Solid State Ionics 21 [4] 305 (1986)
Shmatok	▽	Fizika i Khimiya Stkla 12 [1] 81 (1986)
Efimov	○	Fizika i Khimiya Stkla 2 [2] 151 (1976)
Ivanov	◆	Fizika Tverdogo Tella 9 [5] 2647 (1963)
Sakka	+	J. Non Cryst. Solids 49 [1-3] 103 (1982)
Murthy	◇	J. Am. Ceram. Soc. 47 [9] 444 (1964)
Hanada	▽	J. Ceram. Soc. Jpn. 81 [11] 481 (1973)
Livshits	▣	Fizika i Khimiya Stkla 2 [2] 151 (1976)
Henderson-2	◻	J. Non Cryst. Solids 134 [3] 259 (1991)
Secco	⊕	J. Non Cryst. Solids 238 [3] 244 (1998)
Ruller	⊞	Phy. Chem. Glasses 33 [5] 161 (1992)
Akopyan	▣	Arm. Khim. Zh. 31 [2-3] 120 (1978)

Table A-XVIII. Authors, Symbols and References for Density of $K_2O \cdot GeO_2$ Glasses (Figure 4-15 and 4-16).

Author	Symbol	Reference
Mayer	●	Glastech. Ber. 54 [9] 279 (1981)
Shelby	□	J. Appl. Phys. 50 [1] 276 (1979)
Murthy	▲	J. Am. Ceram. Soc. 47 [9] 444 (1964)
Henderson	▼	Eur. J. Mineral. 14 [4] 733 (2002)
Krupkin	△	Negro. Mater. 7 [9] 1591 (1971)
Verweij	□	J. Mater. Sci. 14 [4] 931 (1979)
Evstrop'ev	○	Advances in Glass Technology, Plenum Press, NY 1962, vol. 2, p.79
Efimov	+	Fizika i Khimiya Stkla 2 [2] 151 (1976)
Sakka	◆	J. Non Cryst. Solids 49 [1-3] 103 (1982)
Ivanov	◇	Fizika Tverdogo Tella 5 [9] 2647 (1963)
Kamiya	■	Res. Rep. Fac. Eng. Mie. 7 107 (1982)
Murthy	▽	Nature 201 [4916] 285 (1964)

Table A-XIX. Authors, Symbols and References for Density of $Rb_2O \cdot GeO_2$ Glasses (Figures 4-17 and 4-18).

Author	Symbol	Reference
Nassau	●	J. Am. Ceram. 65 [4] 197 (1982)
Mayer	□	Glastech. Ber. 54 [9] 279 (1981)
Shelby	▲	J. Appl. Phys. 46 [1] 193 (1975)
Murthy	▼	Nature 201 [4916] 285 (1964)
Henderson	△	Eur. J. Mineral. 14 [4] 733 (2002)
Mundy	▽	Solid State Ionics 21 [4] 305 (1986)
Evstrop'ev	○	Advances in Glass Technology, Plenum Press, NY 1962, vol. 2, p.79
Huang	+	J. Non Cryst. Solids, 255 [1] 103 (1999)

Table A-XX. Authors, Symbols and References for Density of $Cs_2O \cdot GeO_2$ Glasses (Figures 4-19 and 4-20).

Author	Symbol	Reference
Nassau	●	J. Am. Ceram. 65 [4] 197 (1982)
Mayer	□	Glastech. Ber. 54 [9] 279 (1981)
Shelby	▲	J. Appl. Phys. 46 [1] 193 (1975)
Murthy	▼	Nature 201 [4916] 285 (1964)
Di Martino	△	Phys. Chem. Glasses 43C 85 (2002)
Henderson	▽	Eur. J. Mineral. 14 [4] 733 (2002)